

Milan Halenka
Zdeněk Fryšák

Atlas of Thyroid Ultrasonography



Atlas of Thyroid Ultrasonography

Milan Halenka • Zdeněk Fryšák

Atlas of Thyroid Ultrasonography

Milan Halenka, MD, PhD
Department of Internal Medicine III –
Nephrology, Rheumatology and Endocrinology
Faculty of Medicine and Dentistry
Palacky University Olomouc
and University Hospital Olomouc
Olomouc
Czech Republic

Zdeněk Fryšák, MD, CSc
Department of Internal Medicine III –
Nephrology, Rheumatology and Endocrinology
Faculty of Medicine and Dentistry
Palacky University Olomouc
and University Hospital Olomouc
Olomouc
Czech Republic

ISBN 978-3-319-53758-0 ISBN 978-3-319-53759-7 (eBook)
DOI 10.1007/978-3-319-53759-7

Library of Congress Control Number: 2017938120

© Springer International Publishing AG 2017

This work is subject to copyright. All rights are reserved by the Publisher, whether the whole or part of the material is concerned, specifically the rights of translation, reprinting, reuse of illustrations, recitation, broadcasting, reproduction on microfilms or in any other physical way, and transmission or information storage and retrieval, electronic adaptation, computer software, or by similar or dissimilar methodology now known or hereafter developed.

The use of general descriptive names, registered names, trademarks, service marks, etc. in this publication does not imply, even in the absence of a specific statement, that such names are exempt from the relevant protective laws and regulations and therefore free for general use.

The publisher, the authors and the editors are safe to assume that the advice and information in this book are believed to be true and accurate at the date of publication. Neither the publisher nor the authors or the editors give a warranty, express or implied, with respect to the material contained herein or for any errors or omissions that may have been made. The publisher remains neutral with regard to jurisdictional claims in published maps and institutional affiliations.

Printed on acid-free paper

This Springer imprint is published by Springer Nature
The registered company is Springer International Publishing AG
The registered company address is: Gewerbestrasse 11, 6330 Cham, Switzerland

Preface

Diagnosis and treatment of thyroid gland diseases are a very important part of the everyday clinical work of endocrinologists worldwide. Ultrasonography is an essential part of the clinical practice, and its development has largely broadened our clinical options. High-quality resolution ultrasound devices are now available in most hospitals and diagnostic centers around the globe. Ultrasonography can serve as the first diagnostic tool but the figure may sometimes provide the final diagnosis.

This book not only covers the whole spectrum of thyroid and parathyroid gland diseases but also aims to put them into the perspective of general endocrinology practice, utilizing the authors' own experience from long-term teaching of hospital practice.

This atlas is designed as a figure-based book. The authors hope that it serves its readers as a quick reference for clinical practice, not necessarily only in endocrinology practices but also in radiology practices, as well as other clinicians looking for easy-to-access figure information. Ultrasonography is an “expert-based” method partially dependent on the talent of the examiner but it also significantly depends on one's ability, in the right moment, to recall something already seen. As such, we hope that we can help place “first images” in the minds of beginners, indicating both common and rare ultrasonography appearances. Each disease is therefore depicted several times, in several views, to ease the first steps with ultrasonography.

This atlas is derived from its very successful Czech version, and although it is not the first ultrasonography publication, our everyday practice demonstrates the need for current and precise information.

We encourage our readers to employ a lot of patience at the beginning and wish them a great deal of success in their clinical practice.

Olomouc, Czech Republic
Olomouc, Czech Republic

Milan Halenka
Zdeněk Fryšák

Instructions for Readers

Figure Numbering and Marking

- The atlas is divided into chapters according to specific diagnoses. For each diagnosis there are several case reports in different US views.
- In each chapter the figure number corresponds to a single patient with a specific diagnosis. Letters correspond to different US views/cuts (e.g., whole thyroid gland [TG] *transverse*, detail of right lobe [RL] or left lobe [LL], *transverse* or *longitudinal*), in certain cases with CFDS.
- In the upper-right corner there is a pictogram showing the exact probe location.
- Unless stated otherwise the depth of penetration is 3.5 cm.

Atlas Concept

- Each figure is depicted twice on the same page: on the left side (number and small letters) without marks, on the right side (number and small double letters) with marks showing thyroid gland and the US finding. Figure description is below the right figure.
- This design is meant to allow readers to self-test their knowledge.

Acknowledgments

The authors are grateful to our colleagues from the Third Department of Internal Medicine—Nephrology, Rheumatology and Endocrinology, Palacky University Olomouc, Czech Republic. Special thanks go to Charlotte Mlcochova, BA, our experienced registered nurse, for her everyday help with ultrasonography (as a small gift the figures in first chapter are of her own healthy thyroid gland); to Michal Slansky for technical support with completing the figures; to Jan Schovanek, MD, for language and content editing; and to Asst. Prof. Pavel Koranda, MD, PhD, for PET/CT and SPECT/CT imaging in Sect. 7 of Chap. 15 and Chap. 22.

This publication would not be possible without the support of the chief of our clinic, Professor Josef Zadrazil, MD, CSc. And our gratitude also goes to Professor Karel Pacak, MD, PhD, DSc, FACE, for encouragement to prepare the English version.

Contents

Part I Normal Thyroid Gland

1 Normal Ultrasound of Thyroid Gland and Lymph Nodes	3
1.1 Essential Facts	3
1.2 US Characteristics of the Thyroid Gland	3
1.3 Color Flow Doppler Sonography (CFDS) Pattern	4
1.4 A Normal Thyroid Gland Shows	6
1.5 US Characteristics of the Benign or Reactive Cervical Lymph Nodes	6
References	7

Part II Diffuse Thyroid Diseases

1.1 Essential Facts	9
References	9
2 Diffuse Goiter	11
2.1 Essential Facts	11
2.2 US Features of Diffuse Goiter	14
References	15
3 Hashimoto's Thyroiditis	17
3.1 Hashimoto's Thyroiditis: Chronic Lymphocytic Thyroiditis	17
3.1.1 Essential Facts	17
3.1.2 US Features of Hashimoto's Thyroiditis	18
3.2 Hashimoto's Thyroiditis: Goiter	23
3.3 Hashimoto's Thyroiditis: Atrophic Gland	30
3.4 Hashimoto's Thyroiditis: Hashitoxicosis	35
3.4.1 Essential Facts	35
3.4.2 US Features of Hashitoxicosis	35
References	39
4 Graves' Disease	41
4.1 Essential Facts	41
4.2 US Features of Graves' Disease	42
4.3 US Features of Thyroid Gland After Radioiodine ¹³¹ I–Therapy (RIT)	52
References	53
5 Subacute Granulomatous Thyroiditis: de Quervain's Diseases	55
5.1 Essential Facts	55
5.2 US Features of Subacute Granulomatous Thyroiditis	56
References	69







6 Amiodarone-Induced Thyrotoxicosis	71
6.1 Essential Facts	71
6.2 US Findings of Amiodarone-Induced Thyrotoxicosis	76
References	76
 Part III Nodular Goiter: Benign Lesions	
1.1 Thyroid Nodules	77
1.1.1 Essential Facts	77
1.1.2 US Characteristics of Nodules According to the Korean Society of Thyroid Radiology	77
References	78
7 Thyroid Cysts	79
7.1 Essential Facts	79
7.2 US Features of Thyroid Cysts	81
References	91
8 Solid Nodule	93
8.1 Essential Facts	93
8.2 US Features of a Benign Solid Nodule	93
References	103
9 Complex Nodule	105
9.1 Complex Nodule with Cystic Degeneration	105
9.1.1 Essential Facts	105
9.1.2 US Features of Complex Nodules with Cystic Degeneration	105
9.2 Complex Nodule with Calcifications	107
9.2.1 Essential Facts	107
9.2.2 Ultrasound Features of Calcifications	106
References	117
10 Multinodular Goiter	119
10.1 Essential Facts	119
10.2 US Features of Multinodular Goiter	119
References	128
11 Substernal Goiter	129
11.1 Essential Facts	129
11.2 US Characteristics	134
References	134
12 Toxic Multinodular Goiter and Solitary Toxic Adenoma	135
12.1 Essential Facts	135
12.2 US Findings of Toxic Multinodular Goiter or Solitary Toxic Adenoma	140
References	140
 Part IV Nodular Goiter: Suspicious and Malignant Lesions	
1.1 Incidence and Mortality Worldwide According to Data from the International Agency for Research of Cancer World Health Organization—Globocan 2012	141
1.2 Essential Facts According to the 2015 American Thyroid Association (ATA) Guidelines	141

1.3	Clinical Assessment Increasing the Likelihood of Malignancy	142
1.4	US Characteristics of Thyroid Carcinoma	142
1.5	US Classic Features of High Suspicion of Malignancy for Solid Nodules According to the 2015 ATA Guidelines	142
1.6	US Features of High Suspicion of Malignancy for Cystic Nodules According to the 2015 ATA Guidelines	142
1.7	US Features of Malignant Nodules According to the Korean Society of Thyroid Radiology	142
	References	143
13	Lesions with Intermediate Suspicion of Malignancy	145
13.1	Essential Facts	145
13.2	US Criteria of Suspicious and Benign Lesions	148
	References	153
14	Follicular Thyroid Carcinoma	155
14.1	Essential Facts	155
14.2	US Features of FTC According to the 2015 ATA Guidelines	156
	References	163
15	Papillary Thyroid Carcinoma	165
15.1	Papillary Thyroid Microcarcinoma	165
15.1.1	Essential Facts	165
15.1.2	US Features of the Papillary Thyroid Microcarcinoma	165
15.2	Papillary Thyroid Carcinoma: A Small Solitary Nodule ≤ 2 cm	172
15.2.1	Essential Facts	172
15.2.2	US Features of PTC, a Small Nodule ≤ 2 cm	173
15.3	Papillary Thyroid Carcinoma: Medium-Sized and Large Nodules >4 cm	190
15.3.1	Essential Facts	190
15.3.2	US Features of PTC, Medium-Sized and Large Nodules >4 cm	191
15.4	Multifocal Papillary Thyroid Carcinoma	207
15.4.1	Essential Facts	207
15.4.2	US Findings of Multifocal Papillary Thyroid Carcinoma	208
15.5	Papillary Thyroid Carcinoma and Hashimoto's Thyroiditis	214
15.5.1	Essential Facts	214
15.5.2	US Features of Cancerous Thyroid Nodules in the Field of HT	214
15.6	Papillary Thyroid Carcinoma and Graves' Disease or Amiodarone-Induced Thyrotoxicosis	225
15.6.1	Essential Facts	225
15.6.2	US Features of Papillary Thyroid Carcinoma in Graves' Disease	226
15.6.3	US Features of Papillary Thyroid Carcinoma in Amiodarone-Induced Thyrotoxicosis	228
15.7	Synchronous Papillary Thyroid Carcinoma and Parathyroid Adenoma	231
15.7.1	Essential Facts	231
15.7.2	US Features of Parathyroid Adenoma and Papillary Thyroid Carcinoma	231
15.8	Differentiated Thyroid Carcinoma and Extrathyroidal Extension	231
15.8.1	Essential Facts	231
15.8.2	US Features of Extrathyroidal Extension	233
15.9	Papillary Thyroid Carcinoma in Children and Adolescents	236
15.9.1	Essential Facts	236
15.9.2	US Features of Papillary Thyroid Carcinoma in Childhood	243
	References	243

16 Medullary Thyroid Carcinoma	247
16.1 Essential Facts	247
16.2 US Features of Medullary Thyroid Carcinoma	247
References	256
17 Anaplastic Thyroid Carcinoma	257
17.1 Essential Facts	257
17.2 US Features of Anaplastic Thyroid Carcinoma	258
References	263
18 Other Malignancies in Thyroid Gland and Cervical Lymph Nodes	265
18.1 Other Malignancies in Thyroid Gland and Cervical Lymph Nodes: Primary Thyroid Lymphoma	265
18.1.1 Essential Facts	265
18.1.2 US Features of Primary Thyroid Lymphoma	266
18.2 Other Malignancies in Thyroid Gland and Cervical Lymph Nodes: Extramedullary Plasmacytoma	271
18.2.1 Essential Facts	271
18.2.2 US Features of Extramedullary Plasmacytoma in the Thyroid Gland	271
18.3 Other Malignancies in Thyroid Gland and Cervical Lymph Nodes: Malignant Cervical Lymph Nodes, Primary Outside the Thyroid Gland	273
18.3.1 Essential Facts	273
18.3.2 US Features of Metastatic Lymph Nodes	273
18.3.3 US Features of Malignant Lymph Nodes in Lymphomas	281
References	281
19 Metastatic Cervical Lymph Nodes Post Total Thyroidectomy for Thyroid Carcinoma	283
19.1 Essential Facts	283
19.2 US Features of Metastatic Lymph Nodes	284
References	295
Part V Miscellanea	
20 Thyroid Tissue Remnants Post Thyroidectomy	299
20.1 Essential Facts	299
20.2 US Findings of Thyroid Remnants	300
References	310
21 Rare Ultrasound Findings of the Thyroid Gland and Lesions Imitating Goiter	311
21.1 Essential Facts	311
21.2 US Findings of Lesions at the Anterior Neck Space Mimicking Thyroid	313
21.3 US Findings of Artifacts	327
21.4 US Findings of Normal Anatomic Structure of Thyroid Gland Mimic a Lesion	328
References	328

22 Parathyroid Adenoma and Parathyroid Carcinoma	329
22.1 Essential Facts	329
22.2 US Features of Parathyroids	331
References.	363
23 Percutaneous Ethanol Injection Therapy	365
23.1 Method, Indications, and Complications of PEIT	365
23.2 Ultrasound-Guided Percutaneous Ethanol Injection Therapy (US-PEIT) of Thyroid Cysts	366
23.3 Ultrasound-Guided Percutaneous Ethanol Injection Therapy (US-PEIT) of the Parathyroid Gland	372
References.	382
24 Ultrasound-Guided Fine-Needle Aspiration Biopsy (US-FNAB)	383
24.1 Essential Facts	383
24.2 Importance and Benefits of FNAB in the Diagnosis of Nodular Thyroid Disease in the Beginning of the 1990s by Gharib	383
24.3 Diagnostic Yield of FNAB in the Diagnosis of Nodular Thyroid Disease in the Beginning of the 1990s by Gharib	383
24.4 Current FNAB Experience by Dean and Gharib	384
24.5 The Large Analysis of the Brigham and Women's Hospital and Harvard Medical School with a Total of 1985 Patients and FNAB of 3483 Nodules	384
24.6 Recommendations for Diagnostic FNAB of a Thyroid Nodules Based on US Pattern According to the 2015 ATA Guidelines	385
24.7 The Bethesda System for Reporting Thyroid Cytopathology	386
24.8 Basic Equipment Needed for US-FNAB	387
24.9 Description of US-Guided FNAB	388
24.10 Hemorrhage as a FNAB Complication	389
References.	392
25 Thyroid Abscess as a Complication of Fine-Needle Aspiration Biopsy: A Case Report	393
25.1 Essential Facts	393
25.2 The Case Report.	394
References.	396
Index	397

Key: Abbreviations and Symbols in Figures

	<i>Cross</i> , used to indicate lobes of thyroid gland (all figures)
	<i>Arrowhead</i> , used to indicate main US finding—large node, cyst, carcinoma, parathyroid adenoma
	<i>Blank arrowhead</i> , used to indicate main US finding—large lymphatic nodule, parathyroid adenoma
	<i>Arrow</i> , used to indicate main and accessory US finding—small nodule, parathyroid adenoma, dense calcification
	<i>Open arrow</i> , used to indicate accessory US finding—microcalcification, colloid clot, septum
	<i>Mark</i> , used to indicate small lymphatic nodule or small node
TRA	Trachea
CCA	Common carotid artery
IJV	Internal jugular vein
E	Esophagus
NL, nl	Large, small lymphatic nodule
C, c	Large, small cyst
LL, RL	Left Lobe, Right Lobe
PAd	Parathyroid adenoma

List of Abbreviations

AIT	Amiodarone-induced thyrotoxicosis
ASR-W	Age-standardized rate—world
ATA	The American Thyroid Association
ATC	Anaplastic thyroid carcinoma
BCC	Branchial cleft cyst
CCA	Common carotid artery
CFDS	Color flow doppler sonography
CLT	Chronic lymphocytic thyroiditis (= HT—Hashimoto thyroiditis)
CRP	C-Reactive protein
DC	Dermoid cyst
DTC	Differentiated thyroid cancer
DTD	Diffuse thyroid disease
EMP	Extramedullary plasmacytoma
ESR	Erythrocyte sedimentation rate
ETE	Extrathyroidal extension
FLT	Focal lymphocytic thyroiditis
FNAB	Fine-needle aspiration biopsy

FTC	Follicular thyroid carcinoma
FVPTC	Follicular variant of papillary carcinoma
HCC	Hurthle cell carcinoma
HT	Hashimoto's thyroiditis (= CLT—chronic lymphocytic thyroiditis)
IDD	Iodine deficiency disorders
IJV	Internal jugular vein
ITA	Inferior thyroid artery
LL	Left lobe
LN	Lymph node
L/S	Long-to-short axes ratio
MEN 2A	Multiple endocrine neoplasia 2A
MEN 2B	Multiple endocrine neoplasia 2B
MIVAT	Minimally invasive video-assisted technique
MNG	Multinodular goiter
MTC	Medullary thyroid carcinoma
pHPT	Primary hyperparathyroidism
PAd	Parathyroid adenoma
PCa	Parathyroid carcinoma
PEIT	Percutaneous ethanol injection therapy
PET/CT	Positron emission tomography/computed tomography
PSV	Peak systolic velocity
PTC	Papillary thyroid carcinoma
PTL	Primary thyroid lymphoma
PTMC	Papillary thyroid microcarcinoma
RAIU	Radioactive iodine uptake test
RIT	Radioiodine therapy
RL	Right lobe
sHPT	Secondary hyperparathyroidism
SAC	School age children
SGT	Subacute granulomatous thyroiditis
S/L	Short to long axis ratio
SPECT/CT	Single photon emission tomography/computed tomography
SSG	Substernal goiter
STA	Solitary toxic adenoma
Tg-Ab	Thyroglobulin antibody
TMNG	Toxic multinodular goiter
TPO-Ab	Thyroid peroxidase antibody
TSH	Thyroid-stimulating hormone/thyrotropin
TSHR-Ab	Thyroid-stimulating hormone receptor antibody
TT	Total thyroidectomy
Tvol	Thyroid volume (mL)

Part I

Normal Thyroid Gland

1.1 Essential Facts

- The thyroid gland is composed of two lobes connected by a median isthmus.
- 40% of all patients have an accessory lobe—the pyramidal lobe, which is more or less developed. It extends from the isthmus toward the hyoid bone, in front of the thyroid cartilage.
- The thyroid lies in front of and on the sides of the trachea. It is bounded posterolateral by the carotid space, and its anterior and lateral aspects are covered by the strap muscles and the sternocleidomastoid muscles. The posterior surfaces of the lobes are adjacent to the perivertebral space and on the left to the esophagus [1].
- A thyroid lobe has the shape of the rotation ellipsoid. Method of Brunn is widely used to calculate thyroid volume (Tvol). Tvol is a sum of the two lobes each calculated according to the following formula: $V = \text{width} \times \text{depth} \times \text{length} \times 0.479$; or, an optimized correction factor 0.52 can be used [2, 3].
- The contribution of the thyroid isthmus to total gland volume should be ignored [2]. But if the isthmus is >1 cm, its volume should be included [3].
- Caution! Differences in technique (e.g., the pressure applied with the transducer) and in estimation of thyroid anatomy (e.g., inclusion of the thyroid isthmus and estimation of capsule thickness) can produce interobserver errors in Tvol as high as 26% [3].

1.2 US Characteristics of the Thyroid Gland [4]

- The echogenicity: isoechoic, hypoechoic, markedly hypoechoic, and hyperechoic patterns. The strap muscles and submandibular glands were used as a reference for the determination of echogenicity.
- The echotexture: fine, coarse, and micronodulative patterns.
- The glandular vascularity: normal, mildly increased, markedly increased, and decreased patterns.
- The margin of the thyroid: smooth, microlobulated, and macrolobulated patterns.

1.3 Color Flow Doppler Sonography (CFDS) Pattern [5]

- *Pattern 0* (Fig. 5.1dd): absent intraparenchymal (or nodular) vascularity or minimal spots.
- *Pattern I* (Fig. 1.1bb): presence of parenchymal (or nodular) blood flow with patchy uneven distribution.
- *Pattern II* (Fig. 3.15bb): mild increase of color flow Doppler signal with patchy distribution (for nodules: mainly peripheral).
- *Pattern III* (Fig. 4.1bb): markedly increased color flow Doppler signal with diffuse homogeneous distribution, including the so-called “thyroid inferno” [6].

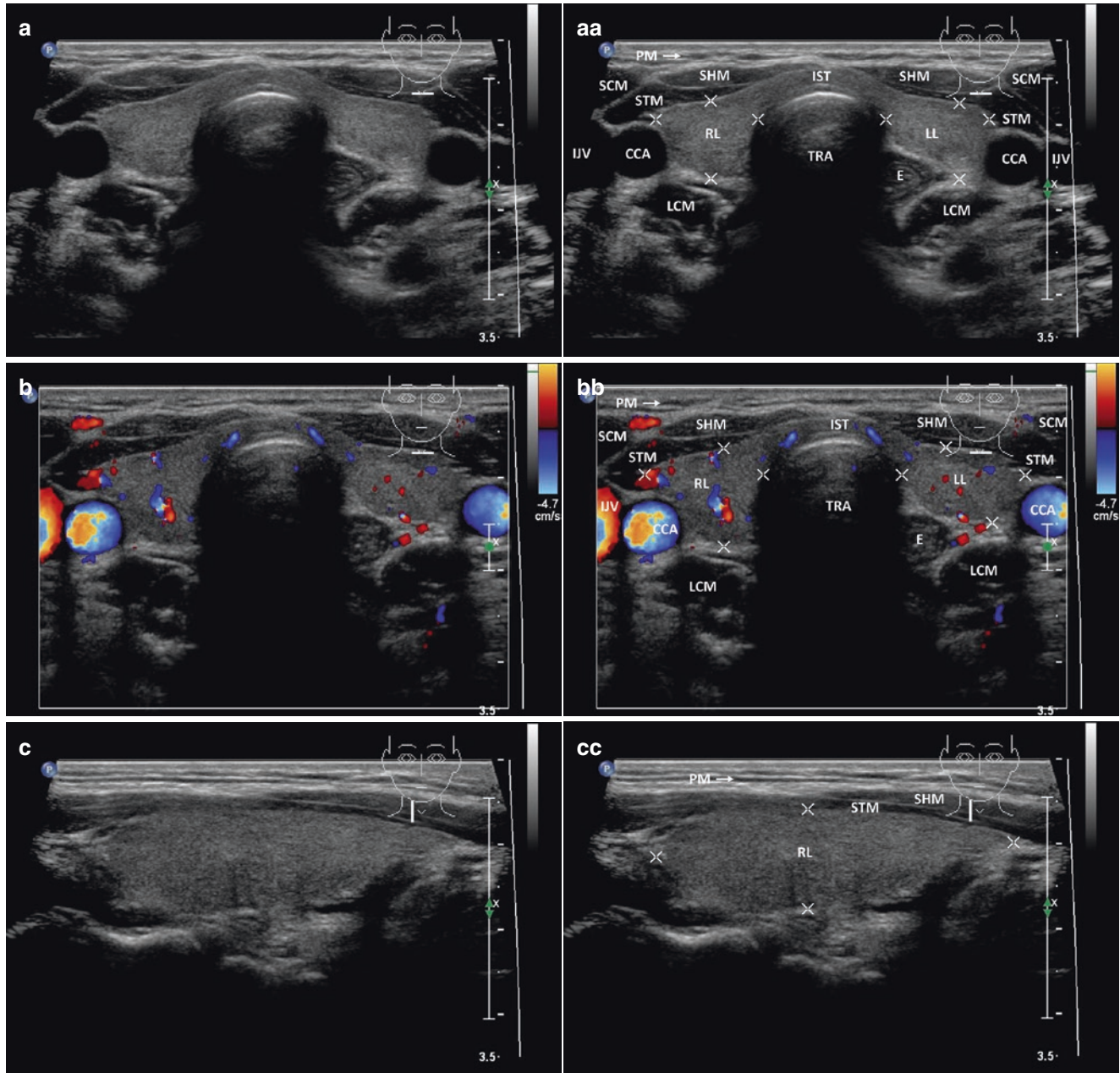
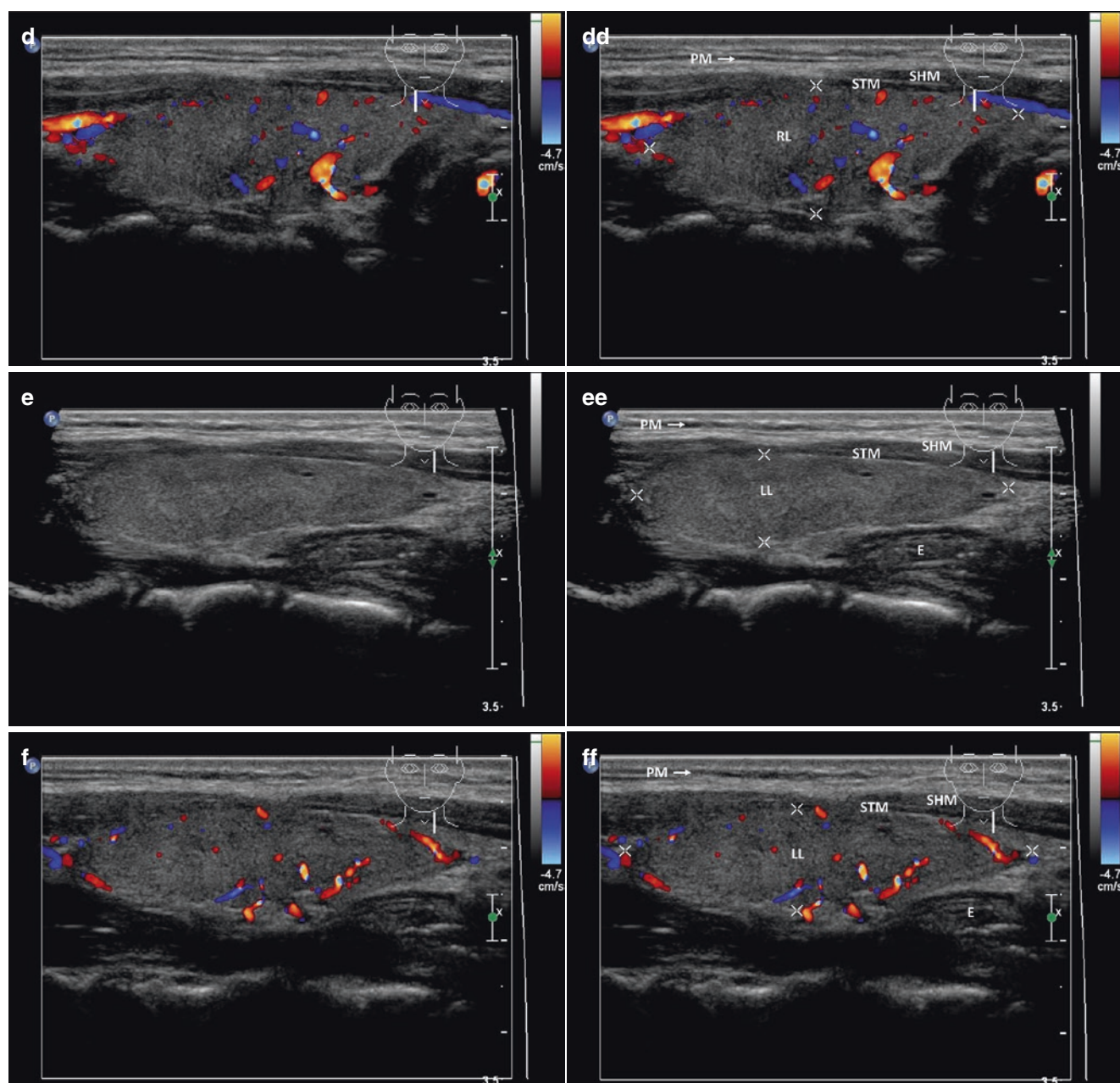


Fig. 1.1 (aa) Thyroid gland and surrounding structures: thyroid gland—homogeneous structure; isoechoic. CCA—common carotid artery; E—esophagus; IJV—internal jugular vein; IST—isthmus; LCM—longus coli muscle; LL—left lobe; PM—platysma muscle, RL—right lobe; SCM—sternocleidomastoid muscle; SHM—sternohyoid muscle; STM—sternothyroid muscle; transverse. (bb) Thyroid

gland and surrounding structures, CFDS: normal parenchymal vascularity, *pattern I*; transverse. (cc) Detail of RL: homogeneous structure; isoechoic; longitudinal. (dd) Detail of RL, CFDS: normal parenchymal vascularity, *pattern I*; longitudinal. (ee) Detail of LL: homogeneous structure; isoechoic; longitudinal. (ff) Detail of LL, CFDS: normal parenchymal vascularity, *pattern I*; longitudinal

**Fig. 1.1** (continued)

1.4 A Normal Thyroid Gland Shows

- Isoechogenicity (the echogenicity is higher compared to overlying strap musculature and similar to parotid or sub-mandibular glands).
- Fine echotexture.
- Absence of scattered microcalcifications.
- Normal vascularity, CFDS—*pattern 0 or 1*.
- Smooth margin.
- On transverse section, a thyroid lobe has a triangular shape, an anteroposterior (AP) diameter from 1 to 2 cm on longitudinal section has an ovoid shape.

1.5 US Characteristics of the Benign or Reactive Cervical Lymph Nodes [7]

- Size: different cut-offs of the nodal size to differentiate reactive and metastatic nodes have been reported (5 mm, 8 mm, and 10 mm).

- Shape: elliptical.
- Short-to-long axis ratio (S/L ratio) <0.5 [7], or long-to-short axis ratio (L/S) >2 [8, 9] (Fig. 1.2bb).
- Margin: unsharp.
- Internal architecture.
 - Echogenicity: hypoechoic.
 - Echogenic hilus (an echogenic intranodal linear structure which is continuous with the adjacent perinodal fat) will demonstrate about 90% of nodes with a maximum transverse diameter >5 mm. Hilus sign (Fig. 1.2aa, bb)—the presence of an echogenic hilus was previously considered a sign of benign disease.
 - Without calcification and necrosis
- Vascular pattern: Approximately 90% of normal lymph nodes with a maximum transverse diameter >5 mm will demonstrate hilar vascularity, or appear apparently avascular.

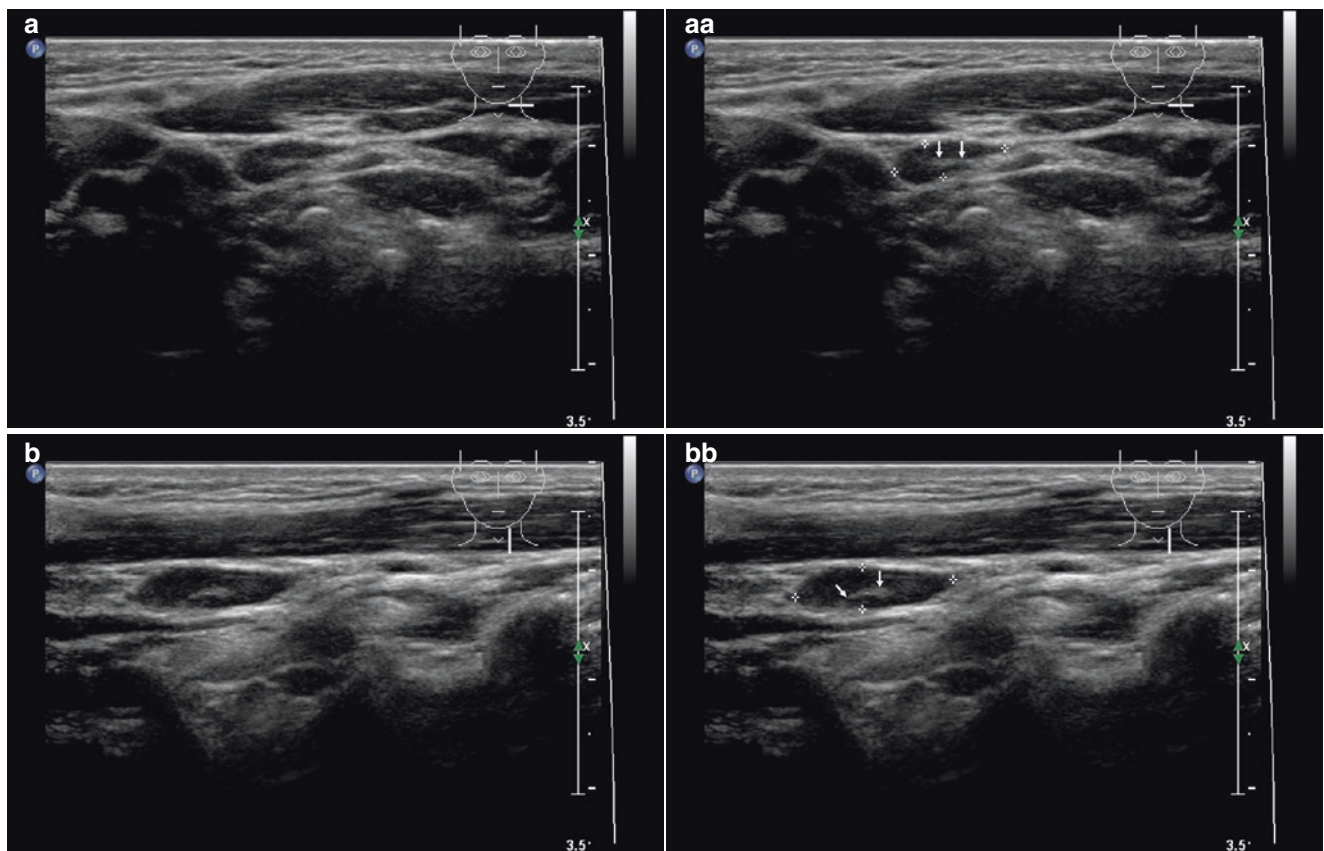


Fig. 1.2 (aa) Normal lymph node: elliptical shape; hypoechoic; hilus sign (arrows); transverse. (bb) Normal lymph node: elliptical shape, L/S ratio >2 (not pathological); hypoechoic; hilus sign (arrows); longitudinal

References

1. Gervasio A, Mujahed I, Biasio A, Alessi S. Ultrasound anatomy of the neck: the infrahyoid region. *J Ultrasound*. 2010;13(3):85–9.
2. Brunn J, Block U, Ruf G, Bos I, Kunze WP, Scriba PC. Volumetric analysis of thyroid lobes by real-time ultrasound. *Dtsch Med Wochenschr*. 1981;106(41):1338–40.
3. Zimmermann MB, Molinari L, Spehl M, Weidinger-Toth J, Podoba J, Hess S, et al. Toward a consensus on reference values for thyroid volume in iodine-replete schoolchildren: results of a workshop on inter-observer and inter-equipment variation in sonographic measurement of thyroid volume. *Eur J Endocrinol*. 2001;144(3):213–20.
4. Kim DW, Eun CK, In HS, Kim MH, Jung SJ, Bae SK. Sonographic differentiation of asymptomatic diffuse thyroid disease from normal thyroid: a prospective study. *AJNR Am J Neuroradiol*. 2010;31(10):1956–60.
5. Bogazzi F, Bartalena L, Brogioni S, Burelli A, Manetti L, Tanda ML, et al. Thyroid vascularity and blood flow are not dependent on serum thyroid hormone levels: studies in vivo by color flow doppler sonography. *Eur J Endocrinol*. 1999;140(5):452–6.
6. Ralls PW, Mayekawa DS, Lee KP, Colletti PM, Radin DR, Boswell WD, et al. Color-flow Doppler sonography in Graves disease: “thyroid inferno”. *AJR Am J Roentgenol*. 1988;150(4):781–4.
7. Ahuja AT, Ying M, Ho SY, Antonio G, Lee YP, King AD, et al. Ultrasound of malignant cervical lymph nodes. *Cancer Imaging*. 2008;8(1):48–56.
8. Solbiati L, Rizzatto G, Bellotti E, Montali G, Cioffi V, Croce F. High-resolution sonography of cervical lymph nodes in head and neck cancer: criteria for differentiation of reactive versus malignant nodes. *Radiology*. 1988;169(P):113–6.
9. Steinkamp HJ, Cornehl M, Hosten N, Pegios W, Vogl T, Felix R. Cervical lymphadenopathy: ratio of long- to short-axis diameter as a predictor of malignancy. *Br J Radiol*. 1995;68(807):266–70.

Diffuse Thyroid Diseases

1.1 Essential Facts

- The natural history of thyroid disorders, including simple goiter, chronic thyroiditis, hyperthyroidism, hypothyroidism, and nodular diseases of the thyroid, indicates they are dynamic and changeable in form, function, appearance, and disappearance. Diffuse thyroid diseases (DTD) are dominant morphologic abnormalities of thyroid gland. The leading disease of the young is diffuse adolescent goiter, and in adults the most common is chronic lymphocytic thyroiditis (CLT), also known as Hashimoto's thyroiditis (HT) [1].
- The WHO 1960 criteria for classification of thyroid size in children defined four grades of goiter: Grade IA—palpable lobes larger than the terminal phalanges of the subject's thumbs; Grade IB—the thyroid visible with the neck extended; Grade II—the thyroid visible with the head in normal position; and Grade III—the thyroid visible at a distance. The WHO 1994 criteria defined two grades of goiter: Grade I—the thyroid palpable but not visible with the head in a normal position; and Grade II—the thyroid visible with the neck in the normal position [2].
- In 1994, World Health Organization/International Council for the Control of Iodine Deficiency Disorders (WHO/ICCIDD) recommended replacing the WHO 1960 four-grade goiter classification with the simplified two-grade system. The WHO 1994 criteria are simpler to use than the 1960 criteria and provide increased sensitivity with only a small reduction in specificity. Like the 1960 criteria, the 1994 criteria overestimate goiter prevalence in areas of mild iodine deficiency disorders (IDD). In areas of mild IDD where goiters are small, US is preferable to palpation to estimate goiter prevalence [3].
- Goiter prevalence in school-age children (SAC) is an important indicator of IDD in a population. A goiter prevalence $\geq 5\%$ in SAC indicates a public health problem. Inspection and palpation have traditionally been used to classify goiters. However, in areas of mild-to-moderate IDD, the sensitivity and specificity of palpation are poor, and measurement of the thyroid volume (Tvol) by US is preferable [4].

References

1. Rallison ML, Dobyns BM, Meikle AW, Bishop M, Lyon JL, Stevens W. Natural history of thyroid abnormalities: prevalence, incidence, and regression of thyroid diseases in adolescents and young adults. *Am J Med.* 1991;91(4):363–70.
2. WHO, UNICEF & ICCIDD. Indicators for assessing iodine deficiency disorders and their control through salt iodization. WHO/NUT/94.6. Geneva: World Health Organization; 1994. http://apps.who.int/iris/bitstream/10665/70715/1/WHO_NUT_94.6.pdf.
3. Zimmermann M, Saad A, Hess S, Torresani T, Chaouki N. Thyroid ultrasound compared with World Health Organization 1960 and 1994 palpation criteria for determination of goiter prevalence in regions of mild and severe iodine deficiency. *Eur J Endocrinol.* 2000;143(6):727–31.
4. Zimmermann MB, Hess SY, Molinari L, De Benoist B, Delange F, Braverman LE, et al. New reference values for thyroid volume by ultrasound in iodine-sufficient schoolchildren: a World Health Organization/Nutrition for Health and Development Iodine Deficiency Study Group Report. *Am J Clin Nutr.* 2004;79(2):231–7.

2.1 Essential Facts

- Diffuse goiter is a generalized thyroid hyperplasia. When measured thyroid volume (Tvol) by US, the goiter is defined by Gutekunst from the year 1988 as Tvol >18 ml in women and Tvol >25 ml in men (Figs. 2.1 and 2.2) [1].
- Normative data of Tvol, showing variations with age, regional factors, and iodine status of the population, have been reported in different populations.
- Iodine deficiency endemic area is defined by the goiter prevalence and the median urinary iodine concentration in a population. The local sex-specific reference values at different ages and body surface areas are not a constant proportion of the WHO/ICCIDD-recommended reference. A further limitation of the WHO/ICCIDD-recommended reference is the lack of normative values for children with small body surface areas (<0.8 m²) commonly found in developing countries [2].
- Epidemiologic study for thyroid abnormalities were performed by Rallison et al. in 4819 school-age children (SAC), ages 11–18 years, from 1965 to 1968. Two-thirds of this original cohort (3121) were re-examined 20 years later, in 1985 and 1986.
 - In the initial examinations (1965–1968), 185 thyroid abnormalities were found (3.7% of the total). These abnormalities were, in order from the most common to the least common: diffuse hypertrophy with normal function (adolescent goiter) in 19.3/1000; CLT in 12.7/1000; and thyroid nodules in 4.6/1000, including two papillary thyroid carcinomas (PTC). Hyperthyroidism or hypothyroidism was found in 1.9/1000.
 - In the follow-up examinations (1985–1986), 298 (10.5%) subjects had thyroid abnormalities (10.5% of the total). These abnormalities were, in order from the most common to least common: CLT in 51.3/1000; simple goiters in 28.7/1000; and nodules in 23.2/1000, which included 10 carcinomas. In addition, 9/1000 had hypothyroidism and 3.9/1000 had hyperthyroidism [3].

Of the 92 subjects with simple or adolescent goiter in 1965–1968, 60% were normal by 1985–1986, 20% were unchanged, approximately 10% had developed CLT, and approximately 3% had developed colloid goiters. Of 61 subjects with CLT, 27% had become normal, about 33% remained unchanged, and 33% had become hypothyroid [3].

- In a study by Hintze et al., a palpation (WHO 1960 palpation criteria) and an ultrasound investigation of the thyroid were performed on 569 unselected elderly subjects greater than 60 years of age from the general population of an iodine-deficient area. Of the subjects, 489 were female and 80 were male.

- By palpation, no thyroid enlargement was noticed in 54% of the subjects; goiter IA (palpable lobes larger than the terminal phalanges of the subject's thumbs) in 18%; goiter IB (visible with the neck extended) in 17%; goiter II (visible with the head in normal position) in 9%; and goiter III (visible at a distance) in 2%.
- Tvol (median) by US was 18.6 ml for the entire group (19.2 ml median in the women and 16.6 ml median in the men). 18% had thyroid nodules and 8% had cystic lesions. The goiter prevalence of 54% in women (>18 ml) and of 23% in men (>25 ml) was obtained. Subjects with goiter demonstrated a significantly lower thyrotropin (TSH) value and a higher thyroglobulin value.

In summary, the study shows a high prevalence of goiter in elderly subjects, a high prevalence of nodules in these thyroids, a negative correlation of goiter volume with TSH, and a positive correlation of goiter volume with the thyroglobulin concentration [4].

- Hormonal changes and metabolic demands during pregnancy result in profound alterations in the biochemical parameters of thyroid function:
 - a marked increase in serum thyroxine-binding globulin levels.
 - a marginal decrease in free hormone concentrations (in iodine-sufficient conditions) that is significantly amplified if there is iodine restriction or overt iodine deficiency.

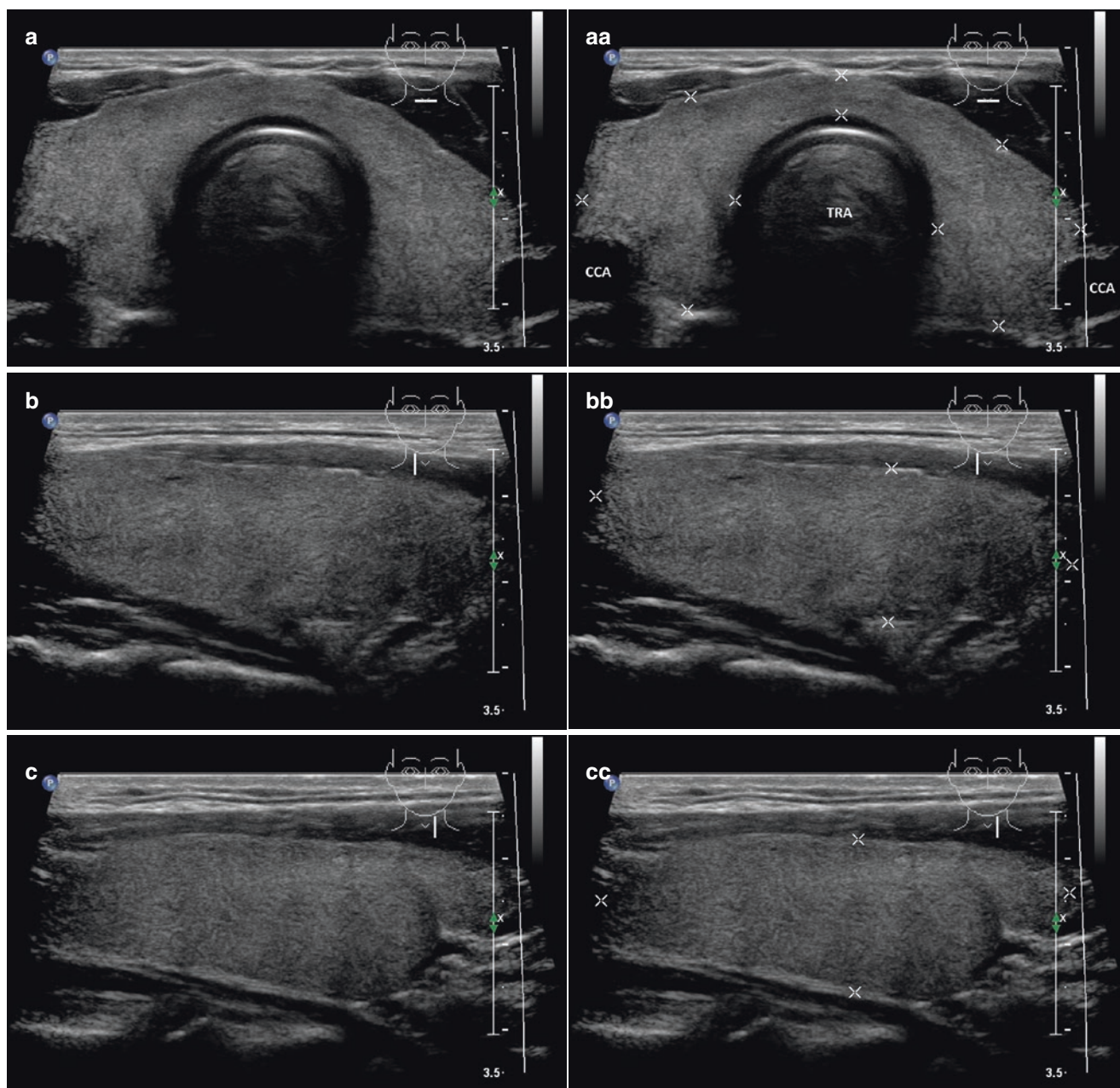


Fig. 2.1 (aa) A 41-year-old man with diffuse goiter: enlarged thyroid gland; homogeneous structure; hyperechoic; thick isthmus 6 mm; Tvol 29 mL, RL 14 mL and LL 14 mL; transverse. (bb) Detail of the RL:

homogeneous structure; hyperechoic; without nodules; longitudinal. (cc) Detail of the LL: homogeneous structure; hyperechoic; without nodules; longitudinal

- a frequent trend toward a slight increase in basal TSH values between the first trimester and the delivery.
- a direct stimulation of the maternal thyroid gland by elevated levels of human chorionic gonadotropin (hCG), which occurs mainly near the end of the first trimester and can be associated with a transient lowering of serum TSH. Goiters formed during gestation may only partially regress after parturition.

Pregnancy, therefore, represents one of the environmental factors that may explain the higher prevalence of goiter

and thyroid disorders in the female population. An iodine-deficient status in the mother also leads to goiter formation in the progeny. When adequate iodine supplementation is given early during pregnancy, it allows for the correction and almost complete prevention of maternal and neonatal goiterogenesis. The ideal dietary allowance of iodine recommended by the WHO is 200 $\mu\text{g}/\text{day}$ for pregnant women [5]. The iodine requirement increases during pregnancy and current recommended intake is in the range of 220–250 $\mu\text{g}/\text{day}$ [6].

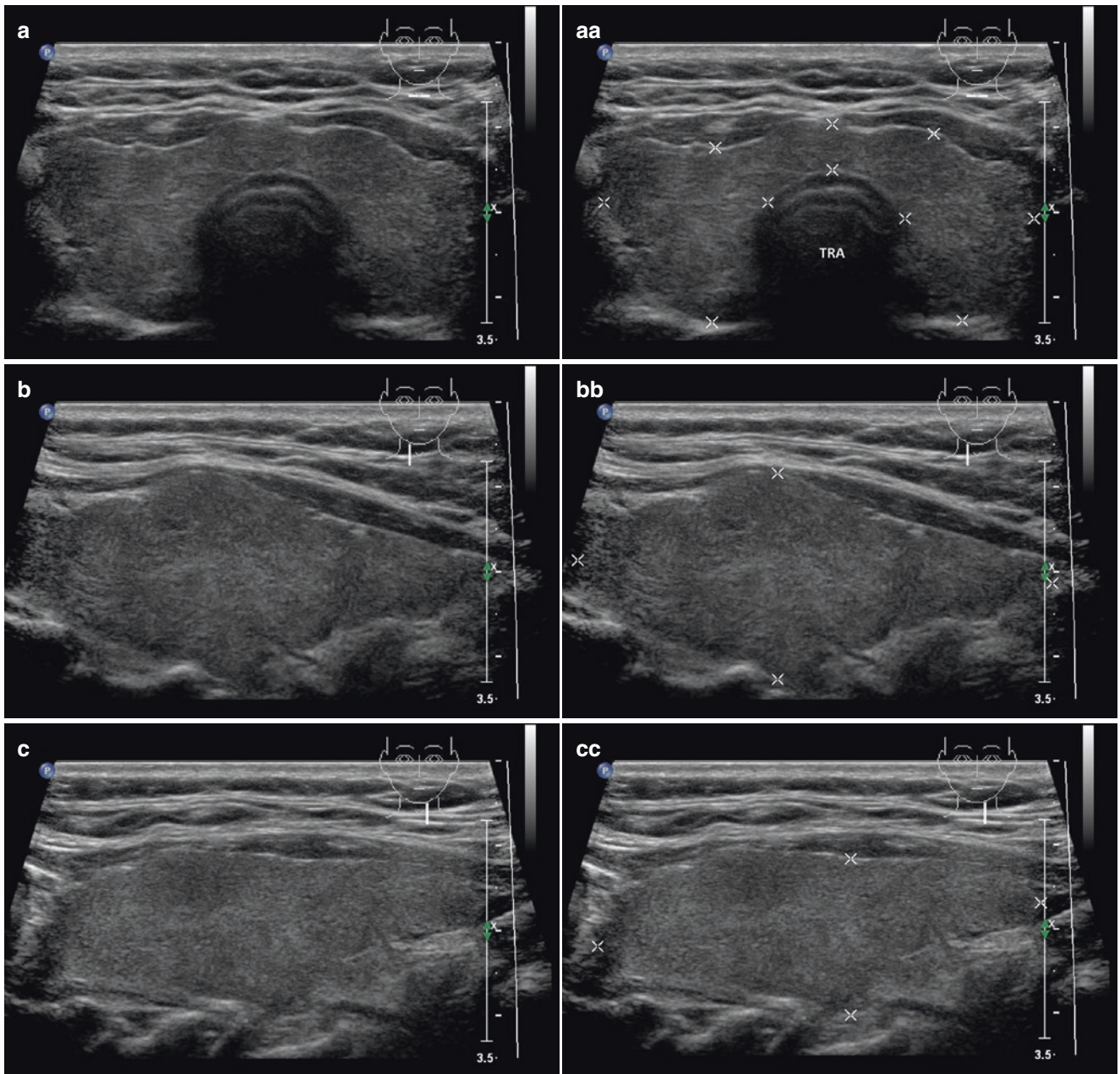


Fig. 2.2 (aa) A 35-year-old woman with diffuse goiter: enlarged thyroid gland; homogeneous structure; hyperechoic; thick isthmus 7 mm; Tvol 24 mL, RL 12 mL and LL 11 mL; transverse. (bb) Detail of the

RL: homogeneous structure; hyperechoic; without nodules; longitudinal. (cc) Detail of the LL: homogeneous structure; hyperechoic; without nodules; longitudinal

- In 1997 the WHO/ICCIDD proposed new references for Tvol in SAC that were based on data from children in iodine-replete countries (Netherlands, Slovakia, France, and Austria). Table 2.1 presents the upper normal limit for Tvol, by age. However, in countries with a high prevalence of child growth retardation, the limits for Tvol shown are unsuitable. In such cases, Tvol is provisionally considered to be more directly a function of total body surface area (Table 2.2) [7].
- However, subsequent reports suggested that the 1997 WHO/ICCIDD references were overestimating the real values. Data of Tvol (medians and P97s) reported in 1999–2000 in iodine-sufficient SAC (United States, Switzerland, and Malaysia) were distinctly lower than those in the European children from the 1997 data. The larger Tvol in the 1997 reference data may have been a residual effect of the iodine deficiency that existed in many European countries up to the early 1990s. Moreover, in 2000 a WHO/

Table 2.1 Upper limit of normal thyroid volume (Tvol) measured by US in iodine-replete children aged 6–15 years, as a function of age, according WHO 1997 [7]

Age (years)	Boys Tvol (ml)	Girls Tvol (ml)
6	5.4	5.0
7	5.7	5.9
8	6.1	6.9
9	6.8	8.0
10	7.8	9.2
11	9.0	10.4
12	10.4	11.7
13	12.0	13.1
14	13.9	14.6
15	16.0	16.1

Table 2.2 Upper limit of normal thyroid volume measured by ultrasonography in iodine-replete children aged 6–15 years as a function of body surface area, according WHO 1997 [7]

Body surface area (m ²)	Boys Tvol (ml)	Girls Tvol (ml)
0.8	4.7	4.8
0.9	5.3	5.9
1.0	6.0	7.1
1.1	7.0	8.3
1.2	8.0	9.5
1.3	9.3	10.7
1.4	10.7	11.9
1.5	12.2	13.1
1.6	14.0	14.3
1.7	15.8	15.6

Table 2.3 Median, 50th percentile (P50) and 97th percentile (P97) values for Tvol measured by ultrasound according to sex and age in an international sample of 6–12 years old children ($n = 3529$) from areas of long-term iodine sufficiency (modified from Zimmermann [8])

Age (years)	Boys Tvol (ml)		Girls Tvol (ml)	
	P50	P97	P50	P97
6 ($n = 468$)	1.60	2.91	1.57	2.84
7 ($n = 561$)	1.80	3.29	1.81	3.26
8 ($n = 579$)	2.03	3.71	2.08	3.76
9 ($n = 588$)	2.30	4.19	2.40	4.32
10 ($n = 528$)	2.59	4.73	2.76	4.98
11 ($n = 492$)	2.92	5.34	3.17	5.73
12 ($n = 313$)	3.30	6.03	3.65	6.59

Table 2.4 Median, 50th percentile (P50) and 97th percentile (P97) values for Tvol measured by ultrasound according to sex and body surface area (BSA) in an international sample of 6–12 year old children ($n = 3529$) from areas of long-term iodine sufficiency (modified from Zimmermann [8])

BSA (m ²)	Boys Tvol (ml)		Girls Tvol (ml)	
	P50	P97	P50	P97
0.7 ($n = 138$)	1.47	2.62	1.46	2.56
0.8 ($n = 493$)	1.66	2.95	1.67	2.91
0.9 ($n = 592$)	1.86	3.32	1.9	3.32
1.0 ($n = 640$)	2.10	3.73	2.17	3.79
1.1 ($n = 536$)	2.36	4.2	2.47	4.32
1.2 ($n = 445$)	2.65	4.73	2.82	4.92
1.3 ($n = 330$)	2.99	5.32	3.21	5.61
1.4 ($n = 174$)	3.36	5.98	3.66	6.40
1.5 ($n = 104$)	3.78	6.73	4.17	7.29
1.6 ($n = 77$)	4.25	7.57	4.76	8.32

ICCIDD workshop on thyroid ultrasound uncovered a large systematic measurement bias in the 1997 references; +30% Tvol at all ages and all body surface areas [8].

- The latest study by Zimmermann, published in 2004, used validated techniques to measure Tvol by US. The subjects were 3500 healthy SAC (6–12 years old) living in six sites on five continents of longstanding iodine sufficiency (Switzerland, Japan, United States, South Africa, Peru, and Bahrain). Compared with previous WHO data for Tvol in SAC from 1997, these new data are more conservative (Tables 2.3 and 2.4). For example, for the boys, both the age- and BSA-specific P97 values for Tvol in this sample is 20% smaller than the corrected 1997 reference values and 15 to 20% smaller than the 1993 WHO reference values. The 1993 (Swedish and German children) and 1997 WHO reference values were based on data from European children. These new international reference values for Tvol by US can be used for goiter screening in the context of IDD monitoring [9].

2.2 US Features of Diffuse Goiter

- Increased thyroid volume, Tvol >18 ml in women and >25 ml in men.
- Homogenous.
- Isoechoic or mild hyperechoic.
- Fine- or middle-grained echotexture.
- Well-defined margin.
- Absence of nodules and calcifications.
- Normal vascularity, CFDS *pattern 0 or I*.
- Very large goiters dislocate adjacent organs—vessel, esophagus, and markedly asymmetric goiter dislocates trachea.
- In a very large goiter, it might be challenging to measure the length of the lobe. It is helpful is to use an image composed from two longitudinal scans, or to use a convex probe.
- Caution! Compared with MR imaging, US underestimates the volume of very large goiter (150–200 ml) by approximately 20% [9].

References

1. Gutekunst R, Becker W, Hehrmann R, Olbricht T, Pfannenstiel P. Ultrasonic diagnosis of the thyroid gland. *Dtsch Med Wochenschr.* 1988;113(27):1109–12.
2. Foo LC, Zulfiqar A, Nafikudin M, Fadzil MT, Asmah AS. Local versus WHO/International Council for Control of iodine deficiency disorders-recommended thyroid volume reference in the assessment of iodine deficiency disorders. *Eur J Endocrinol.* 1999;140(6):491–7.
3. Rallison ML, Dobyns BM, Meikle AW, Bishop M, Lyon JL, Stevens W. Natural history of thyroid abnormalities: prevalence, incidence, and regression of thyroid diseases in adolescents and young adults. *Am J Med.* 1991;91(4):363–70.
4. Hintze G, Windeler J, Baumert J, Stein H, Köbberling J. Thyroid volume and goitre prevalence in the elderly as determined by ultrasound and their relationships to laboratory indices. *Acta Endocrinol* 1991;124(1):12–18.
5. Glinioer D. What happens to the normal thyroid during pregnancy? *Thyroid.* 1999;9(7):631–5.
6. Zimmermann MB. The adverse effects of mild-to-moderate iodine deficiency during pregnancy and childhood: a review. *Thyroid.* 2007;17(9):829–35.
7. Bull World Health Organ. Recommended normative values for thyroid volume in children aged 6-15 years World Health Organization & International Council for Control of Iodine Deficiency Disorders. *Bull World Health Organ.* 1997;75(2):95–7.
8. Zimmermann MB, Hess SY, Molinari L, De Benoist B, Delange F, Braverman LE, et al. New reference values for thyroid volume by ultrasound in iodine-sufficient schoolchildren: a World Health Organization/nutrition for health and development iodine deficiency study group report. *Am J Clin Nutr.* 2004;79(2):231–7.
9. Bonnema SJ, Andersen PB, Knudsen DU, Hegedüs L. MR imaging of large multinodular goiters: observer agreement on volume versus observer disagreement on dimensions of the involved trachea. *AJR Am J Roentgenol.* 2002;179(1):259–66.

3.1 Hashimoto's Thyroiditis: Chronic Lymphocytic Thyroiditis

3.1.1 Essential Facts

- Hashimoto's thyroiditis (HT), also known as chronic lymphocytic thyroiditis (CLT) or autoimmune thyroiditis (AT), is the most frequent cause of hypothyroidism and goiter in iodine sufficient areas [1].
- In addition to classic form, several other clinico-pathological entities are now included under the term of HT: fibrous variant, IgG4-related variant, juvenile form, Hashitoxicosis, and painless thyroiditis (sporadic or post-partum) [2].
- Japanese pathologist Hakaru Hashimoto first described the disease as "*struma lymphomatosa*" in 1912. But the dominant German school of thought in medicine asserted this histology as an early phase of Riedel's thyroiditis. Hashimoto's description was then ignored and forgotten. In 1931, however, Allen Graham et al. reported *struma lymphomatosa* and endorsed Hashimoto's conclusion that it was a disease in its own right. Since then, this disease has been eponymously referred to as "*Hashimoto's thyroiditis*." In 1956 Doniach et al. purified a thyroglobulin antibody (Tg-Ab) from the sera and proposed that HT is an autoimmune disease. In 1962 the concept of HT as organ-specific autoimmune disease was established [3].
- HT is one of the most common organ-specific autoimmune diseases. Its annual incidence is estimated to be between 0.3 and 1.5 cases per 1000 persons, with no significant race-related predominance [1].
- HT affects 1.3% of children and has a female predominance [4].
- Pathologically proven HT is defined as the presence of diffuse lymphocytic infiltration with occasional germinal centers, small thyroid follicles with sparse colloid, and fibrosis [5].
- The diagnosis of HT is defined as elevated thyroid peroxidase (TPO-Ab) and thyroglobulin antibodies (Tg-Ab).

High serum TPO-Ab concentrations are present in more than 90–95% of patients [6].

- In the total population, positive TPO-Ab is detected in $13.0 \pm 0.4\%$, and positive Tg-Ab in $11.5 \pm 0.5\%$. The prevalence of positive antibodies is lower in the disease-free population: TPO-Ab, $11.3 \pm 0.4\%$ and Tg-Ab, $10.4 \pm 0.5\%$. The prevalence of positive TPO-Ab and positive Tg-Ab in the total and disease-free population is higher in women than in men and increases with age, especially among women [7].
- Clinical findings: the presence of a firm, painless, diffusely enlarged gland; a large number of patients with lymphocytic thyroiditis have nodular enlargement [8].
- Long-standing HT causes shrinking and atrophy of the thyroid, but may also lead to diffuse enlargement of the gland and/or formation of nodules. These nodules should be differentiated from PTC and primary thyroidal non-Hodgkin lymphoma, which are possible complications of HT [9].
- Autoimmune thyroid diseases (AITD) like Graves' disease (GD) and HT are complex diseases in which autoimmunity against the thyroid autoantigens develops at a certain genetic background, provoked by exposure to environmental factors. Genetic factors contribute about 70–80% to the pathogenesis, and environmental factors (including infection, stress, iodine, selenium, vitamin D and smoking) contribute about 20–30% to the pathogenesis. Blood relatives of AITD patients carry a risk to contract AITD themselves [10].
- Prevalence of the two major AITD (GD and HT), which are characterized by thyrotoxicosis and hypothyroidism, respectively, is estimated to be 5%. AITD are significantly more common among women than among men, with a w/m ratio ranging from 5:1 to 10:1. Major specific antibodies in HT are TPO-Ab and Tg-Ab, but these antibodies also occur in $\approx 70\%$ of GD patients. Similarly, the major antibody in GD thyroid hormone receptor antibody (stimulating TSHR-Ab) may also occur in a few patients with HT (blocking TSHR-Ab) [11].

- HT is more common in iodine sufficient (e.g., USA) or excess (e.g., Japan) countries. In this condition, the thyroid gland is generally non-tender and firm, and is often enlarged with an irregular texture. Atrophy is often noted in the gland with diffusely infiltrated lymphocytes. The prevalence of HT is as high as 40% in elderly women. Nearly 50% of the patients diagnosed with TPO-Ab are euthyroid, while majority of the other patients have subclinical (mild) hypothyroidism (normal free T4 levels and elevated serum TSH) and only a small minority have severe hypothyroidism. The presence of TPO-Ab predicts the development of overt hypothyroidism at about 2.5% per year. Among the people with elevated TSH and positive TPO-Ab, about 4.5% per year develop overt hypothyroidism [11].
- The Amsterdam AITD cohort is a 5-year follow-up study in a population at risk for AITD, namely in healthy women with one or more first- or second-degree relatives with proven AITD. The mean annual event rate was 1.5%, and the 5-year cumulative event rate was 7.5%. The incidence rate per 1000 women per year was 9.6 for overt hypothyroidism and 3.3 for overt hyperthyroidism [12].
- It is unknown whether in CLT the goitrous (HT) and atrophic forms (primary myxedema) are variants of the same disease or different pathogenic entities. Conventional thyroid-related autoimmune parameters (Tg-Ab and ATPO-Ab) are unable to separate both variants/entities serologically. Other thyroid-specific cytotoxic antibodies, like TSH binding-inhibiting antibodies and TSH function-blocking antibodies, were determined. Analysis of cytotoxicity regarding thyroid size showed a high incidence of cytotoxic antibodies in atrophic disease (Tvol median 6 mL), where cytotoxic antibodies were detectable in 80% vs. 39% in goitrous disease (Tvol median 36 mL) [13].
- Worldwide the most common thyroid disease entity is autoimmune hypothyroidism. Historically this is divided into primary atrophic (primary myxedema) and hypertrophic autoimmune hypothyroidism (CLT-HT). The primary atrophic variant was described in the late 1890s by Ord as “dependent on a destructive affection of the thyroid gland.” In 1912 Hashimoto described the hypertrophic variant later to be known as Hashimoto's disease-thyroiditis (HT). No strict criteria exist to separate the atrophic and the goitrous form of hypothyroidism. Classification is often based on the presence or absence of goiter by clinical examination [14].
- Ord's and Hashimoto's diseases have been reported to be distinct diseases, differing in human leukocyte antigen (HLA) types, the specific autoantibodies involved—blocking TSHR-Ab in the atrophic type of hypothyroidism, TPO-Ab and Tg-Ab in the hypertrophic form, and

importance of humoral vs. cellular immunity for disease development [14].

- Carlé et al., in a Danish population cohort of 247 patients with overt autoimmune hypothyroidism, measured thyroid volume (Tvol) by US. The aim was to verify or disprove whether Ord's and Hashimoto's are in fact two distinct disorders. Patients were divided in quartiles according to Tvol as follows:
 - Women (<6.7, 6.7–11.2, 11.3–17.4, >17.4 mL).
 - Men (<7.4, 7.4–12.3, 12.4–19.0, >19.0 mL).

Patients had smaller Tvol median compared with controls, 11.6 mL vs. 13.5 mL. Tvol, however, showed a Gaussian distribution in both women and men with no bimodal pattern. The patients with the smallest thyroid volumes (<6.7 resp. <7.4 mL) were biochemically more hypothyroid compared with others groups. Among other groups were found no statistically significant differences with regard to either serum TSH levels or serum T4 levels. With increasing Tvol, the levels of circulating antibodies (TPO-Ab, Tg-Ab) correspondingly increased and echostructure became more hypoechoic or even severely hypoechoic. No difference between groups was observed in prevalence of TSHR-Ab or duration of symptoms before hypothyroidism was diagnosed. In primary autoimmune hypothyroidism, Tvol follows a normal distribution. Cases with thyroid atrophy and goiter are only extremes within this distribution and do not represent separate disorders [14].

3.1.2 US Features of Hashimoto's Thyroiditis

- In 1983, French radiologist Espinasse described on US the diffused microechoic character of the thyroid parenchyma. Even though it is nonspecific, it appears thus a valuable sign in the diagnosis of chronic lymphocytic thyroiditis and Graves' disease [15].
- In the same year, Canadian radiologists drew attention to the importance of US in evaluating childhood thyroid disorders. In 25 patients with diffuse thyroid lesions (thyroiditis, Graves' disease, euthyroid goiter, iodine-induced goiter, goitrous cretinism), US revealed only homogeneous thyroid enlargement or a nonspecific patchy echo pattern [16].
- In 1989, German specialists Gutekunst et al. compared clinical, laboratory, and cytological findings with US patterns in 92 patients with CLT. A total of 29% had no clinical symptoms. According to laboratory values 13% of patients had undetectable antimicrosomal antibodies. The functional status according to TSH levels were ≈51% hypothyroid, ≈45% euthyroid and ≈4% hyperthyroid.

Cytology alone was diagnostic in $\approx 91\%$ patients. US revealed a scattered sonolucent echo in $\approx 95\%$ patients, and in $\approx 49\%$ a normal thyroid volume (women <18 mL, men <25 mL). Authors of this pioneering study concluded that US can suggest CLT. If antimicrobial antibodies are undetectable or titres are not significant and/or clinical symptoms are uncertain, FNAB can confirm the US finding [17].

- US is useful for measurement of thyroid size and assessing the echotexture in the HT—CLT patients. The US appearance may vary, which is likely due to the phase and severity of the disease process.
- US imaging of classical HT pattern [1, 18]:
 - An enlarged gland (Figs. 3.4aa and 3.5aa).
 - A diffusely heterogeneous, coarse echotexture (Figs. 3.1aa and 3.4aa).
 - Multiple discrete hypoechoic micronodules ranging from 1 to 6 mm in diameter (Figs. 3.1aa and 3.4aa).
 - Coarse septations from fibrous bands (Figs. 3.1, 3.4, and 3.7)
 - Microlobulated margin (Figs. 3.1bb, 3.2bb and 3.4bb).
 - CFDS may demonstrate slight-to-markedly increased vascularity (Fig. 3.10bb).
 - A presence of perithyroidal satellite lymph nodes, especially the “Delphian” node just cephalad to the isthmus (Figs. 3.9aa and 3.10aa)
- The positive predictive value for micronodulation in diagnosing HT is 94.7% [19].
- Caution! A diffusely heterogeneous, hypoechoic gland is not specific for HT and that may be seen in Graves' disease, and subacute thyroiditis [8].
- Thyroid volume changes throughout the course of Hashimoto's disease. For the evaluation of goiter (Sect. 3.2), Gutekunst applied US criteria from the year 1988: Tvol >18 mL in women (Fig. 3.6), and Tvol >25 mL in men (Figs. 3.5 and 3.7) [20]. However, an exact cut-off is not determined for atrophic form (Sect. 3.3). The most frequently used value is 6 mL used in 1995 in a study, by Bogner, of atrophic (Figs. 3.11–3.14) and goitrous autoimmune thyroiditis [13].
- In a study of 247 patients with overt autoimmune hypothyroidism, Carlé et al. measured Tvol by US, finding that 21% of the patients had goiter, 23% of women had thyroid volume >18 mL, and 12% of men had thyroid volume >25 mL [14].
- Micronodules of HT can increase in size as focal lymphocytic thyroiditis (FLT) and be present as hypoechoic or hyperechoic nodules with ill-defined margins on US. The vascularity is markedly variable, without a distinguishing pattern. These so-called “pseudotumors” constituted 36% of the nodules of focal thyroiditis detected by US and are simulating nodular disease indistinguishable from thyroid cancer or lymphoma. The FLT may represent a milder or earlier presentation of the disease [8].
- It is difficult to discriminate FLT from thyroid cancer if they both have suspicious US findings (*see* Chap. 15). Tg-Ab positivity, presence of a HT pattern (diffusely heterogeneous hypoechogenicity) on US, and absence of calcification in nodules were associated with FLT (specificity of 99% and positive predictive value of 96%, but sensitivity only 45%). However, 20% of FLTs had calcification, which could indicate malignancy. Therefore, absence or presence of calcification in nodules showed relatively low predictive value for FLT. In conclusion, suspicious thyroid nodules with benign cytologic results on initial FNAB could be followed-up only by US, if there is seropositivity of Tg-Ab, no calcifications in nodules, and presence of a HT pattern on US [21].
- The US features and vascularity of nodular HT are extremely variable. In a cohort of 64 patients with HT there occurred a solitary nodule (Figs. 8.5aa and 8.6aa) in 36% and the setting of five or more nodules (Fig. 3.8aa) in 23% of cases. Fifty-five percent of cases of nodular HT occurred within a US background of diffuse HT, and 45% of cases occurred within a US normal thyroid parenchyma. The mean diameter of nodule was 15 ± 7.33 mm. Nodules were most commonly solid in 69% and hypoechoic in 47%. Twenty percent of nodules had calcifications (nonspecific bright reflectors, macrocalcifications, or “eggshell” - Fig. 9.9), and 5% of nodules had colloid cavity (Fig. 3.8aa). The margins were well-defined in 60% and ill-defined in 40% of nodules, and 27% had a hypoechoic halo (Fig. 8.6aa). On CFDS analysis, 35% of nodules were hypervascular, 42% isovascular or hypovascular (Fig. 8.6bb), and 23% avascular [22].
- Currently high-resolution sonography instruments are a useful diagnostic tool for the evaluation of diffuse thyroid disease such as HT. According to Kim et al., a combination of ≥ 3 US features of HT has a high sensitivity and specificity for the identification of HT compared with the use of ≤ 2 US features. No visualization of US features related to HT on real-time thyroid sonography can rule out the existence of asymptomatic HT [23].
- The presence of perithyroidal lymph nodes (LN) is useful in diagnosis of the HT when correlated with US, clinical, and laboratory findings. However, it should be kept in mind that these LN may also correspond to underlying malignant processes, such as PTC and lymphoma. In doubtful cases, FNAB may be required to differentiate between benign (reactionary/inflammatory origin) and malignant LN [18].

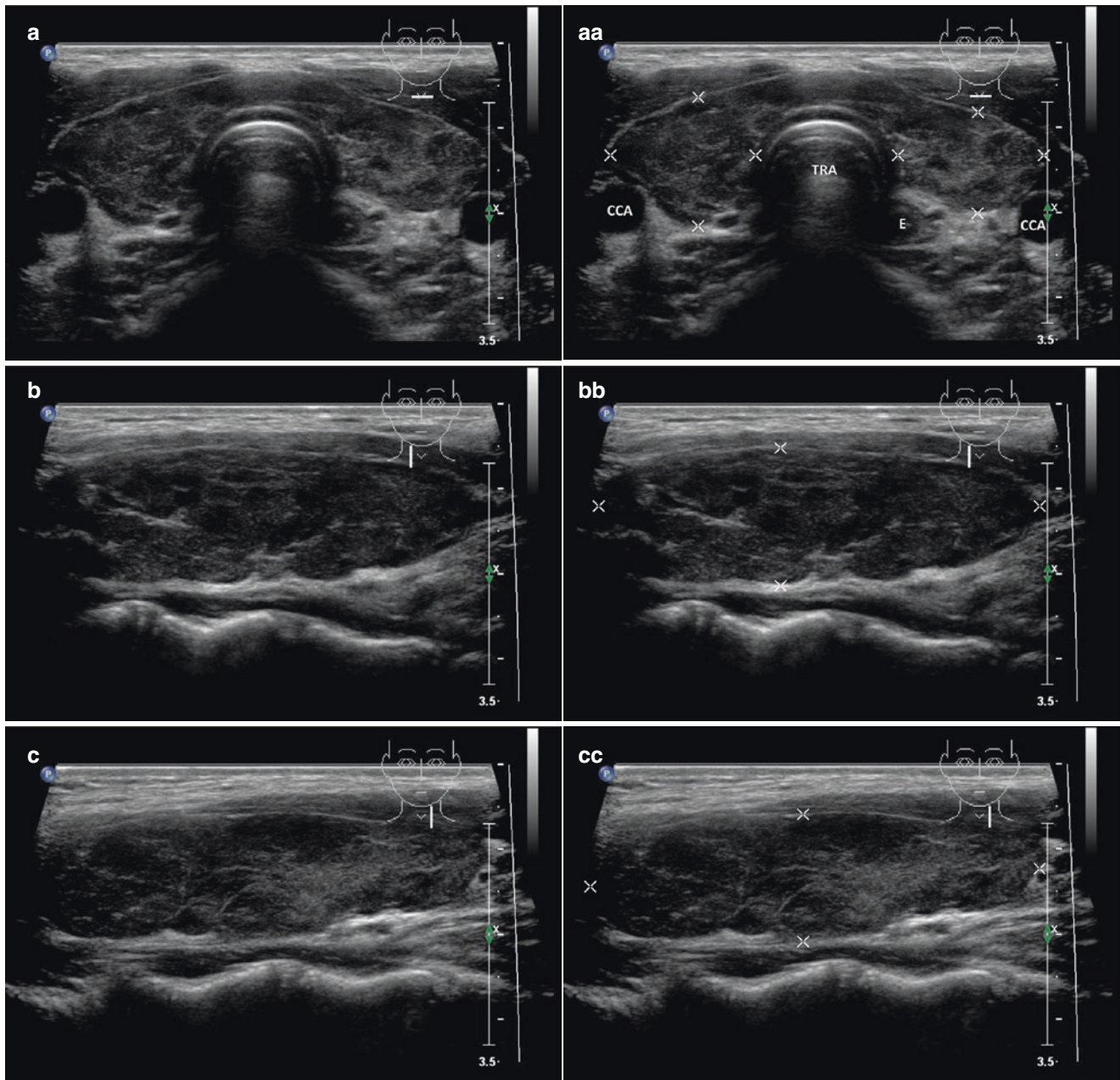


Fig. 3.1 (aa) A 30-year-old woman with Hashimoto's thyroiditis (HT) of upper normal volume. Classic US appearance: inhomogeneous, mostly hypoechoic micronodular structure with thin hyperechoic fibrous septa; dorsally microlobulated margin; Tvol 16 mL, RL 8 mL, and LL 8 mL; transverse. (bb) Detail of RL with classic US appearance

HT: inhomogeneous, mostly hypoechoic micronodular structure with thin hyperechoic fibrous septa; dorsally microlobulated margin; longitudinal. (cc) Detail of LL with classic US appearance HT: inhomogeneous, mostly hypoechoic micronodular structure with thin hyperechoic fibrous septa; dorsally microlobulated margin; longitudinal

- In a study with 223 HT patients, the hypoechogenicity, heterogeneity, and pseudonodular hypoechoic infiltration were associated with significantly higher TPO-Ab. There were no significant correlations between the other US variables (cysts, nodules, and

volume). In addition, an assessment of Tg-Ab levels did not show significant differences in correlation with any of the US variables [24].

- At the onset of HT (Fig. 3.3), classical US pattern is not always present. In Greece, in a study with 105

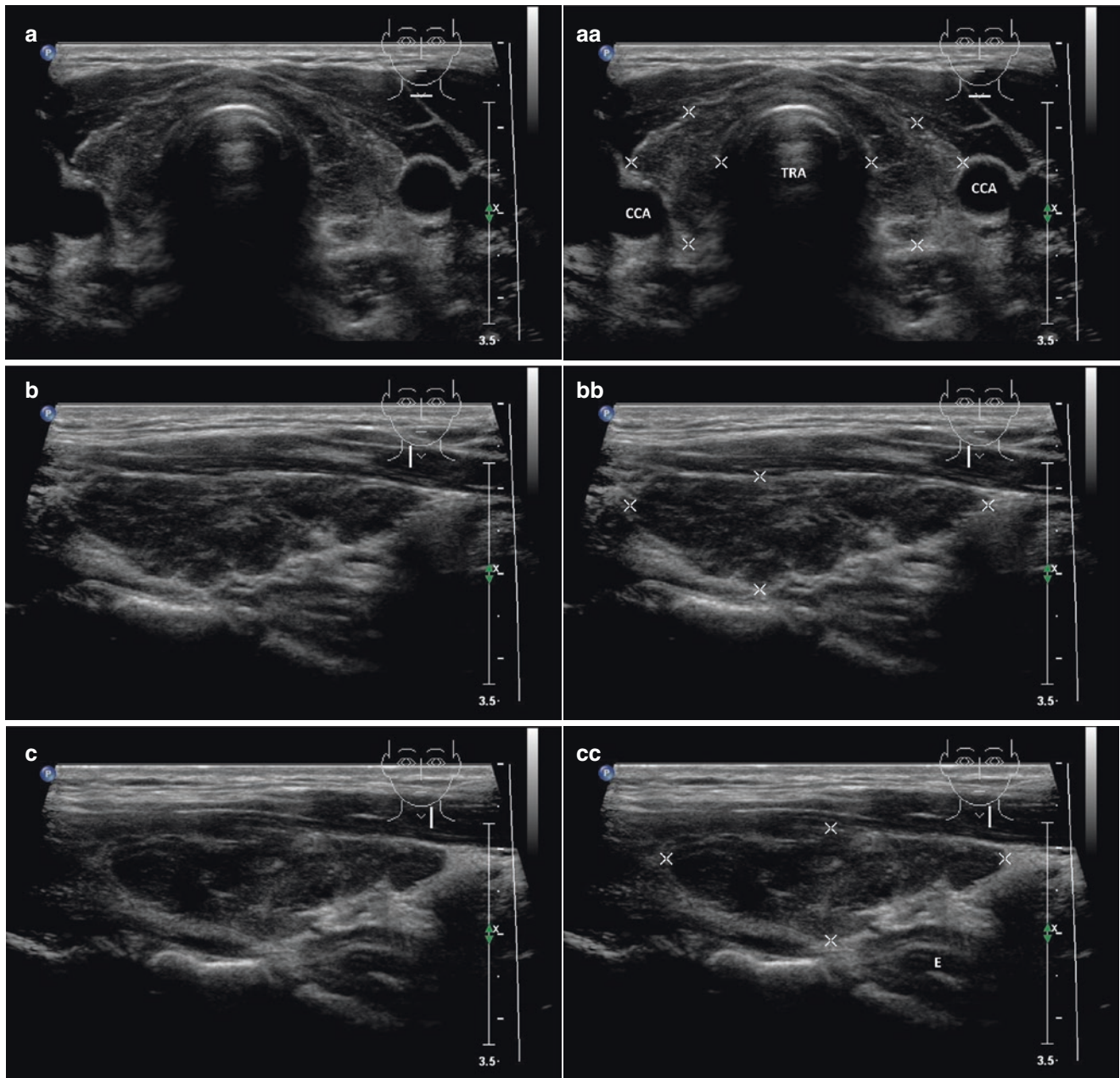


Fig. 3.2 (aa) A 41-year-old woman with Hashimoto's thyroiditis (HT) of lower normal volume and fibrosis. US overall view: coarse structure; mixed echogenicity; hypoechoic micronodular structure with thick hyperechoic fibrous septa and areas; microlobulated margin; Tvol 9 mL, RL 4.5 mL, and LL 4.5 mL; transverse. (bb) Detail of RL with HT and fibrosis: coarse structure; mixed echogenicity; hypoechoic

micronodular structure with thick hyperechoic fibrous septa and areas; microlobulated margin; longitudinal. (cc) Detail of LL with HT and fibrosis: coarse structure; mixed echogenicity; hypoechoic micronodular structure with thick hyperechoic fibrous septa and areas; microlobulated margin; longitudinal

children (23 boys and 82 girls), US findings of HT were present in 37% of the children at diagnosis. Fifty percent of children with normal initial thyroid will develop changes within 7 months; however, character-

istic findings may not develop for over 4 years. Important factors accelerating US changes were goiter, hypothyroidism, and seropositivity for both, TPO-Ab and Tg-Ab [25].

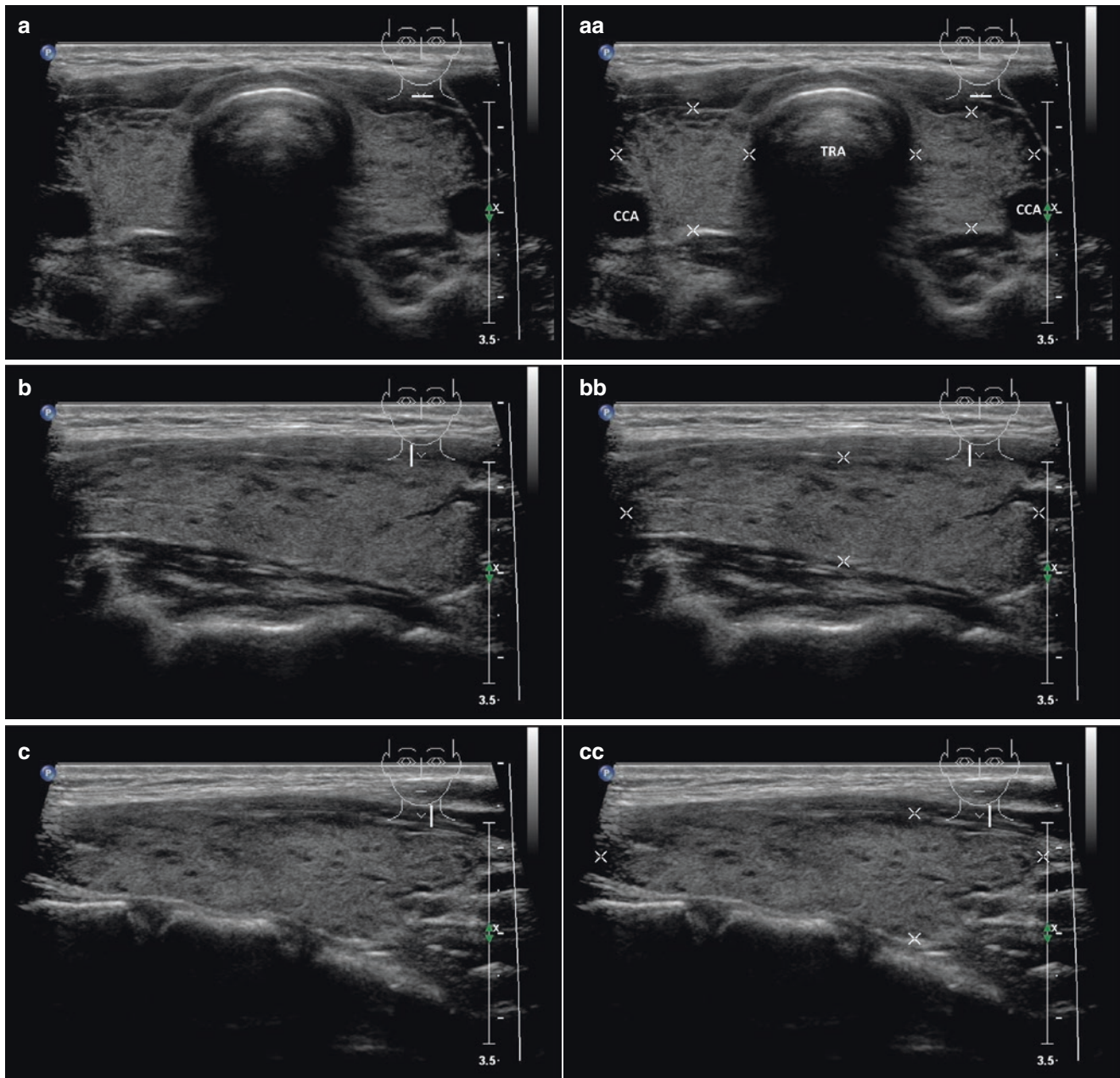


Fig. 3.3 (aa) A 20-year-old woman with Hashimoto's thyroiditis (HT). Initial US appearance: inhomogeneous, mostly isoechoic, sporadically micronodular hypoechoic structure; well-defined smooth margin; Tvol 14 mL, RL 7 mL, and LL 7 mL; transverse. (bb) Detail of RL with HT, initial US appearance: inhomogeneous, mostly

isoechoic, sporadically micronodular hypoechoic structure; well-defined smooth margin; longitudinal. (cc) Detail of LL with HT, initial US appearance: inhomogeneous, mostly isoechoic, sporadically micronodular hypoechoic structure; well-defined smooth margin; longitudinal

3.2 Hashimoto's Thyroiditis: Goiter

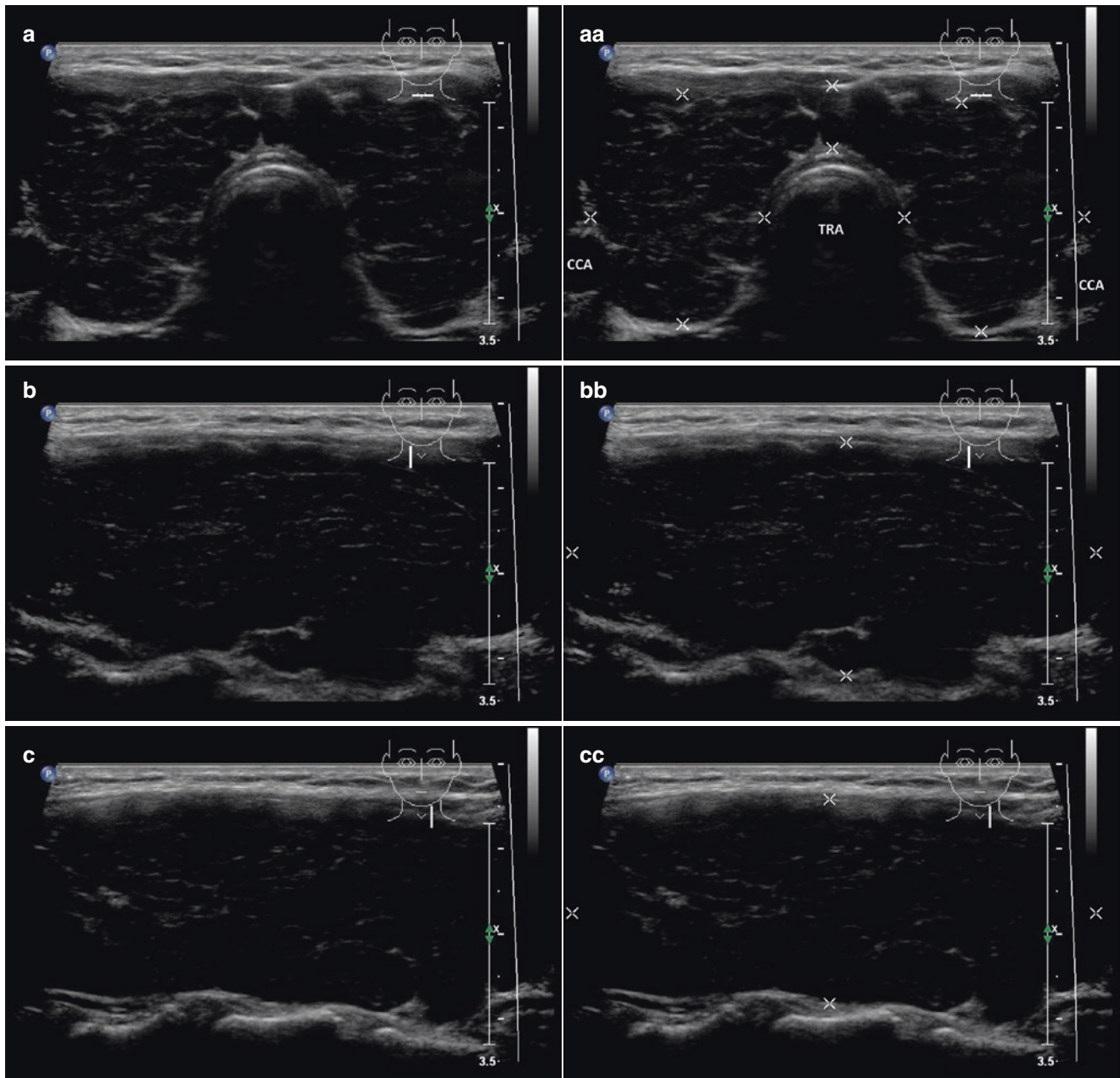


Fig. 3.4 (aa) A 39-year-old woman with Hashimoto's thyroiditis (HT) and goiter volume 40 mL. Classic US appearance: enlarged thyroid gland; inhomogeneous, mostly hypoechoic micronodular structure with thin hyperechoic fibrous septa; microlobulated margin; Tvol 40 mL, isthmus 8 mm, RL 20 mL, and LL 19 mL; transverse. (bb) Detail of RL with classic HT US appearance, goiter: inhomogeneous, mostly

hypoechoic micronodular structure with thin hyperechoic fibrous septa; microlobulated margin; longitudinal. (cc) Detail of LL with classic HT US appearance, goiter: inhomogeneous, mostly hypoechoic micronodular structure with thin hyperechoic fibrous septa; microlobulated margin; longitudinal

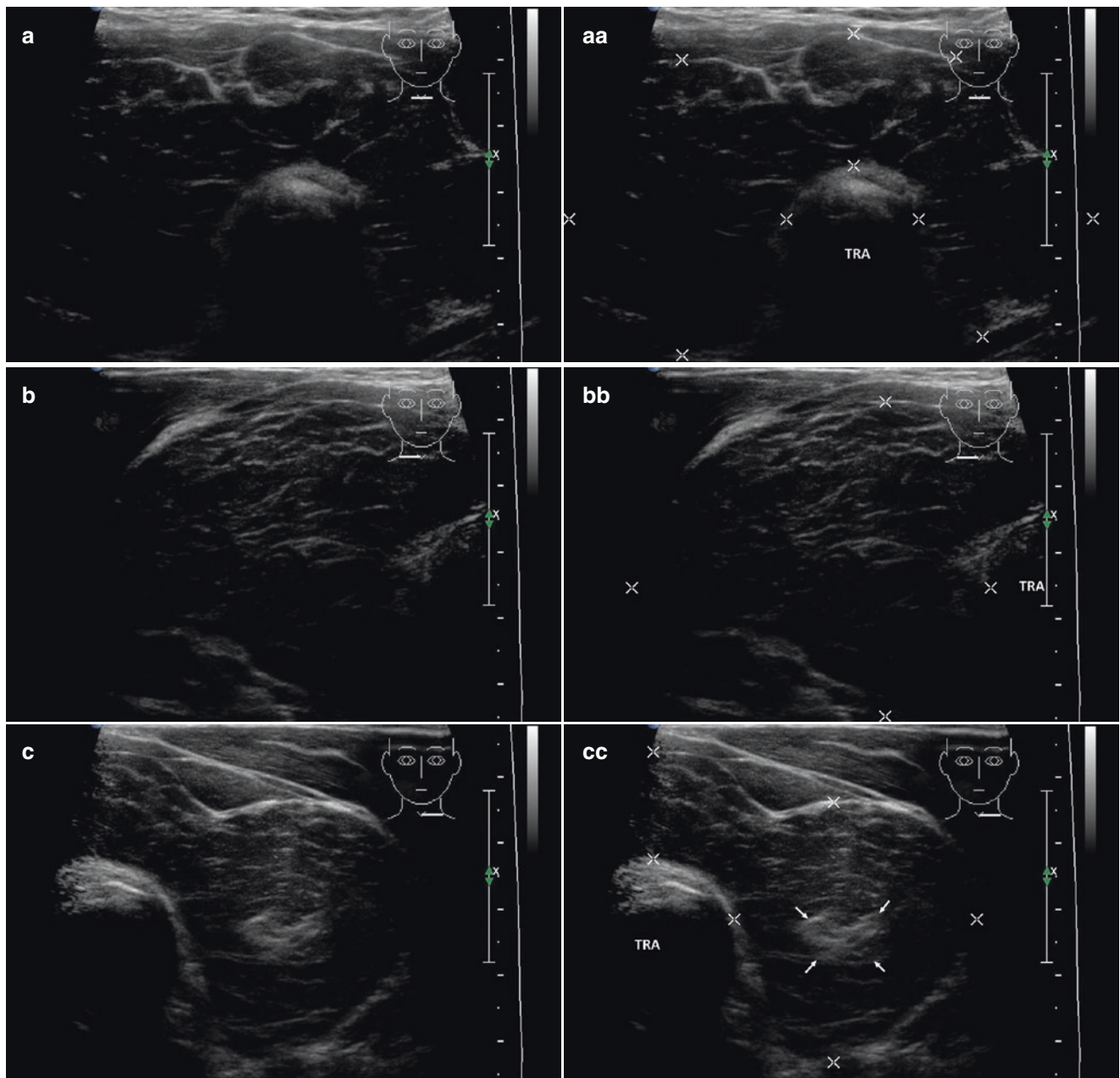


Fig. 3.5 (aa) A 39-year-old man with Hashimoto's thyroiditis (HT) and giant goiter volume approximately 150 mL. Classic US appearance: enlarged thyroid gland; inhomogeneous, mostly hypoechoic micronodular structure with thin hyperechoic fibrous septa; microlobulated margin; Tvol 150 mL, isthmus 20 mm, asymmetry—RL 90 mL and LL 60 mL; transverse, depth of penetration 6 cm. (bb) Detail of RL with classic HT US appearance, giant goiter: inhomogeneous, mostly hypoechoic micronodular structure with thin hyperechoic fibrous septa; microlobulated margin; transverse. (cc) Detail of LL with classic HT US appearance, giant goiter: inhomogeneous, mostly hypoechoic

micronodular structure with thin hyperechoic fibrous septa; in central part focal fibrotic area (*arrows*); microlobulated margin; transverse. (dd) Detail of RL with classic HT US appearance, giant goiter: inhomogeneous, mostly hypoechoic micronodular structure with thin hyperechoic fibrous septa; microlobulated margin; longitudinal. (ee) Detail of LL with classic HT US appearance, giant goiter: inhomogeneous, mostly hypoechoic micronodular structure with thin hyperechoic fibrous septa; in central part focal fibrotic area (*arrows*); microlobulated margin; longitudinal

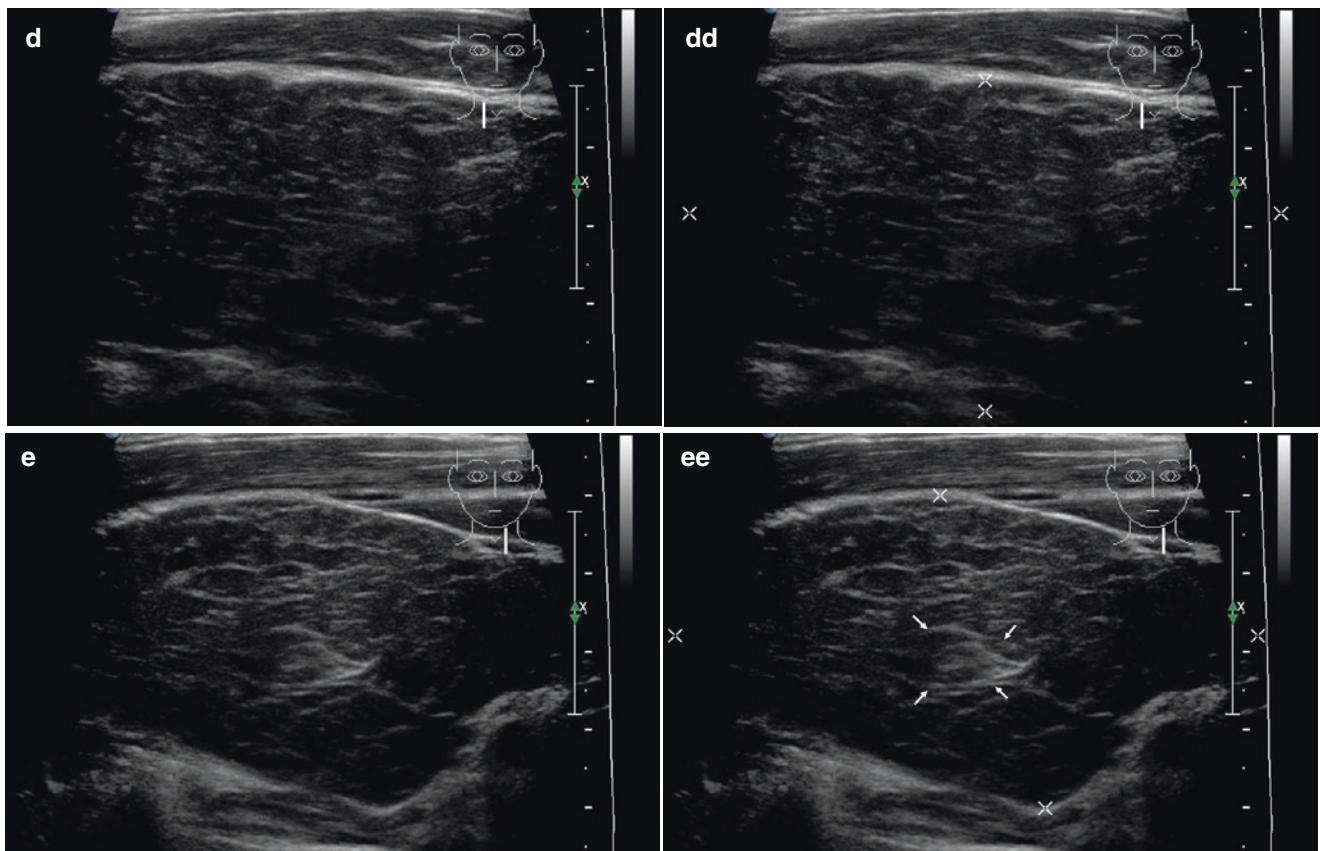


Fig. 3.5 (continued)

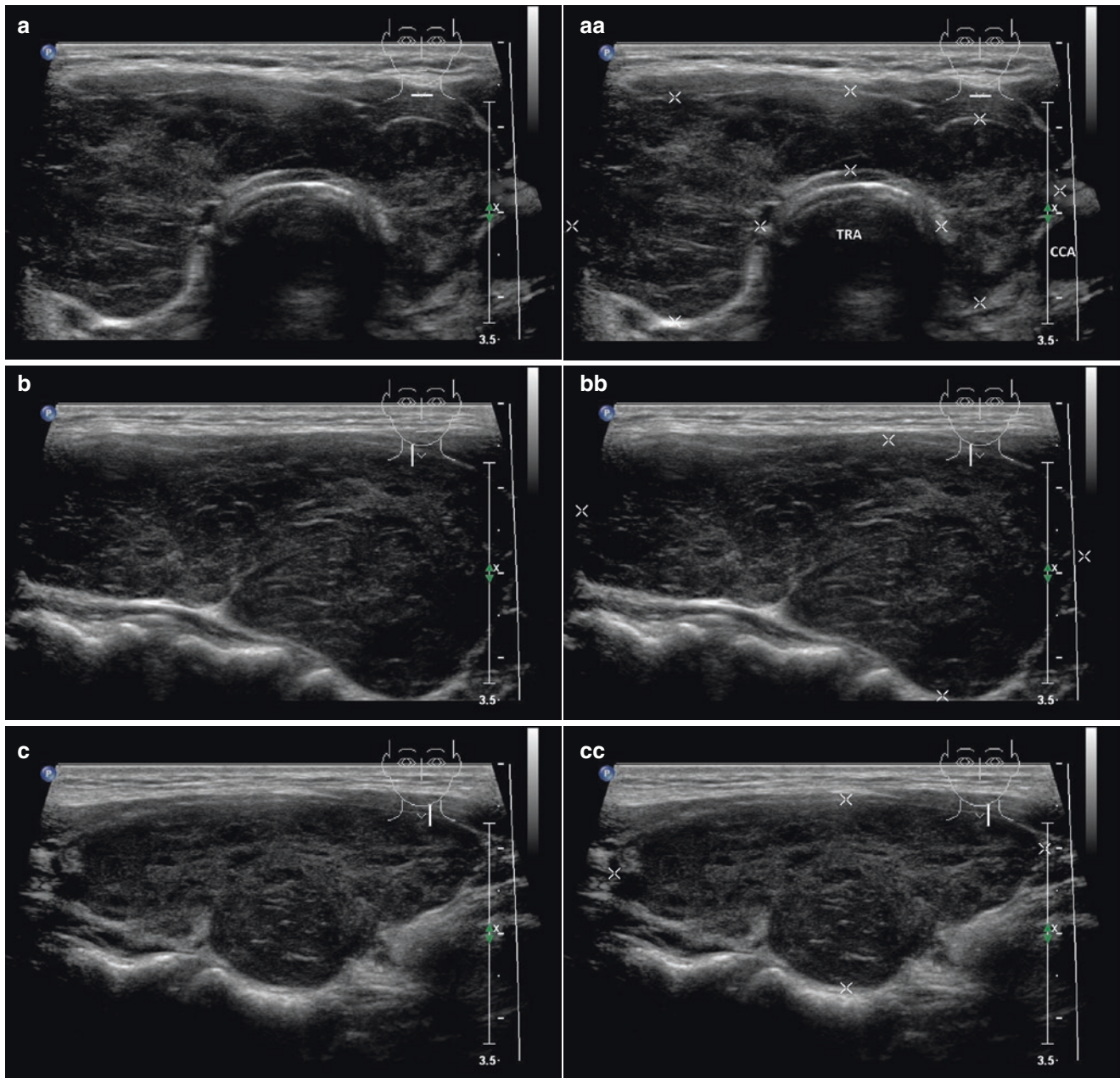


Fig. 3.6 (aa) A 40-year-old woman with Hashimoto's thyroiditis (HT) and asymmetric fibrotic goiter volume 33 mL. US overall view: enlarged thyroid gland; coarse structure; mixed echogenicity; hypoechoic micronodular structure with thick hyperechoic fibrous septa and areas; microlobulated margin; Tvol 33 mL, isthmus 10 mm, asymmetry—RL 20 mL and LL 12 mL; transverse. (bb) Detail of RL

with HT, asymmetric fibrotic goiter: inhomogeneous, mostly hypoechoic micronodular structure with thin hyperechoic fibrous septa; microlobulated margin; longitudinal. (cc) Detail of LL with HT, asymmetric fibrotic goiter: inhomogeneous, mostly hypoechoic micronodular structure with thin hyperechoic fibrous septa; microlobulated margin; longitudinal

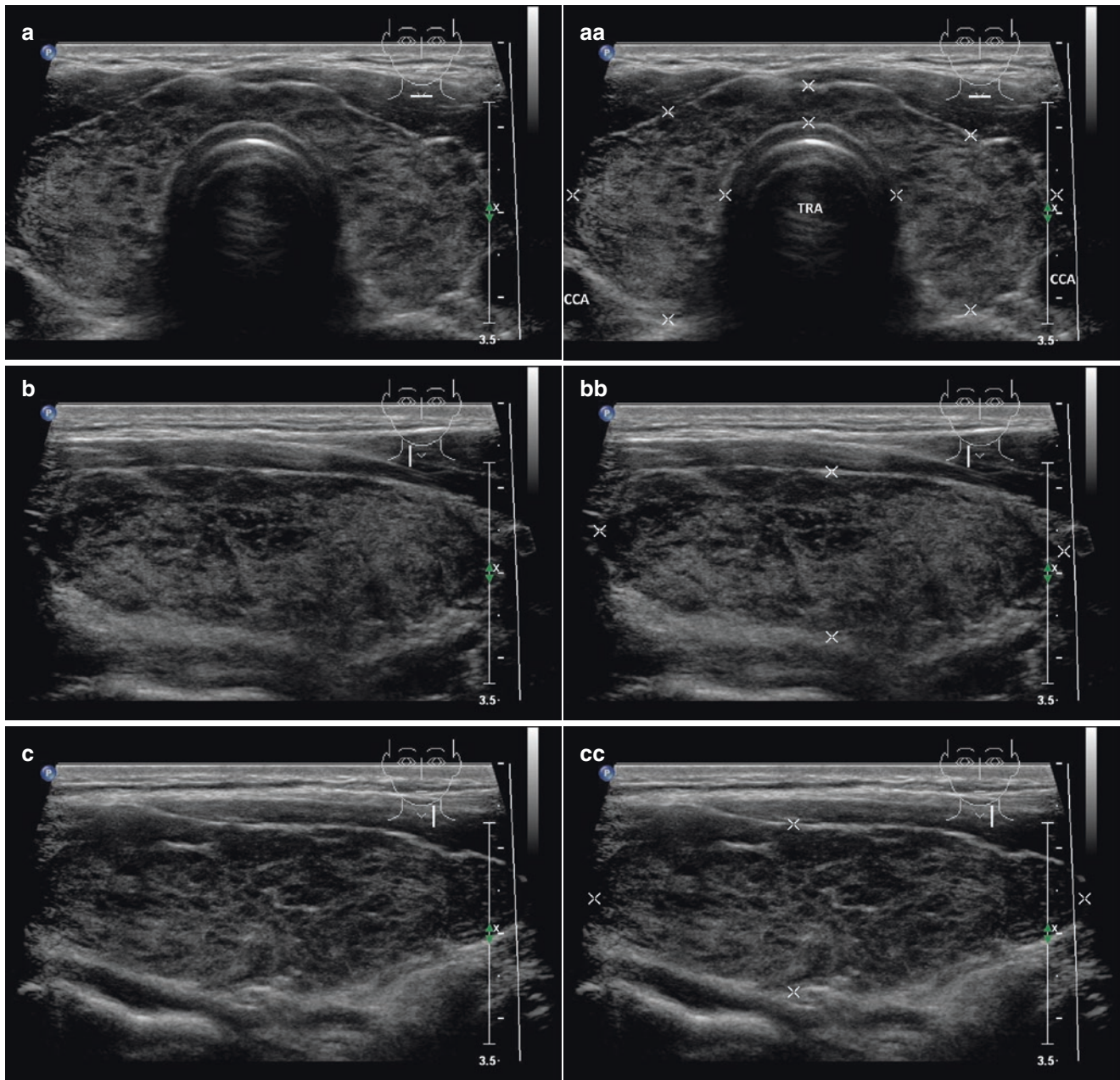


Fig. 3.7 (aa) A 40-year-old man with Hashimoto's thyroiditis (HT) and markedly fibrotic goiter, volume 32 mL. US overall view: enlarged thyroid gland; coarse structure; mostly hyperechoic, sporadically hypoechoic micronodular structure with thick hyperechoic fibrous septa and areas; microlobulated margin; Tvol 32 mL, RL 16 mL and LL 16 mL; transverse. (bb) Detail of RL with HT, markedly fibrotic goiter:

coarse structure; mostly hyperechoic, sporadic hypoechoic micronodular structure with thick hyperechoic fibrous septa and areas; microlobulated margin; longitudinal. (cc) Detail of LL with HT, markedly fibrotic goiter: coarse structure; mostly hyperechoic, sporadic hypoechoic micronodular structure with thick hyperechoic fibrous septa and areas; microlobulated margin; longitudinal

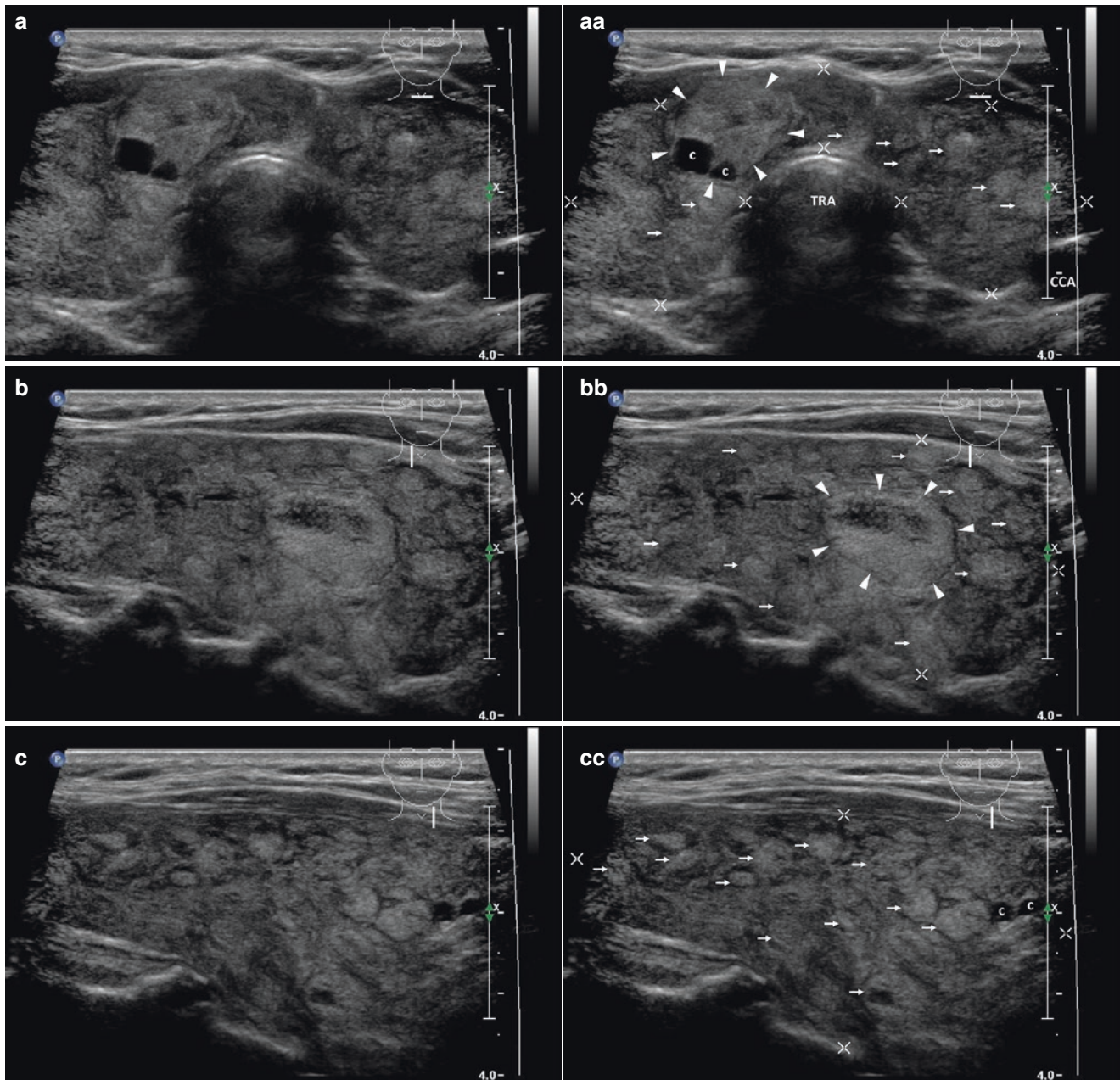


Fig. 3.8 (aa) A 40-year-old man with Hashimoto's thyroiditis (HT) and multinodular goiter, volume 50 mL. US overall view: enlarged thyroid gland—coarse structure; mostly hyperechoic, sporadic hypoechoic micronodular structure; diffusely multiple small solid nodules (*arrows*); one medium-sized complex nodule (*arrowheads*)—size 17×11 mm with small cystic cavities (*c*) in the RL; microlobulated margin; Tvol 50 mL, isthmus 10 mm, RL 26 mL and LL 23 mL; transverse. (bb) Detail of RL with HT and multinodular goiter: coarse structure; mostly

hyperechoic, sporadic hypoechoic micronodular structure; diffusely multiple small solid nodules (*arrows*); one medium-sized complex nodule (*arrowheads*); dorsally ill-defined blurred margin; longitudinal. (cc) Detail of LL with HT and multinodular goiter: coarse structure; mostly hyperechoic, sporadic hypoechoic micronodular structure; diffusely multiple small solid nodules (*arrows*); tiny cystic cavities (*c*); microlobulated margin; dorsally ill-defined blurred margin; longitudinal

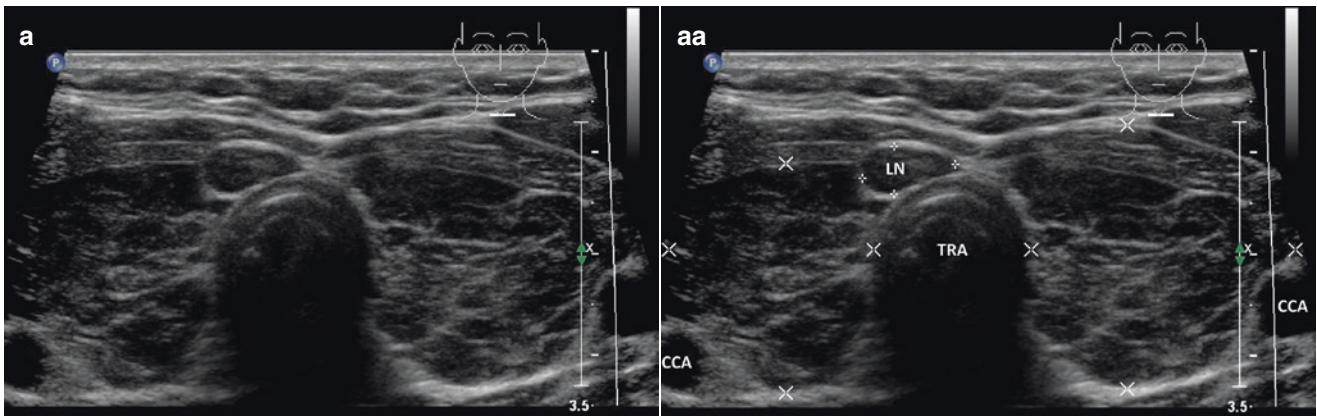


Fig. 3.9 (aa) A 32-year-old woman with Hashimoto's thyroiditis (HT), goiter volume 33 mL and "Delphian" lymph node (LN) adjacent to the isthmus. Classic US appearance: enlarged thyroid gland; inhomogeneous, mostly hypoechoic micronodular structure with thin and thick

hyperechoic fibrous septa; microlobulated margin; nonsuspicious "Delphian" LN in the right isthmus branch—elliptical, size 11×5 mm, L/S ratio >2 (not pathological); hypoechoic; Tvol 33 mL, RL 15 mL and LL 18 mL; transverse

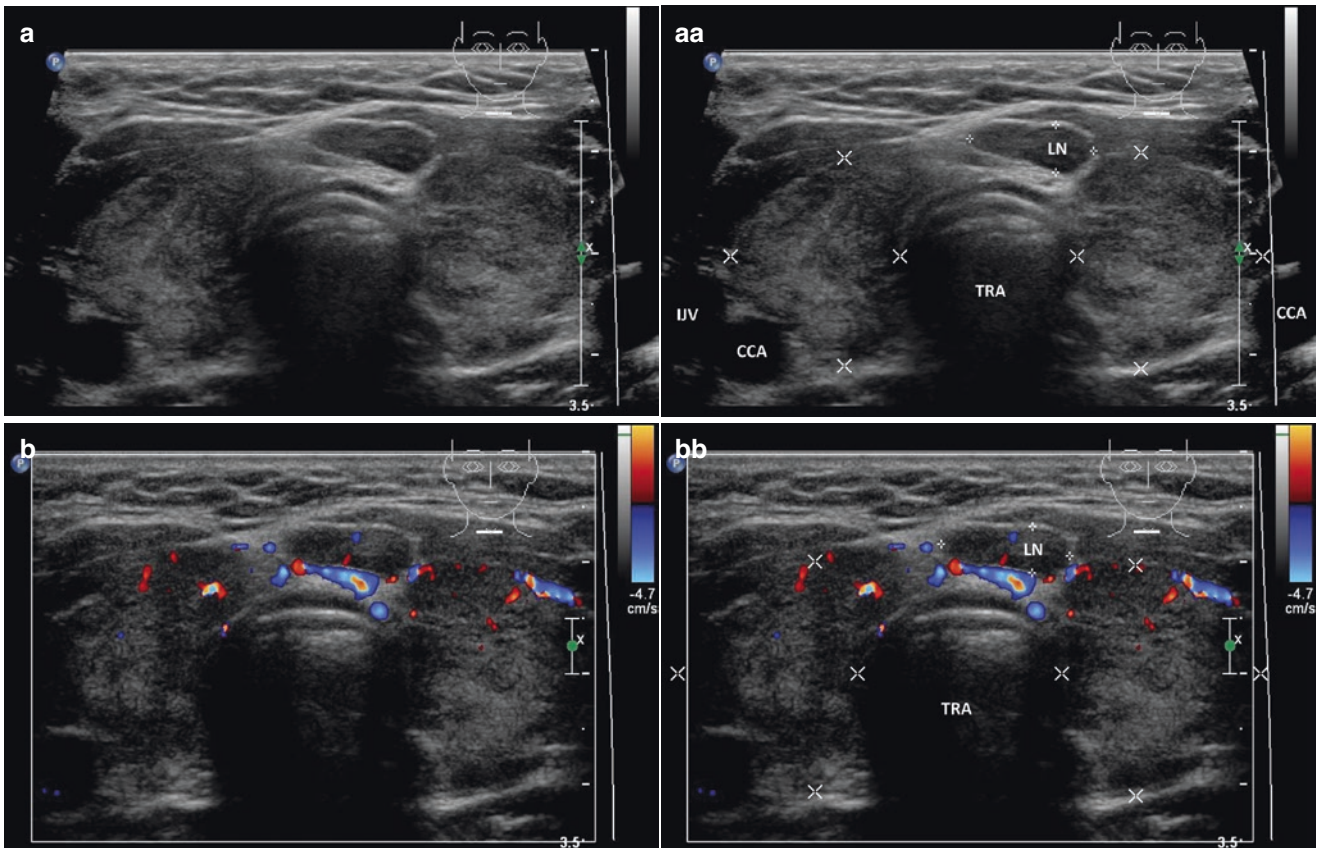


Fig. 3.10 (aa) A 26-year-old woman with Hashimoto's thyroiditis (HT), small goiter volume 21 mL and "Delphian" lymph node (LN) adjacent to the isthmus. Classic US appearance: inhomogeneous structure; mostly isoechoic, sporadic hypoechoic micronodular structure; microlobulated margin; nonsuspicious "Delphian" LN in the left isth-

mic branch—elliptical, size 12×4 mm, L/S ratio >2 (not pathological); hypoechoic; Tvol 21 mL, RL 10 mL and LL 11 mL; transverse. (bb) Detail of HT, small goiter and "Delphian" LN, CFDS: thyroid gland—sporadically parenchymal vascularity, pattern I; LN—minimal hilar vascularity; transverse

3.3 Hashimoto's Thyroiditis: Atrophic Gland

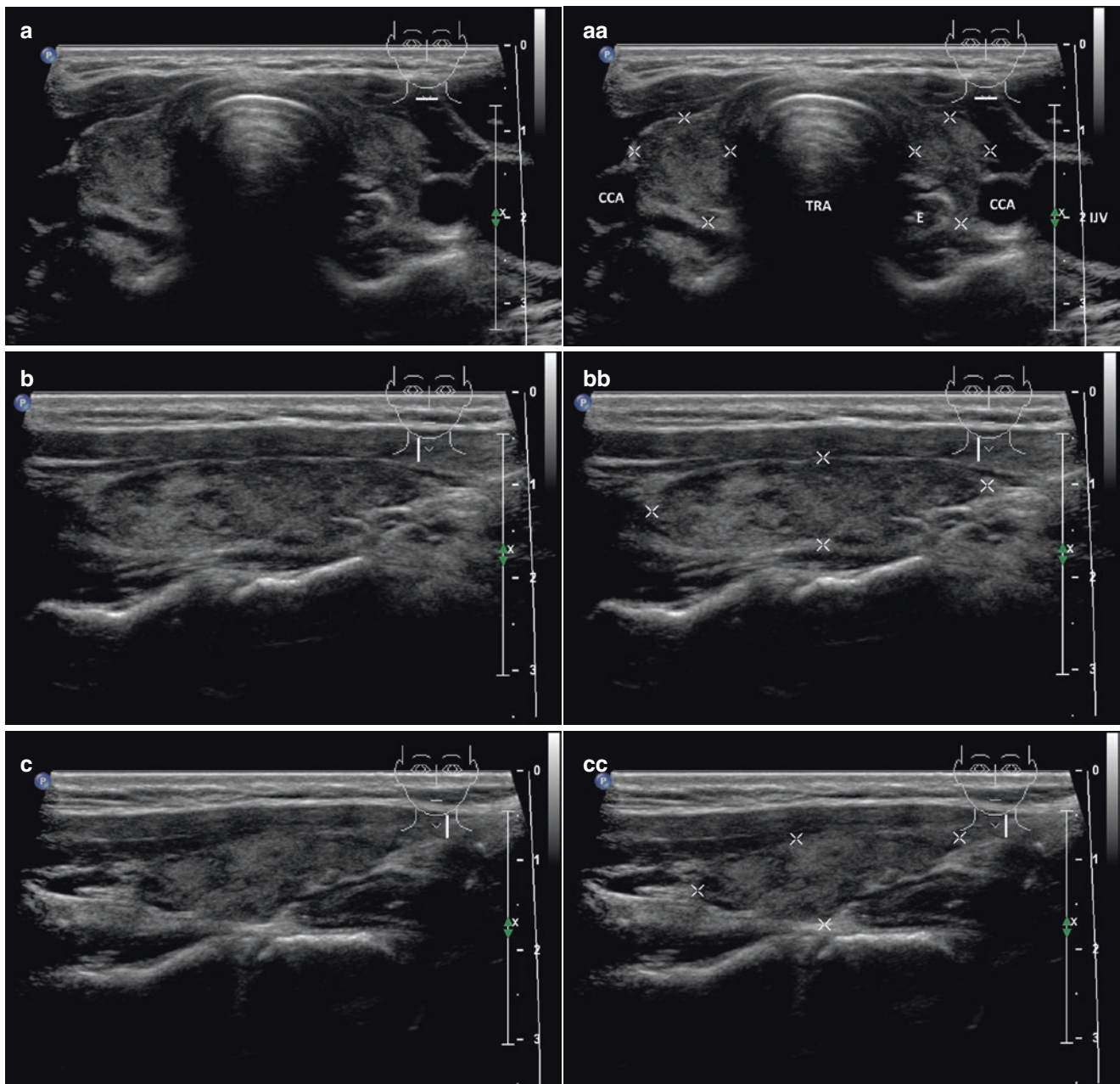


Fig. 3.11 (aa) A 36-year-old woman with Hashimoto's thyroiditis (HT) and atrophic thyroid gland volume 5 mL. US overall view: coarse structure; mixed echogenicity, mostly hyperechoic, sporadic hypoechoic micronodules; well-defined margin; longitudinal. (cc) Detail of LL with atrophic HT: coarse structure; mixed echogenicity, mostly hyperechoic, sporadic hypoechoic micronodules; well-defined margin; Tvol 5 mL, RL 3 mL, and LL 2 mL; transverse. (bb) Detail of RL with atrophic HT: coarse structure;

mixed echogenicity, mostly hyperechoic, sporadic hypoechoic micronodules; well-defined margin; longitudinal. (cc) Detail of LL with atrophic HT: coarse structure; mixed echogenicity, mostly hyperechoic, sporadic hypoechoic micronodules; well-defined microlobulated margin; longitudinal

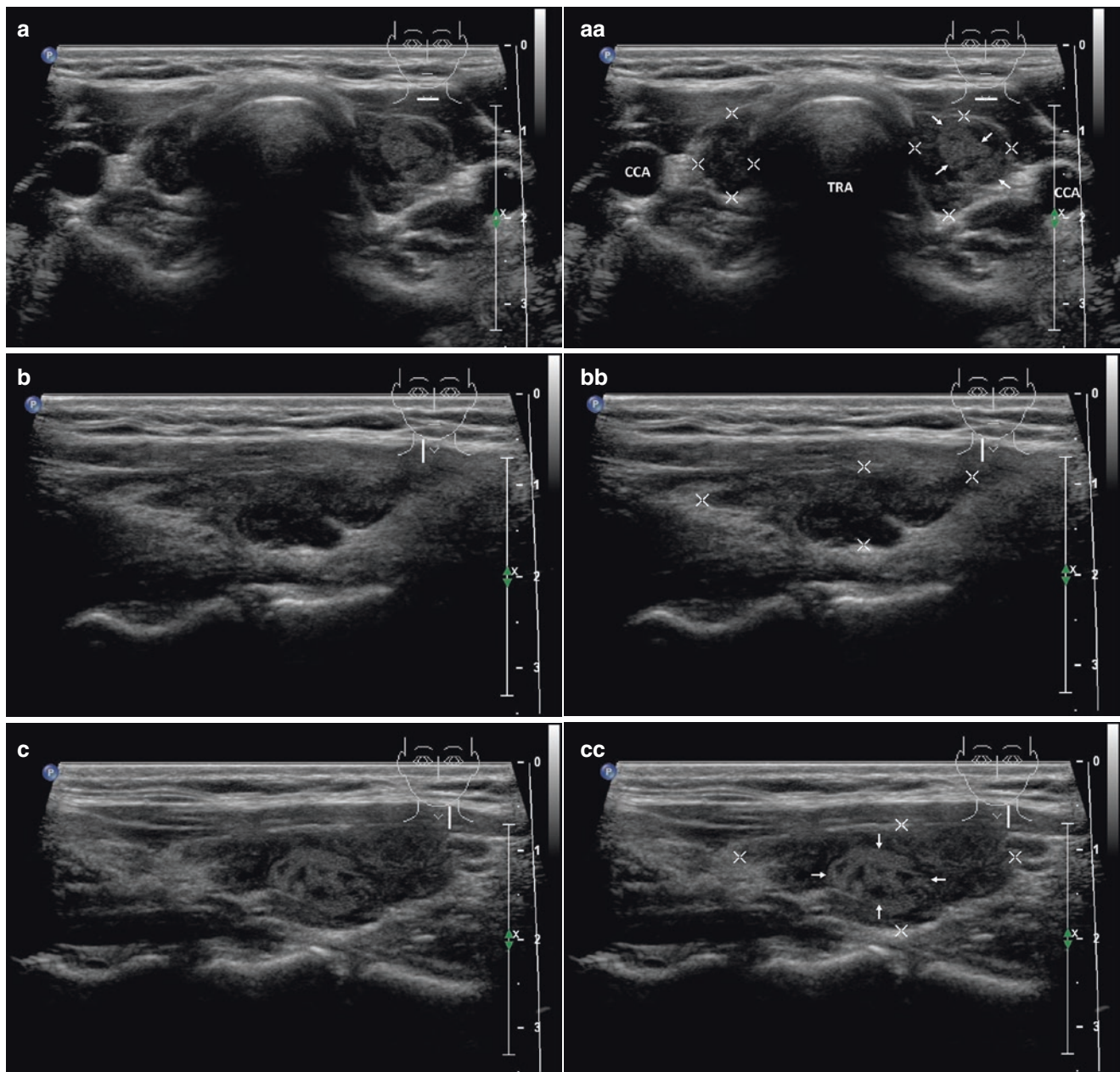


Fig. 3.12 (aa) A 40-year-old woman with HT, atrophic thyroid gland volume 5 mL and a solitary small nodule (*arrows*) in the LL. US overall view: coarse structure; mixed echogenicity, hypoechoic micronodules and hyperechoic fibrotic septa; microlobulated, focally ill-defined margin; nonsuspicious nodule with HT pattern, size $9 \times 7 \times 6$ mm and volume 0.2 mL in the LL—solid, inhomogeneous, hyperechoic with sporadic hypoechoic areas; Tvol 5 mL, RL 2 mL, and LL 3 mL; transverse. (bb) Detail of RL with atrophic HT: coarse structure; hypoechoic

micronodules and hyperechoic fibrotic septa; microlobulated, focally ill-defined margin; longitudinal. (cc) Detail of LL with atrophic HT and small solid nodule: nodule (*arrows*) with HT pattern—solid, inhomogeneous, hyperechoic with sporadic hypoechoic areas; longitudinal. (dd) Detail of LL with atrophic HT and small solid nodule, CFDS: thyroid gland—peripheral and parenchymal vascularity, *pattern I*; nodule (*arrows*)—peripheral vascularity and one central vessel branch, *pattern I*; longitudinal

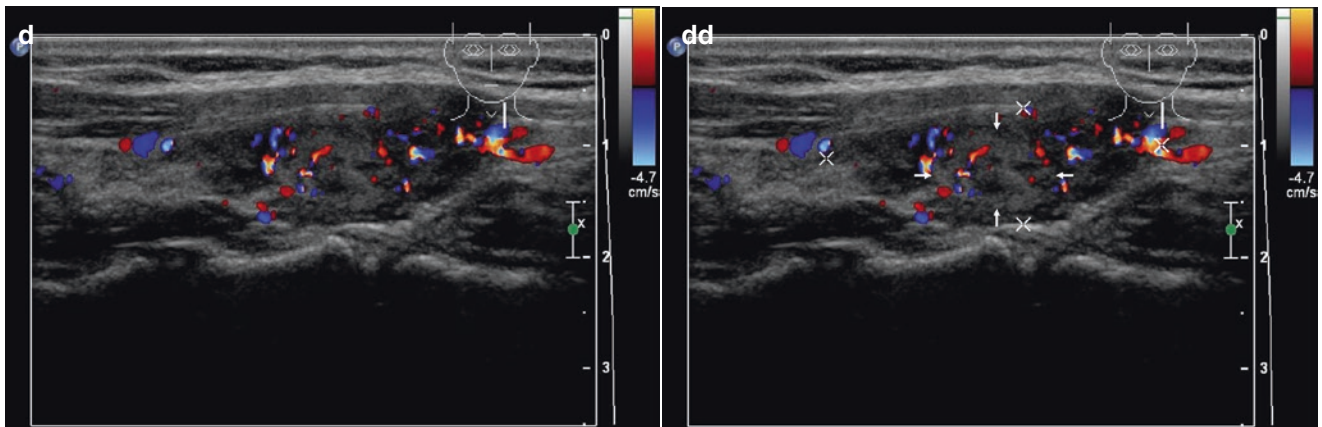


Fig. 3.12 (continued)

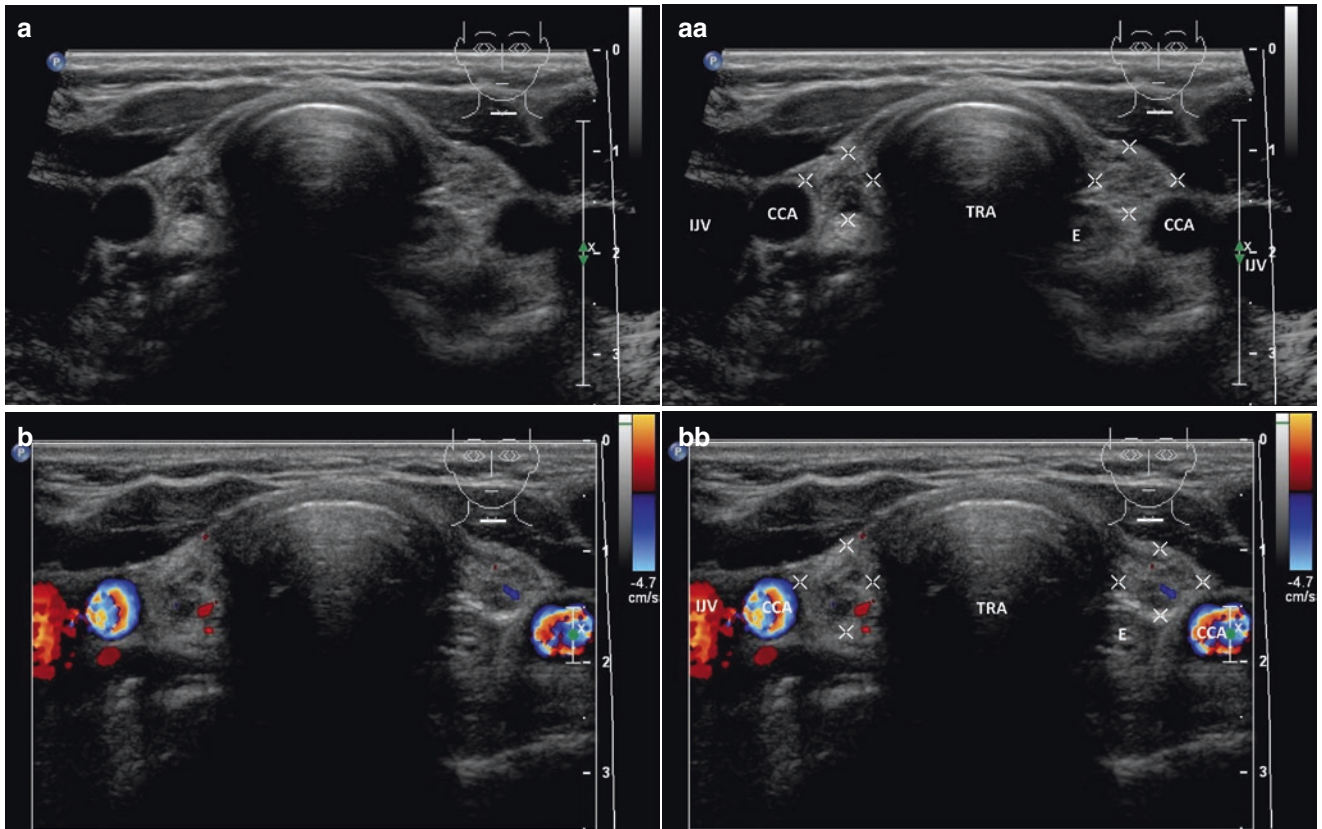
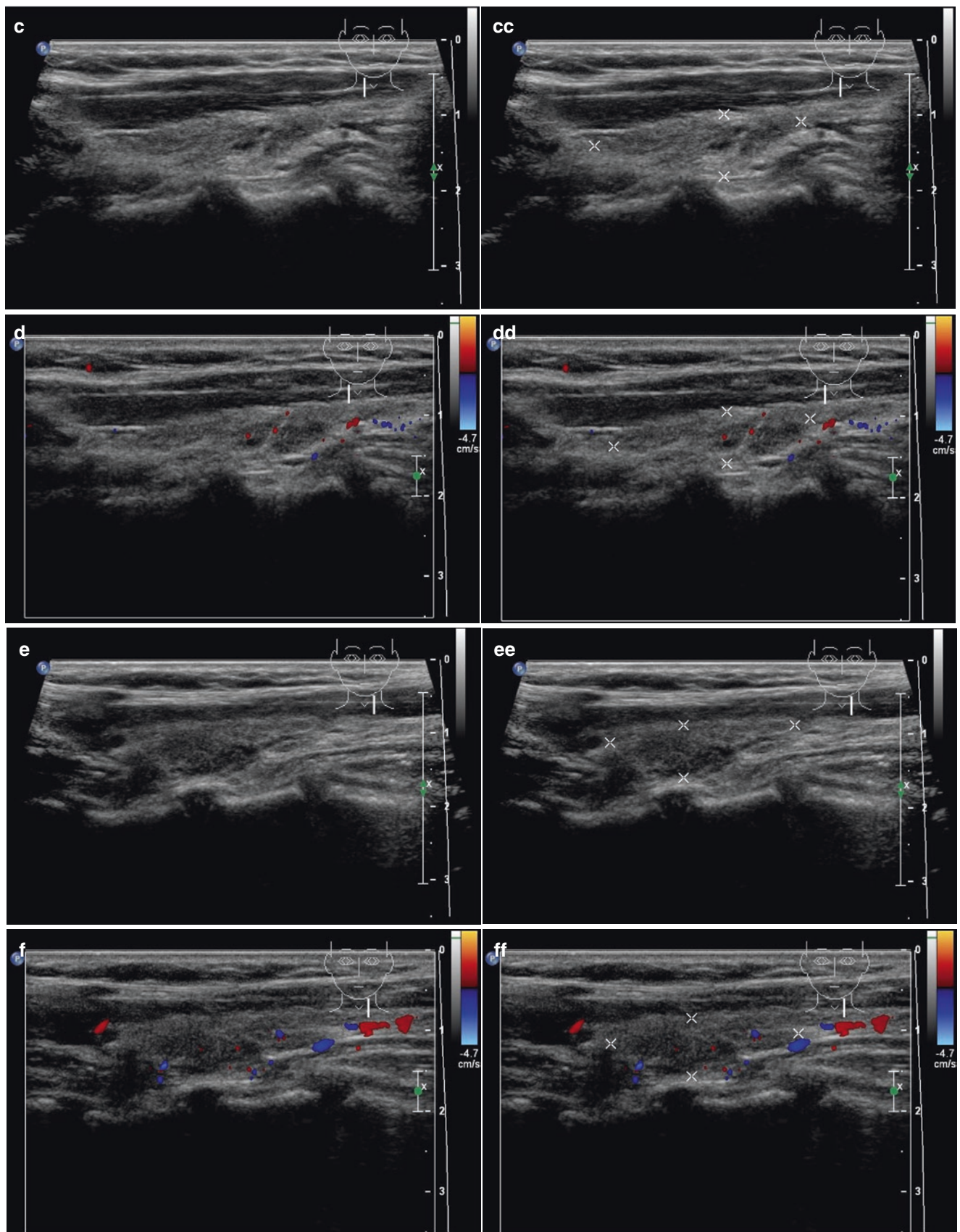


Fig. 3.13 (aa) A 46-year-old woman with HT and markedly atrophic thyroid gland volume 1.5 mL, which is poorly distinguishable from surrounding fibrotic tissue. US overall view: coarse structure; mostly hyperechoic, sporadic hypoechoic micronodules; ill-defined, blurred margin; both lobes in transverse view size 8×7 mm; Tvol 1.5 mL, RL 0.8 mL, and LL 0.7 mL; transverse. (bb) Overall view of markedly atrophic HT, CFDS: minimal vascularity, *pattern 0*; transverse. (cc) Detail of RL with markedly atrophic HT: coarse structure; mostly hyperechoic, sporadic hypoechoic micronodules; ill-defined, blurred

margin, coincides with surrounding fibrotic tissue; in longitudinal view size 28×7 mm; longitudinal. (dd) Detail of RL with markedly atrophic HT, CFDS: minimal vascularity, *pattern 0*; longitudinal. (ee) Detail of LL with markedly atrophic HT: coarse structure; mostly hyperechoic, sporadic hypoechoic micronodules; ill-defined, blurred margin, coincides with surrounding fibrotic tissue; in longitudinal view size 26×7 mm; longitudinal. (ff) Detail of LL with markedly atrophic HT, CFDS: minimal vascularity, *pattern 0*; longitudinal

**Fig. 3.13** (continued)

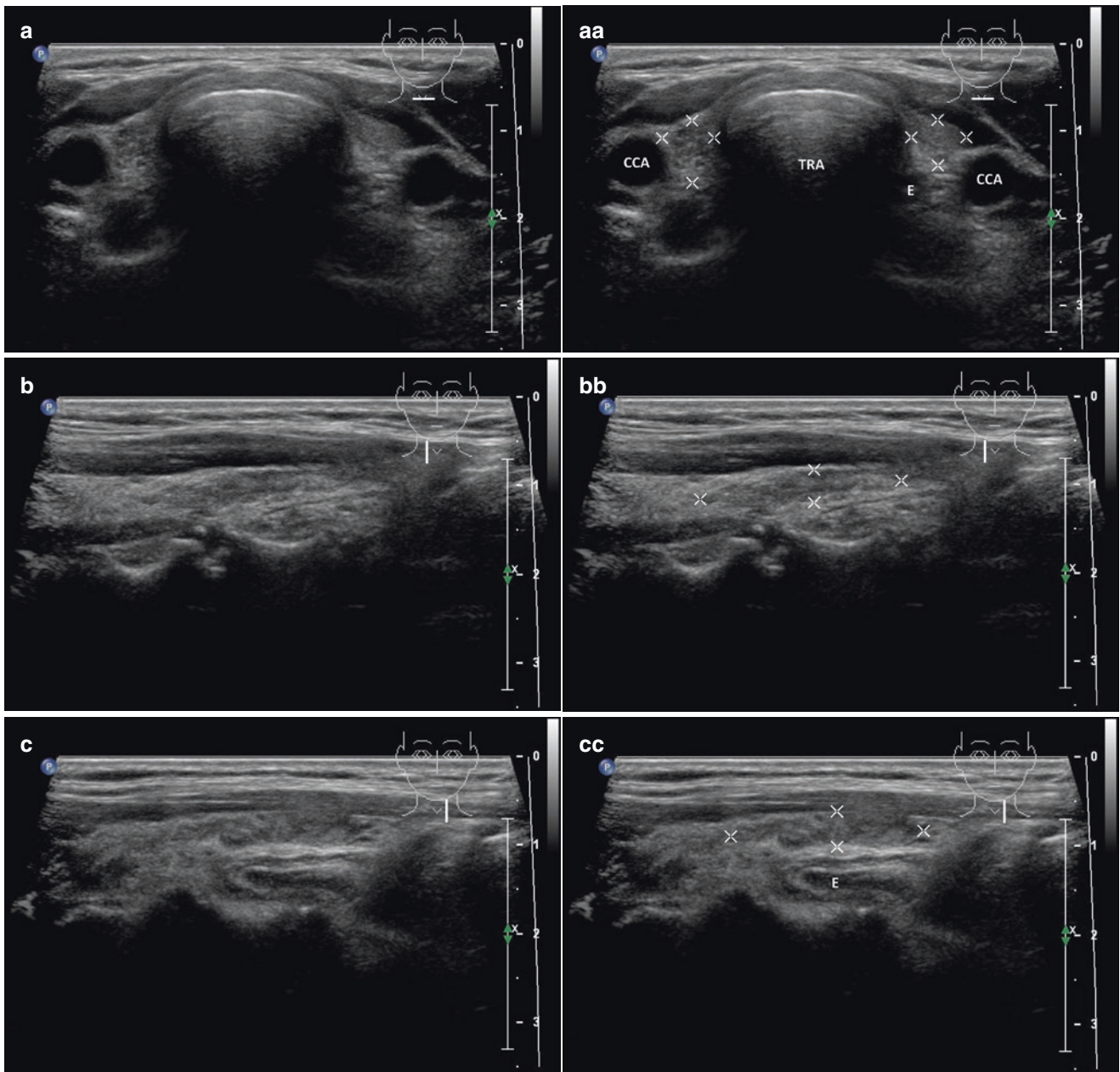


Fig. 3.14 (aa) A 67-year-old woman with HT and “near total” atrophic thyroid gland of volume 1 mL, which almost merged with surrounding fibrotic tissue. US overall view: coarse structure; mostly hyperechoic, sporadic hypoechoic micronodules; ill-defined, blurred margin; in longitudinal view size 24×5 mm; longitudinal. (cc) Detail of LL with “near total” atrophic HT: coarse structure; mostly hyperechoic, sporadic hypoechoic micronodules; ill-defined, blurred margin; in longitudinal view size 22×4 mm; longitudinal. (bb) Detail of RL with “near total”

atrophic HT: coarse structure; mostly hyperechoic, sporadic hypoechoic micronodules; ill-defined, blurred margin; in longitudinal view size 24×5 mm; longitudinal. (cc) Detail of LL with “near total” atrophic HT: coarse structure; mostly hyperechoic, sporadic hypoechoic micronodules; ill-defined, blurred margin; in longitudinal view size 22×4 mm; longitudinal

3.4 Hashimoto's Thyroiditis: Hashitoxicosis

3.4.1 Essential Facts

- Hashitoxicosis is a transient thyrotoxicosis caused by destructive inflammation due to Hashimoto's thyroiditis (HT) damaging the thyroid follicles, and resulting in excess release of thyroid hormone (Fig. 3.15) [26].
- Hashitoxicosis occurs in about 4.5% of patients with HT [26].
- It is a self-limiting form lasting from a period of a few weeks to some months [26].
- During this time, classical symptoms of mild-to-moderate hyperthyroidism may coexist with a diffuse, firm, painless goiter [26].
- Thyroid scintigraphy may show normal or a slightly increased radioiodine uptake [26].
- It is biochemically characterized by elevated titer(s) of TG-Ab and/or TPO-Ab, suppressed TSH, and elevated T4 and T3 [26].
- Differentiation between causes of thyrotoxicosis at time of diagnosis, either hyperthyroidism due to Graves' disease (GD) or destructive thyrotoxicosis due to HT is very important as management of each disease is completely different. Color Flow Doppler Ultrasound (CFDS) is a useful tool [27].

3.4.2 US Features of Hashitoxicosis

- Color Flow Doppler Sonography (CFDS) is a useful, inexpensive, non-invasive and widely available method

for measuring tissue vascularization and blood flow. CFDS can evaluate both qualitative parameters—visual assessment of thyroid vascularity—and quantitative parameters—inferior thyroid arteries peak systolic (PSV), end diastolic (EDV), and mean blood flow velocities [27].

- Both autoimmune thyroid diseases GD and HT have similar US pattern characterized by an enlarged thyroid gland, diffusely heterogeneous echotexture, and predominant hypoechogenicity.
- A diffusely increased thyroid blood flow, so-called “*thyroid inferno*” (Fig. 4.1bb), is pathognomonic of untreated GD and this CFDS pattern identifies the majority of Graves' patients. However, HT during the initial hyperthyroid phase can also present CFDS qualitative pattern (Fig. 3.15 bb) of marked and diffusely increased vascularity similar to GD [28].
- CFDS quantitative parameters are useful in distinguishing thyrotoxicosis in patients with GD and HT. PSV, EDV, and mean velocities of inferior thyroid artery (ITA) in patients with GD were significantly higher than in patients with HT. In studies by Donkol et al. with 26 hyperthyroid patients, by Kurita with 33 hyperthyroid patients, and by Hari Kumar et al. with 65 hyperthyroid patients, CFDS parameters had the sensitivity of 89%, resp. 84%, and resp. 96%, and the specificity 87%, resp. 90%, and resp. 95% to differentiate the two entities [26, 29, 30].
- CFDS parameter PSV with cut-off value of 40–65 cm/s (Fig. 3.15ii) was used to differentiate HT from GD [27, 28].

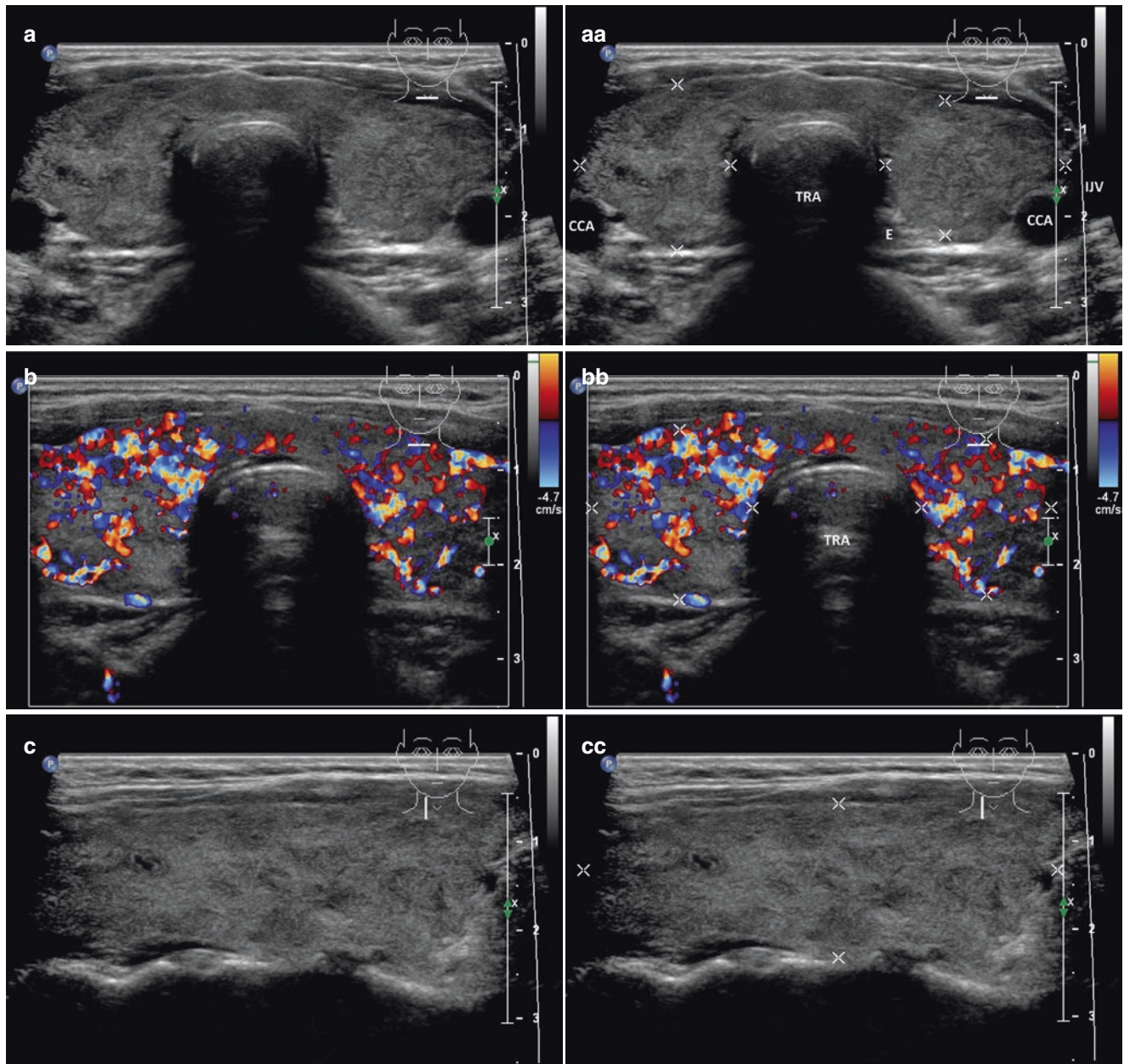
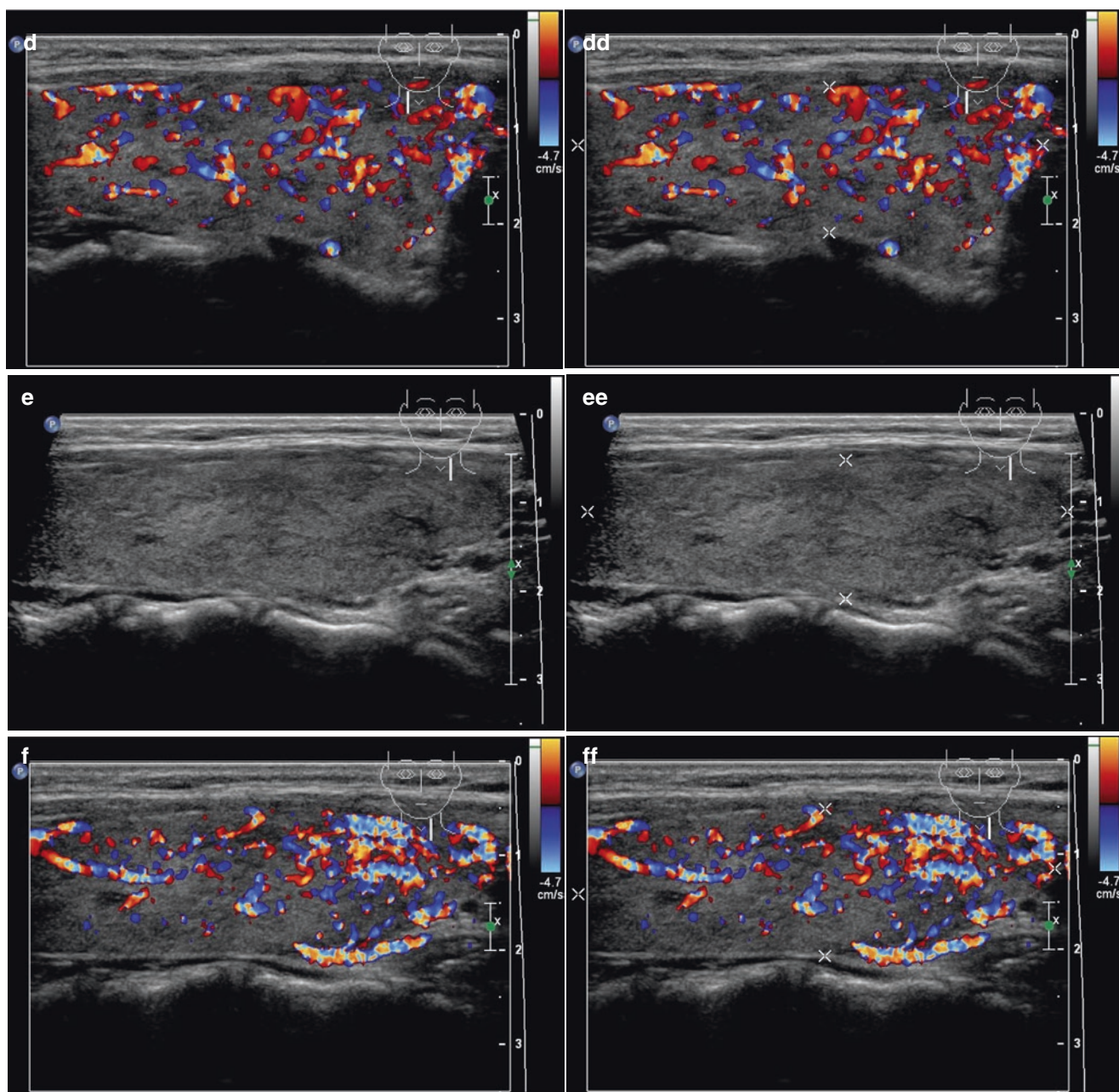


Fig. 3.15 (aa) A 33-year-old woman with Hashimoto's thyroiditis (HT) and hashitoxicosis. US overall view: slightly enlarged thyroid gland; inhomogeneous, mostly isoechoic, sporadic hypoechoic micronodular structure; Tvol 26 mL, RL 14 mL, and LL 12 mL; transverse. (bb) Overall view of HT and hashitoxicosis, CFDS: diffusely increased vascularity, *pattern II*; transverse. (cc) Detail of RL with HT and hashitoxicosis: inhomogeneous, mostly isoechoic, sporadic hypoechoic micronodular structure; longitudinal. (dd) Detail of RL with HT and hashitoxicosis, CFDS: diffusely increased vascularity, *pattern II*; longitudinal. (ee) Detail of LL with HT and hashitoxicosis:

inhomogeneous, mostly isoechoic, sporadic hypoechoic micronodular structure; longitudinal. (ff) Detail of LL with HT and hashitoxicosis, CFDS: diffusely increased vascularity, *pattern II*; longitudinal. (gg) Detail of HT and hashitoxicosis, left inferior thyroid artery (ITA): small lumen located between low pole of LL and left CCA; transverse. (hh) Detail of HT and hashitoxicosis, CFDS in the left ITA: small lumen located between low pole of LL and left CCA; transverse. (ii) Detail of HT and hashitoxicosis, flow parameter measured in the left ITA: peak systolic velocity (PSV) 63.8 cm/s, confirming diagnosis of hashitoxicosis

**Fig. 3.15** (continued)

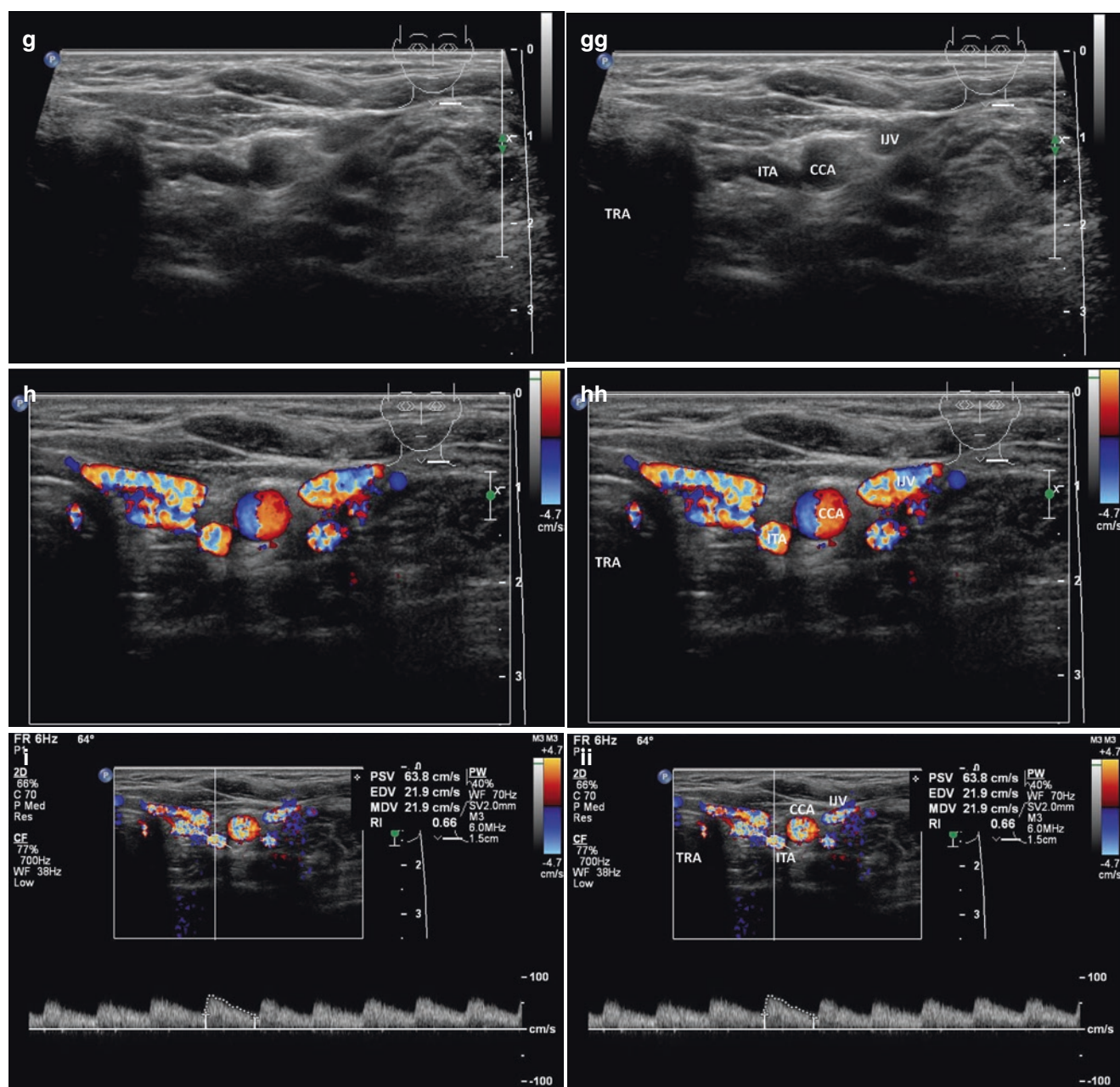


Fig. 3.15 (continued)

References

- Pearce EN, Farwell AP, Braverman LE. Thyroiditis. *N Engl J Med*. 2003;348(26):2646–55.
- Caturegli P, De Remigis A, Rose NR. Hashimoto thyroiditis: clinical and diagnostic criteria. *Autoimmun Rev*. 2014;13(4–5):391–7.
- Hiromatsu Y, Satoh H, Amino N. Hashimoto's thyroiditis: history and future outlook. *Hormones (Athens)*. 2013;12(1):12–8.
- Hong HS, Lee EH, Jeong SH, Park J, Lee H. Ultrasonography of various thyroid diseases in children and adolescents: a pictorial essay. *Korean J Radiol*. 2015;16(2):419–29.
- LiVolsi VA. The pathology of autoimmune thyroid disease: a review. *Thyroid*. 1994;4(3):333–9.
- Singer PA. Thyroiditis. Acute, subacute, and chronic. *Med Clin North Am*. 1991;75(1):61–77.
- Hollowell JG, Staehling NW, Flanders WD, Hannon WH, Gunter EW, Spencer CA, et al. Serum TSH, T(4), and thyroid antibodies in the United States population (1988 to 1994): National Health and Nutrition Examination Survey (NHANES III). *J Clin Endocrinol Metab*. 2002;87(2):489–99.
- Langer JE, Khan A, Nisenbaum HL, Baloch ZW, Horii SC, Coleman BG, et al. Sonographic appearance of focal thyroiditis. *AJR Am J Roentgenol*. 2001;176(3):751–4.
- Caleo A, Vigliar E, Vitale M, Di Crescenzo V, Cinelli M, Carlomagno C, et al. Cytological diagnosis of thyroid nodules in Hashimoto thyroiditis in elderly patients. *BMC Surg*. 2013;13(Suppl 2):S41.
- Wiersinga WM. Clinical relevance of environmental factors in the pathogenesis of autoimmune thyroid disease. *Endocrinol Metab (Seoul)*. 2016;31(2):213–22.
- Dong YH, Fu DG. Autoimmune thyroid disease: mechanism, genetics and current knowledge. *Eur Rev Med Pharmacol Sci*. 2014;18(23):3611–8.
- Strieder TG, Tijssen JG, Wenzel BE, Endert E, Wiersinga WM. Prediction of progression to overt hypothyroidism or hyperthyroidism in female relatives of patients with autoimmune thyroid disease using the thyroid events Amsterdam (THEA) score. *Arch Intern Med*. 2008;168:1657–63.
- Bogner U, Hegedüs L, Hansen JM, Finke R, Schleusener H. Thyroid cytotoxic antibodies in atrophic and goitrous autoimmune thyroiditis. *Eur J Endocrinol*. 1995;132(1):69–74.
- Carlé A, Pedersen IB, Knudsen N, Perrild H, Ovesen L, Jørgensen T, et al. Thyroid volume in hypothyroidism due to autoimmune disease follows a unimodal distribution: evidence against primary thyroid atrophy and autoimmune thyroiditis being distinct diseases. *J Clin Endocrinol Metab*. 2009;94(3):833–9.
- Espinasse P. Thyroid echography in chronic autoimmune lymphocytic thyroiditis. *J Radiol*. 1983;64(10):537–44.
- Bachrach LK, Daneman D, Daneman A, Martin DJ. Use of ultrasound in childhood thyroid disorders. *J Pediatr*. 1983;103(4):547–52.
- Gutekunst R, Hafermann W, Mansky T, Scriba PC. Ultrasonography related to clinical and laboratory findings in lymphocytic thyroiditis. *Acta Endocrinol*. 1989;121:129–35.
- Chaudhary V, Bano S. Thyroid ultrasound. *Indian J Endocrinol Metab*. 2013;17(2):219–27.
- Yeh HC, Futterweit W, Gilbert P. Micronodulation: ultrasonographic sign of Hashimoto thyroiditis. *J Ultrasound Med*. 1996;15(12):813–9.
- Gutekunst R, Becker W, Hehrmann R, Olbricht T, Pfannenstiel P. Ultrasonic diagnosis of the thyroid gland. *Dtsch Med Wochenschr*. 1988;113(27):1109–12.
- Hwang S, Shin DY, Kim EK, Yang WI, Byun JW, Lee SJ, et al. Focal lymphocytic thyroiditis nodules share the features of papillary thyroid cancer on ultrasound. *Yonsei Med J*. 2015;56(5):1338–44.
- Anderson L, Middleton WD, Teefey SA, Reading CC, Langer JE, Desser T, Szabunio MM, et al. Hashimoto thyroiditis: part 1, sonographic analysis of the nodular form of Hashimoto thyroiditis. *AJR Am J Roentgenol*. 2010;195(1):208–15.
- Kim DW, Eun CK, In HS, Kim MH, Jung SJ, Bae SK. Sonographic differentiation of asymptomatic diffuse thyroid disease from normal thyroid: a prospective study. *AJNR Am J Neuroradiol*. 2010;31(10):1956–60.
- Willms A, Bieler D, Wieler H, Willms D, Kaiser KP, Schwab R. Correlation between sonography and antibody activity in patients with Hashimoto thyroiditis. *J Ultrasound Med*. 2013;32(11):1979–86.
- Vlachopapadopoulou E, Thomas D, Karachaliou F, Chatzimarkou F, Memalal L, Vakaki M, et al. Evolution of sonographic appearance of the thyroid gland in children with Hashimoto's thyroiditis. *J Pediatr Endocrinol Metab*. 2009;22(4):339–44.
- Unnikrishnan AG. Hashitoxicosis: a clinical perspective. *Thyroid Res Pract*. 2013;10(Suppl S1):5–6.
- Donkol RH, Nada AM, Boughattas S. Role of color Doppler in differentiation of graves' disease and thyroiditis in thyrotoxicosis. *World J Radiol*. 2013;5(4):178–83.
- Caruso G, Attard M, Caronia A, Lagalla R. Color Doppler measurement of blood flow in the inferior thyroid artery in patients with autoimmune thyroid diseases. *Eur J Radiol*. 2000;36(1):5–10.
- Kurita S, Sakurai M, Kita Y, Ota T, Ando H, Kaneko S, et al. Measurement of thyroid blood flow area is useful for diagnosing the cause of thyrotoxicosis. *Thyroid*. 2005;15(11):1249–52.
- Hari Kumar KV, Pasupuleti V, Jayaraman M, Abhyuday V, Rayudu BR, Modi KD. Role of thyroid Doppler in differential diagnosis of thyrotoxicosis. *Endocr Pract*. 2009;15(1):6–9.

4.1 Essential Facts

- In 1835, Irish physician Robert James Graves published in the London Medical and Surgical Journal a paper titled “*Newly observed affection of the thyroid gland in females*,” in which he described three women who exhibited “violent and long continued palpitations, [whose] eyeballs were apparently enlarged, [and] a beating of the heart could be heard during the paroxysm at some distance from the bed.” With this publication Graves secured his legacy within the annals of clinical endocrinology [1].
- In March 1840, a physician in Merseburg, Germany, Carl Adolph von Basedow, published article in the reputable medical journal of the time, *Heilkunde fuer die Gesamte Medizin*, titled, in German, “*Exophthalmus durch Hypertrophie des Zellgewebes in der Augenhohle*” (“Exophthalmos due to hypertrophy of the cellular tissue in the orbit”). Thereafter, the cardinal symptoms—exophthalmos, goiter, and tachycardia—became known as the “*Merseburger triad*.” Since 1858 Basedow’s disease has been the most commonly used identifying term for the disease on the European continent, while Graves’ disease (GD) is more widely used in the English-speaking world [2].
- Graves’ disease is the most common cause of hyperthyroidism, followed by toxic multinodular goiter. Rarer causes include an autonomously functioning thyroid adenoma and thyroiditis [3].
- Prevalence of hyperthyroidism in women is between 0.5 and 2%, and is 10 times more common in women than in men in iodine-replete communities [3].
- Prevalence data in elderly persons shows a wide range between 0.4 and 2.0% [3].
- Incidence data available for overt hyperthyroidism in men and women from large population studies are comparable, at 0.4 per 1000 women and 0.1 per 1000 men, but the age-specific incidence varies considerably [3].
- GD has the highest incidence in between 20 and 49 years of age, with a secondary peak at the age of 60–69 years. In contrast, the peak age-specific incidence of hyperthyroidism caused by toxic nodular goiter and autonomously functioning thyroid adenomas is >80 years [3].
- Hyperthyroidism is rare in childhood and is most commonly caused by GD. It affects 0.02% of children, or 1 in 5000. The peak incidence occurs from 11 to 15 years of age with a female predominance. A positive family history is common [4].
- GD as a thyroid autoimmunity is caused by stimulatory autoantibodies against the thyrotropin receptor (TSHR-Ab). These antibodies cause uncontrolled and continuous stimulation of the thyroid, leading to excessive synthesis of the thyroid hormones: thyroxine (T4) and triiodothyronine (T3) and its hypertrophy.
- Laboratory findings: Measurements of serum TSH and free thyroxine (fT4) levels are essential for evaluation of hyperthyroidism, and TSHR-Ab shows high specificity of 99% and a sensitivity of 95% for confirmation of GD diagnosis [5].
- Clinical findings: Symptoms of hyperthyroidism and specific features which may point to GD include the presence of a diffuse goiter, ophthalmopathy and pretibial myxedema, and acropachia. Patients with GD usually have diffuse, nontender, symmetrical enlargement of the thyroid gland. Ophthalmopathy, consisting of protrusion of the eyes with periorbital soft-tissue swelling and inflammation, and inflammatory changes in the extraocular muscles resulting in diplopia and muscle imbalance, is clinically evident in 30% of patients with GD [6, 7].
- Hyperthyroidism occurs in approximately 0.2–1.0% of all pregnancies. Gestational transient thyrotoxicosis (GTT) is the most common cause as a result of the thyroid stimulatory actions of human chorionic gonadotropin (hCG). However, for management it is important to distinguish GD found during pregnancy to GTT (no past history or family history of thyroid autoimmunity, no goiter, no ophthalmopathy, TSHR-Ab negative, TPO-Ab negative, may present with hyperemesis, dehydration and electrolyte imbalance, is self-limiting

and usually does not require antithyroid drugs treatment) [6].

- Radioiodine ^{131}I -therapy (RIT) has been used to treat hyperthyroidism since the 1940s. Generally, after 4–6 weeks thyroid function normalizes [5].

4.2 US Features of Graves' Disease

- US imaging of classical GD pattern [4, 12]:
 - An enlarged gland with round-shaped lobes (Fig. 4.1aa), sometimes giant goiter (Fig. 4.4aa).

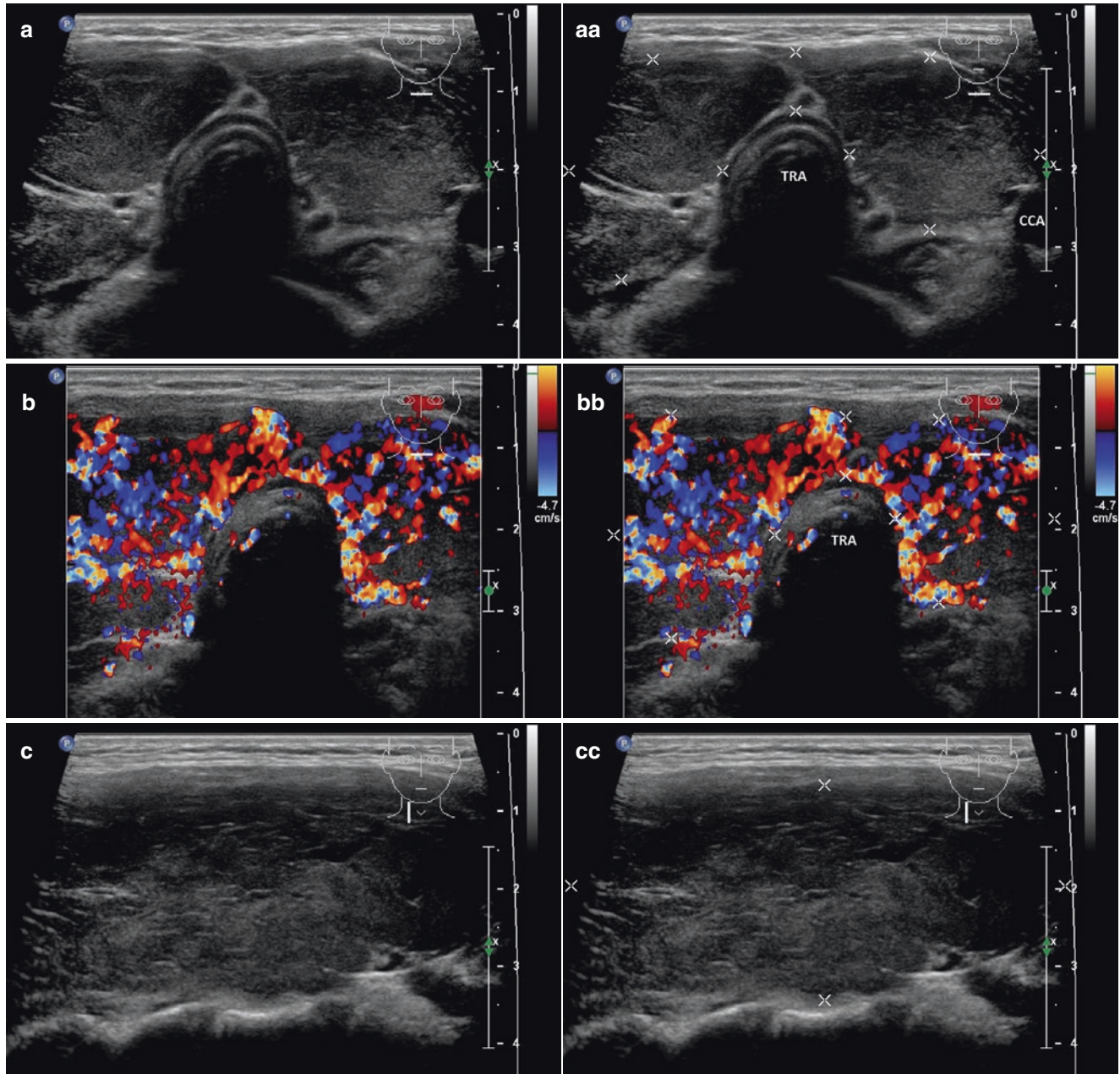


Fig. 4.1 (aa) A 33-year-old woman with Graves' disease (GD) and large goiter volume 65 mL. US overall view: diffusely enlarged thyroid gland with round-shaped lobes; inhomogeneous structure; mixed echogenicity; ventrally mostly hypoechoic micronodular structure; hyperechoic transverse septum at dorsal part of RL; Tvol 65 mL, asymmetry—RL 42 mL and LL 23 mL; transverse, depth of penetration 4.5 cm. (bb) Overall view of GD, CFDS: diffuse hypervascularity, *pattern III*—"thyroid inferno"; transverse. (cc) Detail of RL with GD: coarsened structure; mixed echogenicity; ventrally mostly hypoechoic micronodular structure with short fibrous septa; longitudinal. (dd) Detail of RL with GD,

CFDS: diffuse hypervascularity, *pattern III*—"thyroid inferno"; longitudinal. (ee) Detail of LL with GD: inhomogeneous structure; mostly isoechoic, ventrally hypoechoic micronodular structure; longitudinal. (ff) Detail of LL with GD, CFDS: diffuse hypervascularity, *pattern III*—"thyroid inferno"; longitudinal. (gg) Detail of GD, left inferior thyroid artery (ITA) with two branches: small lumens located between low pole of LL and left CCA; transverse. (hh) Detail of GD, CFDS in the left ITA: small lumens located between low pole of LL and left CCA; transverse. (ii) Detail of GD, flow parameter measured in the left ITA: peak systolic velocity (PSV) 147 cm/s, confirming diagnosis of GD

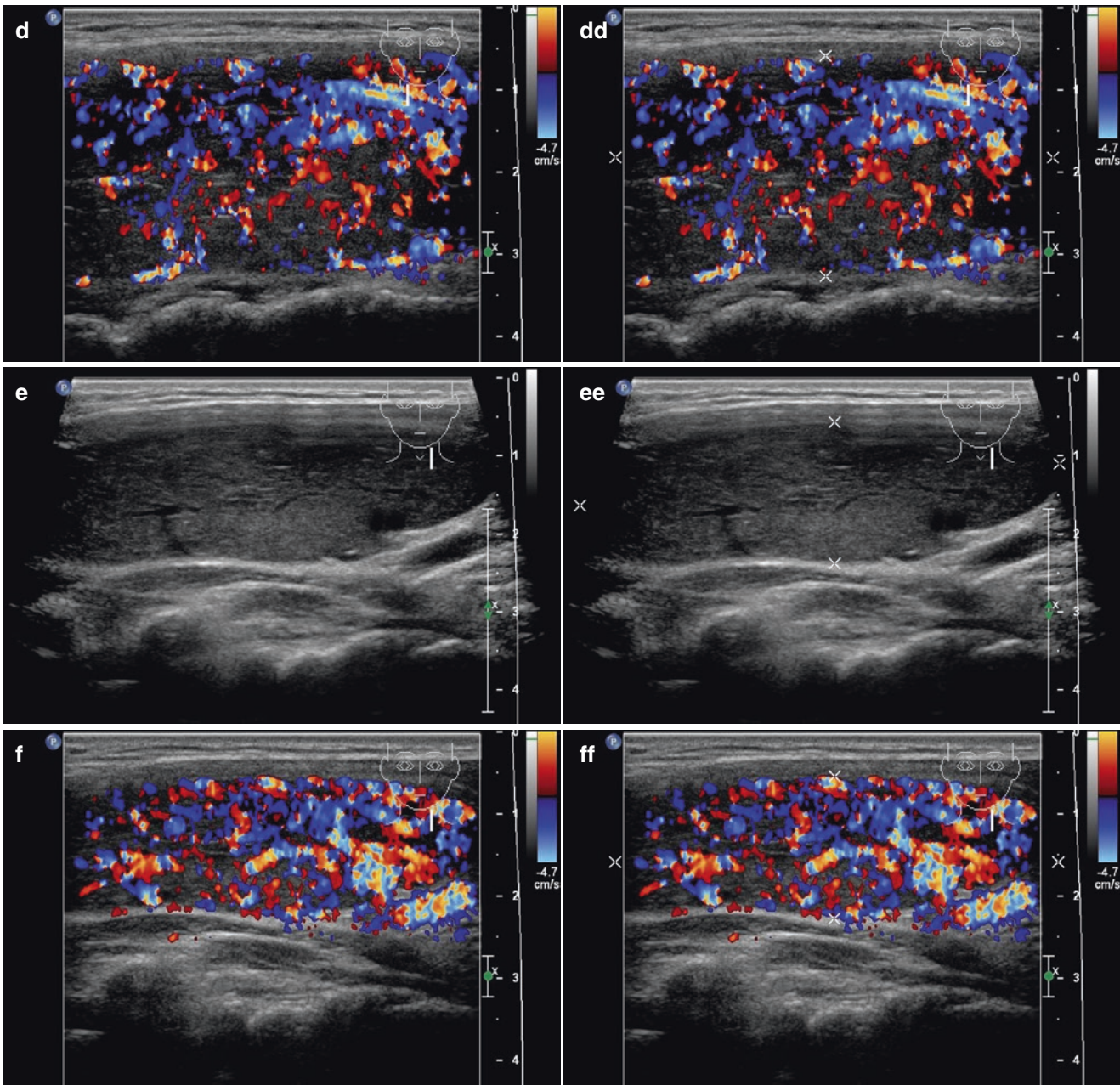


Fig.4.1 (continued)

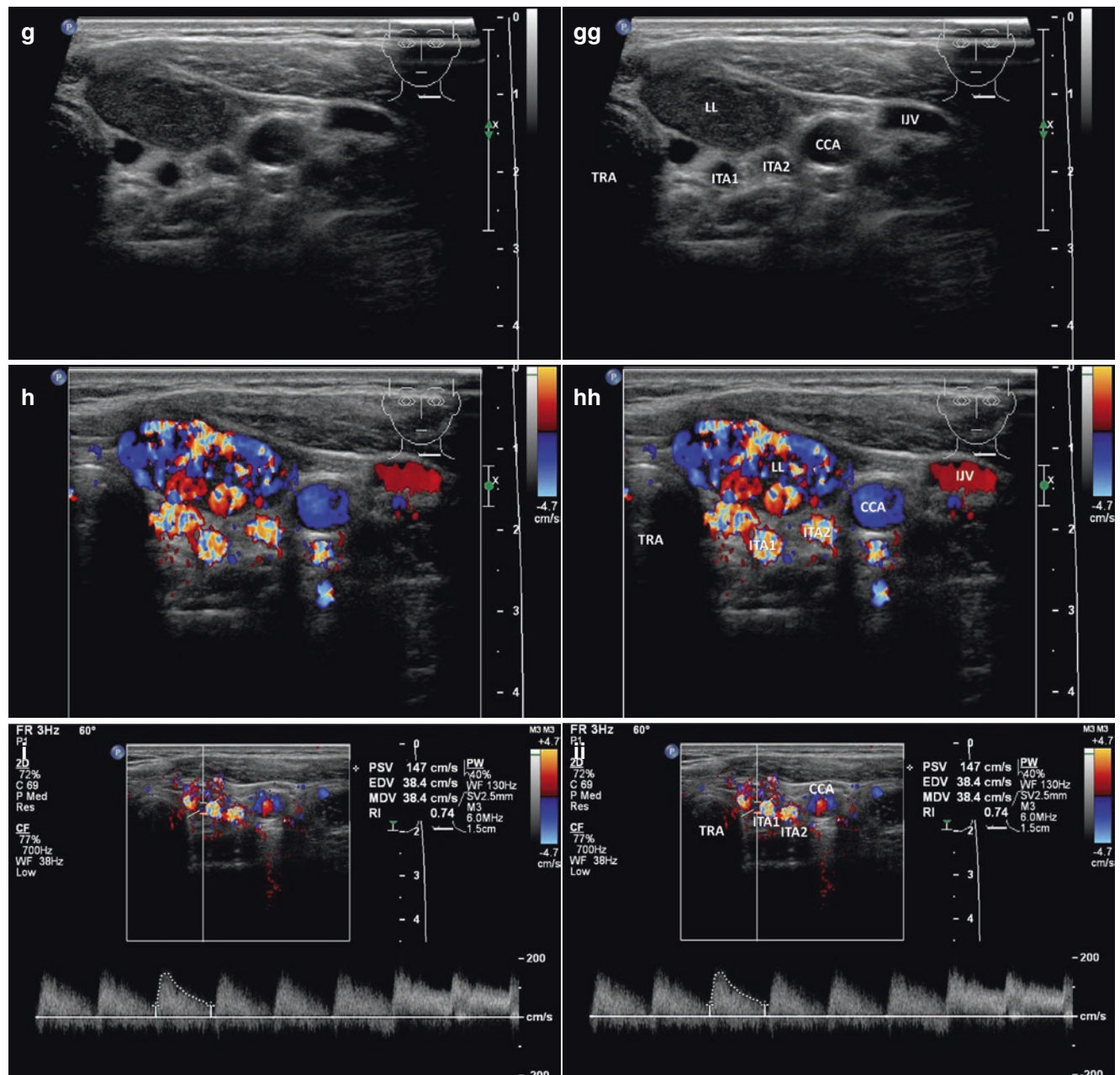


Fig. 4.1 (continued)

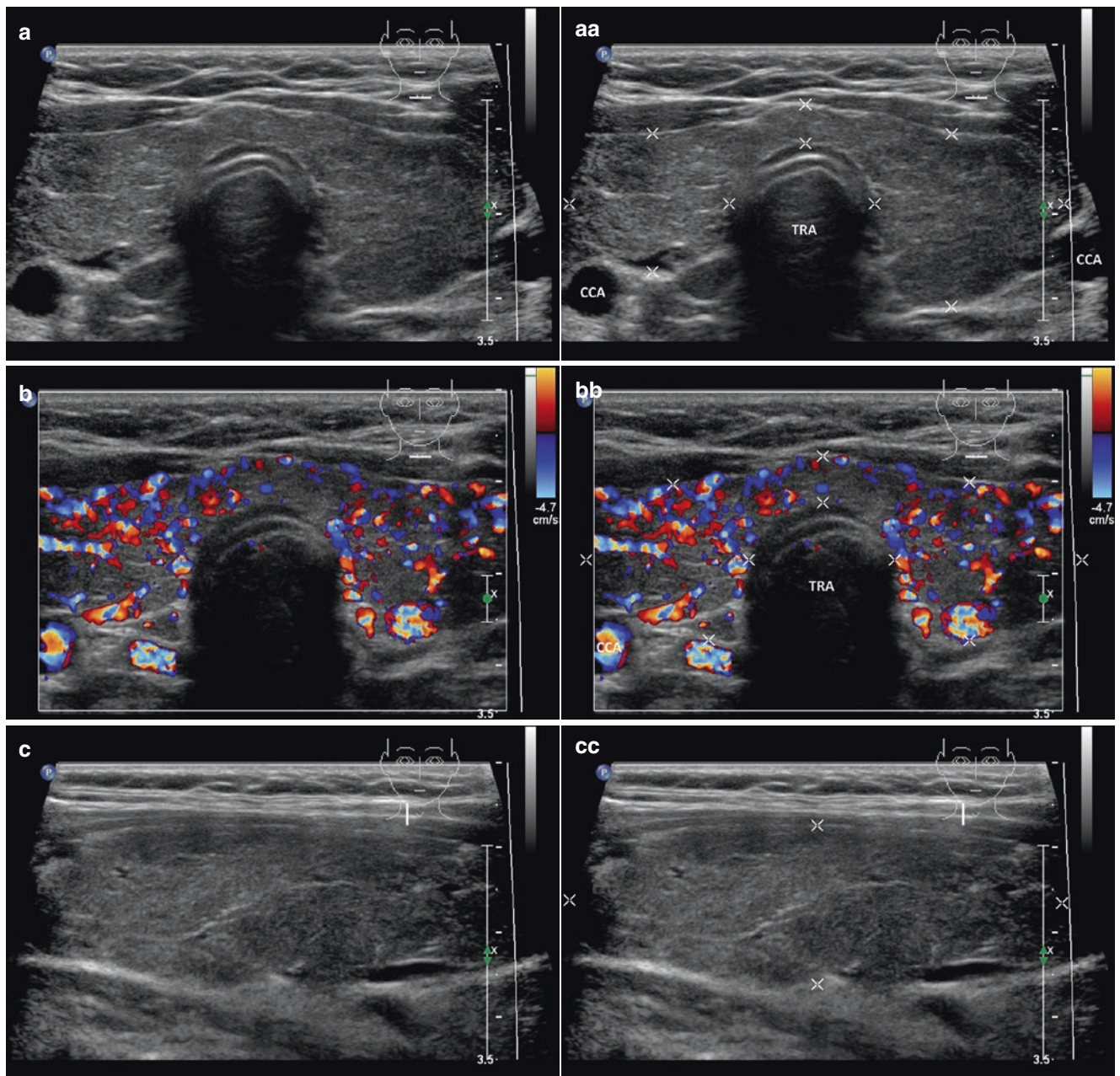


Fig. 4.2 (aa) A 23-year-old woman with Graves' disease (GD) and small goiter volume 32 mL. US overall view: diffusely enlarged thyroid gland; inhomogeneous structure; mostly isoechoic; ventrally sporadic hypoechoic micronodular structure with short fibrous septa; Tvol 32 mL, RL 17 mL and LL 15 mL; transverse. (bb) Overall view of GD, CFDS: diffuse hypervascularity, *pattern III*; transverse. (cc) Detail of RL with GD: inhomogeneous structure; mostly isoechoic; ventrally

sporadic hypoechoic micronodular structure with short fibrous septa; longitudinal. (dd) Detail of RL with GD, CFDS: diffuse hypervascularity, *pattern III*; longitudinal. (ee) Detail of LL with GD: inhomogeneous structure; mostly isoechoic; ventrally sporadic hypoechoic micronodular structure with short fibrous septa; longitudinal. (ff) Detail of LL with GD, CFDS: diffuse hypervascularity, *pattern III*; longitudinal

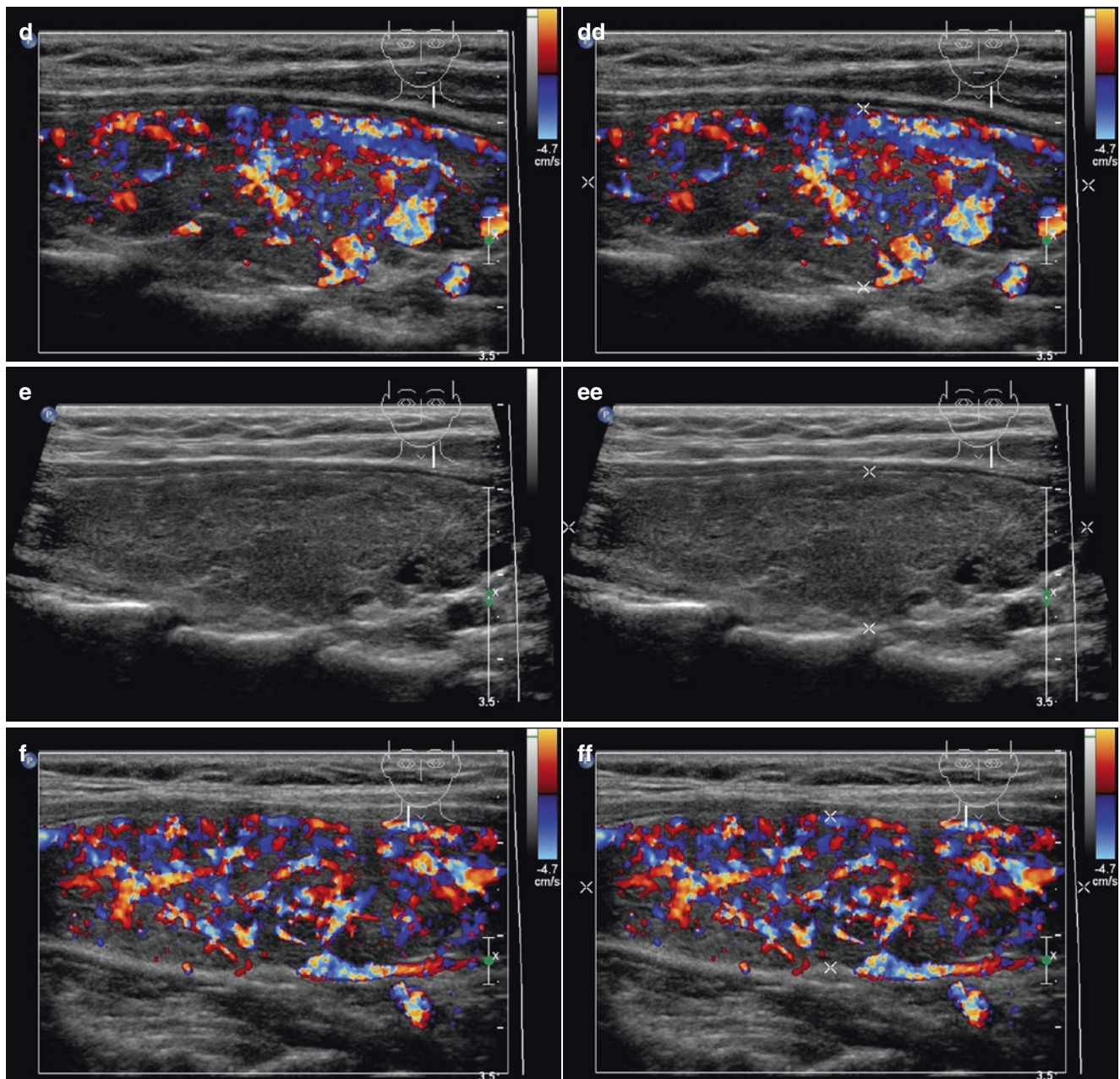


Fig. 4.2 (continued)

- A diffusely heterogeneous or coarse echotexture (Fig. 4.1aa).
- A diffusely hypoechoic (Fig. 4.1aa).
- Typically hypoechoic micronodular structure with short fibrous septa (Figs. 4.2aa and 4.3aa).
- CFDS demonstrate markedly increased vascularity *pattern III*—“thyroid inferno” (Figs. 4.1bb and 4.4bb).
- CFDS parameter peak systolic velocity (PSV) of inferior thyroid artery (ITA) with cut-off value of 65 cm/s, mostly over 150 cm/s (Fig. 4.1ii).

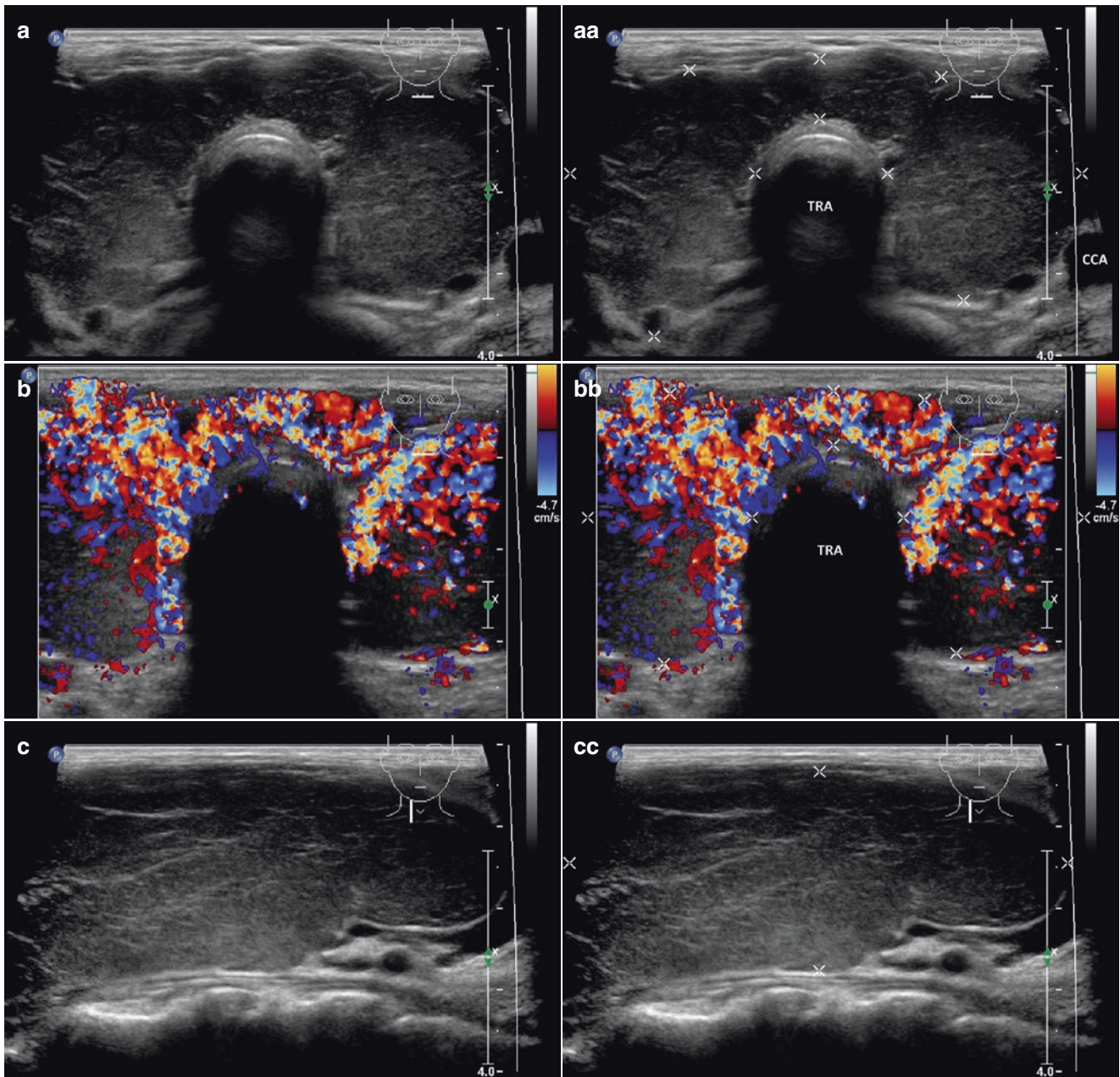


Fig. 4.3 (aa) A 23-year-old woman with Graves' disease (GD) and medium-size goiter volume 47 mL. US overall view: diffusely enlarged thyroid gland with round-shaped lobes; inhomogeneous structure; ventrally mostly hypoechoic micronodular structure with short fibrous septa; Tvol 47 mL, RL 25 mL, and LL 22 mL; transverse, depth of penetration 4 cm. (bb) Overall view of GD, CFDS: diffuse hypervascularity, *pattern III*—"thyroid inferno"; transverse. (cc) Detail of RL with

GD: inhomogeneous structure; ventrally mostly hypoechoic micronodular structure with short fibrous septa; longitudinal. (dd) Detail of RL with GD, CFDS: diffuse hypervascularity, *pattern III*—"thyroid inferno"; longitudinal. (ee) Detail of LL with GD: inhomogeneous structure; ventrally mostly hypoechoic micronodular structure with short fibrous septa; longitudinal. (ff) Detail of LL with GD, CFDS: diffuse hypervascularity, *pattern III*—"thyroid inferno"; longitudinal

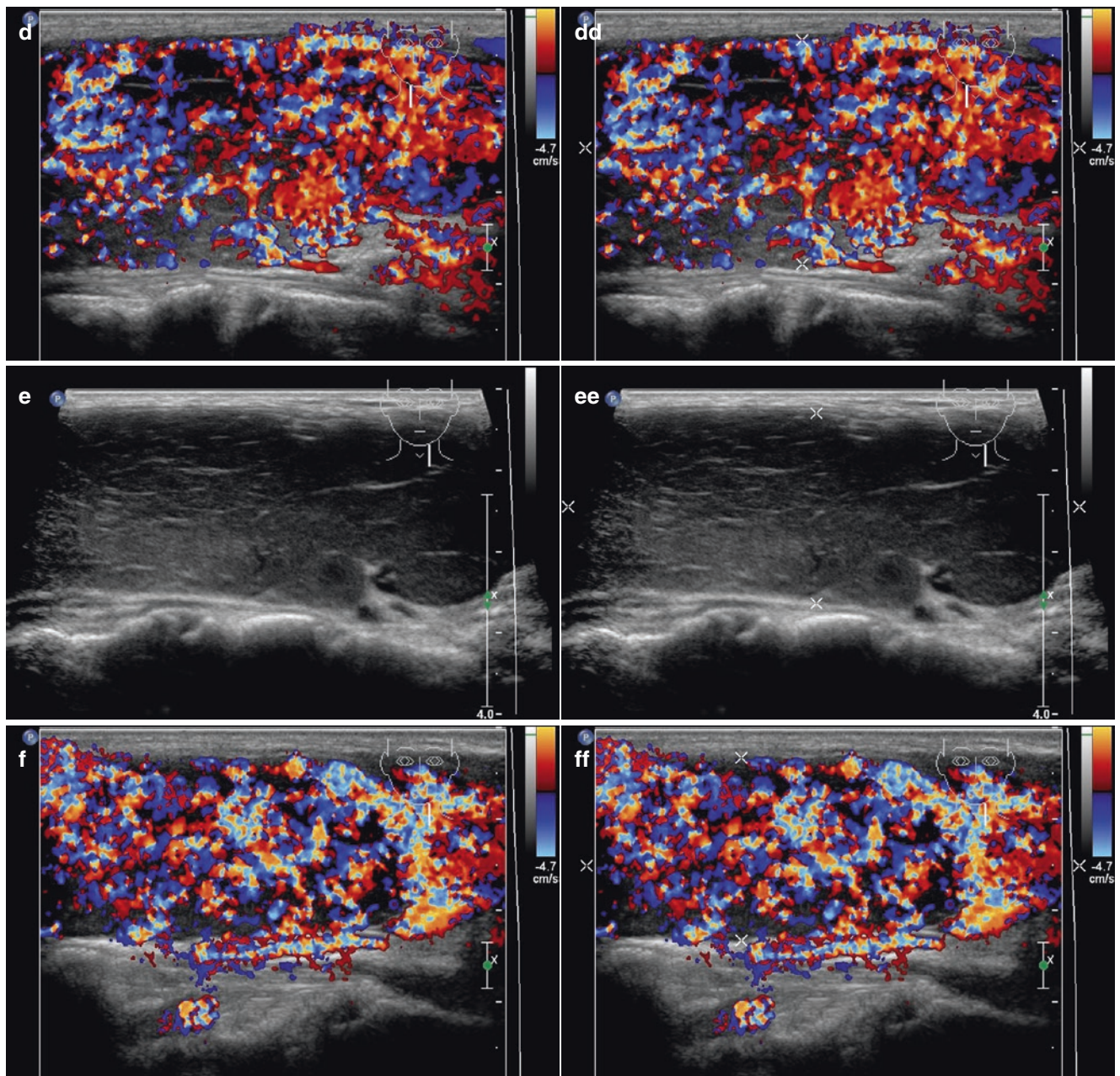


Fig. 4.3 (continued)

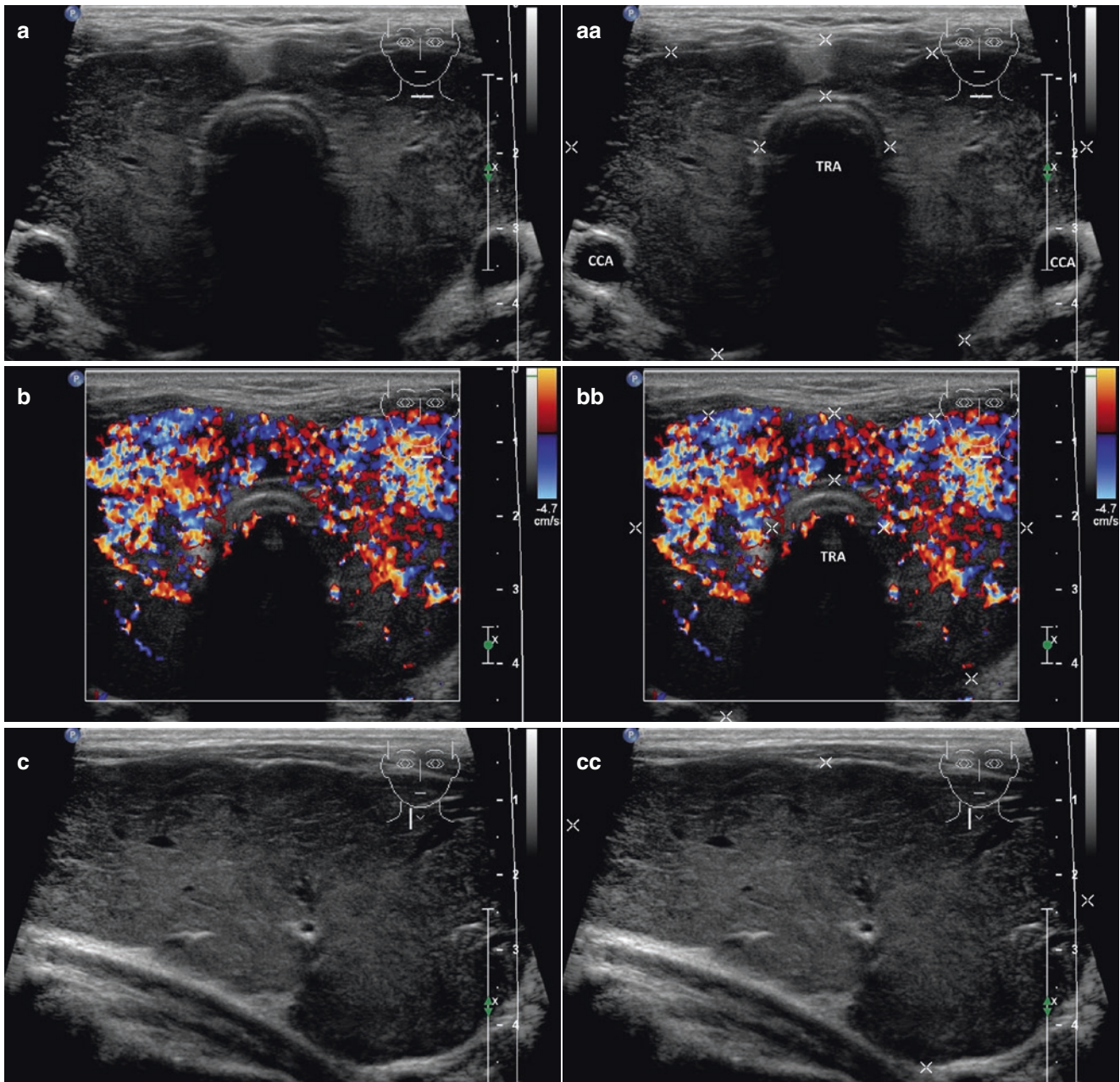


Fig. 4.4 (aa) A 31-year-old man with Graves' disease (GD) and giant goiter volume 96 mL. US overall view: diffusely enlarged thyroid gland with round-shaped lobes; inhomogeneous structure; ventrally mostly hypoechoic micronodular structure with short fibrous septa; Tvol 92 mL, thick isthmus 8 mm, RL 48 mL and LL 43 mL; transverse, depth of penetration 5 cm. (bb) Overall view of GD, CFDS: diffuse hypervascularity, *pattern III*—"thyroid inferno"; transverse. (cc) Detail

of RL with GD: inhomogeneous structure; ventrally mostly hypoechoic micronodular structure with short fibrous septa; longitudinal. (dd) Detail of RL with GD, CFDS: diffuse hypervascularity, *pattern III*—"thyroid inferno"; longitudinal. (ee) Detail of LL with GD: inhomogeneous structure; ventrally mostly hypoechoic micronodular structure with short fibrous septa; longitudinal. (ff) Detail of LL with GD, CFDS: diffuse hypervascularity, *pattern III*—"thyroid inferno"; longitudinal

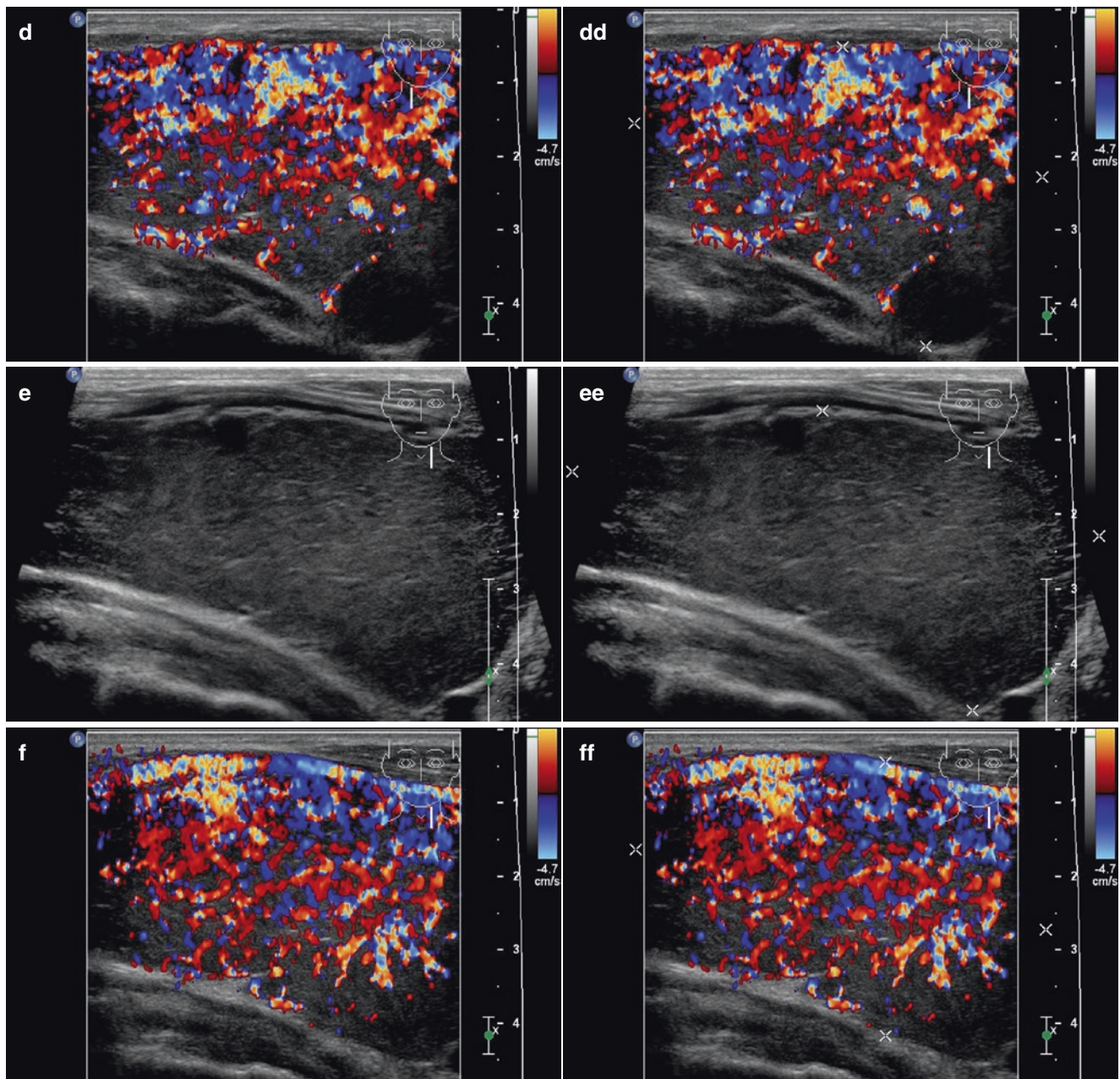


Fig.4.4 (continued)

- In 1983 French radiologist Espinasse described the diffused microechoic character of the thyroid parenchyma, as seen via US, as a nonspecific, although valuable, sign in the diagnosis of CLT and GD [8].
- In 1988 Ralls described that using CFSD in GD patients markedly increased color flow Doppler signal with diffuse homogeneous distribution, the so-called “*thyroid inferno*” (Fig. 4.1bb) [9]; this CFDS pattern is currently classified as *pattern III* (see more in Chap. 1) [10].
- Thyroid US hypoechogenicity is a characteristic of autoimmune thyroid diseases, with an overlap US pattern in patients affected by GD or HT. However, a diffusely increased thyroid blood flow is pathognomonic of untreated GD. CFDS may be useful in distinguishing patients with GD and HT [11].
- CFDS showed a sensitivity of $\approx 89\%$ and a specificity of $\approx 87\%$, a positive predictive value of $\approx 94\%$, a negative predictive value of $\approx 78\%$, and a diagnostic accuracy of $\approx 88\%$ in the differential diagnosis of thyrotoxicosis compared to thyroid scanning by ^{99m}Tc -pertechnetate [11].
- Caruso used CFDS parameter PSV of ITA with cut-off value of 65 cm/s to differentiate between GD and HT; in his study, patients with GD had PSV always over 150 cm/s (186 ± 38 cm/s) [12].
- Vitti et al. reported that about 70% of patients with GD exhibit a low thyroid echogenicity, which is significantly associated with a higher frequency of TSHR-Ab positivity and with the relapse of hyperthyroidism. During a 6-to-18-month follow-up period after methimazole treatment, 83% of patients had a relapse of hyperthyroidism. Recurrence of hyperthyroidism occurred in 93% of patients with thyroid hypoechogenicity and in 55% of those with normal thyroid echogenicity [13].

4.3 US Features of Thyroid Gland After Radioiodine ^{131}I -Therapy (RIT) [14]

- An ultrasound study by English et al. described the typical US features of the thyroid gland in 30 patients with GD after successful RIT. The mean volumes of the right lobe were 2.4 mL (0.6–14) and of the left lobe 1.8 mL (0.4–9.1), with a mean total volume (Tvol) of 4.2 mL (1.3–19.1). Of those who had a pre-treatment US (23%), the percentage reduction in volume was 87%. A substantial majority, 93%, of the glands were hypovascular, with the remaining 7% showing normal vascularity.
- US features of the post-RIT thyroid gland (Fig. 4.5aa):
 - a significantly reduced total thyroid volume (Tvol).
 - hypovascularity.
 - coarse echotexture.
 - hyperechogenicity.

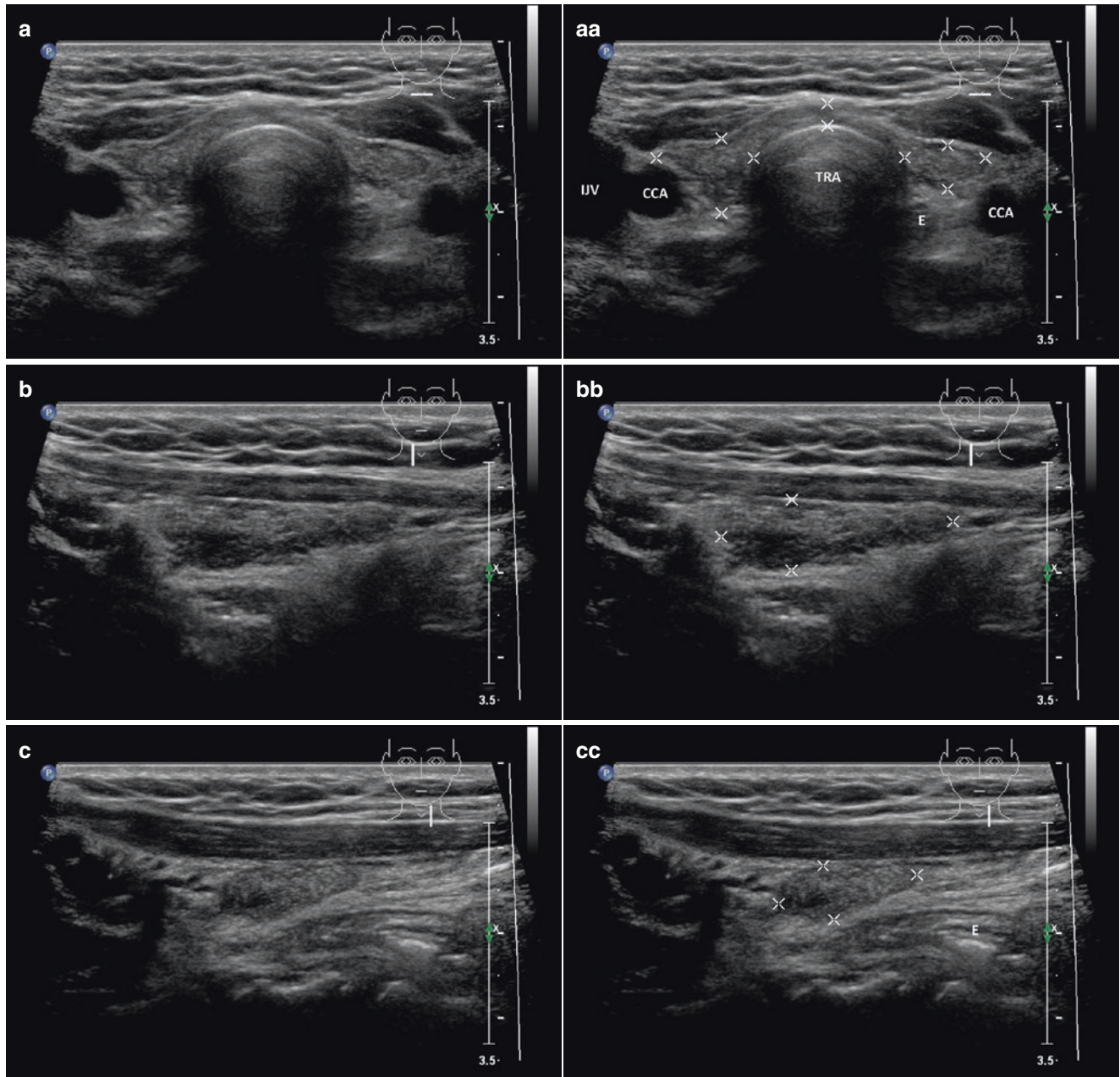


Fig. 4.5 (aa) A 51-year-old woman with Graves' disease (GD), initial volume 32 mL; actually shrunken thyroid gland 2 years post radioactive iodine therapy (RIT): coarse structure; hyperechoic; microlobulated margin; Tvol 5 mL, RL 3 mL, and LL 2 mL; transverse. (bb) Detail of

RL with GD post RIT: coarse structure; hyperechoic; microlobulated margin; longitudinal. (cc) Detail of LL with GD post RIT: coarse structure; hyperechoic; microlobulated margin

References

1. Colman E. Robert Graves and the origins of Irish medical journalism. *Ir J Med Sci*. 2000;169(1):10–1.
2. Duntas LH. A tribute to Carl Adolph von Basedow: to commemorate 150 years since his death. *Hormones (Athens)*. 2004;3(3):208–9.
3. Vanderpump MP. The epidemiology of thyroid disease. *Br Med Bull*. 2011;99:39–51.
4. Hong HS, Lee EH, Jeong SH, Park J, Lee H. Ultrasonography of various thyroid diseases in children and adolescents: a pictorial essay. *Korean J Radiol*. 2015;16(2):419–29.
5. Moon JH, Yi KH. The diagnosis and management of hyperthyroidism in Korea: consensus report of the Korean thyroid association. *Endocrinol Metab (Seoul)*. 2013;28(4):275–9.
6. Okosieme OE, Lazarus J. Hyperthyroidism in Pregnancy. In: De Groot LJ, Beck-Peccoz P, Chrousos G, Dungan K, Grossman A, Herselman JM, Koch C, et al, editors. *Endotext* [Internet]. South Dartmouth (MA): MDText.com, Inc.; 2015.
7. Sharma M, Aronow WS, Patel L, Gandhi K, Desai H. Hyperthyroidism. *Med Sci Monit*. 2011;17(4):RA85–91.
8. Espinasse P. Thyroid echography in chronic autoimmune lymphocytic thyroiditis. *J Radiol*. 1983;64(10):537–44.
9. Ralls PW, Mayekawa DS, Lee KP, Colletti PM, Radin DR, Boswell WD, et al. Color-flow Doppler sonography in Graves disease: “thyroid inferno”. *AJR Am J Roentgenol*. 1988;150(4):781–4.
10. Bogazzi F, Bartalena L, Brogioni S, Burelli A, Manetti L, Tanda ML, et al. Thyroid vascularity and blood flow are not dependent on serum thyroid hormone levels: studies in vivo by color flow doppler sonography. *Eur J Endocrinol*. 1999;140(5):452–6.
11. Donkol RH, Nada AM, Boughattas S. Role of color Doppler in differentiation of Graves’ disease and thyroiditis in thyrotoxicosis. *World J Radiol*. 2013;5(4):178–83.
12. Caruso G, Attard M, Caronia A, Lagalla R. Color Doppler measurement of blood flow in the inferior thyroid artery in patients with autoimmune thyroid diseases. *Eur J Radiol*. 2000;36(1):5–10.
13. Vitti P. Grey scale thyroid ultrasonography in the evaluation of patients with Graves’ disease. *Eur J Endocrinol*. 2000;142(1):22–4.
14. English C, Casey R, Bell M, Bergin D, Murphy J. The sonographic features of the thyroid gland after treatment with radioiodine therapy in patients with Graves’ disease. *Ultrasound Med Biol*. 2016;42(1):60–7.

5.1 Essential Facts

- In 1904 the Swiss surgeon Fritz de Quervain published a complete work about “*Subacute Nonsuppurative Thyroiditis*”. The disease would later be known as “*de Quervain's thyroiditis*” [1].
- The incidence of subacute granulomatous thyroiditis (SGT):
 - 12.1 per 100,000 per year.
 - higher in females (19.1 per 100,000 per year) than in males (4.4 per 100,000 per year).
 - highest in young adulthood (30–40 years), with 24 per 100,000 per year, and middle age (40–50 years), with 35 per 100,000 per year.
 - incidence declines with increasing age [2].
- SGT is most likely caused by a viral infection and is generally preceded by an upper respiratory tract infection.
- Clinical findings: SGT is indicated by painful swelling of the thyroid; at times, the pain begins and may be confined to the one lobe, but usually spreads rapidly to involve the rest of the gland (“creeping thyroiditis”). Pain may radiate to the jaw or the ears, and malaise, fatigue, myalgia, and arthralgia are common. A mild-to-moderate fever is expected, and at times a high fever of 40.0 °C may occur. A transient vocal cord paresis may occur. The disease process may reach its peak within 3–4 days and subside and disappear within a week, but more typically, onset extends over 1–2 weeks and continues with fluctuating intensity for 3–6 weeks. Thyrotoxicosis is present in 50% of patients in the acute phase [3, 4].
- Physical examination: The thyroid gland is typically enlarged, smooth, firm, and tender to palpation [4].
- Laboratory findings: There is a markedly elevated C-reactive protein (CRP), as well as an elevated erythrocyte sedimentation rate (a normal ESR essentially rules out the diagnosis). The leukocyte count is normal or slightly elevated, and levels of thyroid stimulating hormone (TSH) are low to undetectable. Thyroglobulin (TGB) is elevated (a normal level rules out the diagnosis), and the radioactive iodine uptake test (RAIU) is notably low [3, 4].
- Therapy: anti-inflammatory medications and corticosteroids; therapy may improve clinical findings often within 24 h [4].
- Course after therapy: Up to 20% of patients have the recurrence of SGT on discontinuation of prednisone. In 90% or more of patients, there is a complete recovery and a return to normal thyroid function. However up to 5–10% of the patients may become hypothyroid and require permanent replacement with levothyroxine [3, 4].

5.2 US Features of Subacute Granulomatous Thyroiditis [5]

- Unilateral thyroid involvement (Fig. 5.3aa) is more common than bilateral thyroid involvement (Figs. 5.1aa and 5.2aa).
- Thyroid gland is typically enlarged, unilateral (Fig. 5.3aa), or bilateral enlargement (Fig. 5.1aa), but can be normally sized (Fig. 5.2aa).
- In the affected lobe are focally ill-defined heterogeneously hypoechoic areas with an irregular or microlobulated margin (Fig. 5.2aa), without round or ovoid mass formation.
- No hypervascularity (case of thyrotoxicosis) on the CFDS, typically minimal vascularity—*pattern 0* (Fig. 5.1dd); normal (Fig. 5.1jj) or increased vascularity was seen in the recovery stage [6, 7].
- Focal lesion can mimic thyroid carcinoma (Fig. 5.3aa), but the presence of pain or tenderness should allow differentiation of SGT from these other typically nontender entities [7].
- Cytopathological examination for SGT reveals a severe inflammatory area, with non-caseating granulomas.
- Heterogeneity of the thyroid affected by SGT can mimic the changes of Hashimoto thyroiditis as well. The differences are clinical and biochemical [7].
- Characteristic findings of subacute thyroiditis on US in combination with the presence of neck pain can provide a more sensitive and specific diagnosis [7].
- Lesion reduces volume after corticosteroid therapy (Figs. 5.1ii and 5.2gg).
- US performed 3 months or more (Fig. 5.3jj) from the initial US examination shows complete resolution of the changes [7].
- On corticosteroid therapy, symptoms of SGT, the enlargement of thyroid gland, and laboratory signs of inflammation and thyrotoxicosis disappear quickly, in 2–6 weeks, but full normalization of thyroid gland structure during US follow up is slower, taking 2–6 months. SGT is mostly bilateral. Relapse (Fig. 5.3ff) after end of treatment is rare, but may be more severe than the first episode (personal observations).

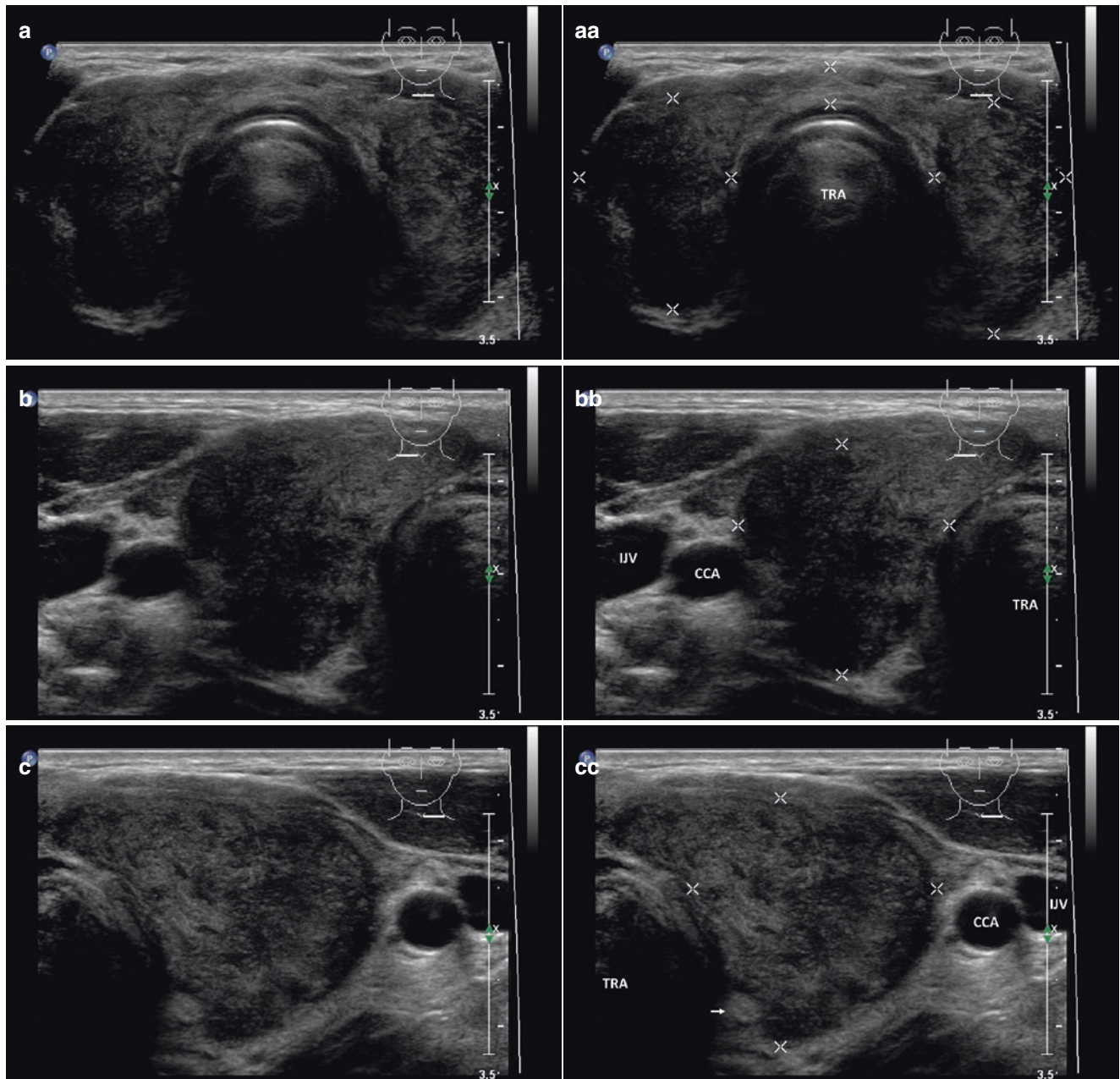


Fig. 5.1 (aa) A 41-year-old man with over 1 month of progressing painful, markedly enlarged, palpable thyroid gland, and currently with a few days of fever up to 39.0 °C. Patient was repeatedly treated unsuccessfully with antibiotics for a suspected pharyngitis. Laboratory tests suggested thyrotoxicosis, elevated ESR and CRP. Initial US scans of subacute granulomatous thyroiditis (SGT) prior to prednisone therapy: large goiter; coarse structure; mixed echogenicity with confluent ill-defined hypoechoic areas; without cervical lymphadenopathy; Tvol 42 mL, isthmus 6 mm, RL 18 mL, and LL 23 mL; transverse. (bb) Detail of the RL: coarse structure; mixed echogenicity with confluent ill-defined hypoechoic areas on the lateral side; transverse. (cc) Detail of the LL: coarse structure; diffusely small ill-defined hypoechoic areas; one small hyperechoic nodule (arrow); transverse. (dd) Overall view of thyroid gland, CFDS: minimal vascularity, *pattern 0*; transverse. (ee) Detail of the RL: coarse structure; mixed echogenicity; in the upper and middle parts, small ill-defined hypoechoic areas; in the lower part, dorsally large ill-defined hypoechoic area imitating nodule (arrowheads); longitudinal. (ff) Detail of the RL, CFDS: minimal vascularity, *pattern 0*; longitudinal. (gg) Detail of the LL: in the upper part inhomogeneous isoechoic structure; in the middle and lower parts

coarse structure, small ill-defined hypoechoic areas; two small hyperechoic nodules (arrows); longitudinal. (hh) Detail of the LL, CFDS: minimal vascularity, *pattern 0*; longitudinal. (ii) After 21-day prednisone therapy in descending dosage regimen, the thyroid was not palpable. Patient felt free of neck pain, without fever. Laboratory tests showed normalized ESR and CRP, but light hypothyroidism. There has been a substantial change in the US finding: size of the thyroid gland markedly decreased; slightly inhomogeneous structure; mostly isoechoic; sporadic patchy ill-defined hypoechoic areas in the RL on the lateral and dorsal sides, in the LL on the lateral side; Tvol 11 mL, RL 6 mL, and LL 5 mL; transverse. (jj) Overall view of thyroid gland, CFDS: minimal vascularity, *pattern 1*; transverse. (kk) Detail of the RL: in the upper part homogeneous isoechoic structure; in the middle and lower parts inhomogeneous structure, mixed echogenicity with small ill-defined hypoechoic areas; longitudinal. (ll) Detail of the RL, CFDS: minimal vascularity, *pattern 1*; longitudinal. (mm) Detail of the LL: mostly homogeneous structure, isoechoic; in the middle and lower parts ventrally an inhomogeneous structure, mixed echogenicity with small ill-defined hypoechoic areas; longitudinal. (nn) Detail of the LL, CFDS: minimal vascularity, *pattern 1*; longitudinal.

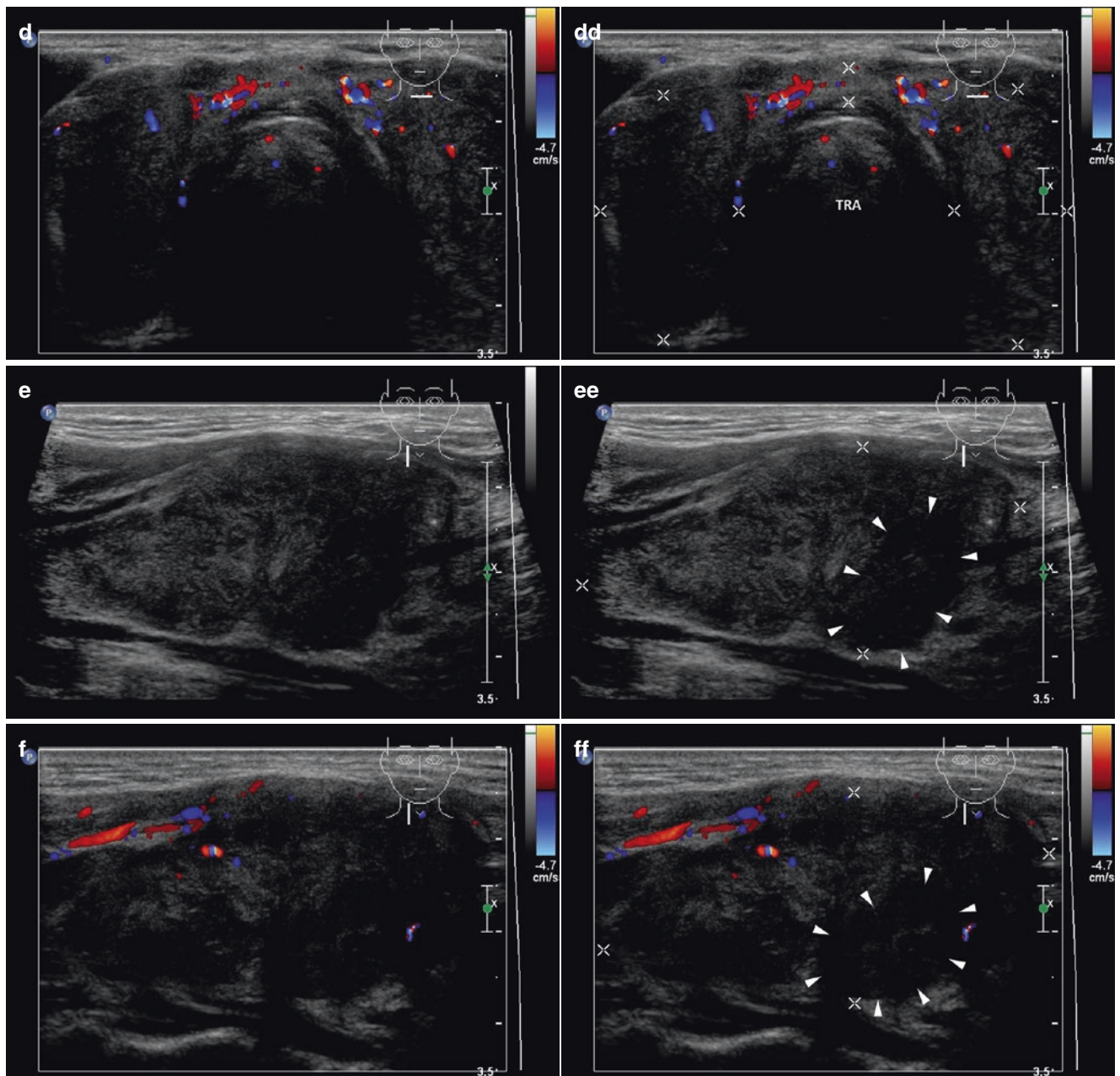
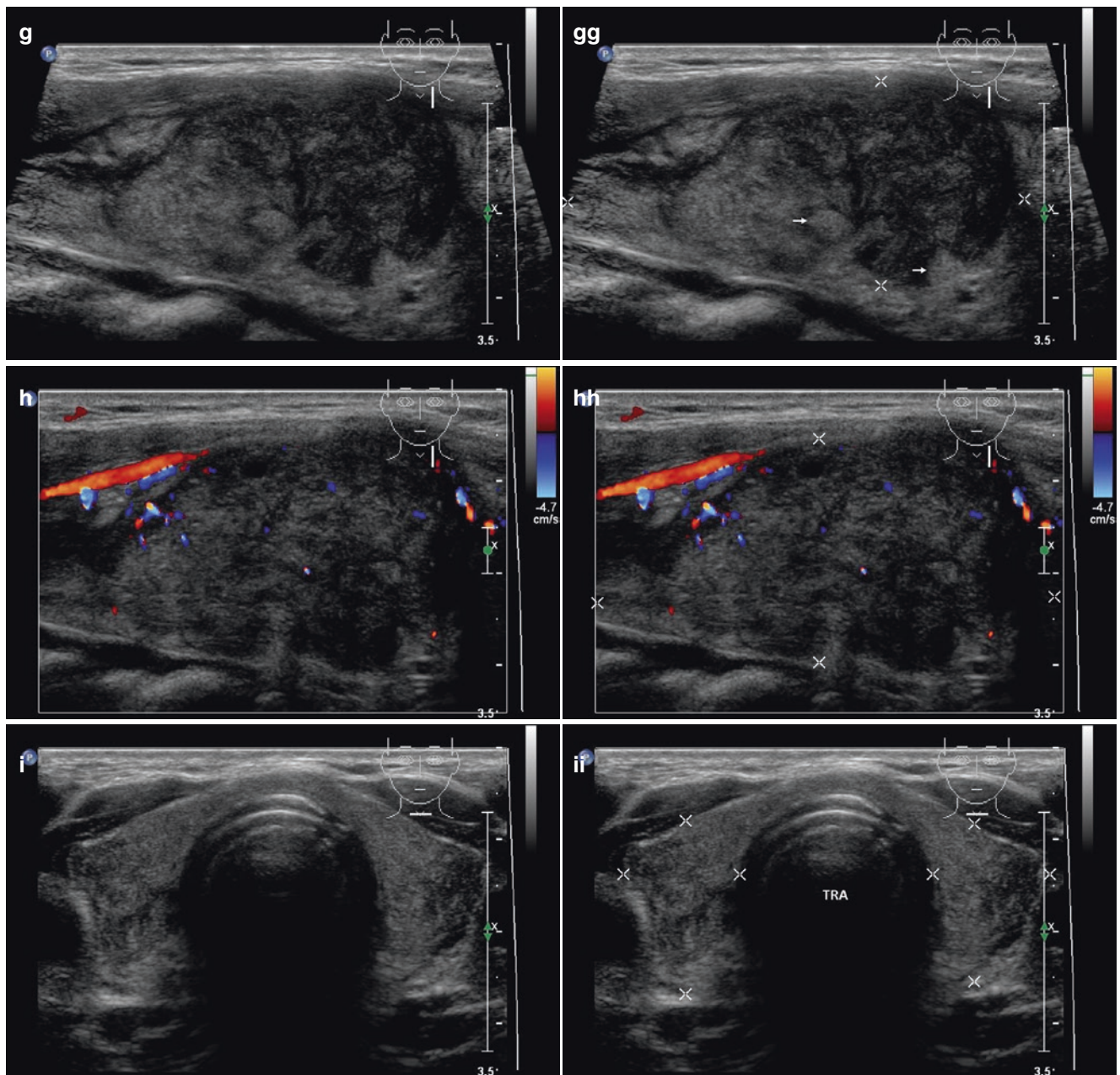


Fig. 5.1 (continued)

**Fig. 5.1** (continued)

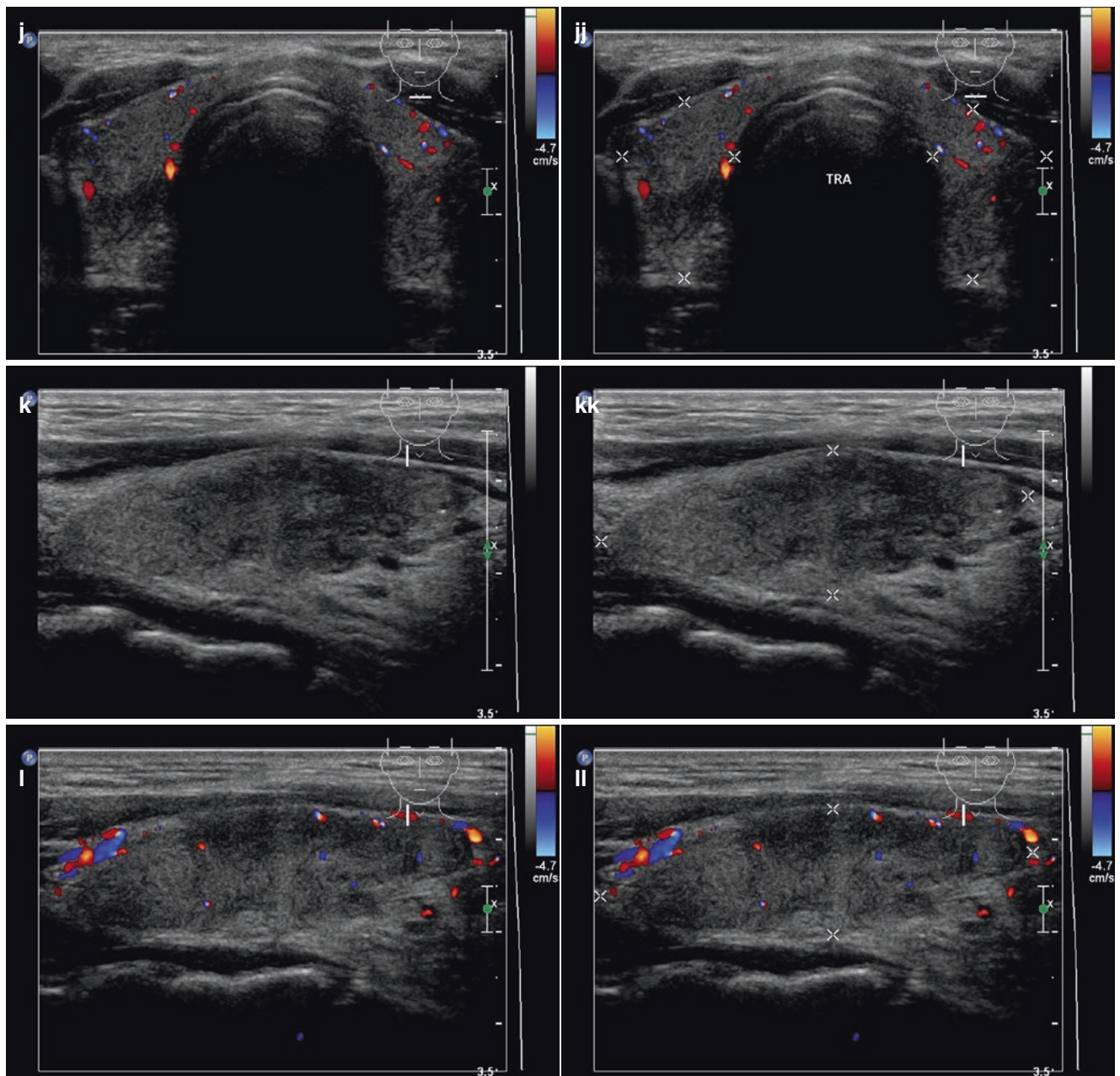


Fig. 5.1 (continued)

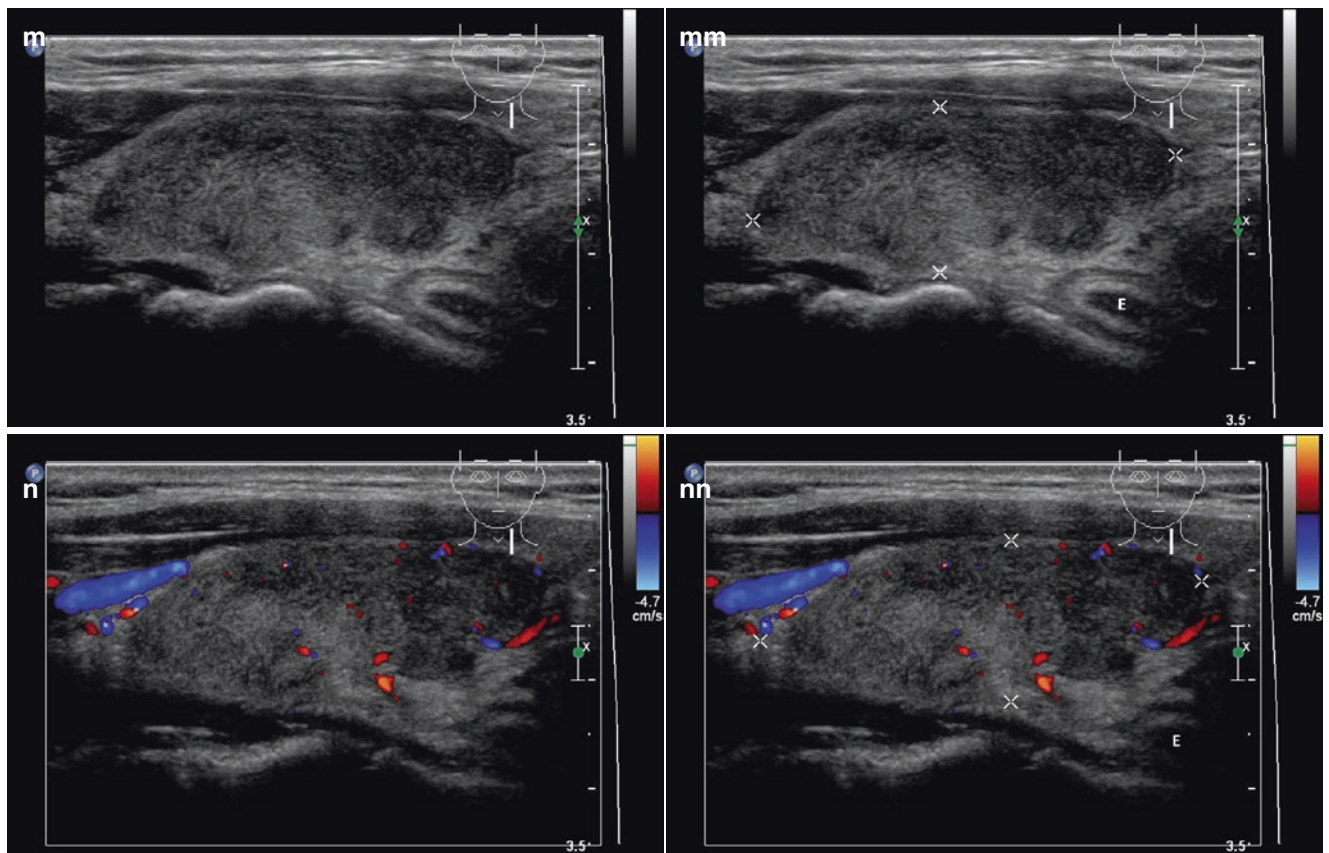


Fig. 5.1 (continued)

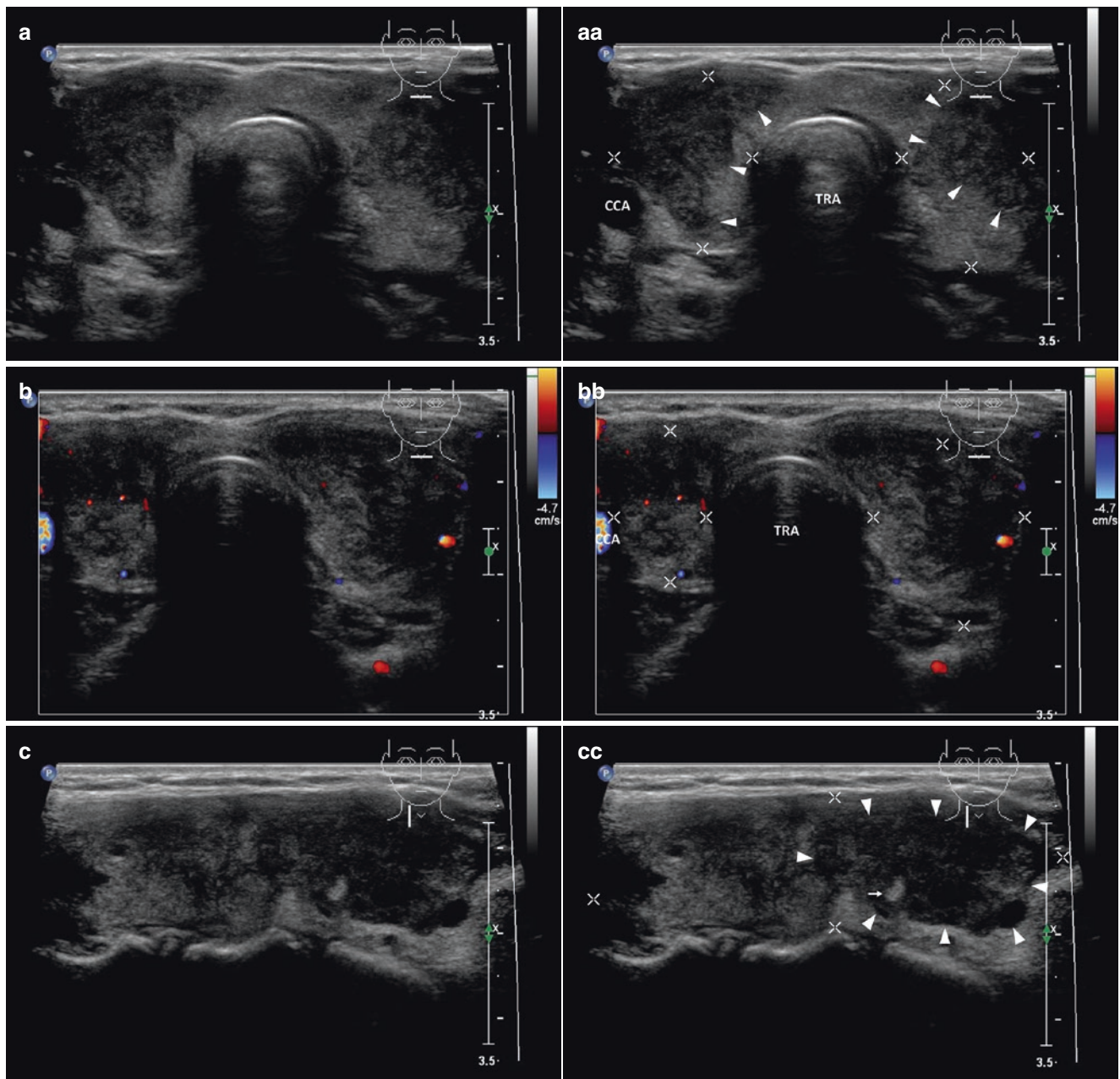


Fig. 5.2 (aa) A 35-year-old woman with a 1-month palpable, painful, slightly enlarged thyroid gland and low-grade fever was unsuccessfully treated with antibiotics for the antecedent upper respiratory tract infection. Laboratory tests suggested thyrotoxicosis and elevated ESR and CRP. Initial US scans of subacute granulomatous thyroiditis (SGT) prior to prednisone therapy: slightly enlarged goiter; normal structure preserved in paratracheal part of lobes and in the isthmus; most of the lobes have coarse structure; mixed echogenicity with confluent ill-defined hypoechoic areas; irregular border between normal and inflammatory tissue (*arrowheads*); no cervical lymphadenopathy; Tvol 20 mL, RL 9 mL, and LL 11 mL; transverse. (bb) Overall view of thyroid gland, CFDS: minimal vascularity, *pattern 0*; transverse. (cc) Detail of the RL: in the upper half inhomogeneous structure; mixed echogenicity; small ill-defined hypoechoic areas; in the lower half coarse structure; ill-defined hypoechoic lesion imitating large nodule (*arrowheads*); small hyperechoic nodule size 3 mm (*arrow*); longitudinal. (dd) Detail of the RL, CFDS: minimal vascularity, *pattern 1*; longitudinal. (ee) Detail of the LL: in the upper and middle parts mostly homogeneous structure, isoechoic; only ventrally inhomogeneous

structure; mixed echogenicity, small, hypoechoic, ill-defined areas; in the lower part coarse structure; confluent ill-defined hypoechoic area imitating nodule (*arrowheads*); longitudinal. (ff) Detail of the LL, CFDS: minimal vascularity, *pattern 0*; longitudinal. (gg) After 49-day prednisone therapy in descending dosage regimen, thyroid was not palpable. The patient felt free of neck pain, without fever. Laboratory tests showed normalized ESR, CRP and normal thyroid function. There has been a substantial change in the US finding: size of the thyroid gland decreased; mostly homogeneous structure; isoechoic; in the RL round ill-defined hypoechoic area (*arrowheads*) and small solid hyperechoic nodule (*arrow*); in the LL tiny ill-defined hypoechoic area; small complex nodule (*arrow*); Tvol 8 mL, RL 4 mL, and LL 4 mL; transverse. (hh) Detail of the RL: mostly homogeneous isoechoic structure; in the middle part ventrally is round inhomogeneous ill-defined hypoechoic area and dorsally small solid, hyperechoic nodule (*arrow*); longitudinal. (ii) Detail of the LL: mostly homogeneous isoechoic structure; in the middle part ventrally is round inhomogeneous ill-defined hypoechoic elongated area; longitudinal

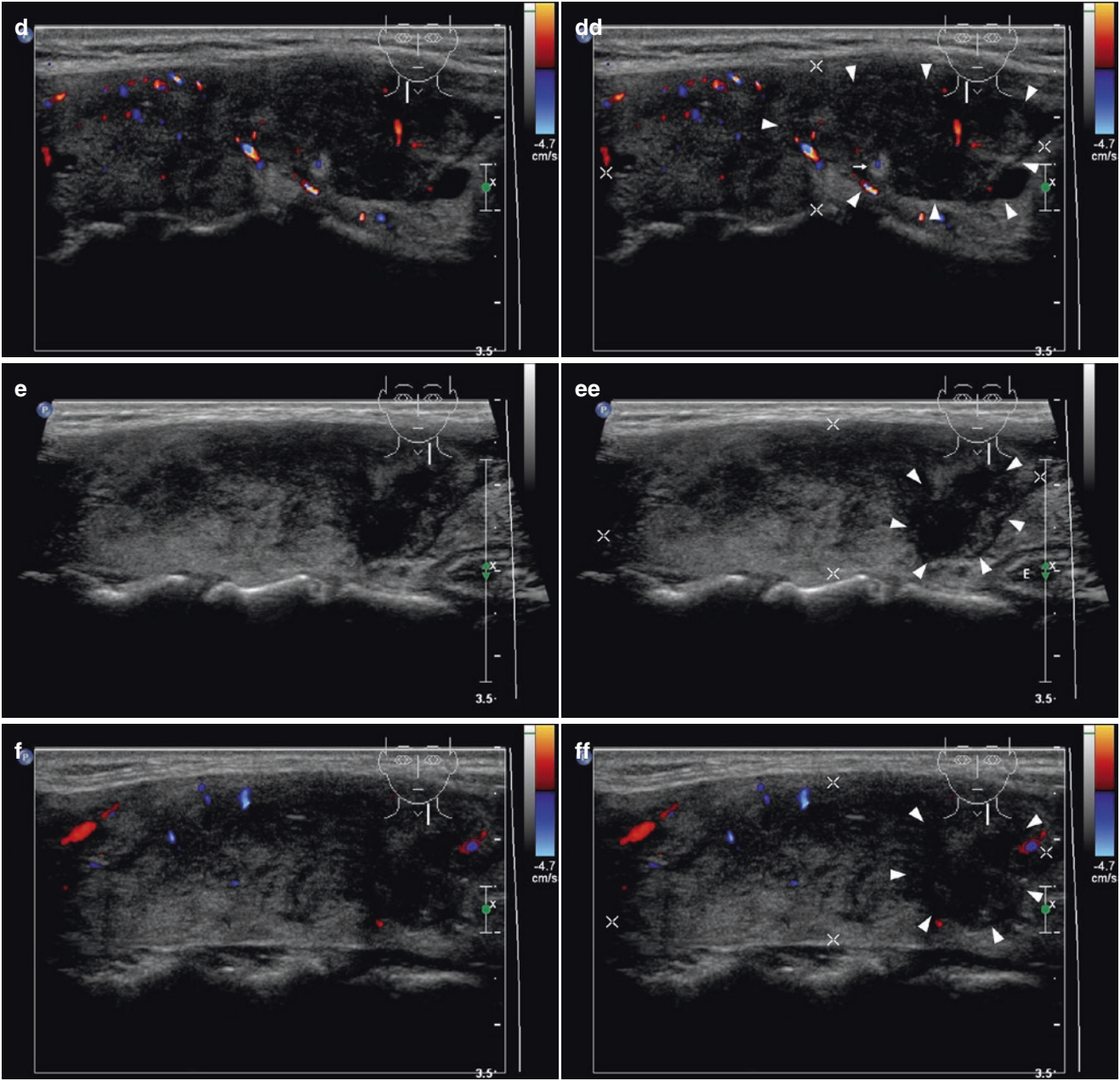


Fig. 5.2 (continued)

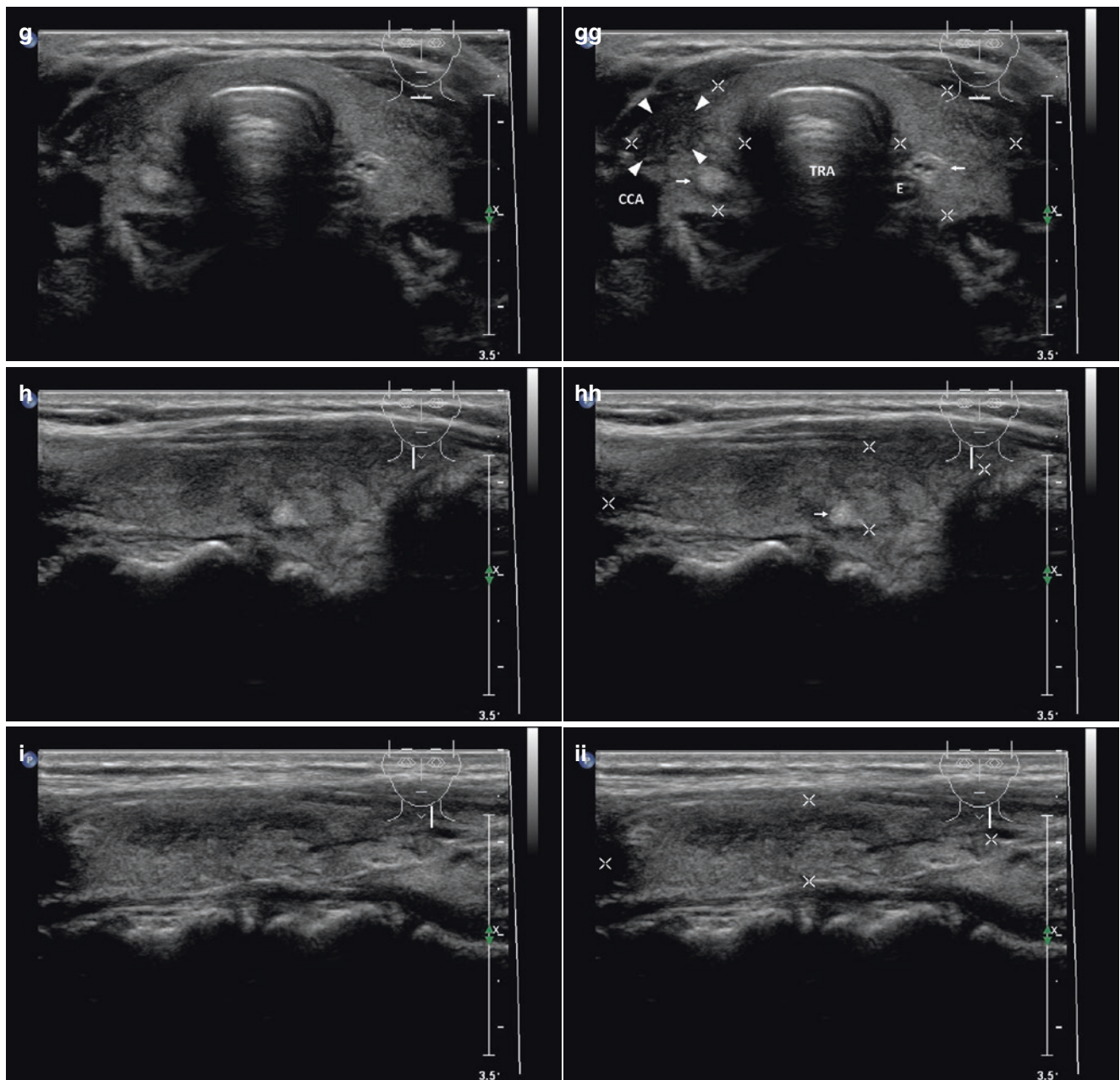


Fig. 5.2 (continued)

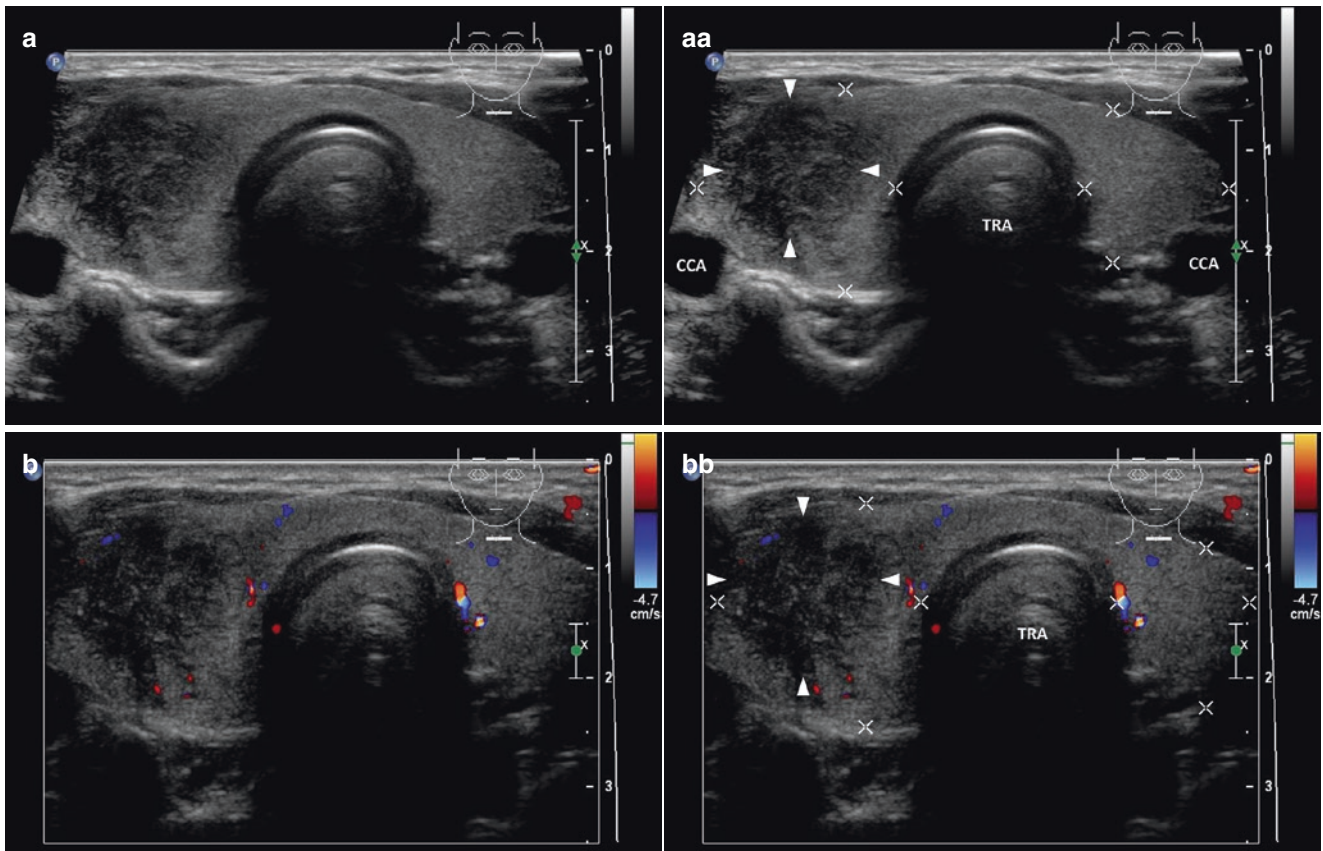


Fig. 5.3 (aa) A 34-year-old woman with 14 days history of painful palpable enlarged RL of the thyroid and with a low-grade fever. Patient was unsuccessfully treated with antibiotics for an acute upper respiratory tract infection. Laboratory tests suggested thyrotoxicosis and elevated ESR and CRP. Initial US scans of the focal subacute granulomatous thyroiditis (SGT) prior to prednisone therapy, slightly enlarged RL: mostly preserved normal structure and echogenicity; large coarse ill-defined hypoechoic lesion, size $27 \times 19 \times 16$ mm and volume 4 mL (arrowheads) in the low half ventrally; LL—normal isoechogenic structure; no cervical lymphadenopathy; Tvol 21 mL, RL 14 mL, and LL 7 mL; transverse. (bb) Overall view of thyroid gland, CFDS: avascular focal hypoechoic lesion and minimal vascularity in the unaffected isoechogenic thyroid gland, *pattern I* (arrowheads); transverse. (cc) Detail of the RL: large coarse ill-defined hypoechoic lesion in the low half ventrally, volume 4 mL (arrowheads); longitudinal. (dd) After 49-day prednisone therapy in descending dosage regimen, the RL was not palpable. The patient felt free of neck pain, without fever. Laboratory tests showed normalized ESR, CRP and normal thyroid function. There has been a substantial change in US finding, size of the RL was decreased: mostly homogeneous isoechoic structure; small homogeneous slightly hypoechoic lesion, size $12 \times 9 \times 5$ mm and volume 0.3 mL (arrowheads) in the low half ventrally; Tvol 14 mL, RL 7 mL, and LL 7 mL; transverse. (ee) Detail of the RL: small homogeneous slightly hypoechoic lesion, volume 0.3 mL (arrowheads) in the low half

ventrally; longitudinal. (ff) Three months after the end of prednisone treatment focal SGT relapsed and spread. Patient complained of symptoms worsening, furthermore pain extended to the whole area of the thyroid gland. US scans showed a new lesion in the RL, but in a different location than the primary focus, and a new attack in the entire LL: slightly enlarged RL—inhomogeneous ill-defined lesion in the upper part, size $22 \times 14 \times 13$ mm and volume 2.5 mL (arrowheads); normal hypoechoic structure and isoechogenicity of the rest of the RL; enlarged LL—inhomogeneous; coarse ill-defined hypoechoic mostly lateral part (arrowheads); no cervical lymphadenopathy; Tvol 23 mL, RL 9 mL, and LL 14 mL; transverse. (gg) Detail of the RL: inhomogeneous ill-defined hypoechoic lesion in the upper part, volume 2.5 mL (arrowheads); longitudinal. (hh) Detail of enlarged LL: coarse hypoechoic structure; small area of normal tissue in the upper part dorsally, borderline between normal and inflammatory tissue (arrowheads); longitudinal. (ii) Detail of the LL, CFDS: minimal vascularity, *pattern I*; longitudinal. (jj) Nine months from the onset of the disease, 4 months from the relapse and 1 month from completion of prednisone therapy in descending dosage regimen, patient was without subjective complaints and all laboratory tests were normal. Follow-up US scan of cured thyroid gland: size decreased; normal structure and echogenicity; no focal changes; Tvol 13 mL, RL 7 mL, and LL 6 mL; transverse. (kk) Detail of the RL: normal structure and echogenicity; longitudinal. (ll) Detail of the LL: normal structure and echogenicity; longitudinal

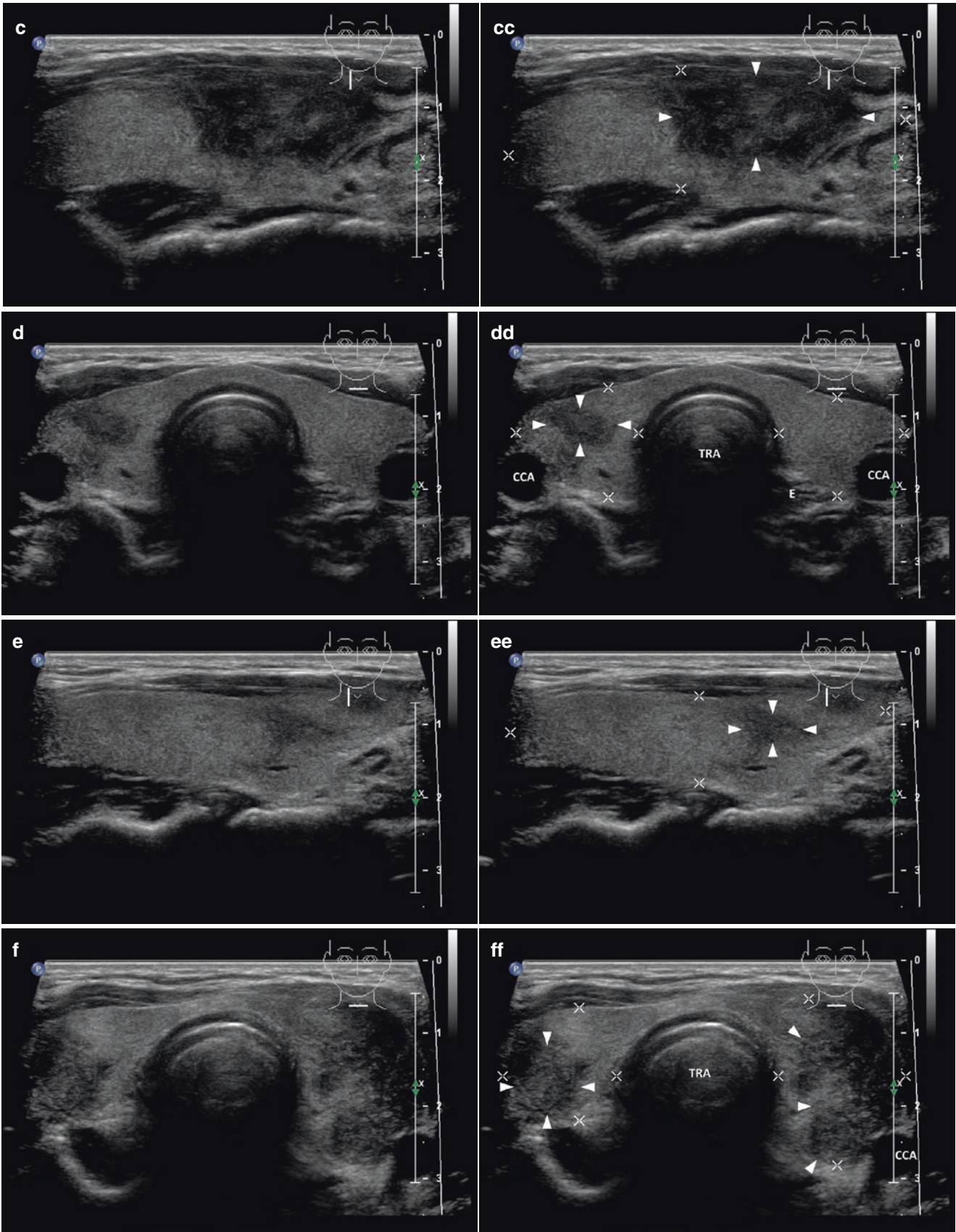
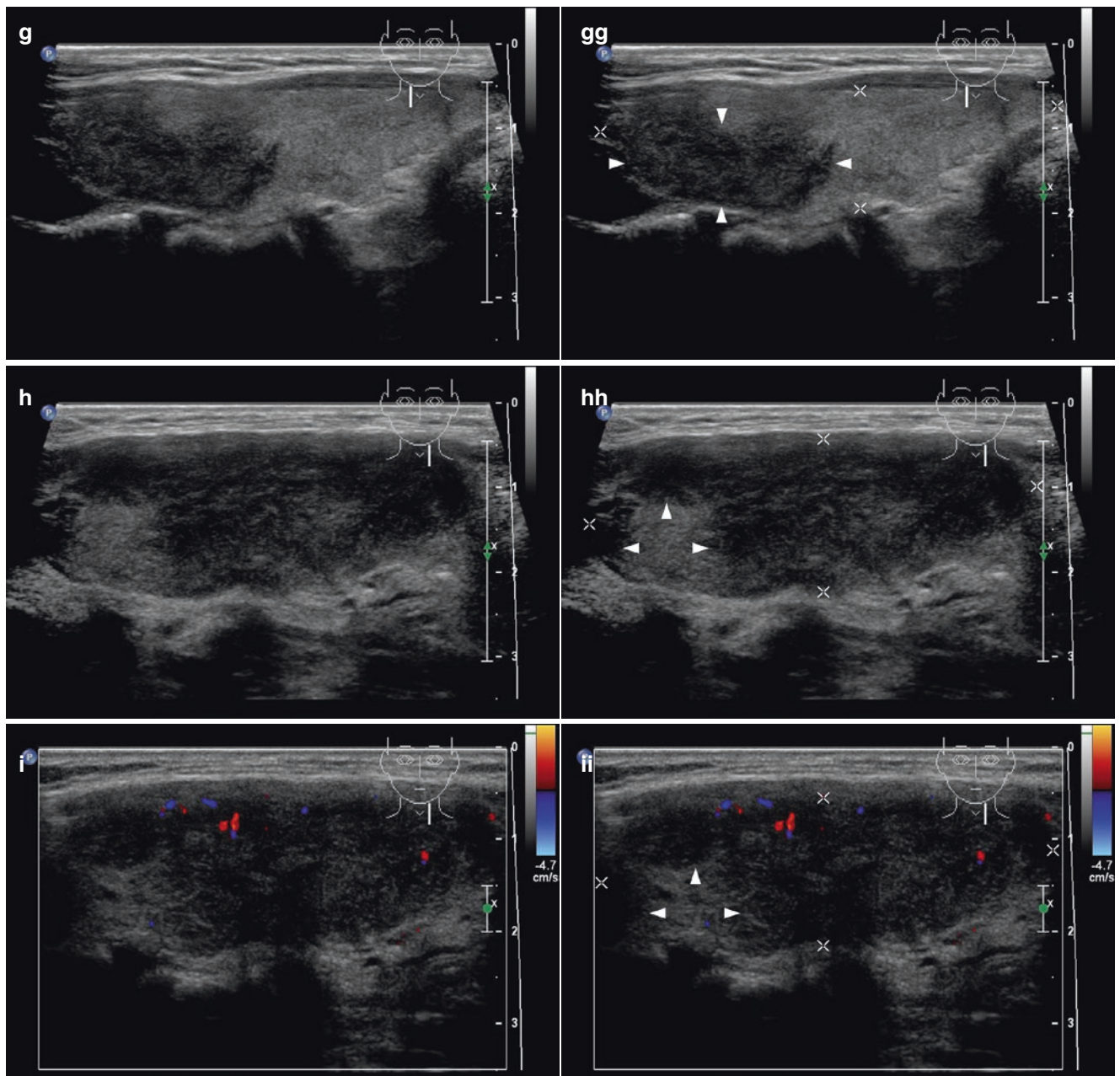


Fig. 5.3 (continued)

**Fig. 5.3** (continued)

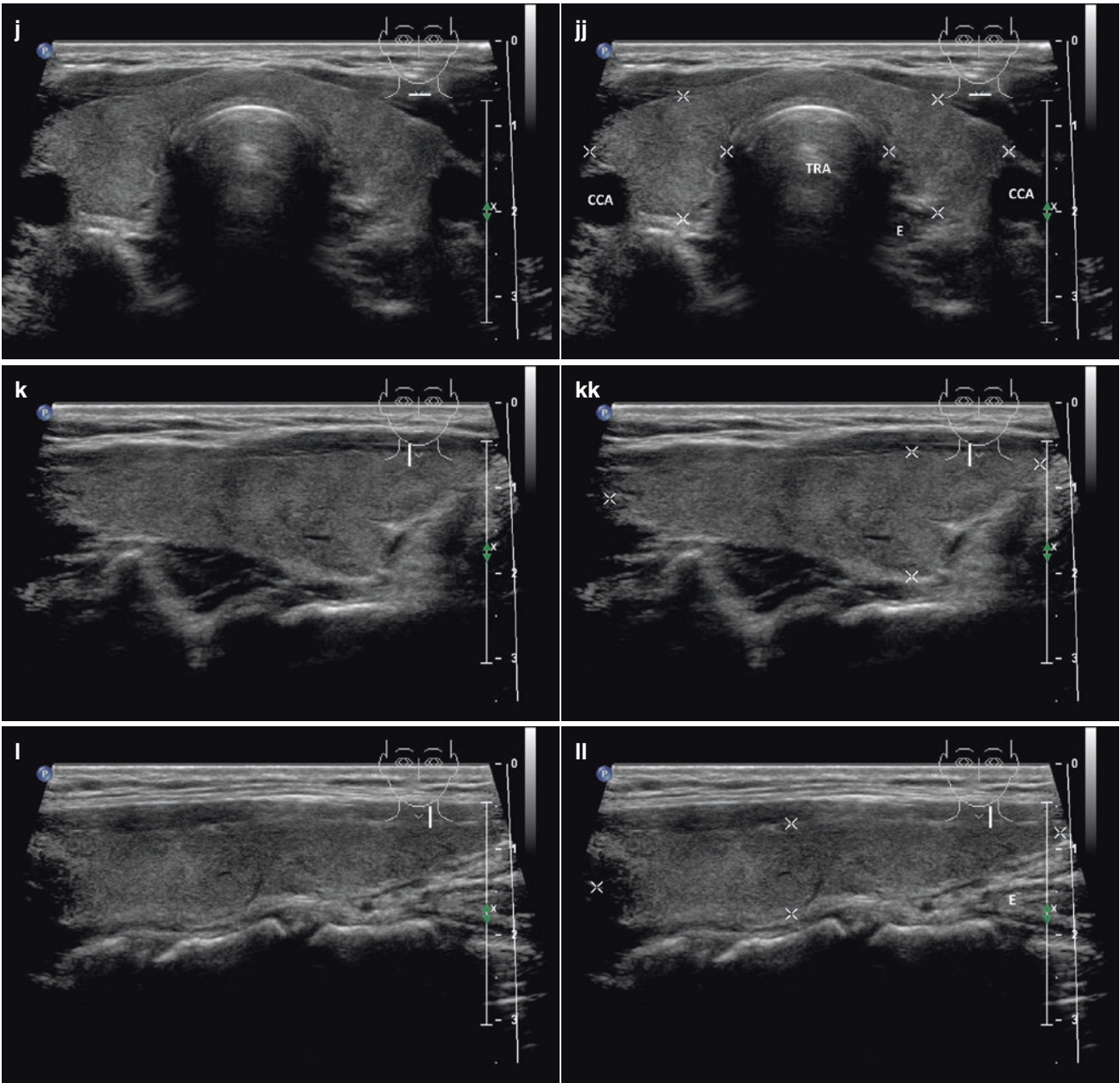


Fig. 5.3 (continued)

References

1. Fritz_de_quervain_md_18681940_stenosing_tendovaginitis at the radial styloid process. Copyright Churchill Livingstone Inc., Medical publisher 2004. Available at: healthorbit.com.
2. Golden SH, Robinson KA, Saldanha I, Anton B, Ladenson PW. Clinical review: prevalence and incidence of endocrine and metabolic disorders in the United States: a comprehensive review. *J Clin Endocrinol Metab*. 2009;94(6):1853–78.
3. Slatosky J, Shipton B, Wahba H. Thyroiditis: differential diagnosis and management. *Am Fam Physician*. 2000;61(4):1047. –52, 1054
4. Hennessey JV. Subacute thyroiditis. In: De Groot LJ, Beck-Peccoz P, Chrousos G, Dungan K, Grossman A, Hershman JM, Koch C, et al, editors. *Source Endotext* [Internet]. South Dartmouth, MA: MDText.com, Inc.; 2015.
5. Park SY, Kim EK, Kim MJ, Kim BM, Oh KK, Hong SW, et al. Ultrasonographic characteristics of subacute granulomatous thyroiditis. *Korean J Radiol*. 2006;7(4):229–34.
6. Zacharia TT, Perumpallichira JJ, Sindhvani V, Chavhan G. Grayscale and color Doppler sonographic findings in a case of subacute granulomatous thyroiditis mimicking thyroid carcinoma. *J Clin Ultrasound*. 2002;30(7):442–4.
7. Frates MC, Marqusee E, Benson CB, Alexander EK. Subacute granulomatous (de Quervain) thyroiditis: grayscale and color Doppler sonographic characteristics. *J Ultrasound Med*. 2013;32(3):505–11.

6.1 Essential Facts

- Amiodarone-induced thyrotoxicosis (AIT) develops in 3% of amiodarone-treated patients in North America. For those living in iodine-depleted areas, the incidence is higher (10%) and the risk also increases with increased dosage.
- Amiodarone is a widely used class III antiarrhythmic drug used in the treatment of recurrent severe ventricular arrhythmias, paroxysmal atrial tachycardia, atrial fibrillation, and maintenance of sinus rhythm after atrial fibrillation cardioversion.
- Thyrotoxicosis is mediated by amiodarone's iodine content. Each 200 mg tablet contains 75 mg of iodine, and approximately 10% of this iodine is released as free iodide daily. Amiodarone accumulates in adipose tissue, cardiac and skeletal muscle, and the thyroid. With long-term treatment, there is a 40-fold increase in plasma and urinary iodide levels, and of elimination half-life of 50 to 100 days [1].
- Amiodarone-induced thyrotoxicosis (AIT) is classified as type 1 or type 2 [1, 2]:
 - AIT type 1 occurs in patients with underlying thyroid pathology such as autonomous nodular goiter or Graves' disease (GD) or Hashimoto's thyroiditis (HT), in which iodine potentiates thyroid hormone synthesis and release.
 - AIT type 2 is a result of amiodarone causing a subacute destructive thyroiditis with release of preformed thyroid hormones into the circulation.
- Occurrence of AIT is usually unpredictable, often sudden, and explosive, occurring either early or long after initiation of amiodarone treatment, mostly after 3 years of treatment. The median time of onset AIT type 1 is 3.5 months, and of AIT type 2, 30 months. It may also develop months after drug withdrawal [2].
- The prevalence of the two main forms has changed over the last 30 years with a current predominance of the AIT type 2 [2].
- Diagnosis of AIT is based on clinical findings (signs and symptoms of thyrotoxicosis) and laboratory results, thyroid radioiodine uptake (RAIU) and US scan [2–4]:
 - Diagnostic criteria AIT type 1 (Fig. 6.1aa): patients with GD, HT, solitary (≥ 1 cm), or multinodular goiter with corresponding laboratory and US findings, including an enhancement of vascularity at CFDS. AIT type 1 responds to combined thionamides and potassium perchlorate therapy.
 - Diagnostic criteria AIT type 2 (Fig. 6.2aa): US criteria—normal or slightly increased thyroid volume without nodules (≥ 1 cm), at CFDS absent hypervascularity. Laboratory criteria—absence of circulating thyroid-directed autoantibodies [anti-thyroglobulin (Tg-Ab), anti-thyroid peroxidase (TPO-Ab), anti-TSH receptor (TSHR-Ab) and RAIU—low/undetectable thyroid radioiodine uptake ($< 5\%$ at 24h). AIT type 2 is responsive to glucocorticoids.
 - Mixed form: A small subset of AIT type 1 patients may have a concomitant destructive process accountable for a longer onset time. This form requires a combination of the two therapeutic regimens.
- Concentration of fT4 and normalized thyroid volume are the main and independent determinants in AIT type 1. Baseline serum fT4 concentration greater than 50 pg/mL and normalized thyroid volume greater than 12 mL/m² is related to a shorter thyrotoxicosis onset time, severity of clinical symptoms, and prolonged response to glucocorticoids [5].

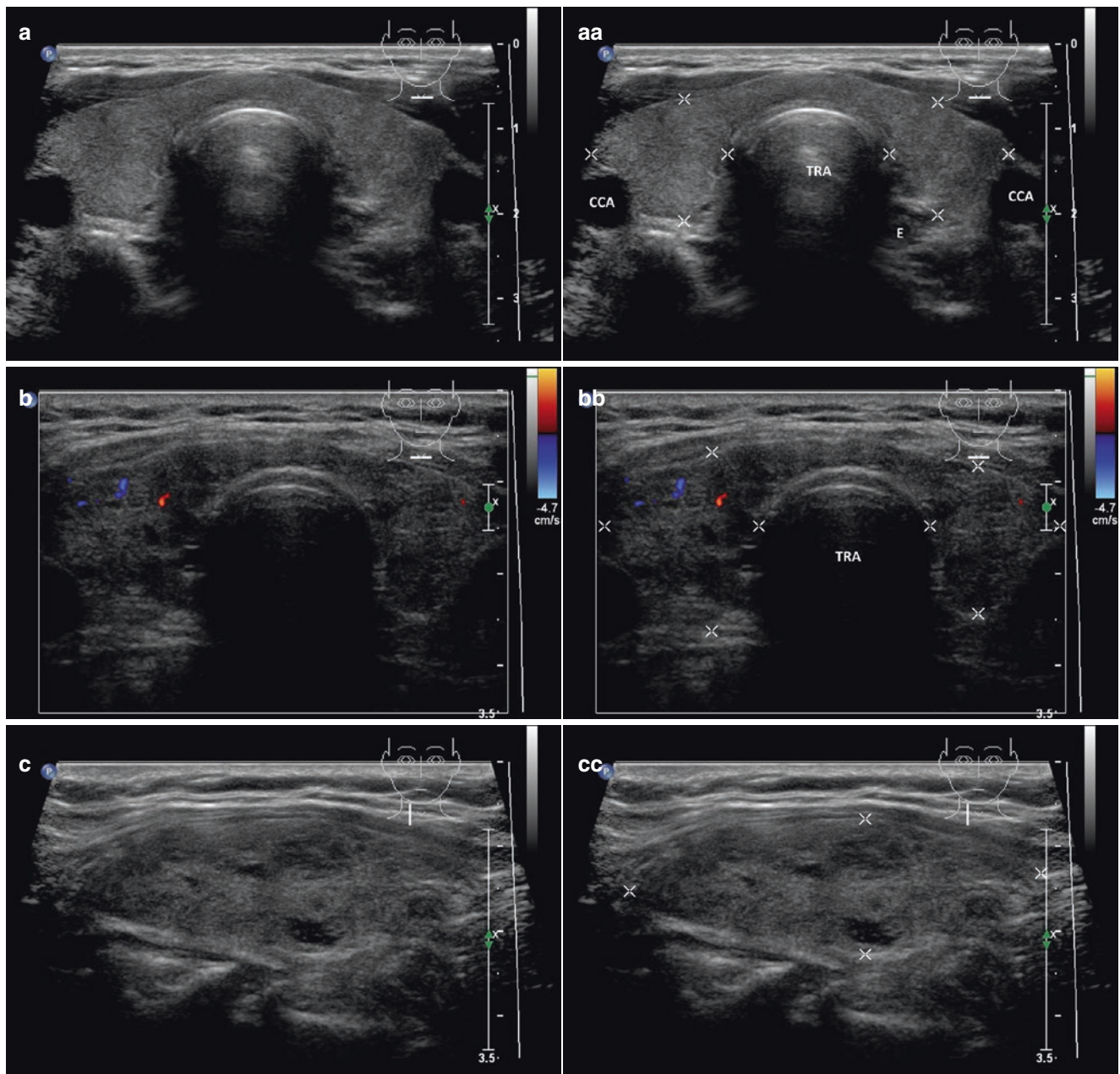


Fig. 6.1 (aa) A 68-year-old woman with amiodarone-induced thyrotoxicosis (AIT) type 1, with underlying Hashimoto's thyroiditis (HT). Laboratory: TSH 0.004 mIU/L (normal: 0.35–4.94), fT₄ 47.9 pmol/L (normal: 9.1–19.1), TPO-Ab 331 kU/L (normal: <4.1), Tg-Ab 54 kIU/L (normal: <4.1). US overall view: small goiter; inhomogeneous structure; mixed echogenicity; diffusely hypoechoic micronodules; Tvol 20 mL, RL 11 mL, and LL 9 mL; transverse. (bb) Overall view of AIT type 1, CFDS: minimal peripheral and parenchymal vascularity, *pattern I* (increased vascularity is more common; AIT mixed form is possible);

transverse. (cc) Detail of RL with AIT type 1: inhomogeneous structure; mixed echogenicity; diffuse hypoechoic micronodules; longitudinal. (dd) Detail of RL with AIT type 1, CFDS: minimal peripheral and parenchymal vascularity, *pattern I*; longitudinal. (ee) Detail of LL with AIT type 1: inhomogeneous structure; mixed echogenicity; diffuse hypoechoic micronodules; longitudinal. (ff) Detail of LL with AIT type 1, CFDS: minimal peripheral and parenchymal vascularity, *pattern I*; longitudinal

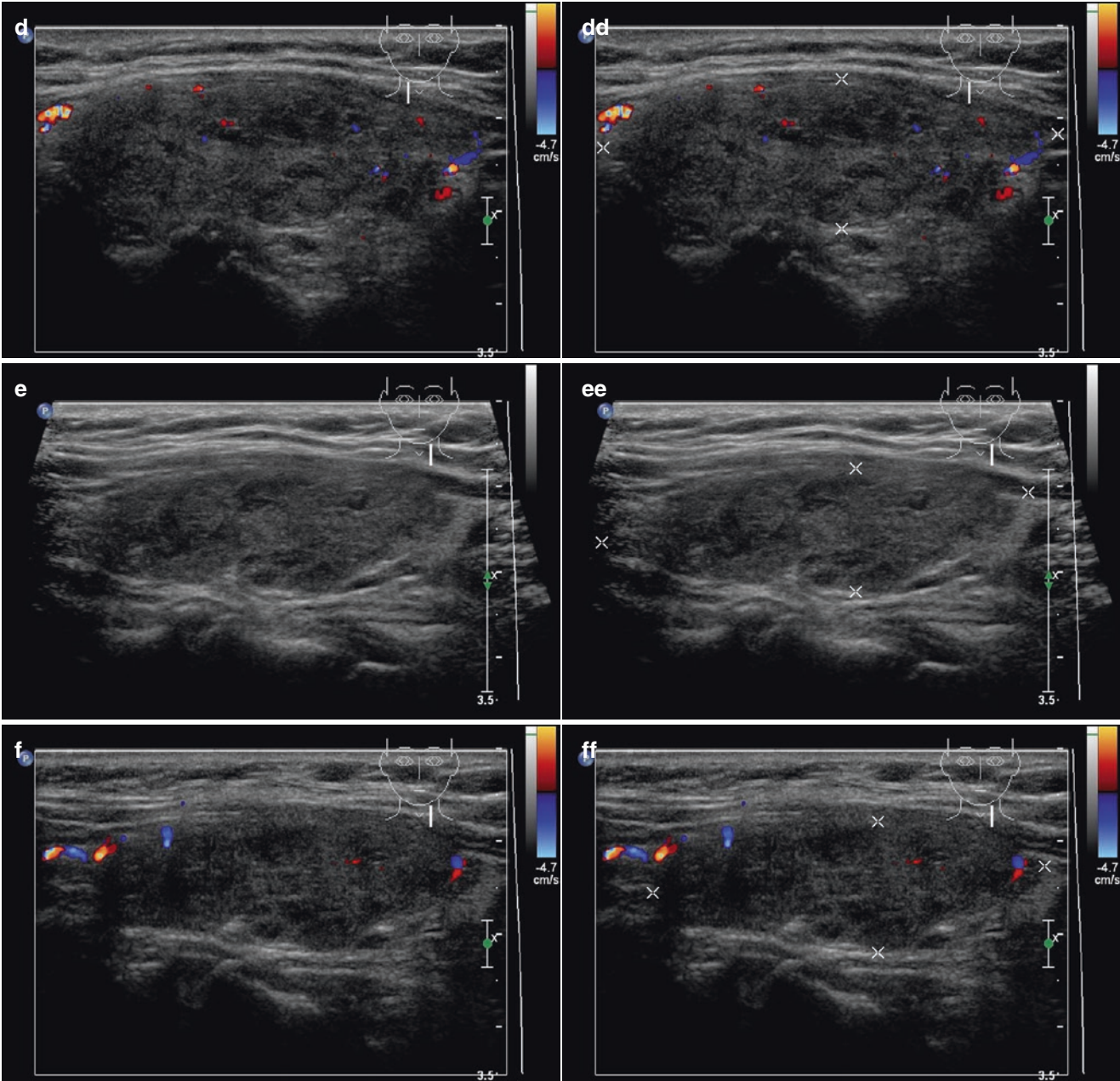


Fig. 6.1 (continued)

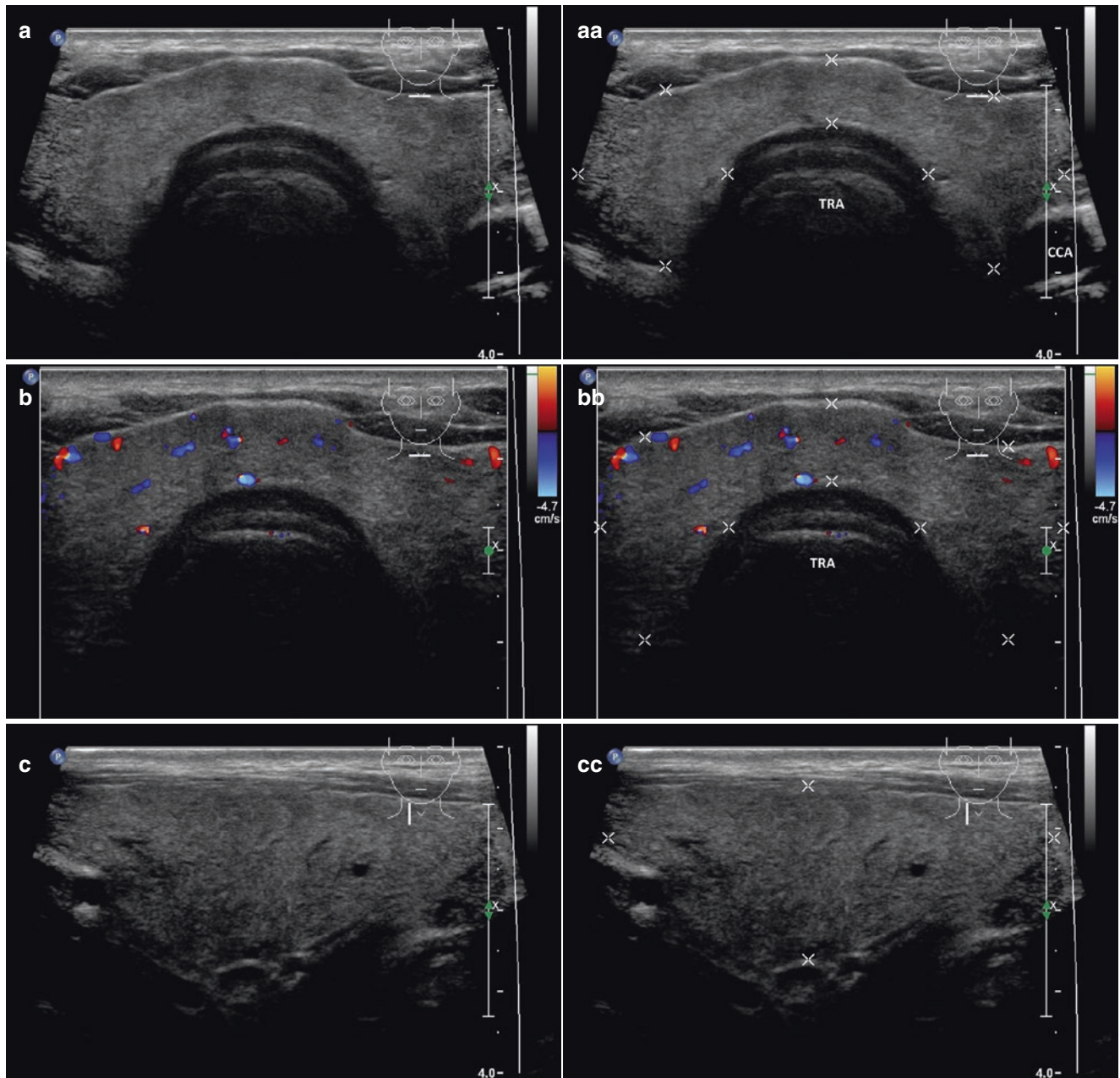
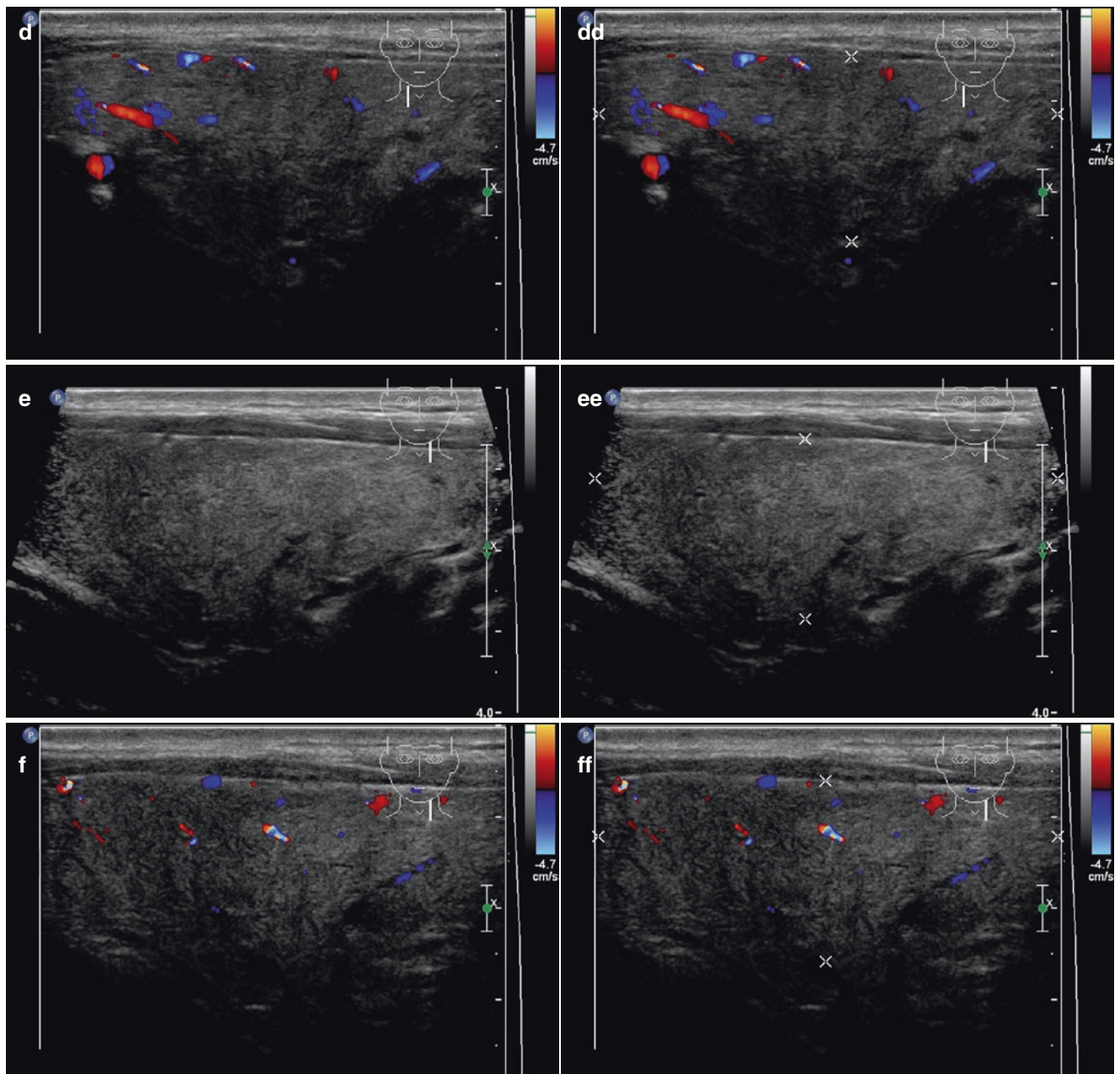


Fig. 6.2 (aa) A 62-year-old man with amiodarone-induced thyrotoxicosis (AIT) type 2. Laboratory: TSH 0.004 mIU/L (normal: 0.35–4.94 mIU/L), fT4 36.7 pmol/L (normal: 9.1–19.1) and normal TPO-Ab, Tg-Ab. US overall view: diffuse goiter without nodules (*the normal volume of the thyroid gland is more common*); homogeneous structure; isoechoic; Tvol 39 mL, RL 19 mL, isthmus 9 mm, and LL 19 mL; transverse. (bb) Overall view of AIT type 2, CFDS: sporadic peripheral and parenchymal vascularity, *pattern I* (*avascular pattern 0 is more com-*

mon); transverse. (cc) Detail of RL with AIT type 2: homogeneous structure; isoechoic; tiny cyst in lower part (*arrow*); longitudinal. (dd) Detail of RL with AIT type 2, CFDS: sporadic peripheral and parenchymal vascularity, *pattern I*; longitudinal. (ee) Detail of LL with AIT type 2: homogeneous structure; isoechoic; longitudinal. (ff) Detail of LL with AIT type 2, CFDS: sporadic peripheral and parenchymal vascularity, *pattern I*; longitudinal

**Fig. 6.2** (continued)

6.2 US Findings of Amiodarone-Induced Thyrotoxicosis [1, 3]

- AIT type 1 (Fig. 6.1aa) shows enlarged thyroid gland with US finding of the underlying thyroid disease.
- CFDS is the main US tool to differentiate and classify AIT. Up to 80% can be classified as AIT type 1 or AIT type 2 [6]:
 - For AIT type 2 (Fig. 6.2bb) is typical *pattern 0*—absent vascularity (due to gland destruction); *see more in Chap. 1*.
 - AIT type 1 (Fig. 6.1bb) may present *pattern I*—uneven patchy parenchymal flow, *pattern II*—diffuse, homogeneous distribution of increased flow, or *pattern III*—markedly increased signal and diffuse homogeneous distribution; *see more in Chap. 1*.

References

1. Tsang W, Houlden RL. Amiodarone-induced thyrotoxicosis: a review. *Can J Cardiol*. 2009;25(7):421–4. Review
2. Tomisti L, Rossi G, Bartalena L, Martino E, Bogazzi F. The onset time of amiodarone-induced thyrotoxicosis (AIT) depends on AIT type. *Eur J Endocrinol*. 2014;171(3):363–8.
3. Bogazzi F, Martino E, Dell'Unto E, Brogioni S, Cosci C, Aghini-Lombardi F, et al. Thyroid color flow doppler sonography and radioiodine uptake in 55 consecutive patients with amiodarone-induced thyrotoxicosis. *J Endocrinol Investig*. 2003;26(7):635–40.
4. Uchida T, Kasai T, Takagi A, Sekita G, Komiya K, Takeno K, et al. Prevalence of amiodarone-induced thyrotoxicosis and associated risk factors in Japanese patients. *Int J Endocrinol*. 2014;2014:534904.
5. Bogazzi F, Bartalena L, Tomisti L, Rossi G, Tanda ML, Dell'Unto E, Aghini-Lombardi F, et al. Glucocorticoid response in amiodarone-induced thyrotoxicosis resulting from destructive thyroiditis is predicted by thyroid volume and serum free thyroid hormone concentrations. *J Clin Endocrinol Metab*. 2007;92(2):556–62.
6. Eaton SE, Euinton HA, Newman CM, Weetman AP, Bennet WM. Clinical experience of amiodarone-induced thyrotoxicosis over a 3-year period: role of colour-flow Doppler sonography. *Clin Endocrinol*. 2002;56(1):33–8.

Nodular Goiter: Benign Lesions

1.1 Thyroid Nodules

1.1.1 Essential Facts

- Thyroid nodules are especially more common in elderly females, patients with iodine deficiency, and patients with a history of neck irradiation [1].
- According to the data from Framingham Heart Study published in 1968, in persons over 60 years of age palpable nodules occurred in 6.4% of women and 1.5% of men [2].
- According to the most recent 2015 ATA Guidelines, current prevalence of palpable thyroid nodules is approximately 5% in women and 1% in men living in iodine-sufficient parts of the world [3].
- High-resolution ultrasound (US) can detect thyroid nodules in 19–68% of randomly selected individuals, with higher frequencies in women and the elderly [3].

1.1.2 US Characteristics of Nodules According to the Korean Society of Thyroid Radiology [1]

1.1.2.1 Nodule Size

- Size of thyroid nodules should be measured in all three dimensions, or only the maximal diameter of the nodule can be measured. It is advisable to locate the calipers at the outer margin of the nodule halo [4].
- About 90% of benign nodules have demonstrated an increase in volume by 15% over a 5-year follow-up period. Cystic

nodules showed slower growth than solid nodules.

- According to the ATA guidelines, a reasonable definition of a growth is a 20% increase in the nodule diameter with a minimum increase in two or more dimensions of at least 2 mm, which is roughly a 50% increase in volume [3].
- The Korean Society of Thyroid Radiology recommends the definition of a nodule growth as a 20% increase in the nodule diameter or a 50% increase in the nodule volume.
- The size of a thyroid nodule is not helpful for distinguishing malignant nodule from benign nodule.

1.1.2.2 Nodule Shape

- Ovoid-to-round (when the anteroposterior diameter of a nodule is equal to or less than its transverse diameter on a transverse or longitudinal plane)
- “*Taller-than-wide*” (when the anteroposterior diameter of a nodule is longer than its transverse diameter on a transverse or longitudinal plane); a typical US feature of malignancy
- Irregular (when a nodule is neither ovoid-to-round nor taller-than-wide)

1.1.2.3 Internal Content

- Solid nodule ($\leq 10\%$ of the cystic portion)
- Predominantly solid nodule ($>10\%$ of the cystic portion and $\leq 50\%$ of the cystic portion)
- Predominantly cystic nodule ($>50\%$ of the cystic portion and $\leq 90\%$ of the cystic portion)

- Cystic nodule (>90% of the cystic portion)
- Spongiform nodule (the aggregation of multiple microcystic components in more than 50% of the volume of the nodule) [5]

1.1.2.4 Echogenicity

- Marked hypoechoic (when a nodule is hypoechoic relative to the adjacent strap muscle); a typical US feature of malignancy
- Hypoechogenicity (when a nodule is hypoechoic relative to the thyroid parenchyma) is a typical US feature of malignancy. However, up to 55% benign nodules are hypoechoic; smaller nodules ≤ 1 cm are more likely to be hypoechoic than the larger ones [3].
- Isoechoic (when a nodule has the same echogenicity as that of the thyroid parenchyma)
- Hyperechoic (when a nodule is echogenic relative to the thyroid parenchyma)

1.1.2.5 Nodule Margin

- Smooth
- Spiculated/microlobulated; a typical US feature of malignancy
- Ill-defined

1.1.2.6 Halo Sign

- The halo is a hypoechoic rim surrounding a nodule (caused by fibrous connective tissue, compressed thyroid tissue, and chronic inflammatory changes).
- Nodules show an accompanying hypoechoic thin or thick halo.
- Although a complete halo is a finding suggestive of a benign nodule (a specificity of 95%), more than a half of benign nodules lack a halo.

1.1.2.7 Calcifications

- Microcalcifications (when there are tiny, punctuate echogenic foci of 1 mm or less either with or

without posterior shadowing); represent typical US feature of malignancy

- Macrocalcifications (when punctuate echogenic foci are larger than 1 mm in size)
- Rim calcifications (when a nodule has peripheral curvilinear or “eggshell” calcification)

1.1.2.8 Vascularity

- Perinodular flow is mainly a characteristic finding for benign nodules (however, it is observed in 22% of malignant nodules).

References

1. Moon WJ, Baek JH, Jung SL, Kim DW, Kim EK, Kim JY, et al., Korean Society of Thyroid Radiology (KSThR), Korean Society of Radiology. Ultrasonography and the ultrasound-based management of thyroid nodules: consensus statement and recommendations. *Korean J Radiol.* 2011;12(1):1–14.
2. Vander JB, Gaston EA, Dawber TR. The significance of nontoxic thyroid nodules. Final report of a 15-year study of the incidence of thyroid malignancy. *Ann Intern Med.* 1968;69(3):537–40.
3. Haugen BR, Alexander EK, Bible KC, Doherty GM, Mandel SJ, Nikiforov YE, et al. 2015 American Thyroid Association Management Guidelines for Adult Patients with Thyroid Nodules and Differentiated Thyroid Cancer: The American Thyroid Association Guidelines Task Force on Thyroid Nodules and Differentiated Thyroid Cancer. *Thyroid.* 2016;26(1):1–133.
4. Frates MC, Benson CB, Charboneau JW, Cibas ES, Clark OH, Coleman BG, et al., Society of Radiologists in Ultrasound. Management of thyroid nodules detected at US: Society of Radiologists in Ultrasound consensus conference statement. *Radiology.* 2005;237(3):794–800.
5. Moon WJ, Jung SL, Lee JH, Na DG, Baek JH, Lee YH, et al., Thyroid Study Group, Korean Society of Neuro- and Head and Neck Radiology. Benign and malignant thyroid nodules: US differentiation – multicenter retrospective study. *Radiology.* 2008;247(3):762–70.

7.1 Essential Facts

- At sonography, 15–25% of solitary thyroid nodules are found to be cystic or predominantly cystic [1, 2].
- Based on the ratio of the liquid portion in nodule, nodules are classified as: mixed predominantly cystic nodule (liquid portion >50% but ≤90% of the nodule volume) or cystic nodule (liquid portion >90% of the nodule volume) [3].
- As thyroid cysts are considered nodules with a liquid component of more than 60% volume; this strict definition is used especially for percutaneous ethanol injection therapy (PEIT) studies; *see more in Chap. 23* [4, 5].
- Thyroid cysts are divided into pure cysts - without internal septa (Fig. 7.1aa) or complex/polyconcamerated cysts - with one or more internal septa (Figs. 7.6aa and 7.8aa) [6].
- In pure cysts the fluid content is colloid only, occasionally with the condensed colloid proteins, while in complex cysts the fluid component may also be the result of degeneration or hemorrhage [6].
- Pure cystic lesions are always thought to be benign; on the contrary, in complex cysts the solid component may represent a 3% risk of malignancy [7].
- Primary thyroid cysts, although rare (<2% of thyroid lesions), are highly likely to be benign [8].

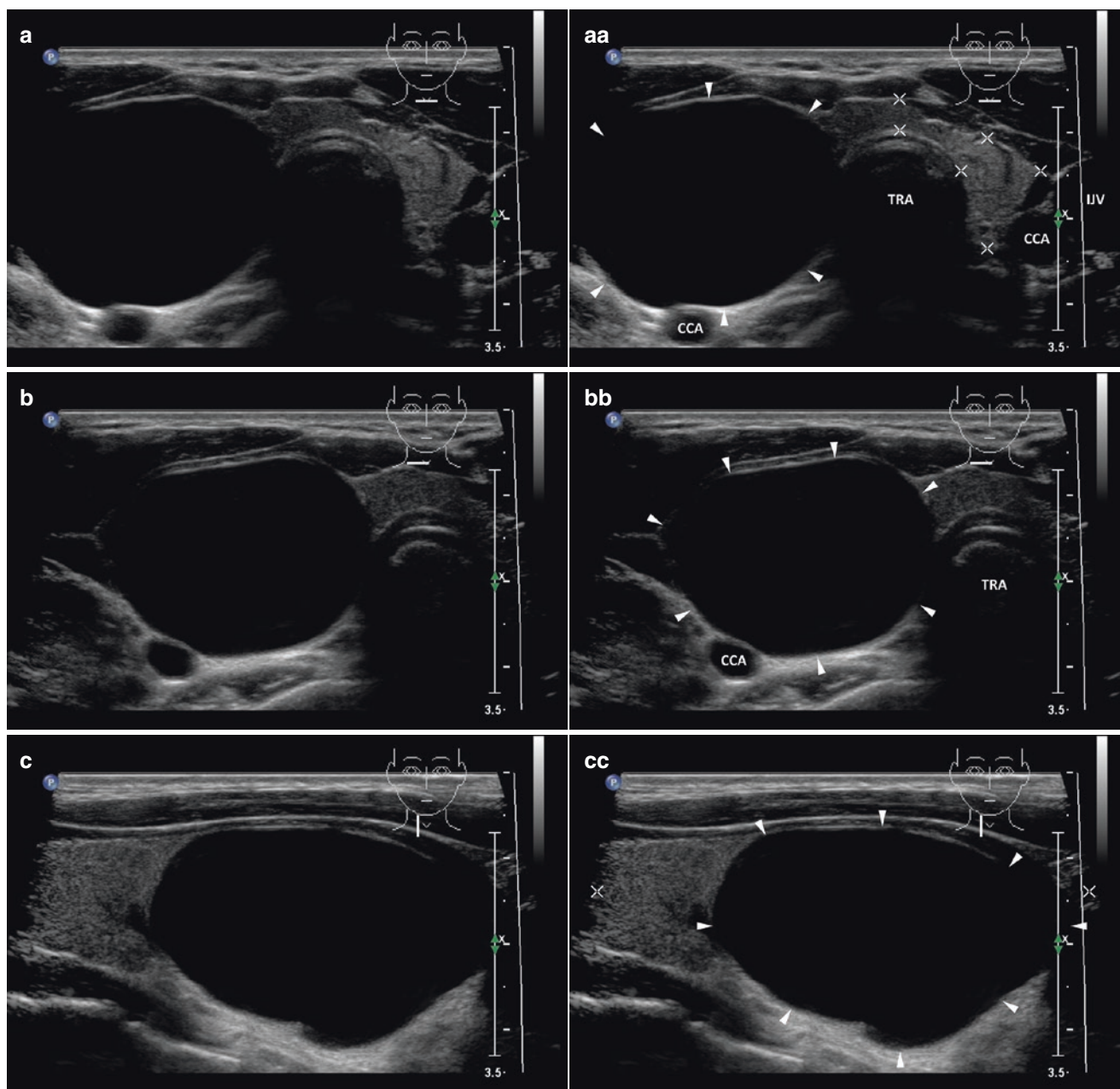


Fig. 7.1 (aa) A 43-year-old woman with a solitary large pure cyst (arrowheads), size $42 \times 31 \times 26$ mm and volume 17 mL in the RL. US overall view: round shape; homogeneously anechoic contents; smooth wall; Tvol 28 mL, asymmetry—RL 24 mL and LL 4 mL; transverse.

(bb) Detail of large pure cyst (arrowheads): ovoid shape; anechoic contents; smooth wall; posterior acoustic enhancement; transverse. (cc) Detail of large pure cyst (arrowheads): ovoid shape; anechoic contents; smooth wall; posterior acoustic enhancement; longitudinal

7.2 US Features of Thyroid Cysts [6]

- Pure cysts (Figs. 7.1aa and 7.2aa):
 - Smooth wall, possibly with focal small solid hyperechoic component (Fig. 7.2aa).
 - Fluid usually appears homogeneously anechoic.
 - Posterior acoustic enhancement (Fig. 7.1cc).
 - Bright hyperechoic reverberation artifacts so-called “comet tails” could be found in the fluid content (condensed colloid proteins).
 - A single “comet tail” artifact within a small cyst is usually called “cat’s eye artifact” (Fig. 7.3bb, cc).
- Complex cysts (Figs. 7.4aa and 7.8aa):
 - Smooth or focally roughened wall (Fig. 7.7aa).
 - Cavity is mostly irregular and separated with thin (Fig. 7.4aa), or thick septa (Figs. 7.5aa and 7.6aa).
- Fluid may be homogeneously anechoic or contain multiple “comet tails” (Fig. 7.9aa, dd).
- Posterior acoustic enhancement (Figs. 7.4aa and 7.10cc).
- If the fluid is the result of hemorrhage, it may change echogenicity over time as the hematoma resolves, appearing isoechoic or hypoechoic and anechoic. Absence of blood flow by CFDS is helpful to distinguish isoechoic liquid from solid hyperechoic part of the cyst wall.
- Hyperechoic debris (Fig. 7.10bb) is often found in liquid content; if there is doubt as to whether the internal content is debris or solid wall thickening, CFDS is helpful to demonstrate absence of blood flow in debris.
- If on US are found suspicious features in the solid part FNAB is required.

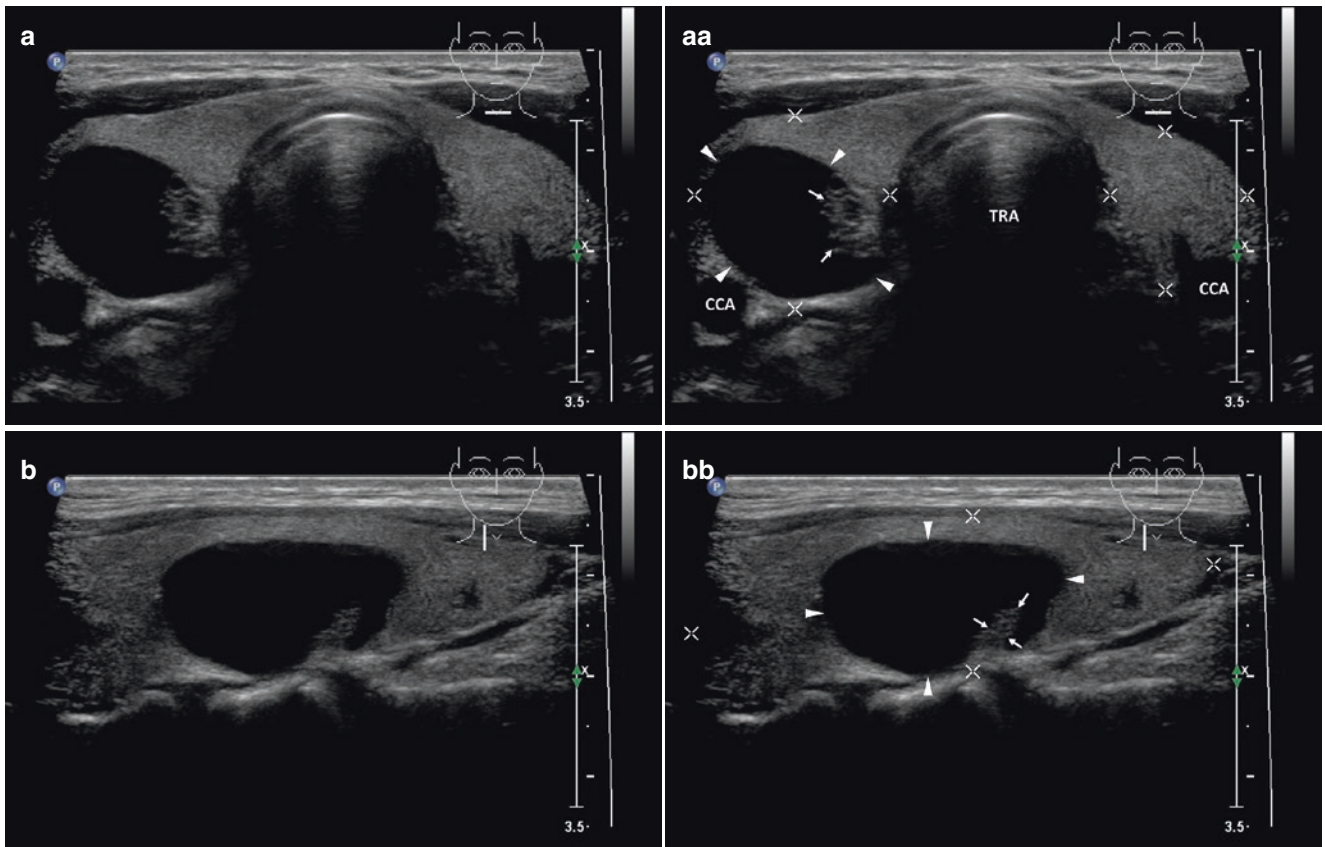


Fig. 7.2 (aa) A 38-year-old woman with a solitary small pure cyst (arrowheads), size $25 \times 20 \times 14$ mm and volume 3.5 mL in the RL: ovoid shape; homogeneously anechoic contents; smooth wall with focal solid hyperechoic component (arrows); Tvol 19 mL, RL 12 mL, and LL

7 mL; transverse. (bb) Detail of small pure cyst (arrowheads): ovoid shape; anechoic contents; smooth wall with focal solid hyperechoic component (arrows) as a polyp extending from the wall; longitudinal

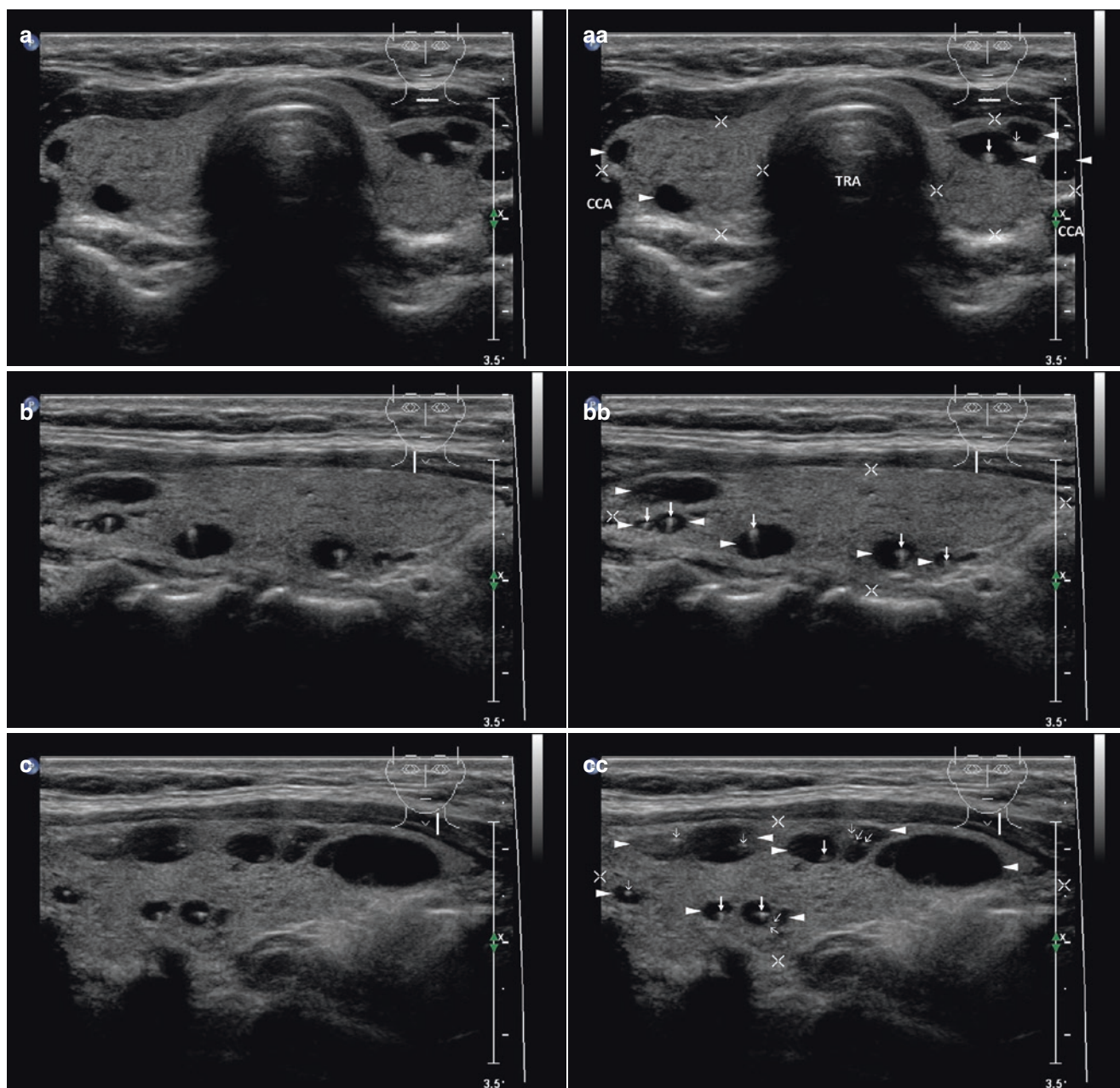


Fig. 7.3 (aa) A 44-year-old woman with multiple tiny cysts (*arrowheads*) sized from 4 to 7 mm bilaterally: round or oval shape; anechoic contents with single comet tails (colloid clot)—“*cat’s eye artifacts*” (*arrows*); Tvol 12 mL, RL 6 mL, and LL 6 mL; transverse. (bb) Detail of the RL with multiple tiny cyst (*arrowheads*): “*cat’s eye artifacts*”

(*arrows*); sporadic tiny colloid clot without tails (*open arrows*); longitudinal. (cc) Detail of the LL with multiple tiny cyst (*arrowheads*): “*cat’s eye artifacts*” (*arrows*); sporadic tiny colloid clot without tails (*open arrows*); longitudinal

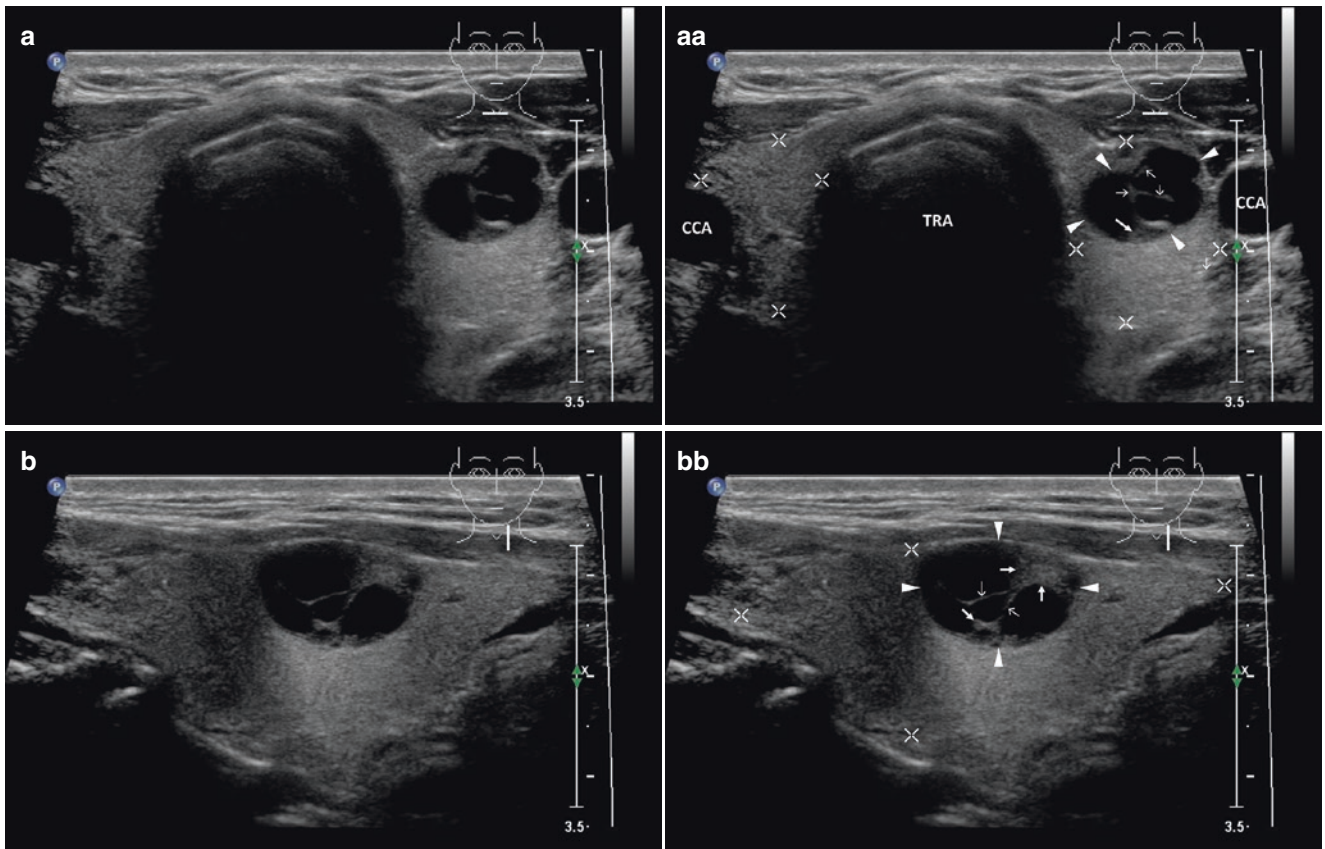


Fig. 7.4 (aa) A 58-year-old man with a small complex septated cyst (arrowheads), size $16 \times 13 \times 10$ mm and volume 1 mL in the LL: ovoid shape; anechoic contents; smooth wall with two focal solid hyperechoic component (arrows) and two thin septa (open arrows); posterior acoustic enhancement; Tvol 19 mL, RL 9 mL and LL 10 mL; transverse. (bb)

Detail of small complex septated cyst (arrowheads): anechoic contents; smooth wall with two focal solid hyperechoic component (arrows) and two thin septa (open arrows); posterior acoustic enhancement; longitudinal

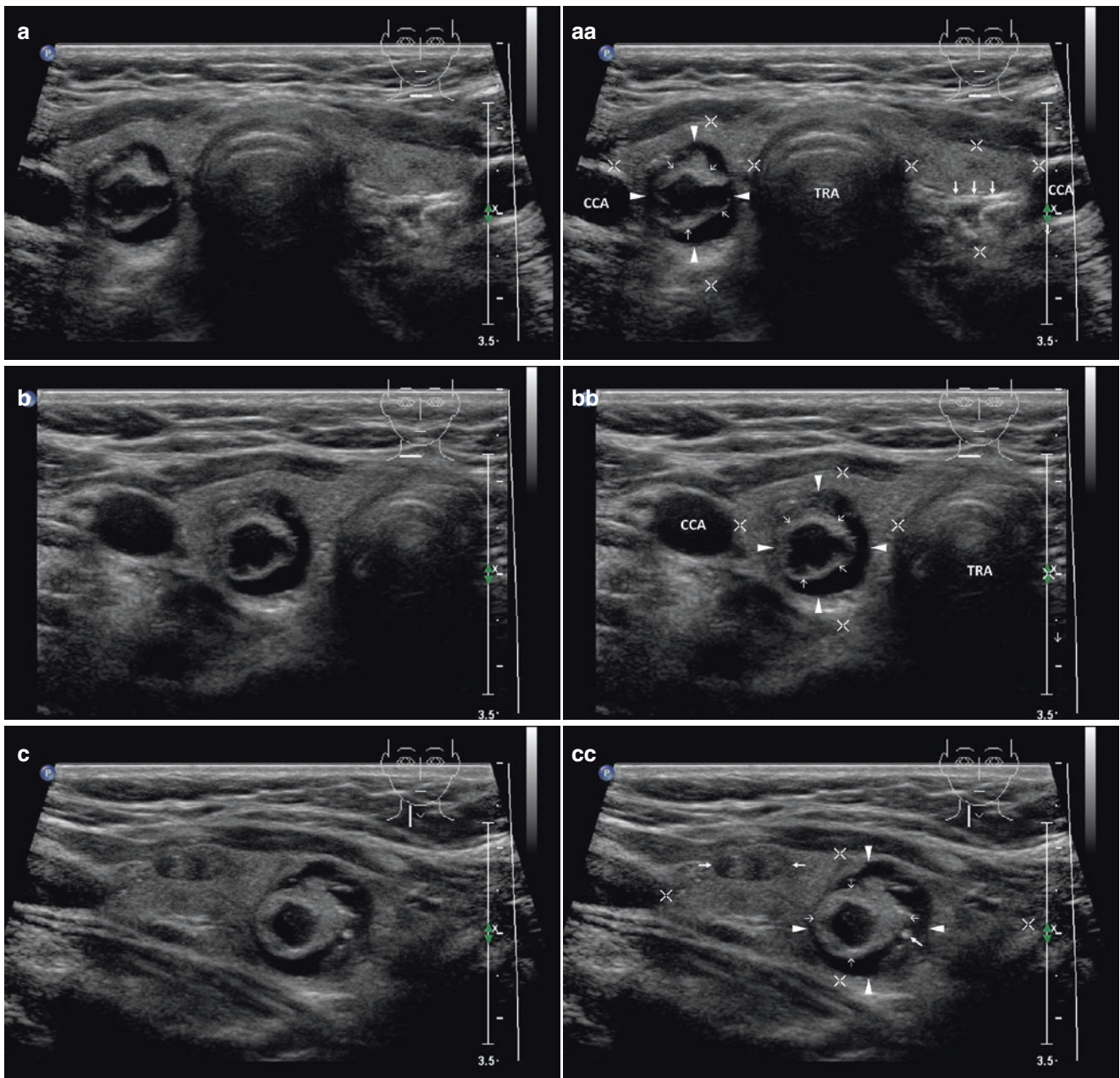


Fig. 7.5 (aa) A 59-year-old woman with small complex septated cyst, “jingle-bell” (arrowheads), size $15 \times 14 \times 12$ mm and volume 1 mL in the RL: round shape; anechoic contents; smooth wall with circular thick hyperechoic septum (open arrows); thick transverse septum (arrows) at the posterior part of LL; Tvol 11 mL, RL 6 mL, and LL 5 mL; transverse. (bb) Detail of small complex septated cyst, “jingle-bell” (arrow-

heads): round shape; anechoic contents; circular thick hyperechoic septum (open arrows); posterior acoustic enhancement; transverse. (cc) Detail of small complex septated cyst, “jingle-bell” (arrowheads): round shape; anechoic contents; circular thick hyperechoic septum (open arrows); colloid clot (arrow); in the upper part another small solid nodule (arrows); longitudinal

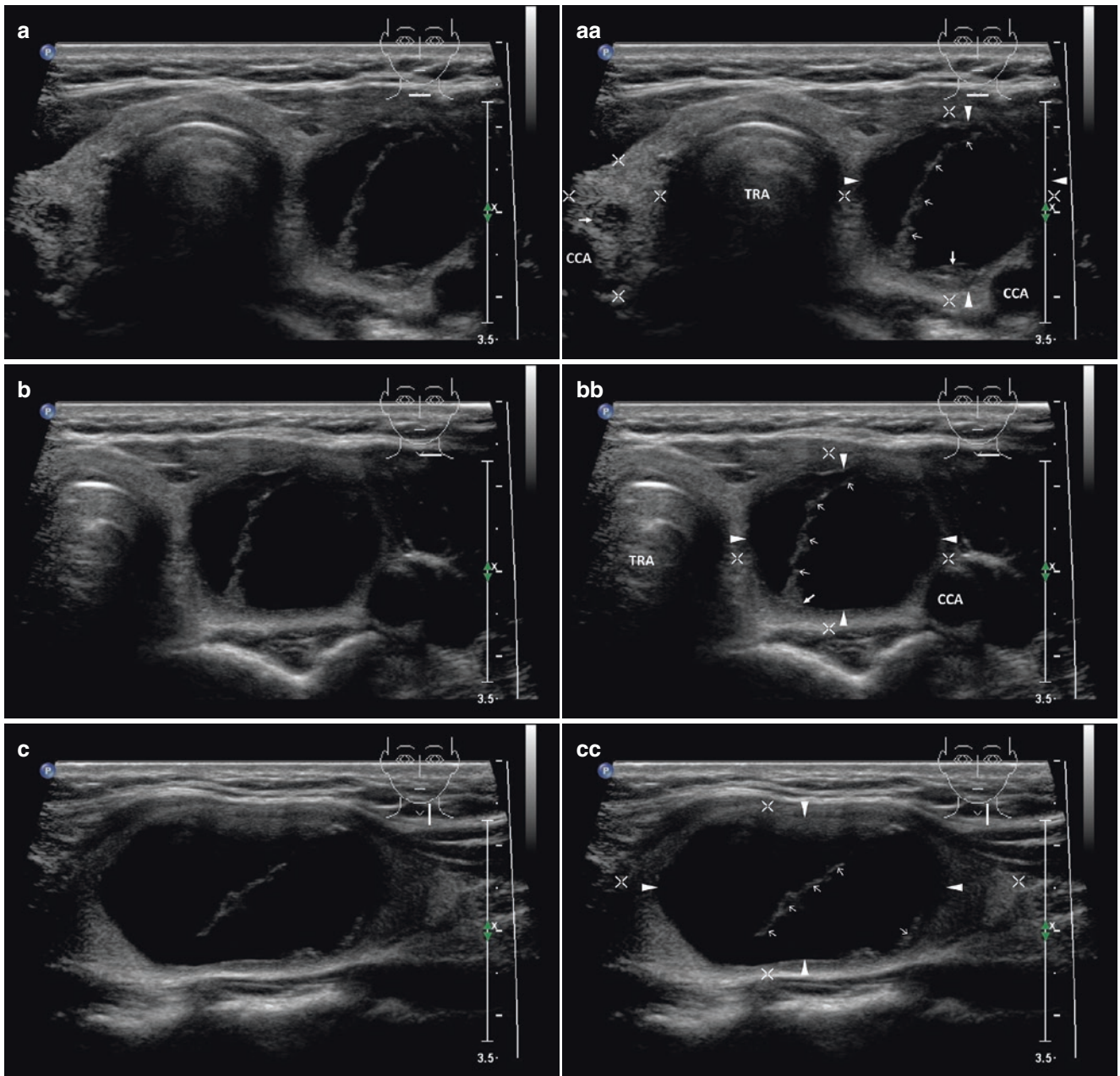


Fig. 7.6 (aa) A 40-year-old woman with a dominant medium-sized complex septated cyst (*arrowheads*), size $38 \times 25 \times 20$ mm and volume 10 mL in the LL of multinodular goiter (MNG); round shape; anechoic contents; smooth wall; thick transverse septum (*open arrows*); tiny complex nodule in the RL; Tvol 21 mL, asymmetry—RL 6 mL and LL 15 mL; transverse. (**bb**) Detail of dominant medium-sized complex sep-

tated cyst (*arrowheads*): ovoid shape; anechoic contents with thick transverse septum (*open arrows*); posterior acoustic enhancement; transverse. (**cc**) Detail of dominant medium-sized complex septated cyst (*arrowheads*): ovoid shape; anechoic contents with thick transverse septum (*open arrows*) and another short thick septum at the lower pole (*open arrows*); posterior acoustic enhancement; longitudinal

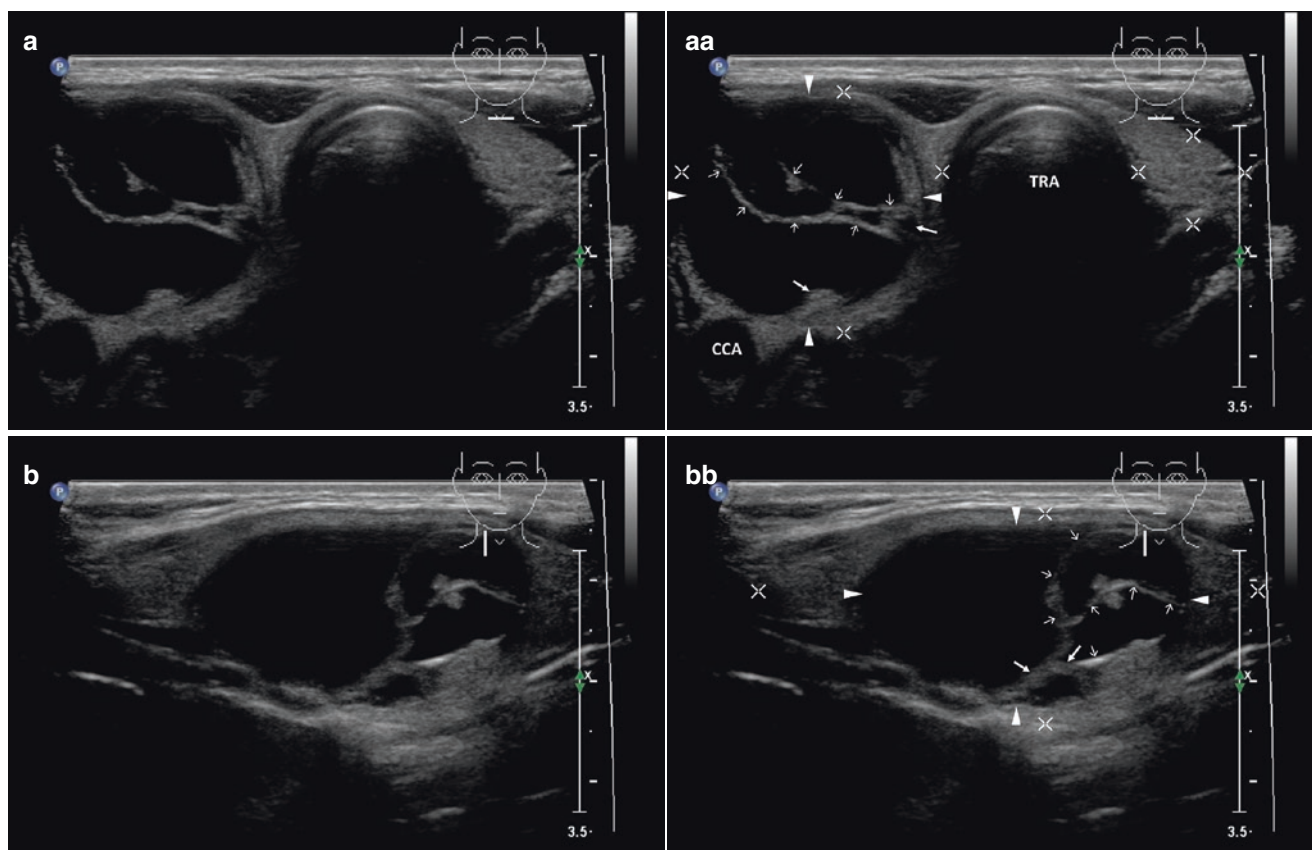


Fig. 7.7 (aa) A 20-year-old woman with a solitary medium-sized complex septated cyst (arrowheads), size $36 \times 32 \times 20$ mm and volume 12 mL in the RL: round shape; anechoic contents; hyperechoic focally thick wall (arrows); transverse thick double septum (open arrows); Tvol 21 mL, asymmetry—RL 19 mL and hypoplastic LL 2 mL; trans-

verse. (bb) Detail of solitary medium-sized complex septated cyst (arrowheads): ovoid shape; anechoic contents; hyperechoic focally thick wall (arrows); thick transverse branching septum (open arrows); posterior acoustic enhancement; longitudinal

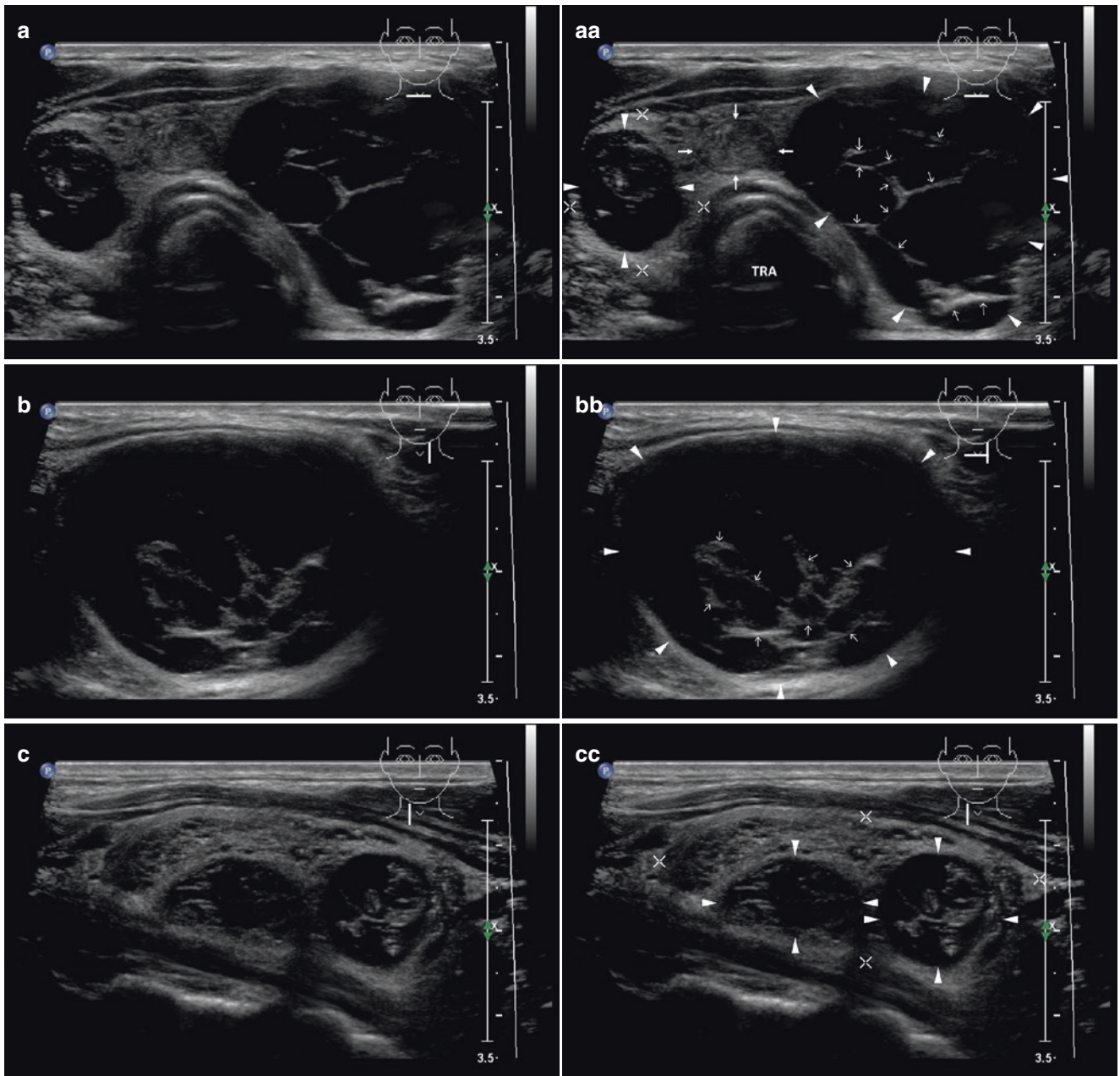


Fig. 7.8 (aa) A 43-year-old man with a dominant complex septated cyst (*arrowheads*) and several small complex cysts in multinodular goiter (MNG), large complex septated cyst, size $40 \times 32 \times 27$ mm and volume 17 mL, occupying the entire LL: anechoic contents; thin hyperechoic wall; multiple thick branching septa (*open arrows*); small solid nodule in the isthmus (*arrows*); small complex septated cyst in the RL (*arrowheads*); Tvol 30 mL, asymmetry—RL 8 mL and LL 22 mL;

transverse. (bb) Detail of the LL with dominant complex septated cyst (*arrowheads*): ovoid shape; anechoic contents; thin hyperechoic wall; multiple thick branching septa (*open arrows*); posterior acoustic enhancement; longitudinal. (cc) Detail of spongiform RL with two small complex septated cyst (*arrowheads*): ovoid, size 18×10 mm and round, size 14×14 mm; anechoic contents with multiple hyperechoic branching septa; moreover multiple tiny cysts; longitudinal

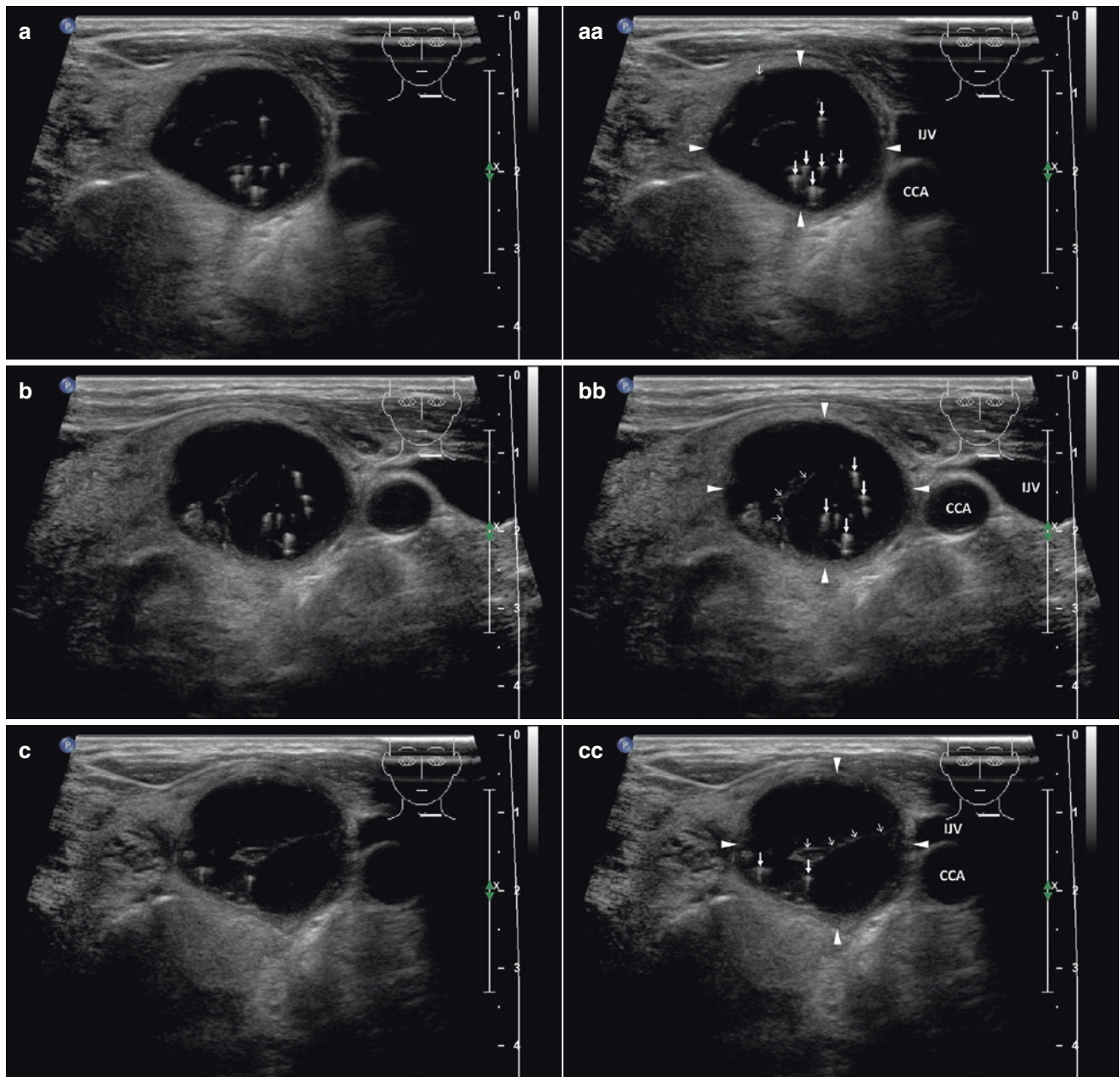
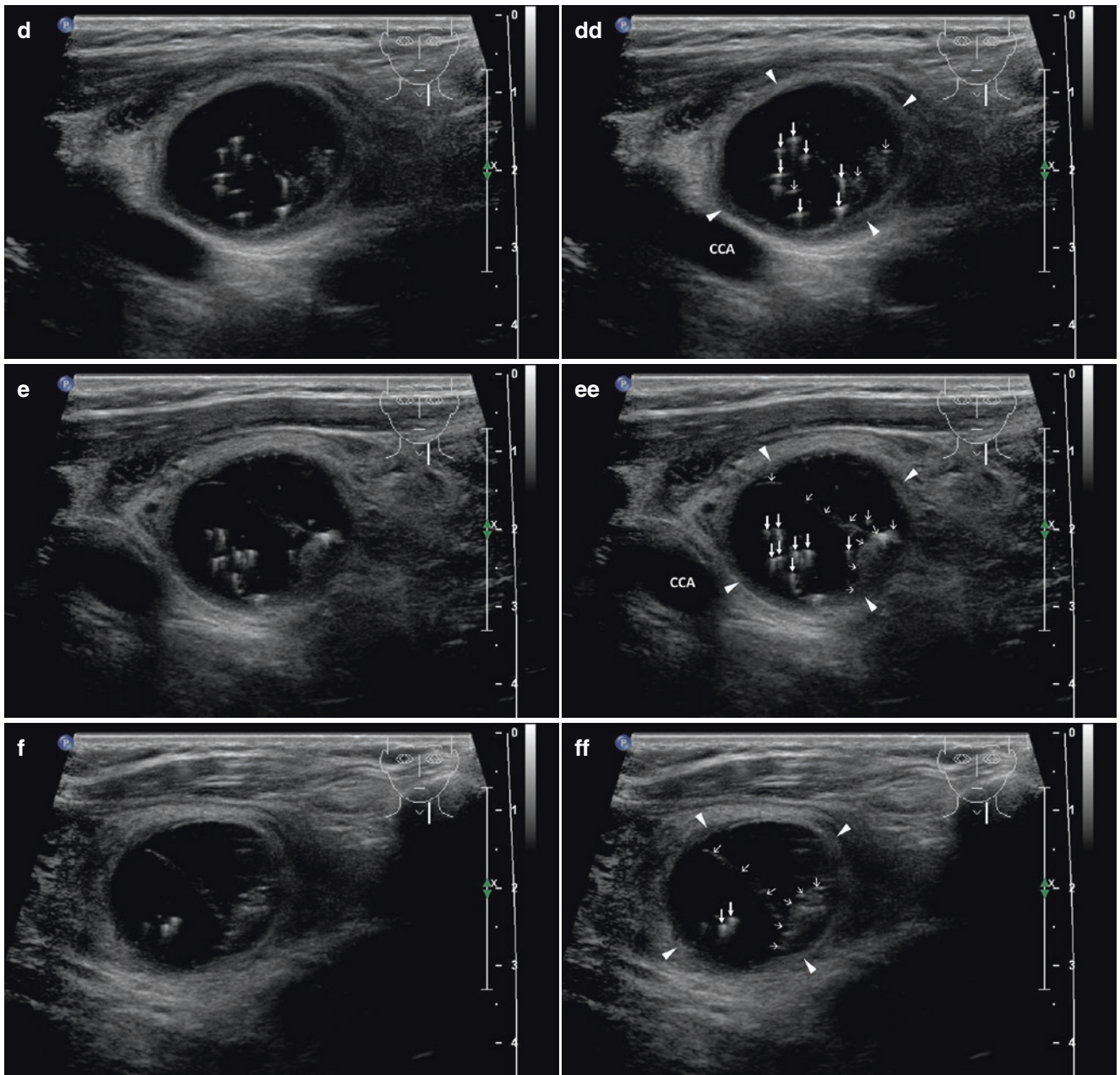


Fig. 7.9 (aa) An 81-year-old woman with multinodular goiter and a dominant medium-sized complex cyst (arrowheads) with comets, size $25 \times 22 \times 18$ mm and volume 5 mL in the LL: round shape; anechoic contents with multiple “comet tails” (arrows); volume of LL 16 mL; transverse. (bb) Detail of medium-sized complex cyst (arrowheads) with cluster of comets and septum: “comet tails” (arrows); sporadic tiny colloid clot without tails (open arrows); smooth wall with focal solid hyperechoic component and thin septum; another transverse view. (cc) Detail of medium-sized complex cyst (arrowheads) with comets and transverse septum: two “comet tails” (arrows); sporadic tiny colloid clot without tails; thick transverse septum (open arrows); another transverse view. (dd) Detail of medium-sized complex cyst (arrow-

heads) with cluster of comets and septum: “comet tails” (arrows); sporadic tiny colloid clot without tails (open arrows); smooth wall with focal solid hyperechoic component and thin septum; longitudinal. (ee) Detail of medium-sized complex cyst (arrowheads) with cluster of comets and septum: “comet tails” (arrows); sporadic tiny colloid clot without tails; smooth wall with focal solid hyperechoic component and thick septum (open arrows); another longitudinal view. (ff) Detail of medium-sized complex cyst (arrowheads) with comets and transverse septum: two “comet tails” (arrows); sporadic tiny colloid clot without tails; smooth wall with focal solid hyperechoic component and thick transverse septum (open arrows); another longitudinal view

**Fig. 7.9** (continued)

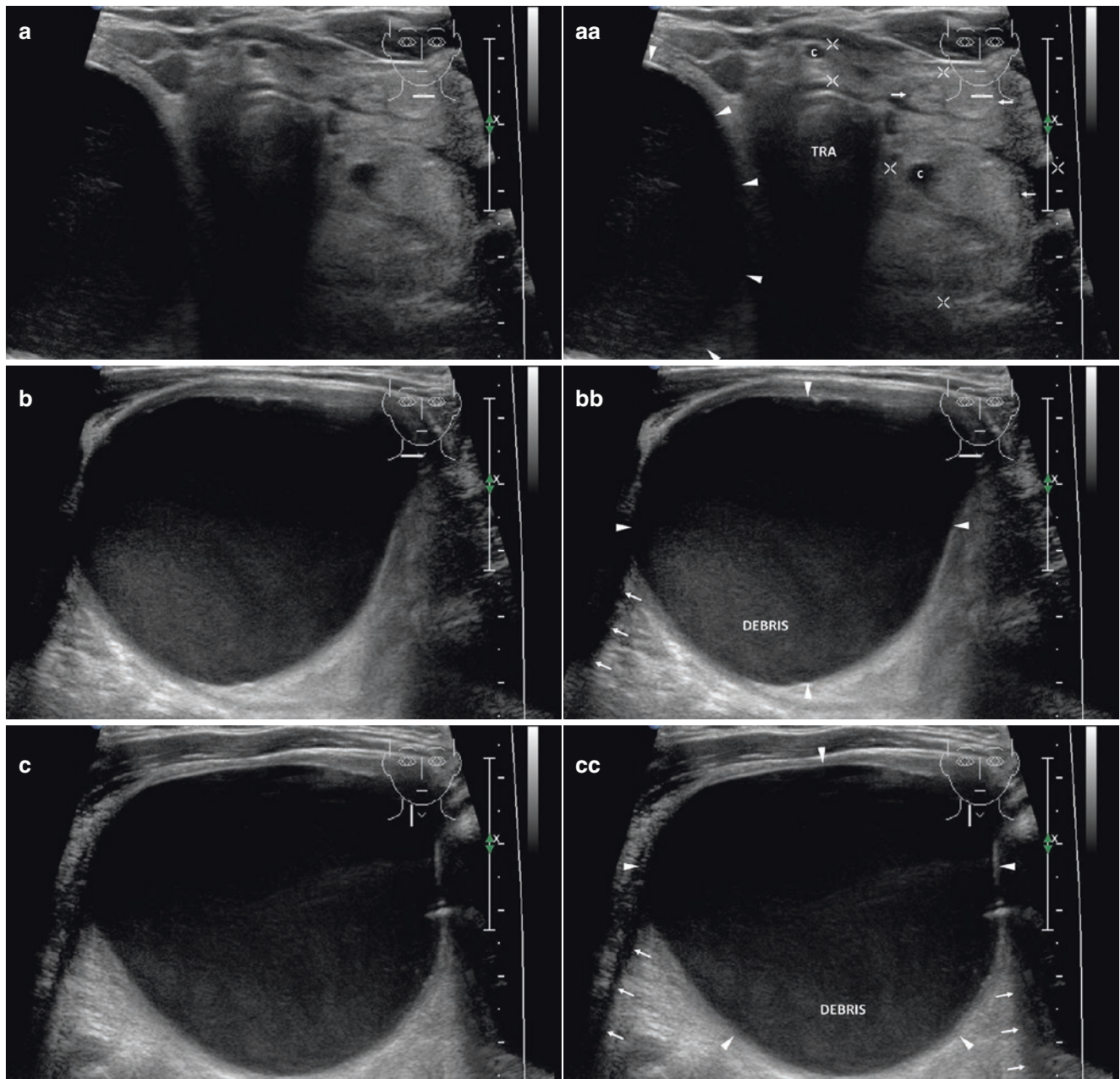


Fig. 7.10 (aa) A 79-year-old man with multinodular goiter (MNG) and a dominant giant complex cyst (*arrowheads*), size $58 \times 56 \times 44$ mm, volume 74 mL, occupying the entire RL. US overall view: medial part of dominant cyst—anechoic contents with hyperechoic debris; hyperechoic smooth wall; posterior acoustic enhancement; multiple solid hyperechoic nodules (*arrows*) and small cysts (*c*) in isthmus and in the LL; Tvol 113 mL, asymmetry—RL 74 mL and LL 37 mL; isthmus 18 mm; transverse; depth of penetration 6 cm. (bb) Detail of dominant

giant complex cyst (*arrowheads*): anechoic contents with hyperechoic debris; hyperechoic smooth wall; posterior acoustic enhancement; acoustic shadow at tangential angle—“ears” (*arrows*); transverse. (cc) Detail of dominant giant complex cyst (*arrowheads*): anechoic contents with hyperechoic debris; hyperechoic smooth wall; posterior acoustic enhancement; acoustic shadow at tangential angle—“ears” (*arrows*); longitudinal

References

1. Del Prete S, Caraglia M, Russo D, Vitale G, Giuberti G, Marra M, et al. Percutaneous ethanol injection efficacy in the treatment of large symptomatic thyroid cystic nodules: ten-year follow-up of a large series. *Thyroid*. 2002;12(9):815–21.
2. Bennedbaek FN, Hegedüs L. Treatment of recurrent thyroid cysts with ethanol: a randomized double-blind controlled trial. *J Clin Endocrinol Metab*. 2003;88(12):5773–7.
3. Moon WJ, Baek JH, Jung SL, Kim DW, Kim EK, Kim JY, et al. Korean Society of Thyroid Radiology (KSThR); Korean Society of Radiology. Ultrasonography and the ultrasound-based management of thyroid nodules: consensus statement and recommendations. *Korean J Radiol*. 2011;12(1):1–14.
4. Cho YS, Lee HK, Ahn IM, Lim SM, Kim DH, Choi CG, et al. Sonographically guided ethanol sclerotherapy for benign thyroid cysts: results in 22 patients. *AJR Am J Roentgenol*. 2000;174(1):213–6.
5. Kim JH, Lee HK, Lee JH, Ahn IM, Choi CG. Efficacy of sonographically guided percutaneous ethanol injection for treatment of thyroid cysts versus solid thyroid nodules. *AJR Am J Roentgenol*. 2003;180(6):1723–6.
6. Andrioli M, Carzaniga C, Persani L. standardized ultrasound report for thyroid nodules: the endocrinologist's viewpoint. *Eur Thyroid J*. 2013;2(1):37–48.
7. Nam-Goong IS, Kim HY, Gong G, Lee HK, Hong SJ, Kim WB, et al. Ultrasonography-guided fine-needle aspiration of thyroid incidentaloma: correlation with pathological findings. *Clin Endocrinol*. 2004;60(1):21–8.
8. Brito JP, Gionfriddo MR, Al Nofal A, Boehmer KR, Leppin AL, Reading C, et al. The accuracy of thyroid nodule ultrasound to predict thyroid cancer: systematic review and meta-analysis. *J Clin Endocrinol Metab*. 2014;99(4):1253–63.

8.1 Essential Facts

- According to The 2015 American Thyroid Association (ATA) Guidelines: isoechoic or hyperechoic solid nodule, or partially cystic nodule with eccentric uniformly solid areas without microcalcifications, irregular margin or extrathyroidal extension, or taller than wide shape prompts low suspicion for malignancy 5–10% [1].
- Caution! About 15–20% of thyroid cancers are isoechoic or hyperechoic on US, and these are generally the follicular variant of papillary thyroid carcinoma (PTC) or follicular thyroid carcinoma (FTC) [1].
 - Homogeneous (Fig. 8.1aa) or coarse structure (Fig. 8.3aa).
 - Isoechogenicity (Fig. 8.1aa) or hyperechogenicity (Fig. 8.3aa).
 - Well-defined, regular margins.
 - Regular thin halo sign (Fig. 8.1aa and Fig. 8.5aa) resp. thick halo sign (Fig. 8.6aa).
 - Perinodular vascularity (Fig. 8.1cc).
 - Sporadic tiny cystic cavities are possible ($\leq 10\%$ of volume) (Fig. 8.4aa).
- According to a large US based study by Moon et al., the US findings for benign nodules were isoechogenicity (sensitivity 56.6%, specificity 88.1%) and spongiform appearance (sensitivity 10.4%, specificity 99.7%); *see more in Chap. 14*. [3].
- FNAB is recommended at size ≥ 1.5 cm; *see more in Chap. 24, Table 24.1*. [1].

8.2 US Features of a Benign Solid Nodule

- US findings for benign nodule (Fig. 8.1aa) [2]:
 - Ovoid, elliptical (“more wide than tall”) (Figs. 8.1aa and 8.2aa) or round shape (Fig. 8.3aa).

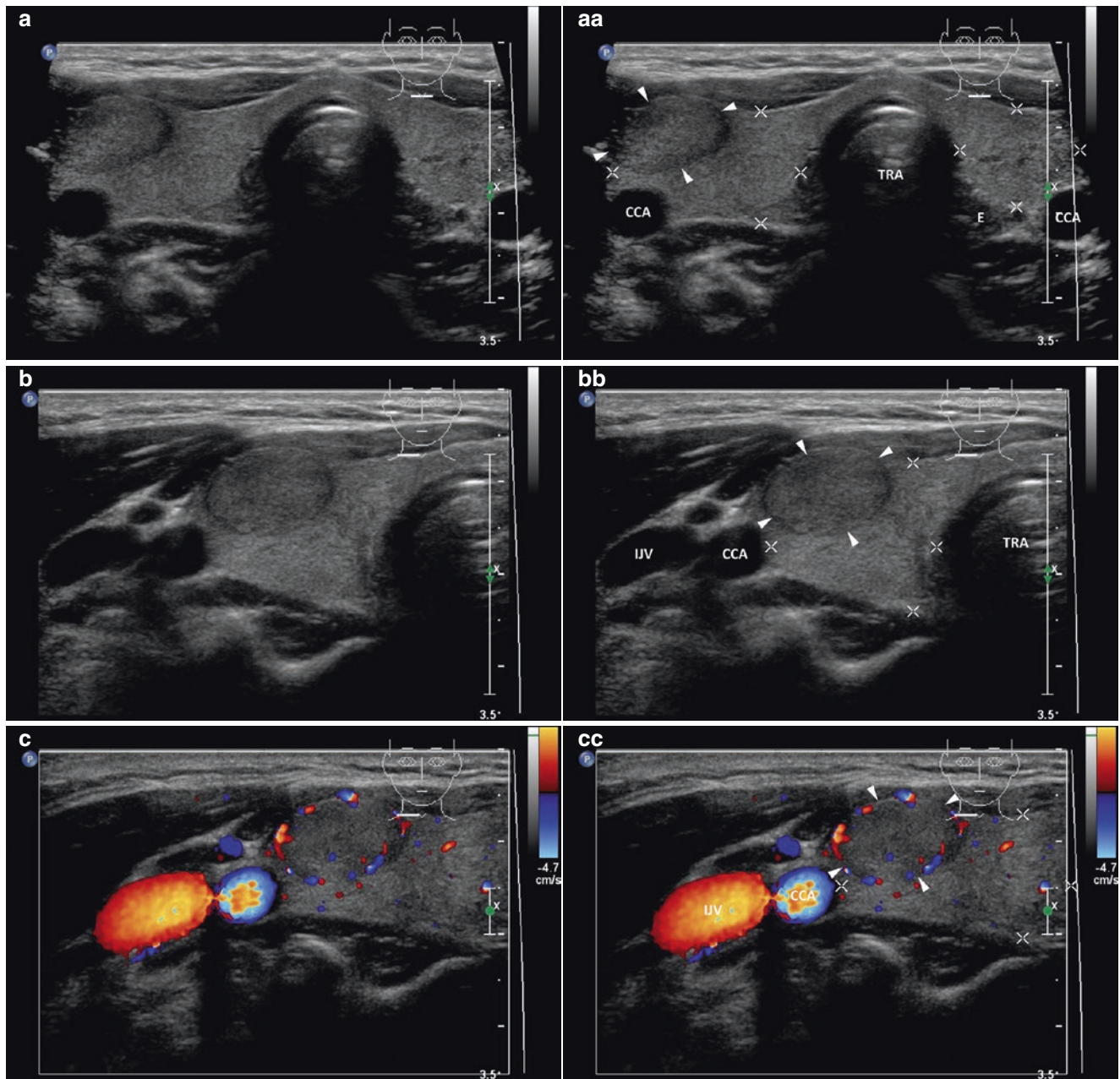


Fig. 8.1 (aa) A 24-year-old woman with solitary solid nodule (*arrowheads*), size $16 \times 14 \times 9$ mm and volume 1 mL in the RL. According to US criteria typically non-suspicious, benign nodule: ovoid shape, “more wide than tall”; homogeneous structure; isoechoic; well-defined with thin halo sign; Tvol 16 mL, RL 9 mL, and LL 7 mL; transverse. (bb) Detail of solitary solid nodule (*arrowheads*): ovoid shape; homogeneous structure; isoechoic; well-defined with thin halo sign. (cc) Detail of solitary solid nodule (*arrowheads*): ovoid shape; homogeneous structure; isoechoic; well-defined with thin halo sign. (ee) Detail of solitary solid nodule (*arrowheads*): ovoid shape; homogeneous structure; isoechoic; well-defined with thin halo sign. (cc) Detail of solitary solid nodule (*arrowheads*): ovoid shape; homogeneous structure; isoechoic; well-defined with thin halo sign.

Detail of solitary solid nodule (*arrowheads*), CFDS: increased vascularity at periphery and sporadic parenchymal vascularity, *pattern I*; transverse. (dd) Detail of solitary solid nodule (*arrowheads*): ovoid shape; homogeneous structure; isoechoic; well-defined with thin halo sign; longitudinal. (ee) Detail of solitary solid nodule (*arrowheads*), CFDS: peripheral vascularity and one intranodal vessel branch, *pattern I*; longitudinal

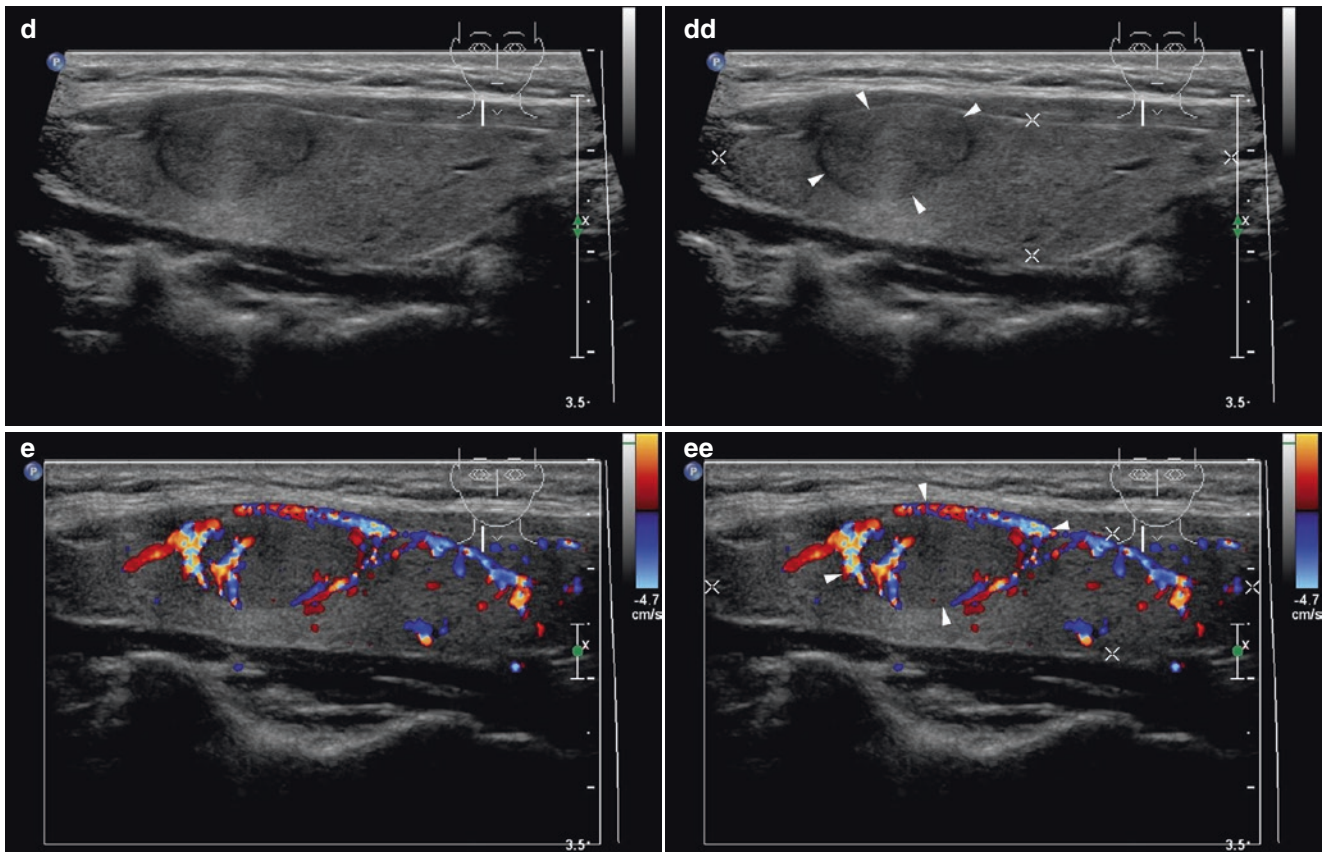


Fig. 8.1 (continued)

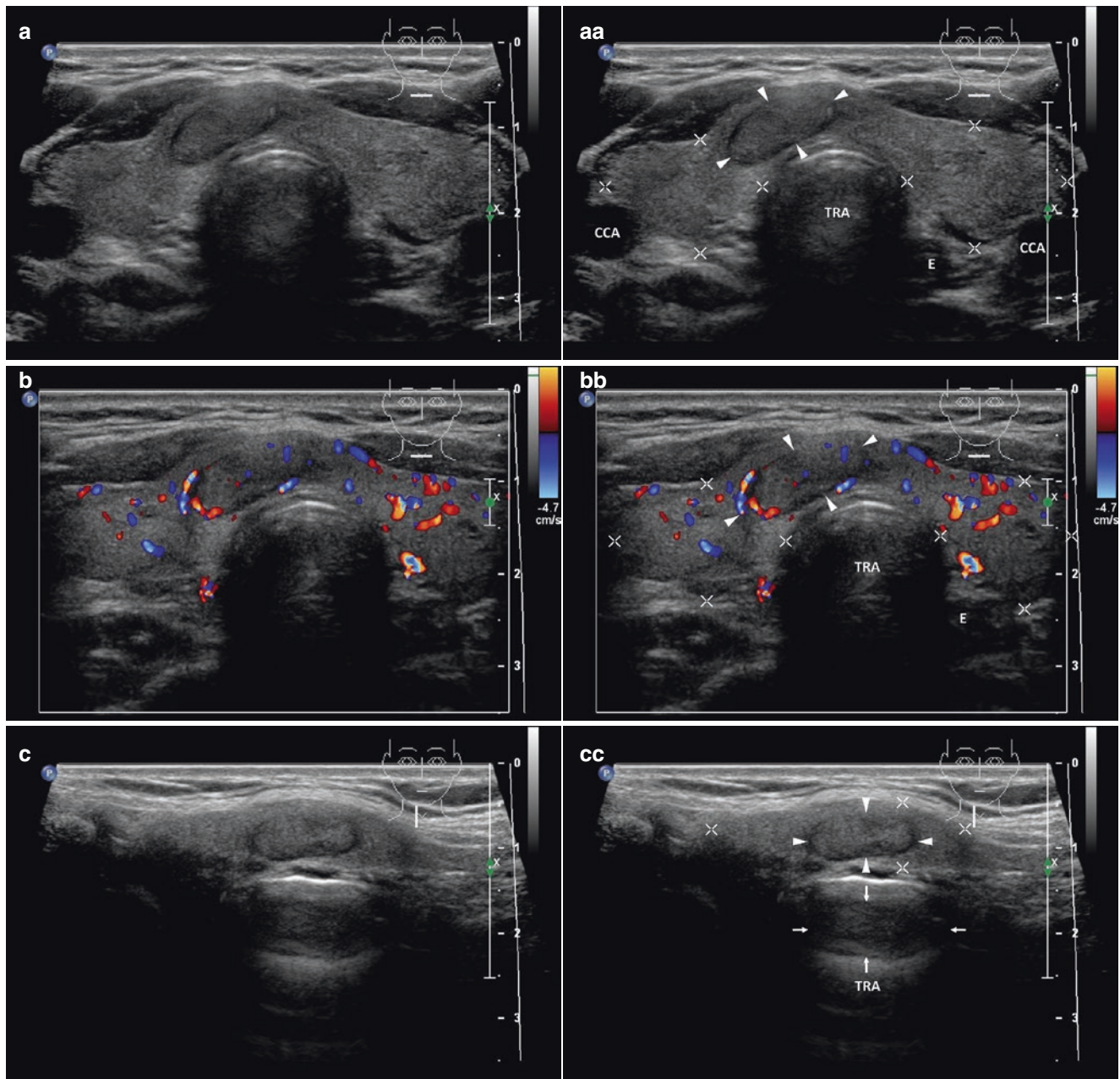
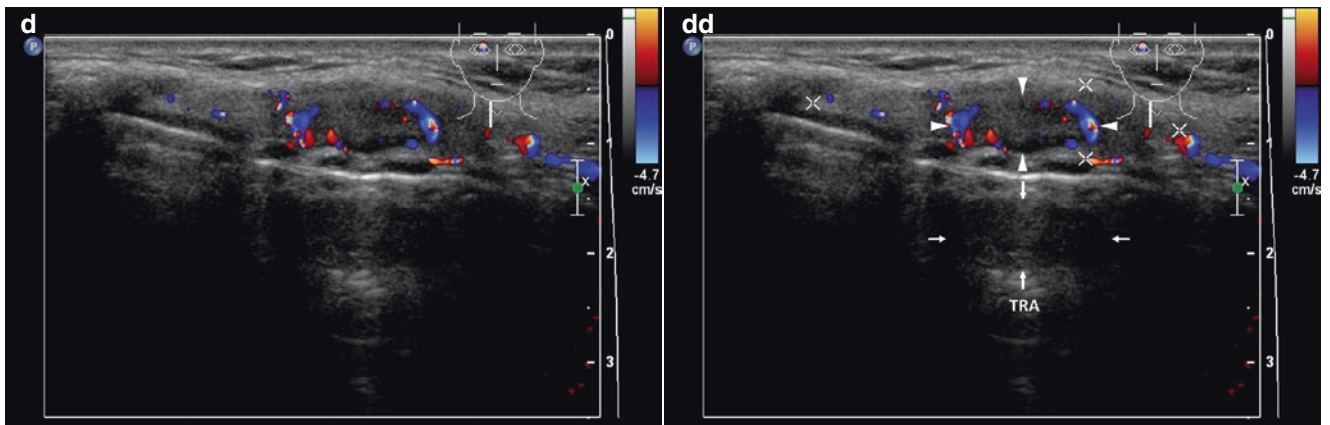


Fig. 8.2 (aa) A 57-year-old woman with solitary solid nodule (*arrowheads*), size $14 \times 13 \times 6$ mm and volume 0.6 mL in the right branch of isthmus. According to US criteria typically non-suspicious, benign nodule: elliptical shape, “more wide than tall”; homogeneous structure; isoechoic; well-defined with thin halo sign; Tvol 19 mL, RL 9 mL, and LL 10 mL; transverse. (bb) Detail of isthmic solitary solid nodule (*arrowheads*), CFDS: peripheral vascularity and minimal parenchymal

vascularity, *pattern I*; transverse. (cc) Detail of isthmic solitary solid nodule (*arrowheads*): ovoid shape; homogeneous structure; isoechoic; well-defined with thin halo sign; slightly enlarged “mirror artifact” (*arrows*) of the nodule visible into the trachea; longitudinal. (dd) Detail of isthmic solitary solid nodule (*arrowheads*), CFDS: increased peripheral vascularity, *pattern I*; slightly enlarged avascular “mirror artifact” (*arrows*) of the nodule, visible into the trachea; longitudinal

**Fig. 8.2** (continued)

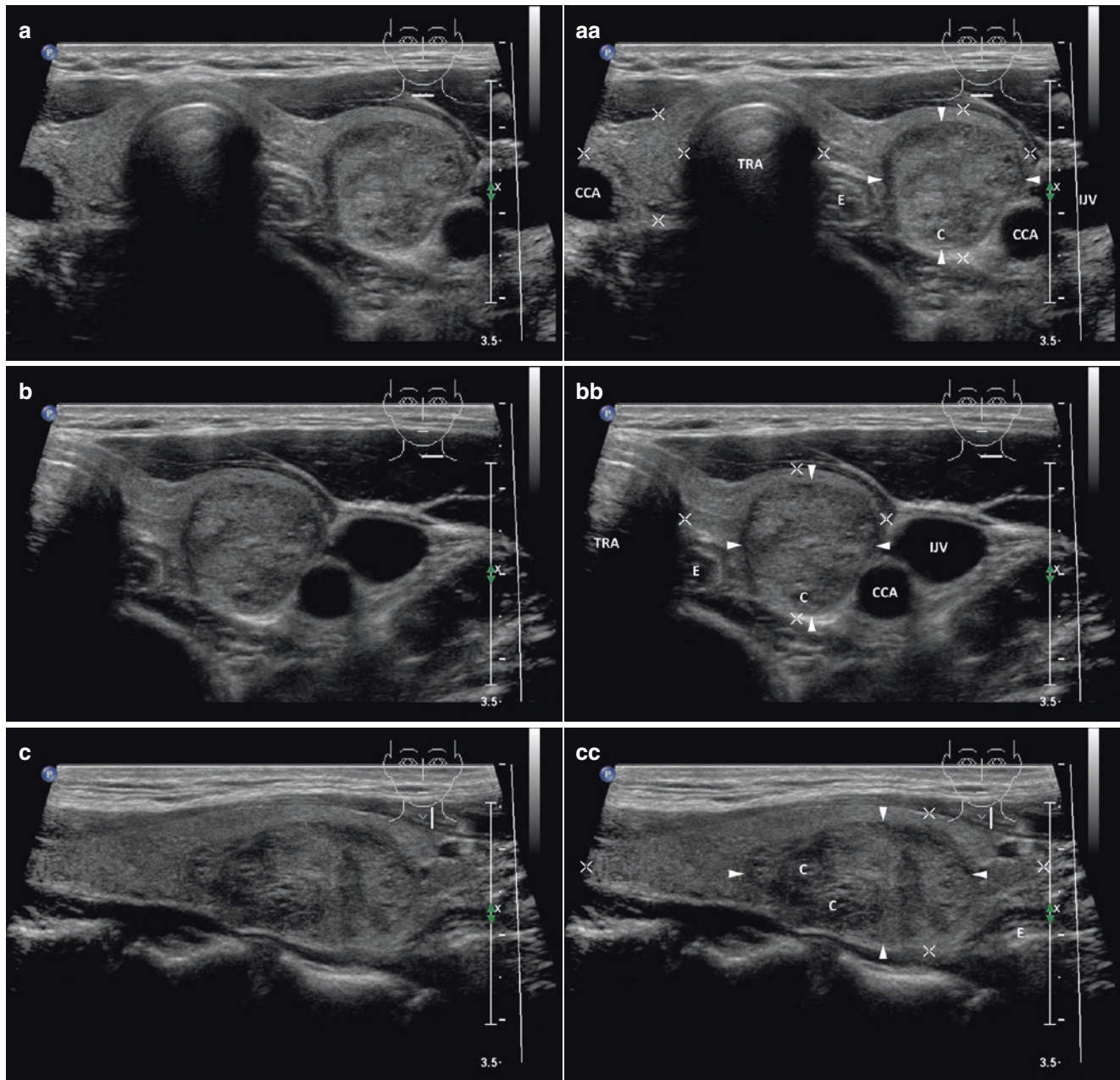


Fig. 8.3 (aa) A24-year-old woman with medium-sized solitary solid nodule (*arrowheads*) with sporadic tiny cystic cavities ($\leq 10\%$ of volume), size $24 \times 16 \times 16$ mm and volume 3 mL in the LL. US overall view: round shape; coarse structure; hyperechoic; sporadic tiny cystic cavities (c); well-defined margin with thin halo sign; Tvol 19 mL, asymmetry—RL 7 mL and LL 12 mL; transverse. (bb) Detail of

medium-sized solitary solid nodule (*arrowheads*): ovoid shape; coarse structure; hyperechoic; sporadic tiny cystic cavities (c); well-defined margin with thin halo sign; transverse. (cc) Detail of medium-sized solitary solid nodule (*arrowheads*): ovoid shape; coarse structure; hyperechoic; sporadic tiny cystic cavities (c); well-defined margin with thin halo sign; longitudinal

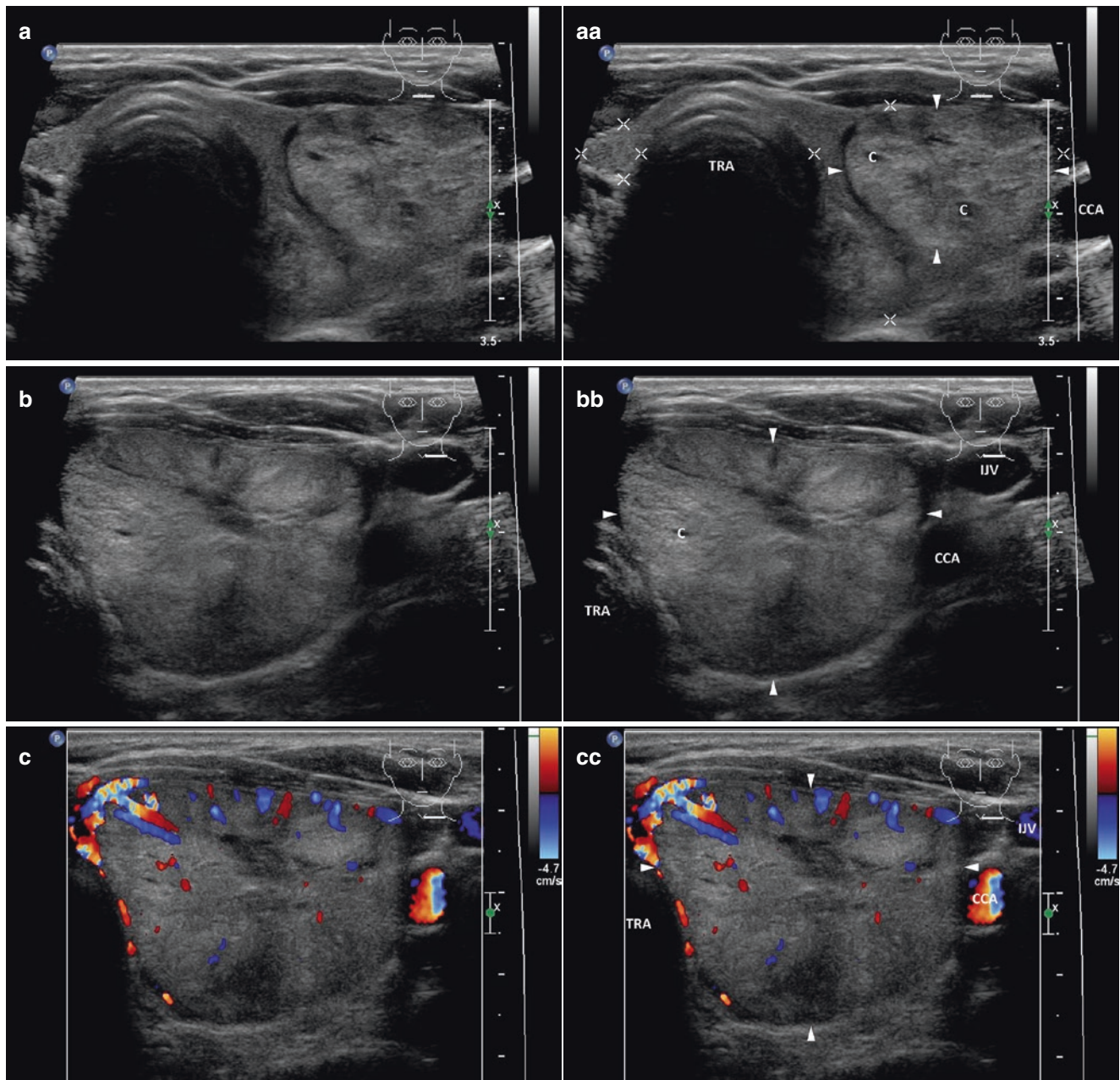


Fig. 8.4 (aa) A 50-year-old woman with large solitary solid nodule (arrowheads) with sporadic tiny cystic cavities ($\leq 10\%$ of volume), size $54 \times 39 \times 30$ mm and volume 33 mL in the LL. US scans: view of upper part of nodule—ovoid shape; size 26×17 mm; coarse structure; hyperechoic; sporadic tiny cystic cavities (c); well-defined with thin halo sign; small right lobe without nodules; trachea pushed to the right; Tvol 40 mL, asymmetry—RL 5 mL and LL 35 mL; transverse. (bb) Detail of large solitary solid nodule (arrowheads): view of central part of nodule—round shape; size 39×30 mm; coarse structure; hyperechoic; spo-

radic tiny cystic cavities (c); well-defined with thin halo sign; transverse; depth of penetration 4.5 cm. (cc) Detail of large solitary solid nodule (arrowheads), CFDS: increased peripheral vascularity and one intranodal vessel branch, *pattern II*; transverse. (dd) Detail of large solitary solid nodule (arrowheads): view of central part of nodule—round shape; size 39×30 mm; coarse structure; hyperechoic; sporadic tiny cystic cavities (c); well-defined with thin halo sign; longitudinal. (ee) Detail of large solitary solid nodule (arrowheads), CFDS: increased peripheral and sporadic intranodal vascularity, *pattern II*; longitudinal

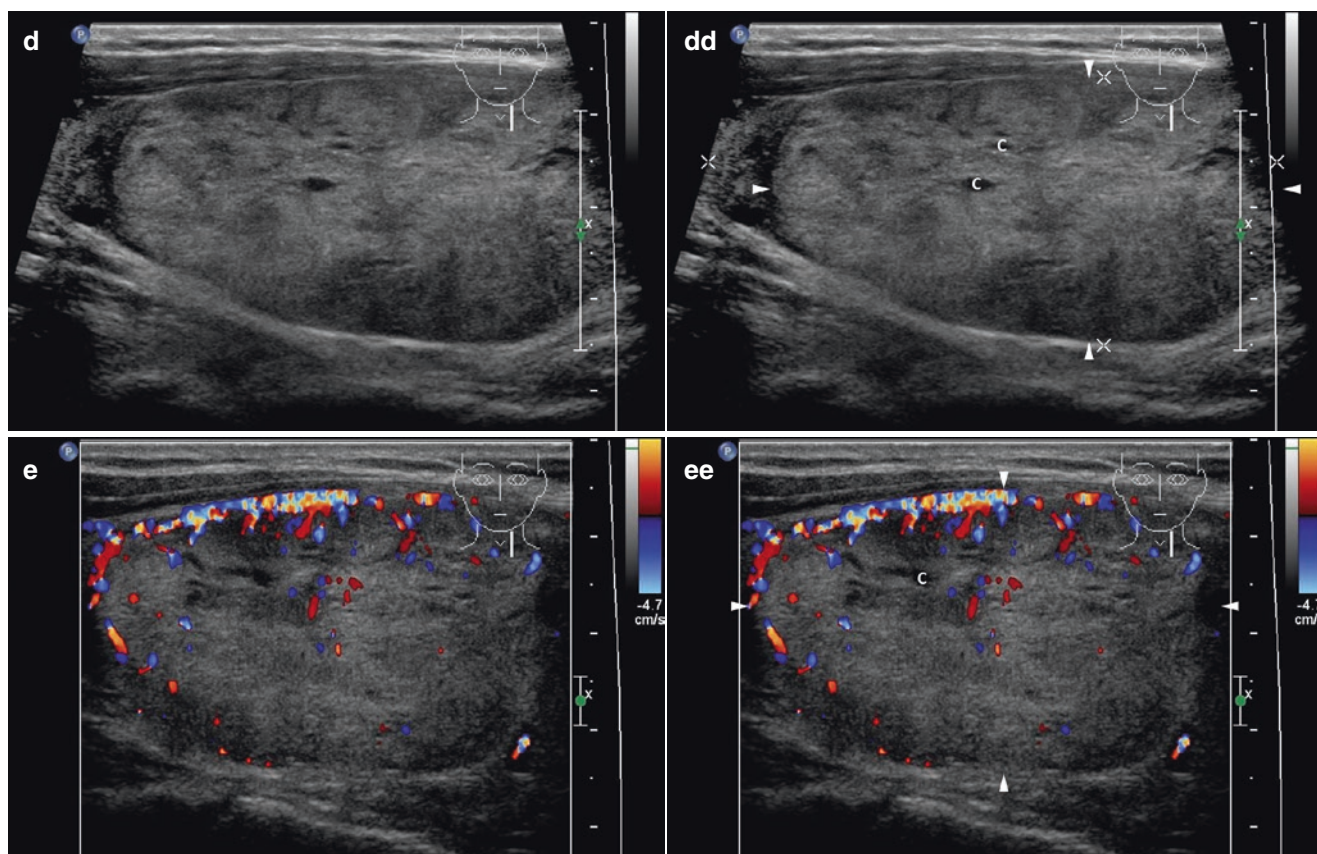


Fig.8.4 (continued)

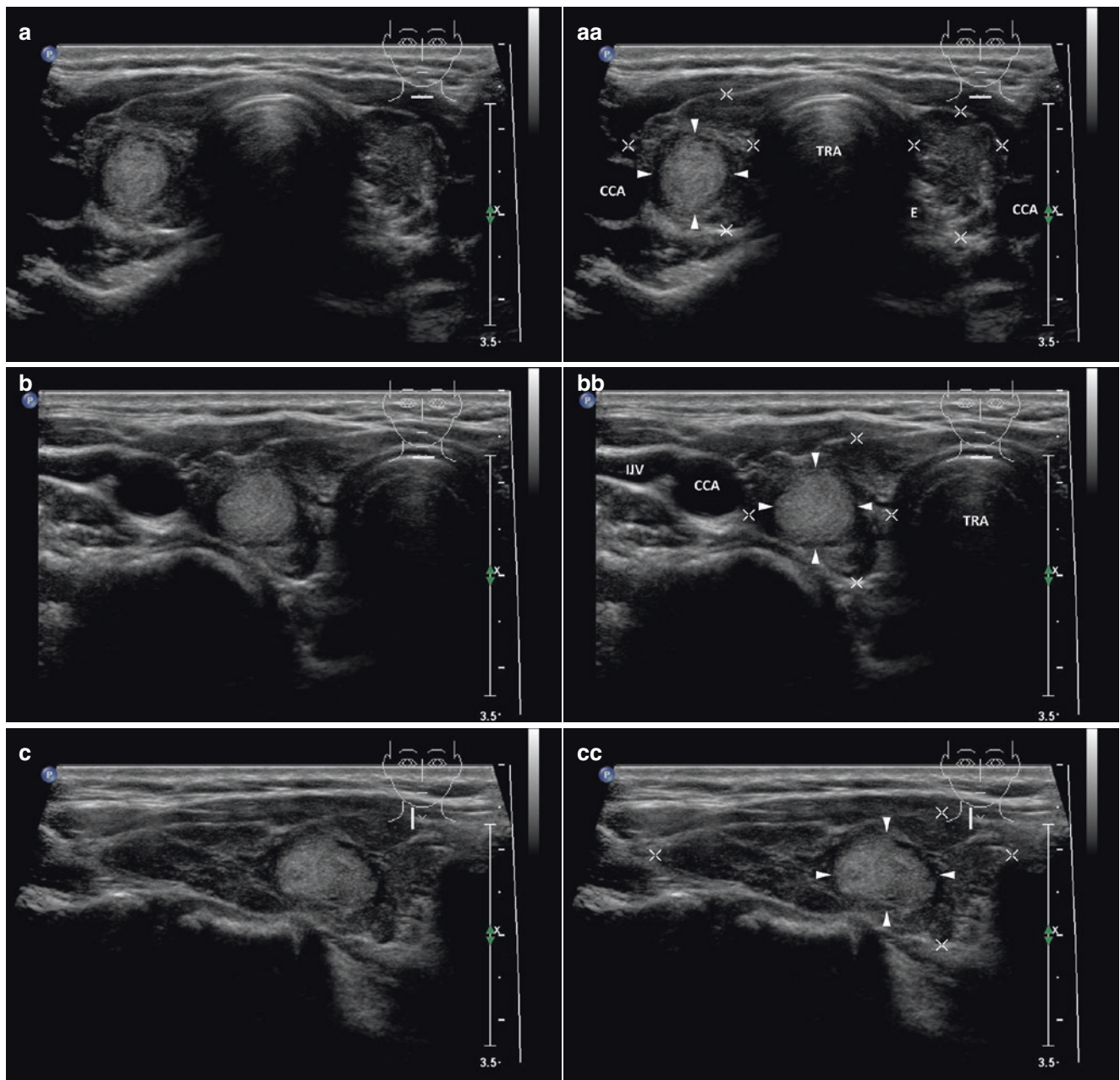


Fig. 8.5 (aa) A 55-year-old woman with Hashimoto's thyroiditis (HT) and small solitary solid nodule (*arrowheads*), size $13 \times 9 \times 8$ mm and volume 0.5 mL in the RL. According to US criteria typically non-suspicious, benign nodule: round shape; homogeneous structure; hyperechoic; well-defined margin with thin halo sign; thyroid gland—inhomogeneous, hypoechoic micronodular structure with thin hyperechoic septa; microl-

obulated margin; Tvol 9 mL, RL 5 mL and LL 4 mL; transverse. (bb) Detail of small solitary solid nodule (*arrowheads*) and HT: round shape; homogeneous structure; hyperechoic; well-defined margin with thin halo sign; transverse. (cc) Detail of small solitary solid nodule (*arrowheads*) and HT: ovoid shape; homogeneous structure; hyperechoic; well-defined margin with thin halo sign; longitudinal

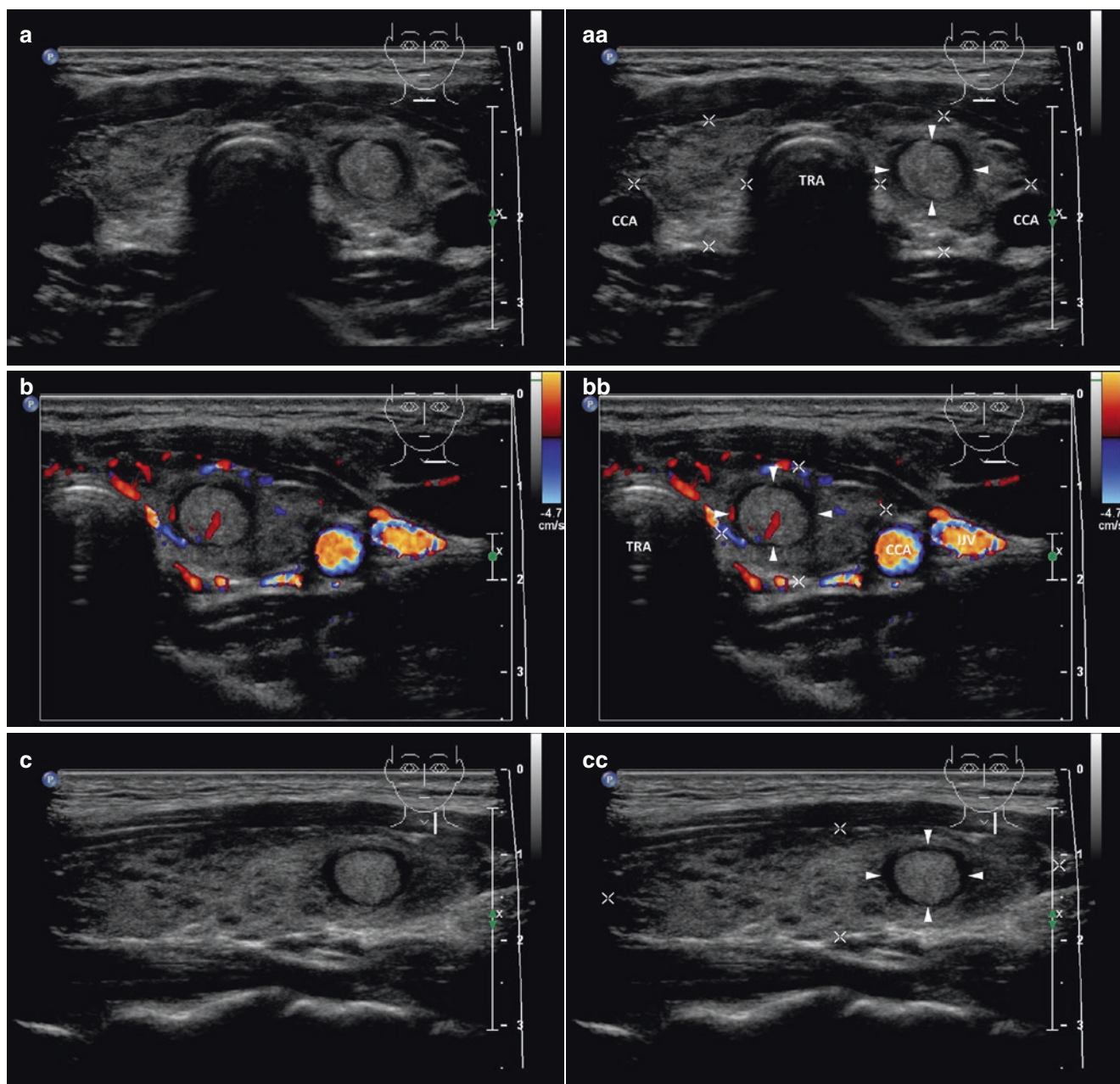


Fig. 8.6 (aa) A 13-year-old girl with Hashimoto's thyroiditis (HT) and tiny solitary solid nodule (*arrowheads*), size $10 \times 9 \times 8$ mm and volume 0.4 mL in the LL. According to US criteria typically non-suspicious, benign nodule: round shape; homogeneous structure; hyperechoic; well-defined margin with thick halo sign; thyroid gland—inhomogeneous, hypoechoic micronodular structure with thin hyperechoic septa; microlobulated margin; Tvol 13 mL, RL 6 mL, and LL 7 mL; transverse. (bb)

Detail of tiny solitary solid nodule (*arrowheads*) and HT, CFDS: sporadic peripheral vascularity and one intranodal vessel branch, *pattern I*; transverse. (cc) Detail of tiny solitary solid nodule (*arrowheads*) and HT: round shape; homogeneous structure; hyperechoic; well-defined margin with thick halo sign; longitudinal. (dd) Detail of tiny solitary solid nodule (*arrowheads*) and HT, CFDS: sporadic peripheral vascularity and one intranodal vessel branch, *pattern I*; longitudinal

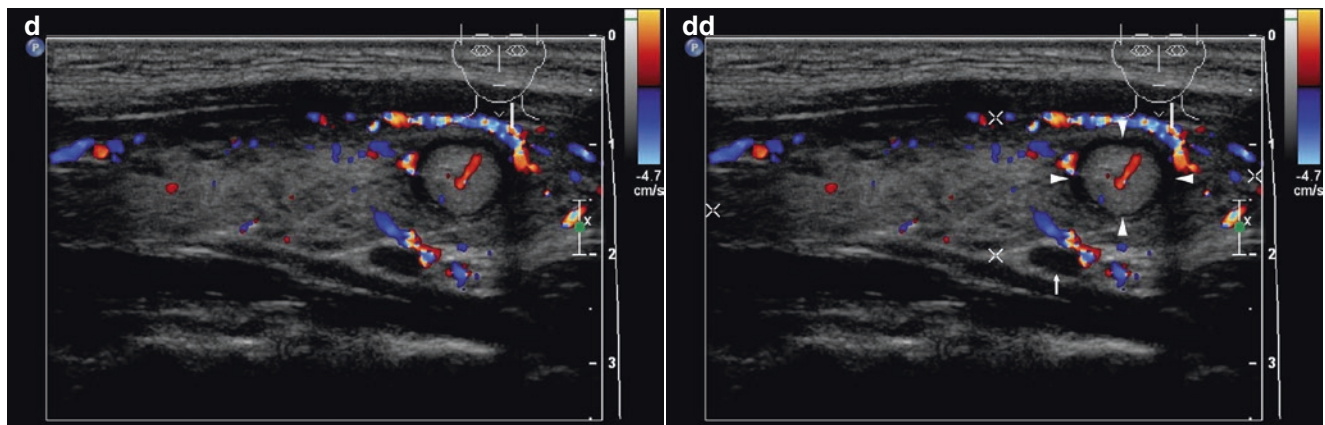


Fig. 8.6 (continued)

References

1. Haugen BR, Alexander EK, Bible KC, Doherty GM, Mandel SJ, Nikiforov YE, et al. 2015 American Thyroid Association Management Guidelines for adult patients with thyroid nodules and differentiated thyroid cancer: The American Thyroid Association Guidelines Task Force on Thyroid Nodules and Differentiated Thyroid Cancer. *Thyroid*. 2016;26(1):1–133.
2. Andrioli M, Carzaniga C, Persani L. Standardized ultrasound report for thyroid nodules: the endocrinologist's viewpoint. *Eur Thyroid J*. 2013;2(1):37–48.
3. Moon WJ, Jung SL, Lee JH, Na DG, Baek JH, Lee YH, Thyroid Study Group. Korean Society of Neuro- and Head and Neck Radiology et al. *Radiology*. 2008;247(3):762–70.

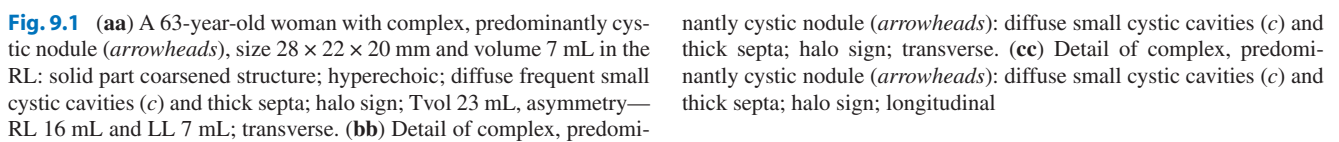
9.1 Complex Nodule with Cystic Degeneration

9.1.1 Essential Facts

- Most cystic lesions of the thyroid result from hemorrhage and subsequent degeneration of preexisting solid nodules [1].
- Incidence of cystic lesions among nodules ranges from 15–37% (Fig. 9.1) [2].
- In McHenry' study of 389 patients, cystic nodules were present in 70 (18%) patients. Thyroidectomy was performed in 28 (40%) of them because of an abnormal or persistently nondiagnostic FNAB or compressive symptoms. Six patients (8.6%) had thyroid carcinoma [3].
- There is a high risk of false negative results when there is a large complex nodule size (≥ 4 cm). It is therefore recommended that FNAB be repeated after 6 months even if the result of the first FNAB is negative [2].
- According to the 2015 American Thyroid Association (ATA) Guidelines: Isoechoic or hyperechoic solid nodule, or partially cystic nodule with eccentric uniformly solid areas without microcalcifications, irregular margin or extrathyroidal extension, or "taller-than-wide" shape prompts low suspicion for malignancy 5–10% [4].
- Spongiform or partially cystic nodules without any of US suspicious features have a low risk of malignancy, <3% [4].

9.1.2 US Features of Complex Nodules with Cystic Degeneration

- For classification of predominantly solid nodule (Fig. 9.2), predominantly cystic nodule (Fig. 9.1), spongiform nodule (Fig. 9.3) and US features of complex nodule cystic part; *see more in introduction to Section III* (part 1.1.2.3) and *Chap. 7* (part 7.2).
- Spongiform and other mixed cystic solid nodules may exhibit bright reflectors on US imaging, caused by colloid crystals or posterior acoustic enhancement of the back wall of a microcystic area. These may be confused with microcalcifications by less proficient sonographers. Therefore, because of potential misclassification, FNAB may still be considered for nodules interpreted as spongiform, but with a larger cut-off size [5].
- The 2015 American Thyroid Association (ATA) Guidelines recommends for spongiform or partially cystic nodules without any of the US suspicious features (Fig. 9.1), FNAB at size ≥ 2 cm. Observation without FNAB may also be considered; *see more in Chap. 24, Table 24.1* [4].



9.2 Complex Nodule with Calcifications

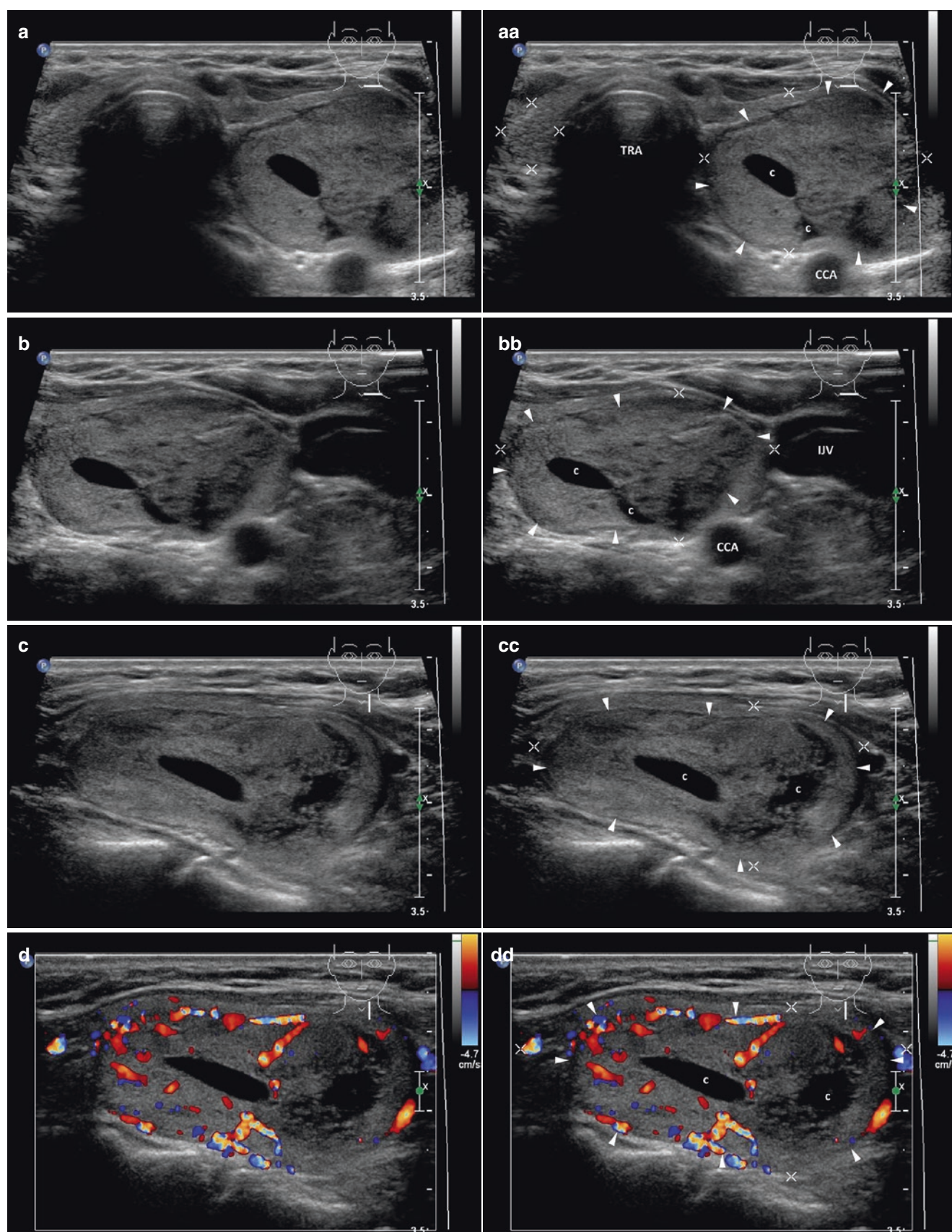
9.2.1 Essential Facts

- Calcification within the thyroid gland is a common finding on US, with the incidence 14–55% [6].
- Histologically, thyroid calcifications are divided into psammomatous (calcium deposits in the epithelium) and dystrophic (amorphous deposits in fibrous tissue) [6].
- Calcification can be detected in both benign and malignant nodules, with malignancy rates of 29–59% [6].
- Benign nodules have dystrophic coarse calcifications, especially with long disease duration [7].
- Peripheral dystrophic calcifications (coarse calcifications shown on US) are more frequently associated with benignity. They can also occur, however, in malignant lesions, up to 18% [6].
- Papillary thyroid carcinoma (PTC) frequently forms psammomatous calcification (fine stippled microcalcifications on US) [6, 8]; (Figs. 15.8bb and 15.9bb)
- Incidence of dystrophic calcifications is higher in older patients, ≥ 45 years of age. Fine stippled psammomatous calcifications predict PTC, particularly in younger patients (<45 years). The sensitivity of dystrophic and psammomatous calcification for the detection of malignancy is 63.5% and 24.3%, respectively; the specificity is 69.8% and 96.8% respectively [8].

- A risk of malignancy in thyroid nodules with calcifications: punctuate calcifications 23.3%, rim calcifications 16.7%, central coarse calcifications 16.7%, without calcifications 8.5% [9].

9.2.2 Ultrasound Features of Calcifications [1]

- Peripheral calcifications are bright echoes observed at the surface of a thyroid nodule.
- Calcifications are categorized according to the shape:
 - Stippled, fine, or coarse nonlinear particles (Fig. 9.7aa).
 - Curvilinear, smooth margin (Fig. 9.5bb).
 - Curvilinear, irregular margin (Fig. 9.4aa).
- Calcifications are categorized according to the extent:
 - Arc or linear calcification is limited to part of the lesion border (Fig. 9.7aa, bb and 9.8aa).
 - Rim calcification involves the entire lesion border—peripheral “eggshell” calcification (Figs. 9.9aa and 9.10aa).
- Intranodular calcification is a hyperechoic structure inside a thyroid nodule, can be coarse (Fig. 9.4aa), linear (Fig. 9.5aa) or “eggshell” (Fig. 9.6aa)
- Acoustic shadows caused by calcifications (Fig. 9.9bb) might worsen visualization of nodule content.



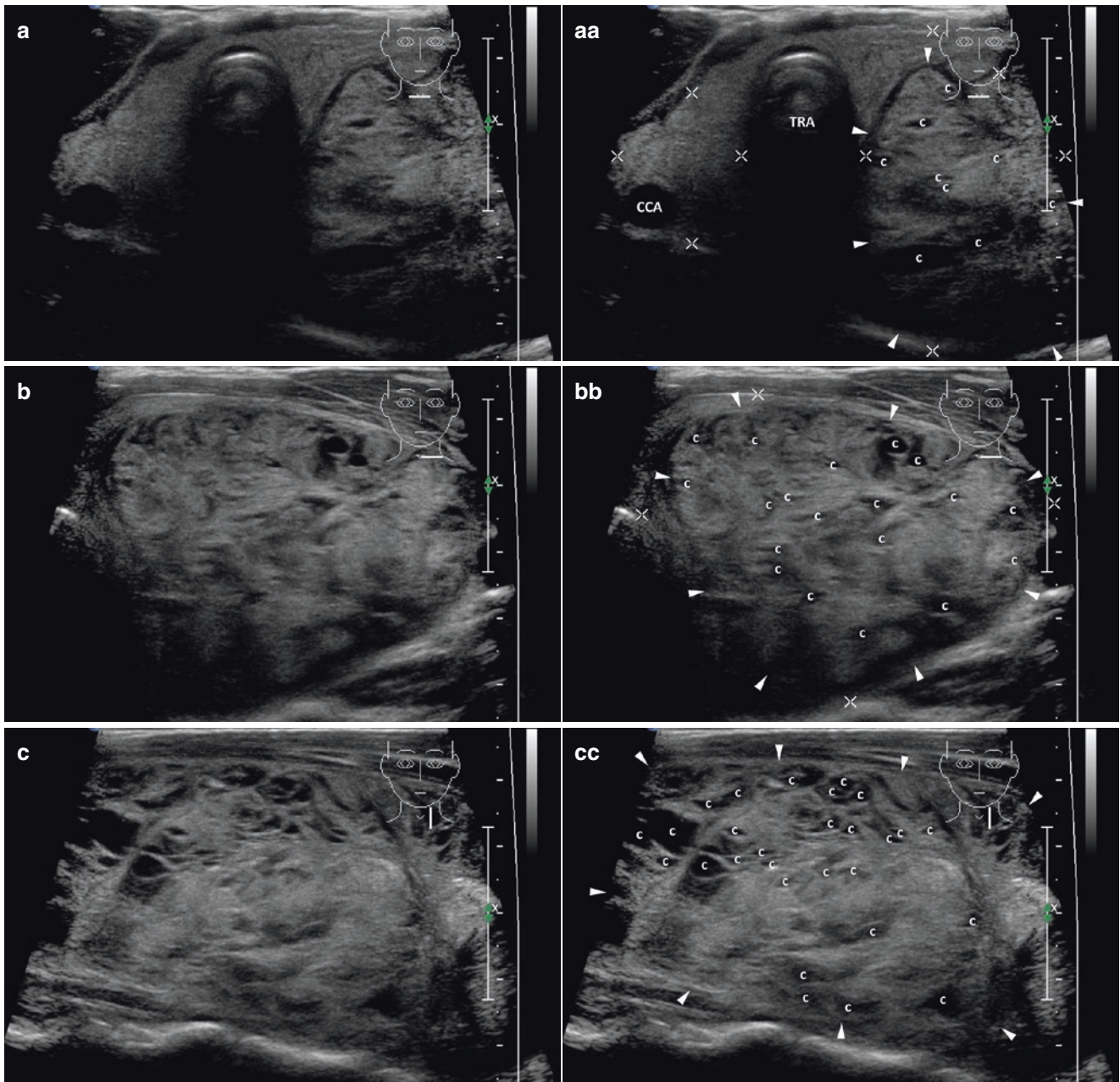


Fig. 9.3 (aa) A 37-year-old man with giant spongiform nodule (*arrowheads*), size $74 \times 57 \times 45$ mm and volume 99 mL in the LL: the solid part coarsened structure; hyperechoic; diffuse multiple small and tiny cystic cavities (*c*), some with hyperechoic septa; irregular halo sign; trachea pushed to the right side; Tvol 119 mL, asymmetry—RL 14 mL and LL 105 mL; transverse; depth of penetration 6 cm. (bb)

Detail of giant spongiform nodule (*arrowheads*): diffuse multiple small and tiny cystic cavities (*c*), some with hyperechoic septa; irregular halo sign; transverse. (cc) Detail of giant spongiform nodule (*arrowheads*): diffuse multiple small and tiny cystic cavities (*c*), some with hyperechoic septa; irregular halo sign; longitudinal

Fig. 9.2 (aa) A 69-year-old woman with large complex, predominantly solid nodule (*arrowheads*), size $45 \times 35 \times 20$ mm and volume 17 mL in the LL: inhomogeneous structure; hyperechoic; sporadic small and tiny cystic cavities (*c*); well-defined margin with thin halo sign; Tvol 29 mL, asymmetry—RL 5 mL and LL 24 mL; transverse. (bb) Detail of complex, predominantly solid nodule (*arrowheads*): sporadic small and tiny

cystic cavities (*c*); well-defined margin with thin halo sign; transverse. (cc) Detail of complex, predominantly solid nodule (*arrowheads*): sporadic small and tiny cystic cavities (*c*); well-defined margin with thin halo sign; longitudinal. (dd) Detail of complex, predominantly solid nodule (*arrowheads*), CFDS: avascular cystic cavities (*c*); increased peripheral vascularity and two intranodal vessel branches, *pattern II*; longitudinal

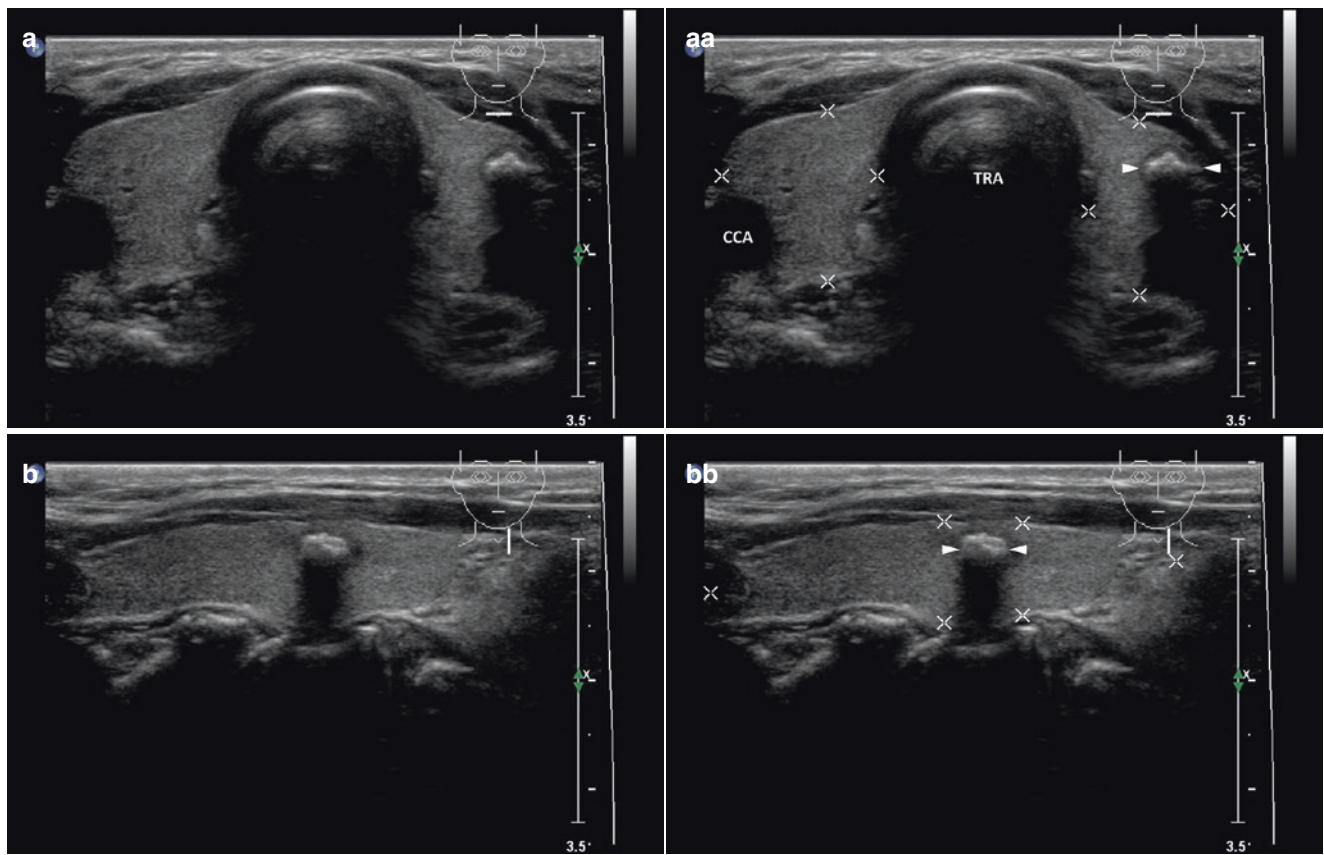


Fig. 9.4 (aa) A 58-year-old woman with a small complex nodule, size $5 \times 5 \times 4$ mm, volume 0.1 mL and intranodular coarse calcification (*arrowheads*) in the LL: coarse hyperechoic structure inside the nodule with prominent acoustic shadow; Tvol 9 mL, RL 5 mL, and LL 4 mL;

transverse. (bb) Detail of complex nodule with coarse intranodular calcification (*arrowheads*): coarse hyperechoic structure inside the nodule with prominent acoustic shadow; longitudinal

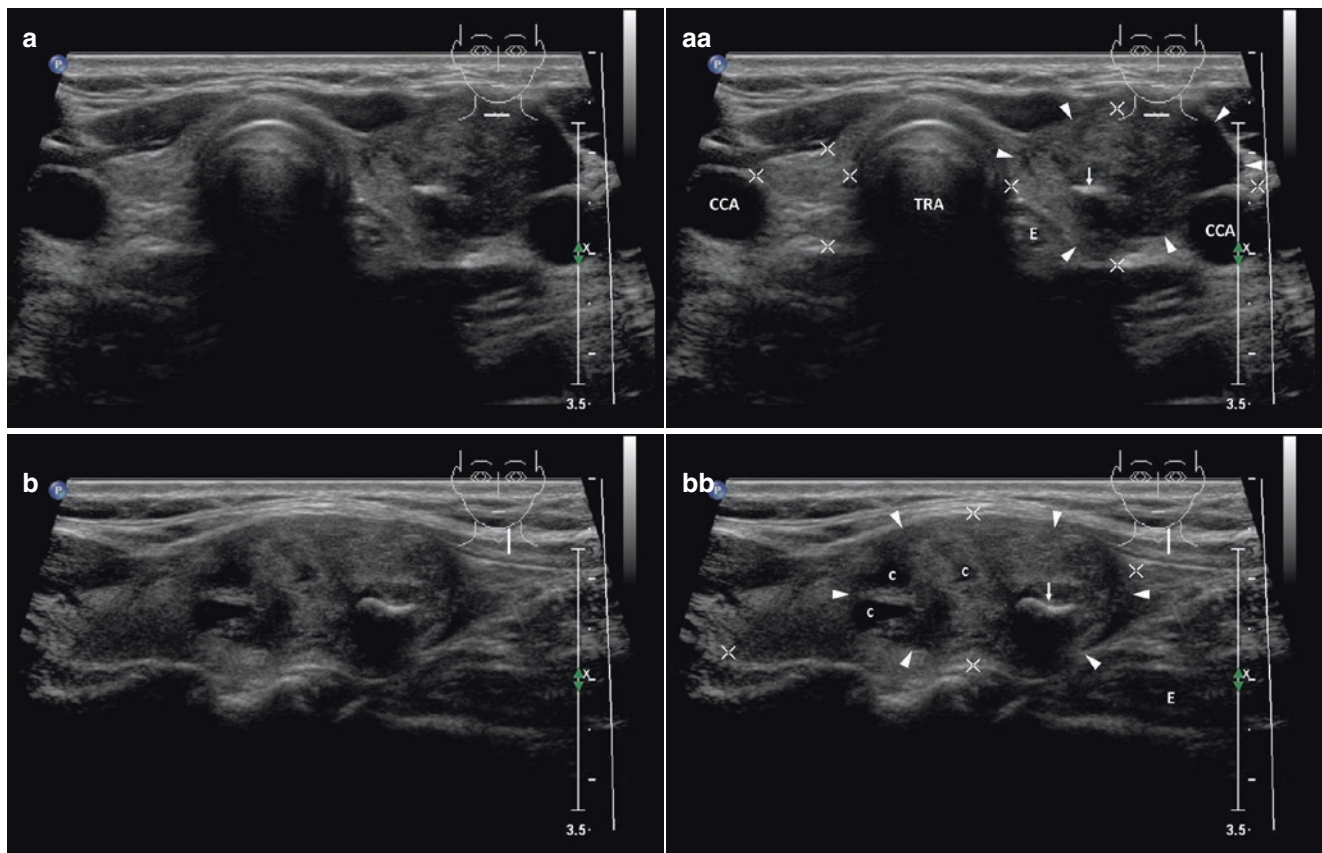


Fig. 9.5 (aa) A 51-year-old woman with a solitary medium-sized complex nodule (*arrowheads*), size $28 \times 18 \times 14$ mm, volume 3.5 mL and intranodular curvilinear calcification in the LL: round, inhomogeneous hyperechoic nodule; linear hyperechoic calcification (*closed arrow*) with acoustic shadow; Tvol 10 mL, asymmetry—RL 3 mL and

LL 7 mL; transverse. (bb) Detail of medium-sized complex nodule (*arrowheads*) with small cystic cavities (*c*) and intranodular curvilinear calcification: in the upper part two small cystic cavities; in the lower part curvilinear hyperechoic calcification (*arrow*) with acoustic shadow; longitudinal

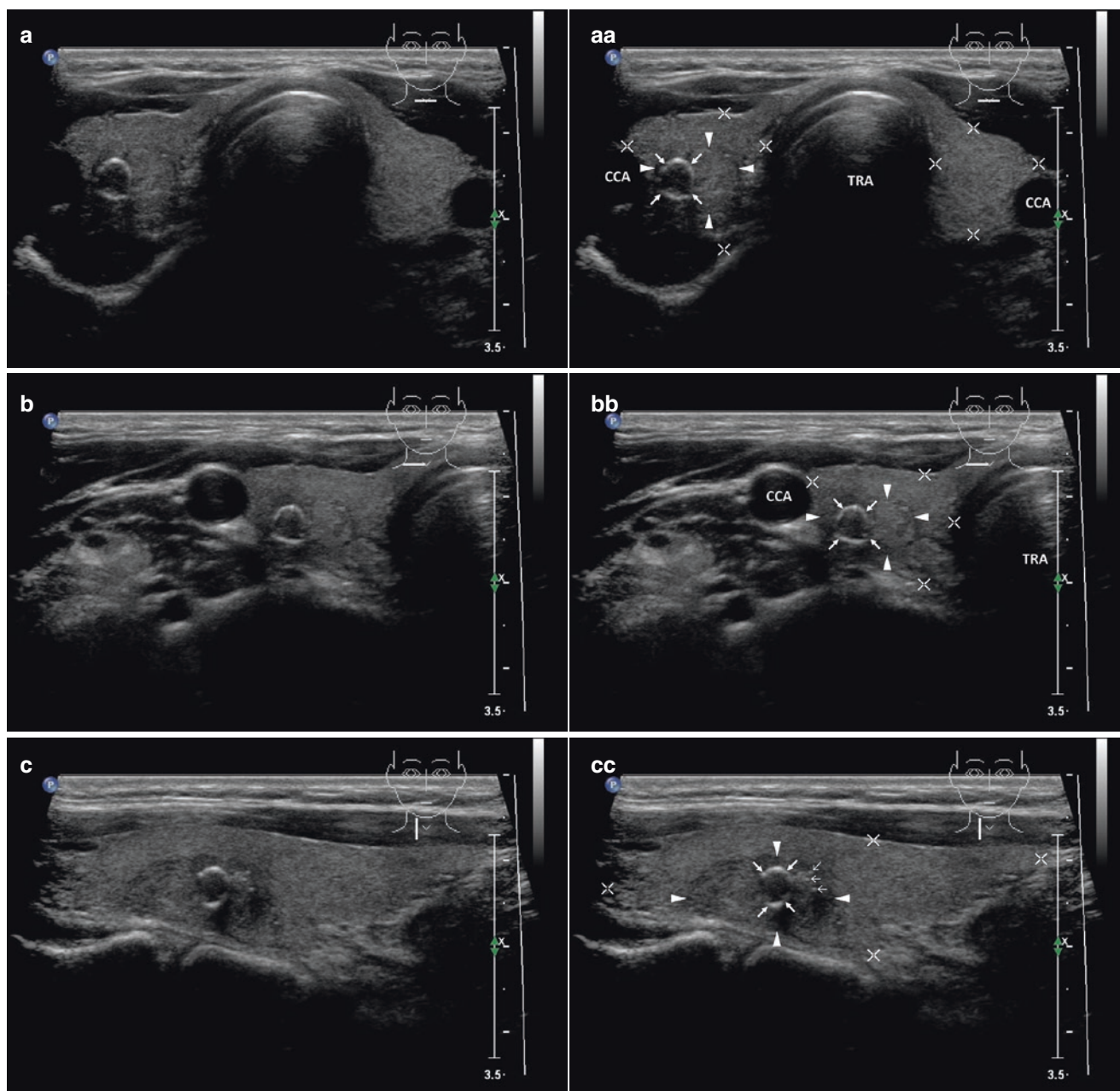


Fig. 9.6 (aa) A 40-year-old woman with a small complex nodule (arrowheads), size $18 \times 12 \times 8$ mm and volume 1 mL with intranodular “eggshell” calcification in the RL: ovoid shape, homogeneous, isoechoic nodule; at periphery small ring of calcification (arrows) with acoustic shadow; Tvol 12 mL, RL 7 mL, and LL 5 mL; transverse. (bb) Detail of complex nodule (arrowheads), with small intranodular “egg-

shell” calcification: small ring of calcification (arrows); transverse. (cc) Detail of complex nodule (arrowheads), with small intranodular “egg-shell” calcification: small ring of calcification (arrows); next to cluster of microcalcifications without acoustic shadow (open arrows); longitudinal

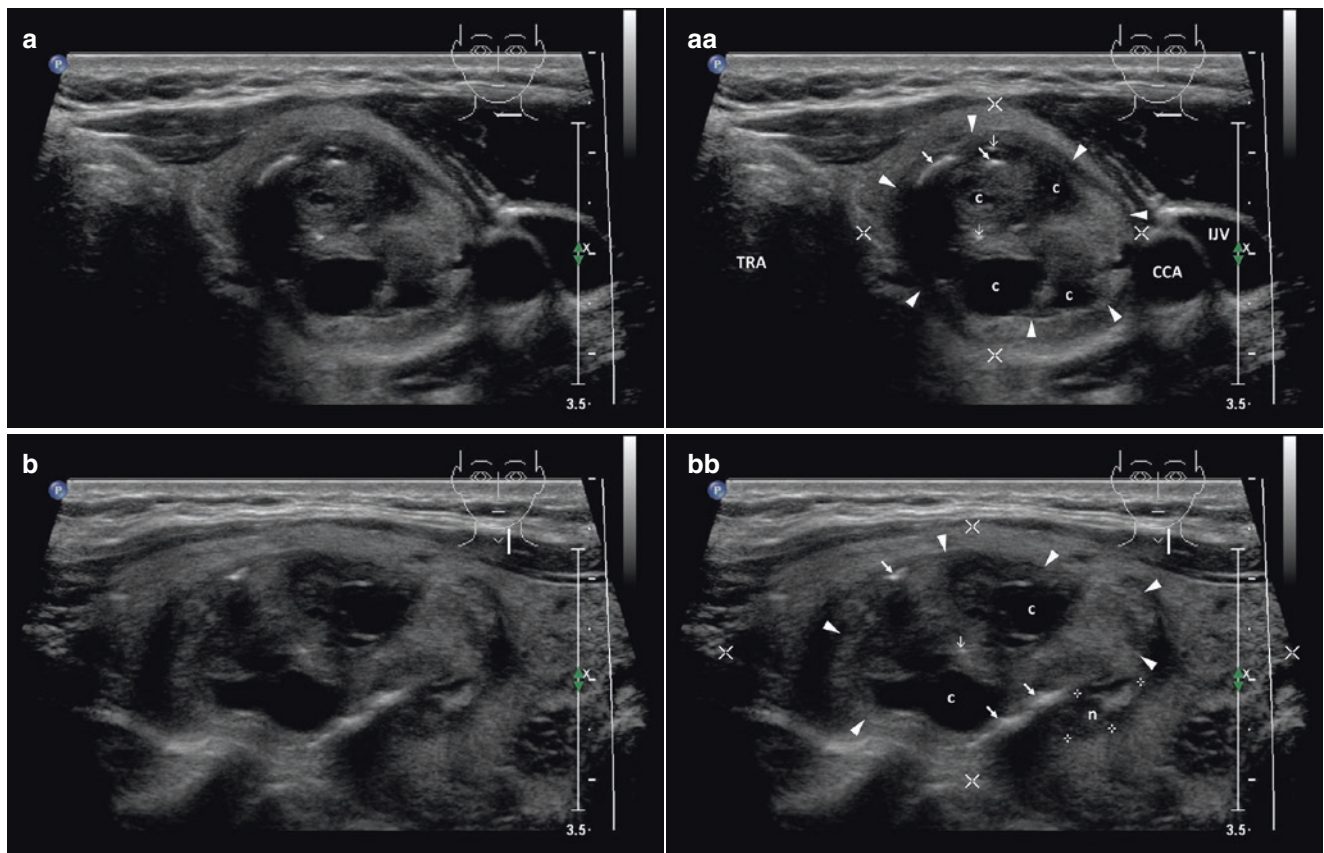


Fig. 9.7 (aa) A 49-year-old woman with large complex, predominantly solid nodule (*arrowheads*), size $38 \times 23 \times 22$ mm and volume 9 mL with peripheral curvilinear calcification in the LL: ovoid, inhomogeneous, hyperechoic nodule; curvilinear and dotted hyperechoic calcification (*arrows*) with acoustic shadow and sporadic microcalcifications (*open arrows*) at periphery and central part; several anechoic cystic

cavities (*c*); Tvol 33 mL, asymmetry—RL 10 mL and LL 23 mL; transverse. (bb) Detail of large complex nodule with peripheral curvilinear calcification: peripheral dotted and linear calcifications (*arrows*), microcalcification in central part (*open arrow*) and two intranodular cystic septated cavities (*c*); longitudinal

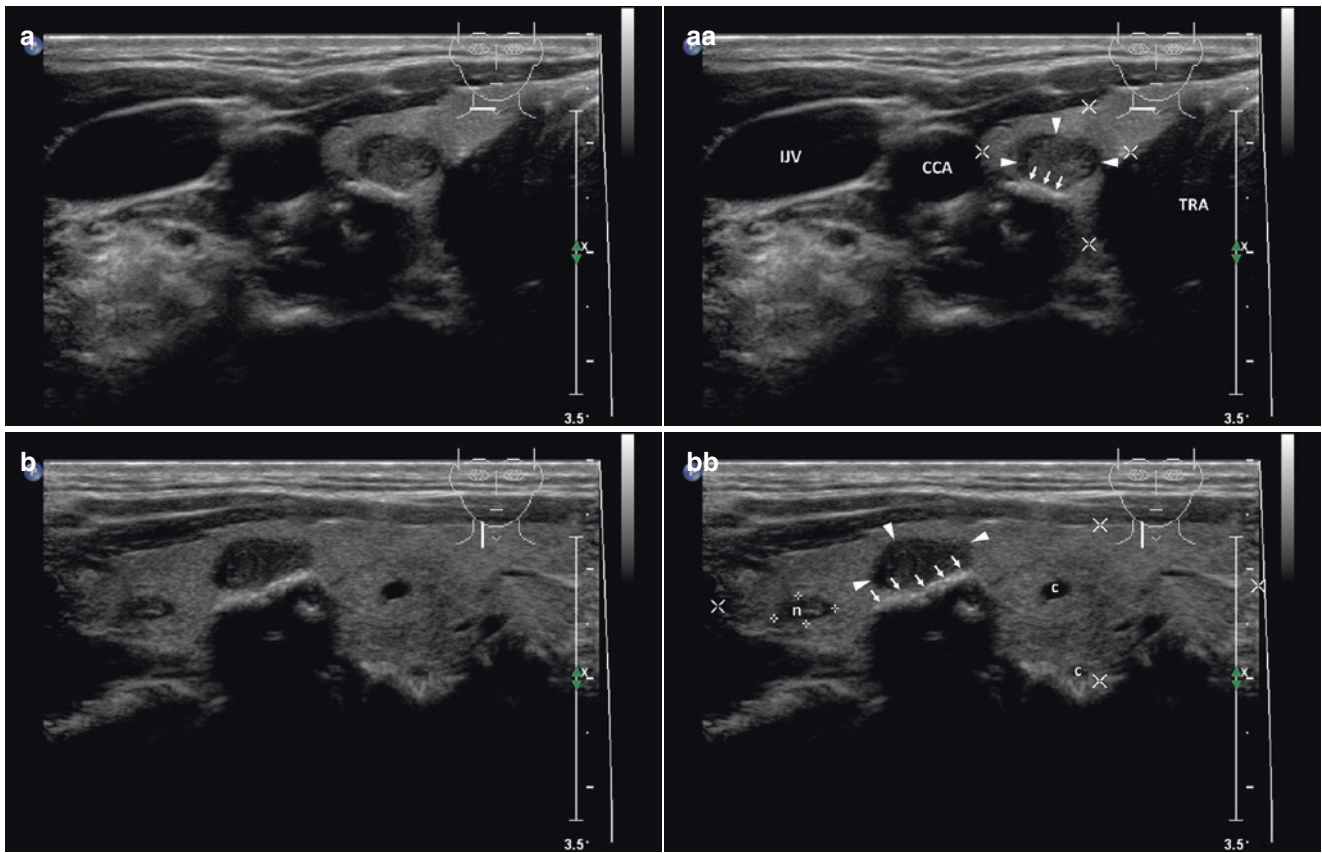


Fig. 9.8 (aa) A 47-year-old woman with a small solid nodule (*arrow-heads*), size $8 \times 7 \times 6$ mm and volume 0.2 mL with peripheral calcification in the RL: ovoid, homogeneous, isoechoic nodule with irregular thin halo sign; at the posterior part peripheral coarse linear calcification (*arrows*) with prominent acoustic shadow; RL 8 mL; transverse. (bb)

Detail of a small complex nodule with peripheral calcification: at the posterior part peripheral coarse linear calcification (*arrows*) with prominent acoustic shadow; another tiny nodule (*n*) and two tiny cystic cavities (*c*); longitudinal

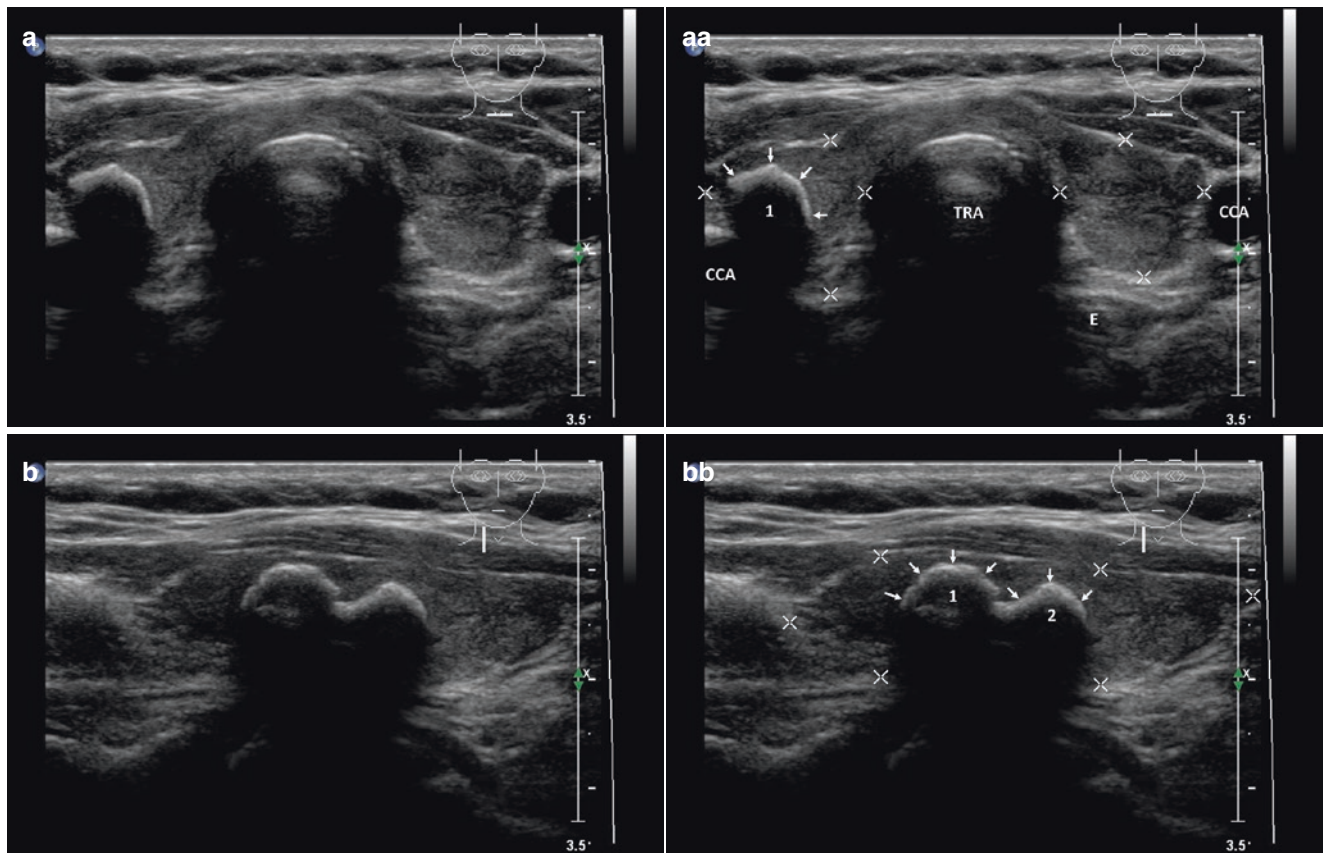


Fig. 9.9 (aa) A 61-year-old woman with a small solid nodule, size $8 \times 8 \times 8$ mm and volume 0.3 mL with peripheral “eggshell” calcification in the RL: nodule with peripheral arc calcification (arrows) and prominent acoustic shadow causing no visualization of intranodular structure; thyroid gland—Hashimoto’s thyroiditis with sporadic

hypoechoic micronodules; Tvol 8 mL, RL 4 mL, and LL 4 mL; transverse. (bb) Detail of two peripheral “eggshell” calcifications: two nodules with peripheral arc calcification (arrows) size 8 and 7 mm and prominent acoustic shadows causing no visualization of internal structure; longitudinal

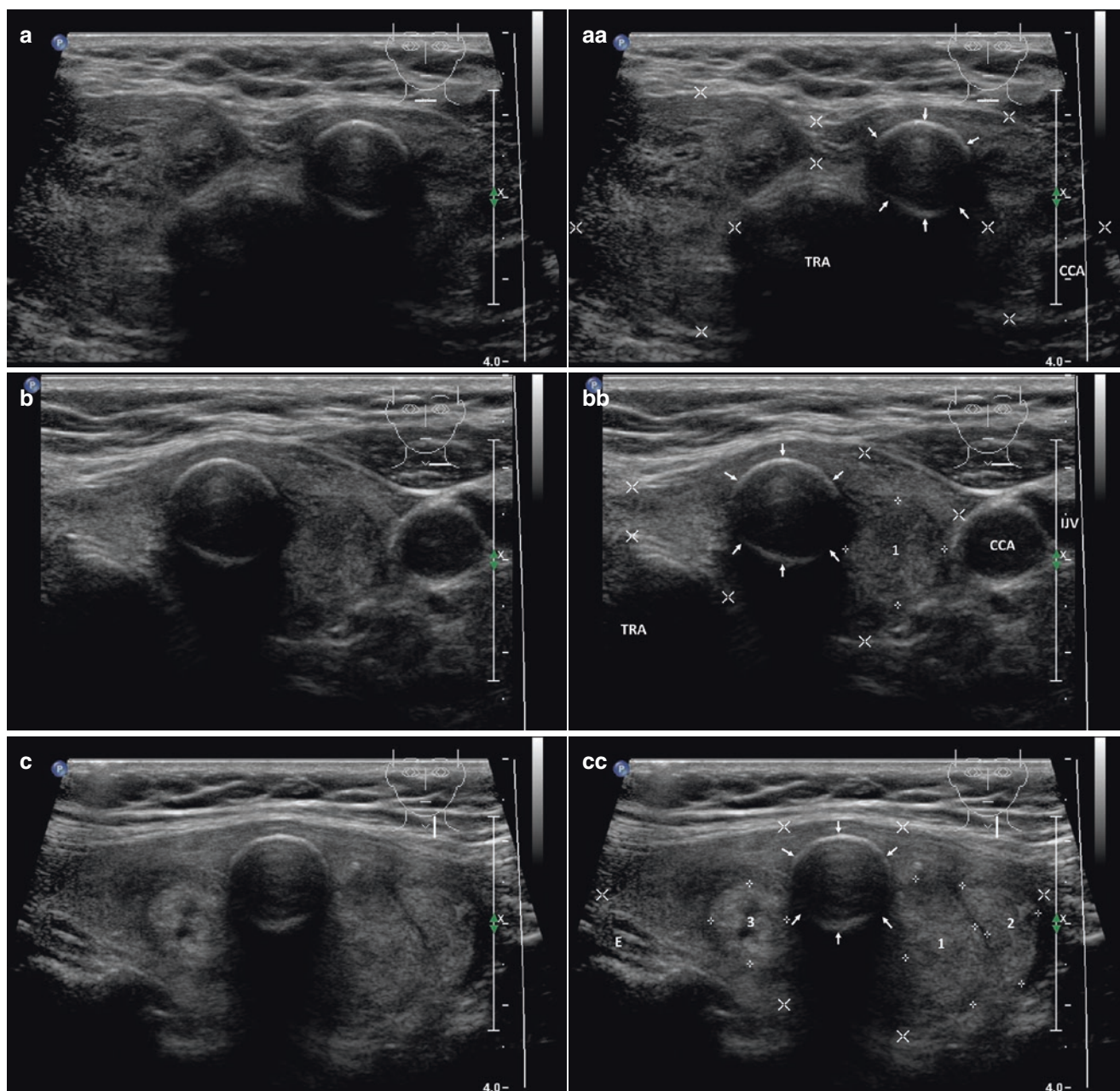


Fig. 9.10 (aa) A 71-year-old woman with multinodular goiter and complex nodule, size $16 \times 16 \times 15$ mm, volume 2 mL with peripheral “eggshell” calcification in the LL: rim peripheral calcification (arrows) with prominent acoustic shadow causing hypoechogenicity of intranodular structure; Tvol 51 mL, RL 26 mL, and LL 25 mL; transverse. (bb) Detail of peripheral “eggshell” calcification: rim peripheral calcifica-

tion (arrows) with prominent acoustic shadow; next to another solid, isoechoic nodule (1) with thin halo sign; transverse. (cc) Detail of peripheral “eggshell” calcification: rim peripheral calcification (arrows) with prominent acoustic shadow; next to three solid hyper-echoic nodules (1, 2, 3) with thin halo sign; longitudinal

References

1. Yasuda K, Ozaki O, Sugino K, Yamashita T, Toshima K, Ito K, et al. Treatment of cystic lesions of the thyroid by ethanol instillation. *World J Surg*. 1992;16(5):958–61.
2. Choi KU, Kim JY, Park DY, Lee CH, Sol MY, Han KT, et al. Recommendations for the management of cystic thyroid nodules. *ANZ J Surg*. 2005;75(7):537–41.
3. McHenry CR, Slusarczyk SJ, Khiyami A. Recommendations for management of cystic thyroid disease. *Surgery*. 1999;126(6):1167–71. discussion 1171–2.
4. Haugen BR, Alexander EK, Bible KC, Doherty GM, Mandel SJ, Nikiforov YE, et al. 2015 American Thyroid Association Management Guidelines for Adult Patients with Thyroid Nodules and Differentiated Thyroid Cancer: The American Thyroid Association Guidelines Task Force on Thyroid Nodules and Differentiated Thyroid Cancer. *Thyroid*. 2016;26(1):1–133.
5. Brito JP, Gionfriddo MR, Al Nofal A, Boehmer KR, Leppin AL, Reading C, et al. The accuracy of thyroid nodule ultrasound to predict thyroid cancer: systematic review and meta-analysis. *J Clin Endocrinol Metab*. 2014;99(4):1253–63.
6. Yoon DY, Lee JW, Chang SK, Choi CS, Yun EJ, Seo YL, et al. Peripheral calcification in thyroid nodules: ultrasonographic features and prediction of malignancy. *J Ultrasound Med*. 2007;26(10):1349–55. quiz 1356–7.
7. Moon WJ, Jung SL, Lee JH, Na DG, Baek JH, Lee YH, et al. Thyroid Study Group, Korean Society of Neuro- and Head and Neck Radiology Benign and malignant thyroid nodules: US differentiation—multicenter retrospective study. *Radiology*. 2008;247(3):762–70.
8. Wang N, Xu Y, Ge C, Guo R, Guo K. Association of sonographically detected calcification with thyroid carcinoma. *Head Neck*. 2006;28(12):1077–83.
9. Frates MC, Benson CB, Doubilet PM, Kunreuther E, Contreras M, Cibas ES, et al. Prevalence and distribution of carcinoma in patients with solitary and multiple thyroid nodules on sonography. *J Clin Endocrinol Metab*. 2006;91(9):3411–7.

10.1 Essential Facts

- Multinodular goiter (MNG) usually means an enlarged thyroid gland containing multiple thyroid nodules. In adults, the normal thyroid gland has a maximum weight of 18–25 g [1].
- In the 1950s, in the era before the ultrasound, prevalence of thyroid nodules at autopsy was: multiple thyroid nodules 37.3%, and solitary nodules 12.2% [2].
- At the end of the twentieth century, in the era of ultrasound, prevalence of thyroid nodularity at autopsy ranged from 30–60%, prevalence on palpation was 13–50%, and US imaging reported prevalence 19–67% [3].
- The risk of malignancy of thyroid nodules occurring within a MNG is the same as in solitary nodule [4].
- Nodules larger than 4 cm in size have 19.3% risk of malignancy [5].
- Surgery is the treatment of first choice in patients with a large MNG. However, in the case of patient ineligibility or preference, radioiodine ^{131}I -therapy (RIT) may be an option. There is a greater effect of RIT on diffuse goiter than on MNG.
- The study by Bonnema et al. followed up with 34 patients with large non-toxic diffuse goiter absent of nodules on ultrasound. They were indicated to RIT for presence of cervical compression and/or cosmetic discomfort. Goiter

volume was reduced from 67.9 ± 28.5 mL to 43.4 ± 18.7 mL after 3 months. By 6 months the goiter volume halved, and on average 3 years post-RIT only $28.1 \pm 2.0\%$ patients remained with same size goiter as initially. However, 36% of patients had become hypothyroid after these 3 years [6].

- RIT has a favorable effect on tracheal compression and inspiratory capacity, but the reduction of Tvol in MNG is only 30–40% [7].

10.2 US Features of Multinodular Goiter

- MNG contains solid (Figs. 10.1bb, 10.3aa), complex (Figs. 10.2bb, 10.3bb), or cystic nodules (Fig. 10.5cc); *see more in Chaps. 7, 8, and 9.*
- Total volume measurement (Tvol) by US is less accurate for large goiters; the Tvol of very large goiter (150–200 ml) can be underestimated by approximately 20%.
- For very large (Fig. 10.4bb) or retrosternal goiters (weight > 100 g, or larger than 150–200 mL), MRI should be preferable method to measure Tvol (with inter- and intra-observer variability 2–4%) [7].
- US-FNAB should be performed in dominant (Fig. 10.6bb) or large nodules; *see more at Chap. 24, Table 24.1* [8].

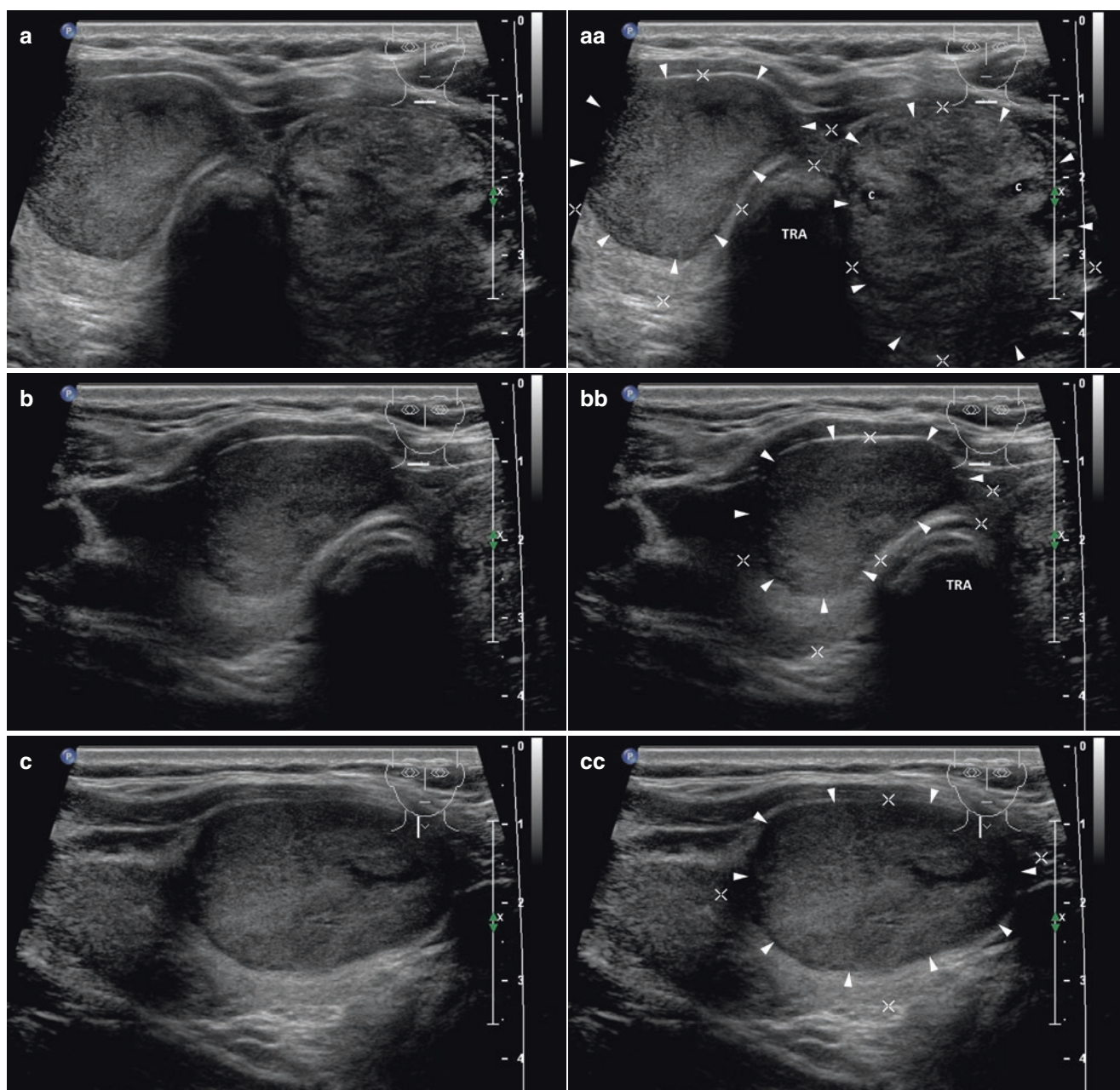


Fig. 10.1 (aa) A 54-year-old man with a large multinodular goiter. Medium-sized solid nodule, size $33 \times 28 \times 17$ mm and volume 8 mL in the RL and large, complex, predominantly solid nodule, size $43 \times 33 \times 31$ mm and volume 23 mL in the LL. US overall view: solid nodule (*arrowheads*)—ovoid shape; homogeneous structure; isoechoic; well-defined margin; complex nodule (*arrowheads*)—round shape; coarse structure; hyperechoic; sporadic small cystic cavities (*c*); well-defined margin with thin halo sign; Tvol 57 mL, asymmetry—RL 20 mL and LL 37 mL; transverse, depth of penetration 5 cm. (bb) Detail of medium-sized solid nodule (*arrowheads*) in the RL: ovoid

shape; homogeneous structure; isoechoic; well-defined margin; transverse. (cc) Detail of medium-sized solid nodule (*arrowheads*) in the RL: ovoid shape; homogeneous structure; isoechoic; well-defined margin; longitudinal. (dd) Detail of large complex nodule (*arrowheads*) in the LL: round shape; coarse structure; hyperechoic; sporadic small cystic cavities (*c*); well-defined margin with thin halo sign; transverse. (ee) Detail of large complex nodule (*arrowheads*) in the LL: round shape; coarse structure; hyperechoic; sporadic small cystic cavities (*c*); well-defined margin with thin halo sign; longitudinal

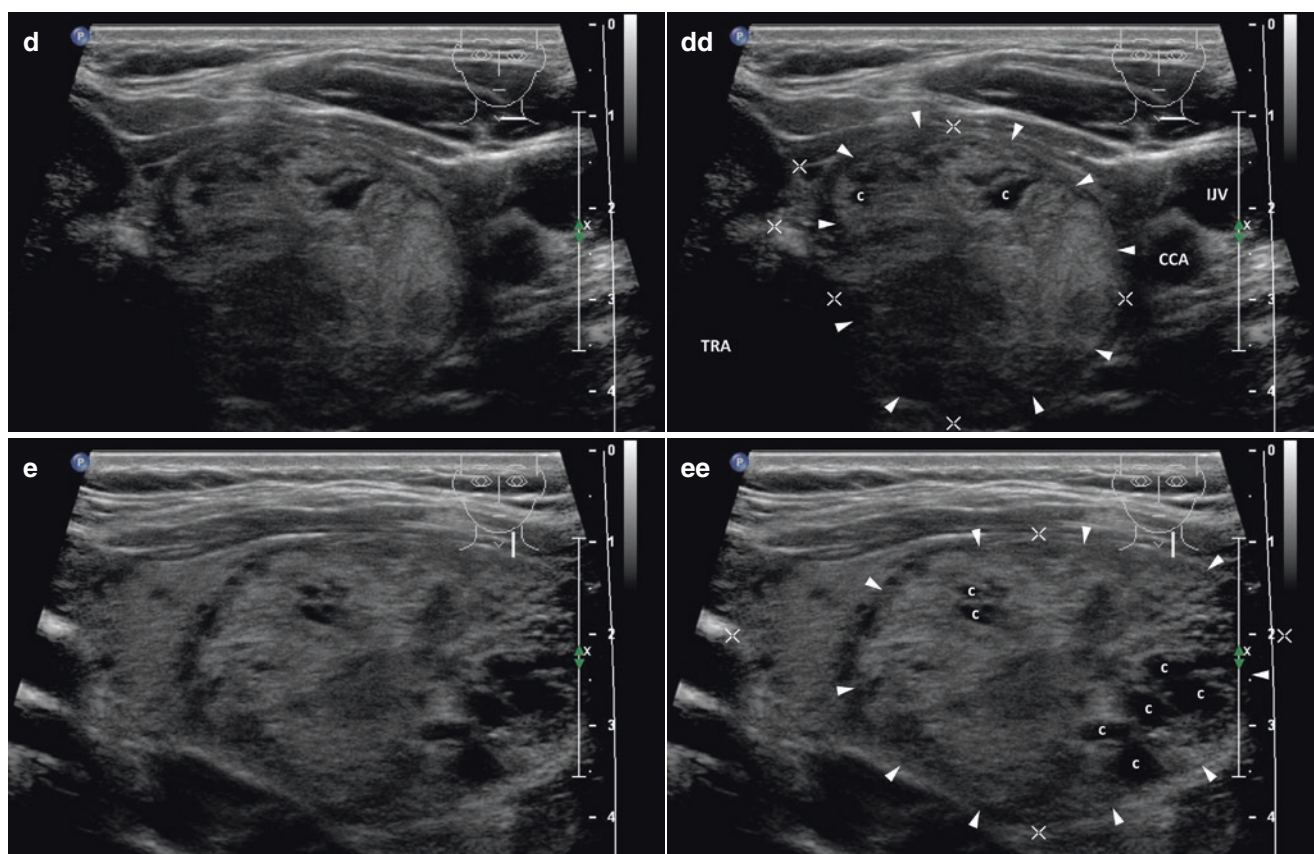


Fig. 10.1 (continued)

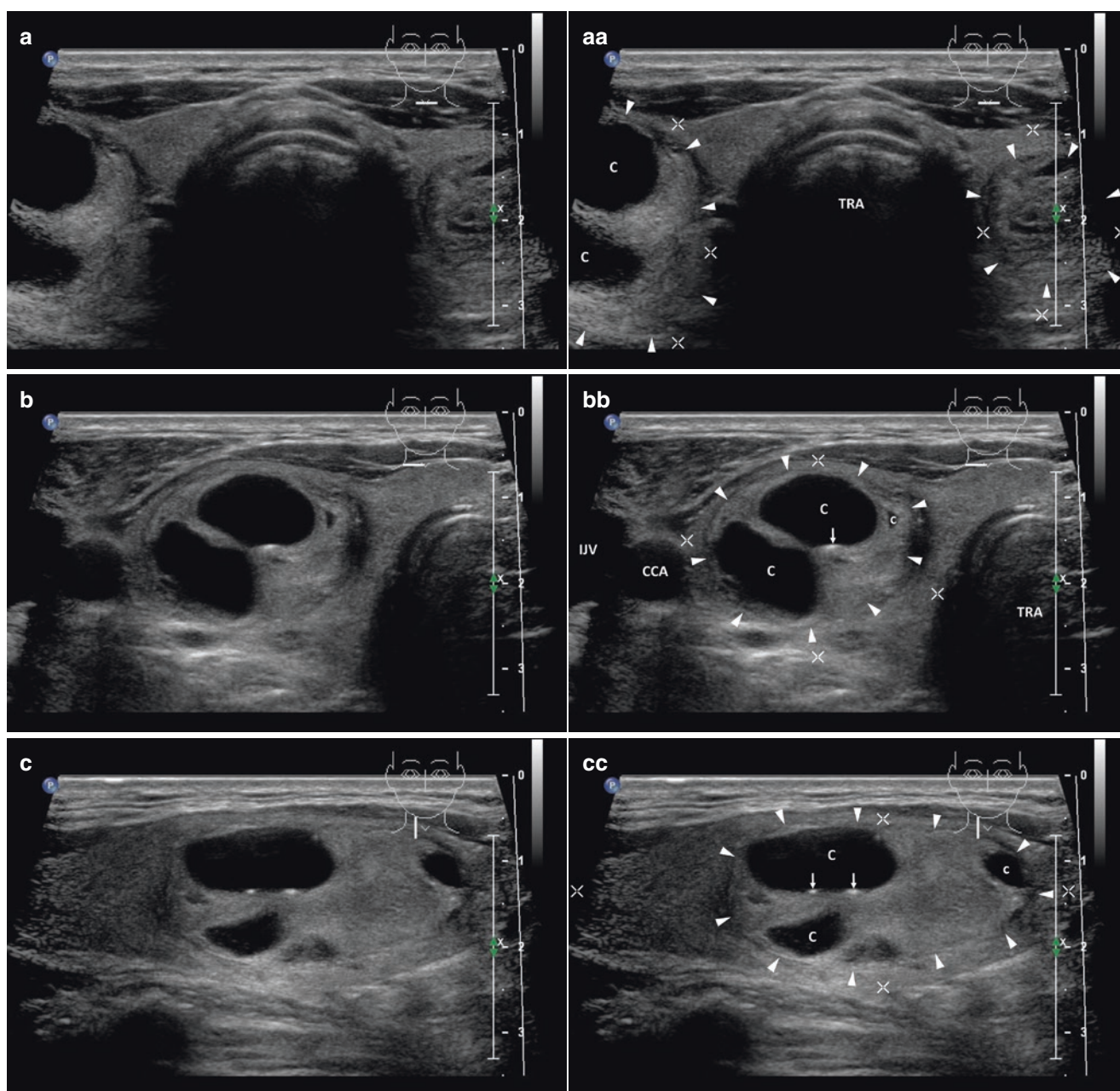


Fig. 10.2 (aa) A 51-year-old man with a large multinodular goiter. Medium-sized, complex, predominantly cystic nodule, size $38 \times 26 \times 19$ mm and volume 10 mL in the RL and small, complex, predominantly solid nodule, size $20 \times 19 \times 15$ mm and volume 3 mL in the LL. US overall view: complex, predominantly cystic nodule (*arrowheads*)—ovoid shape; inhomogeneous structure; hyperechoic; sporadic large cystic cavities (C); well-defined margin; complex, predominantly solid nodule (*arrowheads*)—round shape; coarse structure; hyperechoic; sporadic small cystic cavities (c); Tvol 34 mL, asymmetry—RL 21 mL and LL 13 mL; transverse, depth of penetration 4 cm. (bb) Detail of medium-sized complex nodule (*arrowheads*) in the RL: ovoid shape; inhomogeneous structure; hyperechoic; two large cystic cavities

(C); small dotted and linear calcifications in the cavity wall (*arrows*); well-defined margin with halo sign; transverse. (cc) Detail of medium-sized complex nodule (*arrowheads*) in the RL: ovoid shape; inhomogeneous structure; hyperechoic; three cystic cavities (C), (c); small dotted and linear calcifications at the wall of cavity (*arrows*); well-defined margin with halo sign; longitudinal. (dd) Detail of small complex nodule (*arrowheads*) in the LL: round shape; coarse structure; hyperechoic; sporadic small cystic cavities (c); well-defined margin with thin halo sign; transverse. (ee) Detail of small complex nodule (*arrowheads*) in the LL: round shape; coarse structure; hyperechoic; sporadic small cystic cavities (c); well-defined margin with thin halo sign; longitudinal

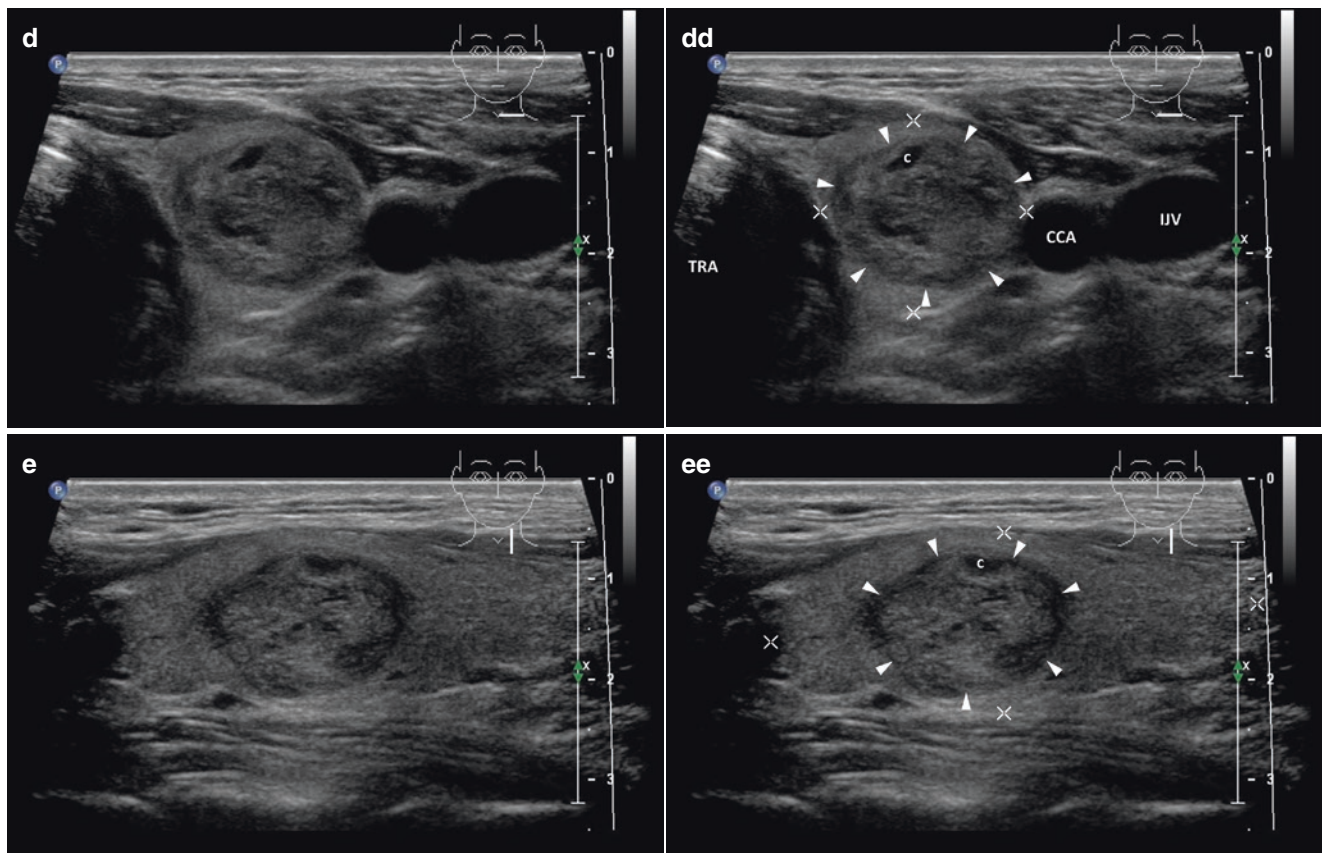


Fig. 10.2 (continued)

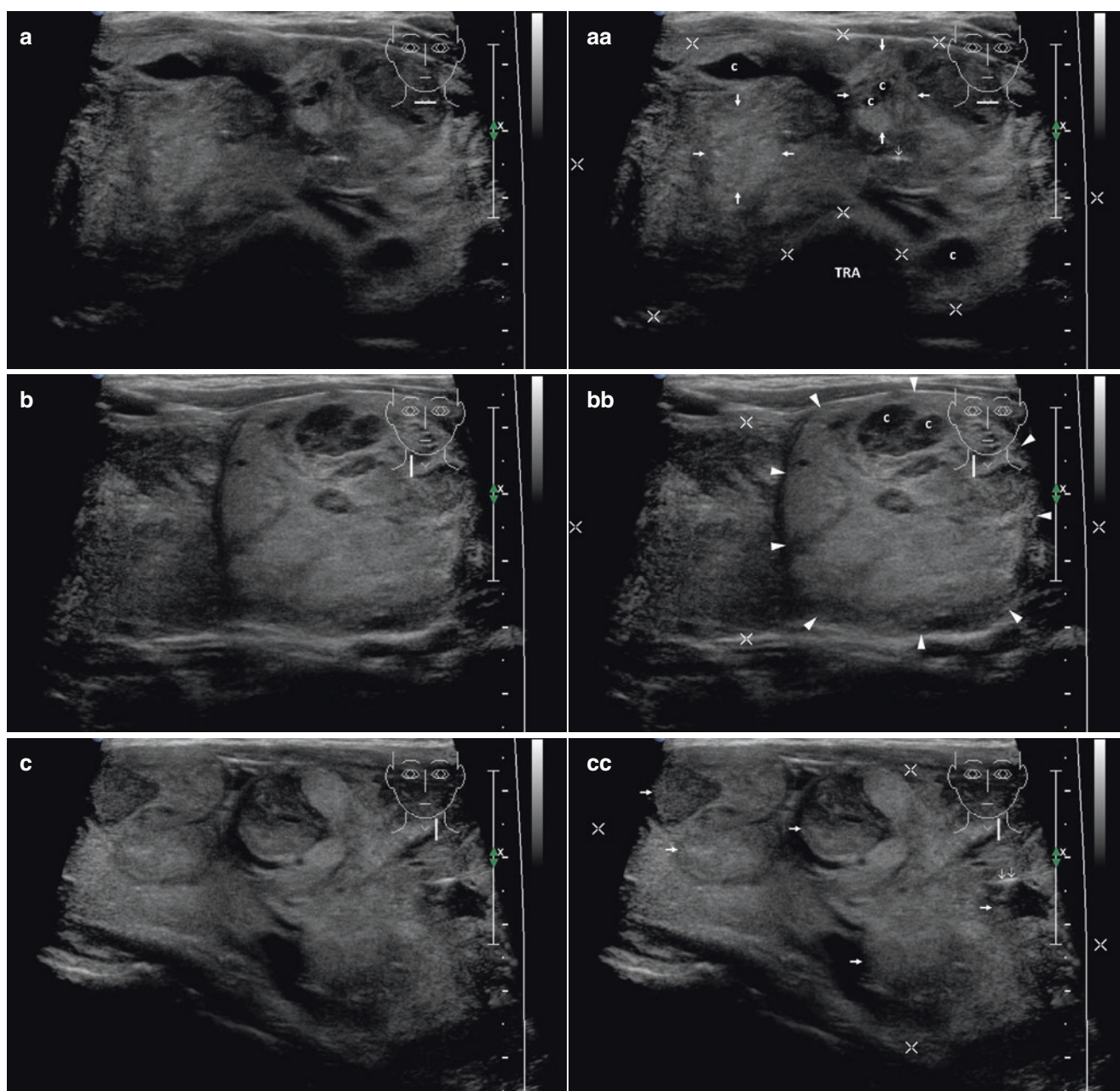
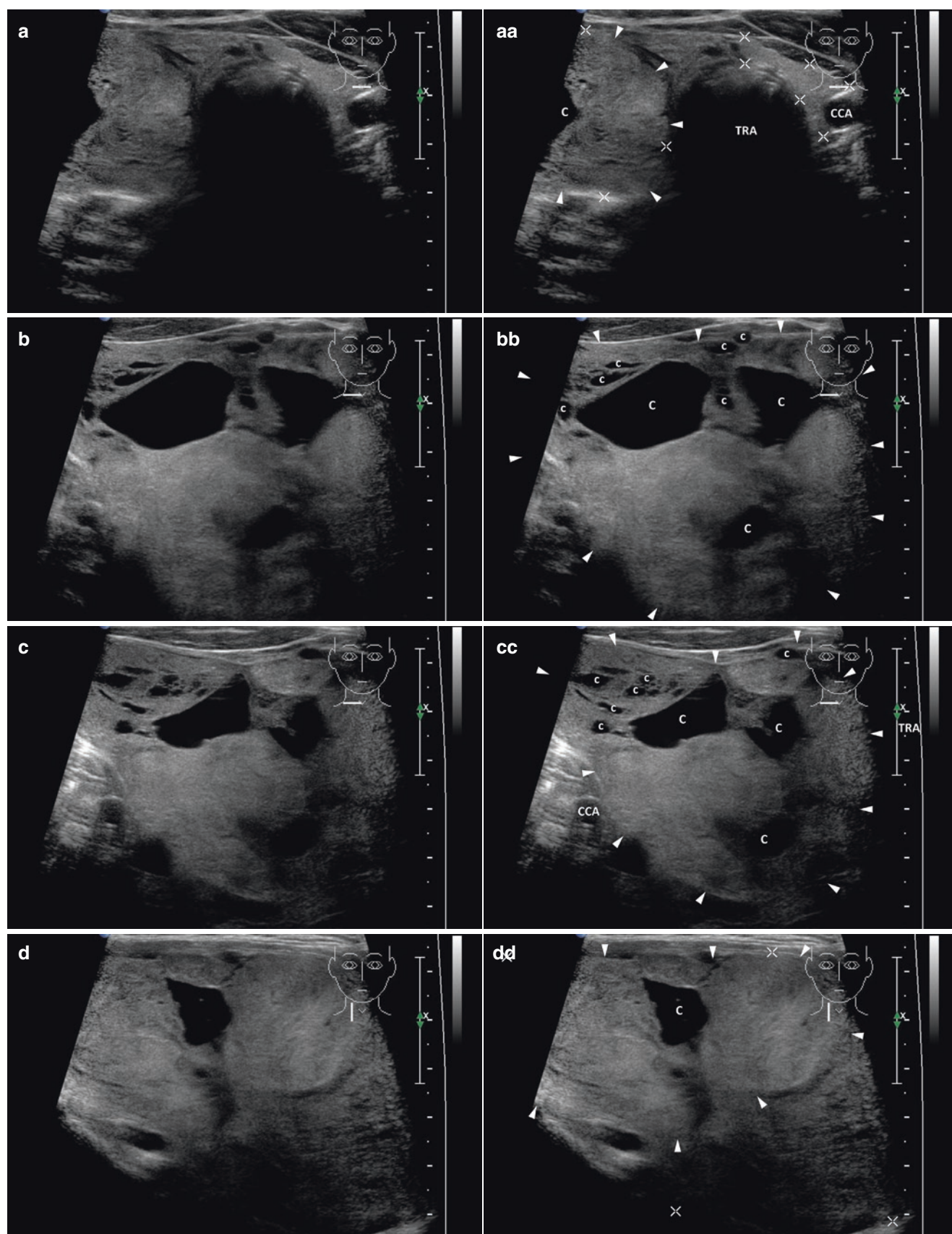


Fig. 10.3 (aa) A 32-year-old man with a giant multinodular goiter, diffusely solid and complex nodules, fairly broad isthmus, trachea pushed dorsally. US overall view: diffusely coarse structure; hyperechoic; solid and complex nodules (arrows) with cystic cavities (c) and microcalcification (open arrow), size from 10 to 30 mm; Tvol 145 mL, asymmetry—RL 95 mL and LL 50 mL, isthmus 30 mm; transverse; depth of penetration 6 cm. (bb) Detail of large complex nodule (arrow-

heads), size 32 × 30 × 28 mm and volume 13 mL in the RL: round shape; coarse structure; hyperechoic; small cystic cavities (c); well-defined margin with thin halo sign; longitudinal. (cc) Detail of the LL with several solid and complex nodules (arrows): round or ovoid shape; inhomogeneous structure; hyperechoic; small cystic cavities (c); linear calcification (open arrow); longitudinal

Fig. 10.4 (aa) A 60-year-old man with a multinodular goiter, giant RL sized approximately 100 × 70 × 50 mm and hypoplastic LL. Trachea pushed to the left side. US overall view: RL—coarse structure; hyperechoic; large cystic cavity (C); LL—homogeneous structure, isoechoic; Tvol 200 mL, asymmetry—RL 195 mL and LL 5 mL, transverse; depth of penetration 7 cm. (bb) Detail of giant RL: coarse structure; hyper-

echoic; large and tiny cystic cavities (C), (c); transverse. (cc) Detail of giant RL: diffuse coarse structure; hyperechoic; large and tiny cystic cavities (C), (c); another transverse view. (dd) Detail of giant RL with large complex nodule (arrowheads): coarse structure; hyperechoic; large cystic cavity (C); longitudinal



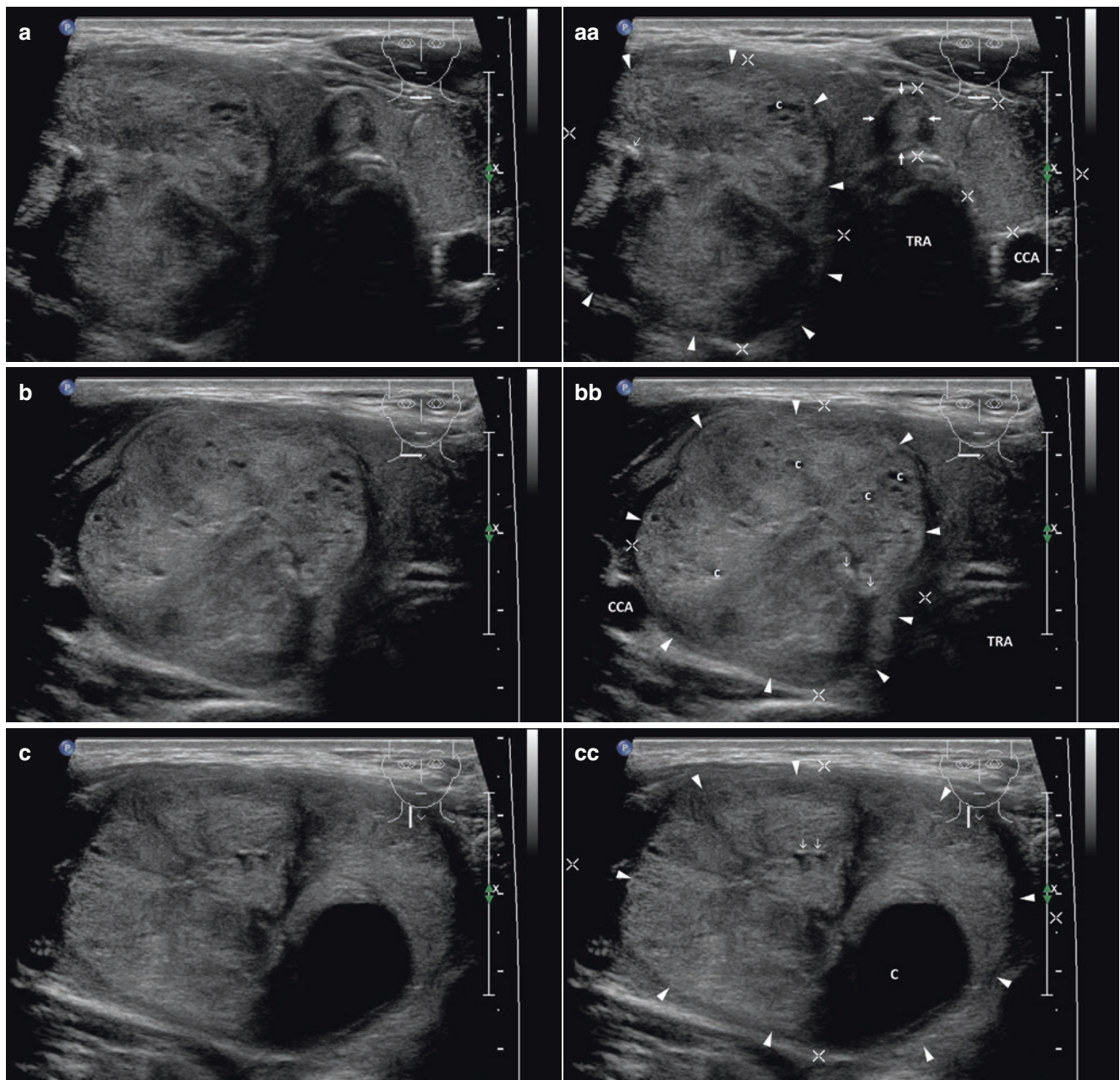


Fig. 10.5 (aa) A 49-year-old man with a large multinodular goiter. Large complex predominantly solid nodule, size $38 \times 36 \times 31$ mm and volume 22 mL in the RL. Trachea pushed to the left side. US overall view: large nodule (*arrowheads*)—round shape; coarse structure; hyperechoic; small cystic cavities (*c*); dotted calcification (*open arrow*); well-defined margin with thin halo sign; small solid hyperechoic nodule (*arrows*) with thin halo sign in isthmus; Tvol 63 mL, asymmetry—RL 55 mL and LL 7 mL, isthmus 10 mm; transverse, depth of

penetration 5 cm. (bb) Detail of large complex nodule in the RL: round shape; coarse structure; hyperechoic; small cystic cavities (*c*); dotted calcification (*open arrows*); well-defined margin with thin halo sign; transverse. (cc) Detail of large complex nodule in the RL: ovoid shape; coarse structure; hyperechoic; large cystic cavity (*C*); dotted calcification (*open arrows*); well-defined margin with thin halo sign; longitudinal

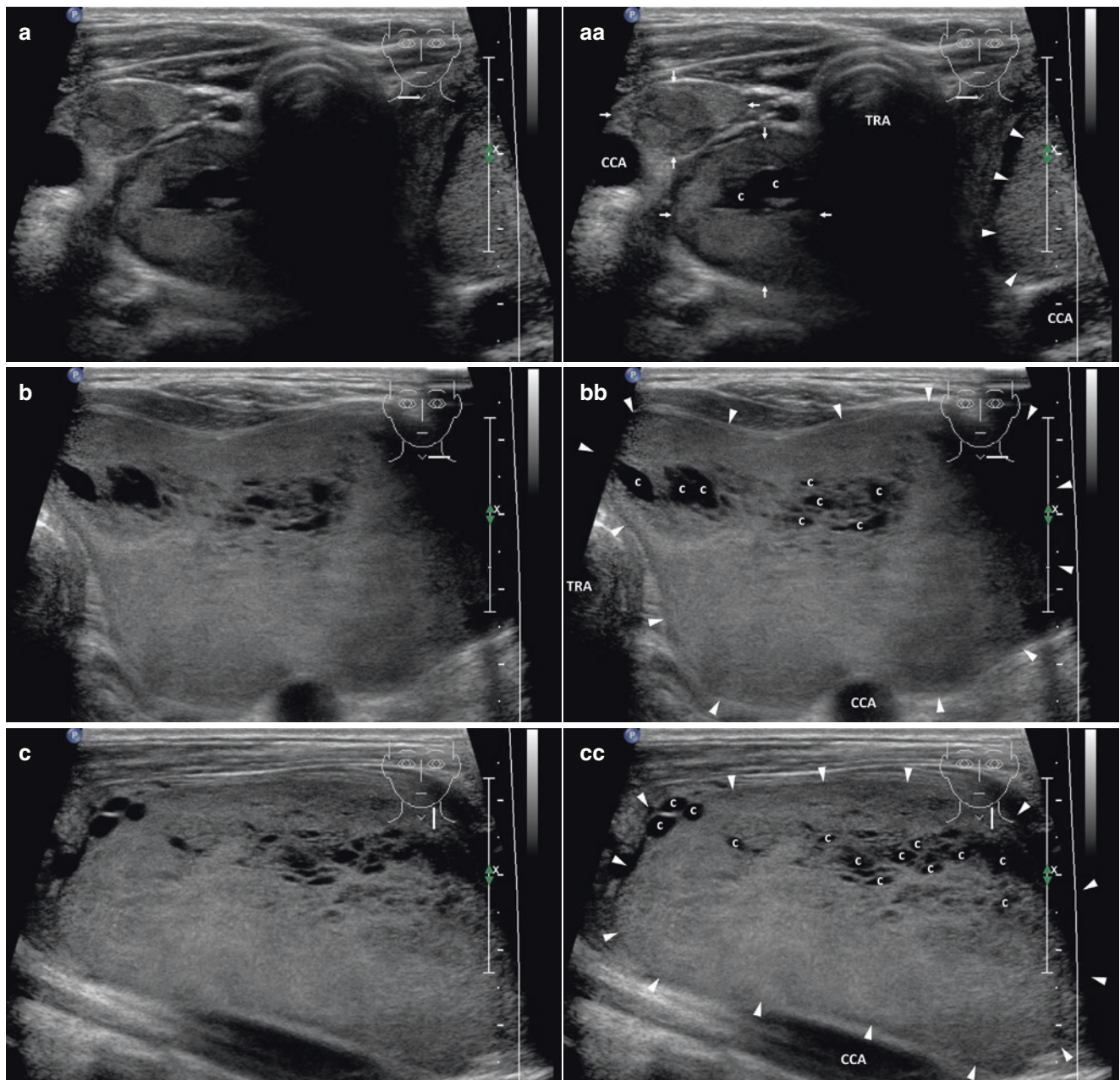


Fig. 10.6 (aa) A 48-year-old man with a multinodular goiter and giant complex nodule, volume 69 mL in the LL. Trachea pushed to the right side. US detail of the RL: solid nodule (*arrows*), volume 5 mL—elliptical shape; inhomogeneous structure; hyperechoic; sporadically tiny cystic cavities; complex predominantly solid nodule (*arrows*), volume 11 mL—round shape; inhomogeneous structure; hyperechoic; small cystic cavities (*c*); part of giant complex nodule (*arrowheads*) in the LL; Tvol 105 mL, asymmetry—RL 31 mL and LL 73 mL, isthmus

10 mm; transverse, depth of penetration 5 cm. (bb) Detail of giant complex, predominantly solid nodule, size 61 × 59 × 37 mm and volume 69 mL in the LL: round shape; inhomogeneous structure; markedly hyperechoic; spongiform band of multiple small and tiny cystic cavities (*c*); transverse. (cc) Detail of giant complex, predominantly solid nodule in the LL: round shape; inhomogeneous structure; markedly hyperechoic; spongiform band of multiple small and tiny cystic cavities (*c*); longitudinal

References

1. Finke R, Schleusener H, Hierholzer K. The thyroid gland. In: Greger R, Windhorst U, editors. *Comprehensive human physiology: from cellular mechanisms to integration*. New York: Springer; 2013. p. 453.
2. Mortensen JD, Woolner LB, Bennett WA. Gross and microscopic findings in clinically normal thyroid glands. *J Clin Endocrinol Metab*. 1955;15(10):1270–80.
3. Tan GH, Gharib H. Thyroid incidentalomas: management approaches to nonpalpable nodules discovered incidentally on thyroid imaging. *Ann Intern Med*. 1997;126(3):226–31.
4. Tollin SR, Mery GM, Jelveh N, Fallon EF, Mikhail M, Blumenfeld W, Perlmutter S. The use of fine-needle aspiration biopsy under ultrasound guidance to assess the risk of malignancy in patients with a multinodular goiter. *Thyroid*. 2000;10(3):235–41.
5. McCoy KL, Jabbour N, Ogilvie JB, Ohori NP, Carty SE, Yim JH. The incidence of cancer and rate of false-negative cytology in thyroid nodules greater than or equal to 4 cm in size. *Surgery*. 2007;142(6):837–44. discussion, 844 e1–3.
6. Bonnema SJ, Nielsen VE, Hegedüs L. Long-term effects of radioiodine on thyroid function, size and patient satisfaction in non-toxic diffuse goitre. *Eur J Endocrinol*. 2004;150(4):439–45.
7. Bonnema SJ, Bartalena L, Toft AD, Hegedüs L. Controversies in radioiodine therapy: relation to ophthalmopathy, the possible radio-protective effect of antithyroid drugs, and use in large goitres. *Eur J Endocrinol*. 2002;147(1):1–11.
8. Haugen BR, Alexander EK, Bible KC, Doherty GM, Mandel SJ, Nikiforov YE, et al. 2015 American Thyroid Association Management Guidelines for adult patients with thyroid nodules and differentiated thyroid cancer: The American Thyroid Association Guidelines Task Force on Thyroid Nodules and Differentiated Thyroid Cancer. *Thyroid*. 2016;26(1):1–133.

11.1 Essential Facts

- According to the most commonly used definition, the substernal goiter (SSG) or retrosternal goiter (RSG) is one with more than 50% of its mass lying below the thoracic inlet [1].
- Prevalence of SSG (depending of definition) ranges from 2–19% among all patients with a goiter [2].
- Intrathoracic goiters account for 3.1–5.8% of all mediastinal masses [3].
- Primary SSG (Fig. 11.1aa) (an ectopic thyroid tissue detached from a cervical thyroid mass, receiving blood supply from mediastinal vessel) is very rare (1%). Secondary SSG (Fig. 11.2aa) is more common as a part of multinodular goiter, with its portion extending retrosternally [4].
- Patients are generally in the fifth decade of life, and women predominate.
- Many patients experience dysphagia (52%), shortness of breath (52%), voice issues (11%), and chest pressure (12%) [5].
- In a large analysis of 80 patients with SSG, postoperative histology revealed multinodular goiter in 51%, follicular adenoma in 35%, Hashimoto's thyroiditis in 5%, and occult papillary carcinoma 1.6% [6].
- Some prospective studies document the incidence of carcinoma development in SSG at 1.3–3.7 new cases per 1000 patients [7].
- The incidence of thyroid cancer in SSG is not higher than the incidence of cancer in cervical goiters [8].

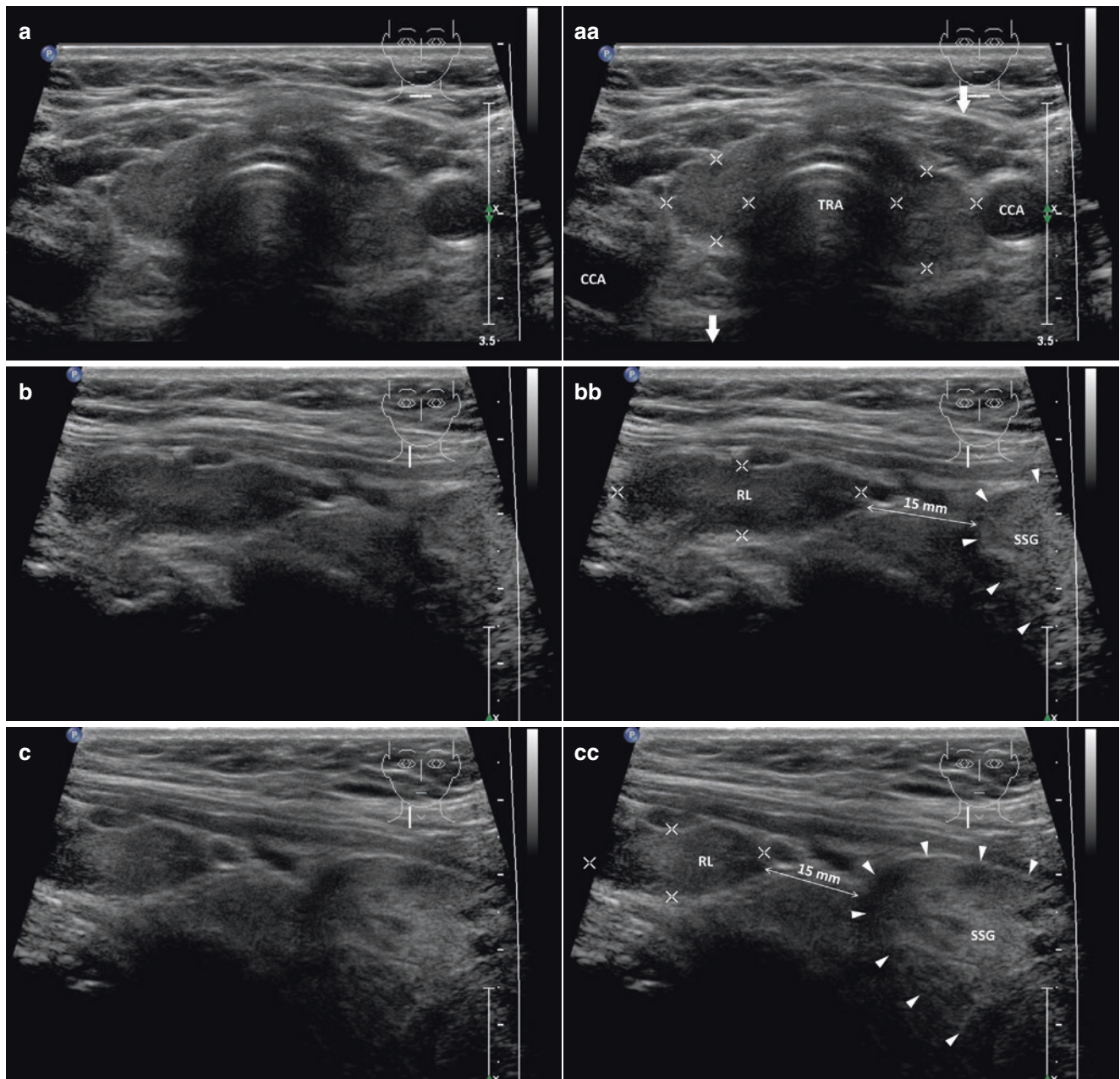


Fig. 11.1 (aa) A 50-year-old woman with primary substernal multinodular goiter (SSG), size $55 \times 53 \times 35$ mm and volume 53 mL (entirely visible and measured by US) on the right side. US overall view of atrophic thyroid gland in thyroid bed: homogeneous structure; isoechoic; Tvol 5 mL, RL 3 mL, and LL 2 mL; transverse. Note: pictogram—*thick arrow* indicates location of SSG (*not shown*)—caudally from the current probe position. (bb) Detail of atrophic RL and upper pole of SSG: atrophic RL—homogeneous structure; isoechoic; upper pole of SSG—

coarse structure; hyperechoic; clear 15 mm space between low pole of the RL and upper pole of SSG; longitudinal, depth of penetration 5 cm. (cc) Detail of space between atrophic RL and upper pole of SSG: clear 15 mm space between low pole of the RL and upper pole of SSG; longitudinal. (dd) Detail of separated SSG: solid; inhomogeneous structure; hyperechoic; probe inclined retrosternally; transverse. (ee) Detail of separated SSG: solid; inhomogeneous structure; hyperechoic; probe inclined retrosternally; longitudinal

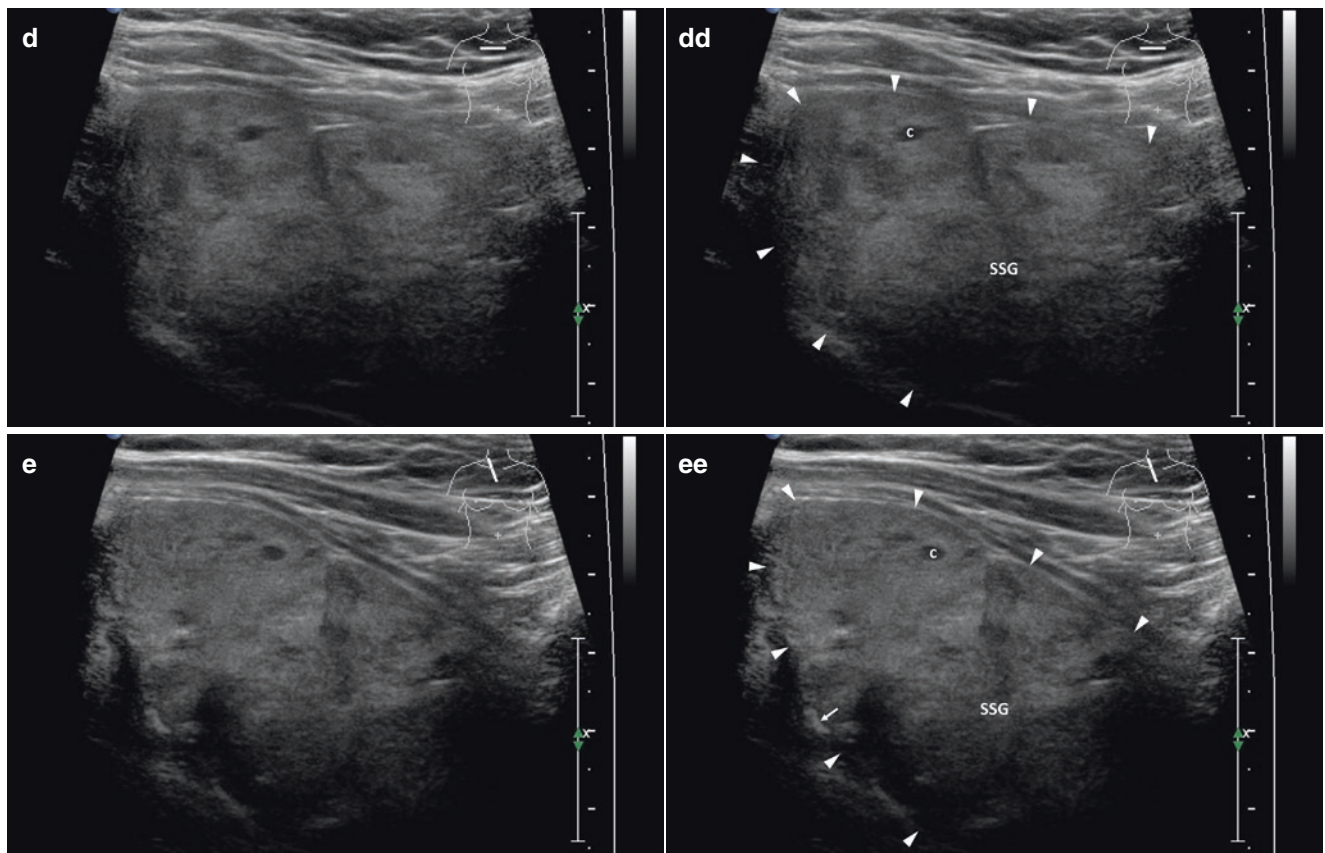


Fig. 11.1 (continued)

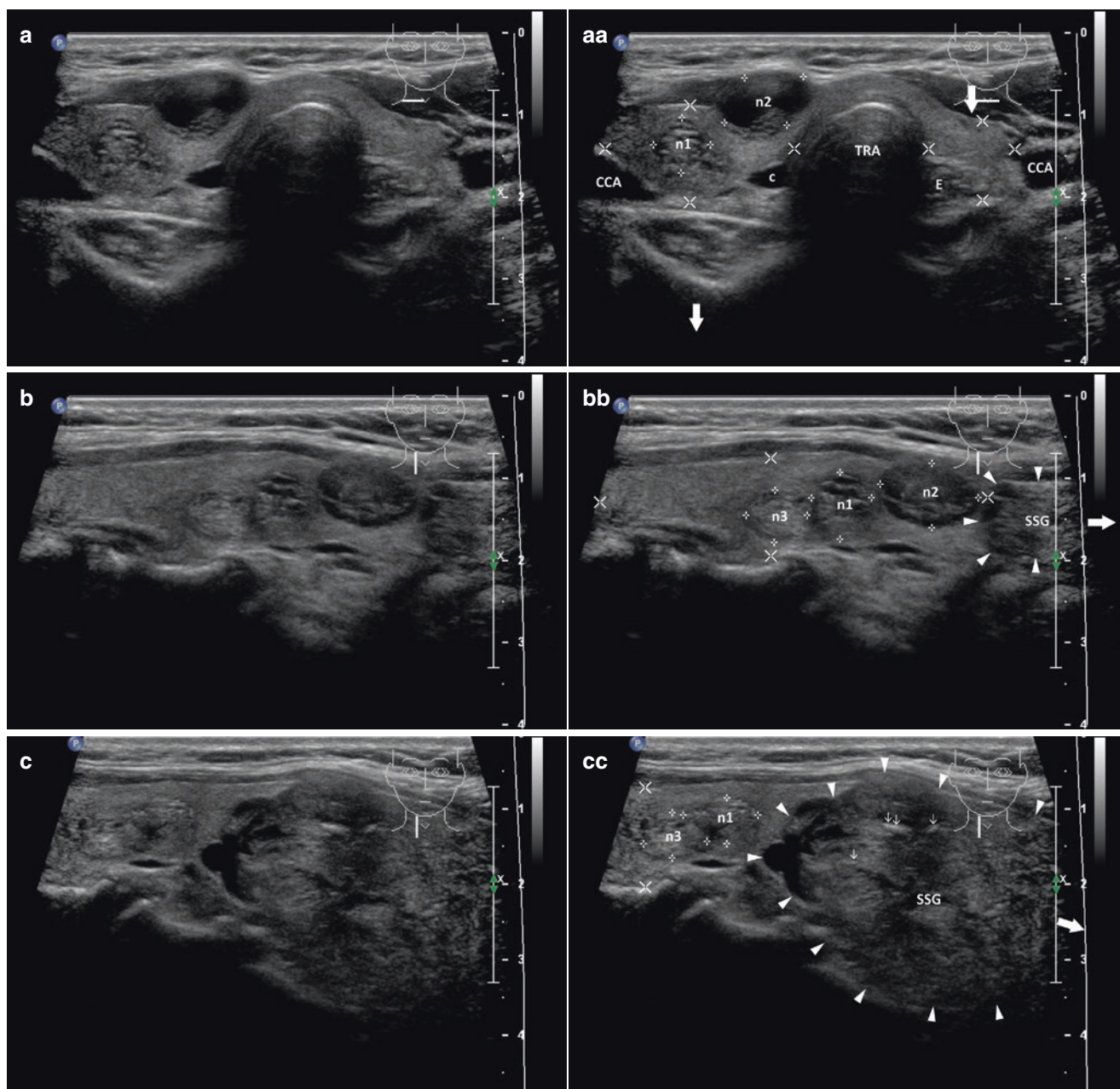
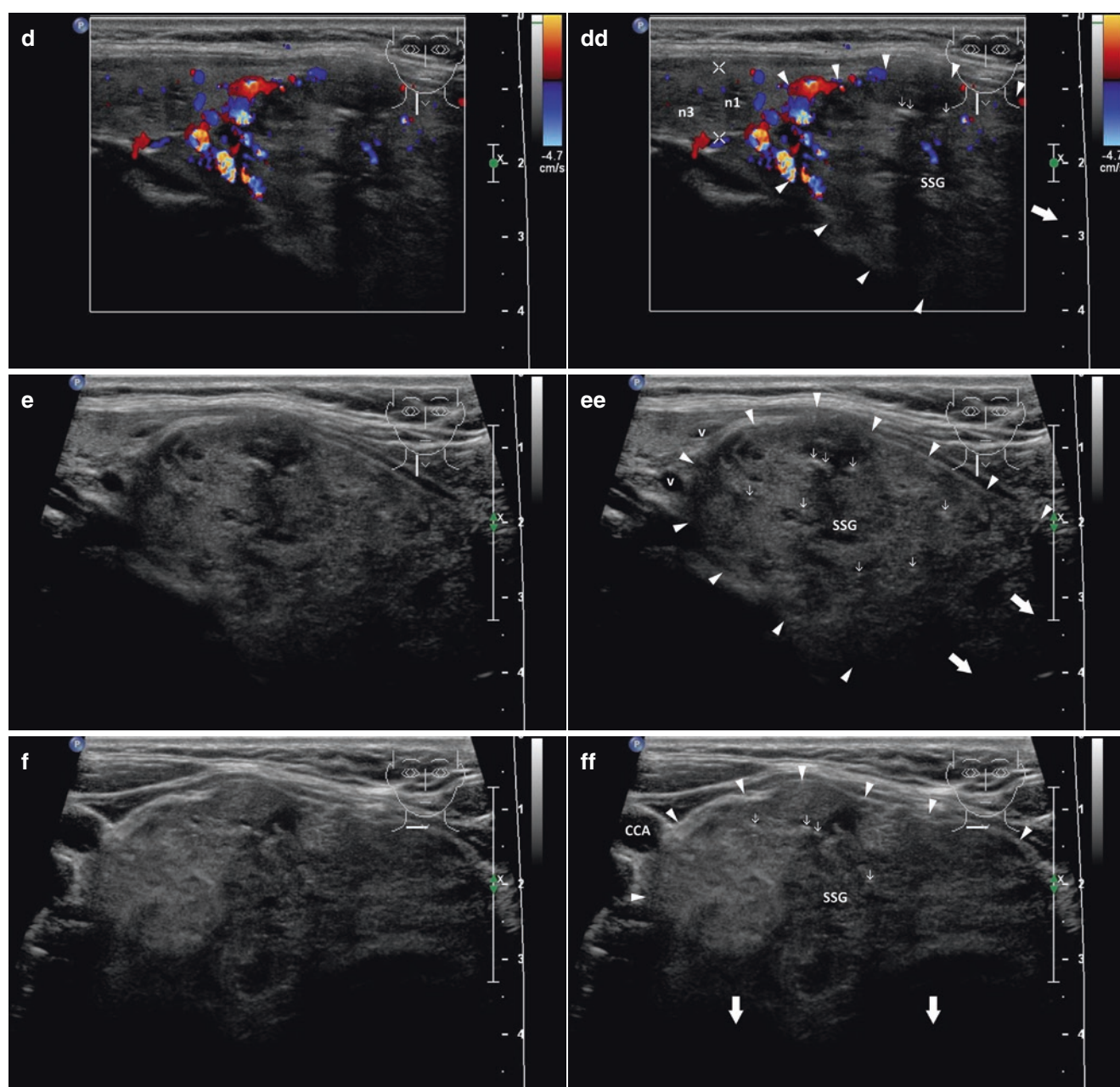


Fig. 11.2 (aa) A 50-year-old woman with secondary substernal multinodular goiter (SSG), size 55 × 54 × 33 mm and volume 52 mL (visible part as measured by US) on the right side. US scan of multinodular thyroid gland (MNG) with small nodules: inhomogeneous structure; isoechoic; small complex nodule (*n1*, *n2*) and tiny cyst (*c*) in the RL; part of the SSG not visible on US (*thick arrows*); Tvol 13 mL, RL 8 mL and LL 5 mL; transverse. Note: pictogram—*thick arrow* indicates location of SSG (*not shown*)—caudally from the current probe position. (bb) Detail of the RL of MNG with small nodules: one solid (*n3*) and two complex nodules (*n1*, *n2*) size from 6 to 11 mm; the lower pole continues into SSG (*arrowheads*); longitudinal; depth of penetration 4 cm; part of the SSG not visible on US (*thick arrow*). (cc) Detail of direct connection between low pole of the RL and upper part of SSG: undulated border (*arrowheads*); coarse multinodular structure of

retrosternal part; linear calcification and sporadic microcalcifications (*open arrows*); part of the SSG not visible on US (*thick arrow*); longitudinal. (dd) Detail of direct connection between low pole of the RL and upper part of SSG, CFDS: increased vascularity at the undulated border (*arrowheads*); longitudinal. (ee) Detail of almost complete retrosternal part of SSG: solid; coarse multinodular structure; hyperechoic; linear calcification and sporadic microcalcifications (*open arrows*); lumen of small vein (*v*) at the undulated border; part of the SSG not visible on US (*thick arrow*); probe inclined retrosternally; longitudinal. (ff) Detail of almost complete retrosternal part of SSG: solid; coarse multinodular structure; hyperechoic; sporadic microcalcifications (*open arrows*); part of the SSG not visible on US (*thick arrows*); probe inclined retrosternally; transverse

**Fig. 11.2** (continued)

11.2 US Characteristics

- On US scan, only the cervical and the upper part of SSG are visible (Fig. 11.1ee). It is possible to assess the structure and presence of nodes, and to eventually perform a FNAB.
- Retrosternal part of SSG is not easily imaged by US due to artifact generated by bony structures. Also, intrathoracic nodules are inaccessible to FNAB; making malignancy exclusion difficult.
- In the case of primary SSG we can see a space between the eutopic thyroid gland and retrosternally localized SSG (Fig. 11.1bb, cc).
- Computed tomography (CT) helps to evaluate the volume, extension, nodal disease, signs of malignancy such as irregular borders or microcalcifications, and assessing for mass effect by the trachea.

substernal goiter based on risk factors for an extracervical surgical approach. *Head Neck*. 2011;33(6):792–9.

3. Kanzaki R, Higashiyama M, Oda K, Okami J, Maeda J, Takenaka A, et al. Surgical management of primary intrathoracic goiters. *Gen Thorac Cardiovasc Surg*. 2012;60(3):171–4.
4. Hegedüs L, Bonnema SJ. Approach to management of the patient with primary or secondary intrathoracic goiter. *J Clin Endocrinol Metab*. 2010;95(12):5155–62.
5. Nankee L, Chen H, Schneider DF, Sippel RS, Elfenbein DM. Substernal goiter: when is a sternotomy required? *J Surg Res*. 2015;199(1):121–5.
6. Katlic MR, Grillo HC, Wang CA. Substernal goiter. Analysis of 80 patients from Massachusetts General Hospital. *Am J Surg*. 1985;149(2):283–7.
7. Hardy RG, Bliss RD, Lennard TW, Balasubramanian SP, Harrison BJ. Management of retrosternal goitres. *Ann R Coll Surg Engl*. 2009;91(1):8–11.
8. White ML, Doherty GM, Gauger PG. Evidence-based surgical management of substernal goiter. *World J Surg*. 2008;32(7):1285–300.

References

1. Katlic MR, Wang CA, Grillo HC. Substernal goiter. *Ann Thorac Surg*. 1985;39(4):391–9.
2. Mercante G, Gabrielli E, Pedroni C, Formisano D, Bertolini L, Nicoli F, et al. CT cross-sectional imaging classification system for

12.1 Essential Facts

- Toxic adenomas are benign monoclonal thyroid tumors autonomously secreting excess of thyroid hormone. Thyrotoxicosis may develop in patients with a single autonomous thyroid nodule as the solitary toxic adenoma - STA (Fig. 12.1) or in those with multiple autonomous nodules as toxic multinodular goiter - TMNG (Fig. 12.2), also known as Plummer's disease (first described by Henry Plummer in 1913). Nodular autonomy typically progresses gradually, leading first to subclinical, and then to overt, hyperthyroidism. Remission is rare [1].
- Toxic multinodular goiter (TMNG) is found more frequently in the iodine-deficient regions and accounts for 37% of thyrotoxicosis cases in Sweden. On the other hand, the frequency is relatively low in countries with excess iodine intake, and accounts for only 6.2% of thyrotoxicosis cases in Iceland and 0.3% in Japan [2].
- A Danish population-based study by Carlé et al. found the prevalence of TMNG to be 44% and STA 5.7% of all nosological types of hyperthyroidism [3].
- TMNG is diagnosed by ^{99m}Tc or ^{123}I scintigraphy, which shows diffuse inhomogeneous tracer uptake reflecting areas of hyperfunction and hypofunction within the thyroid gland [2].
- Clinical findings: Ophthalmopathy and other stigmata of Graves' disease are absent [1]. TMNG is responsible for the majority of cases of thyrotoxicosis in the elderly. There is a relative paucity of typical hyperadrenergic symptoms in older patients with hyperthyroidism, who instead may present with unexplained weight loss, neurocognitive changes, or cardiovascular effects. Of particular concern is the elevated risk of atrial fibrillation [4].
- Physical examination: single palpable thyroid nodule, usually at least 2.5 cm in size, or a multinodular goiter [1].
- Laboratory findings: Antithyroid antibodies are absent [1]. Biochemically, the development of autonomous function in a nodular goiter is the first evidence of the "sub-clinical" hyperthyroidism (suppression of serum TSH with normal serum concentrations of thyroid hormones), later followed by overt hyperthyroidism with elevation of serum-free T3 and free T4 [4].
- Radioactive iodine treatment using ^{131}I of TMNG or STA is well accepted. Total thyroidectomy is the only appropriate procedure for the surgical management of hyperthyroidism [1].

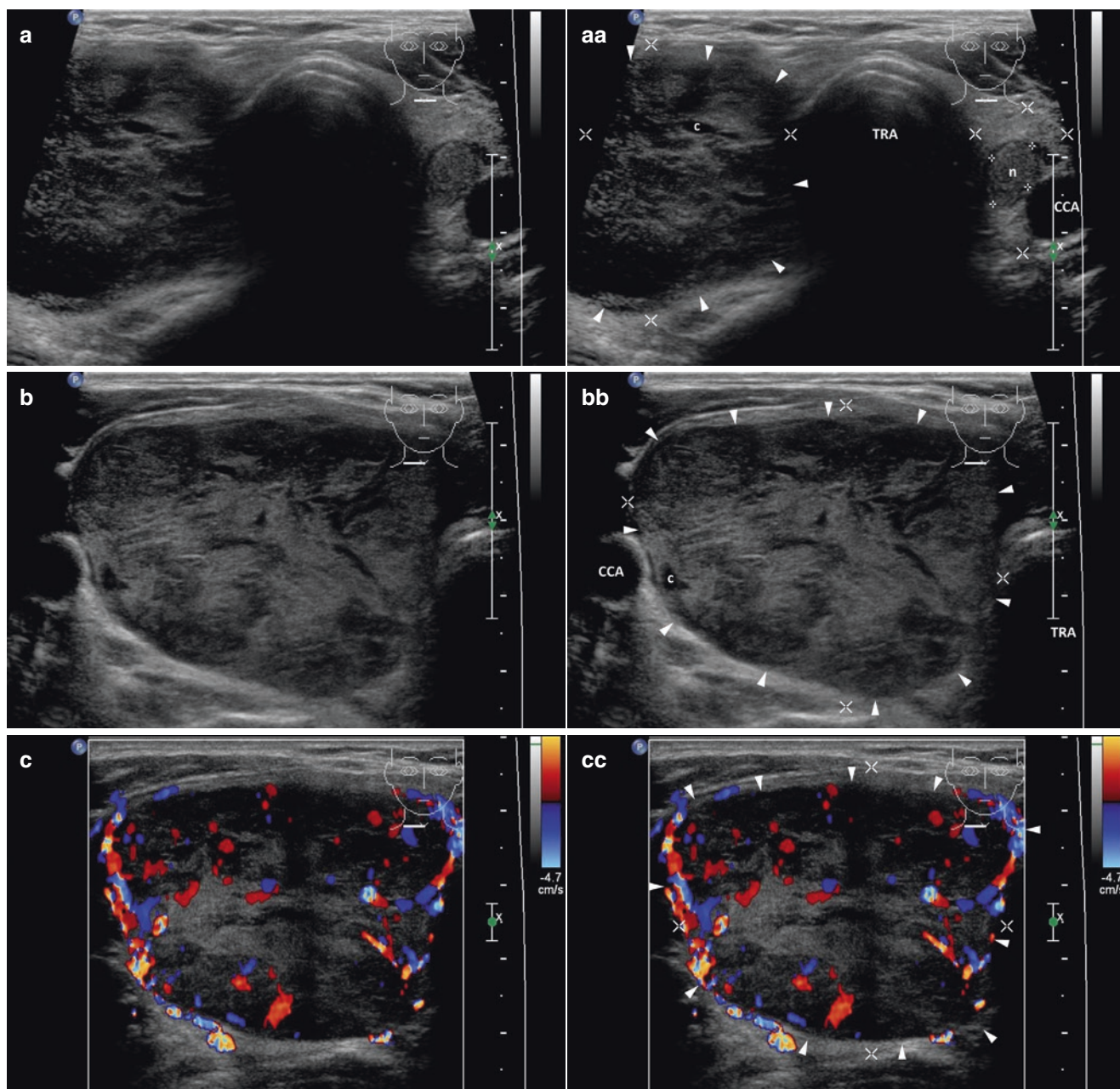


Fig. 12.1 (aa) An 81-year-old man with a giant solitary toxic adenoma—STA (arrowheads), size $65 \times 48 \times 37$ mm and volume 59 mL in the RL of multinodular goiter. US overall view: STA—round shape; coarse structure; mixed echogenicity, mostly hyperechoic; sporadic tiny cystic cavities (c); well-defined margin with thin halo sign; small, solid, isoechoic nodule (n) with halo sign in the LL; Tvol 80 mL, asymmetry—RL 72 mL and LL 8 mL; transverse; depth of penetration 5 cm. (bb) Detail of STA (arrowheads): round shape; coarse structure; mixed

echogenicity, mostly hyperechoic; sporadic tiny cystic cavities (c); well-defined margin with thin halo sign; transverse. (cc) Detail of STA (arrowheads), CFDS: diffusely increased vascularity, *pattern III*; transverse. (dd) Detail of STA (arrowheads): round shape; coarse structure; mixed echogenicity, mostly hyperechoic; sporadic tiny cystic cavities (c); well-defined margin with thin halo sign; longitudinal. (ee) Detail of STA (arrowheads), CFDS: diffusely increased vascularity, *pattern III*; longitudinal

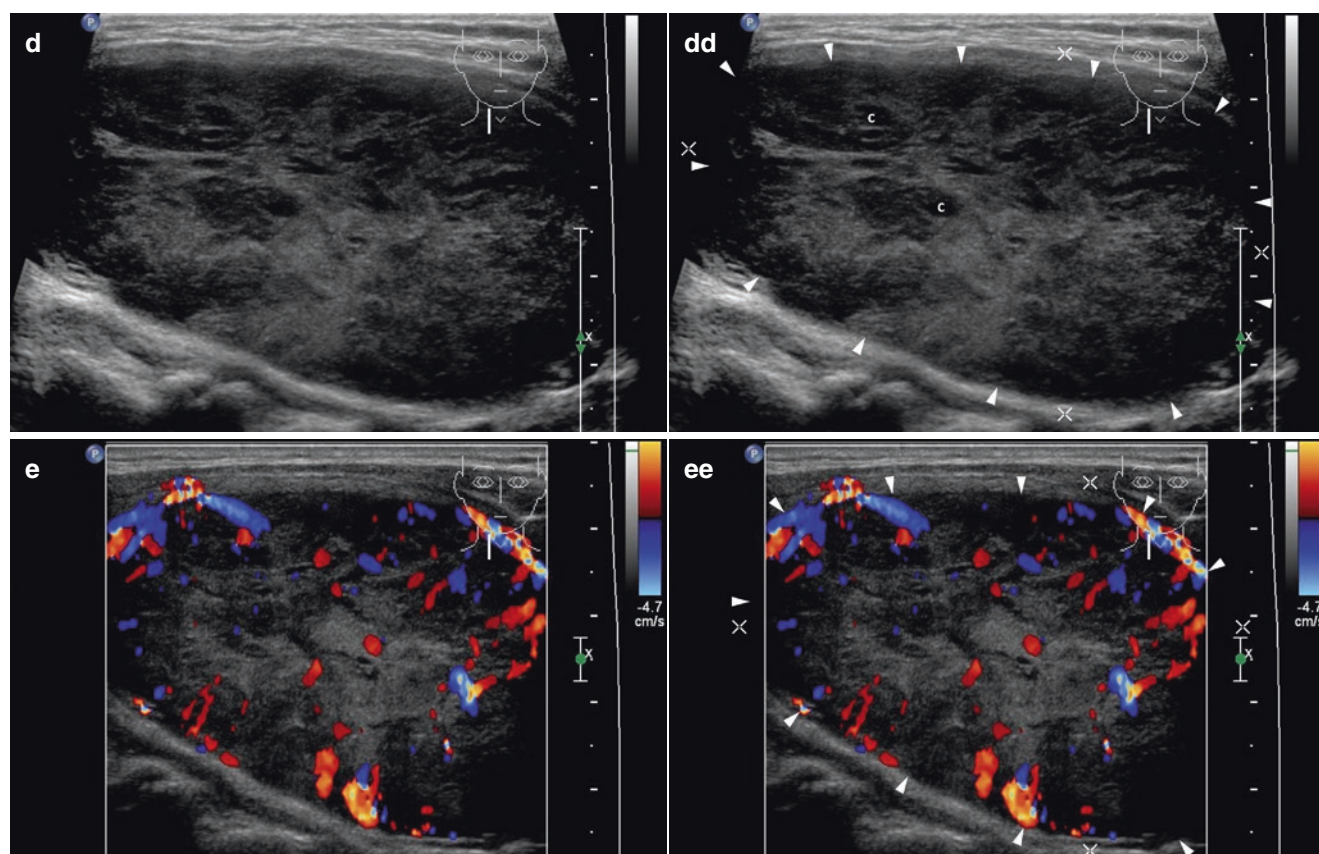


Fig. 12.1 (continued)

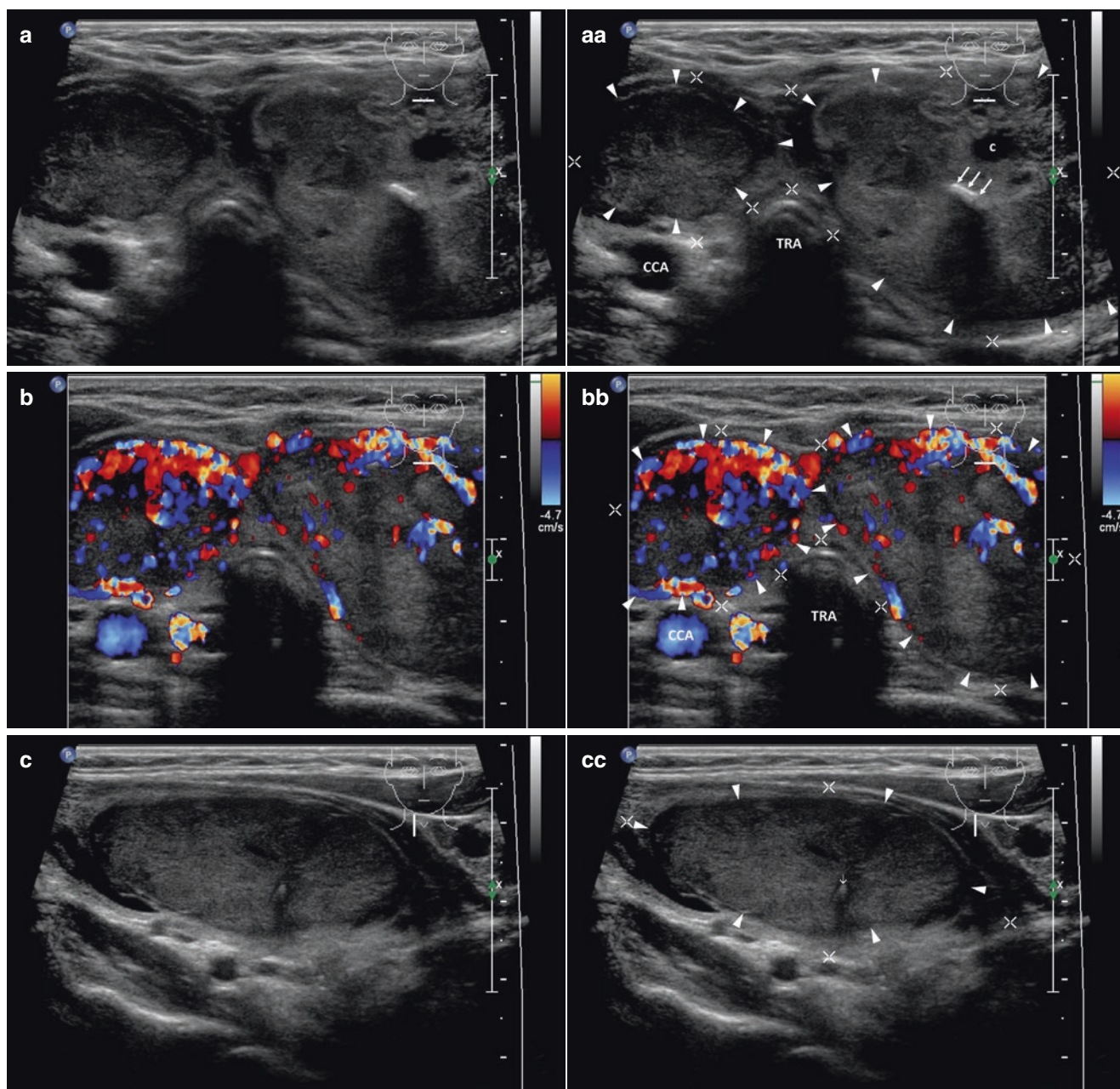
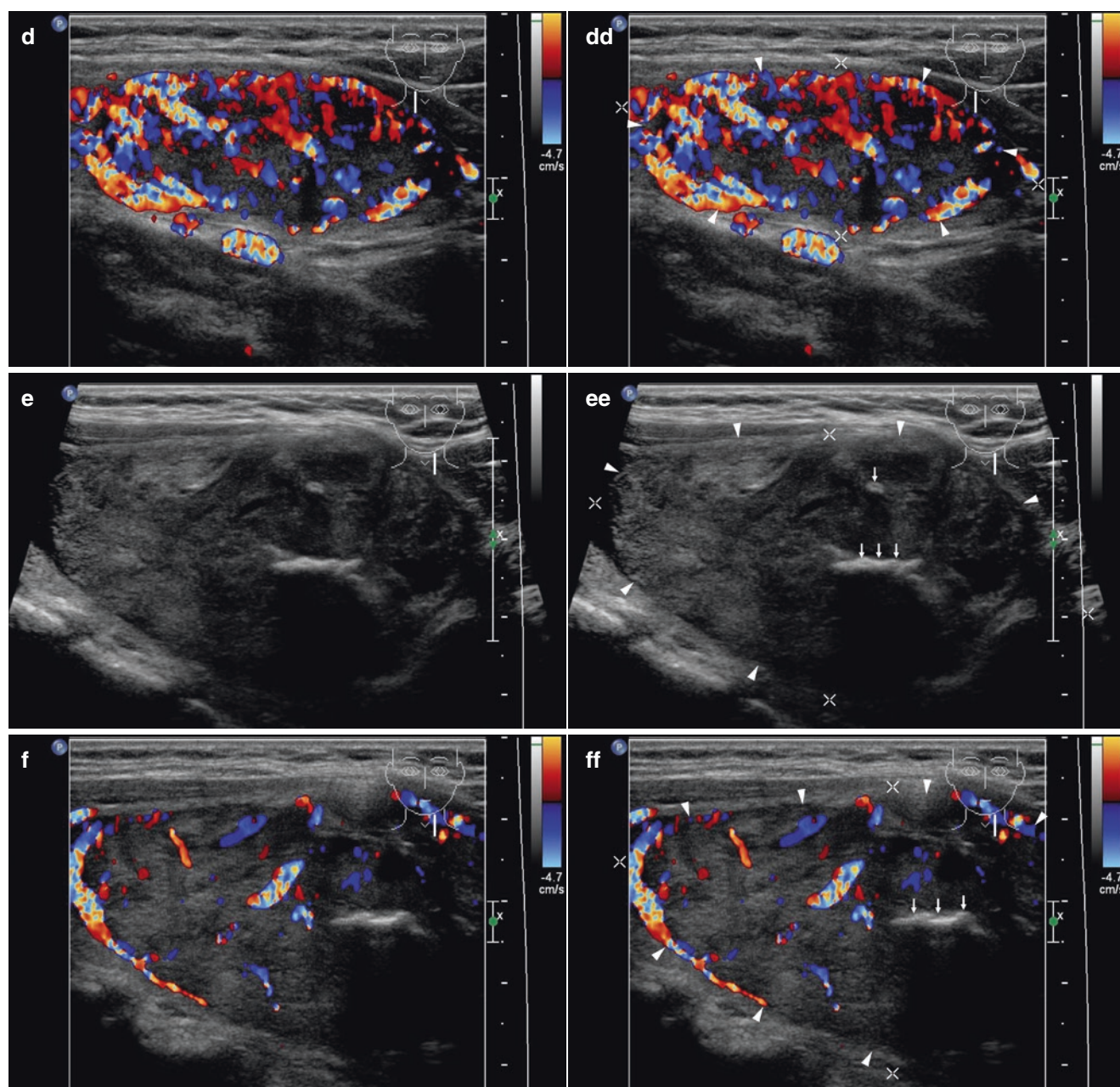


Fig. 12.2 (aa) A 30-year-old woman with toxic multinodular goiter (TMNG)—medium-sized toxic nodule (arrowheads), size $40 \times 21 \times 18$ mm, volume 9 mL in the RL and large toxic nodule (arrowheads), size $55 \times 49 \times 32$ mm, volume 46 mL in the LL. US overall view: nodule in the RL—round shape; inhomogeneous structure; mostly hyperechoic; well-defined margin with thin halo sign; complex nodule in the LL—ovoid shape; coarse structure; hyperechoic; sporadic tiny cystic cavities (c) and intranodular coarse linear calcification (arrows); well-defined margin with thin halo sign; Tvol 72 mL, asymmetry—RL 17 mL and LL lobe 55 mL; transverse; depth of penetration 5 cm. (bb) Overall view of thyroid gland, CFDS: solid nodule (arrowheads) in the RL—diffuse hypervascularity, *pattern III*; complex nodule (arrowheads) in the LL—diffusely increased vascularity, *pattern II*;

transverse. (cc) Detail of the RL with solid toxic nodule (arrowheads): elliptical shape; inhomogeneous; hyperechoic; intranodular microcalcification (open arrow) with acoustic shadow; well-defined margin with thin halo sign; longitudinal. (dd) Detail of the RL with solid toxic nodule (arrowheads), CFDS: diffusely hypervascularity, *pattern III*; longitudinal. (ee) Detail of the LL with complex toxic nodule (arrowheads): ovoid shape; coarse structure; hyperechoic; sporadic tiny cystic cavities (c) and intranodular coarse linear calcification with prominent acoustic shadow and dotted calcification with slight acoustic shadow (arrows); longitudinal. (ff) Detail of the LL with complex toxic nodule (arrowheads), CFDS: diffusely increased vascularity, *pattern II*; longitudinal.

**Fig. 12.2** (continued)

12.2 US Findings of Toxic Multinodular Goiter or Solitary Toxic Adenoma

- US findings of SAT and TMNG:
 - US shows enlarged but otherwise normal-appearing thyroid multinodular goiter, sometimes with degenerative changes—cystic cavities and calcifications (Fig. 12.2aa).
 - Solitary nodule has a size ≥ 2.5 , more commonly >3 cm (Fig. 12.1aa).
 - Enlarged thyroid gland with multiple nodules (Fig. 12.2aa).
 - CFDS evaluation reveals blood flow within the rim of the nodules and intraparenchymally (Figs. 12.1cc, 12.2bb).
- US follow-up: Solitary autonomous nodules in adult patients characteristically progress slowly over many years, with toxicity rarely developing in nodules less than 2.5 cm in diameter and occurring primarily in nodules 3 cm or larger. Hyperfunctioning thyroid nodules in children and adolescents have a more rapidly progressive course than those in adults and should be treated by thyroid lobectomy at the time of diagnosis [5].
- US only shows the nodule but does not confirm the diagnosis. Thyroid scintigraphy employs radioiodine or ^{99m}Tc -technetium-pertechnetate in order to differentiate hyperfunctioning nodules, also referred as “autonomous,” “autonomously-functioning,” or “hot” nodules [6].
- A literature review of surgical patients with solitary hyperfunctioning thyroid nodules managed by thyroid resection revealed an estimated 3.1% prevalence of malignancy. Histological diagnosis of papillary thyroid carcinoma

(PTC) in $\approx 57\%$, follicular thyroid carcinoma (FTC) in $\approx 36\%$, and Hurthle cell carcinoma (HCC) in $\approx 8\%$. Mean nodule size of 4.13 ± 1.68 cm. Of these, 78% were in females and mean age at time of diagnosis was 47 years. Laboratory assessment revealed T3 elevation in 76.5%, T4 elevation in 51.9%, and subclinical hyperthyroidism in 13% of patients. Thus, hot thyroid nodules harbor a low but not negligible rate of malignancy. Compared to individuals with benign hyperfunctioning thyroid nodules, those with malignant hyperfunctioning nodules are younger and more predominantly female. There are not any specific characteristics that could be used to distinguish between malignant and benign hot nodules [6].

References

1. Sharma M, Aronow WS, Patel L, Gandhi K, Desai H. Hyperthyroidism. *Med Sci Monit.* 2011;17(4):RA85–91.
2. Kahara T, Shimizu A, Uchiyama A, Terahata S, Tajiri J, Nishihara E, et al. Toxic multinodular goiter with low radioactive iodine uptake. *Intern Med.* 2011;50(16):1709–14.
3. Carlé A, Pedersen IB, Knudsen N, Perrild H, Ovesen L, Rasmussen LB, et al. Epidemiology of subtypes of hyperthyroidism in Denmark: a population-based study. *Eur J Endocrinol.* 2011;164(5):801–9.
4. Samuels MH, Franklyn JA. Hyperthyroidism in aging. In: De Groot LJ, Beck-Peccoz P, Chrousos G, Dungan K, Grossman A, Hershman JM, et al., editors. *Endotext* [Internet]. South Dartmouth, MA: MDText.com, Inc.; 2015.
5. Thomas Jr CG, Croom 3rd RD. Current management of the patient with autonomously functioning nodular goiter. *Surg Clin North Am.* 1987;67(2):315–28.
6. Mirfakhraee S, Mathews D, Peng L, Woodruff S, Zigman JM. A solitary hyperfunctioning thyroid nodule harboring thyroid carcinoma: review of the literature. *Thyroid Res.* 2013;6(1):7.

Nodular Goiter: Suspicious and Malignant Lesions

1.1 Incidence and Mortality Worldwide According to Data from the International Agency for Research of Cancer World Health Organization—Globocan 2012 [1]

- Thyroid carcinoma currently ranks worldwide 18th among all malignancies and 21st in mortality of this disease. It is the most frequent malignancy of the endocrine system.
- In 2012, a total of 298,102 thyroid cancer patients were diagnosed throughout the world. The global incidence was 4.2 for both genders (4.0 age-standardized rate—world [ASR-W]), 6.6 for females (6.1 ASR-W) and 1.9 for males (1.9 ASR-W).
- In 2012, a total of 39,771 subjects died of thyroid carcinoma. The global mortality was 0.6 for both genders (0.5 ASR-W), 0.8 for females (0.6 ASR-W) and 0.4 for males (0.3 ASR-W).

1.2 Essential Facts According to the 2015 American Thyroid Association (ATA) Guidelines [2]

- According to most recent 2015 ATA Guidelines, thyroid cancer occurs in 7–15% of cases depending on age, sex, radiation exposure history, family history, and other factors.

- Differentiated thyroid cancer (DTC), which includes papillary (PTC) and follicular cancer (FTC), comprises the vast majority (>90%) of all thyroid cancers.
- In the United States, approximately 63,000 new cases of thyroid cancer were predicted to be diagnosed in 2014, compared with 37,200 in 2009 when the last ATA guidelines were published. The yearly incidence has nearly tripled from 4.9 per 100,000 in 1975 to 14.3 per 100,000 in 2009.
- Almost the entire change has been attributed to an increase in the incidence of papillary thyroid cancer (PTC). Moreover, 25% of the new thyroid cancers diagnosed in 1988–1989 were ≤ 10 mm compared with 39% of the new thyroid cancer diagnoses in 2008–2009.
- Nonpalpable nodules detected on US or other anatomic imaging studies are termed incidentally discovered nodules or “incidentalomas.”
- Nonpalpable nodules have the same risk of malignancy as do US-confirmed palpable nodules of the same size.
- The likelihood of a nodule being malignant is approximately twice as high in a solitary compared with a nonsolitary nodule and more than 1.5 times as high in a man than in a woman [3].
- In patients with multiple nodules, the cancer rate per nodule decreases, but the decrease is approximately proportional to the number of nodules so that the overall rate of cancer per patient, 10–13%, is the same as that in patients with a solitary nodule [4].

- The vast majority of non-medullary DTC occur sporadically; only 5–10% have a familial occurrence.
- Generally, only nodules ≥ 10 mm should be evaluated, since they have a greater potential to develop into clinically significant cancers. Occasionally, there may be nodules < 10 mm that require further evaluation because of clinical symptoms or associated lymphadenopathy. *Recommendations for diagnostic FNAB see in detail in Chap. 24, Table 24.1.*

1.3 Clinical Assessment Increasing the Likelihood of Malignancy [5]

- Patient's history: prior head and neck irradiation (especially during childhood, with a relative risk of 8.7 at 1 Gy for x-rays and gamma radiation) (Fig. 15.3.2aa), reports of rapid growth, dysphagia, dysphonia, male gender, presentation at extremes of age (< 20 or > 70 years), and a family history of MTC or multiple endocrine neoplasia (MEN).
- Physical examination findings: nodules size > 4 cm (19.3% risk of malignancy), firmness to palpation, fixation of the nodule to adjacent tissues, cervical lymphadenopathy > 1 cm, and vocal fold immobility.

1.4 US Characteristics of Thyroid Carcinoma

- According to the ATA, the vast majority (82–91%) of thyroid cancers are solid [2].
- In a retrospective review of 360 consecutively surgically removed thyroid cancers at the Mayo clinic, 88% were solid or minimally cystic ($< 5\%$), 9% were $< 50\%$ cystic, and only 3% were more than 50% cystic [6].
- According to the Korean Society of Thyroid Radiology, a mainly cystic nodule is rare in thyroid carcinoma, but a cystic component is found in 13–26% of all thyroid carcinomas. Approximately 5% of all partially cystic nodules have been reported to be malignant. In this case, the presence of a solid component with vascularity, an eccentric location of the solid portion, or microcalcifications may suggest malignant nodule and especially PTC [7].

1.5 US Classic Features of High Suspicion of Malignancy for Solid Nodules According to the 2015 ATA Guidelines [2]

- A typical high-suspicion nodule is a solid hypoechoic nodule or a solid hypoechoic component in a partially cystic nodule with one or more of the following features:
 - Irregular margins (specifically defined as infiltrative, microlobulated, or spiculated)
 - Microcalcifications
 - “Taller-than-wide” shape (anteroposterior-to-transverse ratio > 1)
 - Disrupted rim calcifications with small extrusive hypoechoic soft tissue component
 - Evidence of extrathyroidal extension

1.6 US Features of High Suspicion of Malignancy for Cystic Nodules According to the 2015 ATA Guidelines [2]

- FNAB decision-making for partially cystic thyroid nodules must be tempered by their lower malignant risk. The evidence linking US features with malignancy in this subgroup of nodules is less robust [2].
- US features with a higher risk of malignancy of cystic nodule [6, 8]:
 - An eccentric rather than concentric position of the solid component along the cyst wall
 - An acute rather than obtuse angle interface of the solid component and cyst
 - The presence of microcalcifications
 - Lobulated margins (less robust risk factor)
 - Increased vascularity of the solid portion (less robust risk factor)

1.7 US Features of Malignant Nodules According to the Korean Society of Thyroid Radiology [7]

- Rapid growth of thyroid nodules can be seen in anaplastic thyroid carcinoma, lymphoma, sarcoma, and rarely for high-grade carcinoma.
- Approximately 5% of all partially cystic nodules are malignant; a mainly cystic nodule is rare in

thyroid carcinoma. A cystic component, however, is found in 13–26% of all thyroid carcinomas.

- “*Taller-than-wide*” shape (a specificity of 89–93%)
- Spiculated/microlobulated margin is a highly suggestive finding (a specificity of 92%).
- Marked hypoechogenicity is highly specific for malignant nodule (a specificity of 92–94%).
- Microcalcifications are highly suggestive for malignant nodule (a specificity of 86–95%).
- Intranodular hypervascularity is observed in 6%–74% of thyroid carcinomas, but perinodular flow is observed in 22% of malignant nodules.
- Extracapsular extension is observed in 36% of all thyroid carcinomas.
- Although a completely even halo is a finding suggestive of a benign nodule, 10–24% of all PTC have a complete or incomplete halo sign.

References

1. Web portal: International Agency for Research of Cancer World Health Organization. Globocan 2012: Estimated cancer incidence, mortality and prevalence worldwide in 2012. <http://globocan.iarc.fr>.
2. Haugen BR, Alexander EK, Bible KC, Doherty GM, Mandel SJ, Nikiforov YE, et al. 2015 American Thyroid Association Management Guidelines for Adult Patients with Thyroid Nodules and Differentiated Thyroid Cancer: The American Thyroid Association Guidelines Task Force on Thyroid Nodules and Differentiated Thyroid Cancer. *Thyroid*. 2016;26(1):1–133.
3. Frates MC, Benson CB, Doubilet PM, Kunreuther E, Contreras M, Cibas ES, et al. Prevalence and distribution of carcinoma in patients with solitary and multiple thyroid nodules on sonography. *J Clin Endocrinol Metab*. 2006;91(9):3411–7.
4. Frates MC, Benson CB, Charboneau JW, Cibas ES, Clark OH, Coleman BG, et al. Management of thyroid nodules detected at US: Society of Radiologists in Ultrasound consensus conference statement. *Radiology*. 2005;237(3):794–800.
5. Bomeli SR, LeBeau SO, Ferris RL. Evaluation of a thyroid nodule. *Otolaryngol Clin North Am*. 2010;43(2):229–38. vii.
6. Henrichsen TL, Reading CC, Charboneau JW, Donovan DJ, Sebo TJ, Hay ID. Cystic change in thyroid carcinoma: prevalence and estimated volume in 360 carcinomas. *J Clin Ultrasound*. 2010;38(7):361–6.
7. Moon WJ, Baek JH, Jung SL, Kim DW, Kim EK, Kim JY, et al., Korean Society of Thyroid Radiology (KSThR), Korean Society of Radiology. Ultrasonography and the ultrasound-based management of thyroid nodules: consensus statement and recommendations. *Korean J Radiol*. 2011;12(1):1–14.
8. Kim DW, Lee EJ, In HS, Kim SJ. Sonographic differentiation of partially cystic thyroid nodules: a prospective study. *AJNR Am J Neuroradiol*. 2010;31(10):1961–6.

13.1 Essential Facts

- Up to 55% of benign nodules are hypoechoic compared to thyroid parenchyma; hypoechogenicity alone, therefore, is not a diagnostic sign of malignancy. In addition, benign nodules ≤ 1 cm are more likely to be hypoechoic than larger nodules [1].
- According to the 2015 American Thyroid Association (ATA) Guidelines [1]:
 - Intermediate suspicion of malignancy (estimated risk 10–20%) is attached to a hypoechoic solid nodule with a smooth regular margin (Fig. 13.1aa), but without microcalcifications, extrathyroidal extension, or “*taller-than-wide*” shape. This appearance has the highest sensitivity (60–80%) for papillary thyroid carcinoma (PTC), but a lower specificity than the preceding high suspicion pattern, and FNAB should be considered for these nodules ≥ 1 cm to refute malignancy.
 - Low suspicion malignancy risk (estimated risk 5–10%): isoechoic or hyperechoic solid nodule, or partially cystic nodule with eccentric uniformly solid areas without microcalcifications, irregular margin or extrathyroidal extension, or “*taller-than-wide*” shape prompts low suspicion for malignancy. Only about 15–20% of thyroid cancers are isoechoic or hyperechoic on US, and these are generally the follicular variant of PTC or follicular thyroid carcinoma (FTC). Fewer than 20% of these nodules are partially cystic. Therefore, these appearances are associated with a lower probability of malignancy and observation may be warranted until the size is ≥ 1.5 cm.

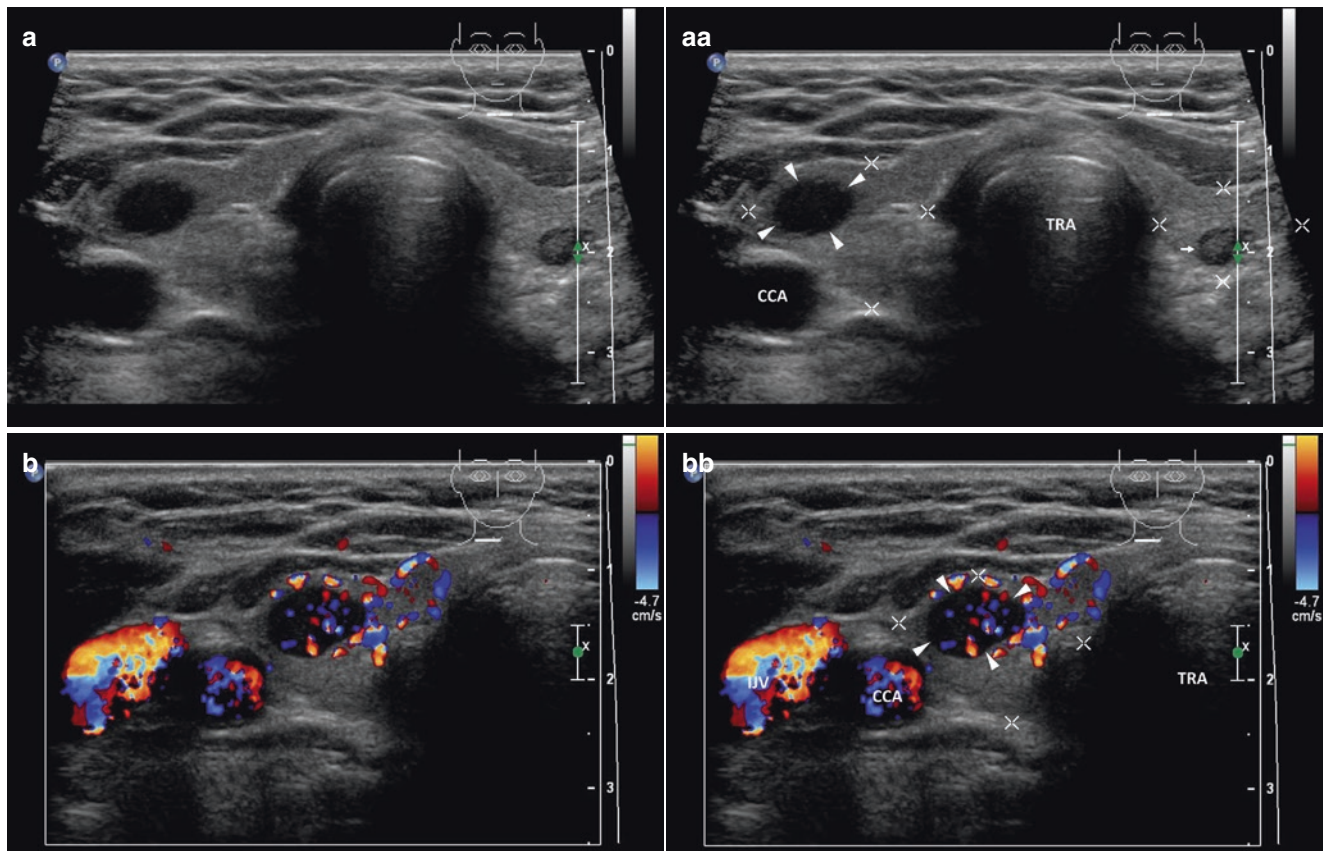


Fig. 13.1 (aa) A 58-year-old woman with a suspicious small solid nodule (arrowheads) in the RL, size $12 \times 8 \times 6$ mm and volume 0.3 mL. Post-thyroidectomy histology: benign hyperplastic nodule. US overall view: elliptical shape; homogeneous; hypoechoic; without microcalcifications; well-defined margin; tiny nonsuspicious nodule in the LL—homogeneous, isoechoic with halo sign; Tvol 12 mL, RL 7 mL, and LL 5 mL; transverse. (bb) Detail of suspicious small solid

nodule (arrowheads), CFDS: diffusely increased vascularity, *pattern II*; transverse. (cc) Detail of suspicious small solid nodule (arrowheads): homogeneous structure; hypoechoic; well-defined margin; longitudinal. (dd) Detail of suspicious small solid nodule (arrowheads), CFDS: increased peripheral vascularity and one intranodal vessel branch, *pattern II*; longitudinal

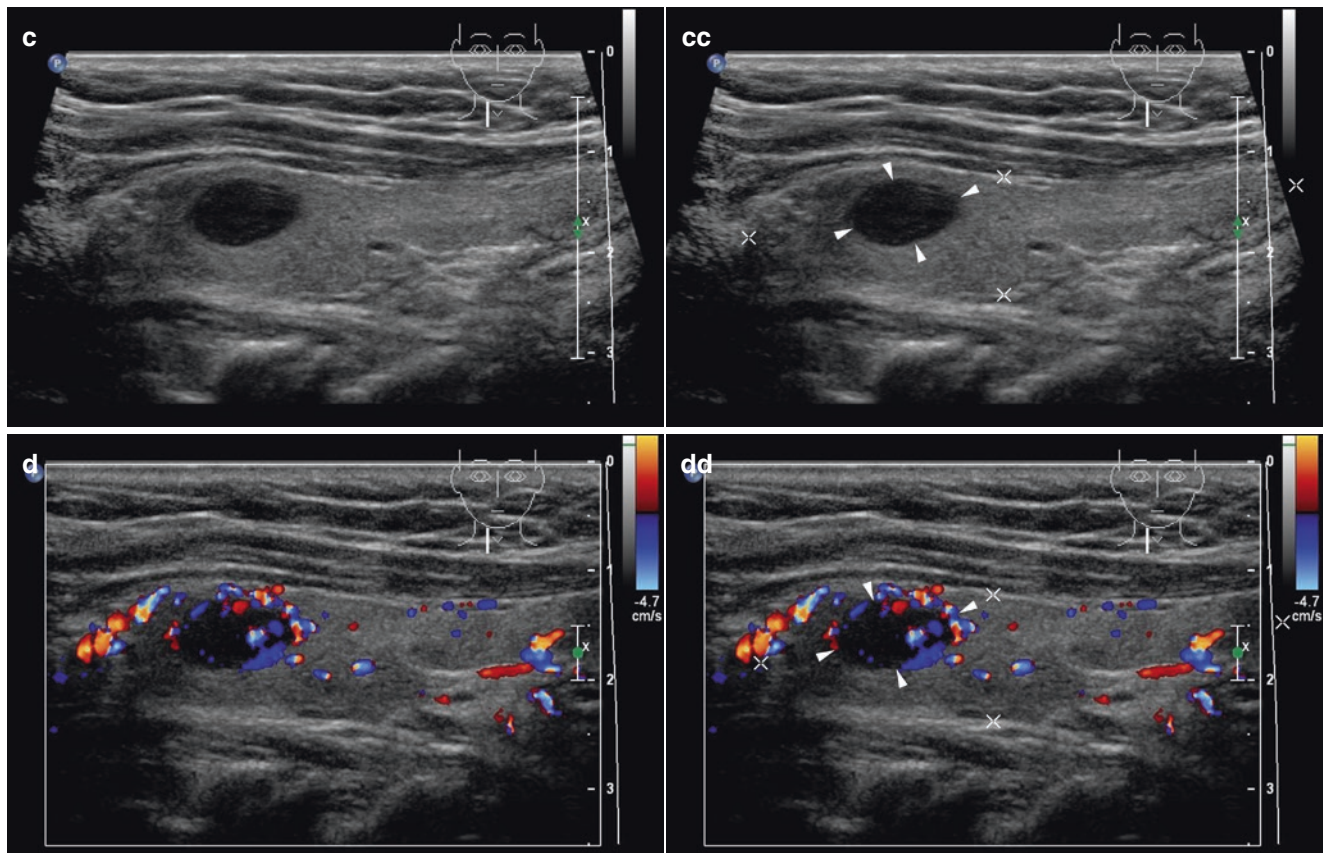


Fig. 13.1 (continued)

13.2 US Criteria of Suspicious and Benign Lesions [2]

- Using tissue diagnosis as the reference standard, a study by Monn et al. evaluated the diagnostic accuracy of US criteria for depiction of benign and malignant thyroid nodules. A total of 849 nodules (360 malignant, 489 benign) were diagnosed at surgery or FNAB:
- Statistically significant findings of malignancy:
 - Taller-than-wide shape (sensitivity 40.0%, specificity 91.4%).
 - Spiculated margin (sensitivity 48.3%, specificity 91.8%).
 - Marked hypoechogenicity (sensitivity 41.4%, specificity 92.2%) (Fig. 13.2ee).
 - Microcalcifications (sensitivity 44.2%, specificity 90.8%) (Fig. 13.3aa).
 - Macrocalcifications (sensitivity 9.7%, specificity 96.1%).
- US findings of benign nodules:
 - Isoechogenicity (sensitivity 56.6%, specificity 88.1%).
 - Spongiform appearance (sensitivity 10.4%, specificity 99.7%).
- Presence of at least one malignant US finding had a sensitivity of 83.3%, a specificity of 74%, and a diagnostic accuracy of 78%. For thyroid nodules with a diameter of ≤ 1 cm, the sensitivity of microcalcifications was lower than that in larger nodules (36.6 vs. 51.4%).

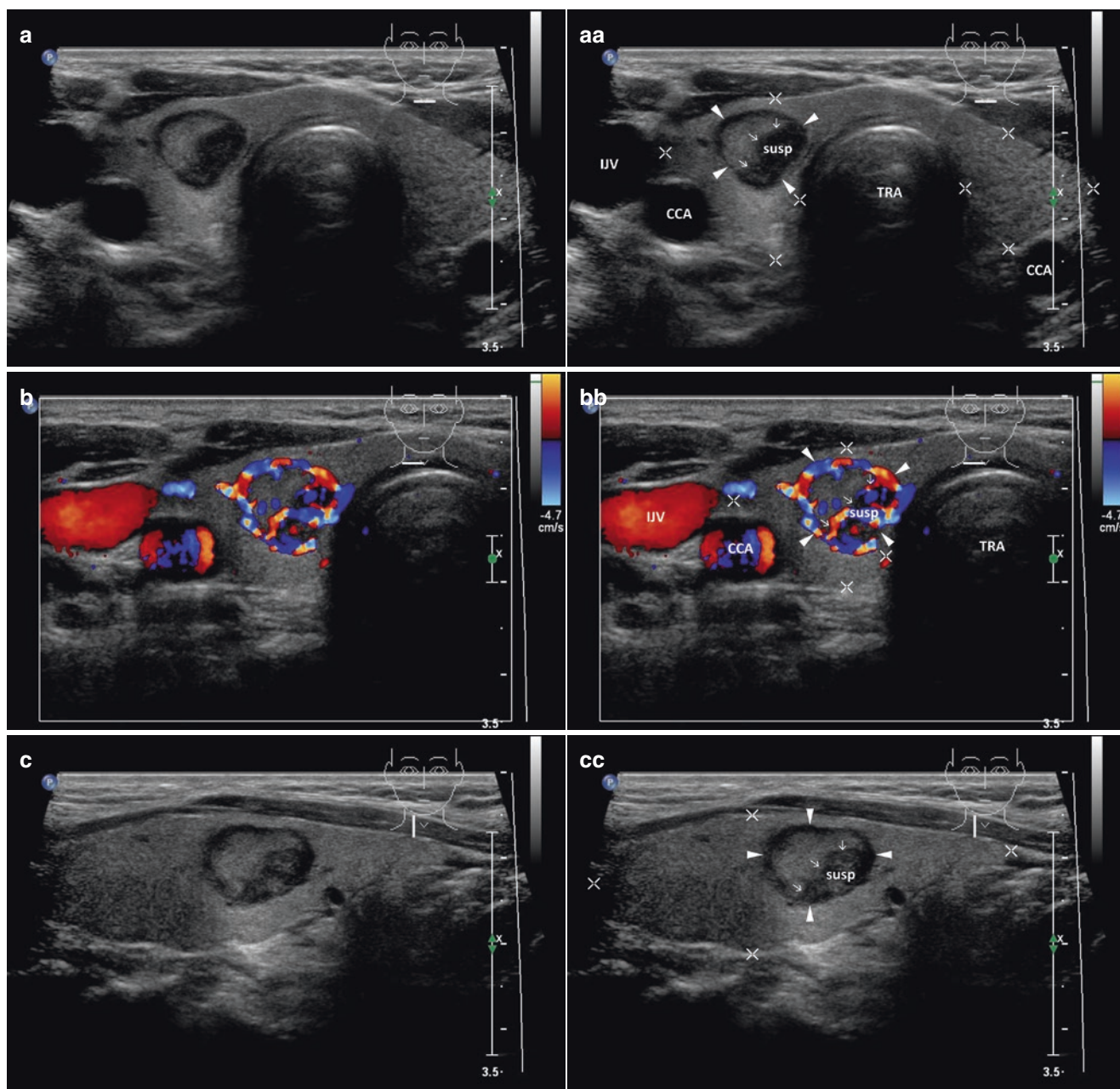


Fig. 13.2 (aa) A 48-year-old woman with a suspicious solitary small solid nodule (*arrowheads*) in the RL, size $13 \times 10 \times 9$ mm and volume 0.7 mL. Post-thyroidectomy histology: benign hyperplastic nodule. US overall view: round shape; one half homogeneous and isoechoic with halo sign; the other half inhomogeneous and mostly hypoechoic; microlobulated border between halves (*open arrows*); without microcalcifications; well-defined margin; Tvol 11 mL, RL 6 mL, and LL 5 mL; transverse. (bb) Detail of suspicious solitary small solid nodule (*arrowheads*), CFDS: increased peripheral vascularity and focal hypervascularity in hypoechoic half, *pattern II-III*; transverse. (cc) Detail of

suspicious solitary small solid nodule (*arrowheads*): ovoid shape; one half homogeneous and isoechoic with halo sign; the other half inhomogeneous and mostly hypoechoic; microlobulated border between halves (*open arrows*); longitudinal. (dd) Detail of suspicious solitary small solid nodule (*arrowheads*), CFDS: increased peripheral vascularity and focal hypervascularity in hypoechoic half, *pattern II-III*; longitudinal. (ee) Detail of suspicious solitary small solid nodule (*arrowheads*), US-FNAB procedure: tip of needle (*long arrow*) just in the center of hypoechoic part; zoom view, transverse

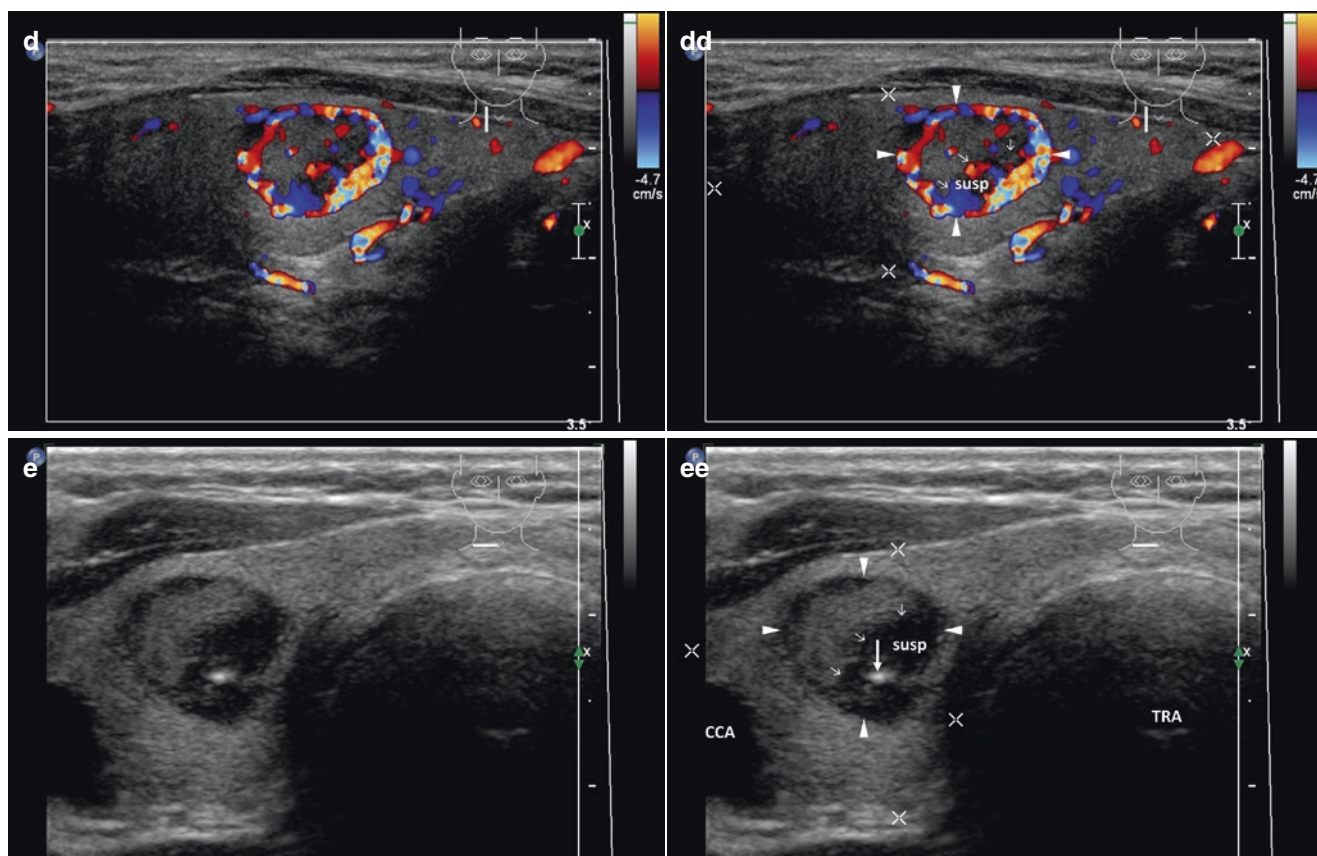


Fig. 13.2 (continued)

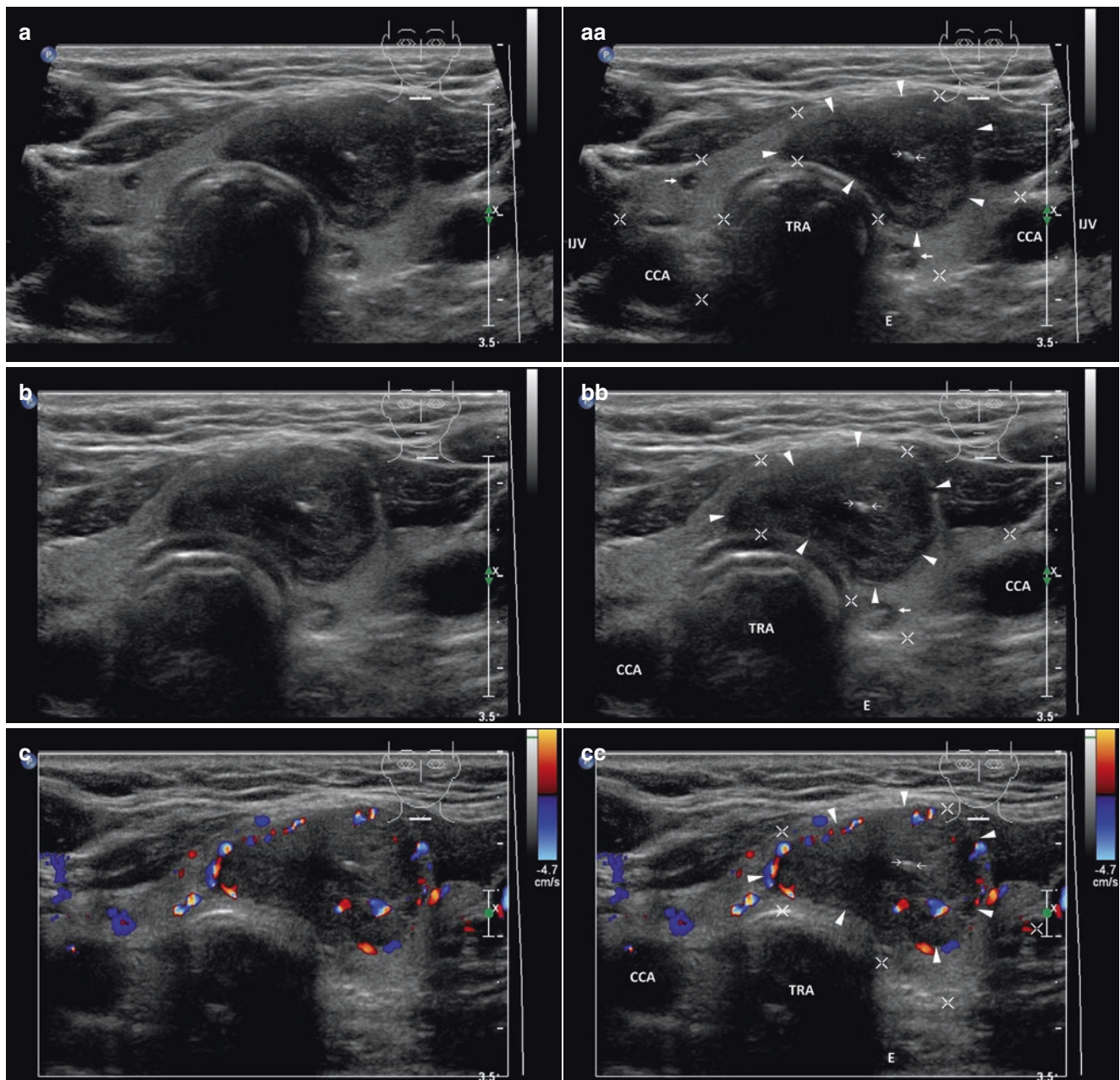


Fig. 13.3 (aa) A 67-year-old woman with a suspicious medium-sized solid nodule (*arrowheads*), in the LL and left branch of isthmus, size $25 \times 23 \times 15$ mm and volume 4.5 mL in multinodular goiter (MNG). Post-thyroidectomy histology: benign hyperplastic nodule. US scans: ovoid shape; homogeneous; hypoechoic; central microcalcifications (*arrows*); well-defined margin; tiny nonsuspicious complex nodules bilaterally (*arrows*); Tvol 12 mL, RL 6 mL, and LL 6 mL; transverse. (bb) Detail of suspicious medium-sized solid nodule (*arrowheads*): ovoid shape; homogeneous; hypoechoic; central microcalcifications (*arrows*); nodule protrusion ventrally with contour bulging, but without interrupting continuity of the capsule; transverse. (cc) Detail of suspi-

cious medium-sized solid nodule (*arrowheads*), CFDS: normal peripheral vascularity and sporadic central vascularity, *pattern I*; nodule protrusion ventrally with contour bulging, but no vessel invasion into muscles; transverse. (dd) Detail of suspicious medium-sized solid nodule (*arrowheads*): ovoid shape; homogeneous; hypoechoic; one central microcalcification (*arrow*); nodule protrusion ventrally with contour bulging, but without interrupting continuity of the capsule; focally lobulated margin; longitudinal. (ee) Detail of suspicious medium-sized solid nodule (*arrowheads*), CFDS: normal peripheral vascularity and sporadic central vascularity, *pattern I*; nodule protrusion ventrally with contour bulging, but no vessel invasion into muscles; longitudinal

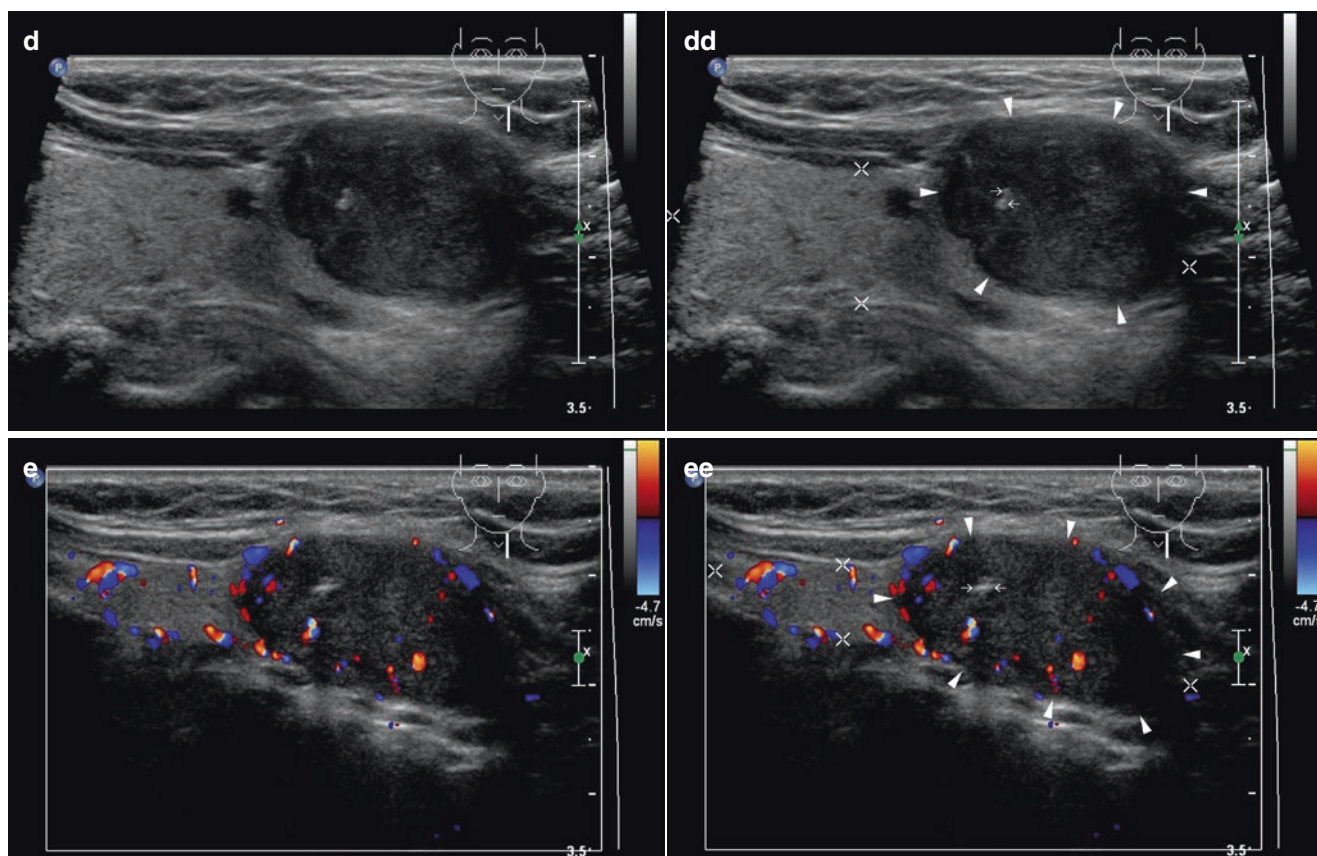


Fig. 13.3 (continued)

References

1. Haugen BR, Alexander EK, Bible KC, Doherty GM, Mandel SJ, Nikiforov YE, et al. 2015 American Thyroid Association Management Guidelines for adult patients with thyroid nodules and differentiated thyroid cancer: The American Thyroid Association Guidelines Task Force on Thyroid Nodules and Differentiated Thyroid Cancer. *Thyroid*. 2016;26(1):1–133.
2. Moon WJ, Jung SL, Lee JH, Na DG, Baek JH, Lee YH, et al.; Thyroid Study Group, Korean Society of Neuro- and Head and Neck Radiology. Benign and malignant thyroid nodules: US differentiation—multi-center retrospective study. *Radiology* 2008;247(3):762–770.

14.1 Essential Facts

- A follicular thyroid carcinoma (FTC) accounts for 10–32% of differentiated thyroid carcinomas (DTC); the rest is papillary thyroid carcinoma (PTC) [1].
- In a large demographic study in the USA the second most common histologic type among all sex and racial/ethnic groups was FTC ranges 9–23%. Both PTC and FTC rates are consistently two to three times higher among females than males. Incidence rates tended to be higher among White than among Black subjects, and among White non-Hispanic subjects than among White Hispanic or Asian Pacific Islander subjects [2].
- In iodine-deficient areas the relative rate of FTC tends to be even higher, up to 40% of the cases [3].
- More recently, a decreased incidence of FTC has been reported. This decrease is probably due to more accurate histological diagnosis (exclusion of atypical follicular adenoma, identification of follicular variants of PTC) and also to iodine supplementation programs [3].
- FTC has been classified as minimally invasive (MI-FTC), which has limited capsular and/or vascular invasion, and as widely invasive (WI-FTC), which has widespread infiltration of adjacent thyroid tissue and/or blood vessels. WI-FTC has larger primary tumors, and had a higher incidence of extrathyroidal extension, lymph node metastasis, and distant metastasis (50%) [1, 3].
- LN involvement in FTC is uncommon, ranging from 0–10% [3].
- DTC (PTC and FTC) have similarities in their clinically indolent behavior, management, and outcome. However, there are distinct differences between these two carcinomas: Patients with FTC tend to be older, present with more advanced disease, and have a poorer survival rate [1].
- FTC has a higher risk of developing distant metastases (28.8%) and mortality (17.2%) compared with PTC (8.9% resp. 7.6%) [1].
- The recurrences of PTC and FTC are most frequent at the extremes of age (<20 and >59 years), but their mortality rates successively increased in patients aged >40 years [4].
- The overall 5-year relative survival rate for PTC and FTC is greater than 90%; FTC, therefore, has a poorer prognosis compared to PTC. The mortality rate ranges from 5–15% even if the disease is confined to the thyroid at the time of diagnosis [5].
- For a more detailed comparison of both cancers, see Sect. 15.2 of Chap. 15.
- Hürthle cell carcinoma (HCC) has generally been considered to be a variant of FTC. HCC occurs in an older age group, is more aggressive with distant metastasis, and has a poorer prognosis than non-HCC [3]. HCC accounts for 3–5% of all thyroid cancers [7, 8]. In a study by Kushchayeva et al. [9] the 10-year disease-free interval was 75% for FTC and 40.5% for HCC and the 10-year cause-specific mortality was 20% for FTC and 51% for HCC patients [9]. Increasing age, male sex, and increasing tumor size substantially decrease survival of patients with HCC [7].

14.2 US Features of FTC According to the 2015 ATA Guidelines [6]

- For FTC, apply the same 2015 ATA criteria as for others suspected nodes (Fig. 14.1aa).
- FTC exhibits some differences in US features:
 - Nodules are more likely to be isoechoic to hyperechoic (Fig. 14.3aa).
 - Noncalcified (Fig. 14.1aa).
 - Round (width greater than anteroposterior dimension) (Fig. 14.2aa).
 - Regular smooth margins (Fig. 14.3aa).
- Similarly, the follicular variant of papillary cancer (FVPTC) has the same appearance as FTC.
- Distant metastases are rarely observed arising from FTC < 2 cm in diameter, which therefore justifies a higher size cutoff for hyperechoic nodules.
- In FTC, intranodular vascularity correlates with malignancy.
- HCCs show a spectrum of US appearances from predominantly hypoechoic to hyperechoic lesions; from peripheral blood flow with no internal flow to extensively vascularized lesions. The most frequent pattern (Fig. 14.4aa) is predominantly isoechoic, containing hypoechoic areas, without calcifications and with internal or peripheral (Fig. 14.4dd) vascularity [10].

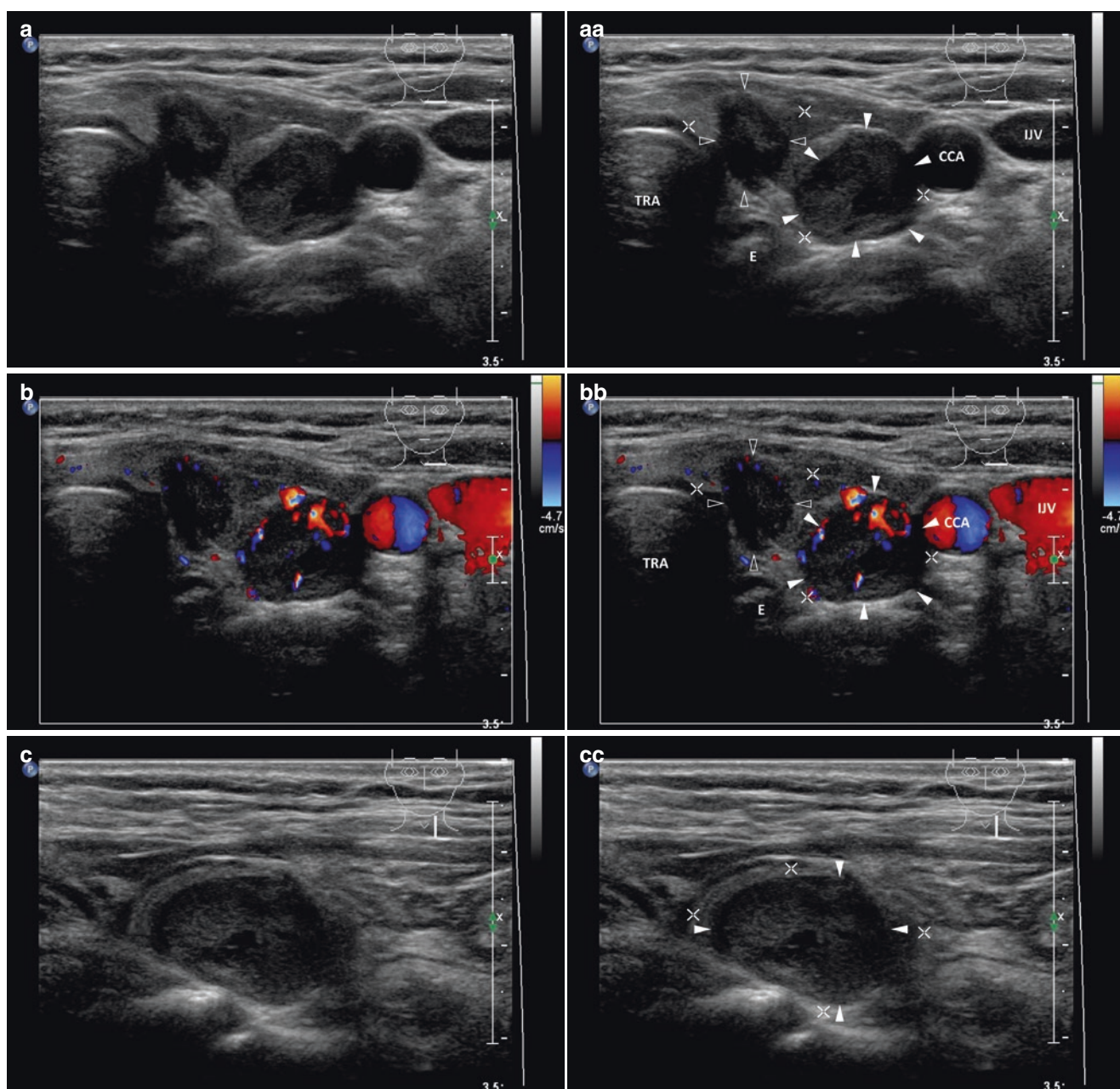


Fig. 14.1 (aa) A 76-year-old woman with two follicular thyroid carcinomas (FTCs) in the LL—micro FTC, size $9 \times 9 \times 8$ mm, volume 0.5 mL and small FTC, size $19 \times 15 \times 12$ mm, volume 2 mL: micro FTC (blank arrowheads)—“taller-than-wide” shape; small FTC (arrowheads)—round shape; both with the same US appearance—solid; inhomogeneous structure; mostly hypoechoic; smooth margin; LL 8 mL; transverse. (bb) Detail of two FTCs, CFDS: micro FTC (blank arrowheads)—minimal vascularity at periphery, *pattern 0*; small FTC

(arrowheads)—increased central and peripheral vascularity, *pattern II*; transverse. (cc) Detail of small FTC (arrowheads): ovoid shape; longitudinal. (dd) Detail of small FTC (arrowheads), CFDS: increased central and peripheral vascularity, *pattern II*; longitudinal. (ee) Detail of micro FTC (blank arrowheads): “taller-than-wide” shape; longitudinal. (ff) Detail of micro FTC (blank arrowheads), CFDS: minimal peripheral vascularity, *pattern 0*; longitudinal

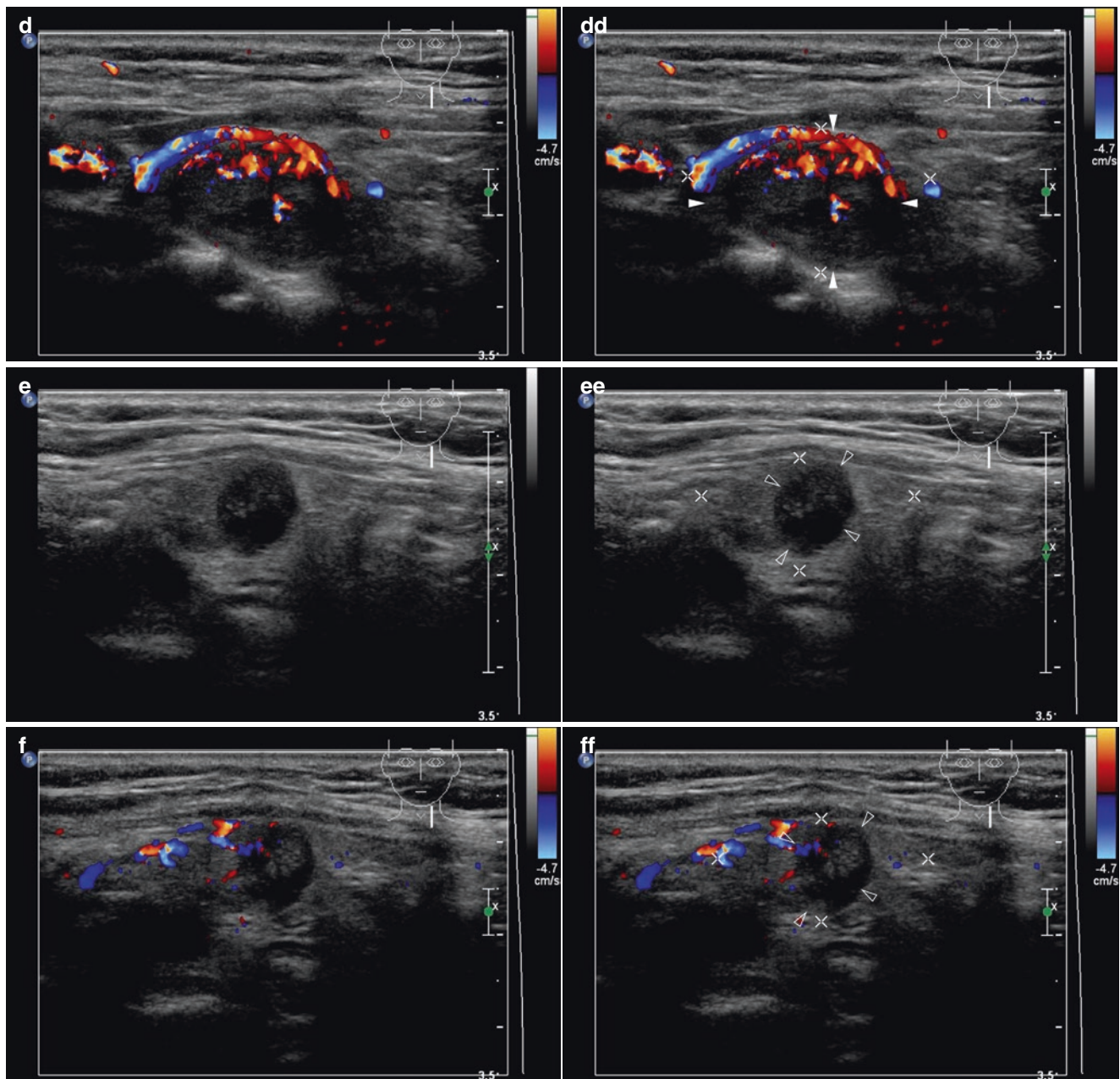
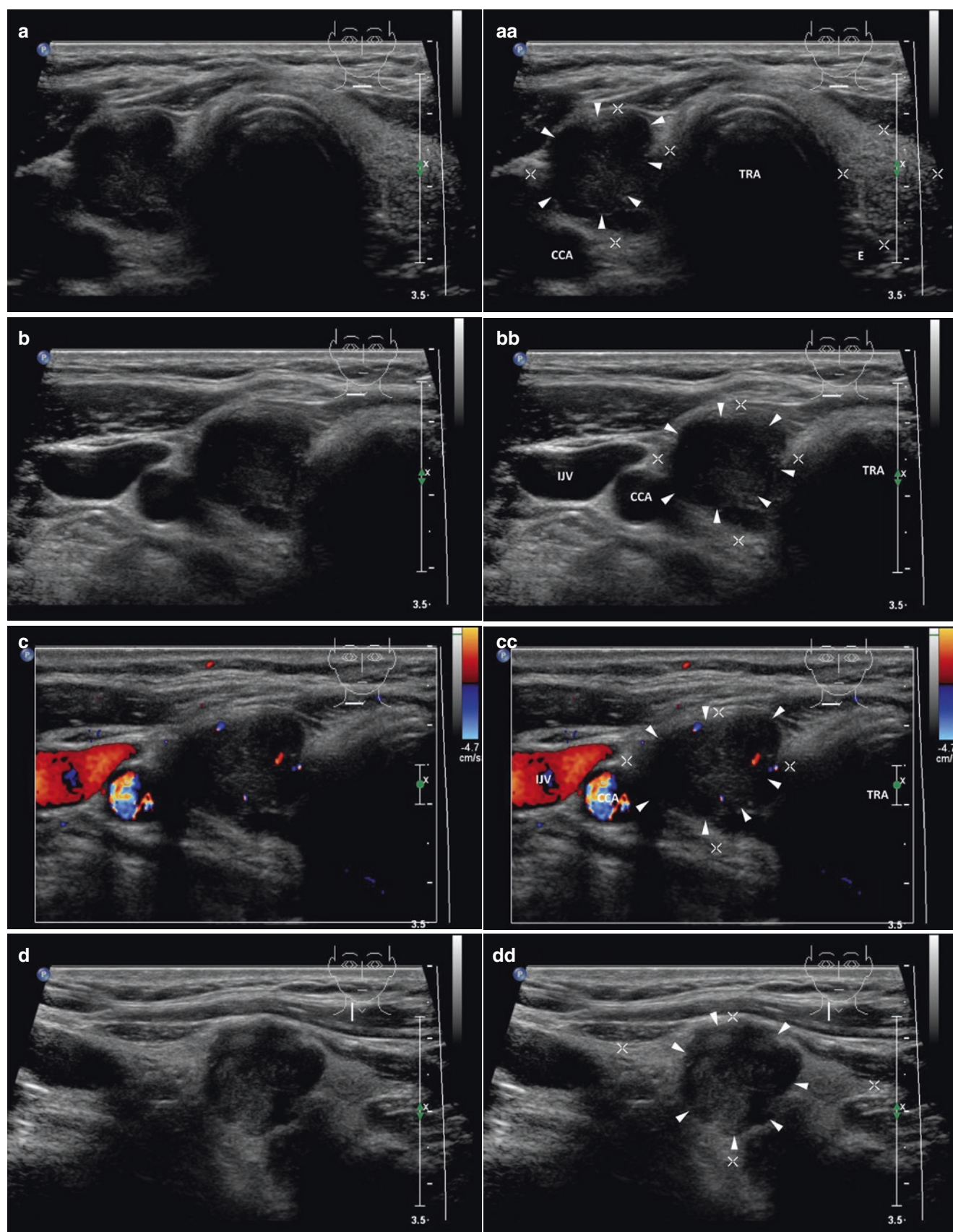


Fig. 14.1 (continued)

Fig. 14.2 (aa) A 67-year-old man with a solitary, medium-sized follicular thyroid carcinoma—FTC (arrowheads) in the RL, size $22 \times 17 \times 15$ mm and volume 3 mL: solid; round shape; inhomogeneous structure; mostly hypoechoic; microlobulated margin; Tvol 18 mL, RL 10 mL, and LL 8 mL; transverse. (bb) Detail of medium-sized FTC (arrowheads): round shape; inhomogeneous structure; mostly

hypoechoic; microlobulated margin; transverse. (cc) Detail of medium-sized FTC (arrowheads), CFDS: minimal vascularity at periphery, pattern 0; transverse. (dd) Detail of medium-sized FTC (arrowheads): round shape; inhomogeneous structure; mostly hypoechoic; microlobulated margin; longitudinal



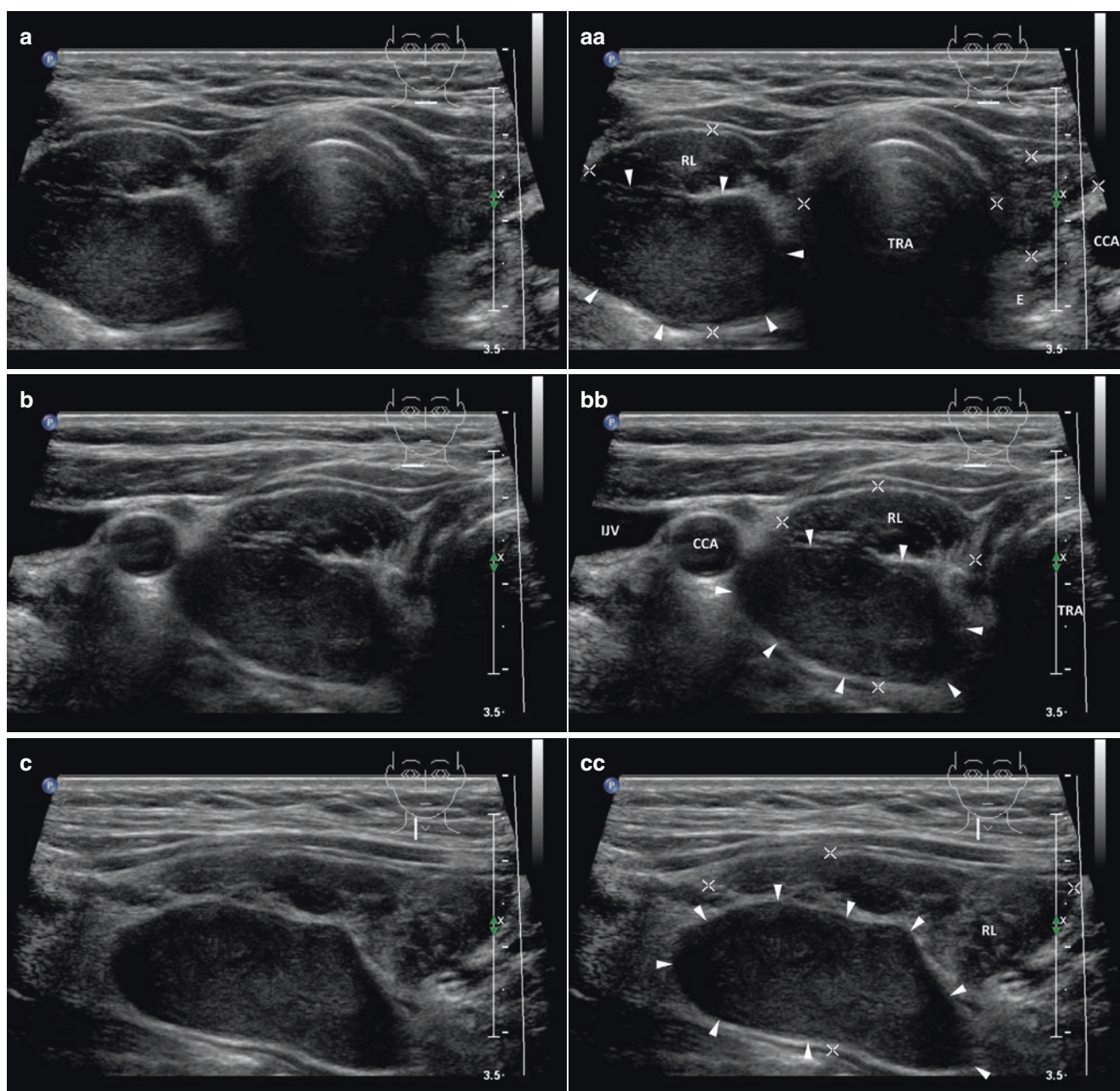


Fig. 14.3 (aa) A 69-year-old woman with Hashimoto's thyroiditis (HT) and a solitary large follicular thyroid carcinoma—FTC (arrowheads) in the RL, size $34 \times 29 \times 15$ mm and volume 8 mL; solid; elliptical shape; inhomogeneous structure; mixed echogenicity, mostly hypoechoic at periphery; well-defined margin; thyroid gland—classic HT US appearance; Tvol 16 mL, RL 9 mL, and LL 7 mL; transverse. (bb) Detail of large FTC (arrowheads) located dorsally in the upper part of the RL: elliptical shape; inhomogeneous structure; mixed echogenicity, mostly hypoechoic at periphery; well-defined margin; transverse. (cc) Detail of large FTC (arrowheads) located dorsally in the upper part of the RL: elliptical shape; inhomogeneous structure; mixed echogenicity, mostly hypoechoic at periphery; well-defined margin; transverse. (dd) Detail of large FTC (arrowheads) located dorsally in the upper part of the RL: elliptical shape; inhomogeneous structure; mixed echogenicity, mostly hypoechoic at periphery; well-defined margin; transverse. (ee) Detail of large FTC (arrowheads) located dorsally in the upper part of the RL: elliptical shape; inhomogeneous structure; mixed echogenicity, mostly hypoechoic at periphery; well-defined margin; transverse. (ff) Detail of large FTC (arrowheads) located dorsally in the upper part of the RL: elliptical shape; inhomogeneous structure; mixed echogenicity, mostly hypoechoic at periphery; well-defined margin; transverse.

genicity, mostly hypoechoic at periphery; well-defined margin; transverse. (cc) Detail of large FTC (arrowheads) located dorsally in the upper part of the RL: elliptical shape; inhomogeneous structure; mixed echogenicity, mostly hypoechoic at periphery; well-defined margin; RL—classic HT US appearance; transverse. (dd) Detail of large FTC (arrowheads) located dorsally in the upper part of the RL, CFDS: avascular, only focus of hilar and central vascularity, pattern 0-I; longitudinal

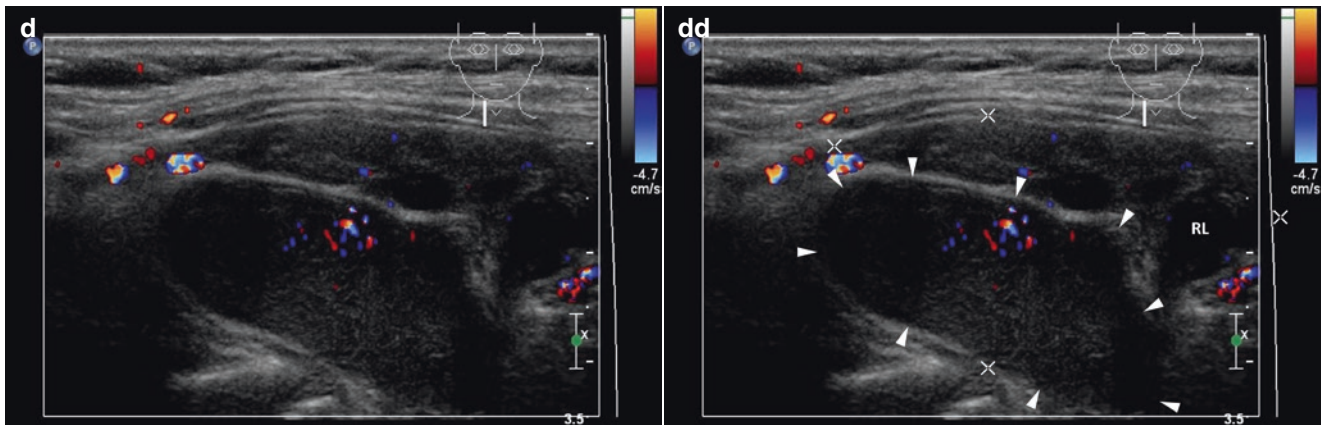


Fig. 14.3 (continued)

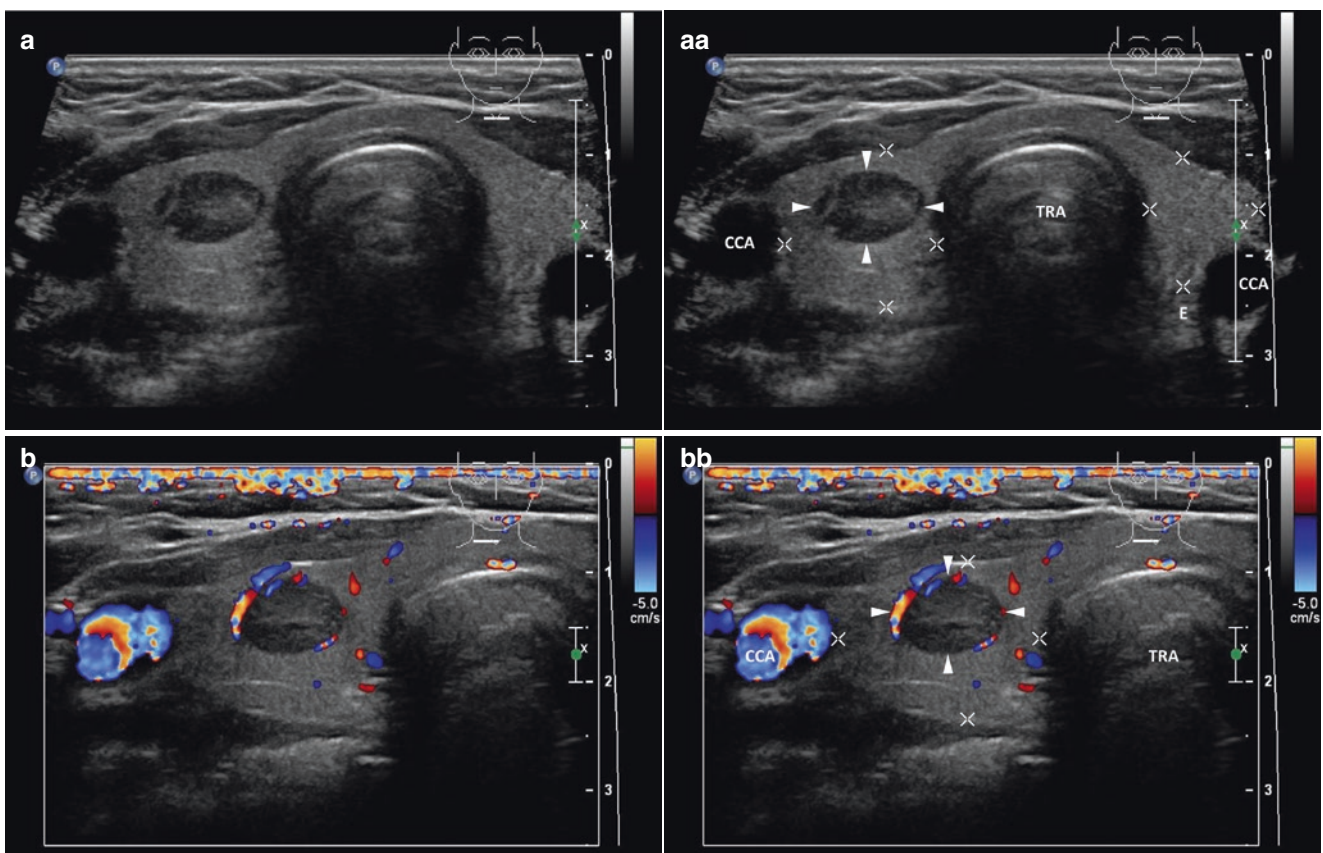


Fig. 14.4 (aa) A 56-year-old woman with a solitary Hürthle cell carcinoma (HCC)—microcarcinoma (*arrowheads*) in the RL, size $12 \times 11 \times 7$ mm and volume 0.5 mL; solid; elliptical shape; inhomogeneous structure; mixed echogenicity, mostly hypoechoic at periphery; well-defined margin; Tvol 12 mL, RL 7 mL, and LL 5 mL; transverse. (bb) Detail of HCC microcarcinoma (*arrowheads*) in the RL, CFDS:

peripheral vascularity, *pattern I*; transverse. (cc) Detail of HCC microcarcinoma (*arrowheads*) in the RL: solid; elliptical shape; inhomogeneous structure; mixed echogenicity, mostly hypoechoic at periphery; longitudinal. (dd) Detail of HCC microcarcinoma (*arrowheads*) in the RL, CFDS: peripheral vascularity, *pattern I*; longitudinal

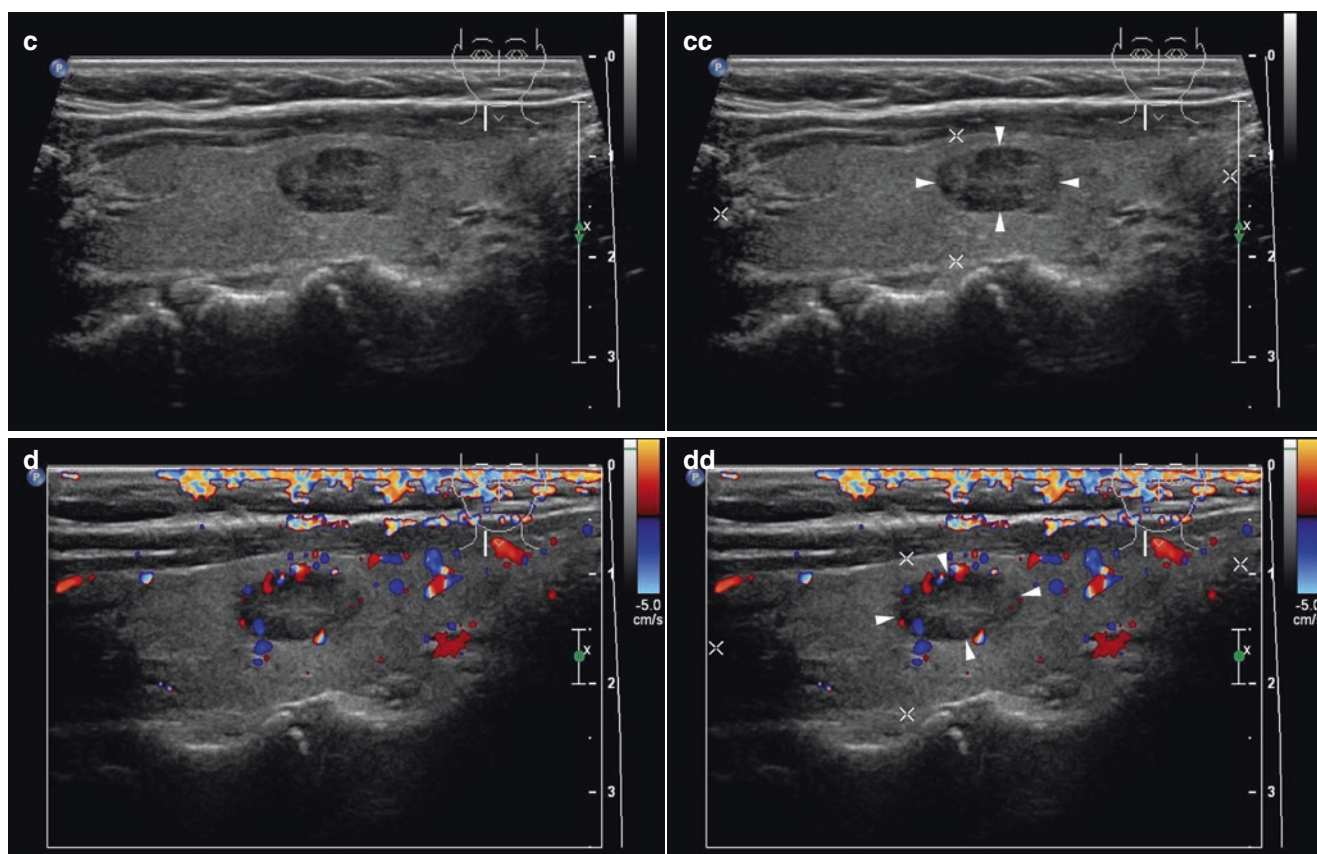


Fig. 14.4 (continued)

References

1. Chow SM, Law SC, Mendenhall WM, Au SK, Yau S, Yuen KT, et al. Follicular thyroid carcinoma: prognostic factors and the role of radioiodine. *Cancer*. 2002;95(3):488–98.
2. Enewold L, Zhu K, Ron E, Marrogi AJ, Stojadinovic A, Peoples GE, et al. Rising thyroid cancer incidence in the United States by demographic and tumor characteristics, 1980–2005. *Cancer Epidemiol Biomark Prev*. 2009;18(3):784–91.
3. De Crea C, Raffaelli M, Sessa L, Ronti S, Fadda G, Bellantone C, et al. Actual incidence and clinical behaviour of follicular thyroid carcinoma: an institutional experience. *Sci World J*. 2014;2014:952095.
4. Mazzaferri EL. An overview of the management of papillary and follicular thyroid carcinoma. *Thyroid*. 1999;9(5):421–7.
5. Hassan A, Khalid M, Riaz S, Nawaz MK, Bashir H. Follicular thyroid carcinoma: disease response evaluation using American Thyroid Association Risk Assessment Guidelines. *Eur Thyroid J*. 2015;4(4):260–5.
6. Haugen BR, Alexander EK, Bible KC, Doherty GM, Mandel SJ, Nikiforov YE, et al. 2015 American Thyroid Association Management Guidelines for Adult Patients with Thyroid Nodules and Differentiated Thyroid Cancer: The American Thyroid Association Guidelines Task Force on Thyroid Nodules and Differentiated Thyroid Cancer. *Thyroid*. 2016;26(1):1–133.
7. Bhattacharyya N. Survival and prognosis in Hürthle cell carcinoma of the thyroid gland. *Arch Otolaryngol Head Neck Surg*. 2003;129(2):207–10.
8. Stojadinovic A, Ghossein RA, Hoos A, Urist MJ, Spiro RH, Shah JP, et al. Hürthle cell carcinoma: a critical histopathologic appraisal. *J Clin Oncol*. 2001;19(10):2616–25.
9. Kushchayeva Y, Duh QY, Kebebew E, D'Avanzo A, Clark OH. Comparison of clinical characteristics at diagnosis and during follow-up in 118 patients with Hurthle cell or follicular thyroid cancer. *Am J Surg*. 2008;195(4):457–62.
10. Maizlin ZV, Wiseman SM, Vora P, Kirby JM, Mason AC, Filipenko D, et al. Hurthle cell neoplasms of the thyroid: sonographic appearance and histologic characteristics. *J Ultrasound Med*. 2008;27(5):751–7.

15.1 Papillary Thyroid Microcarcinoma

15.1.1 Essential Facts

- Analysis of the thyroid cancer incidence from 1980 to 2005 (the Surveillance, Epidemiology and End Results/SEER/program of the National Cancer Institute) showed that half of the overall increase in PTC rates is due to rising rates of very small ≤ 1.0 cm cancers, so-called papillary thyroid microcarcinomas (PTMC) [1].
- Prevalence of subclinical PTMC is 1.9–11.7 per 100,000 females; that is about 1000 times higher than that of clinical thyroid carcinoma [2].
- PTMC represents 43% of PTC in patients >45 years of age and 34% in patients <45 years of age [3].
- The detection rate of PTMC (measuring 3–9.9 mm) in autopsy studies is 0.5–5.2% [2].
- Hay et al. at Mayo Clinic investigated 900 patients with PTMC in the period 1945–2004, with a mean follow-up of 17.2 years. Despite tumors being found multifocal in 23%, associated with cervical metastatic lymph nodes (LNs) in 31% and in 0.3% with distant metastases at diagnosis, the 20-year and 40-year tumor recurrence rates were only 6% and 8%, respectively [4].
- Currently, post-surgical follow-up of patients with PTMC shows disease-specific mortality rates $<1\%$, cervical metastatic LNs 2–6%, and distant recurrence rates 1–2%. These excellent results are more related to the indolent nature of the disease rather than to the effectiveness of treatment [4, 5].
- PTMC mostly showed stable tumor size on average follow-up by US on 5-year follow-up, whereas only 5% showed tumor enlargement (>3 mm) and 8% on 10-year follow-up. Only 1.7% and 3.8% of patients at

5-year and 10-year follow-up showed evidence of LN metastases [2].

- Subclinical low-risk PTMCs (no evidence of extrathyroidal extension, cervical metastatic LNs, or distant metastases) often have an indolent course and could be observed without immediate need for surgery. Older patients with subclinical low-risk PTMC may be the best candidates for observation only. PTMC in young patients (<40 years of age) is significantly more progressive, but the cause-specific survival is reported to be excellent. These patients can also be candidates for close US follow-up since it would not be too late for surgery if their subclinical PTMC turned into clinical disease [2].
- Meta-analyses revealed that central cervical metastatic LNs (at level C-VI) are associated with male gender, younger age (<45 years), larger tumor size (>5 mm), multifocality, and extrathyroidal extension [6].
- When patients with PTMC and PTC were compared, no differences were observed in age, gender, and multifocality. PTMC is associated with less frequent bilaterality, cervical metastatic LNs, thyroid capsule invasion, and disease recurrence, and has a higher rate of incidental diagnosis [7].

15.1.2 US Features of the Papillary Thyroid Microcarcinoma

- For PTMC, apply the same 2015 ATA criteria as for other suspected nodules [8].
- Typical features of PTMC [9]:
 - 50% of PTMC nodules have a well-defined margin and 50% have an ill-defined margin (and half of those

display, on histology, infiltration into the surrounding thyroid tissue (Figs. 15.2aa and 15.4aa).

- Halo sign in $\approx 6\%$ (Figs. 15.3aa and 15.4aa).
- No cystic changes.
- Microcalcifications in 50% (Figs. 15.1aa and 15.2aa).

- Isoechogenicity (on histology, predominantly follicular structures with large proportion of colloid) (Figs. 15.3aa and 15.4aa).
- Heterogeneous echogenicity (on histology, fibrous stroma proportion of $>20\%$) (Fig. 15.4aa)
- Cervical metastatic LNs (2–6%) (Fig. 15.4dd).

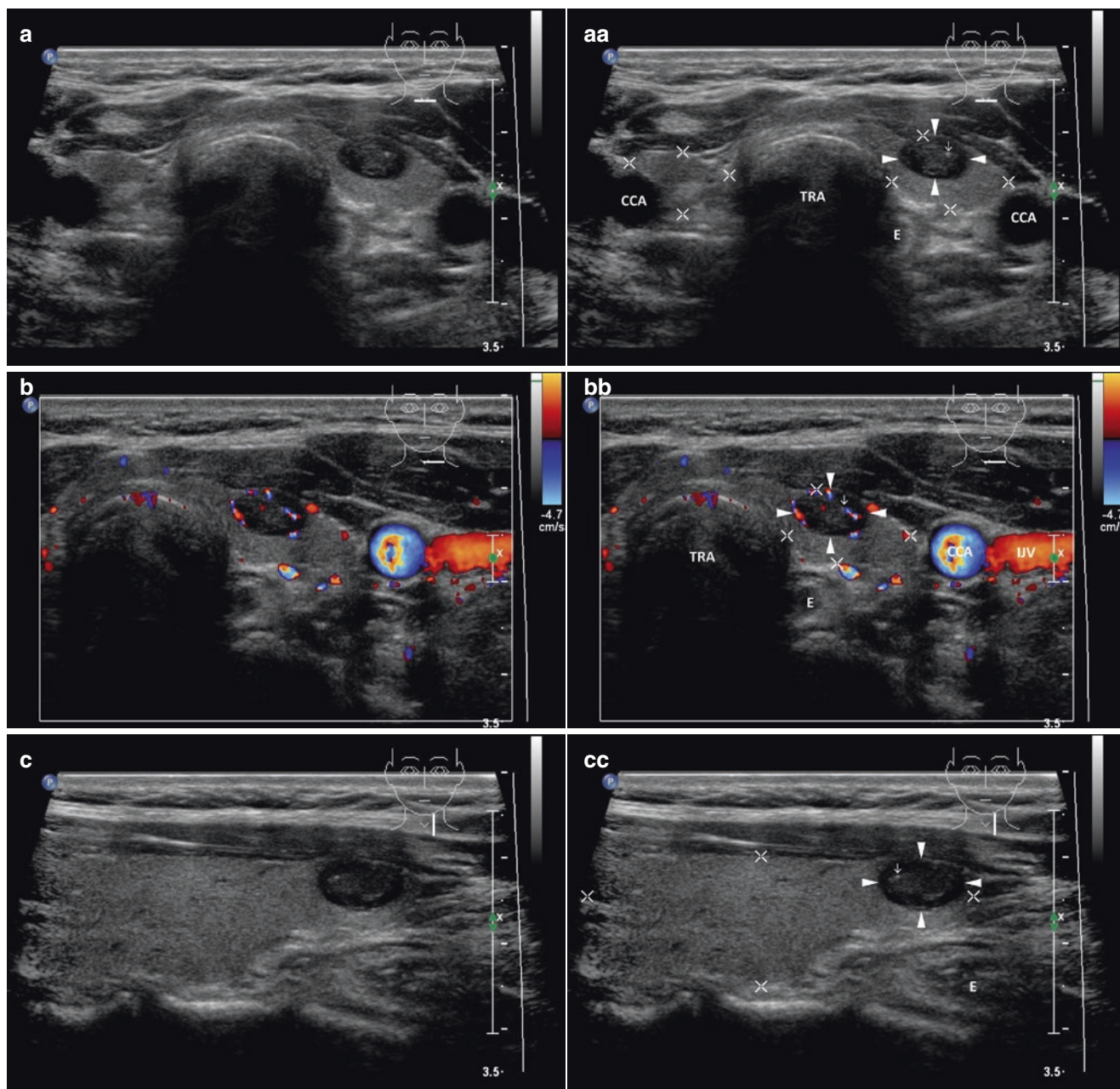


Fig. 15.1 (aa) A 44-year-old woman with a solitary papillary thyroid microcarcinoma—PTMC (arrowheads) in the LL, size $10 \times 8 \times 6$ mm and volume 0.3 mL: solid; elliptical shape; homogeneous; hypoechoic; one microcalcification (open arrow); well-defined, smooth margin; Tvol 12 mL, RL 6 mL, and LL 6 mL; transverse. (bb) Detail of solitary

PTMC (arrowheads), CFDS: peripheral vascularity and one central vessel branch, *pattern I*; transverse. (cc) Detail of solitary PTMC (arrowheads): hypoechoic; one microcalcification (open arrow); longitudinal. (dd) Detail of solitary PTMC (arrowheads), CFDS: peripheral vascularity and one central vessel branch, *pattern I*; longitudinal

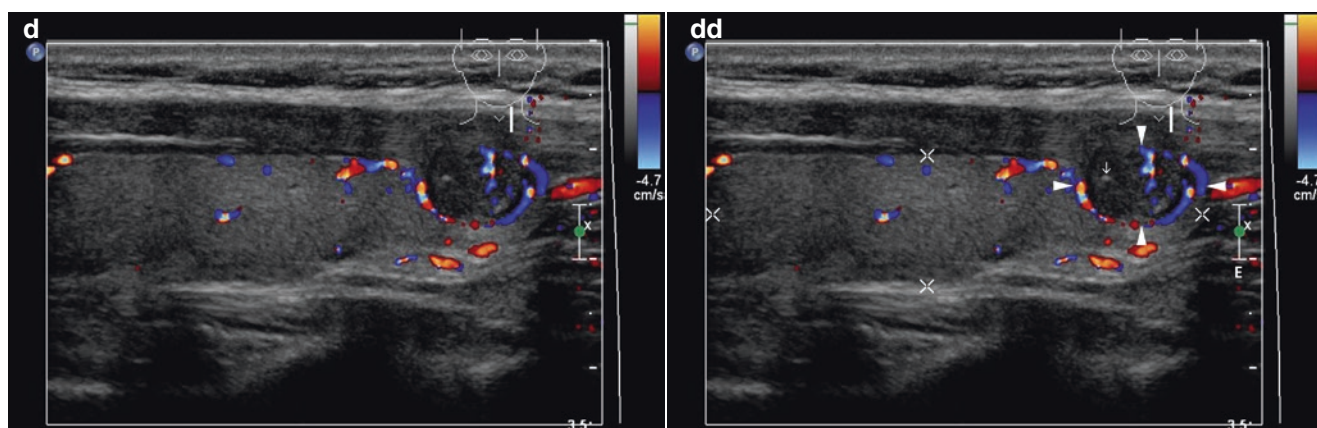


Fig. 15.1 (continued)

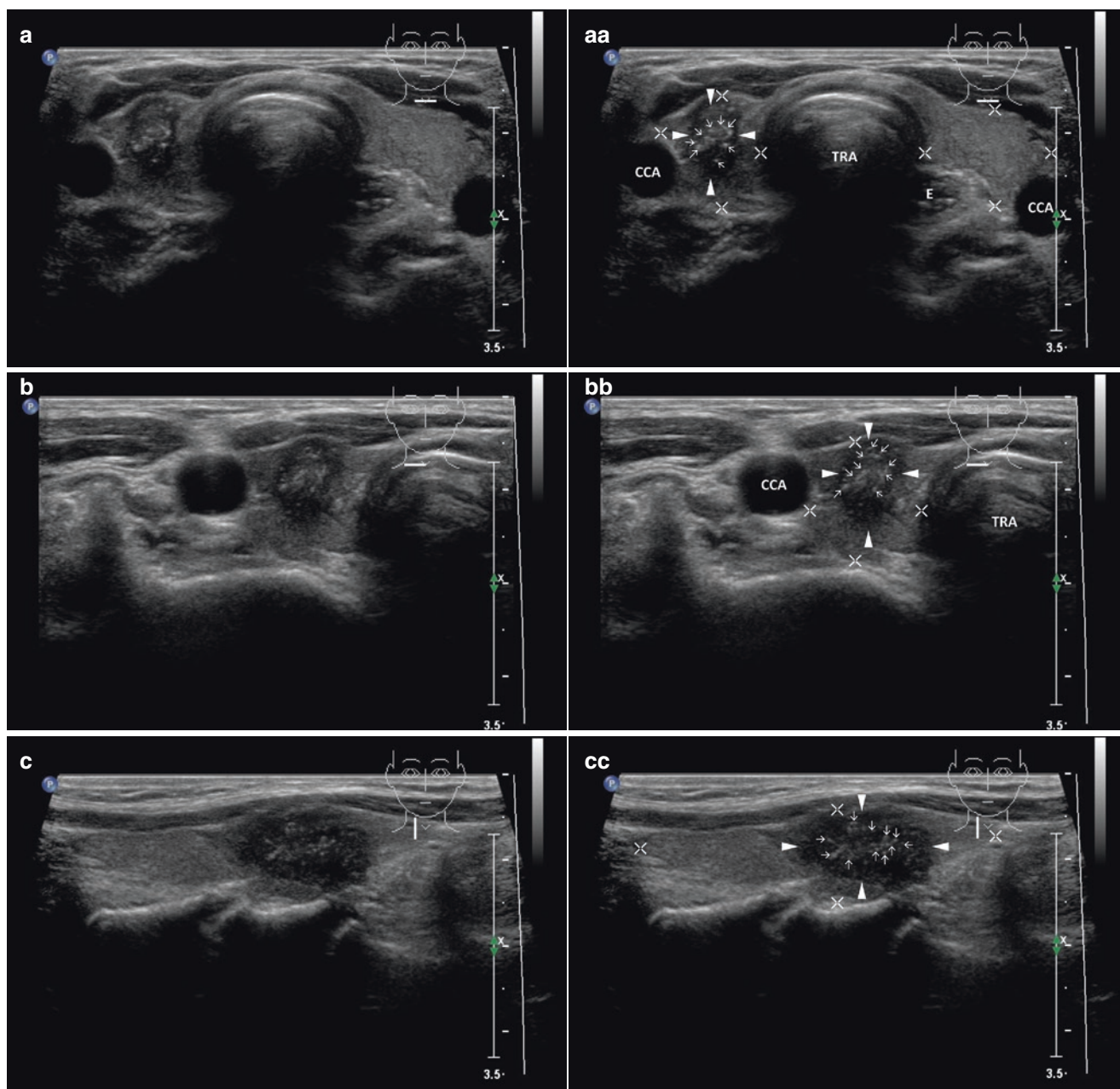


Fig. 15.2 (aa) A 63-year-old woman with a solitary papillary thyroid microcarcinoma—PTMC (arrowheads) in the RL, size $10 \times 9 \times 6$ mm and volume 0.3 mL: solid; “taller than wide” shape; coarse structure; hypoechoic; cluster of microcalcifications in the center (open arrows); blurred margin; Tvol 8 mL, RL 4 mL and LL 4 mL; transverse. (bb)

detail of solitary PTMC (arrowheads): solid; “taller-than-wide” shape; coarse structure; hypoechoic; cluster of microcalcifications in the center (open arrows); blurred margin; transverse. (cc) Detail of solitary PTMC (arrowheads): solid; coarse structure; hypoechoic; cluster of microcalcifications in the center (open arrows); blurred; longitudinal

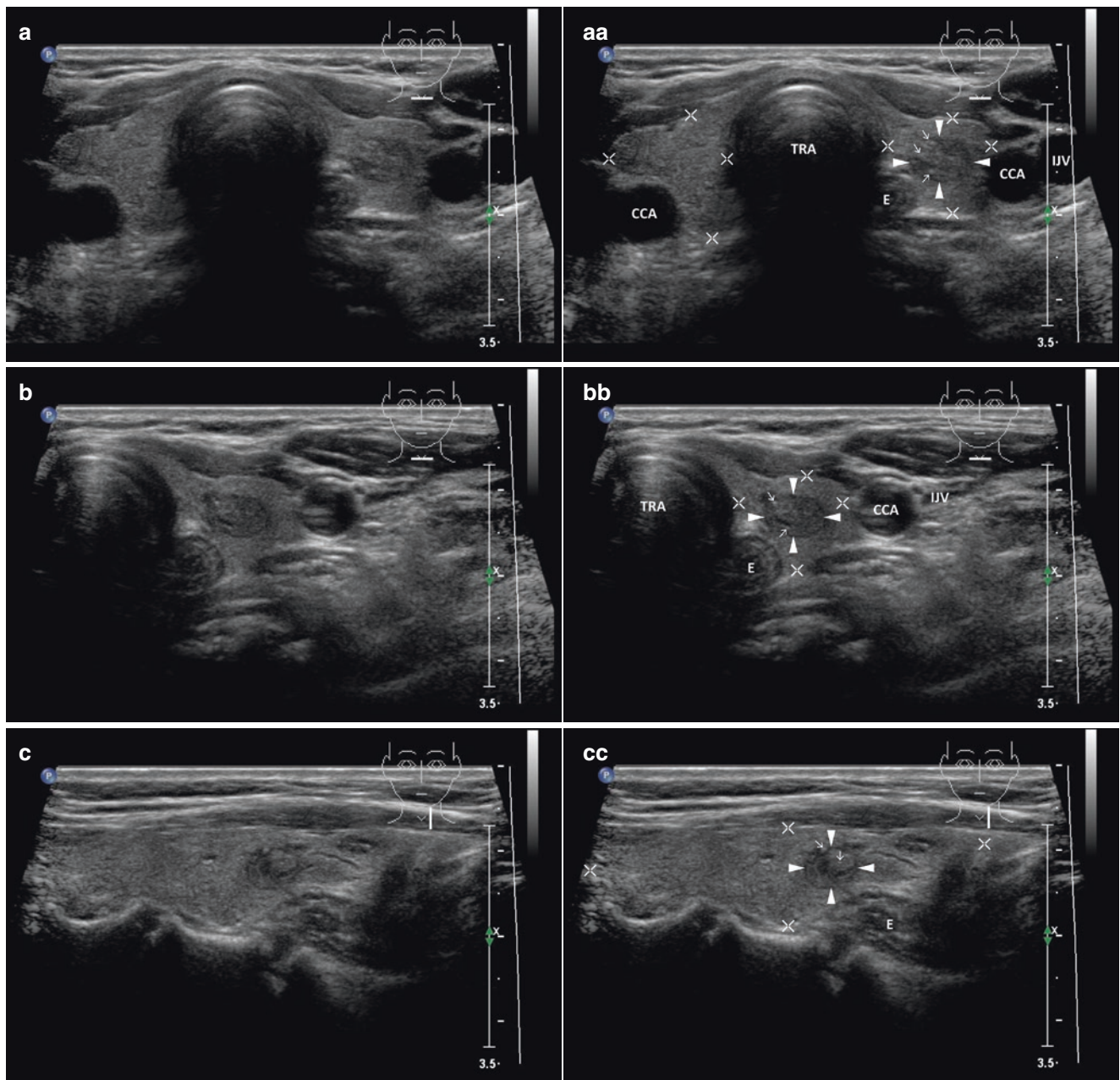


Fig. 15.3 (aa) A 62-year-old woman with a solitary papillary thyroid microcarcinoma—PTMC (arrowheads) in the LL, size $8 \times 7 \times 6$ mm and volume 0.2 mL: solid; round shape; inhomogeneous structure; isoechoic; sporadically hyperechoic punctuation (open arrows); thin halo sign; Tvol 8 mL, RL 4 mL, and LL 4 mL; transverse. (bb) Detail of solitary PTMC (arrowheads): inhomogeneous structure; isoechoic;

sporadically hyperechoic punctuation (open arrows); well-defined margin with thin halo sign; transverse. (cc) Detail of solitary PTMC (arrowheads): inhomogeneous; isoechoic; sporadically hyperechoic punctuation (open arrows); well-defined margin with thin halo sign; longitudinal

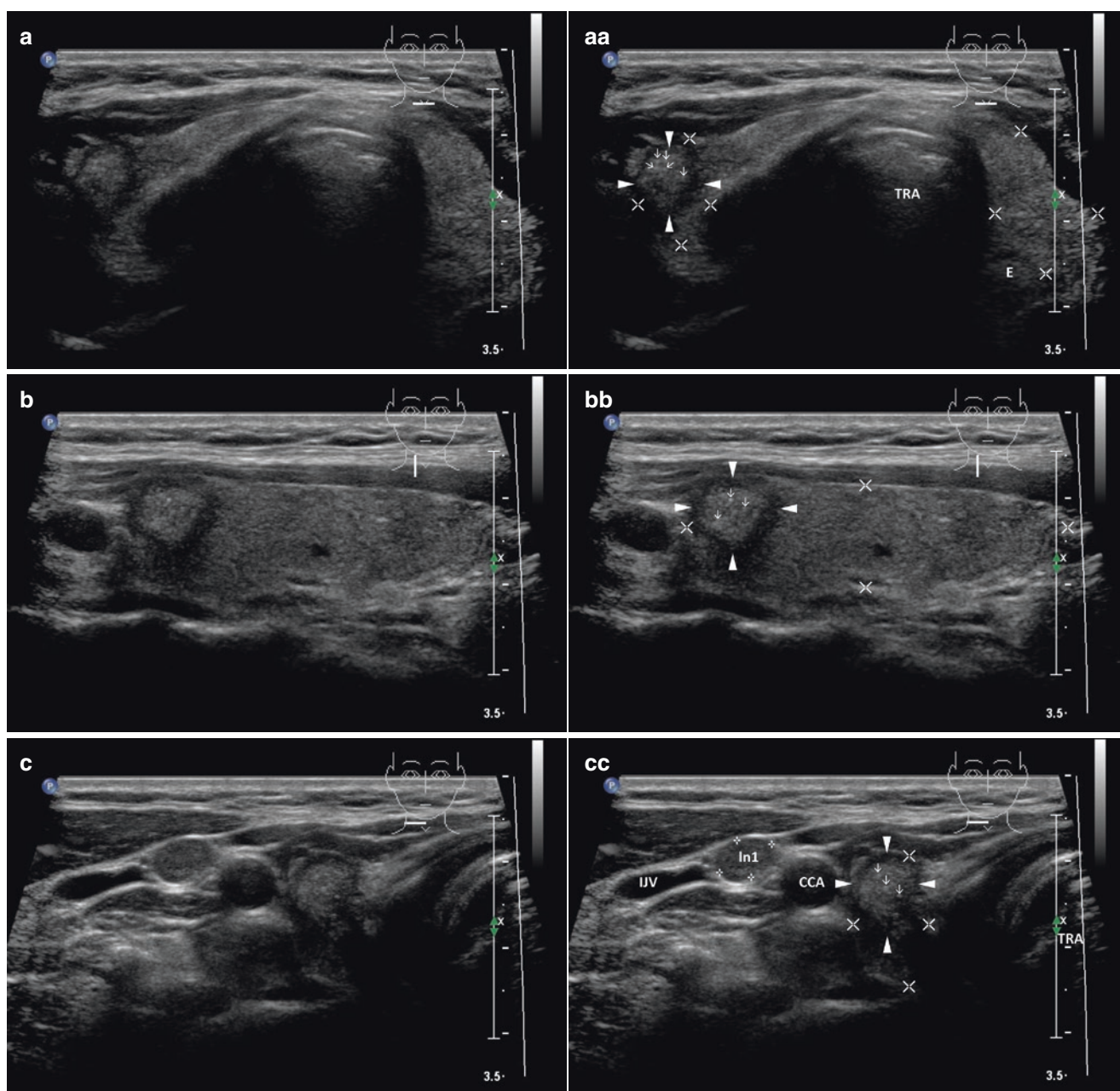


Fig. 15.4 (aa) A 30-year-old woman with a solitary, papillary thyroid microcarcinoma (PTMC) in the RL, size $10 \times 9 \times 8$ mm, volume 0.4 mL and small metastatic cervical lymph nodes (LNs) along right IJV, at level C-III. Overall view of thyroid gland: PTMC (arrowheads)—solid; “taller-than-wide” shape; inhomogeneous structure; isoechoic; central hyperechoic punctuation (open arrows); ill-defined margin with thick halo sign; Tvol 14 mL, RL 7 mL, and LL 7 mL; transverse. (bb) Detail of solitary PTMC (arrowheads): inhomogeneous structure; isoechoic; central hyperechoic punctuation (open arrows); ill-defined margin with thick halo sign; longitudinal. (cc) Detail of solitary PTMC and meta-

static cervical LNs: PTMC (arrowheads)—“taller-than-wide” shape; inhomogeneous structure; isoechoic; central hyperechoic punctuation (open arrows); one small oval hyperechoic metastatic ln1 (marks) between the right IJV and CCA; transverse. (dd) Detail of two metastatic cervical LNs: ln1, ln2 (marks)—solid; elliptical shape; size 19×7 mm and 16×6 mm, L/S ratio > 2 (not pathological); inhomogeneous structure; hyperechoic; no hilus sign; lumen of small vein (v) between LNs; longitudinal. (ee) Detail of two metastatic cervical LNs, CFDS: ln1, ln2 (marks)—increased mixed (peripheral and central) vascularity; lumen of small vein (v) between LNs; longitudinal

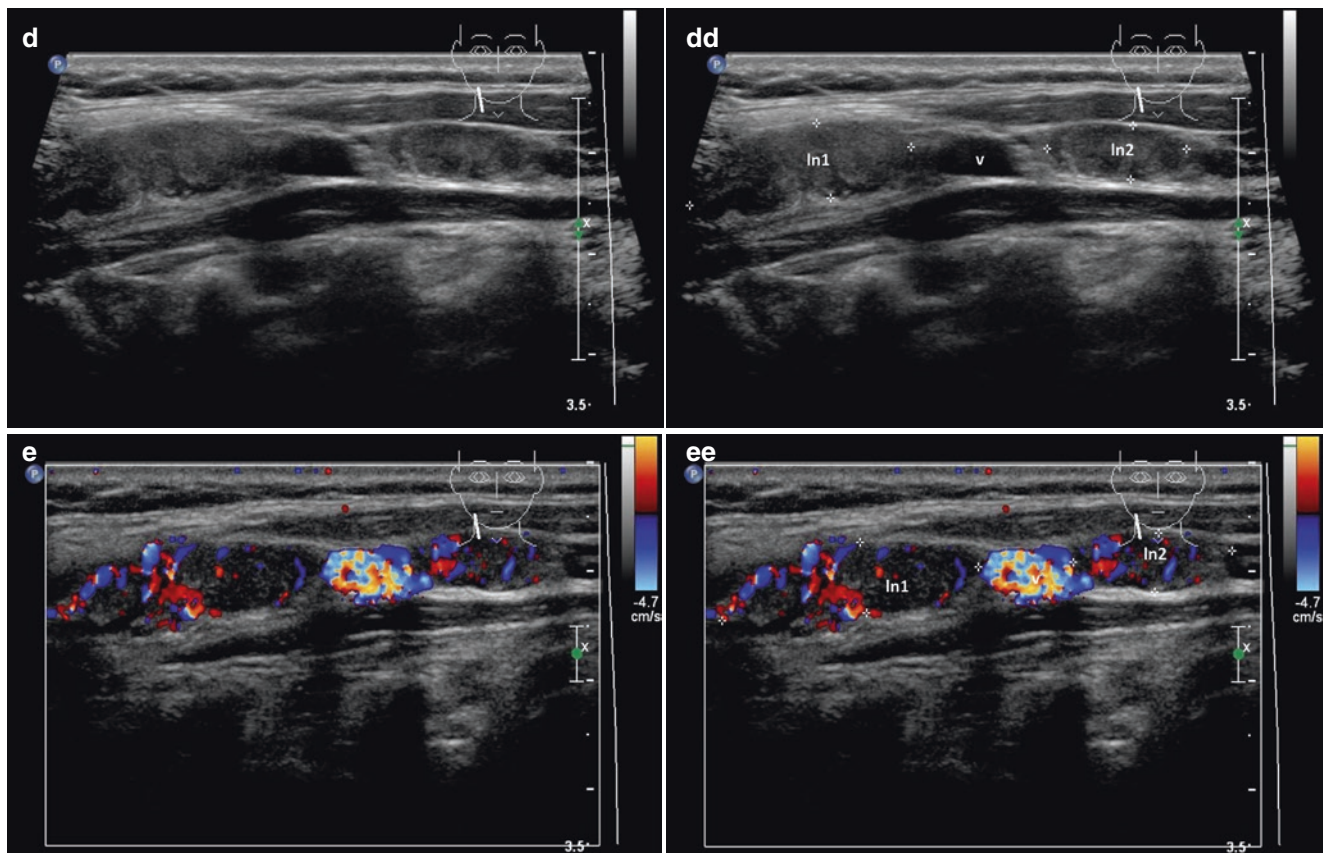


Fig. 15.4 (continued)

15.2 Papillary Thyroid Carcinoma: A Small Solitary Nodule ≤ 2 cm

15.2.1 Essential Facts

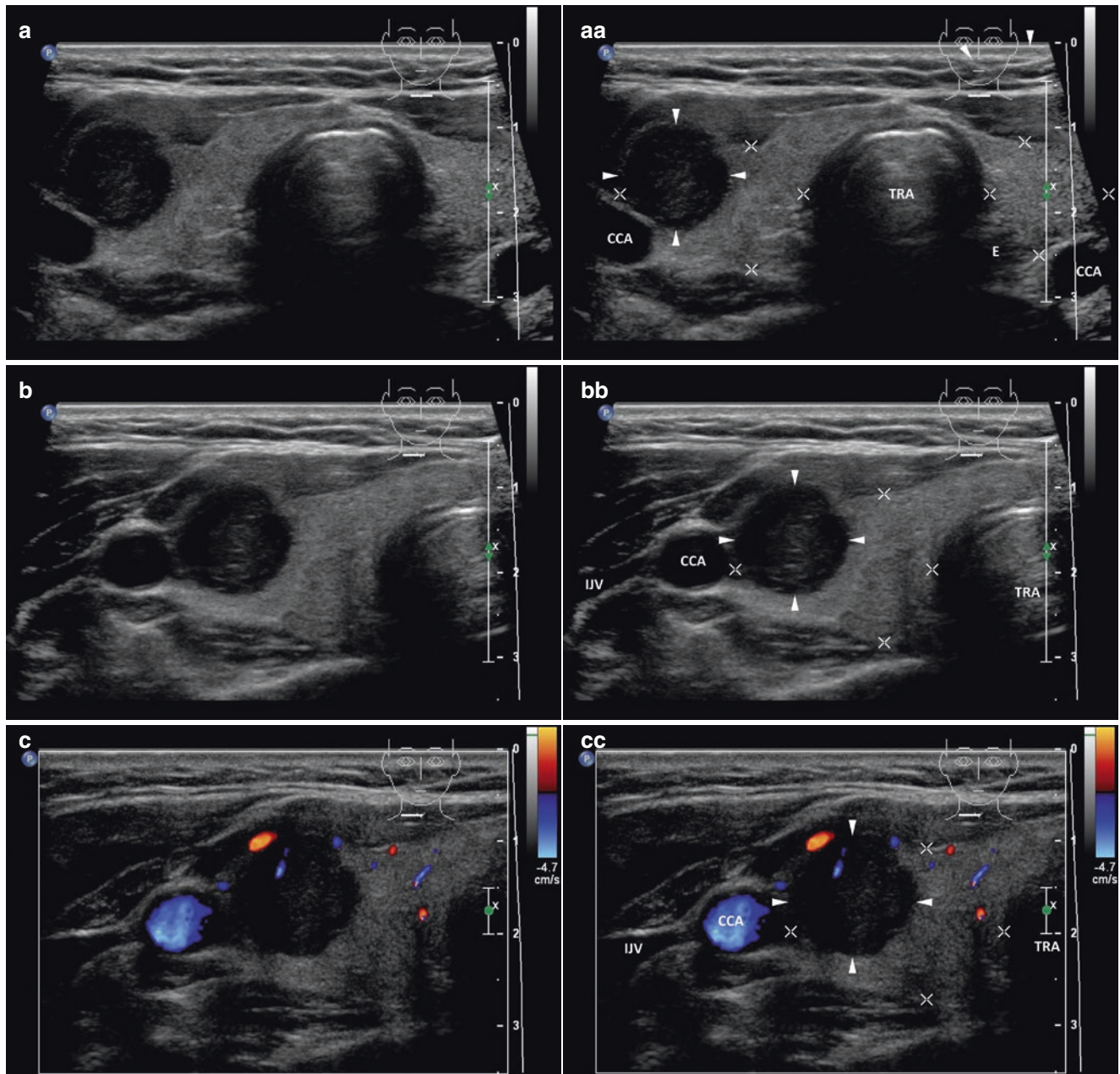
- The most common histological type of thyroid cancer among all sex and racial/ethnic groups is papillary thyroid carcinoma (PTC), range: 65–88% [1].
- PTC rate is consistently two to three times higher among females than males. The highest rates occurred among females aged 40–59, but the steepest increases were observed among those aged 60–79. Age-specific rates among men rise more slowly, peaking at ages 60–69 years for both genders; then decline at ages ≥ 80 years [1, 10].
- The youngest (<20 years) and oldest (≥ 80 years) age groups each accounts for only 2–3% of the PTC [1].
- Features predicting a poor prognosis of PTC patients: old age, extrathyroidal and/or extranodal extension, palpable lymph node (LN) and/or distant metastases, and large tumor size [11].
- Tg-Ab positive patients with no postoperative decrease in the Tg-Ab level have a poor prognosis of disease-free survival [12].
- PTC prognosis is excellent, reflecting a 5- and 10-year survival rate of 90–95% [13].
- Recurrence of PTC develops in about 20% of patients [14].
- PTC tends to metastasize through the lymphatic system, with cervical metastatic LNs occurring in 40–60%, and vascular invasion occurs in 2–14% [13].
- The vascular invasion was found in 3.3% of pure PTC, compared with 20.9% of cases of the follicular variant of papillary carcinoma (FVPTC) [13].
- The incidence of PTC is growing at a faster rate than any other malignancy. Nearly 50% of the increase proved to be PTC of 1 cm or smaller, and 87% were ≤ 2 cm. However, thyroid cancer mortality has remained flat, implying that these small cancers would not likely have progressed to be life-threatening. This dramatic rise in subclinical disease has been attributed largely to more frequent and widespread use of imaging of the head and neck for unrelated investigations, with the unanticipated discovery of these incidental cancers [15].
- Comparison PTC vs. FTC (both differentiated thyroid carcinomas) [16]:
 - Higher incidence 3.9:1.
 - Manifestation in a younger age, median age, 44 vs. 49.
 - Higher female-male ratio, 4.5 vs. 2.9.
 - Smaller primary tumor size, median 2 cm vs. 3.5 cm.
 - Higher incidence of multifocal disease, 28.3% vs. 18.1%.
 - Frequent extrathyroidal extension, 39.4% vs. 14%.
 - More cervical metastatic LNs, 33.3% vs. 12.1%.
 - Less distant metastases 8.9% vs. 28.8%.
 - The 10-year cause-specific survival, freedom from distant metastasis, and locoregional failure figures for PTC compared with FTC were 92.1% vs. 81%, 90.8% vs. 72.3%, and 78.5% vs. 83%.

Fig. 15.5 (aa) A 43-year-old woman with a solitary small papillary thyroid carcinoma—PTC (*arrowheads*) in the RL, size $15 \times 14 \times 14$ mm and volume 1.5 mL. US overall view: solid nodule—round shape; homogeneous structure; hypoechoic; well-defined margin; Tvol 18 mL, RL 10 mL, and LL 8 mL; transverse. (bb) Detail of solitary small PTC (*arrowheads*): solid nodule—round shape; homogeneous structure; hypoechoic; well-defined margin; transverse. (cc) Detail of solitary

small PTC (*arrowheads*), CFDS: minimal peripheral vascularity and one central vessel branch, *pattern I*; transverse. (dd) Detail of solitary small PTC (*arrowheads*): solid nodule—round shape; homogeneous structure; hypoechoic; well-defined margin; longitudinal. (ee) Detail of solitary small PTC (*arrowheads*), CFDS: minimal peripheral vascularity and one central vessel branch, *pattern I*; longitudinal

15.2.2 US Features of PTC, a Small Nodule ≤ 2 cm [8]

- Typical US features:
 - Marked hypoechogenicity (Figs. 15.5aa and 15.6aa).
 - Microcalcifications (Figs. 15.8bb, 15.9aa, and 15.12aa).
 - “Taller-than-wide shape” (anteroposterior-to-transverse ratio >1) (Figs. 15.7aa, 15.8aa, and 15.9bb).
 - Irregular margins (microlobulated, or spiculated) (Fig. 15.8cc).
 - Intranodular hypervascularity (Figs. 15.13cc and 15.14ee).
- Rare US features:
 - Follicular variant of papillary carcinoma (FVPTC) is more likely to be iso- to hyperechoic (Fig. 15.12aa).
 - Disrupted rim calcifications with small extrusive hypoechoic soft tissue component (Fig. 15.10aa).
 - Possible complete or incomplete halo sign (Figs. 15.11aa and 15.13aa).
 - Cystic degeneration (Fig. 15.14aa).
 - Cervical metastatic LNs.
- **See more at Section IV:** US classic features of high suspicion of malignancy for solid nodules according to the 2015 ATA Guidelines [8].



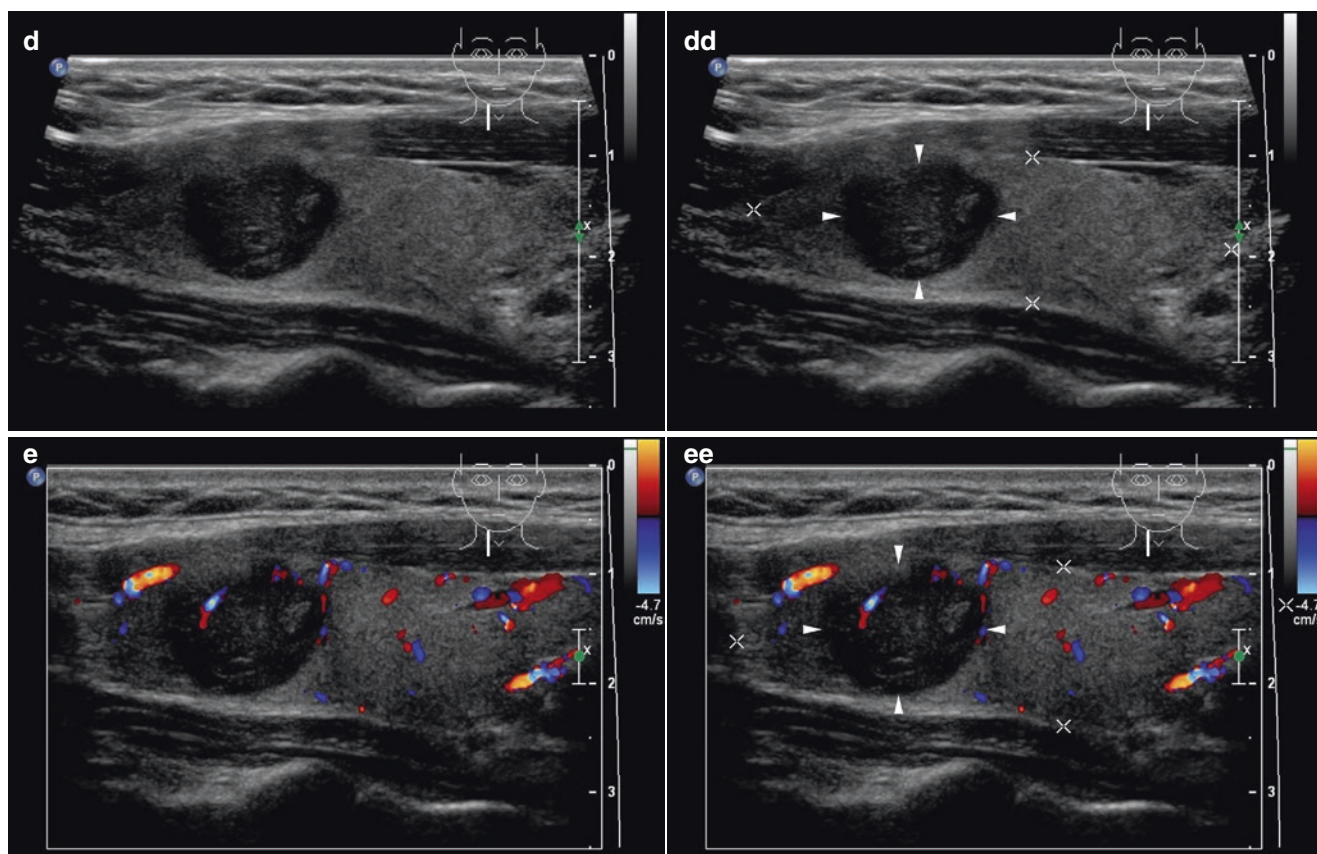


Fig. 15.5 (continued)

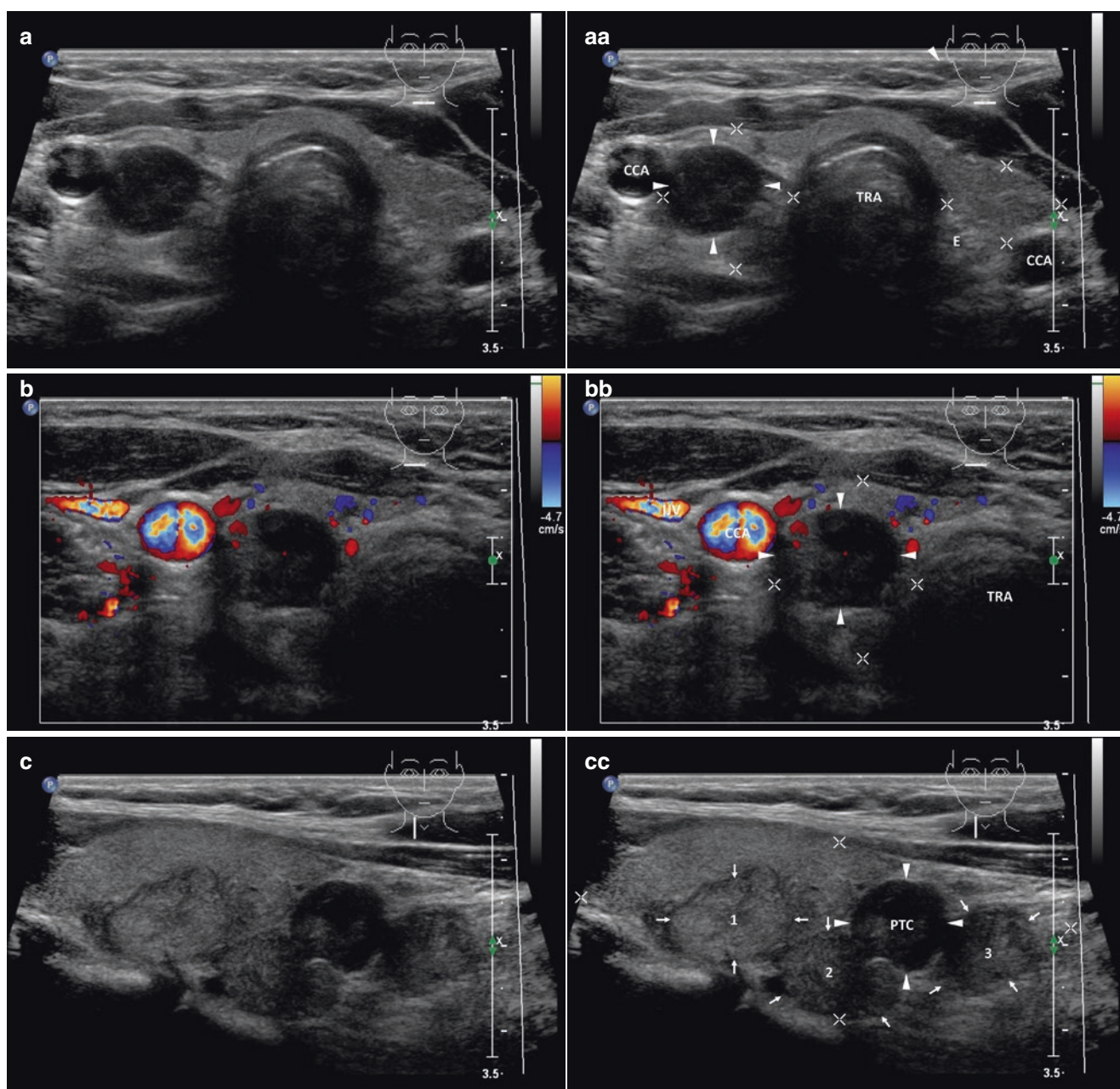


Fig. 15.6 (aa) A 37-year-old woman with multinodular goiter (MNG) and a small papillary thyroid carcinoma—PTC (arrowheads) in the RL, size $13 \times 12 \times 12$ mm and volume 1 mL. US overall view: solid nodule—round shape; homogeneous structure; hypoechoic; well-defined margin; Tvol 10 mL, RL 6 mL, and LL 4 mL; transverse. (bb) Detail of small PTC (arrowheads), CFDS: minimal peripheral and intranodular

vascularity, *pattern I*; transverse. (cc) Detail of small PTC (arrowheads) in MNG, RL: PTC—solid nodule; round shape; homogeneous structure; hypoechoic; well-defined margin; three nonsuspicious nodules (1, 2, 3)—solid; round or ovoid shape; homogeneous structure; hyperechoic; well-defined margin with halo sign; longitudinal

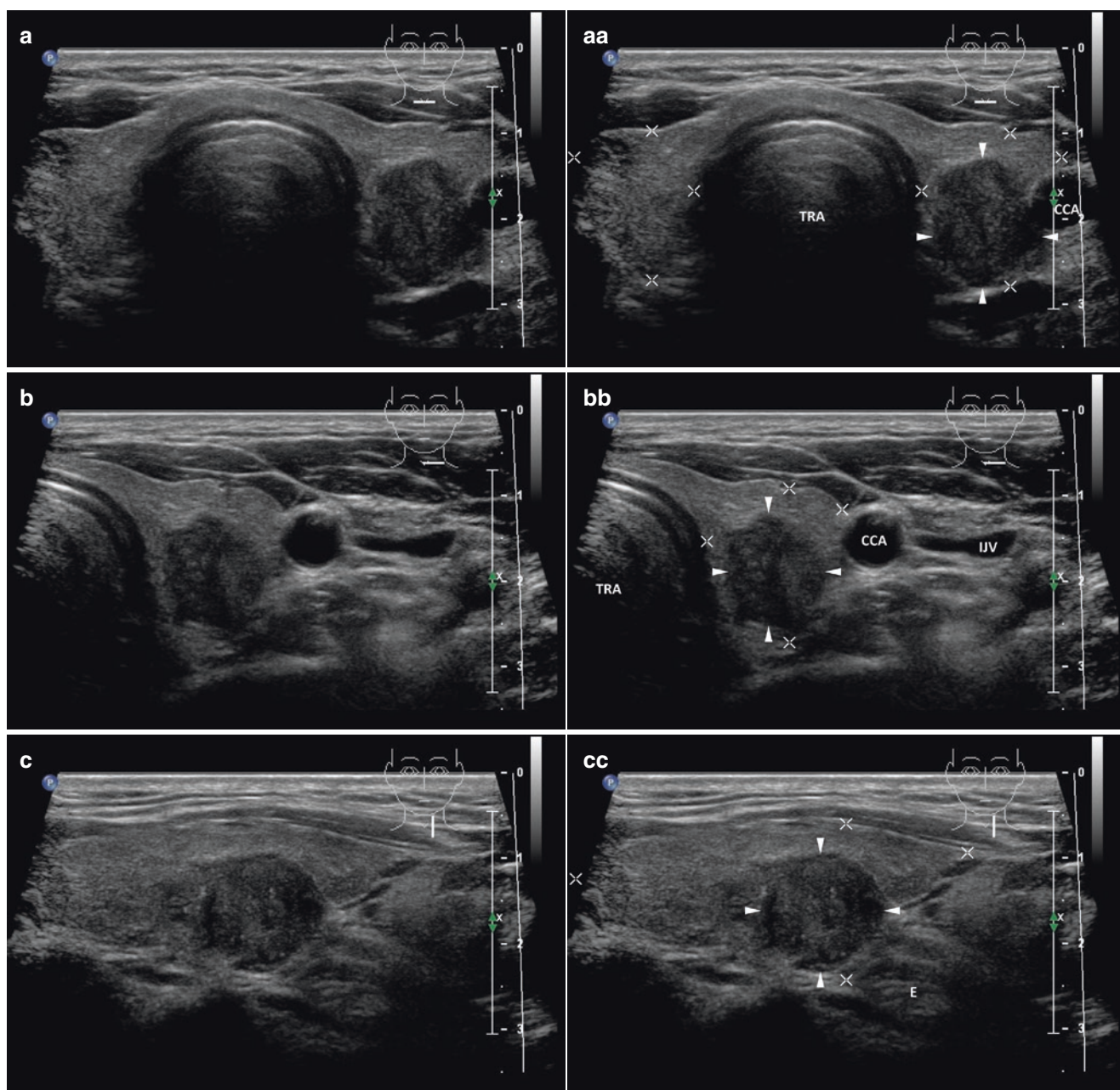
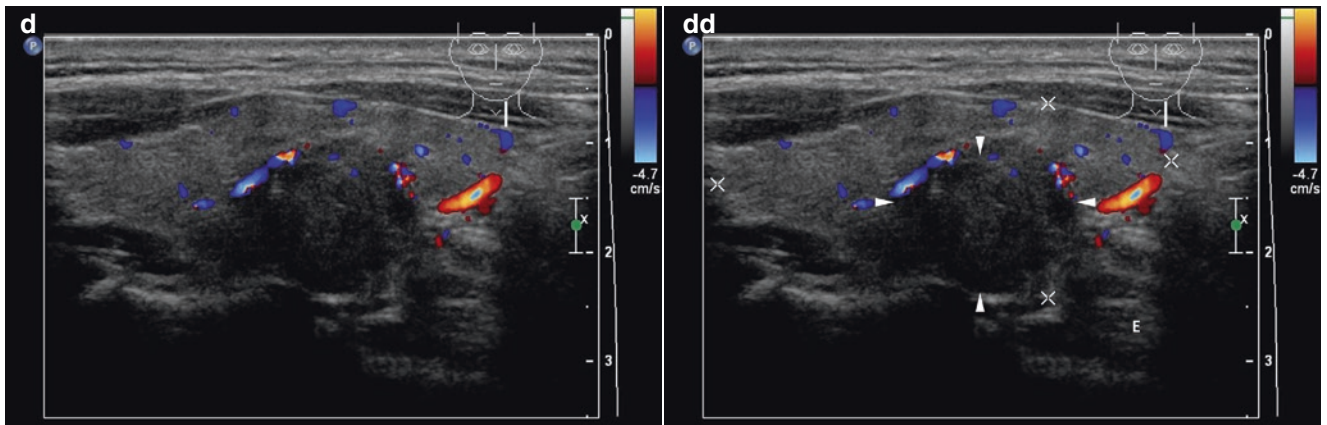


Fig. 15.7 (aa) A 44-year-old man with a solitary small papillary thyroid carcinoma—PTC (*arrowheads*), size $19 \times 14 \times 11$ mm and volume 1.5 mL in the LL. US overall view: solid nodule—“taller-than-wide” shape; inhomogeneous structure; slightly hypoechoic; diffusely hyperechoic punctuation; blurred margin; Tvol 20 mL, RL 10 mL, and LL 10 mL; transverse. (bb) Detail of solitary small PTC (*arrowheads*): solid nodule—“taller-than-wide” shape; inhomogeneous structure;

slightly hypoechoic; diffusely hyperechoic punctuation; blurred margin; transverse. (cc) Detail of solitary small PTC (*arrowheads*): solid nodule—“taller-than-wide” shape; inhomogeneous structure; slightly hypoechoic; diffusely hyperechoic punctuation; blurred margin; longitudinal. (dd) Detail of solitary small PTC (*arrowheads*), CFDS: minimal peripheral vascularity, *pattern I*; longitudinal

**Fig. 15.7** (continued)

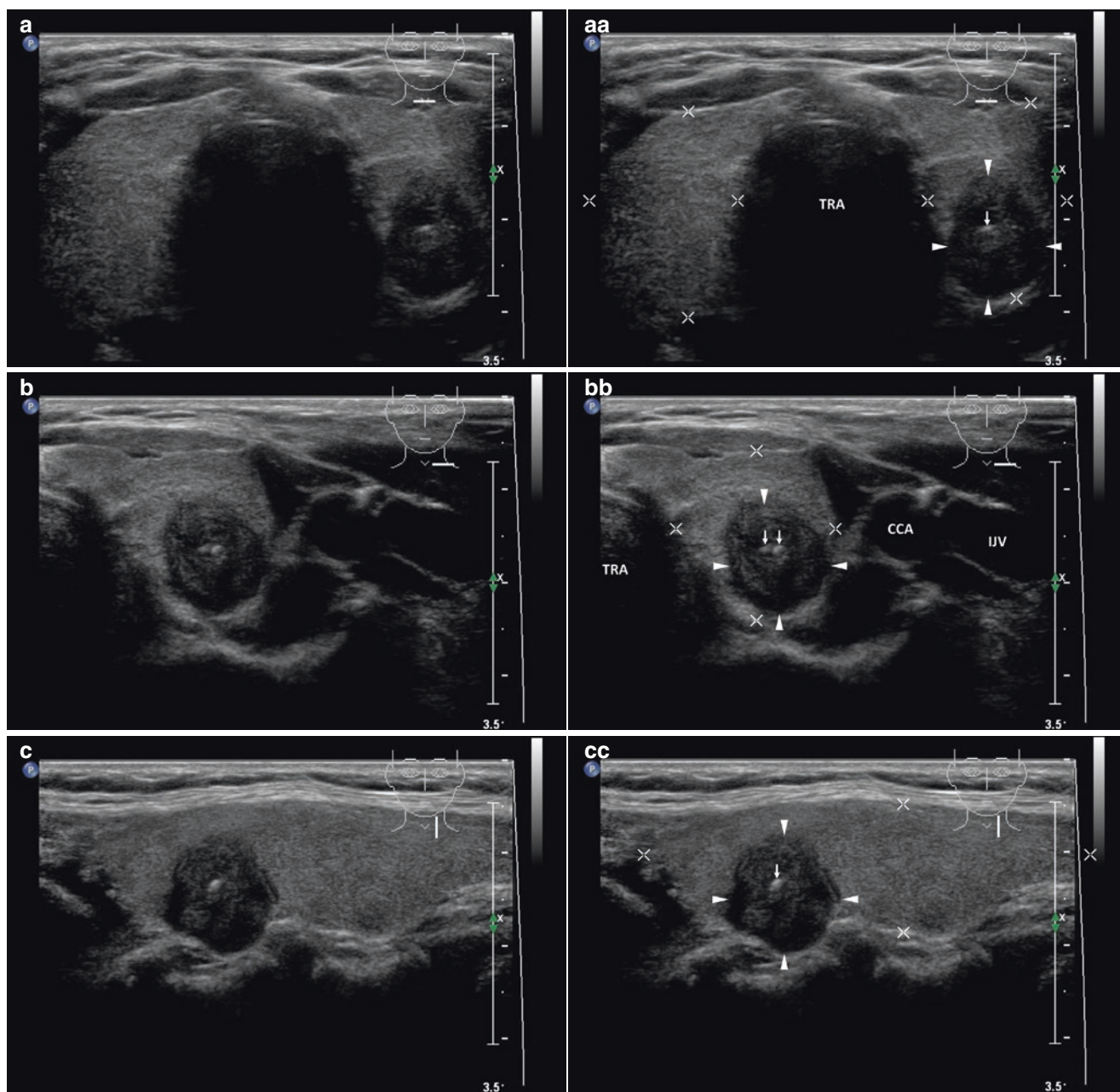


Fig. 15.8 (aa) A 48-year-old man with a solitary small papillary thyroid carcinoma—PTC (*arrowheads*) in the LL, size $19 \times 14 \times 11$ mm and volume 1.5 mL. US overall view: solid nodule—“taller-than-wide” shape; inhomogeneous structure; hypoechoic; central microcalcifications (*arrow*); microlobulated margin; Tvol 22 mL, RL 11 mL, and LL 11 mL; transverse. (bb) Detail of solitary small PTC (*arrowheads*): solid nodule—“taller-than-wide” shape; inhomogeneous structure;

hypoechoic; central microcalcifications (*arrow*); microlobulated margin; transverse. (cc) Detail of solitary small PTC (*arrowheads*): solid nodule—“taller-than-wide” shape; inhomogeneous structure; hypoechoic; central microcalcifications (*arrow*); microlobulated margin; longitudinal. (dd) Detail of solitary small PTC (*arrowheads*), CFDS: minimal peripheral vascularity, *pattern I*; longitudinal

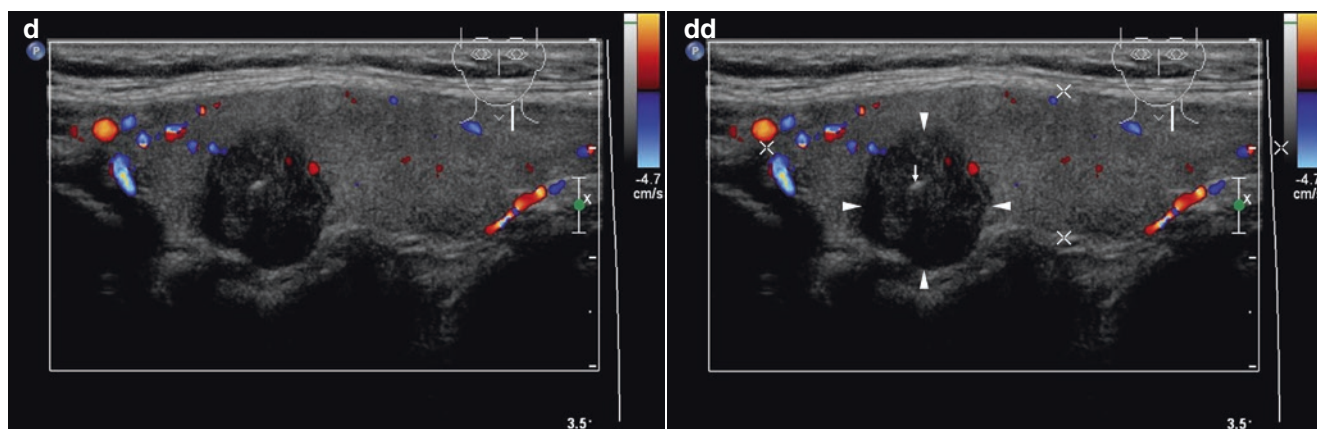


Fig. 15.8 (continued)

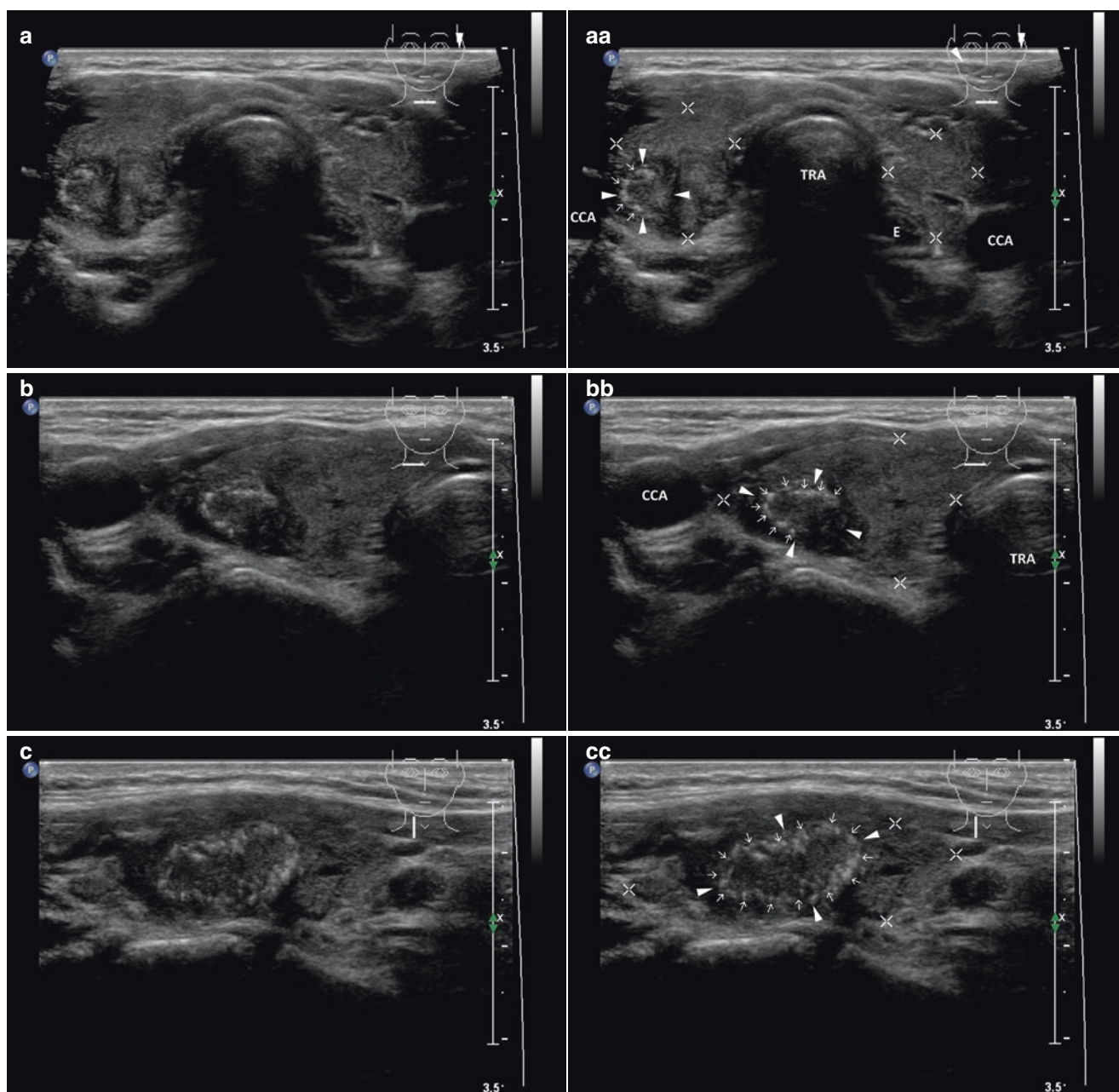


Fig. 15.9 (aa) A 38-year-old man with a solitary small papillary thyroid carcinoma—PTC (*arrowheads*) in the RL, size $17 \times 14 \times 7$ mm and volume 1 mL. US overall view: solid nodule—oval shape; inhomogeneous structure; slightly hypoechoic; diffusely hyperechoic punctuation; peripheral arc of microcalcifications (*arrows*); blurred margin; Tvol 22 mL, RL 7 mL, and LL 5 mL; transverse. (bb) Detail of solitary small PTC (*arrowheads*): solid nodule—oval shape; inhomogeneous

structure; slightly hypoechoic; diffusely hyperechoic punctuation; peripheral arc of microcalcifications (*arrows*); blurred margin; transverse. (cc) Detail of solitary small PTC (*arrowheads*): solid nodule—oval shape; inhomogeneous structure; slightly hypoechoic; diffuse hyperechoic punctuation; peripheral circular rim of microcalcifications (*arrows*); blurred margin; longitudinal

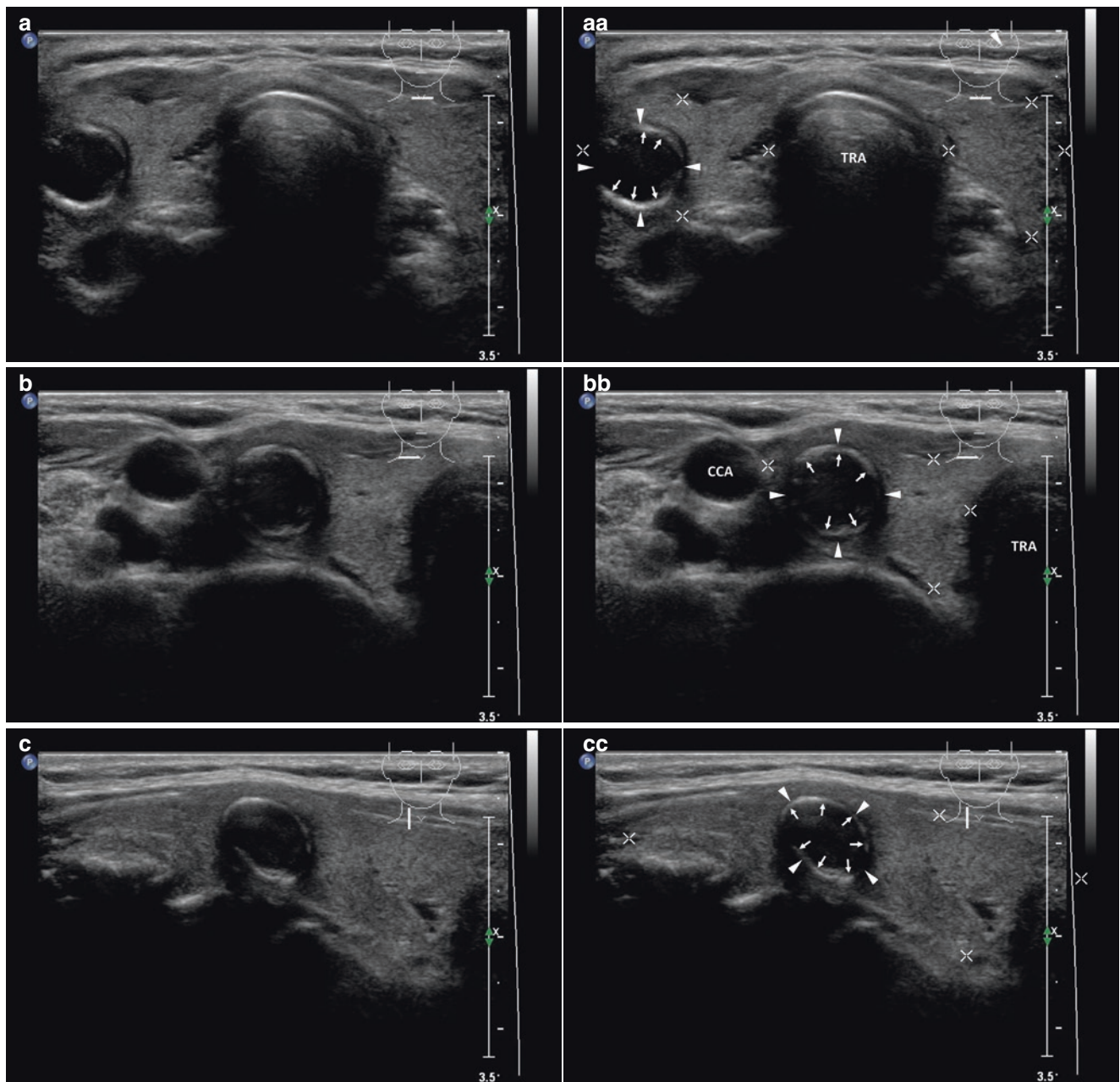


Fig. 15.10 (aa) A 55-year-old man with a solitary small papillary thyroid carcinoma—PTC (arrowheads) in the RL, size $15 \times 11 \times 11$ mm and volume 1 mL. US overall view: interrupted rim peripheral “eggshell” calcification (arrows) with prominent acoustic shadow causing hypoechogenicity of intranodular structure; Tvol 15 mL, RL 7 mL, and LL 8 mL; transverse. (bb) Detail of solitary small PTC (arrowheads):

interrupted rim peripheral “eggshell” calcification (arrows) with prominent acoustic shadow causing hypoechogenicity of intranodular structure; transverse. (cc) Detail of solitary small PTC (arrowheads): interrupted rim peripheral “eggshell” calcification (arrows) with prominent acoustic shadow causing hypoechogenicity of intranodular structure; longitudinal

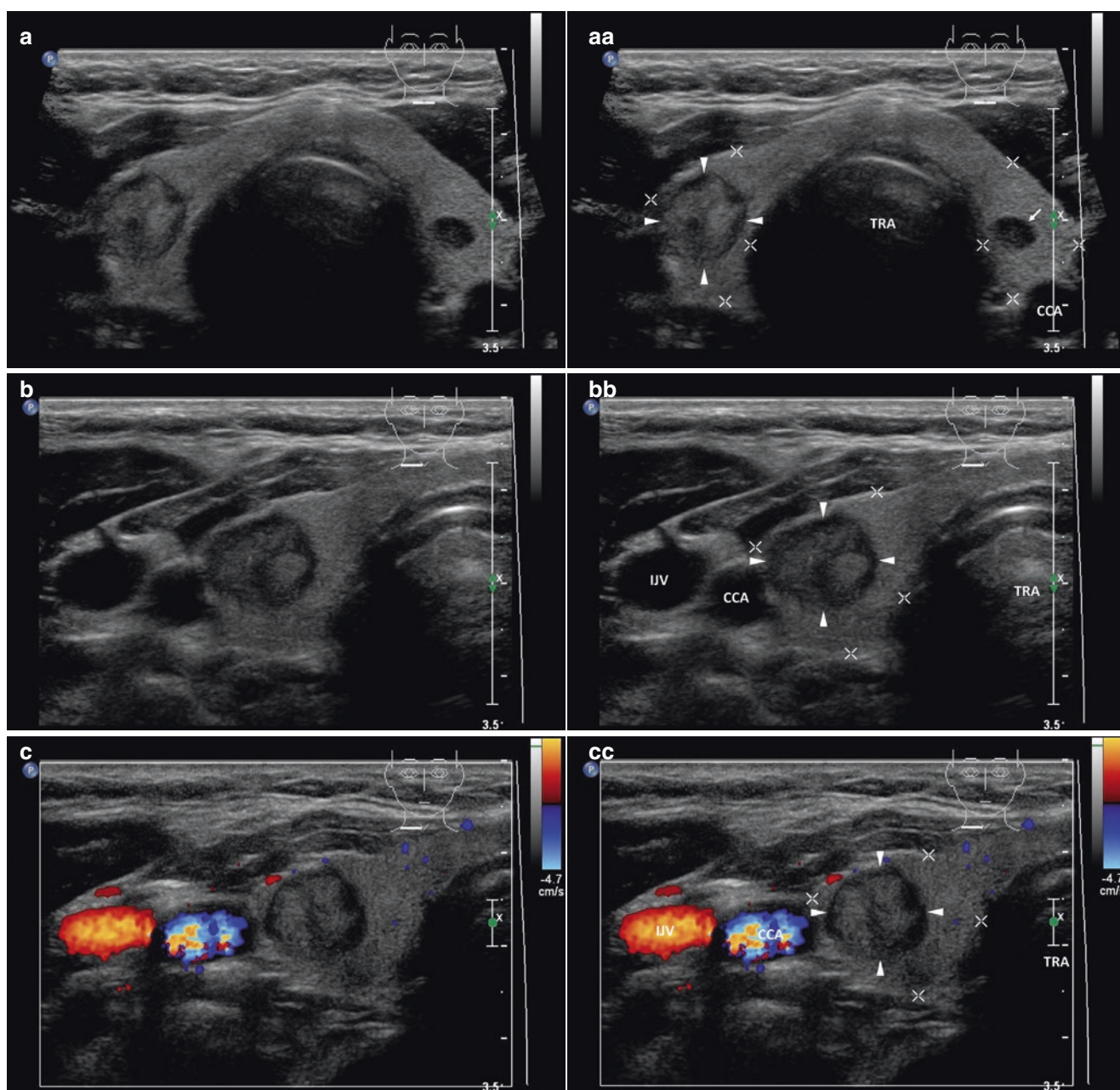


Fig. 15.11 (aa) A 43-year-old woman with a small papillary thyroid carcinoma—PTC (arrowheads) in the RL, size $12 \times 12 \times 11$ mm and volume 1 mL. US overall view: solid nodule—round shape; homogeneous structure; mostly isoechoic; centrally tiny hypoechoic area; well-defined margin; irregular thick halo sign; tiny hypoechoic nodule in the LL; Tvol 13 mL, RL 7 mL, and LL 6 mL; transverse. (bb) Detail of solitary small PTC (arrowheads): solid nodule—round shape; homoge-

neous structure; mostly isoechoic; centrally tiny hypoechoic area; well-defined margin; irregular thick halo sign; transverse. (cc) Detail of small PTC (arrowheads), CFDS: avascular node, *pattern 0*; transverse. (dd) Detail of solitary small PTC (arrowheads): solid nodule—round shape; homogeneous structure; mostly isoechoic; centrally tiny hypoechoic area; well-defined margin; irregular thick halo sign; longitudinal

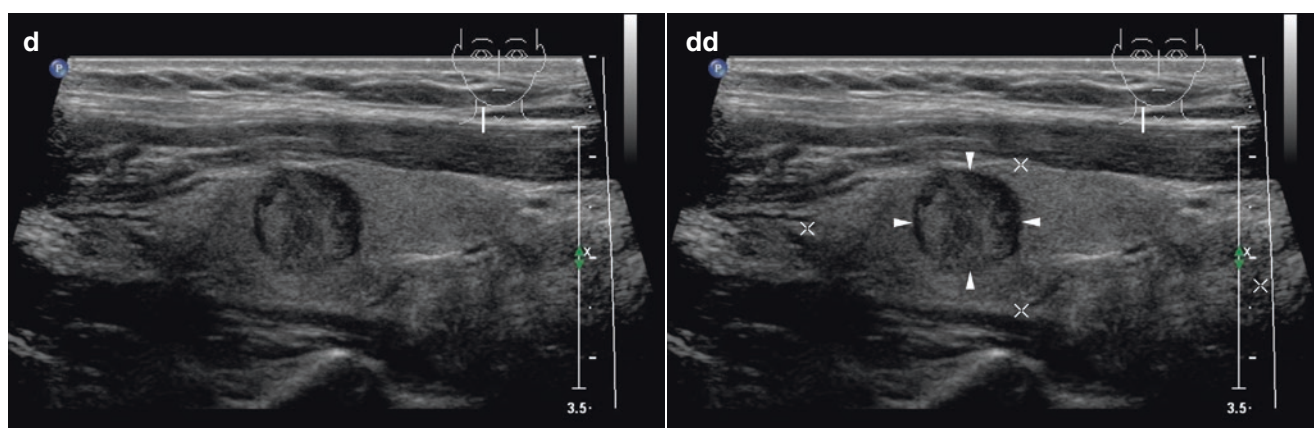


Fig. 15.11 (continued)

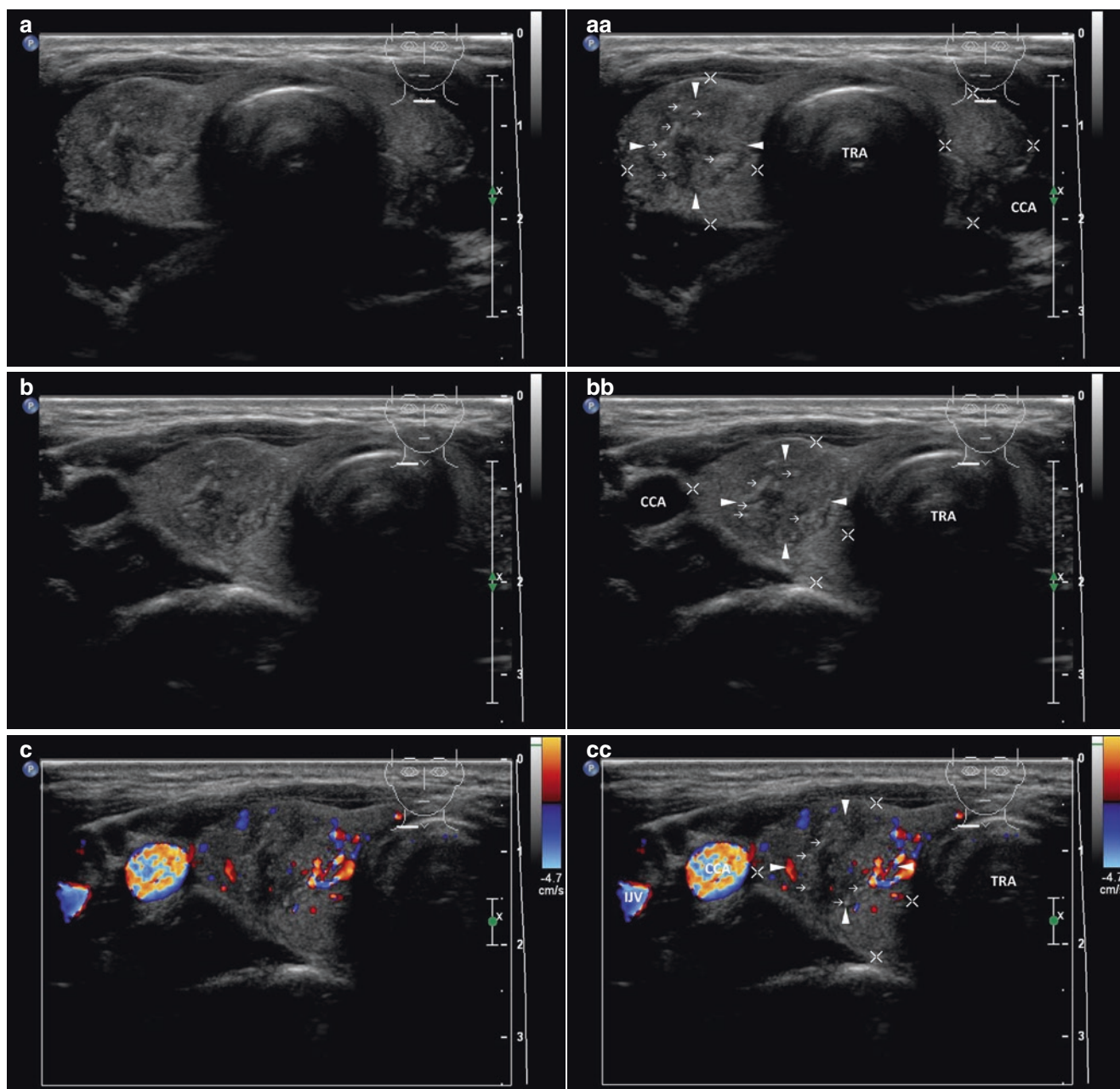


Fig. 15.12 (aa) A 44-year-old man with a solitary small papillary thyroid carcinoma, follicular variant—FVPTC (arrowheads) in the RL, size $13 \times 12 \times 12$ mm and volume 1 mL. US overall view: solid nodule—round shape; inhomogeneous structure; isoechoic; diffusely hyperechoic punctuation; centrally tiny hypoechoic area; blurred margin; Tvol 8 mL, RL 5 mL, and LL 3 mL; transverse. (bb) Detail of solitary small FVPTC (arrowheads): solid nodule—round shape; inhomogeneous structure; isoechoic; diffusely hyperechoic punctua-

tion; centrally tiny hypoechoic area; blurred margin; transverse. (cc) Detail of small FVPTC (arrowheads), CFDS: focally increased peripheral and intranodular vascularity, *pattern II*; transverse. (dd) Detail of solitary small FVPTC (arrowheads): solid nodule—round shape; inhomogeneous structure; isoechoic; diffusely hyperechoic punctuation; centrally tiny hypoechoic area; blurred margin; longitudinal. (ee) Detail of small FVPTC (arrowheads), CFDS: peripheral vascularity, *pattern I*; transverse.

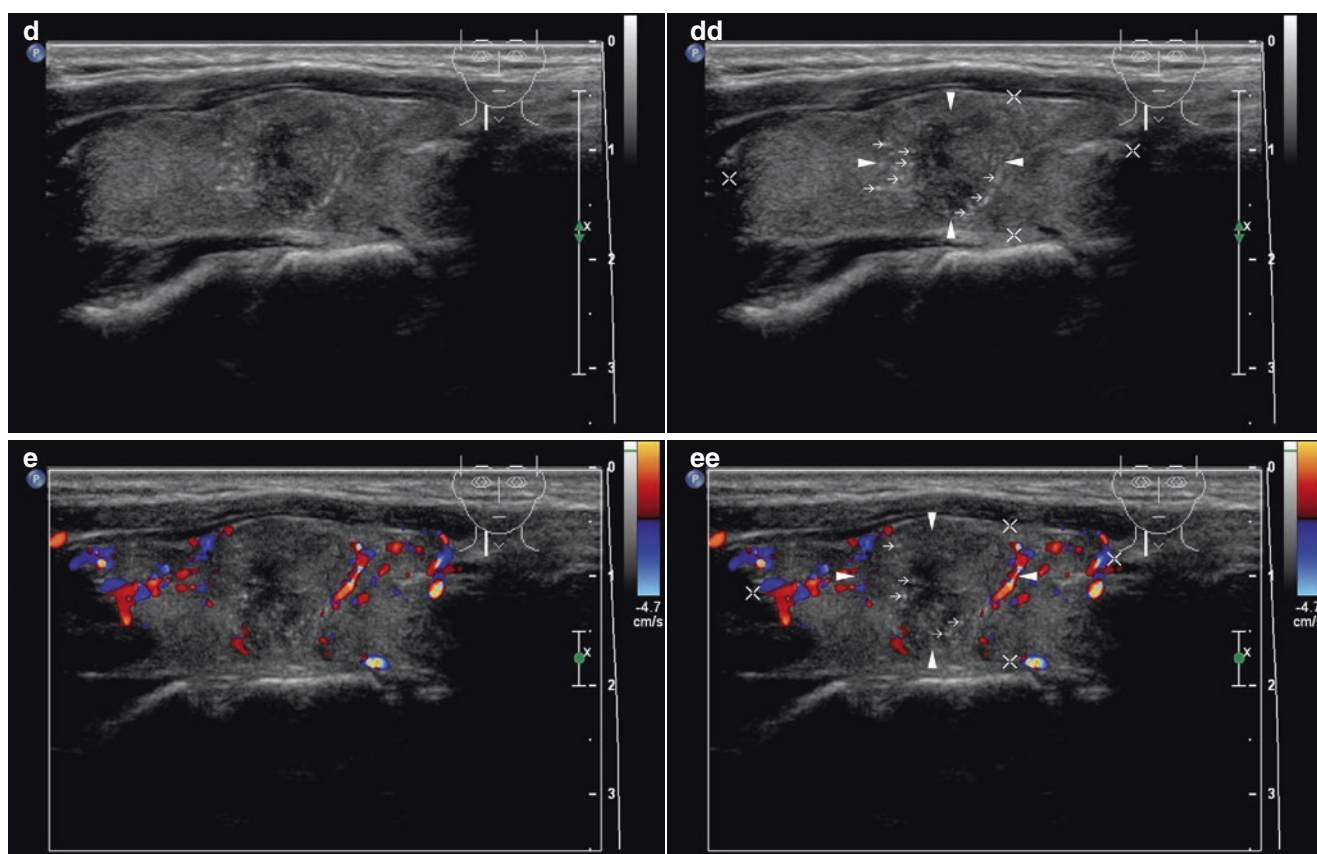


Fig. 15.12 (continued)

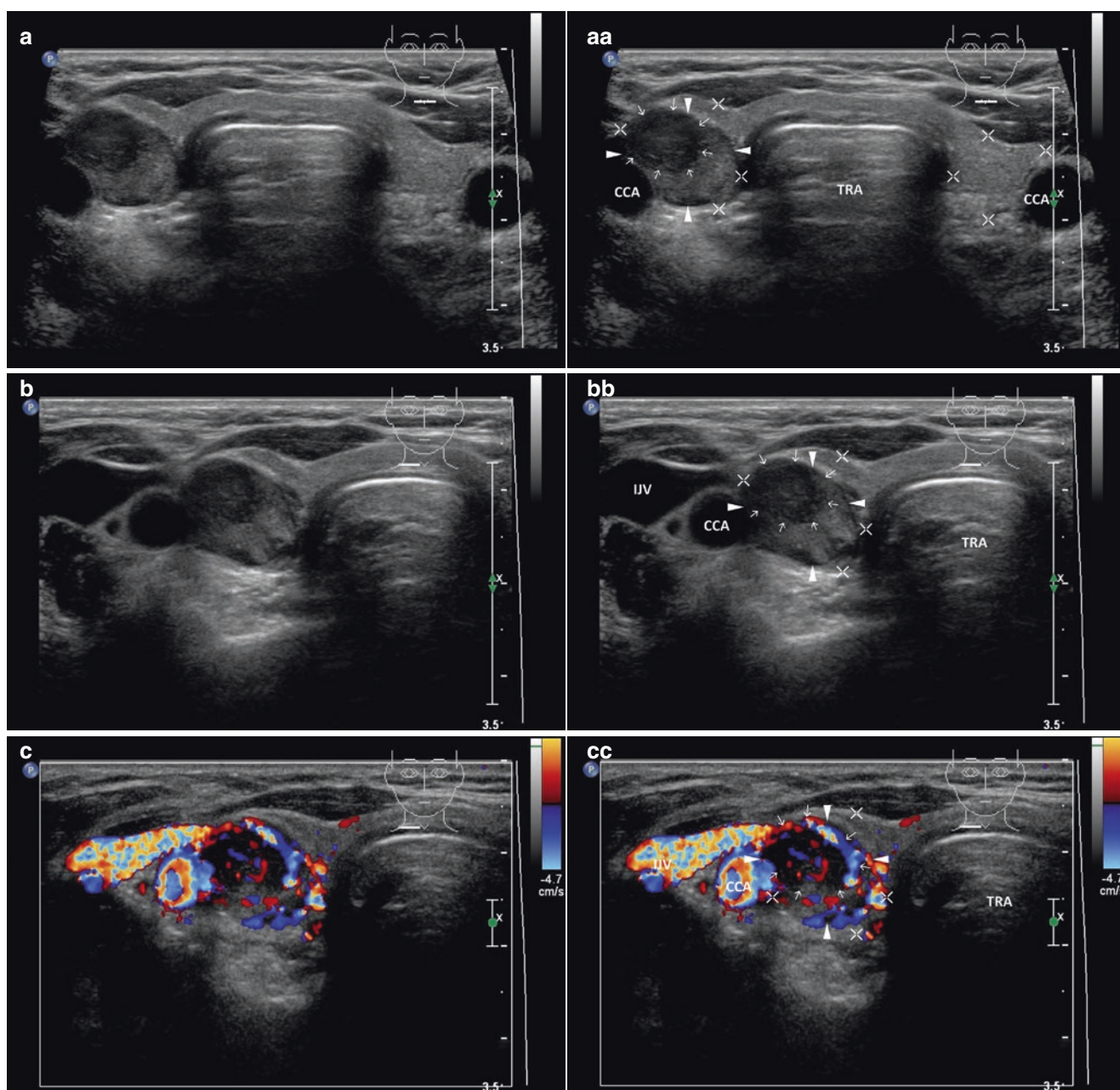


Fig. 15.13 (aa) A 56-year-old woman with a solitary small papillary thyroid carcinoma—PTC (arrowheads) in the RL, size $19 \times 14 \times 11$ mm and volume 1.5 mL. US overall view: solid nodule—ovoid shape; homogeneous structure; mostly isoechoic; small round hypoechoic area at periphery “nodule in a nodule” appearance; well-defined margin; thin halo sign around isoechoic part; Tvol 13 mL, RL 7 mL, and LL 6 mL; transverse. (bb) Detail of solitary small PTC (arrowheads): solid nodule—ovoid shape; homogeneous structure; mostly isoechoic; small round hypoechoic area (open arrows): at periphery like “nodule in a nodule” appearance; well-defined margin; thin halo sign around

isoechoic part; transverse. (cc) Detail of small PTC (arrowheads), CFDS: increased peripheral vascularity and markedly in intranodular hypoechoic “nodule” (open arrows), pattern II; transverse. (dd) Detail of solitary small PTC (arrowheads): solid nodule—ovoid shape; homogeneous structure; mostly isoechoic; small round hypoechoic area (open arrows) at periphery “nodule in a nodule” appearance; well-defined margin; thin halo sign around isoechoic part; longitudinal. (ee) Detail of small PTC (arrowheads), CFDS: increased peripheral vascularity and markedly in intranodular hypoechoic “nodule” (open arrows), pattern II; longitudinal

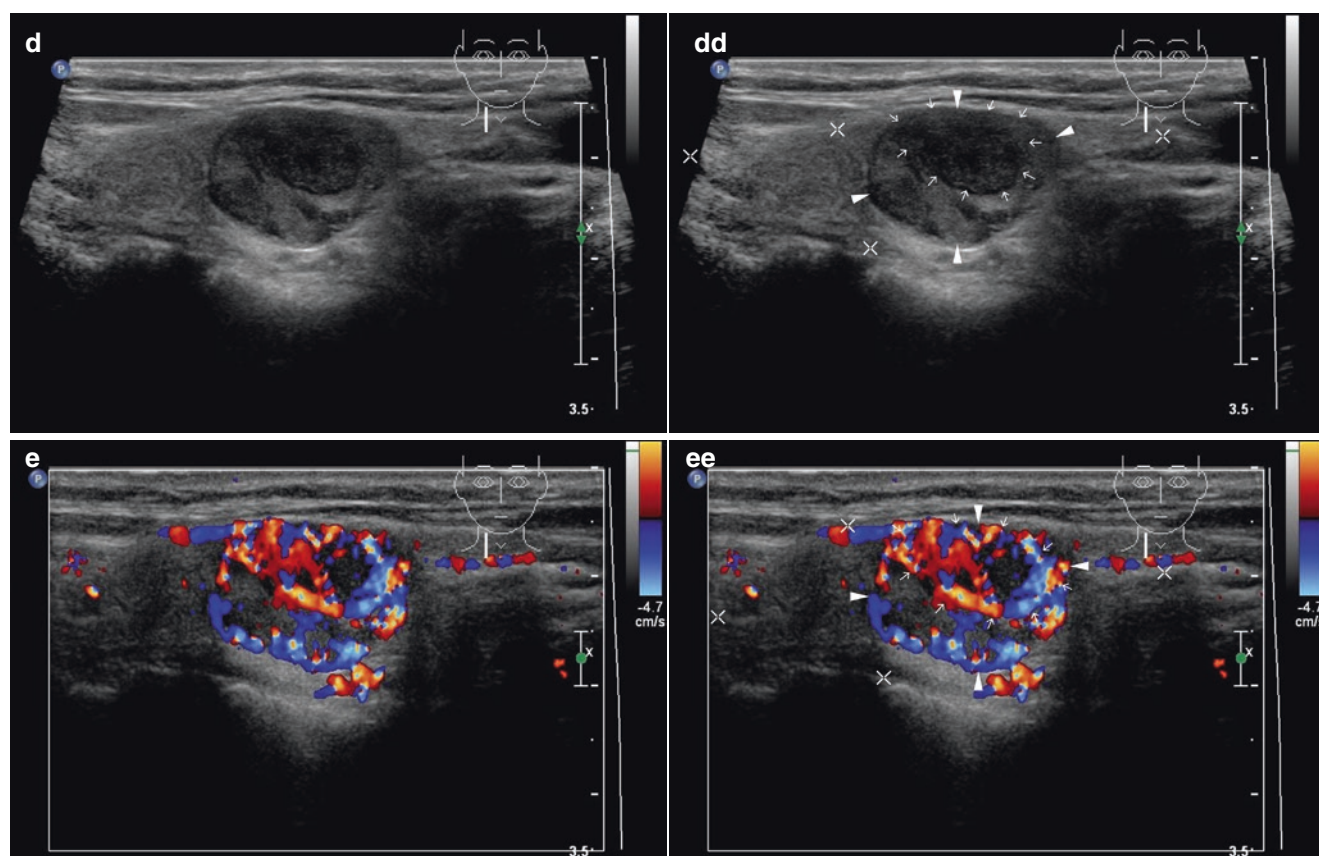


Fig. 15.13 (continued)

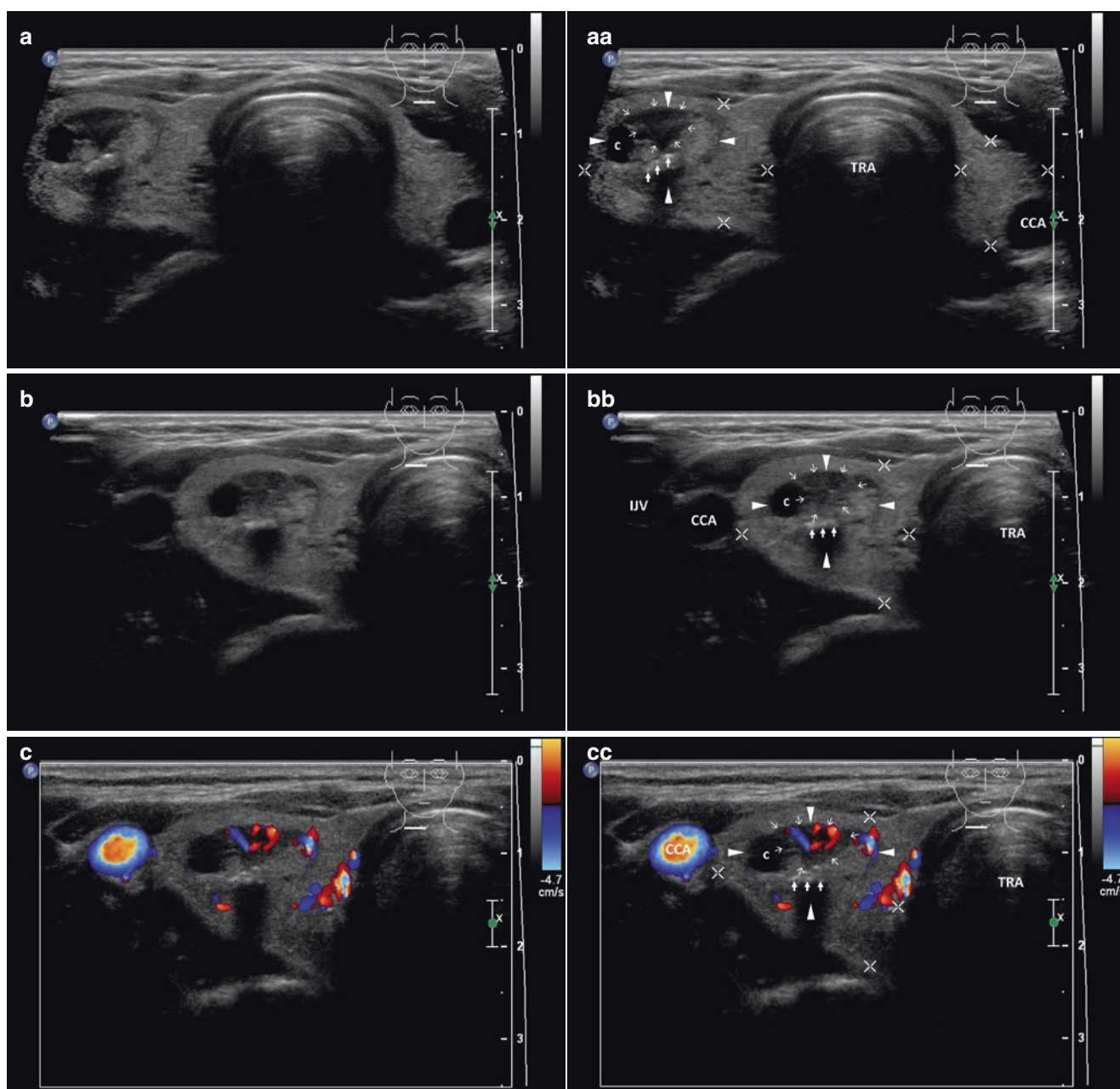
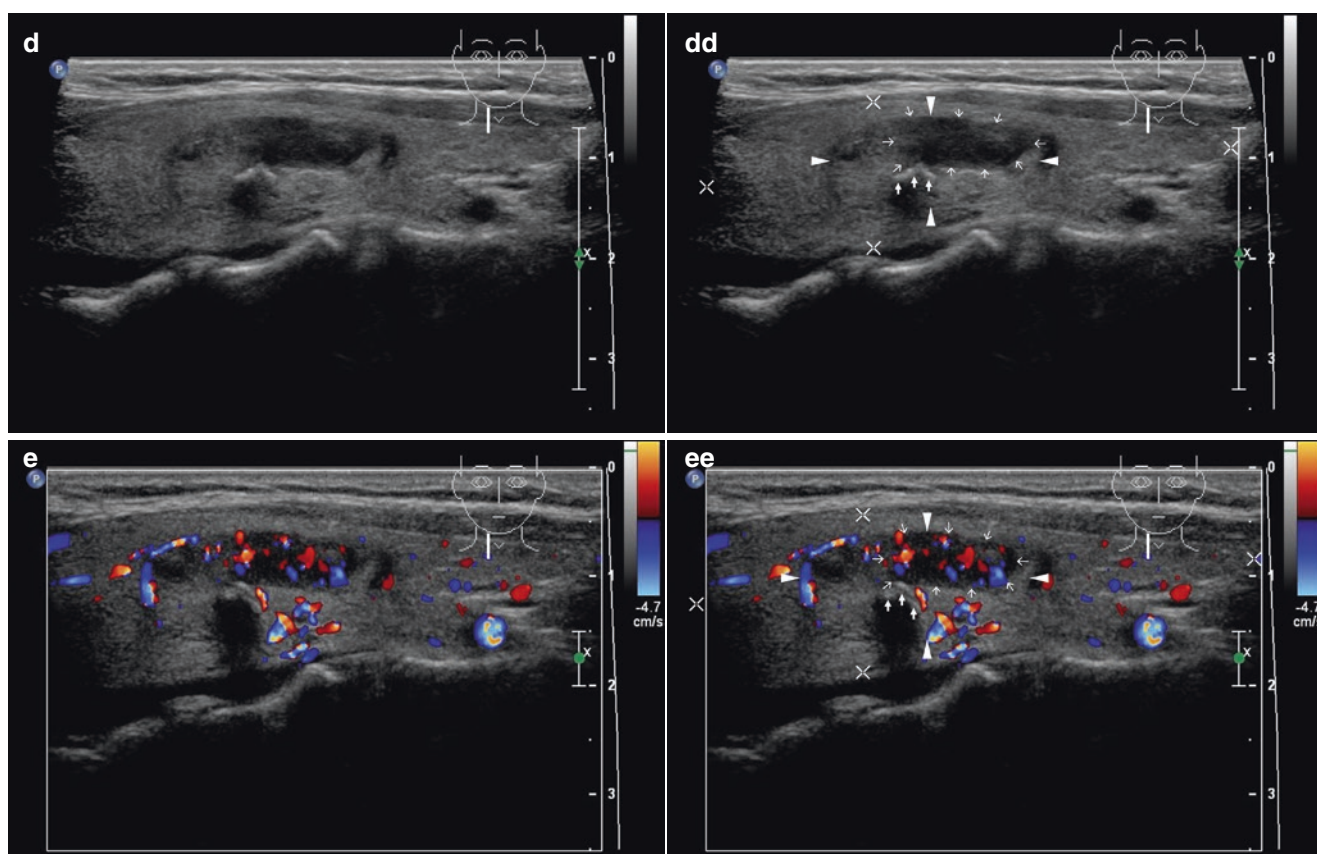


Fig. 15.14 (aa) A 34-year-old woman with a solitary small papillary thyroid carcinoma—PTC (arrowheads) in the RL, size $23 \times 15 \times 11$ mm and volume 2 mL. US overall view: complex, predominantly solid nodule—ovoid shape; solid part inhomogeneous structure; mostly hyperechoic; central coarse linear calcification (arrow) with acoustic shadow; suspicious small hypoechoic part (open arrows) above calcification; small cystic cavity (c) at periphery; blurred margin; Tvol 13 mL, RL 7 mL, and LL 6 mL; transverse. (bb) Detail of solitary small PTC (arrowheads): complex, predominantly solid nodule—ovoid shape; solid part inhomogeneous structure; mostly hyperechoic; central coarse linear calcification (arrow) with acoustic shadow; suspicious small hypoechoic part above calcification; small cystic cavity (c) at periphery;

blurred margin; transverse. (cc) Detail of small PTC (arrowheads), CFDS: sporadic peripheral vascularity and markedly increased intranodular vascularity in hypoechoic part (open arrows), pattern II; transverse. (dd) Detail of solitary small PTC (arrowheads): complex, predominantly solid nodule—ovoid shape; solid part inhomogeneous structure; mostly hyperechoic; central coarse linear calcification (arrow) with acoustic shadow; suspicious small hypoechoic part (open arrows) above calcification; blurred margin; longitudinal. (ee) Detail of small PTC (arrowheads), CFDS: sporadic peripheral vascularity and markedly increased intranodular vascularity in hypoechoic part (open arrows), pattern II; longitudinal

**Fig. 15.14** (continued)

15.3 Papillary Thyroid Carcinoma: Medium-Sized and Large Nodules >4 cm

15.3.1 Essential Facts

- Recent data shows that incidence of papillary thyroid carcinoma (PTC) has rapidly increased for large size tumors (>4.0 cm) as well as for papillary thyroid microcarcinomas (PTMC) (≤ 1 cm) [10].
- Greater nodule size influences risk of malignancy, although the increase in absolute risk between small (1.0–1.9 cm) and large (>4.0 cm) nodules is modest. Notably, a threshold effect is detected at approximately 2.0 cm in nodule diameter [17].
- Thereafter, larger nodule size imparts no further malignant risk, even if 4.0 cm or larger. However, larger nodules, if cancerous, are significantly more likely to be FTC or HCC (or other rare malignancies) in comparison with smaller nodules [17].
- PTC is largely predetermined at its inception and does not transform with growth [17].
- On the contrary, the distribution of FTC and HCC increased linearly from 6% in nodules 1–1.9 cm to 15% in nodules >4 cm in diameter [17].
- In retrospective analysis of large thyroid nodules >4 cm the accuracy of US-FNAB was higher in nodules with US features suspicious of malignancy compared to nodules without these features. The accuracy improved as the number of these features increased. The overall false negative rate of nodules that appeared benign on US was 11.9%, of mixed nodules (7.7%), of solid nodules (17.9%) and of nodules with any microcalcification or macrocalcification (33.3%). In nodules without suspicious features of malignancy, the false negative rate of US-FNAB was zero percent. If nodules exhibit any suspicious features, potential false negative results of FNAB should be kept in mind and surgery may be considered [18].
- Comparison of US features of thyroid nodules in selection of thyroid nodules for FNAB, in relation to the nodule's size [19]:
 - Suspicious small nodules ≤ 1.5 cm show hypoechogenicity, microcalcifications, solitary occurrence and height-to-width ratio as independent risk factors for malignancy. Ideally, all lesions presenting at least one of the above-mentioned features should be biopsied (sensitivity 98%, specificity 44%).
 - In large nodules >1.5 cm, the US criteria were less sensitive. Large nodules primarily selected for FNAB should be hypoechoic, more tall-than-wide, or contain microcalcifications (sensitivity 84%, specificity 72%).
- Relapse risk in patients without metastases in the LN ranges between 0 and 9%, while clinically and US positive LN are associated with higher recurrence rates of 10–42% [14].
- Reported US accuracy for staging of the cervical lateral metastatic LNs in PTC ranges 85–90% [20].
- According to Noguchi et al., metastatic NL are present in 90% of patients with PTC; however, 57% of these were <3 mm [21].
- Metastatic LNs occur early and often in PTC, initially located in compartment VI (C-VI; central neck compartment bordered laterally by the carotid arteries, superiorly by the hyoid bone, and inferiorly at or just below the sternal notch), followed soon by spread to C-III and C-IV (low and mid internal jugular lymph nodes from the base of the neck at and slightly below the clavicle extending superiorly to the level of the hyoid bone) [15].
- In study by Machens, 296 patients (134 PTCs, 162 medullary thyroid carcinomas—MTCs) underwent total thyroidectomy in conjunction with a standard resection of at least the cervicocentral LN compartment. Of 10,446 sampled lymph nodes, 1641 were positive for malignancy (16%). The ipsilateral cervicolateral compartment was involved almost as often as the cervicocentral compartment in primary PTC (29% vs. 32%), reoperative PTC (21% vs. 37%), primary MTC (34% vs. 34%), and reoperative MTC (49% vs. 65%). The contralateral cervicolateral and mediastinal compartments were more rarely affected, and were least affected in the primary setting [22].

15.3.2 US Features of PTC, Medium-Sized and Large Nodules >4 cm [8]

- Typical US features:
 - Mixed echogenicity (Fig. 15.16aa), hyperechoic (Fig. 15.17aa) or slightly hypoechoic (Fig. 15.15aa), rarely marked hypoechogenicity (Fig. 15.19aa).
 - Microcalcifications (Figs. 15.15aa, 15.17aa, and 15.20aa).
 - Round (Fig. 15.16aa), oval (Fig. 15.17bb) or elliptical shape—“more wide than tall” (Fig. 15.18aa) or irregular shape (Fig. 15.21aa), rather than “*Taller-than-wide shape*”.
 - Irregular margins (microlobulated or spiculated) (Fig. 15.18aa) or ill-defined, lobulated margin (Fig. 15.21aa) or blurred (Fig. 15.21dd), rarely well-defined margin (Fig. 15.19aa).
 - Intranodular hypervascularity (Figs. 15.15cc, 15.16cc, and 15.18cc).
- Often cervical metastatic LNs (Figs. 15.15ff, 15.16ee, and 15.17dd), sometimes with degenerative and necrotic changes (Figs. 15.18ff, 15.21ff, gg).
- Rarely US features:
 - Follicular variant of papillary carcinoma (FVPTC) is more likely to be iso- to hyperechoic (Fig. 15.20aa).
 - More often rim or intranodal macrocalcifications (Figs. 15.16aa, 15.18bb, and 15.21bb).
 - More often cystic degeneration (Figs. 15.18aa and 15.21cc).
 - Rarely complete or incomplete halo sign (Figs. 15.17bb and 15.18aa).
 - Occasionally multiple PTC with “daughter” small PTC (Fig. 15.19dd).

See more in Section IV: US classic features of high suspicion of malignancy for solid nodules according to the 2015 ATA Guidelines [8].

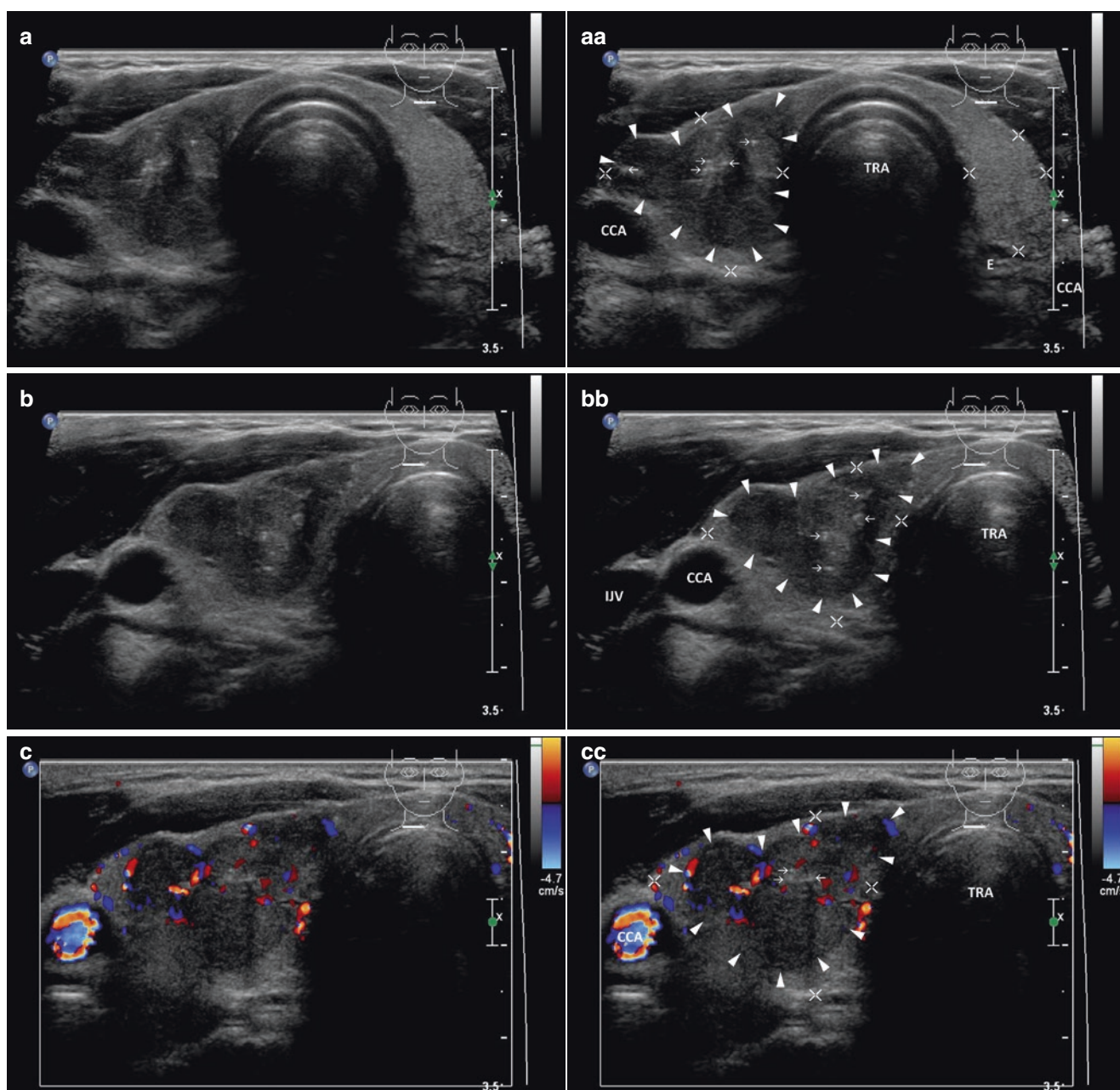
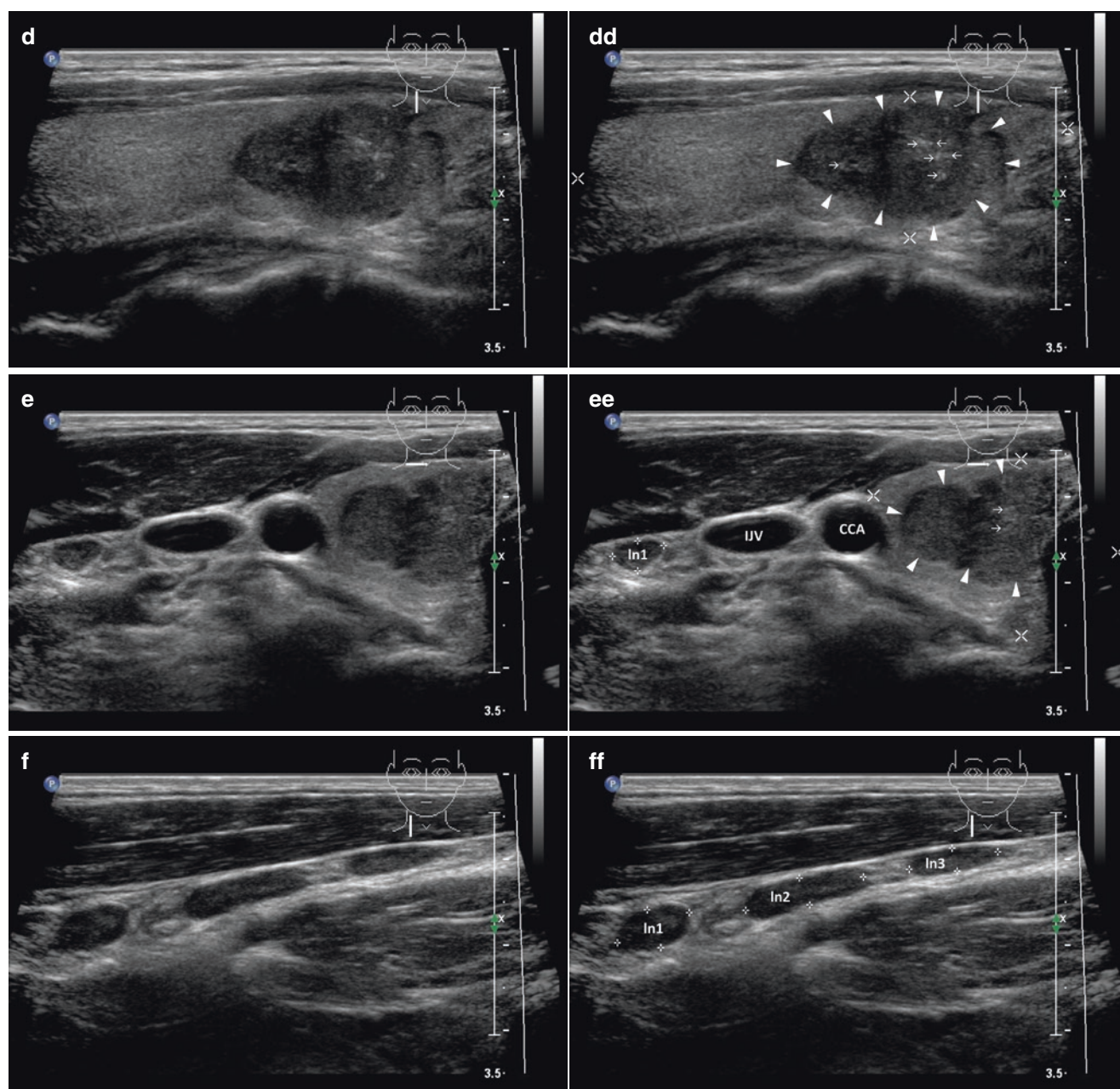


Fig. 15.15 (aa) A 30-year-old man with a solitary medium-sized papillary thyroid carcinoma—PTC (arrowheads) in the RL, size $27 \times 25 \times 16$ mm and volume 5 mL. Moreover small metastatic cervical lymph nodes (LN) along the right IJV at level C-III, IV. US overall view: solid nodule—irregular shape, inhomogeneous structure; isoechoic or slightly hypoechoic; foci of microcalcifications (open arrows); lobulated blurred margin; Tvol 18 mL, asymmetry—RL 12 mL and LL 6 mL; transverse. (bb) Detail of solitary medium-sized PTC (arrowheads): solid nodule—irregular shape, inhomogeneous structure; isoechoic or slightly hypoechoic; foci of microcalcifications (open arrows); lobulated blurred margin; transverse. (cc) Detail of solitary medium-sized PTC (arrowheads), CFDS: increased peripheral and

intranodular vascularity, pattern II; transverse. (dd) Detail of solitary medium-sized PTC (arrowheads): solid nodule—inhomogeneous structure; isoechoic or slightly hypoechoic; foci of microcalcifications (open arrows); lobulated blurred margin; longitudinal. (ee) Detail of solitary medium-sized PTC (arrowheads) and one tiny metastatic LN at level C-III: ln1—round shape, size 5 mm; homogeneous structure; hyperechoic; no hilus sign; transverse. (ff) Detail of three small metastatic LN at level C-III, IV: ln1—oval shape, size 9×5 mm; ln2—elliptical shape, size 15×4 mm and ln3—size 11×3 mm, L/S ratio ≈ 2 (not pathological); homogeneous structure; hyperechoic; no hilus sign; longitudinal

**Fig. 15.15** (continued)

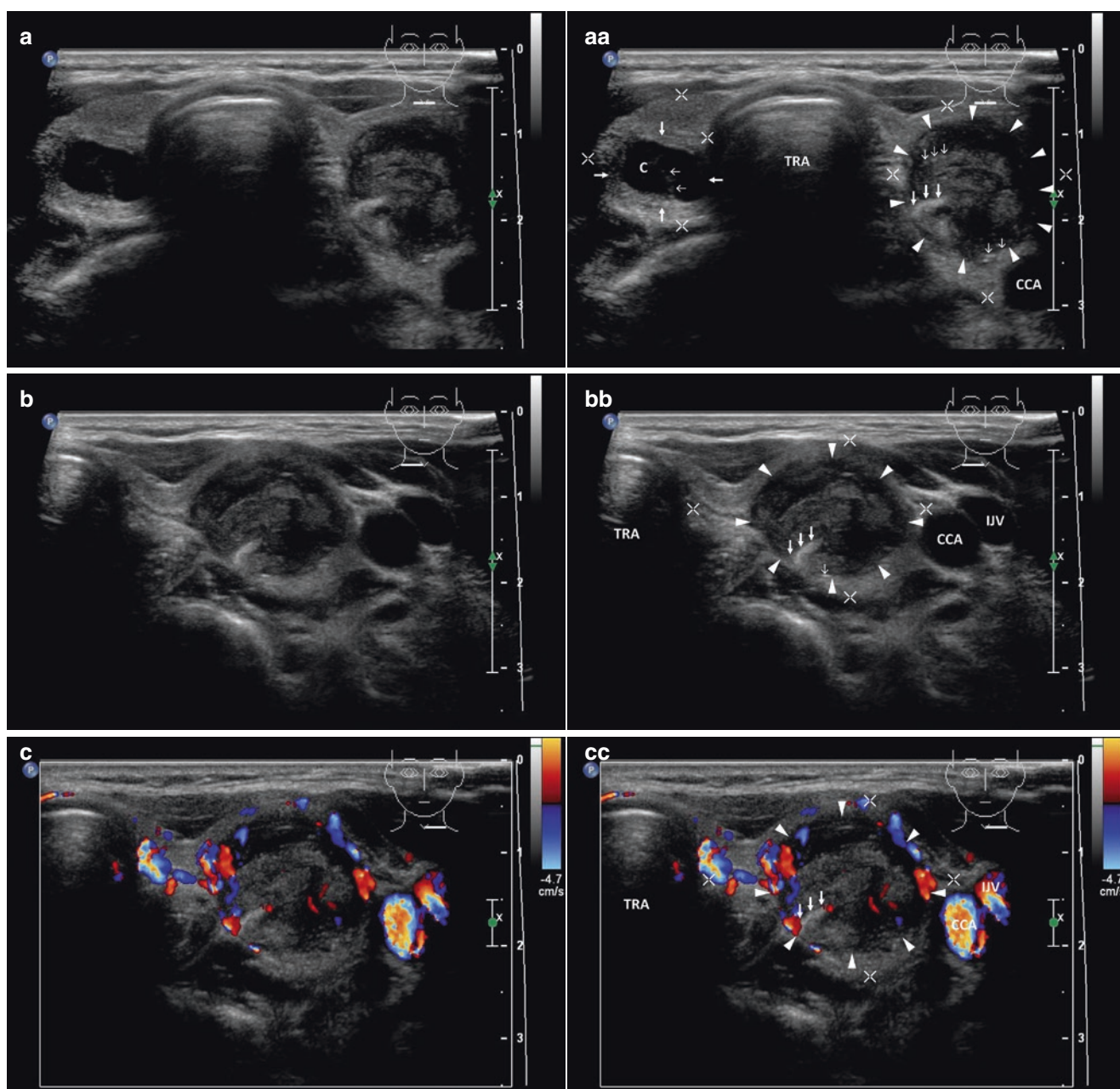
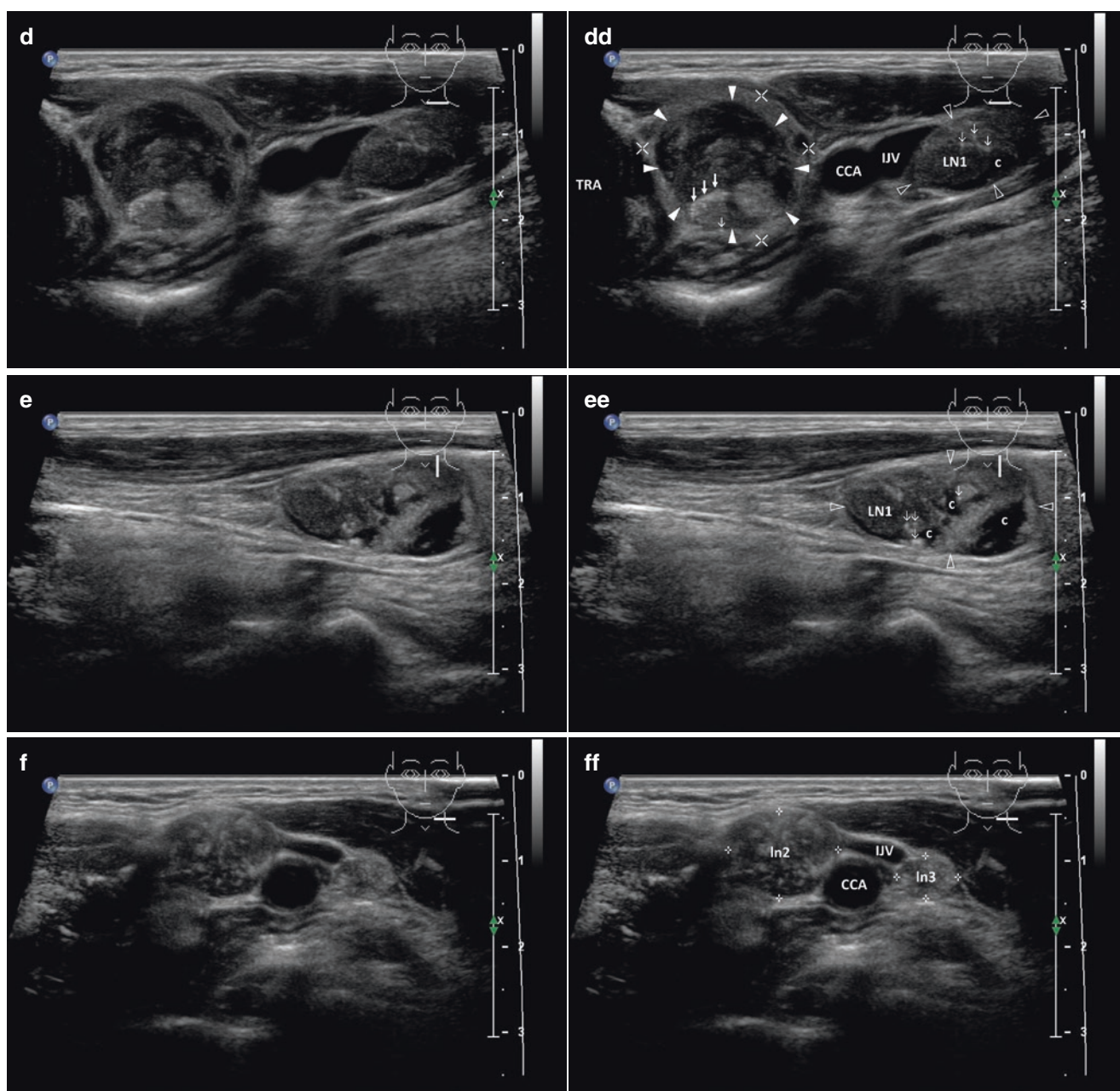


Fig. 15.16 (aa) A 42-year-old woman with multinodular goiter and medium-sized papillary thyroid carcinoma—PTC in the LL, size $28 \times 20 \times 18$ mm and volume 5 mL. Moreover small metastatic cervical lymph nodes (LN) along the left IJV at level C-II, III. Personal history: 20 years post radiotherapy for Hodgkin's lymphoma. US overall view: suspicious solid nodule (arrowheads) in the LL—round shape; inhomogeneous structure; mixed echogenicity with irregular hypoechoic areas; linear calcifications at periphery (arrows); microlobulated margin; non-suspicious complex nodule in the RL—hyperechoic; central septated cystic cavity (c); well-defined margin with thin halo sign; Tvol 18 mL, asymmetry—RL 12 mL and LL 6 mL; transverse. (bb) Detail of medium-sized PTC (arrowheads) in the LL: solid nodule—suspicious solid nodule (arrowheads) in the LL—round shape; inhomogeneous structure; mixed echogenicity with irregular hypoechoic areas; linear

calcifications at periphery (arrows); microlobulated margin; transverse. (cc) Detail of medium-sized PTC (arrowheads) in the LL, CFDS: increased peripheral and sporadic intranodular vascularity, pattern II; transverse. (dd) Detail of medium-sized PTC (arrowheads) and one metastatic LN1 (blank arrowheads) at level C-III: LN1—elliptical shape, size 16×10 mm; inhomogeneous structure; solid part hyperechoic; central hyperechoic punctuation; sporadic cystic (c) necrosis; no hilus sign; transverse. (ee) Detail of metastatic LN1 (blank arrowheads) at level C-III: elliptical shape, size 23×10 mm, L/S ratio ≈ 2 (not pathological); inhomogeneous structure; solid part hyperechoic; central hyperechoic punctuation; sporadic cystic (c) necrosis; no hilus sign; longitudinal. (ff) Detail of two tiny metastatic LN at level C-II: Ln2—oval shape, size ≈ 10 mm and Ln3—size ≈ 6 mm; homogeneous structure; hyperechoic; no hilus sign; transverse

**Fig. 15.16** (continued)

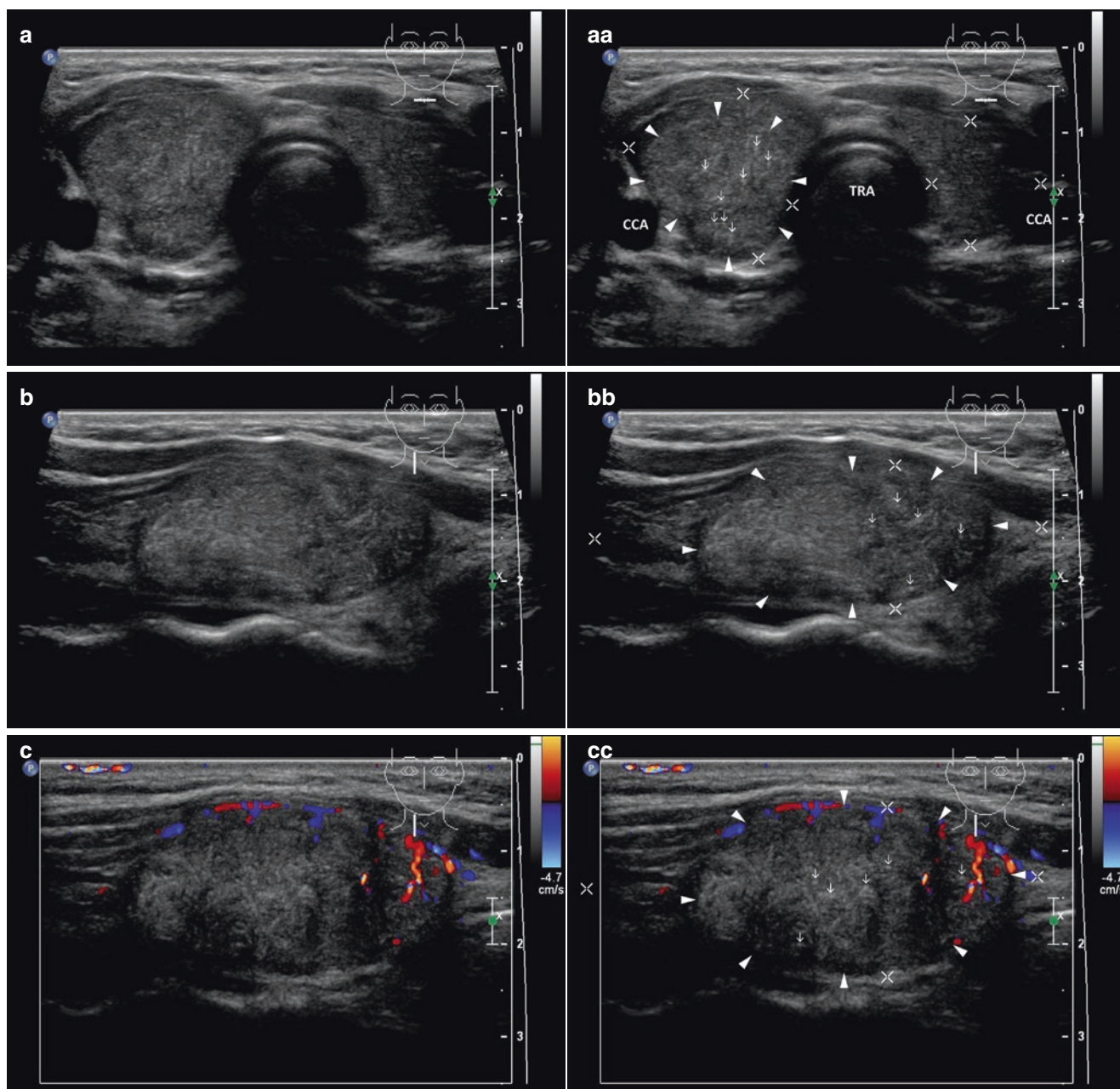
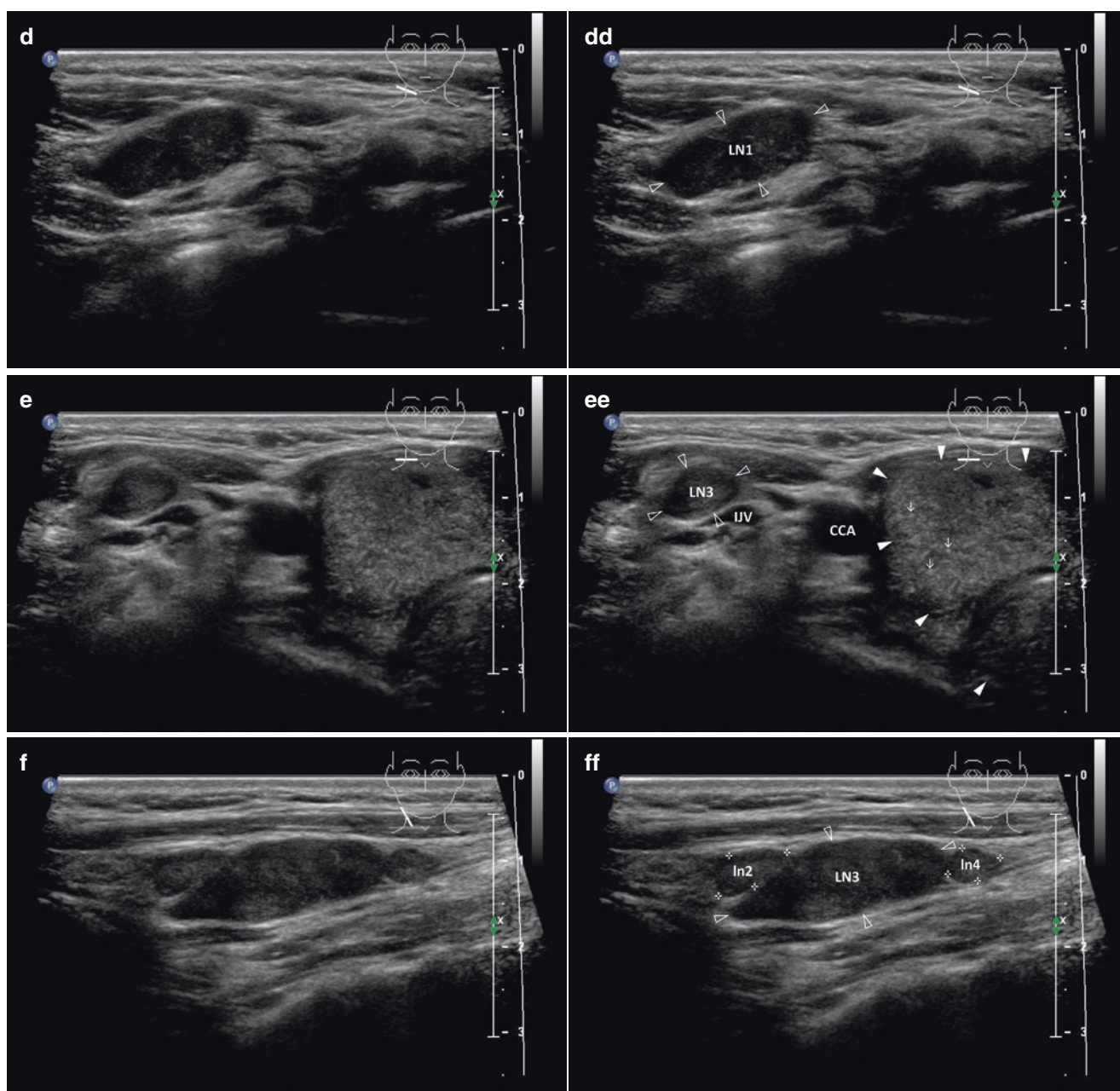


Fig. 15.17 (aa) A 27-year-old woman with a solitary medium-sized papillary thyroid carcinoma—PTC (*arrowheads*) in the RL, size $34 \times 21 \times 20$ mm and volume 7.5 mL. Moreover small metastatic cervical lymph nodes (LN) along the right IJV at level C-II, III. US overall view: solid nodule—oval shape, inhomogeneous structure; hyperechoic; diffusely hyperechoic punctuations (*open arrows*); well-defined margin; incomplete thin halo sign; Tvol 15 mL, asymmetry—RL 10 mL and LL 5 mL; transverse. (bb) Detail of solitary medium-sized PTC (*arrowheads*): solid nodule—oval shape, inhomogeneous structure; hyperechoic; diffusely hyperechoic punctuations (*open arrows*); well-defined margin; incomplete thin halo sign; longitudinal. (cc) Detail of solitary medium-sized PTC (*arrowheads*), CFDS: sporadic

peripheral and intranodular vascularity, *pattern I*; longitudinal. (dd) Detail of a lone metastatic LN at level C-II: LN1—elliptical shape, size 18×9 mm; inhomogeneous structure; slightly hyperechoic; no hilus sign; transverse. (ee) Detail of solitary medium-sized PTC (*arrowheads*) and another small metastatic LN at level C-III: LN3—oval shape, size 14×9 mm; homogeneous structure; hyperechoic; no hilus sign; transverse. (ff) Detail of three small metastatic LN at level C-III: tiny ln2—elliptical shape, size 7×3 mm; small LN3—elliptical shape, size 25×9 mm, L/S ratio ≈ 2 (*not pathological*); and tiny ln4, size 5 mm; all LNs—homogeneous structure; hyperechoic; no hilus sign; longitudinal

**Fig. 15.17** (continued)

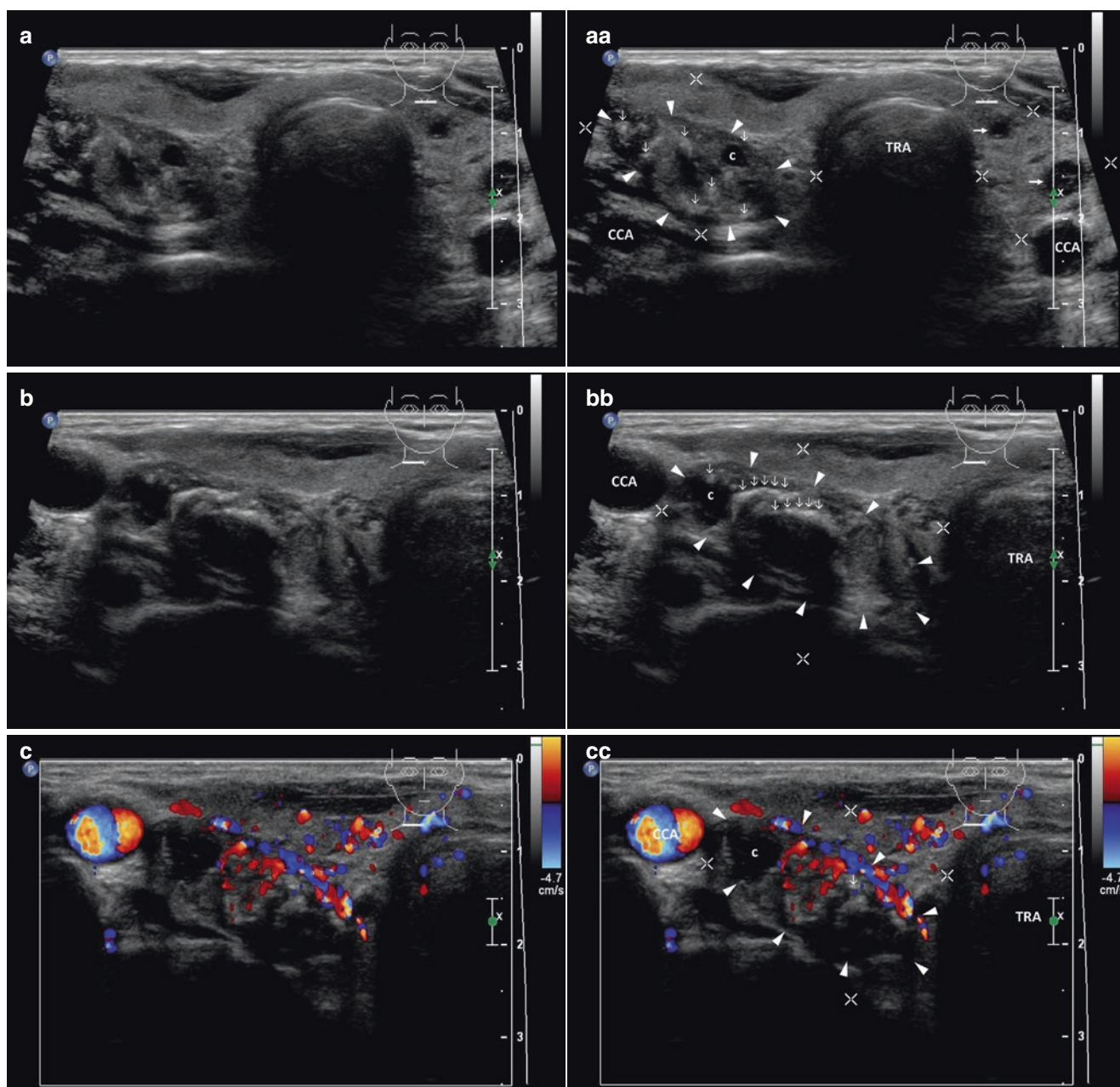
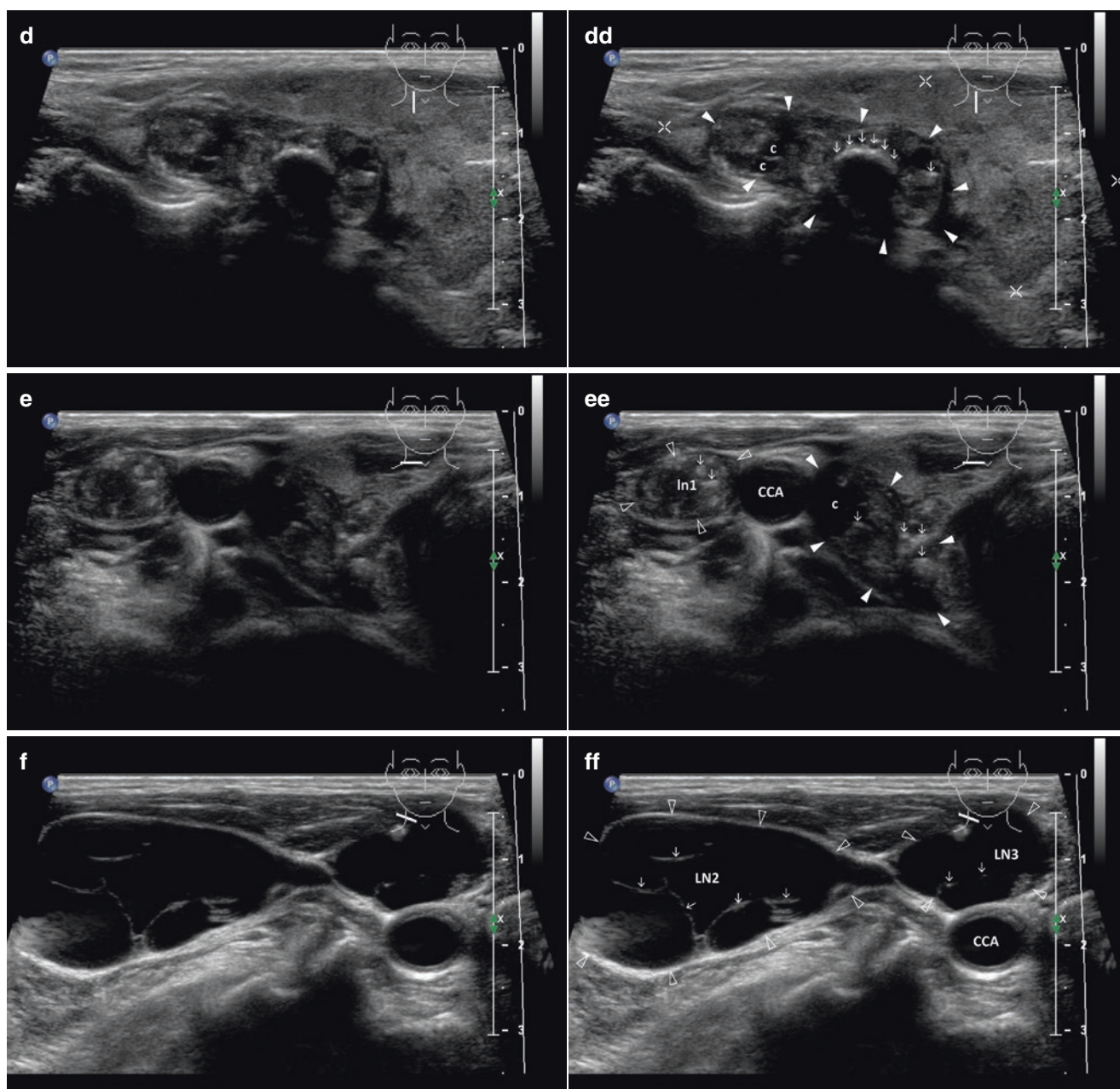


Fig. 15.18 (aa) An 80-year-old woman with a solitary medium-sized papillary thyroid carcinoma—PTC (arrowheads) in the RL, size $34 \times 32 \times 14$ mm and volume 8 mL. Moreover metastatic cervical lymph nodes (LN) along the right CCA at level C-II, III. US overall view: complex nodule—elliptical shape, “more wide than tall”; coarse structure; mixed echogenicity, solid part mostly hyperechoic with multiple microcalcifications (open arrows), small irregular cystic cavities (c); microlobulated margin; incomplete thin halo sign; Tvol 33 mL, asymmetry—RL 29 mL and LL 8 mL; transverse; depth of penetration 4 cm. (bb) Detail of medium-sized PTC (arrowheads): complex nodule—coarse structure; solid part mostly hyperechoic with coarse linear calcifications (line of open arrows) and multiple microcalcifications (open arrows) with acoustic shadow, small irregular cystic cavities (c); microlobulated margin; incomplete thin halo sign; transverse. (cc) Detail of medium-sized PTC (arrowheads), CFDS: increased vascular-

ity, pattern II; transverse. (dd) Detail of medium-sized PTC (arrowheads): complex nodule—coarse structure; solid part mostly hyperechoic with coarse curvilinear calcifications (line of open arrows) with acoustic shadow and single microcalcification (open arrow), small irregular cystic cavities (c); microlobulated margin; incomplete thin halo sign; longitudinal. (ee) Detail of medium-sized PTC and solid metastatic LN along the right CCA at level C-III: complex nodule—coarse structure; multiple microcalcifications (open arrows), small cystic cavities (c) hypoechoic periphery; Ln 1—oval shape; size 12×8 mm; coarse structure; hyperechoic; multiple microcalcifications (open arrows); no hilus sign; transverse. (ff) Detail of two large metastatic LN with cystic necrosis along the right CCA at level C-II: LN2—size 36×18 mm and LN3—size 17×11 mm, L/S ratio ≈ 2 (not pathological); completely anechoic contents with sporadic septa; no hilus sign; transverse

**Fig. 15.18** (continued)

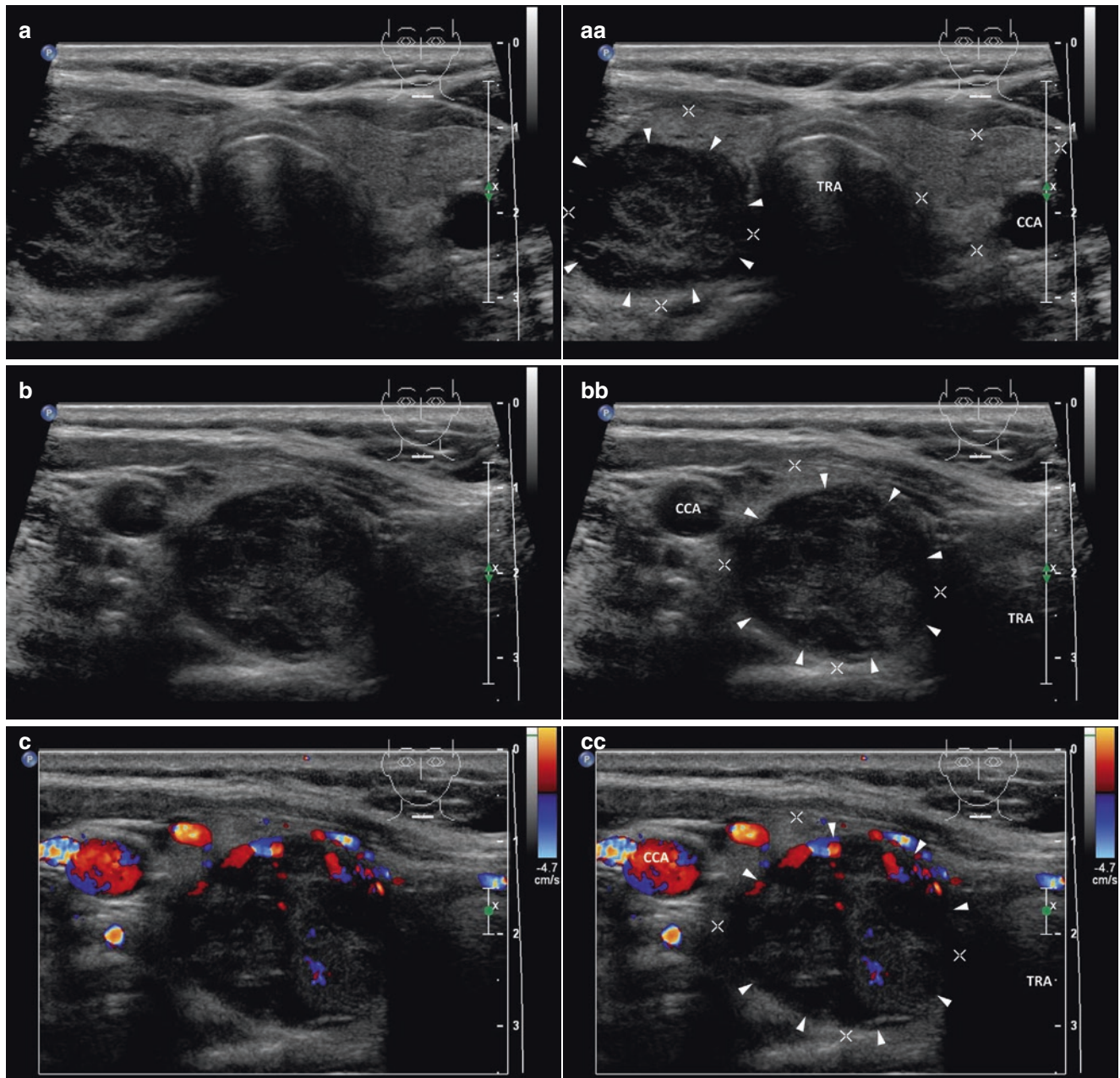


Fig. 15.19 (aa) A 61-year-old woman with a medium-sized papillary thyroid carcinoma—PTC (arrowheads) in the RL, size $35 \times 23 \times 21$ mm and volume 9 mL. No metastatic cervical lymph nodes. US overall view: solid nodule—inhomogeneous structure; mixed echogenicity, central mostly hyperechoic and markedly hypoechoic periphery; well-defined margin; Tvol 26 mL, asymmetry—RL 19 mL and LL 7 mL; transverse. (bb) Detail of medium-sized PTC (arrowheads): solid nodule—inhomogeneous structure; central mostly hyperechoic and mark-

edly hypoechoic periphery; well-defined margin; transverse. (cc) Detail of medium-sized PTC (arrowheads), CFDS: sporadic peripheral and central vascularity, *pattern I*; transverse. (dd) Detail of medium-sized PTC (arrowheads): solid nodule—inhomogeneous structure; central mostly hyperechoic and markedly hypoechoic periphery; well-defined margin; “daughter” small nodule (arrows), size 11×7 mm with the same pattern next to the upper pole of PTC; longitudinal

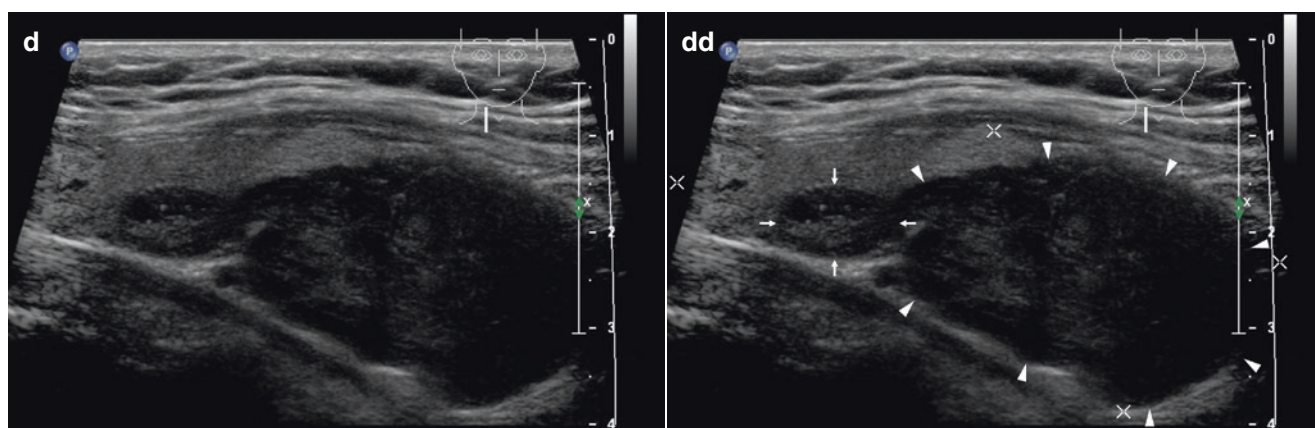


Fig. 15.19 (continued)

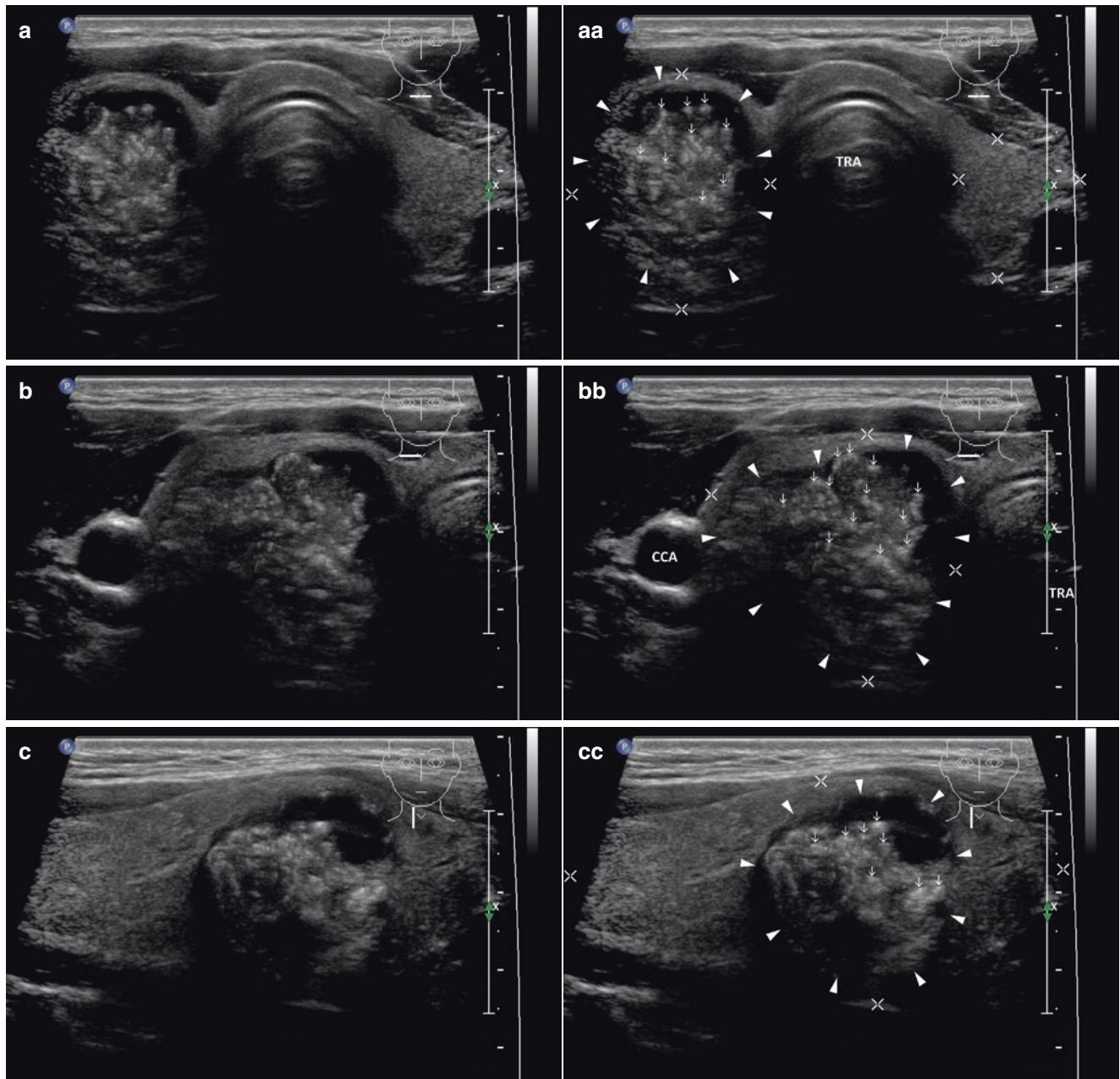
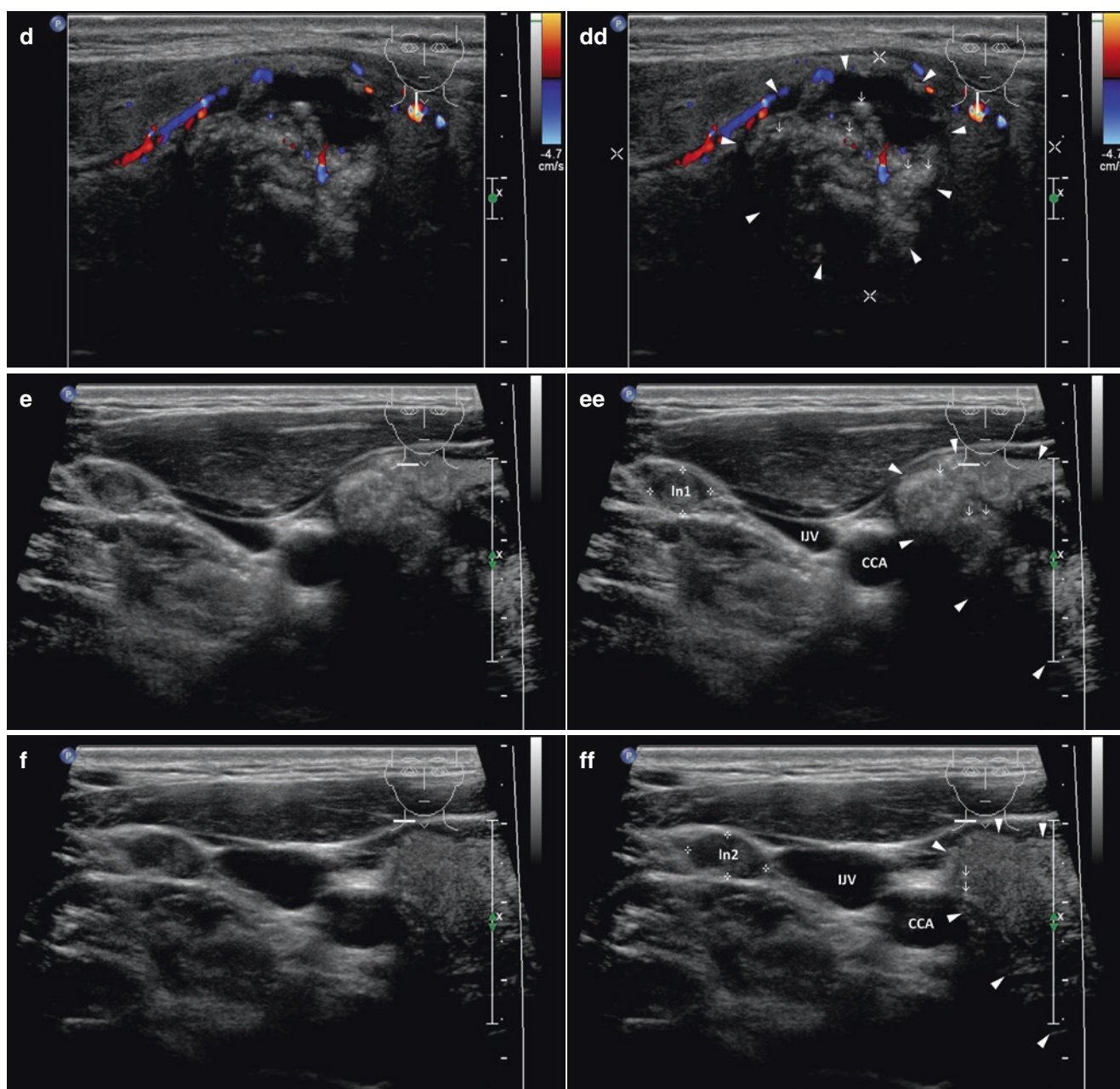


Fig. 15.20 (aa) A 33-year-old man with a solitary medium-sized papillary thyroid carcinoma, follicular variant—FVPTC (arrowheads) in the RL, size $34 \times 33 \times 27$ mm and volume 15 mL. Moreover tiny metastatic cervical lymph nodes (LN) along the right IJV at level C-III. US overall view: solid nodule; round shape; coarse structure; mixed echogenicity, central hyperechoic with multiple microcalcifications (open arrows), hypoechoic periphery; ill-defined, lobulated margin; Tvol 33 mL, asymmetry—RL 29 mL and LL 8 mL; transverse; depth of penetration 4 cm. (bb) Detail of medium-sized FVPTC (arrowheads): solid nodule; round shape; coarse structure; mixed echogenicity, central hyperechoic with multiple microcalcifications (open arrows), laterally with acoustic shadow, hypoechoic periphery; ill-defined, lobulated mar-

gin; transverse. (cc) Detail of medium-sized FVPTC (arrowheads): solid nodule; round shape; coarse structure; mixed echogenicity, central hyperechoic with multiple microcalcifications (open arrows) with acoustic shadow, hypoechoic periphery; ill-defined, lobulated margin; longitudinal. (dd) Detail of medium-sized FVPTC (arrowheads), CFDS: minimal vascularity, pattern 0; longitudinal. (ee) Detail of medium-sized FVPTC and tiny metastatic LNs: ln1—round shape; size 7×5 mm, long-to-short axis ratio ≈ 1 ; hyperechoic; no hilus sign; transverse. (ff) Detail of medium-sized FVPTC and tiny metastatic LNs: ln2—elliptical shape; size 10×5 mm, L/S ratio ≈ 2 (not pathological); hyperechoic; no hilus sign; transverse.

**Fig. 15.20** (continued)

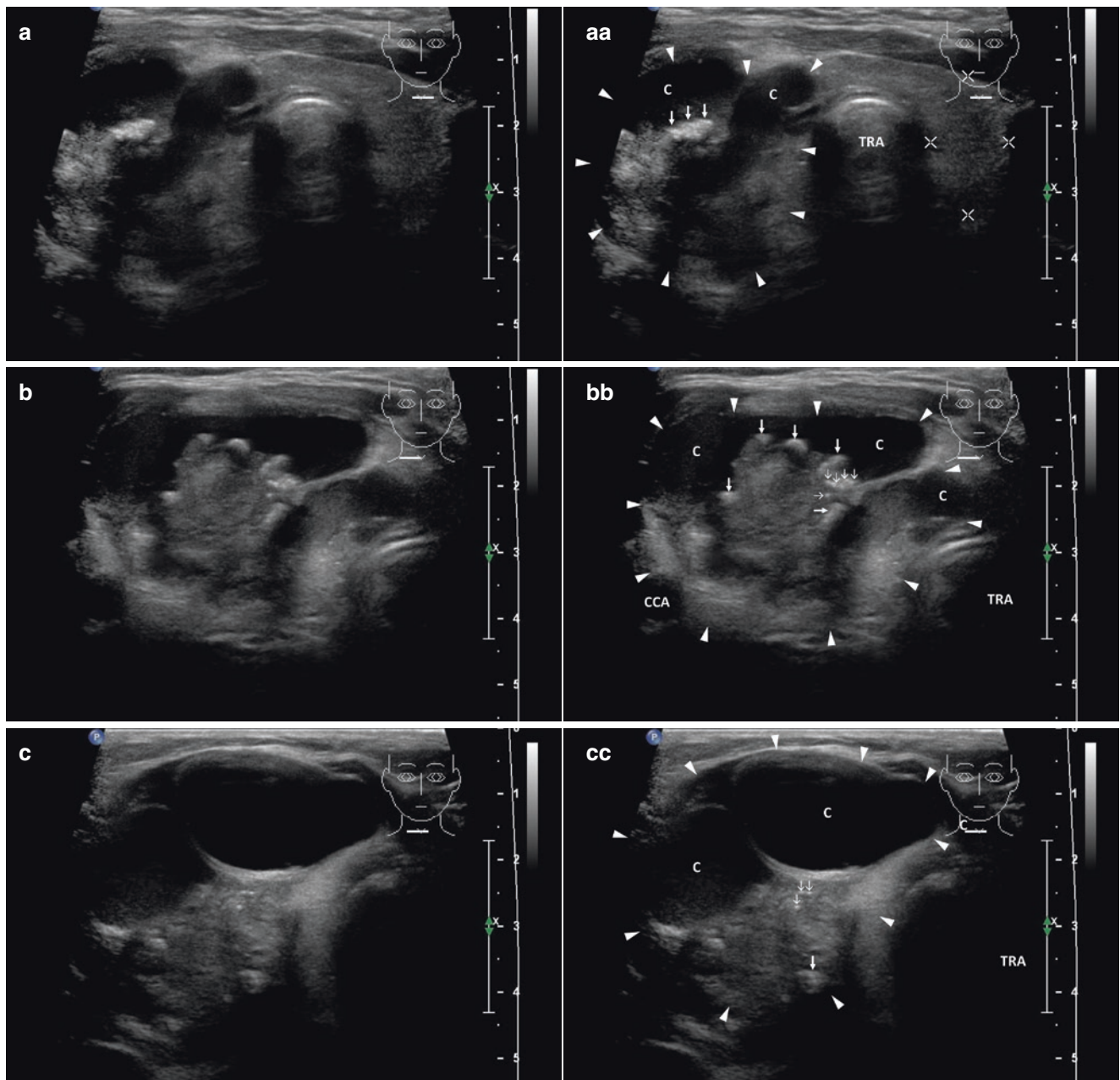
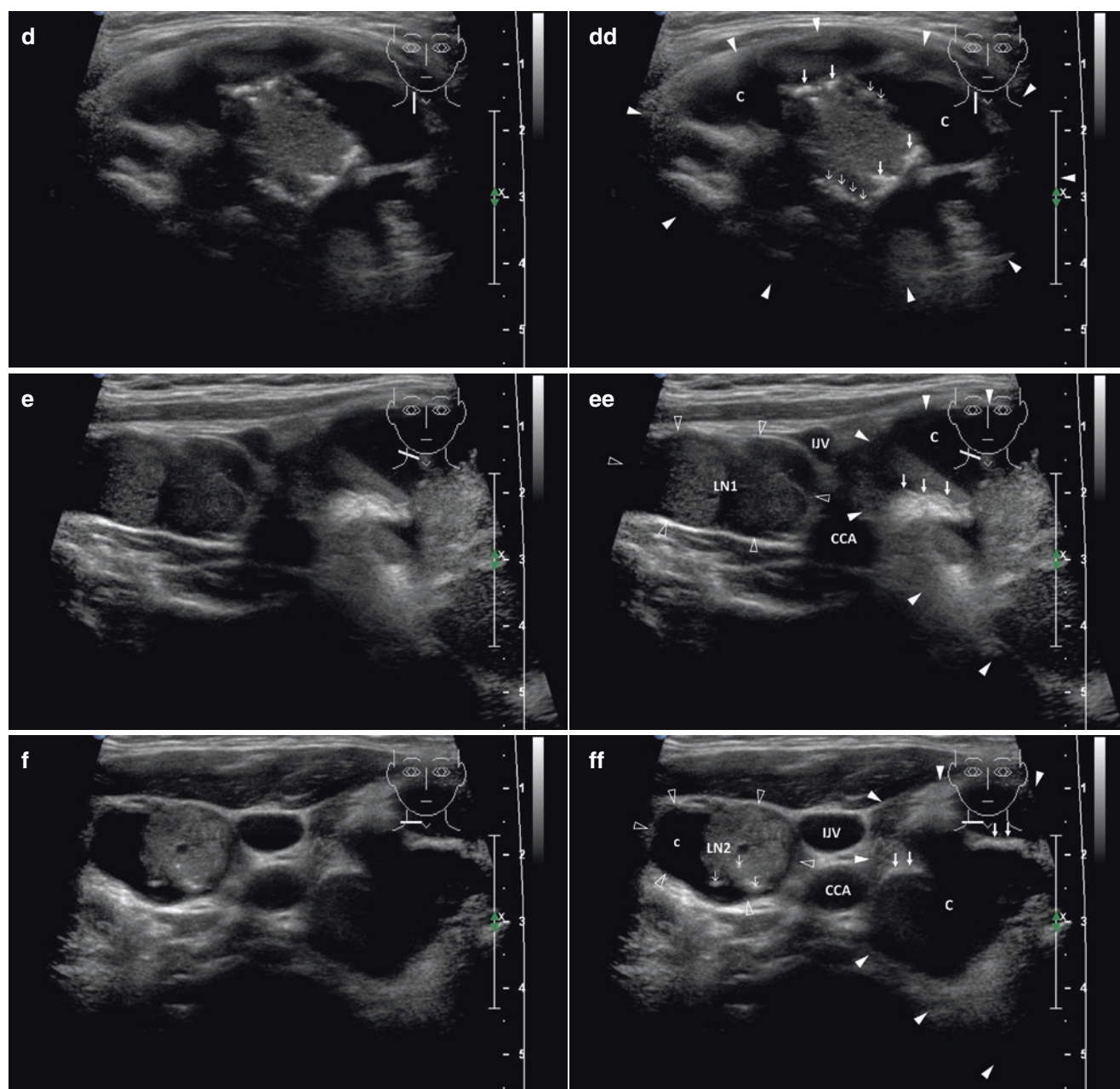


Fig. 15.21 (aa) A 52-year-old woman with a solitary giant papillary thyroid carcinoma—PTC (*arrowheads*) consist of entire RL, size $60 \times 47 \times 38$ mm and volume 56 mL. Moreover metastatic cervical lymph nodes (LN) along the right CCA at level C-II, III, IV. US overall view: complex nodule—irregular shape; coarse structure; solid part hyperechoic with multiple coarse calcifications (*arrows*) with acoustic shadow, large irregular cystic cavities (C); ill-defined, lobulated margin; normal structure of LL; trachea and LL push to the left; Tvol 33 mL, asymmetry—RL 56 mL and LL 9 mL; transverse; depth of penetration 6 cm. (bb) Detail of giant PTC (*arrowheads*): complex nodule—irregular shape; coarse structure; solid part hyperechoic with multiple coarse calcifications (*arrows*), multiple irregular cystic cavities (c); ill-defined, lobulated margin; transverse. (cc) Detail of giant PTC (*arrowheads*), another view: complex nodule—irregular shape; coarse structure; solid part hyperechoic with multiple coarse calcifications (*open arrows*), large cystic cavities (C); ill-defined, lobulated or blurred margin; transverse. (dd) Detail of giant PTC (*arrowheads*): complex nodule—irregular shape; coarse structure; solid part hyperechoic with multiple coarse calcifications (*arrows*) with acoustic shadow, multiple irregular cystic cavities (C); ill-defined, lobulated or blurred margin; longitudinal. (ee) Detail of giant PTC and large solid metastatic LN size $43 \times 25 \times 15$ mm and volume 8 mL along the right IJV and CCA at level C-II: lateral part of PTC (*arrowheads*); LN

1—elliptical shape; homogeneous structure; hyperechoic; no hilus sign; compressing IJV; transverse. (ff) Detail of giant PTC and medium-sized complex metastatic LN with cystic necrosis, size $26 \times 22 \times 16$ mm and volume 4.5 mL along the right IJV and CCA at level C-III: lateral part of PTC (*arrowheads*) with cystic cavity (C); LN2—elliptical shape; inhomogeneous structure; solid part hyperechoic; microcalcifications (*open arrows*); irregular cystic cavity (c); no hilus sign; transverse. (gg) Detail of giant PTC and large complex metastatic LN with cystic and coagulation necrosis (*arrows*), size $37 \times 35 \times 23$ mm and volume 16 mL along the right CCA at level C-IV: lateral part of PTC (*arrowheads*) with cystic cavity (c); LN3—elliptical shape; inhomogeneous structure; hypoechoic with debris and coarse hyperechoic foci without acoustic shadow (*arrows*); no hilus sign; transverse. (hh) Detail of medium-sized complex metastatic LN2 with cystic necrosis at level C-III and large complex metastatic LN3 with cystic and coagulation necrosis (*arrows*) at level C-IV: LN2—microcalcifications (*open arrows*); irregular cystic cavity (c); LN3—hypoechoic with debris and coarse hyperechoic foci without acoustic shadow (*arrows*); longitudinal. (ii) Detail of medium-sized complex metastatic LN2 with cystic necrosis at level C-III and large complex metastatic LN3 with cystic and coagulation necrosis at level C-IV, CFDS: both LNs hilar vascularity; longitudinal

**Fig. 15.21** (continued)

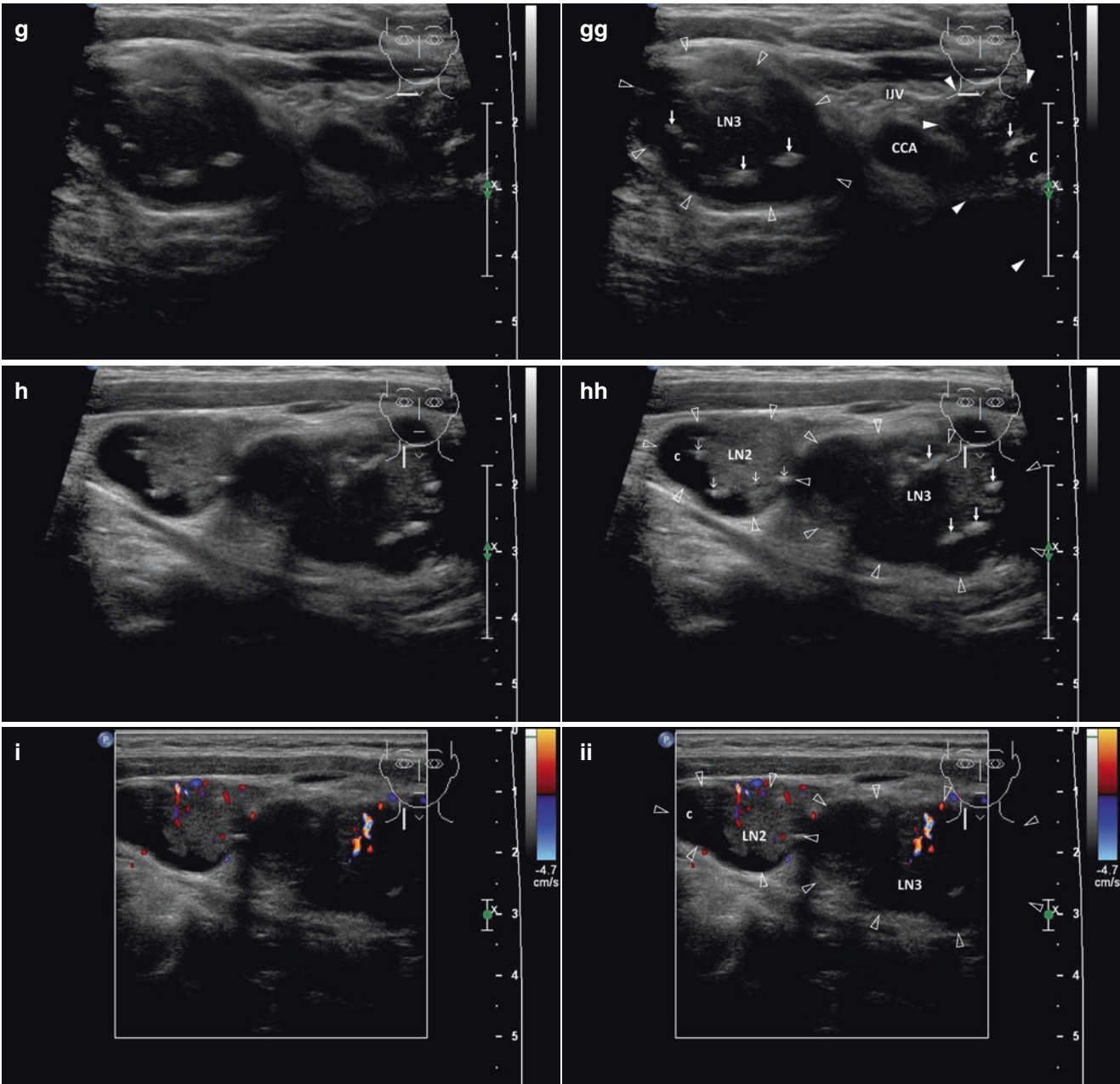


Fig. 15.21 (continued)

15.4 Multifocal Papillary Thyroid Carcinoma

15.4.1 Essential Facts

- A retrospective study by Tam et al. [23] of 912 patients who underwent thyroidectomy for papillary thyroid carcinoma (PTC), found multifocal PTC in 308 patients ($\approx 34\%$). Capsular invasion, extrathyroidal extension, and cervical metastatic lymph nodes (LNs) were significantly more common in patients with multifocal tumors compared to patients with unifocal PTC. Multifocal papillary thyroid microcarcinomas (PTMC) with the total tumor diameter of all foci >10 mm confer a similar risk of aggressive histopathological behavior as unifocal PTC >10 mm [23].
- A retrospective study by Zhu et al. [24] of 763 patients with PTC who underwent total thyroidectomy with bilateral central neck dissection, identified 277 PTC patients with Hashimoto's thyroiditis (HT). There were not any significant differences in incidence of cervical lateral metastatic LNs (at level C-II, III, IV) between the multifocal PTC-associated with HT and the classic multifocal PTC. However, a significantly reduced risk of cervical central metastatic LNs (at level C-VI) was observed in the multifocal PTC-associated with HT compared to classic multifocal PTC cases (35.7% vs. 72.4%). HT was associated with increased prevalence of multifocality and capsular invasion. In contrast, HT was associated with a reduced risk of cervical central metastatic LNs in PTC and multifocal PTC patients, which indicated a potential protective effect [24].
- A retrospective analysis by Al Afif et al. [25] considered 227 patients with multifocal PTC who underwent total or hemi-thyroidectomy with central neck dissection. They found a significant association between the multifocal PTC and the cervical central metastatic LNs positivity, increasing proportionally with the number of foci. These findings recognize multifocality as a sign of tumor aggressiveness [25].

15.4.2 US Findings of Multifocal Papillary Thyroid Carcinoma

- PTCs frequently occur as two (Fig. 15.22 and 15.23) or more separate foci within (Fig. 15.24) the thyroid gland (18–87%). However, those multifocal tumors are often undetected by preoperative radiologic evaluations. In study by So et al. [26], multifocal PTMCs were detected in 100 of 277 patients ($\approx 36\%$). Sensitivity and specificity of preoperative US were 42.7% and 92.2% for multifocal tumors. Sensitivity and specificity of preoperative CT were 29.4% and 95.5% for multifocal tumors. Sensitivity and specificity of preoperative US were 49.0% and 93.5% for bilateral tumors. Sensitivity and specificity of preoperative CT were 28.6% and 100% for bilateral tumors [26].
- For multifocal PTC apply the same 2015 ATA criteria as for solitary suspected nodule [8]; *see more at Section IV.*
- For cervical metastatic LNs (Figs. 15.22cc and 15.24ee) *see more at Chap. 18, Sect. 18.3 and Chap. 19.*

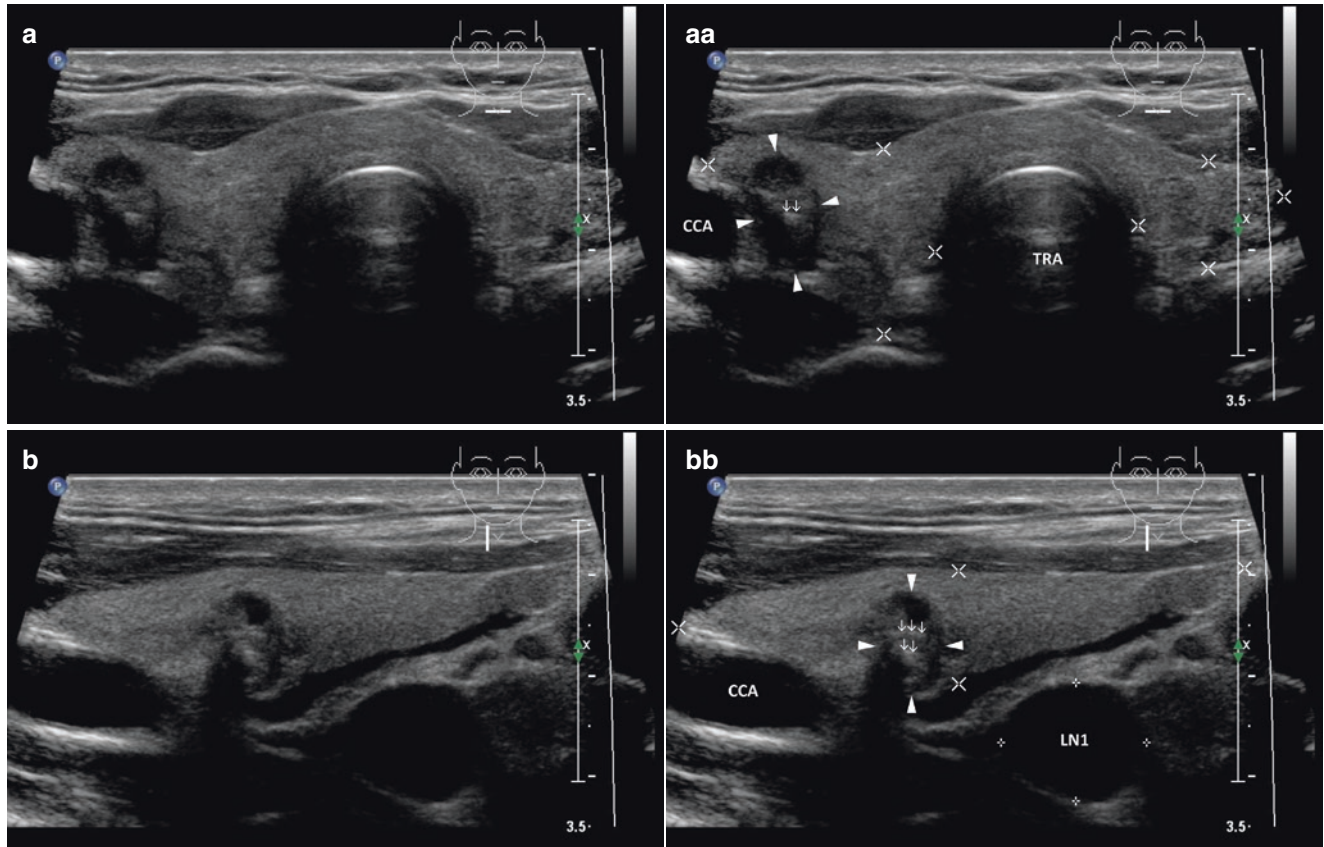
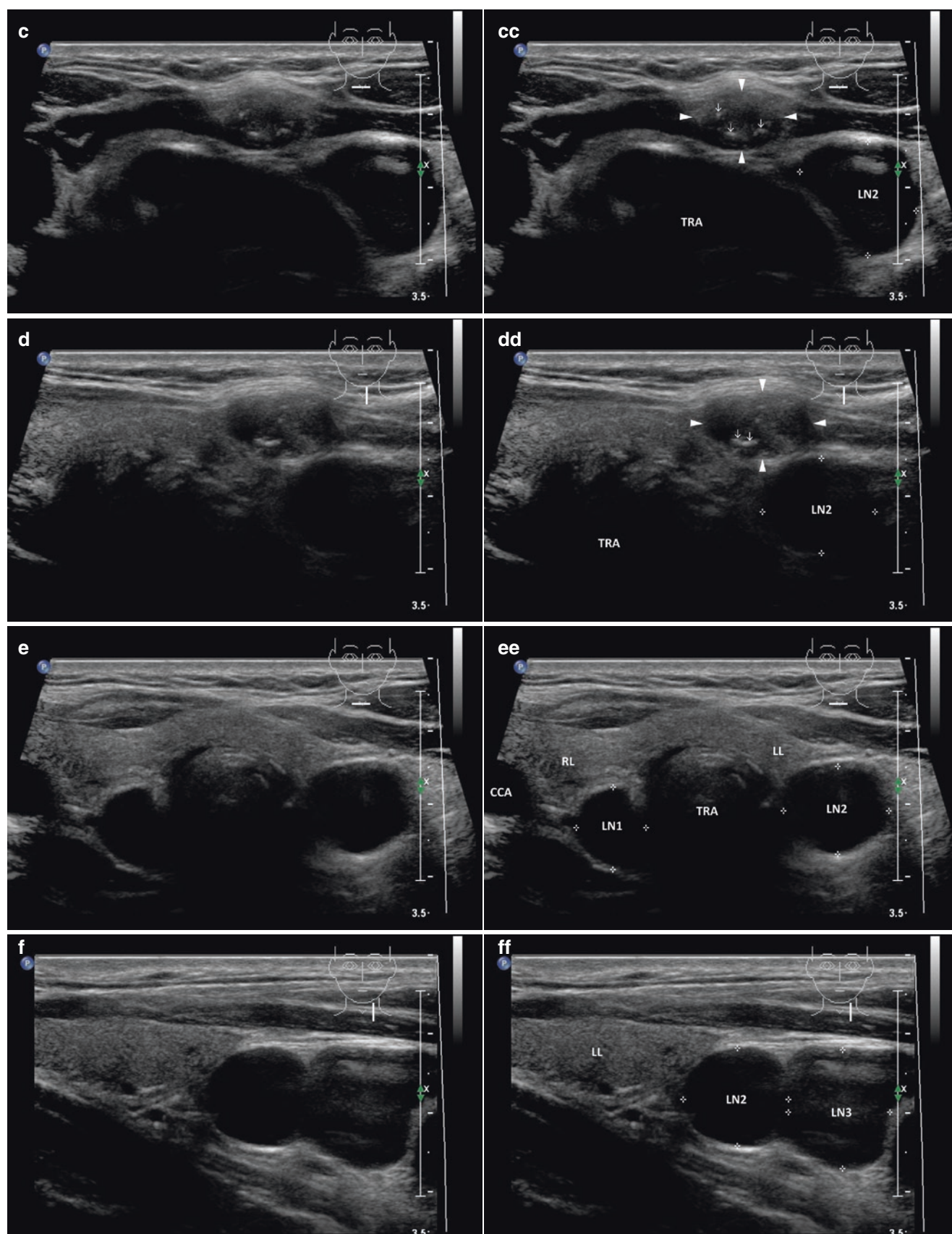


Fig. 15.22 (aa) A 37-year-old man with a multifocal papillary thyroid carcinoma (PTC)—papillary thyroid microcarcinoma (PTMC) in the RL and small papillary thyroid carcinoma (PTC) in the isthmus and three cervical metastatic lymph nodes (LN) bilaterally. US scan of PTMC (arrowheads), size $12 \times 9 \times 8$ mm and volume 0.4 mL in the RL: solid nodule; “taller-than-wide” shape; inhomogeneous structure; hypoechoic; centrally microcalcifications (open arrows); ill-defined blurred margin; Tvol 21 mL, RL 11 mL, and LL 10 mL; transverse. (bb) Detail of PTMC in the RL and metastatic LN along the right CCA at level C-VI: PTMC (arrowheads)—solid nodule; “taller-than-wide” shape; inhomogeneous structure; hypoechoic; centrally microcalcifications (open arrows); ill-defined blurred margin; metastatic LN1 (marks)—round shape; size 15×12 mm, L/S ratio ≈ 1 ; homogeneous structure; hypoechoic; no hilus sign; longitudinal. (cc) Detail of small PTC size $15 \times 12 \times 9$ mm, volume 0.8 mL in low side of isthmus and metastatic LN in the low neck at level C-VI: PTC (arrowheads)—solid

nodule; round shape; coarse structure; mostly hypoechoic; peripheral microcalcifications (open arrows); ill-defined blurred margin; metastatic LN2 (marks)—round shape; homogeneous structure; hypoechoic; hyperechoic band, no hilus sign; transverse. (dd) Detail of PTC in low side of isthmus and metastatic LN on the low neck at level C-VI: PTC (arrowheads)—solid nodule; ovoid shape; coarse structure; mostly hypoechoic; peripheral microcalcifications (open arrows); ill-defined blurred margin; metastatic LN2 (marks)—round shape, size 14×13 mm, L/S ratio ≈ 1 ; homogeneous structure; hypoechoic; no hilus sign; longitudinal. (ee) Detail of two metastatic LNs under low poles bilaterally at level C-VI: metastatic LN1, LN2 (marks)—round shape, L/S ratio ≈ 1 ; homogeneous structure; hypoechoic; no hilus sign; transverse. (ff) Detail of two metastatic LNs under low pole of the LL at level C-VI: metastatic LN2 (marks) size 14×13 mm, LN3 (marks) size 16×16 mm—round shape, L/S ratio ≈ 1 ; homogeneous structure; hypoechoic; no hilus sign; longitudinal

**Fig. 15.22** (continued)

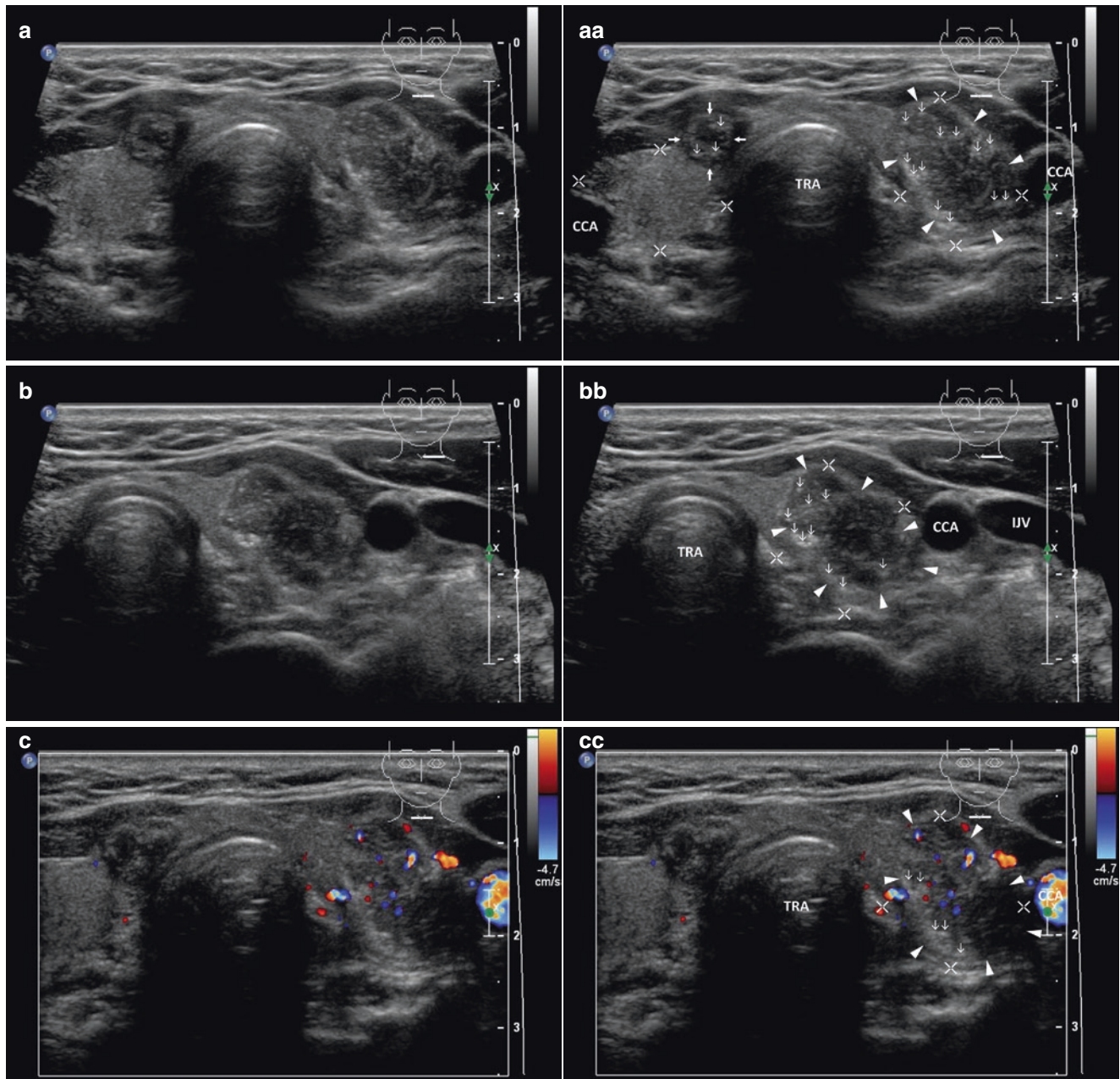
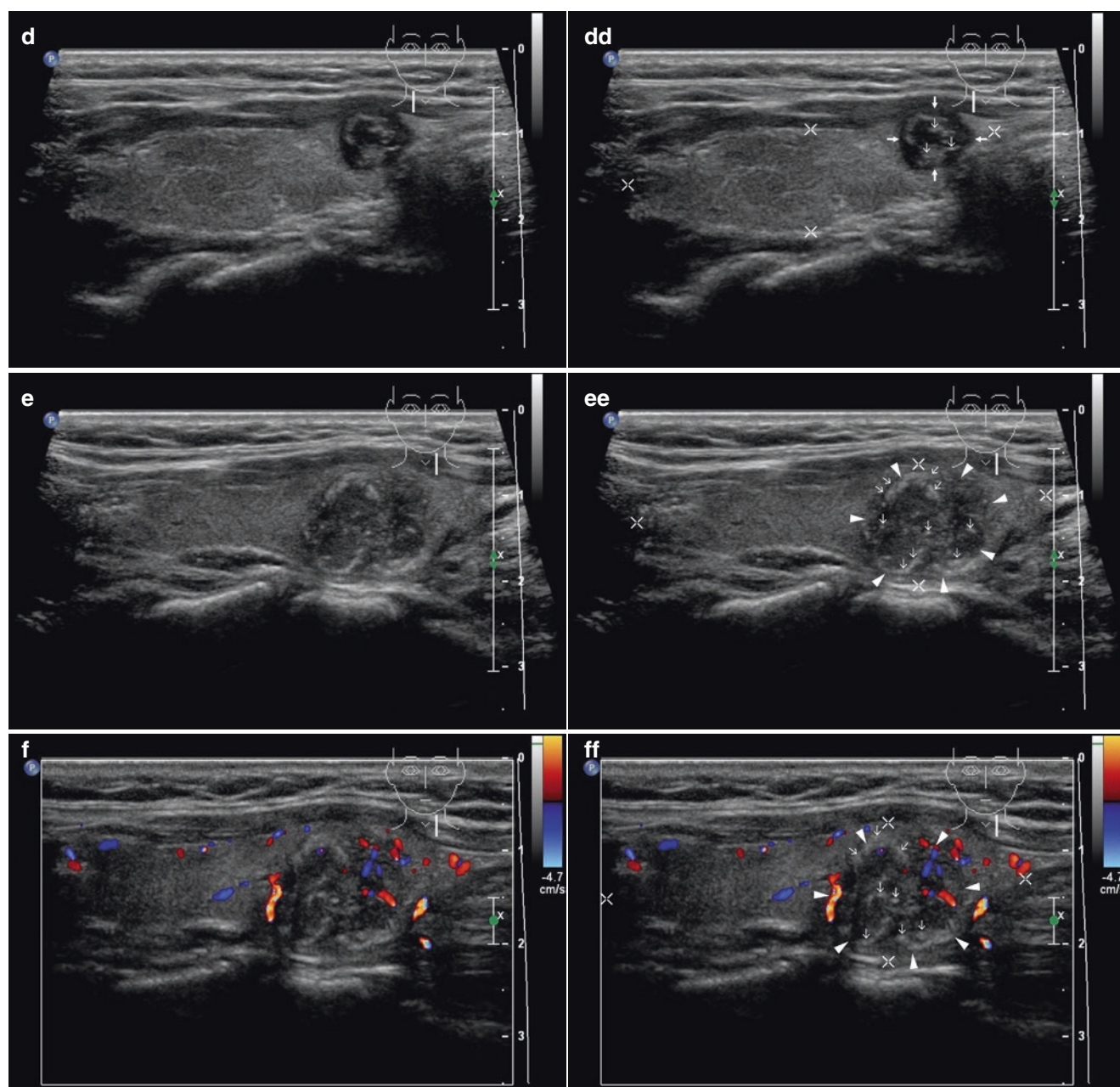


Fig. 15.23 (aa) A 48-year-old woman with a multifocal papillary thyroid carcinoma (PTC)—papillary thyroid microcarcinoma (PTMC) size $8 \times 7 \times 6$ mm, volume 0.2 mL in the RL and medium-sized papillary thyroid carcinoma (PTC) size $18 \times 15 \times 14$ mm, volume 2 mL in the LL; *without cervical metastatic lymph nodes*. US overall view: PTMC (arrows)—solid nodule; round shape; inhomogeneous structure; mixed echogenicity; sporadic microcalcifications (*open arrows*); well-defined margin; thin halo sign; PTC (arrowheads)—solid nodule; “taller-than-wide” shape; coarse structure; mixed echogenicity; diffusely microcalcifications (*open arrows*); ill-defined blurred margin; Tvol 15 mL, RL 7 mL, and LL 8 mL; transverse. (bb) Detail of medium-sized PTC (arrowheads) in the LL: solid nodule; “taller-than-wide”

shape; coarse structure; mixed echogenicity; diffusely microcalcifications (*open arrows*); ill-defined blurred margin; transverse. (cc) Overall view of PTMC and PTC, CFDS: PTMC (arrows)—avascular, *pattern 0*; PTC (arrowheads)—sporadic peripheral and parenchymal vascularity, *pattern 1*; transverse. (dd) Detail of PTMC (arrows) in the RL: solid nodule; round shape; inhomogeneous structure; mixed echogenicity; centrally sporadic microcalcifications (*open arrows*); well-defined margin; thin halo sign; longitudinal. (ee) Detail of PTC (arrowheads) in the LL: solid nodule; round shape; coarse structure; mixed echogenicity; diffusely microcalcifications (*open arrows*); ill-defined blurred margin; longitudinal. (ff) Detail of PTC in the LL, CFDS: sporadic peripheral and parenchymal vascularity, *pattern 1*; longitudinal

**Fig. 15.23** (continued)

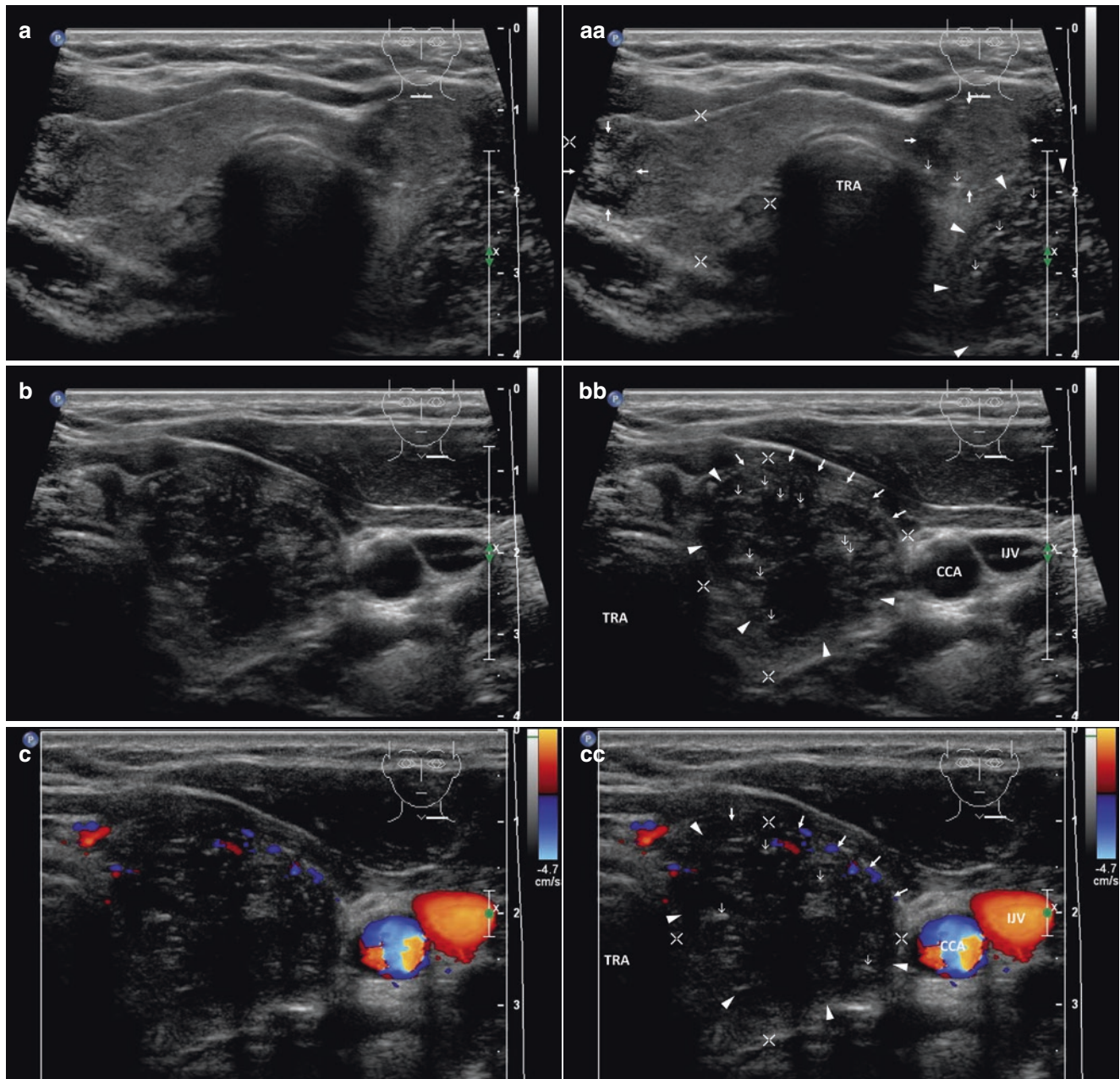
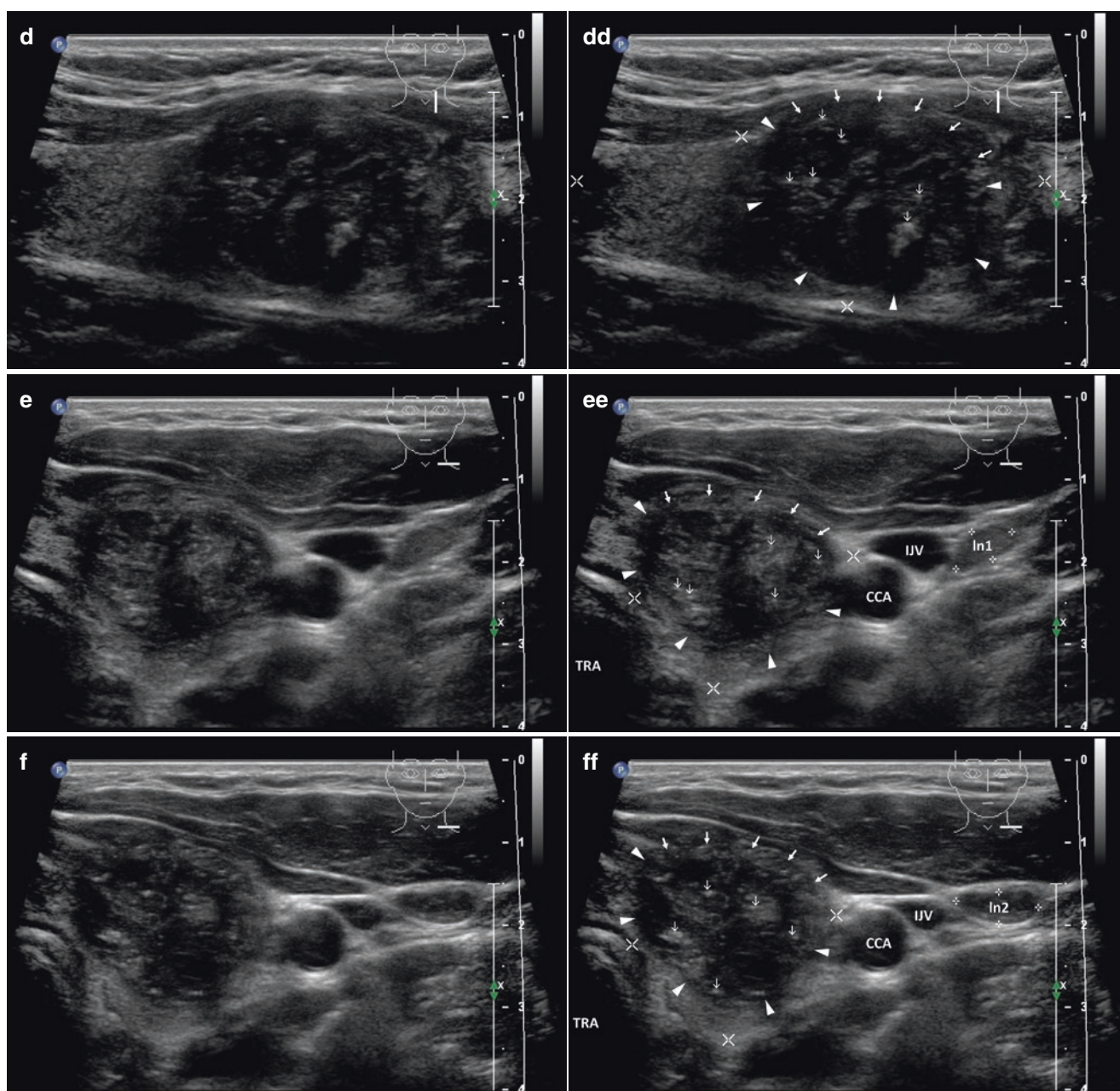


Fig. 15.24 (aa) A 33-year-old man with a multifocal papillary thyroid carcinoma (PTC)—dominant large PTC, size $31 \times 24 \times 23$ mm, volume 9 mL in the LL and two small PTCs in the RL and LL sized ≈ 10 mm. Moreover cervical metastatic lymph nodes (LN) along the left IJV at level C-IV. US overall view: large PTC (arrowheads) in the LL dorsally—solid nodule; “taller-than-wide” shape; coarse structure; hypoechoic; diffusely microcalcifications (open arrows); ill-defined blurred margin; small PTC (arrows) in the LL ventrally—solid nodule; round shape; homogeneous structure; isoechoic; sporadic microcalcifications (open arrows) at periphery; ill-defined margin; small PTC (arrows) in the RL—solid nodule; round shape; inhomogeneous structure; hypoechoic; centrally microcalcifications (open arrows); ill-defined slurred margin; Tvol 31 mL, RL 11 mL, and LL 20 mL; transverse. (bb) Detail of large PTC (arrowheads) in LL: solid nodule; “taller-than-wide” shape; coarse structure; hypoechoic; diffusely microcalcifications (open arrows); ill-defined blurred margin; tumor

protrusion ventrally with contour bulging and interrupting continuity of the capsule (arrows); transverse. (cc) Detail of large PTC (arrowheads) in LL, CFDS: sporadic peripheral vascularity, pattern I; transverse. (dd) Detail of large PTC (arrowheads) in LL: solid nodule; “taller-than-wide” shape; coarse structure; hypoechoic; diffusely microcalcifications (open arrows); ill-defined blurred margin; tumor protrusion ventrally with contour bulging and interrupting continuity of the capsule (arrows); longitudinal. (ee) Detail of large PTC (arrowheads) in LL and two tiny metastatic LNs along the left IJV at level C-IV: ln1 (marks)—elliptical shape, size 9×4 mm, L/S ratio > 2 (not pathological); homogeneous structure; hyperechoic; no hilus sign; transverse. (ff) Detail of large PTC (arrowheads) in LL and two tiny metastatic LNs along the left IJV at level C-IV: ln2 (marks)—elliptical shape, size 10×4 mm, L/S ratio > 2 (not pathological); homogeneous structure; hyperechoic; no hilus sign; transverse

**Fig. 15.24** (continued)

15.5 Papillary Thyroid Carcinoma and Hashimoto's Thyroiditis

15.5.1 Essential Facts

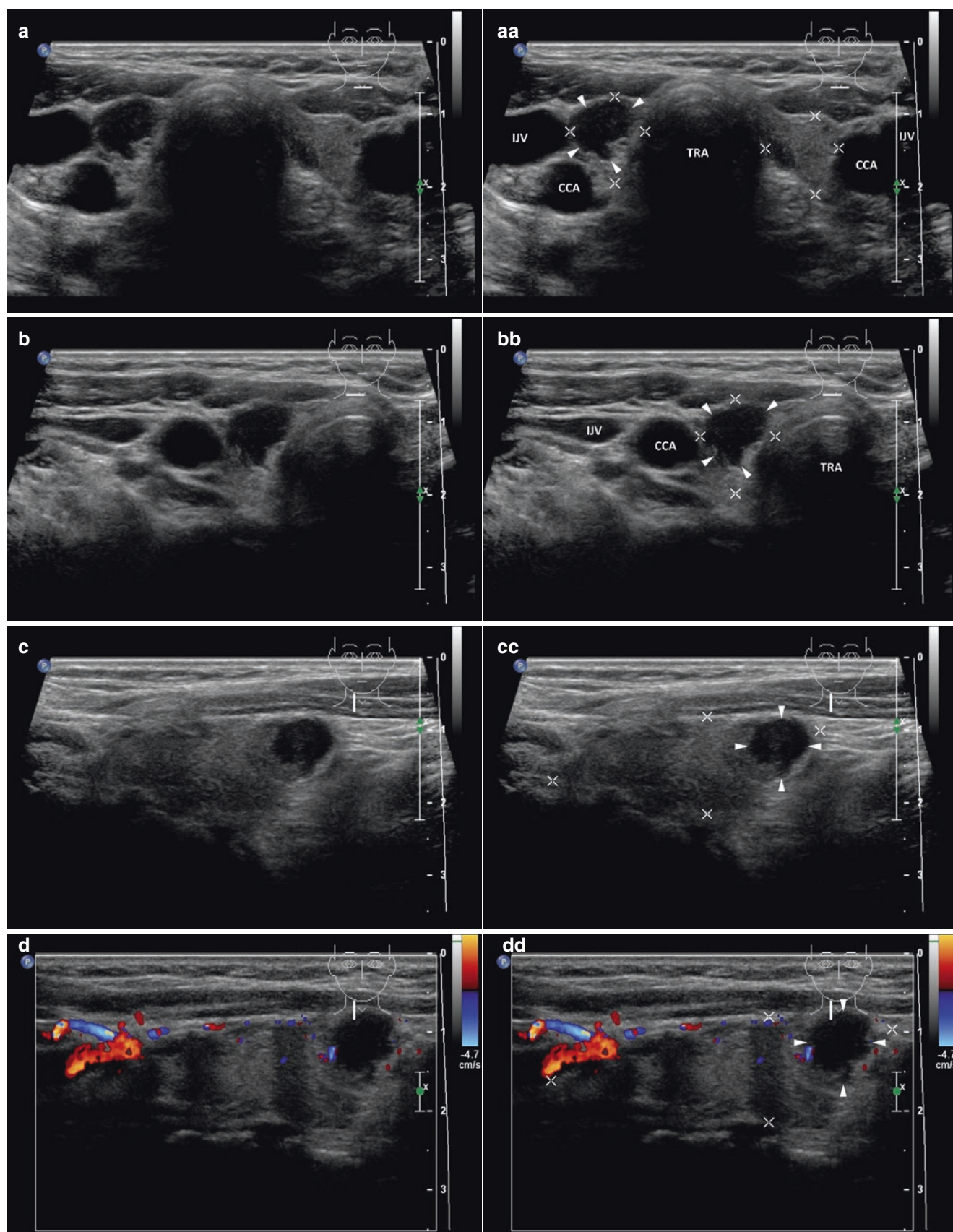
- Coexistence of Hashimoto's Thyroiditis (HT)—chronic lymphocytic thyroiditis (CLT)—and papillary thyroid carcinoma (PTC) was first reported in 1955 [27].
- According to a Japanese study with 626 patients, CLT was suggested as a predisposing factor for PTC. Prevalence of CLT was significantly higher in patients with PTC than in patients with adenomatous goiter; in Japanese females (63%) and males (50%), white females (76%), and African American females (46%) [28].
- Although the prognosis of patients with PTC is excellent, patient outcome is influenced by: patient age at diagnosis; stage of PTC; tumor size; presence of cervical node or distant metastasis; extrathyroidal extension; delay in diagnosis; extent of thyroidectomy; and postoperative radioiodine ablation.
- In a Korean study with 1357 PTC patients, 359 (26.5%) had coexisting CLT. Compared to patients without CLT, patients with CLT were younger, predominantly female, and had a small tumor size and a lower extrathyroidal extension rate at the time of surgery, which are the most important and well-known prognostic variables for thyroid cancer mortality. Coexistent CLT in PTC patients reduced the risk of recurrence (relapse-free 5-year survival rate $\approx 98.5\%$ vs. $\approx 95\%$ in patients without CLT), CLT was not an independent predictive factor for recurrence [29].
- There is no consensus on the association between PTC and HT. Meta-analysis of 38 eligible studies including 10,648 PTC cases reported a histologically proven association in 2471 (23.2%) PTCs. HT was more frequently observed in PTCs than in benign thyroid diseases and other carcinomas (OR = 2.8 and 2.4). PTCs with coexisting HT were significantly related to female patients (OR = 2.7), multifocal involvement (OR = 1.5), no extrathyroidal extension (OR = 1.3), and no LN metastasis (OR = 1.3). Moreover, PTCs with HT were significantly associated with long recurrence-free survival (HR = 0.6). PTC patients with HT have favorable clinicopathological characteristics compared to PTCs without HT. However, patients with HT needed to be carefully monitored for the development of PTC [30].

15.5.2 US Features of Cancerous Thyroid Nodules in the Field of HT

- US features of cancerous thyroid nodules are not significantly different in patients with HT compared to those without HT [31–33].
- Certain characteristics are emphasized. The cancerous nodules are:
 - most often solid (Figs. 15.25aa and 15.26aa).
 - most often hypoechoic (Figs. 15.25aa and 15.26aa).
 - with smooth margins (Figs. 15.25aa and 15.26aa).
 - without the “halo” sign (Figs. 15.25aa and 15.26aa).
 - without internal calcifications (Figs. 15.25aa and 15.26aa).
 - multifocal PTC (Fig. 15.28cc).
- Less frequent US findings:
 - intranodal microcalcifications (Fig. 15.29bb), peripheral arc of microcalcifications (Fig. 15.28cc).
 - thick halo sign (Fig. 15.28bb).
 - ill-defined, blurred margin (Figs. 15.27cc and 15.31bb).
 - extrathyroidal extension, contour bulging (Fig. 15.29bb).
 - cervical metastatic LNs (Figs. 15.30dd and 15.31dd).
 - diffuse sclerosing variant of PTC (Fig. 15.31aa)
- When the appearance of cancerous thyroid nodules in HT patients with a homogeneous gland were compared to those with a heterogeneous gland, the only US feature that reached statistical significance was the margin of the nodule. The cancerous nodules in patients with a heterogeneous gland were more likely to have irregular or poorly defined margins [33].
- To the contrary, another US study reported that the frequency of dense calcification in patients with HT was significantly higher and frequency of psammoma bodies was less than in PTC patients without HT. On the other hand, PTC with HT had more irregular shapes and ill-defined edges of the borders with less hypoechogenicity and calcification than PTC without HT, but the difference was not significant. Any type of US-detected calcification types may represent a risk for PTC [34].

Fig. 15.25 (aa) A 32-year-old woman with Hashimoto's thyroiditis (HT) and a solitary papillary thyroid microcarcinoma—PTMC (*arrowheads*) in the RL, size $10 \times 9 \times 8$ mm and volume 0.4 mL: PTMC—solid nodule; round shape; homogeneous structure; hypoechoic; well-defined margin, focally lobular; *no microcalcifications*; thyroid gland—mostly homogeneous structure; isoechoic, only sporadic hypoechoic micronodular structure; Tvol 7 mL, RL 4 mL, and LL 3 mL; transverse. **(bb)** Detail of RL with HT and PTMC (*arrowheads*):

solid nodule; round shape; homogeneous structure; hypoechoic; well-defined margin, focally lobular; transverse. **(cc)** Detail of RL with HT and PTMC (*arrowheads*): solid nodule; round shape; homogeneous structure; hypoechoic; well-defined margin, focally lobular; longitudinal. **(dd)** Detail of RL with HT and PTMC (*arrowheads*), CFDS: nodule—avascular with one peripheral vessel only, *pattern 0*; thyroid gland—minimal vascularity, *pattern 0*; longitudinal



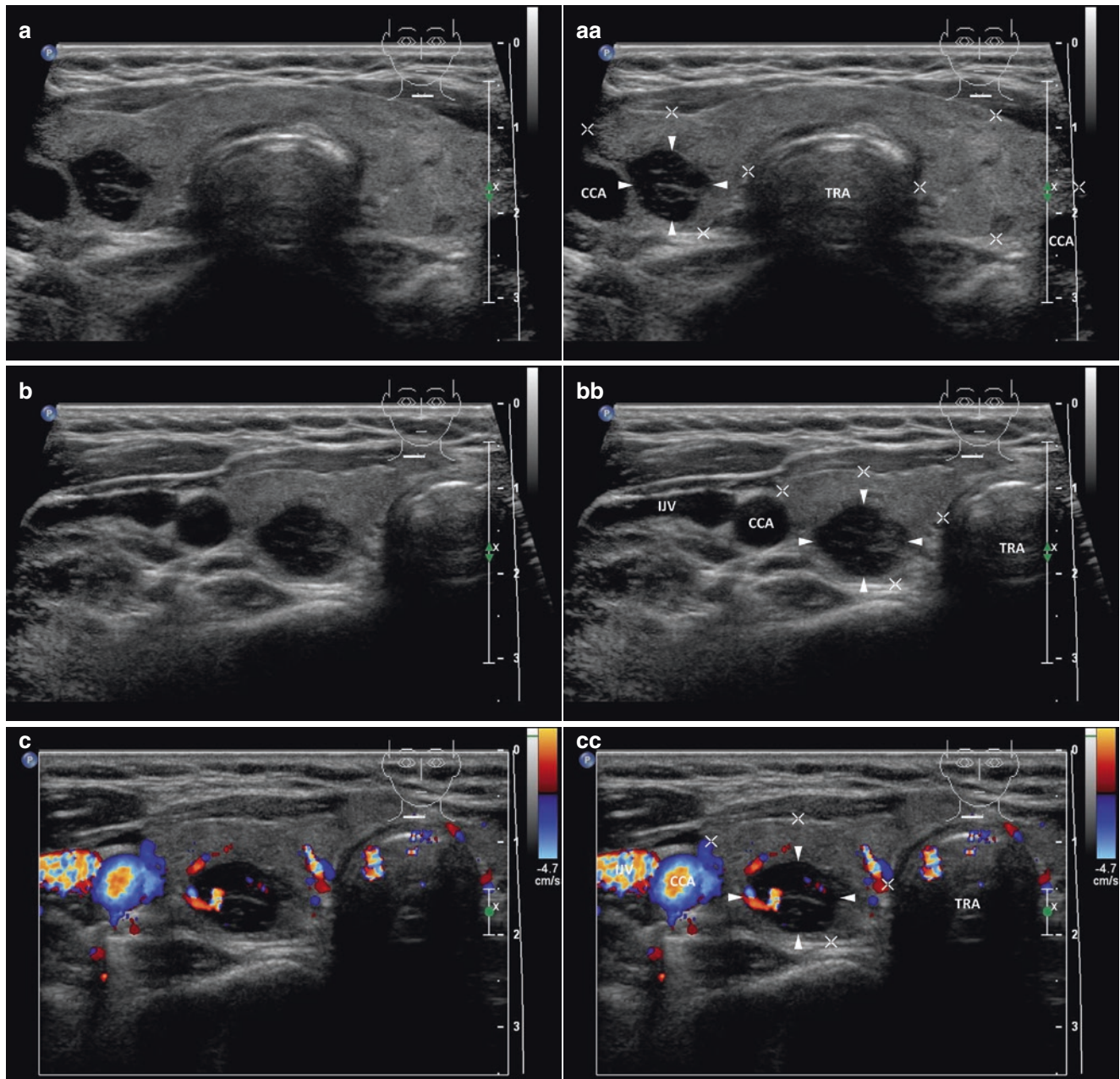


Fig. 15.26 (aa) A 52-year-old woman with Hashimoto's thyroiditis (HT) and a solitary small papillary thyroid carcinoma—PTC (arrowheads) in the RL, size $18 \times 11 \times 9$ mm and volume 1 mL: PTC—solid nodule; round shape; inhomogeneous structure; hypoechoic with hyperechoic fibrous septa; well-defined margin; *no microcalcifications*; thyroid gland—mostly homogeneous structure; isoechoic, only sporadic hypoechoic micronodular structure; Tvol 15 mL, RL 8 mL, and LL 7 mL; transverse. (bb) Detail of RL with HT and small PTC (arrowheads): solid nodule; round shape; inhomogeneous structure; hypoechoic with hyperechoic fibrous septa; well-defined margin; trans-

verse. (cc) Detail of RL with HT and small PTC (arrowheads), CFDS: nodule—focally peripheral vascularity and one intranodal vessel branch, *pattern I*; thyroid gland—sporadic peripheral and parenchymal vascularity, *pattern I*; longitudinal. (dd) Detail of RL with HT and small PTC (arrowheads): solid nodule; round shape; inhomogeneous structure; hypoechoic with hyperechoic fibrous septa; microlobulated margin; transverse. (ee) Detail of RL with HT and small PTC (arrowheads), CFDS: nodule—focally peripheral vascularity and one intranodal vessel branch, *pattern I*; thyroid gland—sporadic peripheral and parenchymal vascularity, *pattern I*; longitudinal

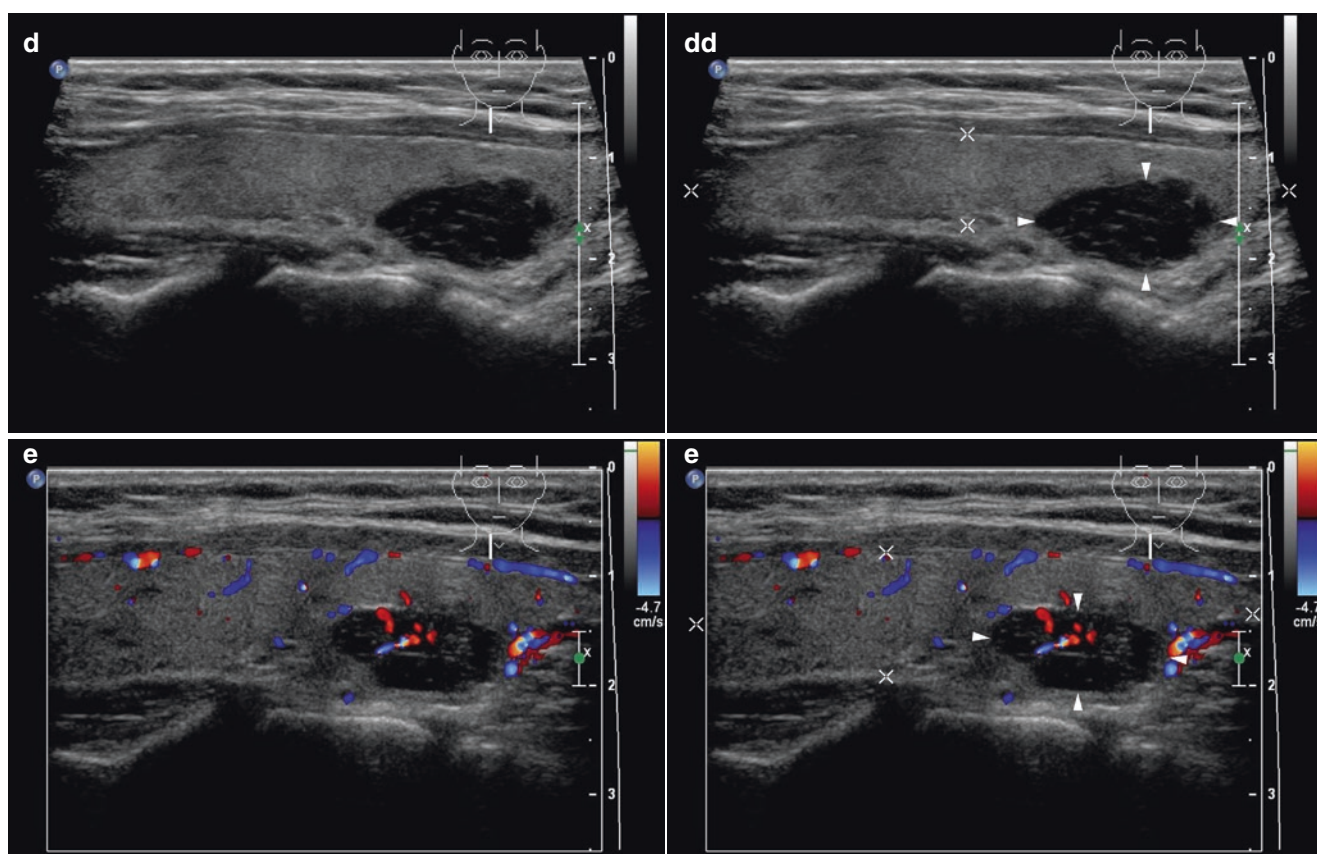


Fig. 15.26 (continued)

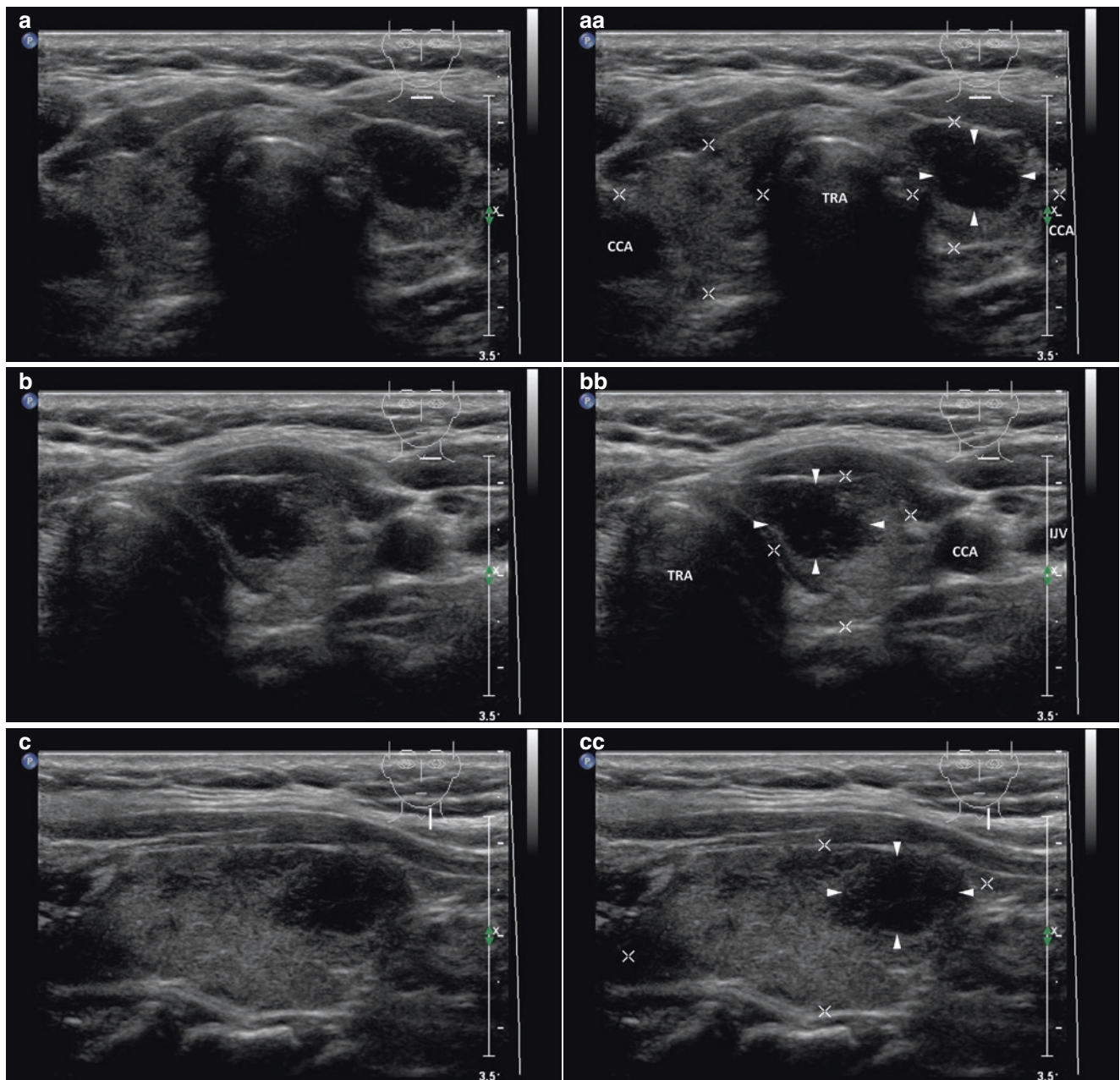


Fig. 15.27 (aa) A 62-year-old woman with Hashimoto's thyroiditis (HT) and a solitary small papillary thyroid carcinoma—PTC (arrow-heads) in the LL, size $15 \times 14 \times 9$ mm and volume 1 mL: PTC—solid nodule; round shape; inhomogeneous structure; hypoechoic with sporadic hyperechoic fibrotic areas; ill-defined margin; no microcalcifications; thyroid gland—mostly homogeneous isoechoic, only sporadic hypoechoic micronodular structure; Tvol 13 mL, RL 6 mL, and LL

7 mL; transverse. (bb) Detail of LL with HT and small PTC (arrow-heads): solid nodule; round shape; inhomogeneous structure; hypoechoic with sporadic hyperechoic fibrotic areas; ill-defined blurred margin; transverse. (cc) Detail of LL with HT and small PTC (arrow-heads): solid nodule; round shape; inhomogeneous structure; hypoechoic with sporadic hyperechoic fibrotic areas; ill-defined blurred margin; longitudinal

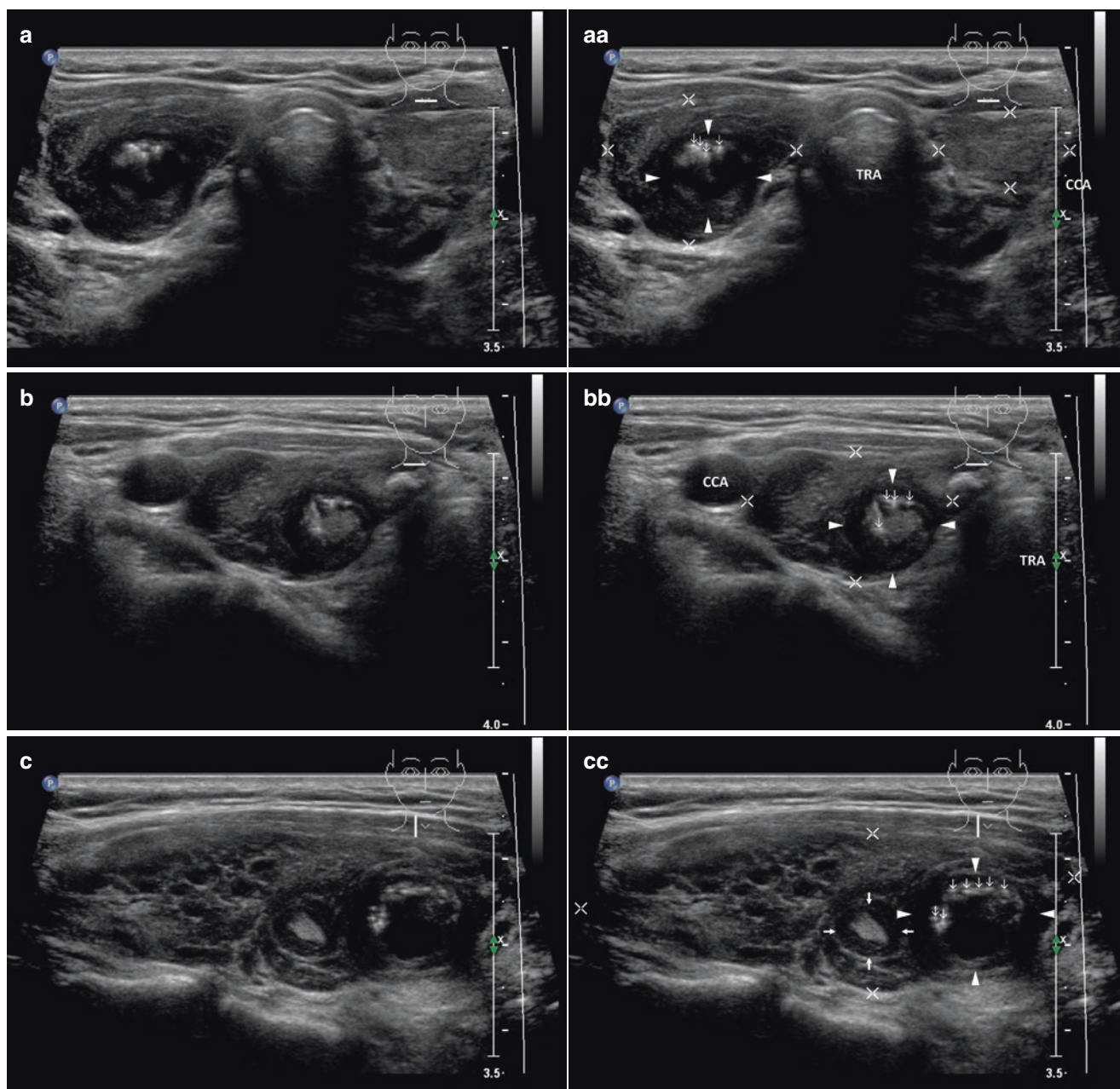


Fig. 15.28 (aa) A 49-year-old woman with Hashimoto's thyroiditis (HT) and a small papillary thyroid carcinoma—PTC (arrowheads) in the RL, size $14 \times 11 \times 11$ mm and volume 0.6 mL, moreover one PTMC: PTC—solid nodule; round shape; inhomogeneous structure; peripheral arc of microcalcifications (open arrows) with acoustic shadow; ill-defined margin; thick halo sign; thyroid gland—diffusely hypoechoic micronodular structure and hyperechoic fibrous septa; Tvol 29 mL, RL 14 mL, and LL 15 mL; transverse. (bb) Detail of RL with HT and small PTC (arrowheads): solid nodule; round shape; inhomogeneous structure; mixed echogenicity; peripheral arc of microcalcifications (open arrows); ill-defined margin; thick halo sign; transverse.

(cc) Detail of RL with HT and small PTC (arrowheads), moreover PTMC (arrows) size 6×5 mm: PTC—solid nodule; round shape; inhomogeneous structure; mixed echogenicity; peripheral arc of microcalcifications (open arrows) with acoustic shadow; ill-defined margin; thick halo sign; PTMC (arrows)—next to another small nodule—solid, hypoechoic, with central hyperechoic fibrous area (without shadow); longitudinal

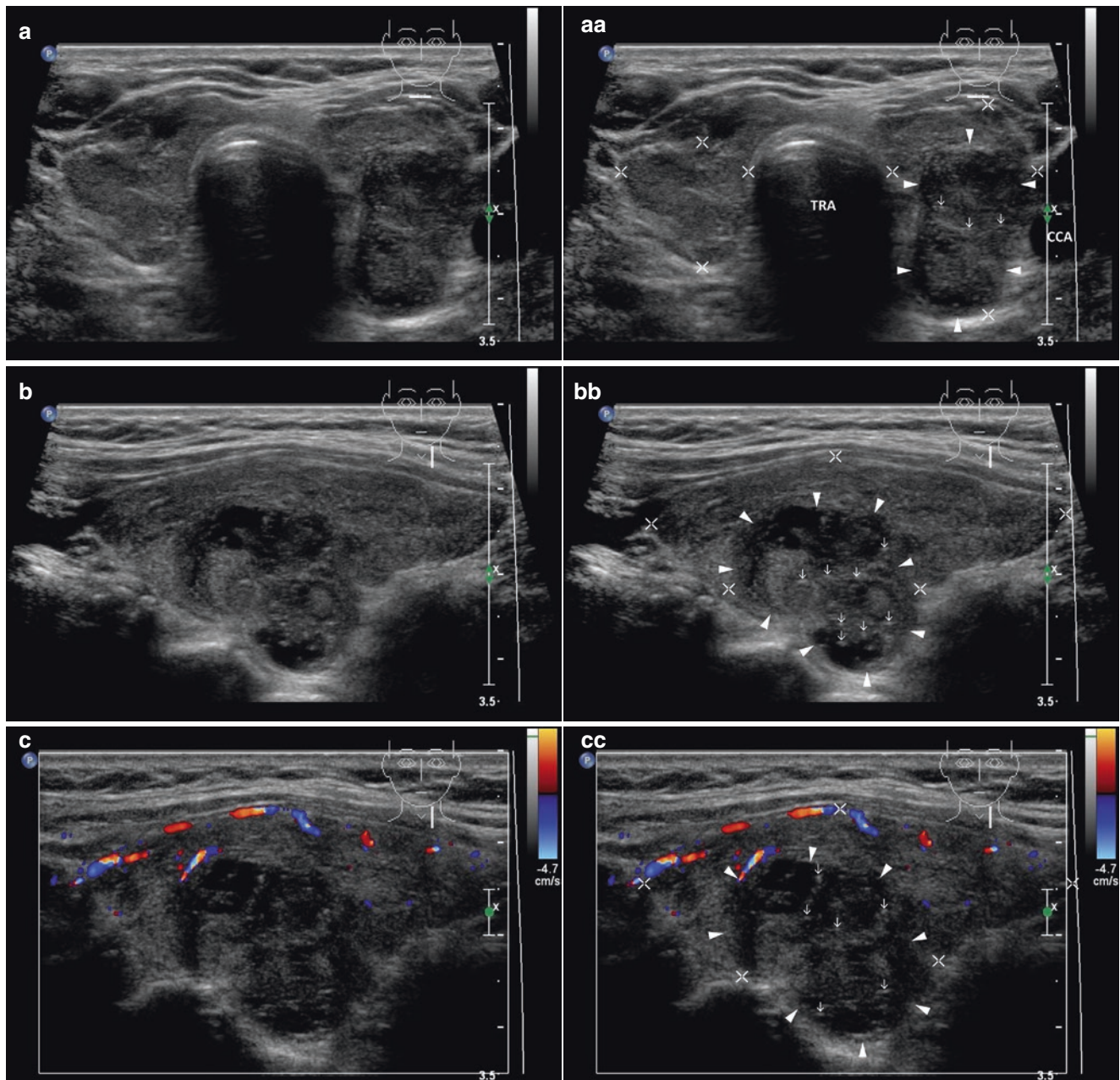


Fig. 15.29 (aa) A 67-year-old woman with Hashimoto's thyroiditis (HT) and a solitary medium-sized papillary thyroid carcinoma, follicular variant (FVPTC) in the LL, size $24 \times 20 \times 13$ mm and volume 3 mL: PTC—solid nodule; “taller-than-wide” shape; inhomogeneous structure; mixed echogenicity; sporadic microcalcifications (*open arrows*); ill-defined microlobulated margin; tumor protrusion dorsally with contour bulging and without interrupting continuity of the capsule; longitudinal. (cc) Detail of LL with HT and medium-sized FVPTC, CFDS: nodule—avascular with one peripheral vessel only, *pattern 0*; thyroid gland—mostly homogeneous structure; isoechoic, only sporadic hypoechoic micronodular structure; Tvol 19 mL, RL 7 mL, and LL

12 mL; transverse. (bb) Detail of LL with HT and medium-sized FVPTC: solid nodule; “taller-than-wide” shape; inhomogeneous structure; mixed echogenicity; sporadic microcalcifications (*open arrows*); ill-defined microlobulated margin; tumor protrusion dorsally with contour bulging and without interrupting continuity of the capsule; longitudinal. (cc) Detail of LL with HT and medium-sized FVPTC, CFDS: nodule—avascular with one peripheral vessel only, *pattern 0*; thyroid gland—sporadic peripheral and parenchymal vascularity, *pattern 1*; longitudinal

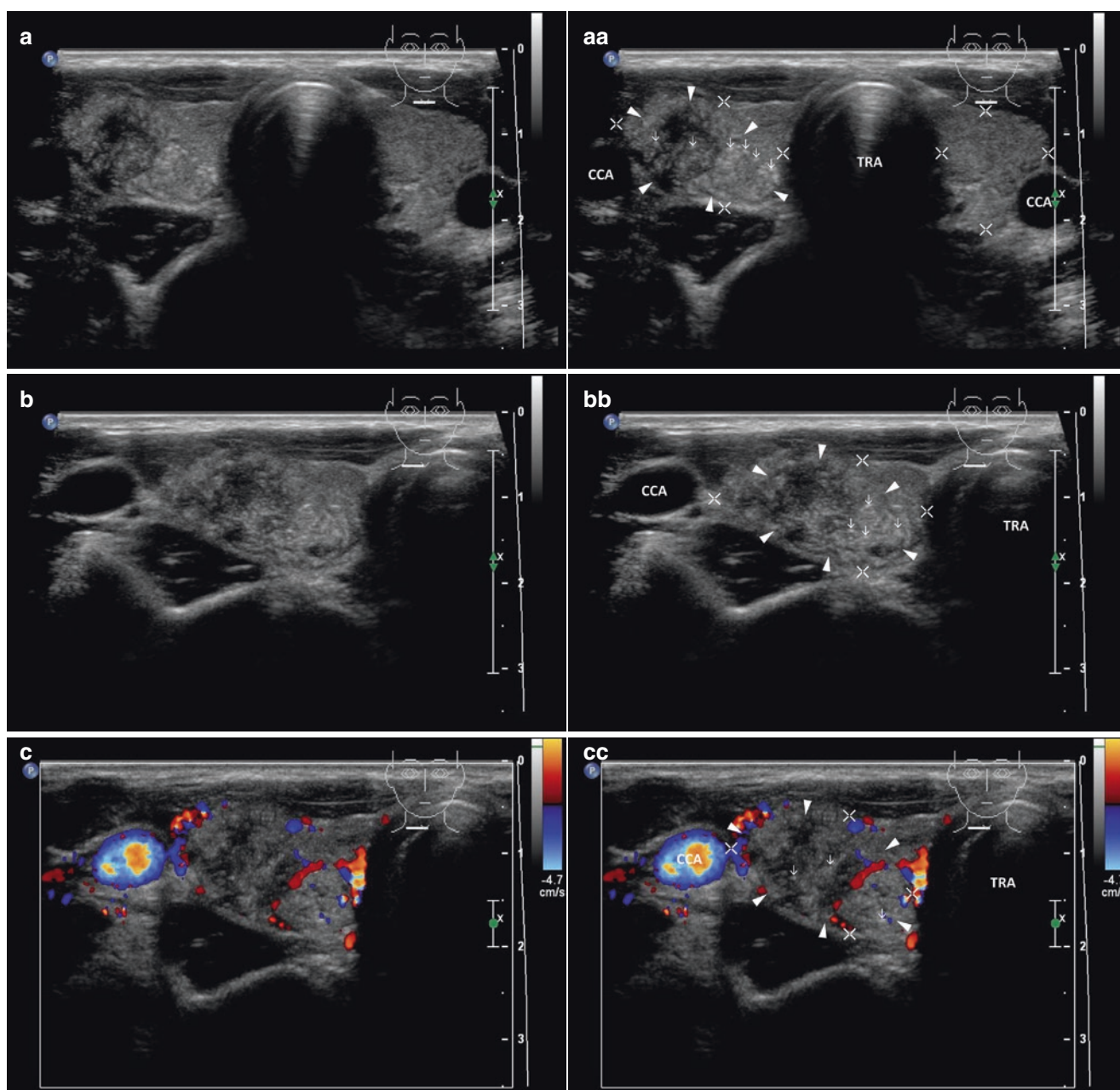


Fig. 15.30 (aa) A 24-year-old woman with Hashimoto's thyroiditis (HT) and a solitary medium-sized papillary thyroid carcinoma (PTC) in the RL, size $25 \times 23 \times 12$ mm and volume 3.5 mL, moreover small metastatic cervical lymph nodes (LN) just under the low pole at level C-VI: PTC (arrowheads)—solid nodule; ovoid shape; coarse structure; mostly isoechoic; central prominent ill-defined mostly hypoechoic area; diffusely microcalcifications (open arrows); ill-defined blurred margin; thyroid gland—mostly homogeneous structure; isoechoic, only sporadic hypoechoic micronodular structure; Tvol 15 mL, RL 9 mL, and LL 6 mL; transverse. (bb) Detail of RL with HT and medium-sized PTC (arrowheads): solid nodule; ovoid shape; coarse structure; mostly isoechoic; central prominent ill-defined mostly hypoechoic area; diffusely microcalcifications (open arrows); ill-defined slurred margin; transverse. (cc) Detail of RL with HT and medium-sized PTC (arrow-

heads), CFDS: nodule—focally peripheral vascularity and one intranodal vessel branch, *pattern I*; transverse. (dd) Detail of RL with HT and medium-sized PTC (arrowheads) and two small metastatic LNs at level C-VI: PTC—solid nodule; ovoid shape; coarse structure; mostly isoechoic; central prominent ill-defined mostly hypoechoic area; diffusely microcalcifications (open arrows); ill-defined blurred margin; metastatic Ln1, Ln2 (marks) just under the low pole—elliptical shape, size 11×5 mm and 9×5 mm, L/S ratio ≈ 2 (not pathological); homogeneous structure; hyperechoic; no hilus sign; longitudinal. (ee) Detail of RL with HT and medium-sized PTC (arrowheads) and two small metastatic LNs at level C-VI, CFDS: nodule—focally peripheral vascularity and one intranodal vessel branch (but not in hypoechoic part), *pattern I*; metastatic Ln1, Ln2 (marks)—mixed (hilar and peripheral) hypervascularity; longitudinal

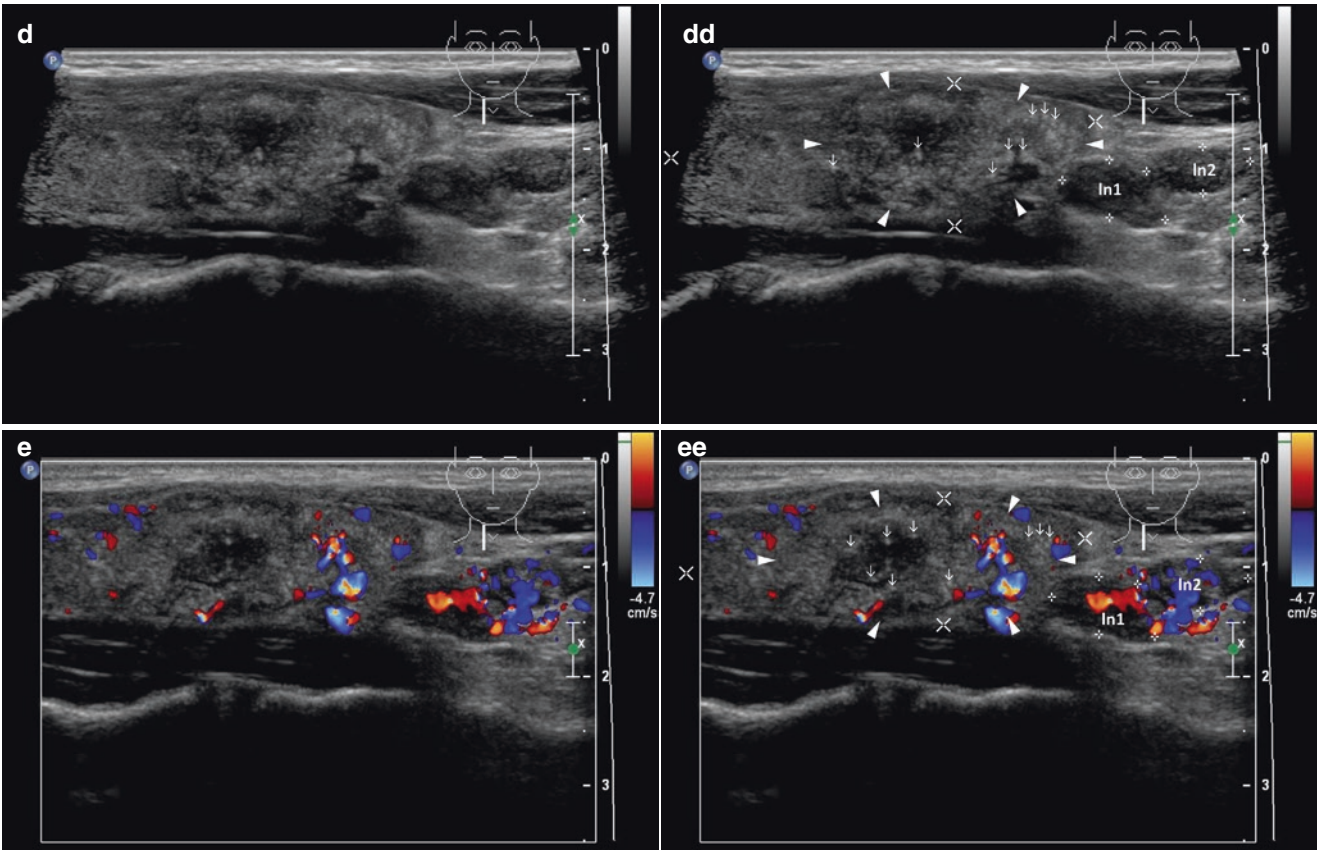


Fig. 15.30 (continued)

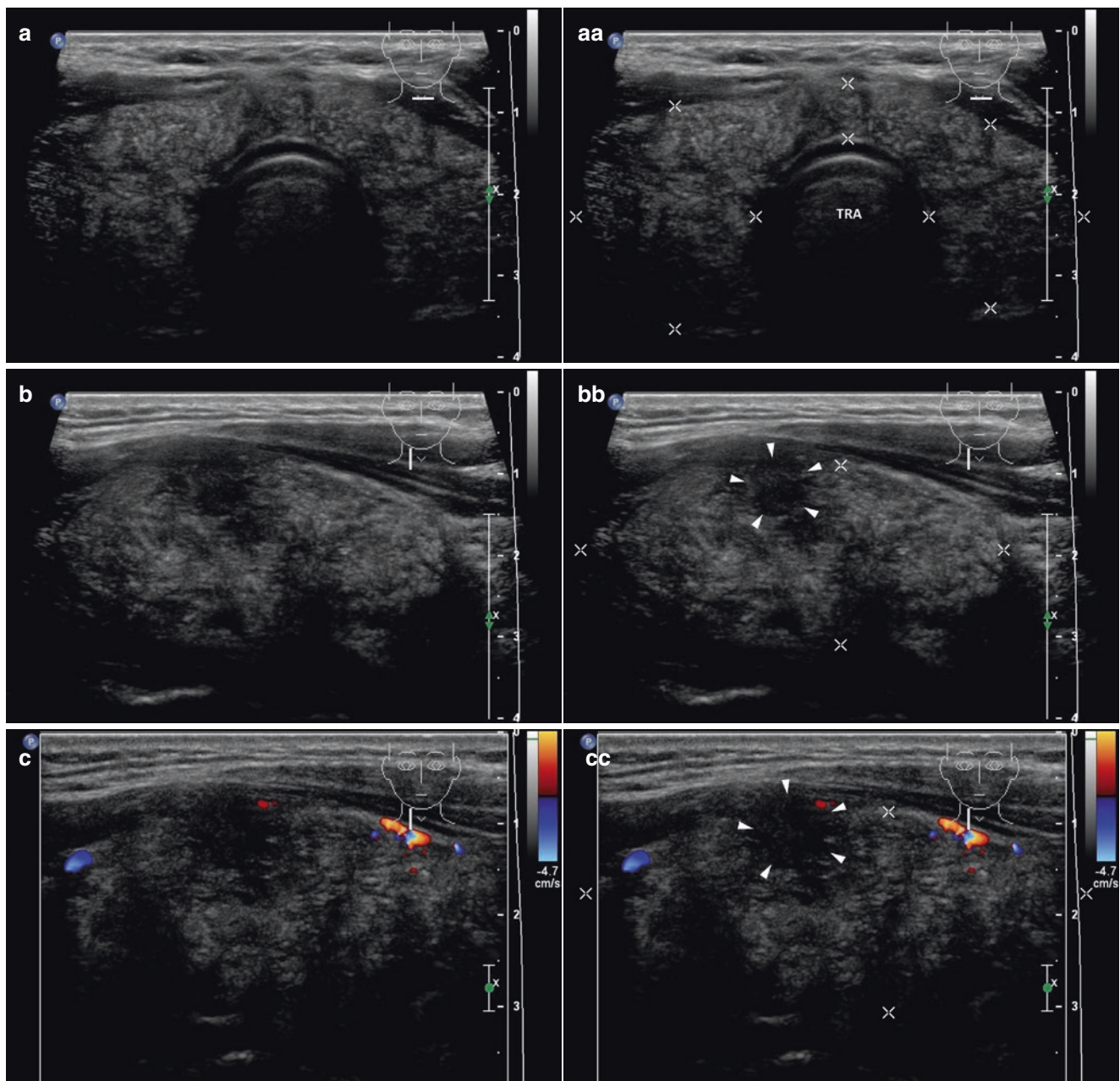


Fig. 15.31 (aa) A 31-year-old man with Hashimoto's thyroiditis (HT) and a diffuse sclerosing variant of papillary thyroid carcinoma—PTC (confirmed histologically) in the RL. Moreover small metastatic cervical lymph nodes (LNs) along the right IJV at level C-II, III: thyroid gland—inhomogeneous structure; diffusely hypoechoic micronodular structure; *without suspicious foci*; Tvol 38 mL, isthmus 7 mm, RL 20 mL, and LL 17 mL; transverse. (bb) Detail of RL with HT and small suspicious lesion (*arrowheads*), size 12 × 8 mm in the central part ventrally, the site of FNAB (suspicious cytology): oval, inhomogeneous, hypoechoic area with ill-defined blurred margin; longitudinal. (cc)

Detail of RL with HT and small suspicious lesion (*arrowheads*), CFDS: avascular hypoechoic area, *pattern 0*; longitudinal. (dd) Detail of RL with HT and diffuse PTC and one metastatic LN at level C-III: LN3 (*blank arrowheads*)—elliptical shape; size 19 × 12 mm, L/S ratio ≈ 2 (*not pathological*); inhomogeneous structure; hyperechoic; no hilus sign; transverse. (ee) Detail of RL with HT and diffuse PTC and three metastatic LNs at level C-II, III: LN1 (*blank arrowheads*)—elliptical shape, size 19 × 8 mm, L/S ratio ≈ 2 (*not pathological*); LN2 (*marks*)—round, size 9 mm and LN3 (*blank arrowheads*)—elliptical shape, size 19 × 12 mm; all LNs hyperechoic; no hilus sign; transverse

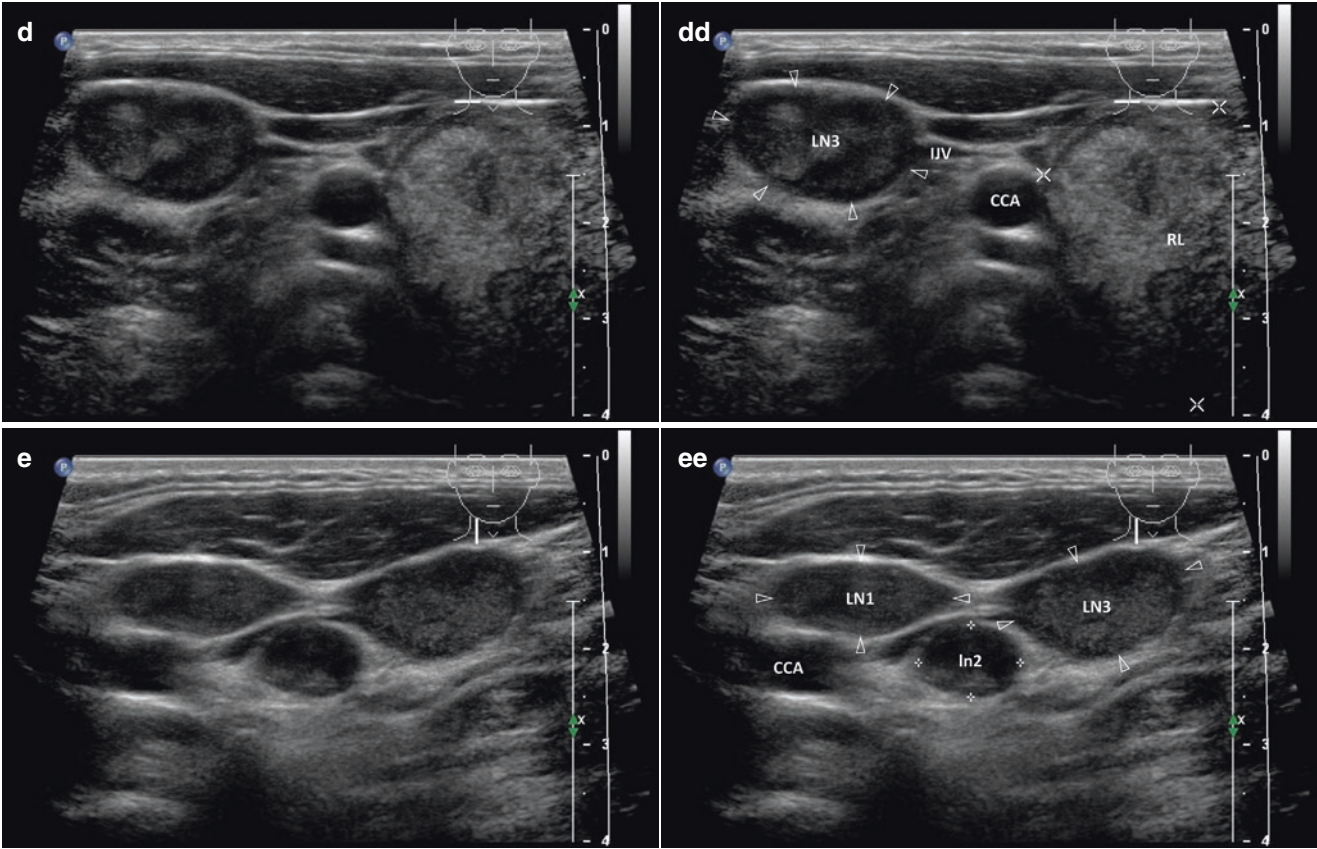


Fig. 15.31 (continued)

15.6 Papillary Thyroid Carcinoma and Graves' Disease or Amiodarone-Induced Thyrotoxicosis

15.6.1 Essential Facts

- Incidence of thyroid nodule in Graves' disease (GD) patients varies from 10 to 35% [35].
 - Prevalence of differentiated thyroid cancer (DTC) in GD patients ranges from 0.3 to 16.6% [35].
 - Taneri et al. reported that incidence of DTC in patients with GD is 3–8%. However, it increases up to 15% in the patients with thyroid nodule. Hyperthyroidism apparently does not protect patients from DTC as reported previously. In contrast, hyperthyroidism with concurrent thyroid cancer can be diagnosed after pathological examination of unsuspected nodules. In published series DTCs were incidental diagnosis in 90% of cases. Total thyroidectomy for GD patients with nodules is preferable [36].
 - Controversy remains regarding the pathogenic relationship between DTC and GD. It is well known that the binding of thyroid-stimulating hormone (TSH) to its receptors might promote growth of cancer cells in euthyroid patients with thyroid carcinoma. In GD, in which serum TSH is suppressed, other thyroid stimulating autoantibodies (TS-Ab) activate the TSH receptor. The autoimmune responses to TS-Abs are closely linked to angiogenesis, which plays a crucial role in tumor growth and development [37, 38].
 - Close relationship of TSH receptor to the stimulating antibodies (TSHR-Ab) seen in GD has led to the perception that thyroid cancer may become more aggressive as a result of stimulation by these autoantibodies [39].
 - Cappelli et al., in a retrospective study with 2449 patients undergoing thyroidectomy for any type of hyperthyroidism, assessed coexisting thyroid cancer. Thyroid cancer was diagnosed more frequently in patients with GD (6.5%) than in those with solitary toxic adenoma (SAT) (4.4%) or toxic multinodular goiter (TMNG) (3.9%).
- Lymph nodes involvement was found in 56% of the patients with GD, in 23% of those with TMNG, and in none of those with SAT. Distant metastases were found in one patient with GD. Tumors associated with GD seem to be more aggressive than those associated with TMNG or SAT [40].
- GD patients with DTC have a worse clinical outcome than euthyroid patients with DTC [39, 40].
 - A retrospective study by Lee of 779 patients with GD who underwent thyroidectomy in intervals of 20 years found prevalence of PTC at 7.9% (50 women and 8 men). Twenty-six cases (3.3%) were clinically overt thyroid carcinomas and 32 (4.2%) were incidentalomas. The 10-year overall and disease-free survival rates were $\approx 96\%$ and $\approx 91\%$, respectively, showing favorable treatment outcomes in these patients, and the severity of thyrotoxicosis and serum thyroid hormone levels did not affect the prognosis. Predicting factors for recurrence in DTC patients with concurrent GD were: age >45 years; tumor size >10 mm; multiplicity; extracapsular invasion; and clinical overt carcinoma [35].
 - Presence of DTC in thyroidectomy specimens removed for AIT is very rare. Inaba et al. reported occult PTC in MNG and Amiodarone-induced thyrotoxicosis type 1. US showed a slightly enlarged MNG. In the left upper lobe, a 7-mm lesion with low echogenicity, small calcifications, and an irregular margin were observed. FNAB was performed and cytology revealed suspicious PTC. Amiodarone should be carefully commenced in cases with MNG [41]. Saad et al. described occult PTC and Amiodarone-induced thyrotoxicosis type 2. Physical and ultrasound examination revealed a normal-sized thyroid gland without discernible nodules. The specimen of the right lobe after thyroidectomy revealed two small nodules, 0.6 and 0.3 cm in size. Both nodules were diagnosed as the follicular variant of papillary thyroid carcinoma (FVPTC). Tumors revealed any genetic alterations. Amiodarone induced distortion of thyroid construction, necrosis, apoptosis, and may contribute to thyroid carcinogenesis [42].

15.6.2 US Features of Papillary Thyroid Carcinoma in Graves' Disease

- US findings for GD: diffuse heterogeneous and hypoechoic enlargement of the thyroid. CFDS imaging reveals a hypervascular pattern [43].

- US typical features of high suspicion nodule (Fig. 15.32aa): a solid hypoechoic nodule, irregular margin, microcalcifications, taller-than-wide shape and increased vascularity [8].

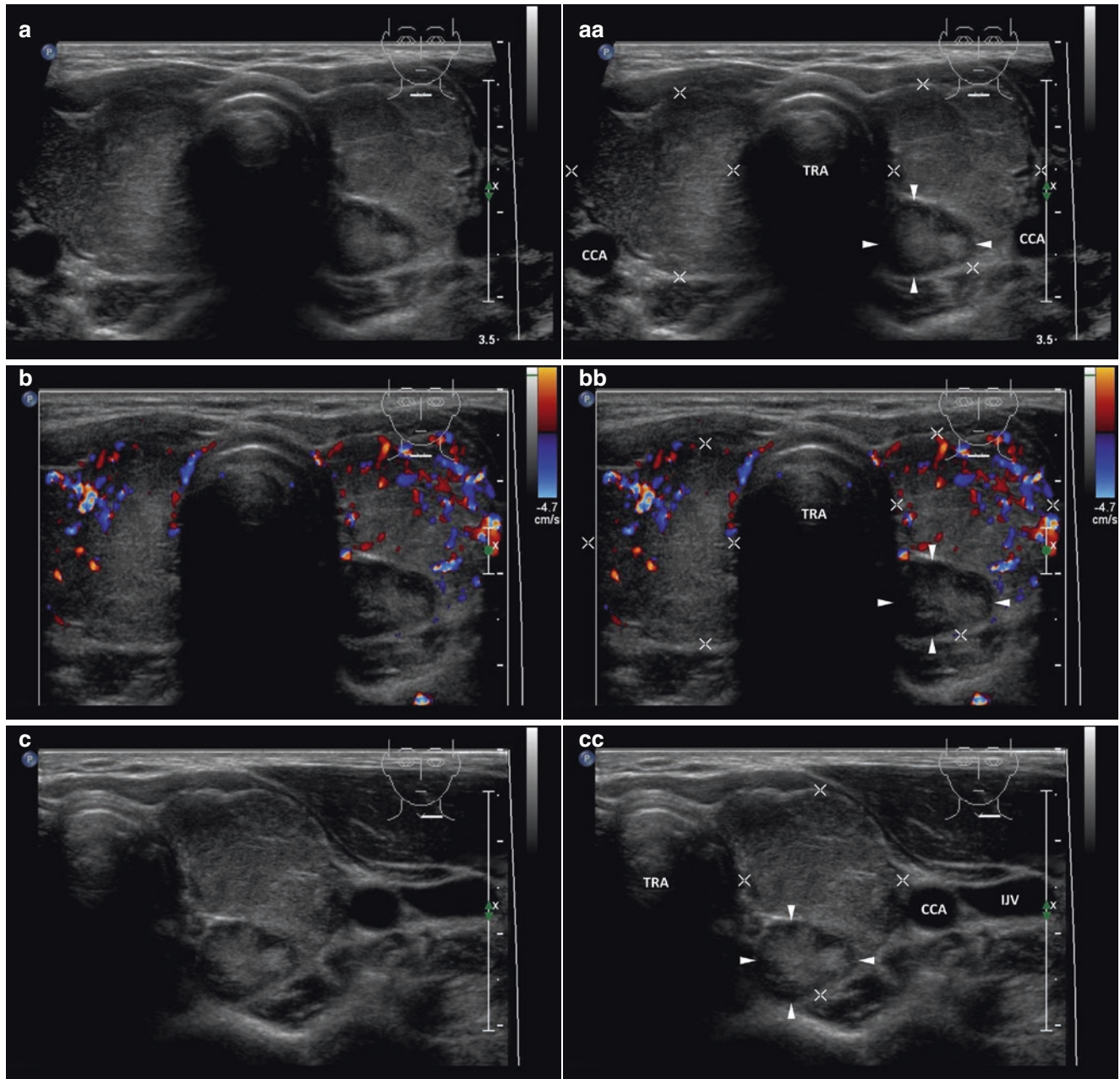
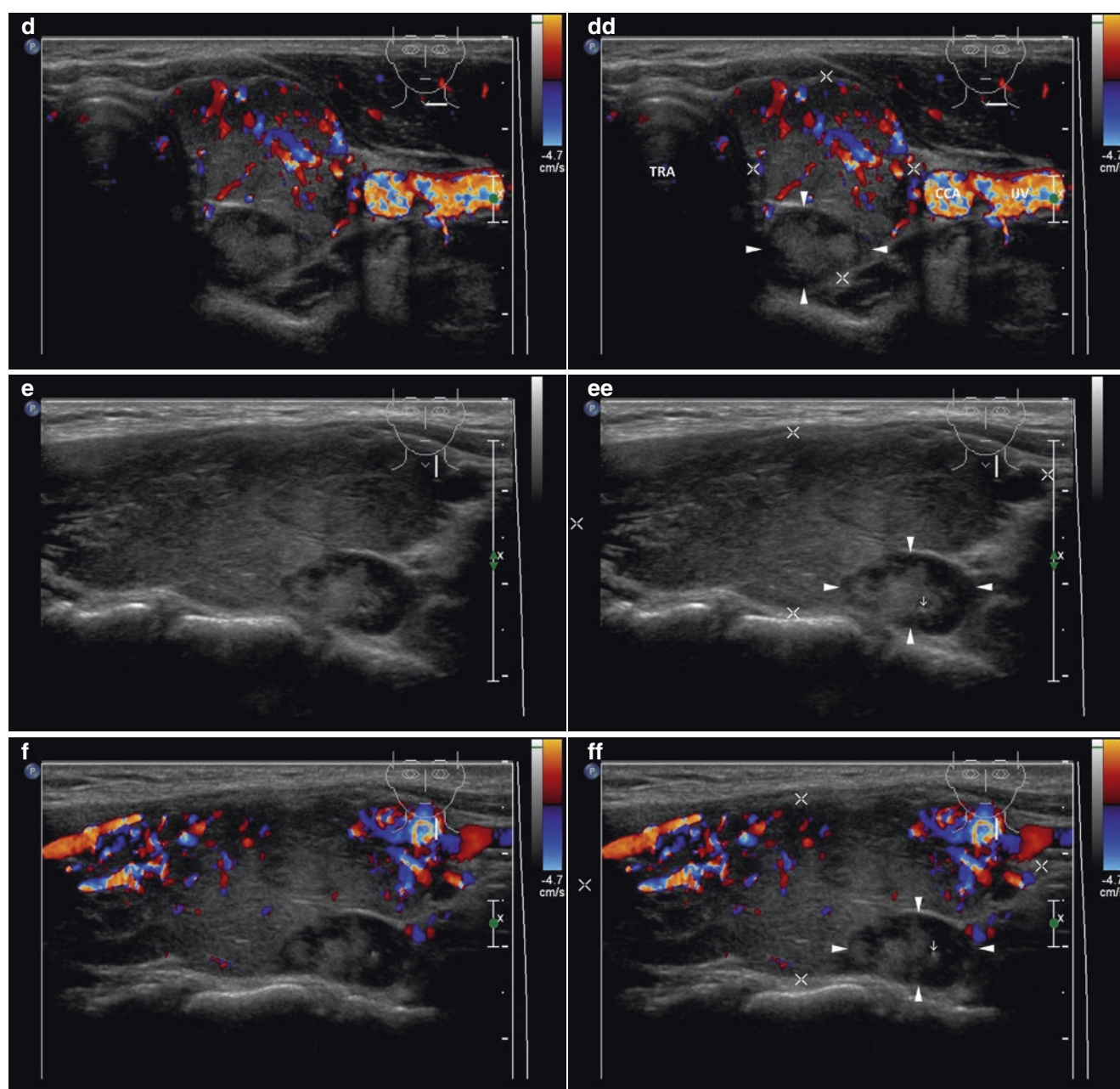


Fig. 15.32 (aa) A 32-year-old woman with Graves' disease (GD) and a small papillary thyroid carcinoma—PTC (arrowheads) in the LL, size $14 \times 10 \times 9$ mm and volume 0.7 mL: PTC—solid nodule; round shape; centrally homogeneous isoechoic structure; slightly inhomogeneous and hypoechoic at periphery; well-defined margin; thyroid gland—both lobes mostly homogeneous, isoechoic, only ventrally inhomogeneous hypoechoic micronodular structure; Tvol 26 mL, RL 14 mL, and LL 12 mL; transverse. (bb) Overall view of GD and small PTC (arrowheads), CFDS: increased vascularity, mostly ventrally in hypoechoic parts, *pattern II*; transverse. (cc) Detail of LL with GD and small PTC

(arrowheads): solid nodule; round shape; centrally homogeneous isoechoic structure; slightly inhomogeneous and hypoechoic at periphery, well-defined margin; transverse. (dd) Detail of LL with GD and small PTC (arrowheads), CFDS: PTC—avascular nodule, *pattern 0*; thyroid gland—*pattern II*; transverse. (ee) Detail of LL with GD and small PTC (arrowheads): solid; round shape; centrally homogeneous isoechoic structure; slightly inhomogeneous and hypoechoic at periphery; well-defined margin; longitudinal. (ff) Detail of LL with GD and small PTC (arrowheads), CFDS: PTC—avascular nodule, *pattern 0*; thyroid gland—*pattern II*; longitudinal

**Fig. 15.32** (continued)

15.6.3 US Features of Papillary Thyroid Carcinoma in Amiodarone-Induced Thyrotoxicosis

- US typical features of high suspicion nodule (Fig. 15.33aa): a solid hypoechoic nodule, irregular margin, microcalcifications, taller-than-wide shape, and increased vascularity [8].

- However, DTCs are mostly small and occult incidentalomas hidden in a MNG or by US not detectable [41, 42].

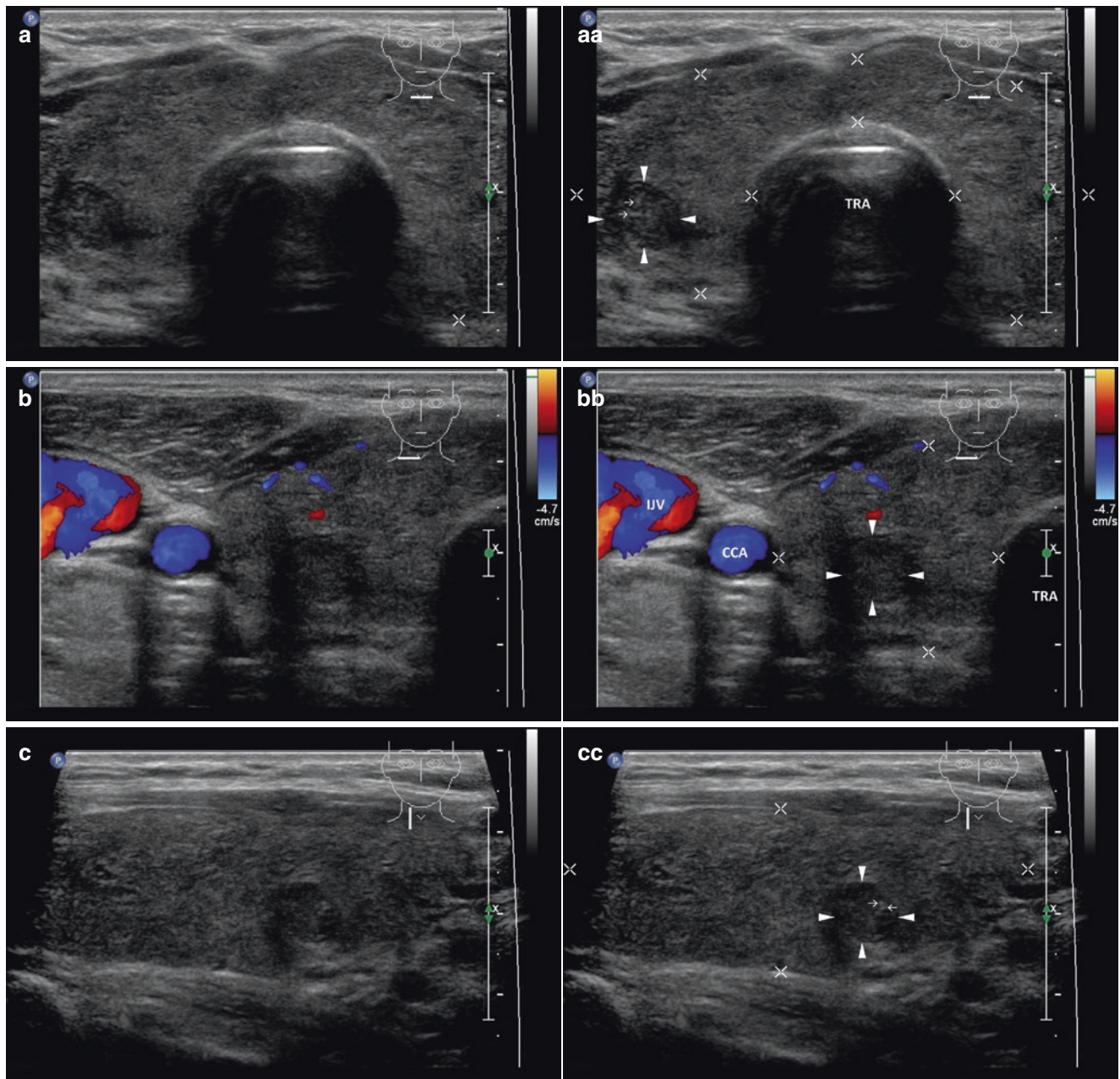


Fig. 15.33 (aa) A 55-year-old man with amiodarone-induced thyrotoxicosis (AIT), type 2 (normal TPO-Ab, Tg-Ab) and occult papillary thyroid microcarcinoma—PTMC (arrowheads), in the RL, size $9 \times 8 \times 8$ mm and volume 0.3 mL: PTMC—solid nodule; round shape; slightly inhomogeneous structure; mostly isoechoic, only hypoechoic at periphery; well-defined margin; thyroid gland—enlarged thyroid gland, homogeneous structure; isoechoic; Tvol 45 mL, isthmus 9 mm, RL 23 mL, and LL 21 mL; transverse. (bb) Detail of RL with AIT, type

2 and PTMC (arrowheads), CFDS: PTMC—avascular nodule, *pattern 0*; thyroid gland—minimal vascularity, *pattern 0*; transverse. (cc) Detail of RL with AIT, type 2 and PTMC (arrowheads): solid nodule; round shape; slightly inhomogeneous structure; mostly isoechoic, only hypoechoic at periphery; sporadically hyperechoic punctuations (open arrow); well-defined margin; longitudinal. (dd) Detail of RL with AIT, type 2 and PTMC (arrowheads), CFDS: PTMC—avascular nodule, *pattern 0*; thyroid gland—minimal vascularity, *pattern 0*; longitudinal

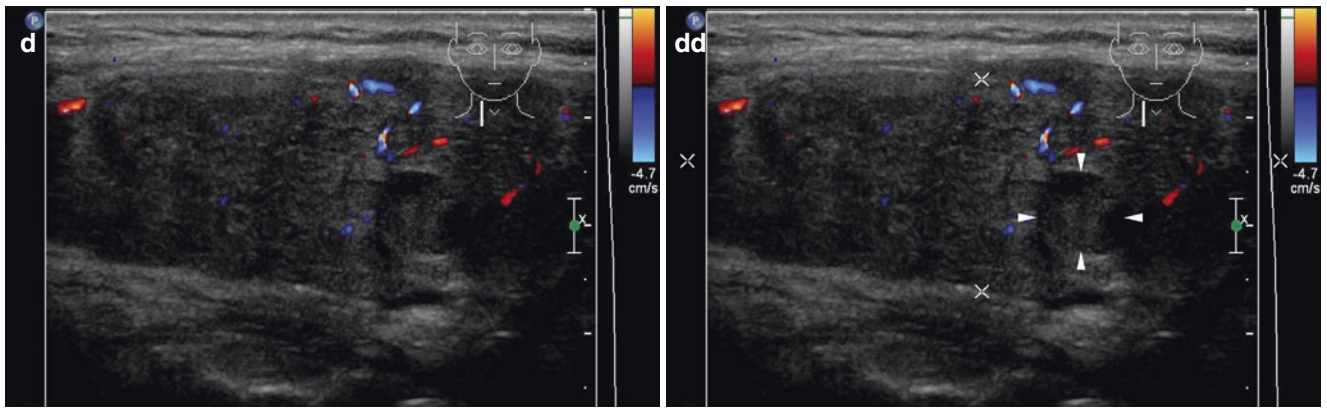


Fig. 15.33 (continued)

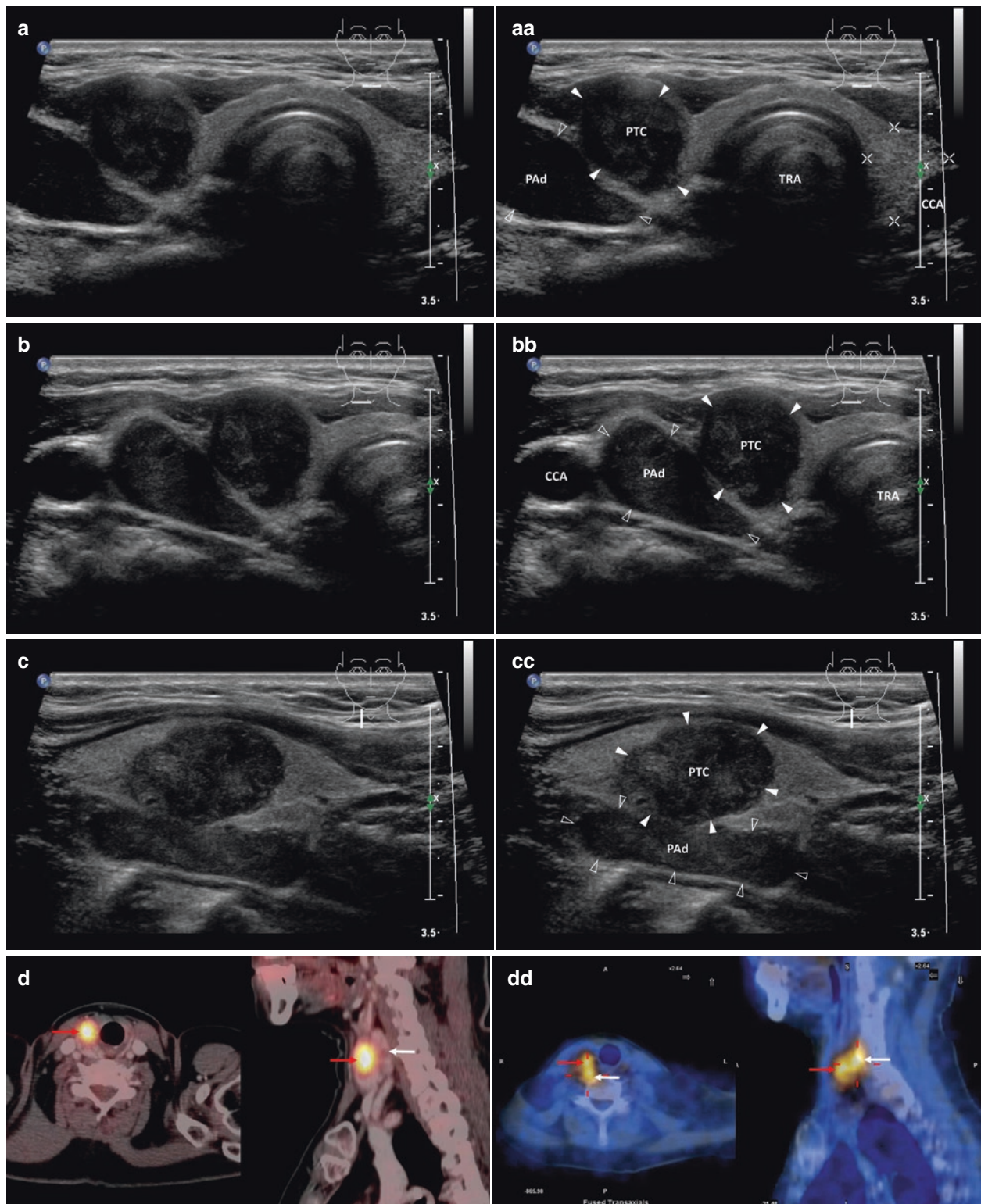


Fig. 15.34 (aa) A 57-year-old woman with a solitary papillary thyroid carcinoma (PTC) in the LL, size $21 \times 17 \times 14$ mm, volume 3 mL and right superior parathyroid adenoma (PAd), size $34 \times 25 \times 12$ mm, volume 5 mL. Overall US view: PTC (arrowheads)—solid; “taller-than-wide” shape; homogeneous structure; hypoechoic; microlobulated margin; PAd (blank arrowheads) located behind the lobe—wedge-like shape; solid; homogeneous structure; hypoechoic; Tvol 12 mL, RL 6 mL, and LL 6 mL; transverse. (bb) Detail of solitary PTC and right superior PAd: PTC (arrowheads)—“taller-than-wide” shape; homogeneous structure; hypoechoic; microlobulated margin; PAd (blank arrowheads) located behind the RL—wedge-like shape; homogeneous structure; hypoechoic;

transverse. (cc) Detail of solitary PTC and right superior PAd: PTC (arrowheads)—ovoid shape; homogeneous structure; hypoechoic; microlobulated margin; PAd (blank arrowheads) located behind the RL; markedly elongated shape; homogeneous structure; hypoechoic; longitudinal. (d) ¹⁸F-FDG PET/CT transverse and sagittal view: increased ¹⁸F-FDG uptake in PTC in the RL of thyroid gland (red arrow), without ¹⁸F-FDG accumulation in PAd (white arrow) behind the RL. (Image courtesy of Pavel Koranda, MD, PhD) (dd) ^{99m}Tc-MIBI SPECT/CT transverse and sagittal view: increased ^{99m}Tc-MIBI uptake in PTC in the RL of thyroid gland (red arrow) and in PAd (white arrow) behind the RL. (Image courtesy of Pavel Koranda, MD, PhD)

15.7 Synchronous Papillary Thyroid Carcinoma and Parathyroid Adenoma

15.7.1 Essential Facts

- Coincidence of thyroid disease and primary hyperparathyroidism (pHPT) is known. In a 1999 study of 13,000 patients with thyroid disease, Wagner et al. [44] found a 0.3% incidence of PHPT, while in 2008 Morita et al. [45] reported a 3.1% incidence of pHPT among 326 patients.
- On the contrary, the rate of incidentally detected thyroid pathology in patients with pHPT has been reported to range from 17 to 84%. Frequency of malignant thyroid lesions in population with pHPT ranges from 2 to 12% [46].
- In large preoperative study by Milas [47], 40% of pHPT patients (477/1195) had coexisting thyroid disease, whether identified at parathyroidectomy (39%; 327/845) or by US (43%; 150/350). Colloid nodules/goiters accounted for nearly half of thyroid pathology, followed by follicular adenomas, papillary cancer, thyroiditis, and intrathyroidal parathyroids [47].
- Today, minimally invasive, targeted parathyroidectomy (MIP) has achieved wide acceptance among endocrine surgeons. With MIP, however, the surgeon may not be able to examine the entire thyroid gland for associated pathology. To improve the diagnostic success for most thyroid pathologies, US should be used in addition to ^{99m}Tc-MIBI scan. In 2009, Heizmann et al. evaluated the value of MIP in respect to coexisting thyroid findings and their impact on preoperative workup for pHPT. This study includes 30 patients treated for pHPT. Ten patients (33%) had a concurrent thyroid finding that required additional thyroid surgery. Four patients of those with thyroid and parathyroid pathology on the same side received unilateral exploration. Two patients (7%) with negative localization results underwent bilateral neck exploration. Eighteen patients (60%) met the criteria for open MIP [46].
- In studies of patients undergoing surgery for pHPT, the incidence of thyroid cancer was 2.1–17.6%. The two largest studies were carried out by Linos et al. in 1982, and by Milas et al. in 2005. Linos showed a 2.5% incidence of thyroid carcinoma among 2058 patients operated for pHPT [48], while Milas found a 4.6% incidence in 1195 patients. Frequently, carcinomas were not known preoperatively and were only detected by histological examination of resected nodular goiters [47].

15.7.2 US Features of Parathyroid Adenoma and Papillary Thyroid Carcinoma

- The US findings typical for PAd; *see more in Chap. 22* [49].
- US classic features of high suspicion of malignancy for solid nodules according The 2015 ATA Guidelines; *see Chap. 24, Table 24.1* [8].
- Caution! PAd could be mistaken for a metastatic cervical lymph node.
- US-FNAB from both lesions (Fig. 15.34bb) needs to be performed. The analysis of parathormone in aspirate form PAd may be helpful to confirm the diagnosis [50].

15.8 Differentiated Thyroid Carcinoma and Extrathyroidal Extension

15.8.1 Essential Facts

- Well-differentiated thyroid cancer (DTC—PTC, FTC) most commonly presents as an intrathyroidal tumor. However, extrathyroidal extension (ETE) occurs in approximately 6–13% of patients and carries a significantly negative impact on survival. The 10-year survival drops to 41%, as compared to 91% in patients without ETE [51].
- Patients with ETE were more likely to fail treatment and to die of their disease than patients without ETE (77% vs. 34% and 71% vs. 13%). Local, regional, and distant failures were more prominent among patients with ETE than among those without ETE (48% vs. 9%, 41% vs. 16%, and 37% vs. 11%). Survival of patients with ETE was adversely affected by non-papillary histology, distant metastasis, age greater than 45 years, tumor size >4 cm, and incomplete excision. After stratification for age, survival in older patients was not affected by tumor size or incomplete excision, while in younger patients tumor size or the presence of distant metastasis did not adversely affect survival. Patients younger than 45 years with negative margins had a similar survival to patients without ETE [52].
- Retrospective study by McCaffrey of 262 patients treated for invasive PTC was designed to define more clearly the significance of ETE of PTC on survival. The most common structures invaded were muscle, 53%; trachea, 37%; laryngeal nerve, 47%; esophagus, 21%; larynx, 12%; and other sites, 30%. Complete tumor removal was accomplished in 56% of cases. The overall survival was 79% at 5 years, 63% at 10 years, and 54% at 15 years [53].

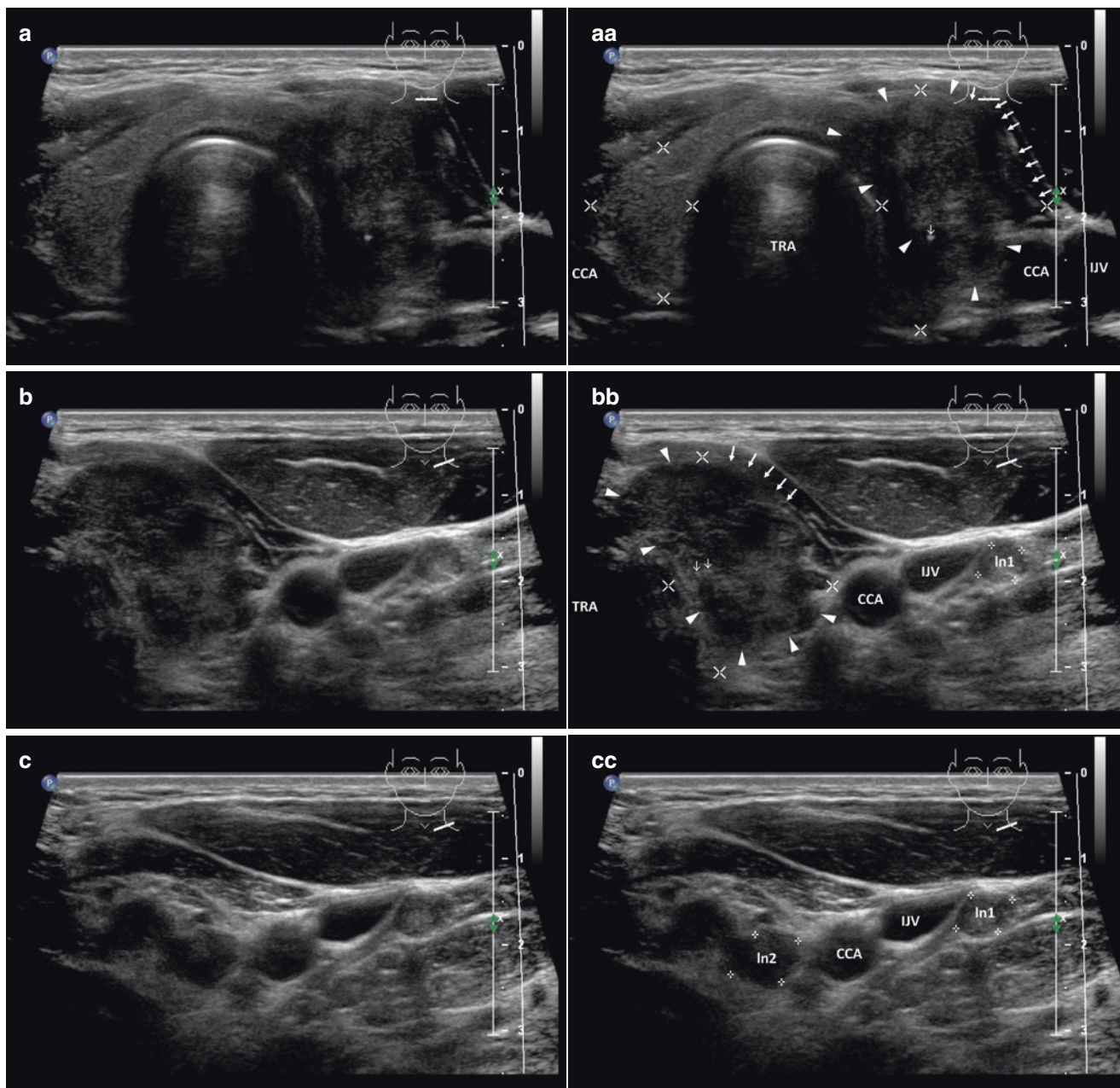
- A retrospective review by Shah et al., which was undertaken to analyze prognostic factors of survival, examines 931 previously untreated patients (630 female and 301 male, an average age of 43 years of age, 532 patients less than 45 years of age) with DTC (731 had PTC and 200 had FTC, 153 lesions >4 cm) treated over a 50-year period. On presentation ETE was noted in 71 patients, multifocal lesions in 159 patients, regional lymph node metastases in 451 patients, and distant metastases in 45 patients. Ten-year survival for all patients was 87%. Favorable prognostic factors using univariate analysis included female gender, multifocal primary tumors, and regional metastatic LNs. Adverse prognostic factors included age >45 years, FTC, ETE, tumor size >4 cm, and the presence of distant metastases. On multivariate analysis, the only factors that affected the prognosis were patient age, histology, tumor size, ETE, and distant metastases [54].
- Papini et al., in his study, correlated US with the results of US-FNAB and pathologic staging of surgically removed thyroid cancers in 494 consecutive patients with non-palpable thyroid nodules (8–15 mm). Thyroid malignancies were observed in 18 of 195 (9.2%) solitary thyroid nodules and in 13 of 207 (6.3%) multinodular goiters. Cancer prevalence was similar in nodules >10 mm or <10 mm (9.1% vs. 7.0%). ETE (pT4 at TNM staging) was present in 11 of 31 cancers (35.5%) without significant differences between tumors smaller and greater than 10 mm (33.3% vs. 36.8%). Nodal involvement was found in 6 of 31 (19.4%) [55].
- PTC, FTC and HCC also have well-documented microscopic characteristics of microinvasion affecting the great cervical vein [56, 57].
- Invasion of IJV with hypervascular tumor thrombosis is an extremely rare situation in PTC [58–60].
- Aggressive local invasion is relatively common in anaplastic carcinoma (Figs. 17.1aa and 17.2aa), lymphoma, and sarcoma [61, 62].
- Patients with tumor thrombi were more likely to have pulmonary metastasis than those without (33.3% vs. 0.9% respectively) [56].

Fig. 15.35 (aa) A 38-year-old man with a medium-sized papillary thyroid carcinoma—PTC in the LL and isthmus, size 25 × 23 × 17 mm, volume 5 mL and extrathyroidal extension (ETE) into muscles. Moreover tiny metastatic lymph nodes (LN) in the left low neck at level C-IV. US overall view: PTC (arrowheads)—solid nodule; “taller-than-wide” shape; coarse structure; mostly hypoechoic; microcalcification (open arrow); microlobulated margin; tumor protrusion ventrally with interrupting continuity of the capsule and invasion into muscles (arrows); Tvol 22 mL, RL 8 mL, and LL 14 mL; transverse. (bb) Detail of medium-sized PTC with ETE into muscles and metastatic LNs at level C-IV: PTC (arrowheads)—solid nodule; “taller-than-wide” shape; coarse structure; mostly hypoechoic; microcalcification (open arrows); tumor protrusion ventrally with contour bulging and interrupting continuity of the capsule (arrows); tiny metastatic Ln1 (marks) next to the left IJV size 6 × 5 mm—round shape; homogeneous structure; hyperechoic; no hilus sign; transverse. (cc) Detail of two tiny metastatic LNs at level C-VI and IV: Ln2 (marks) next to the left CCA, size

7 × 6 mm and Ln1 (marks) next to the left IJV, size 6 × 5 mm—round shape; homogeneous structure; hyperechoic; no hilus sign; transverse. (dd) Detail of medium-sized PTC (arrowheads) with ETE into muscles: solid nodule; coarse structure; mostly hypoechoic; microcalcification (open arrows); tumor protrusion ventrally with contour bulging and interrupting continuity of the capsule (arrows); longitudinal. (ee) Detail of medium-sized PTC (arrowheads) with ETE into muscles, CFDS: sporadic peripheral and central vascularity, pattern I; tumor protrusion ventrally with contour bulging and interrupting continuity of the capsule (arrows); longitudinal. (ff) Detail of medium-sized PTC with ETE into muscles and metastatic LNs at level C-VI: PTC (arrowheads)—solid nodule; “taller-than-wide” shape; coarse structure; mostly hypoechoic; microcalcification (open arrows); tumor protrusion ventrally with contour bulging and interrupting continuity of the capsule (arrows); tiny metastatic Ln2 (marks) under the low pole of the LL, size 7 × 6 mm—round shape; homogeneous structure; hyperechoic; no hilus sign; longitudinal

15.8.2 US Features of Extrathyroidal Extension

- Kamaya et al. analyzed 62 patients with PTC, 16 of whom had pathologically proven ETE; presence of capsular abutment had 100% sensitivity for detection of ETE. Conversely, lack of capsular abutment had a 100% negative predictive value for excluding ETE [63]:
 - Contour bulging (Fig. 15.31cc) has 88% sensitivity for detection of ETE and its absence has an 87% negative predictive value.
 - Loss of the echogenic capsule (Figs. 15.35aa, 17.1aa, and 17.2aa) is the best predictor of ETE, with 75% sensitivity, 65% specificity, and an 88% negative predictive value.
- Vascularity beyond the capsule (Fig. 17.1cc, ee) has 89% specificity, but sensitivity of only 25%.
- Tumor thrombus in the internal jugular vein presents [56, 60]:
 - Solid hyperechoic mass (Fig. 15.36aa)
 - CFDS—vascularity continues beyond imaginary border of thyroid carcinoma into hyperechoic thrombus (Fig. 15.36bb)
 - CFDS shows residual flow through lumen of IJV (Fig. 15.36bb)
 - In acute thrombosis enlarged lumen fills with markedly hypoechoic mass with absent flow, non-compressible by probe (Fig. 17.2dd).



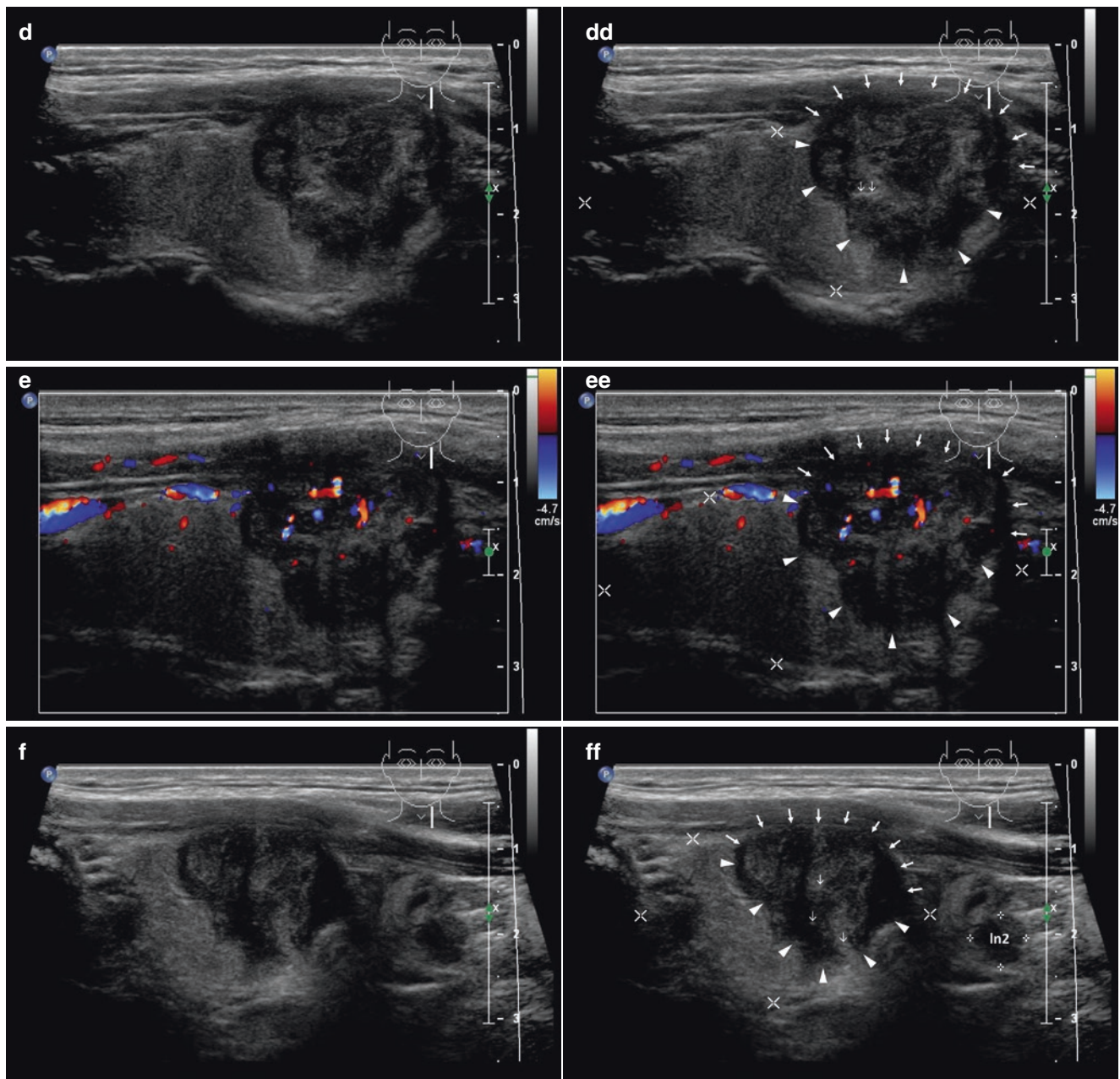
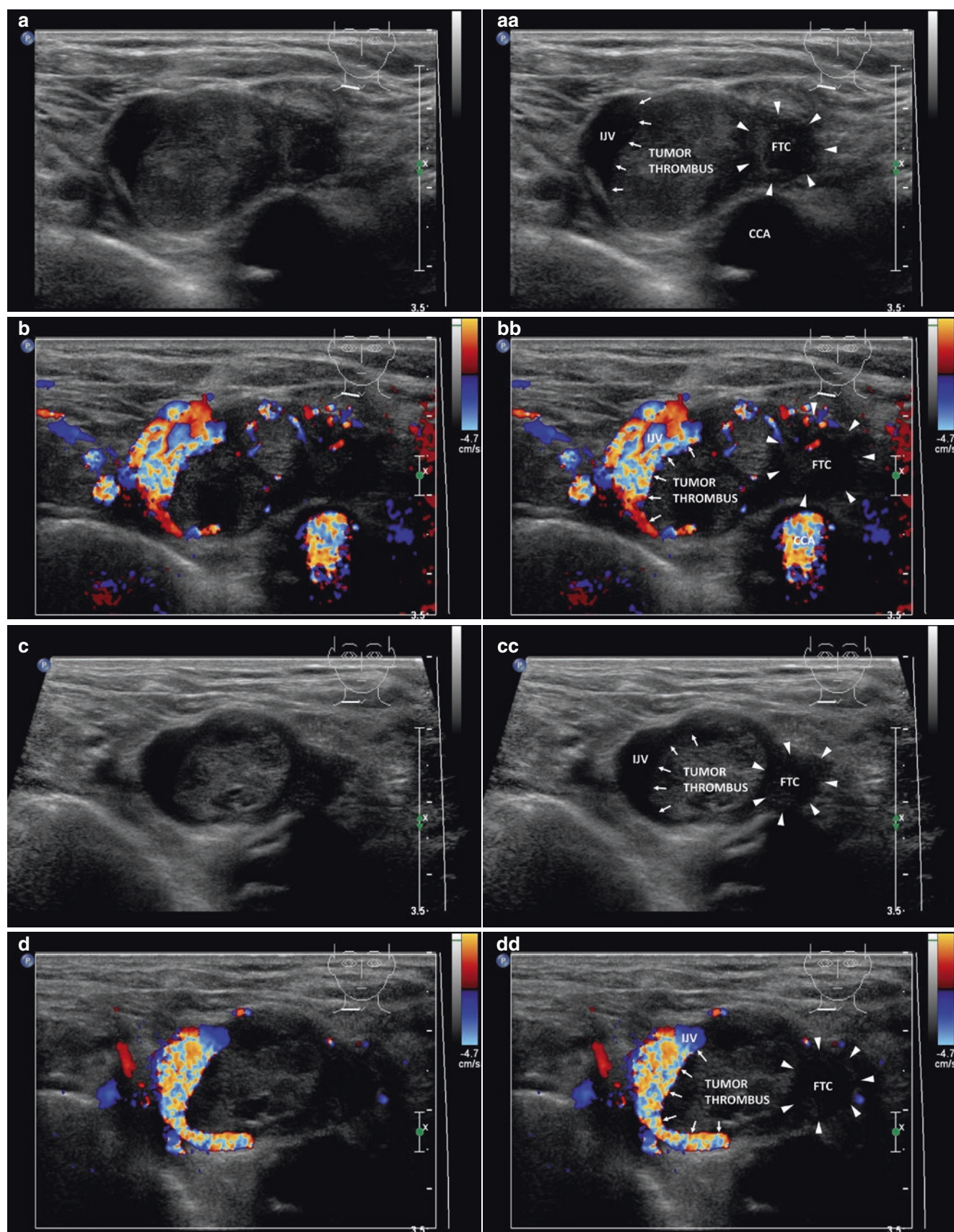


Fig. 15.35 (continued)

Fig. 15.36 (aa) An 87-year-old woman 7 year post thyroidectomy for follicular thyroid carcinoma (FTC) with history of several weeks palpable mass in the right lower anterior neck. US scans revealed recurrences of FTC (confirmed by FNAB), size $24 \times 21 \times 14$ mm, volume 3.5 mL and thrombus in the right IJV, size $21 \times 18 \times 14$ mm, volume 2.5 mL: recurrent FTC (*arrowheads*)—inhomogeneous, mostly hypoechoic lesion in the right thyroid bed invading the wall of IJV and hyperechoic thrombus; preserved crescent-shaped anechoic lumen (*arrows*); transverse. (**bb**) Detail of recurrent FTC and tumor thrombus in the right IJV, CFDS: increased vascularity in hypoechoic FTC (*arrowheads*) continues beyond imaginary border into hyperechoic thrombus; preserved

flow through crescent-shaped lumen (*arrows*); transverse. (**cc**) One year post radiotherapy, detail of recurrent FTC and tumor thrombus in the right IJV; FTC size $16 \times 15 \times 13$ mm, volume 1.5 mL and thrombus size $18 \times 16 \times 13$ mm, volume 2 mL: recurrent FTC (*arrowheads*)—well-defined, homogeneous, hypoechoic lesion in the right thyroid bed; well-distinguished thrombus—inhomogeneous, mostly hyperechoic; preserved crescent-shaped anechoic lumen (*arrows*); transverse. (**dd**) One year post radiotherapy, detail of recurrent FTC and tumor thrombus in the right IJV, CFDS: no vascularity in thrombus or recurrent FTC (*arrowheads*); preserved flow through crescent-shaped lumen (*arrows*); transverse



15.9 Papillary Thyroid Carcinoma in Children and Adolescents

15.9.1 Essential Facts

- Thyroid cancer (TC) is the most common endocrine malignancy, but due to its rare occurrence in the pediatric population, the cancer risk of childhood thyroid nodules is incompletely defined, and optimal management of children with suspected nodules is debated [64].
- The youngest (<20 years) age groups account for only 2–3% of all papillary thyroid carcinomas (PTC) [1].
- In contrast to the 5–15% cancer rate reported for adults with thyroid nodules, reports of cancer prevalence in children with thyroid nodules vary widely, ranging from 3 to 70% even among the most comprehensive series [64].
- Results of a 14-year study by Gupta et al. reported risk of sporadic thyroid cancer approximately 1.6-fold higher in children (22%; 28/125 biopsied nodules) compared to adults (14%). Suspected thyroid nodules are more common in adolescents (13–18 years) than in children of younger age, and the female-to-male ratio is 5.2:1. Pediatric nodules are larger at presentation and more often solitary. The US abnormalities of calcifications and abnormal lymph nodes are strongly associated with cancer but have a low sensitivity (0.07–0.36) due to their rare occurrence [64].
- Available pediatric data of TC are extremely limited. The latest 25-year review study, published in 2016 by Ho and Zacharin, identified 46 patients: 39 (84.8%) had PTC, 5 (10.9%) had FTC, and 2 (4.3%) had MTC (MEN2B). Thirty-three (71.7%) had childhood radiation exposure (17 females) with thyroid malignancy occurring 6–37 years later. The smallest nodule size found on surveillance to have thyroid malignancy was 4 mm. TC in patients <16 years of age was seen in 22 patients (47.8%). Sixteen (32.6%) had metastases [65].
- In previous study published in 2006 by Babcock, the most common pediatric thyroid malignancy was PTC in 80% cases, 5–10% are familial and autosomal dominant, 17% FTC, and 2–3% MTC, often diagnosed in patients with MEN2A, 2B syndrome [66].
- Radiation exposure in childhood (for cancer treatment) is clearly linked to risk of TC. In a review study by Gow et al., 17 patients had TC as a second neoplasm after being treated for: acute lymphoblastic leukemia (6 patients); Hodgkin's disease (5 patients); central nervous system tumor (2 patients); Wilms' tumor (1 patient); retinoblastoma (1 patient); non-Hodgkin's lymphoma (1 patient); and neuroblastoma (1 patient). Patients with secondary TC presented at a median age of 21.5 years (range 15.3–42.6 years), a median of 16.2 years (range 0.9–29.2 years) after diagnosis of the primary cancer. Lesions of secondary TC arising after childhood cancer appear to have similar presentations and outcomes when compared with primary carcinomas and can be therefore managed in the same manner [67].
- TC in children tends to present at a more advanced stage than that in adults and with a higher frequency of lymph node (LN) and pulmonary metastases. Distant metastasis is less common than regional LN involvement, and the lung is the most common site of distant metastasis. Pediatric patients with PTC have a good prognosis. A study by Grigsby et al. observed 56 children and adolescents (43 girls and 13 boys, age 4–20 years) with PTC. At diagnosis, 15 (27%) patients had disease confined to the thyroid, 34 (60%) had additional metastatic LNs (Figs. 15.37cc and 15.39) to the neck or upper mediastinum, and 7 (13%) also had lung metastasis. The overall survival rate was 98% and the 10-year progression-free survival rate was 61%. Nineteen patients (34%) experienced a recurrence of their PTC at times ranging from 8 months to 14.8 years (mean, 5.3 years). None of those with disease confined to the thyroid developed recurrent disease. The recurrence rate was 50% (17/34) in patients with metastatic LNs and 29% (2/7) in patients with lung metastasis. Tumor characteristics such as thyroid capsule invasion (Figs. 15.38aa, bb), soft tissue invasion, and tumor location at diagnosis (thyroid only vs. thyroid and metastatic LNs vs. thyroid, metastatic LNs, and lung metastasis) were significant for developing recurrent disease. Patients younger than 15 years old at diagnosis were more likely to have more extensive tumor at diagnosis than patients who were 15 years of age and older [68].
- In a study by Corrias et al. the observed prevalence of thyroid nodules and TC of 365 children with Hashimoto's thyroiditis (HT) were 31.5% and 3%, respectively. PTC was the only histotype detected [69].
- In a study of 228 children with HT (Skarpa et al.), 63 (28%) had a goiter, 32 (14%) had thyroid nodules, and 3 (1.3%) had PTC [70].

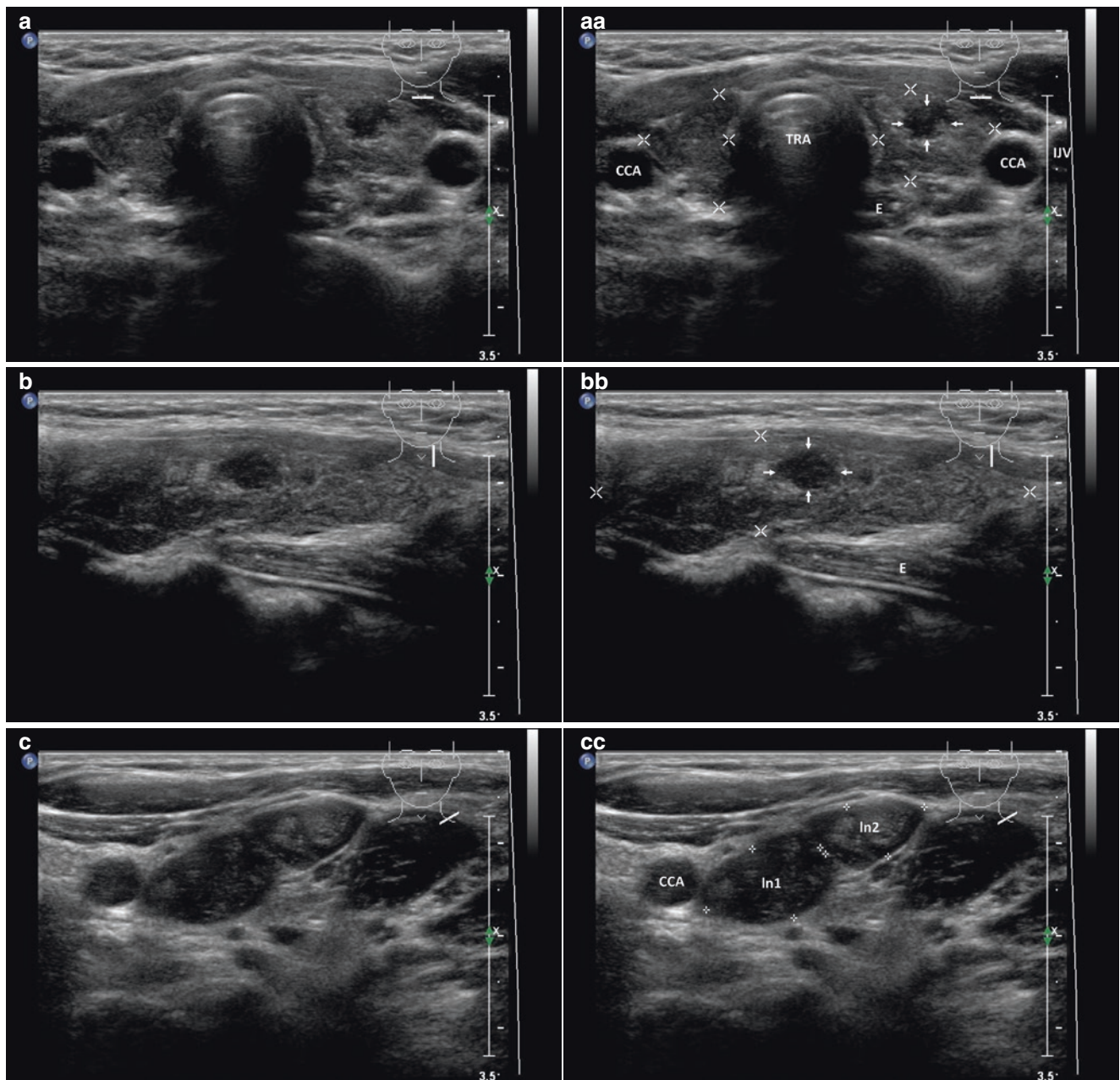
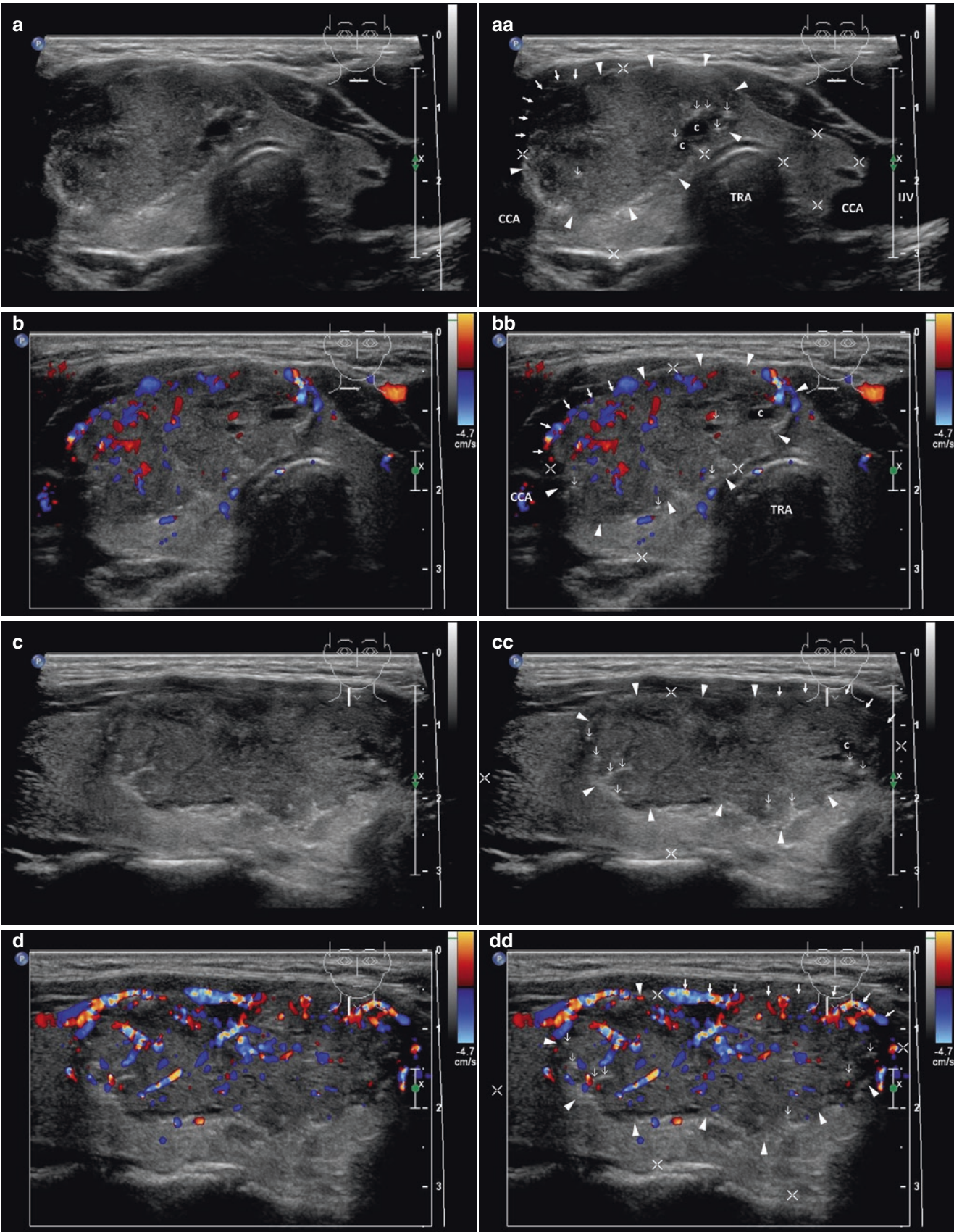


Fig. 15.37 (aa) A 15-year-old girl with Hashimoto's thyroiditis and a solitary tiny papillary thyroid microcarcinoma—PTMC (arrows) in the LL, size $6 \times 5 \times 4$ mm and volume 0.1 mL. Moreover metastatic lymph nodes (LNs) next to the left CCA at level C-IV. US overall view: PTMC—solid; round shape; inhomogeneous structure; hypoechoic; microlobulated margin; thyroid gland—microlobulated hypoechoic

structure; Tvol 8 mL, RL 4 mL, and LL 4 mL; transverse. (bb) Detail of solitary PTMC (arrows): solid; round shape; inhomogeneous structure; hypoechoic; microlobulated margin; longitudinal. (cc) Detail of two metastatic LNs size 20×12 mm and 16×10 mm next to the left CCA at level C-IV: In1, In2 (marks) elliptical shape; inhomogeneous structure; hypoechoic; no hilus sign; transverse



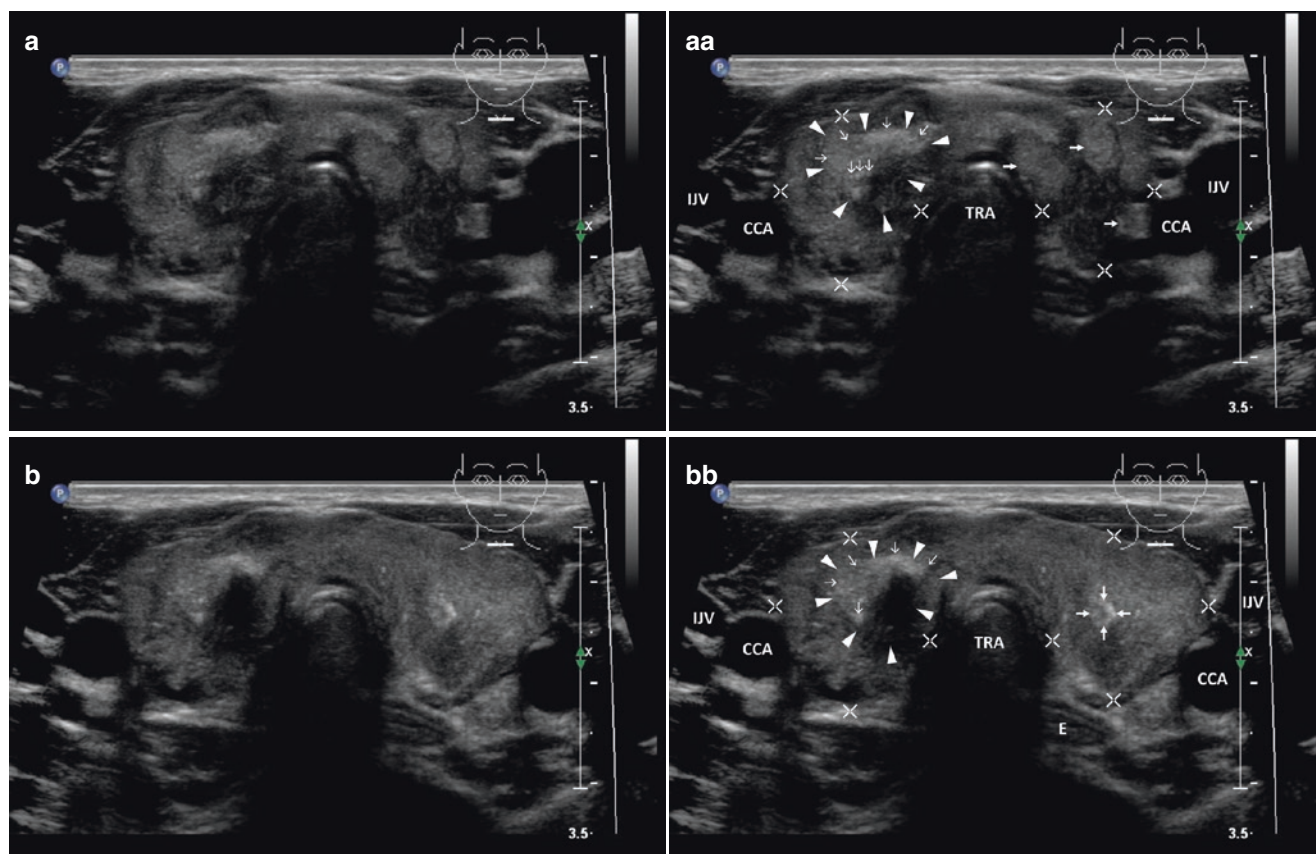


Fig. 15.39 (aa) A 16-year-old boy with Hashimoto's thyroiditis (HT) and a multifocal papillary thyroid carcinoma (PTC) in both lobes. Moreover multiple metastatic lymph nodes (LNs) on the neck at levels C-II, III, IV bilaterally at level C-VI. US scans: suspicious solid nodule (arrowheads) in the RL—coarse structure with dense cluster of microcalcifications and acoustic shadow (open arrows); ill-defined margin; small solid hyperechoic nodules (arrows) in the LL; focal microlobulated hypoechoic structure of HT in bilaterally; Tvol 14 mL, RL 9 mL, and LL 5 mL; transverse. (bb) Another transverse overall view of HT and multifocal PTC: suspicious solid nodule (arrowheads) in the RL—coarse structure with dense cluster of microcalcifications (open arrows) and acoustic shadow; ill-defined margin; tiny suspicious nodule (arrows) in the LL, coarse structure with cluster of microcalcifications; transverse. (cc) Overall view of HT and multifocal PTC, CFDS: diffusely increased vascularity, *pattern II*; transverse. (dd) Detail of HT and multifocal PTC in the RL: suspicious solid nodule (arrowheads), size 12 × 9 mm—coarse structure with dense cluster of microcalcifications and acoustic shadow; ill-defined margin; longitudinal. (ee) Detail of HT and multifocal PTC in the RL, CFDS: diffusely increased vascularity, *pattern II*; focal hypervascularity in suspicious nodule (arrowheads); transverse. (ff) Detail of two metastatic LNs (blank arrowheads) in the upper right neck next to IJV and CCA in level C-II: LN1—elliptical shape, size 18 × 12 mm and LN2—oval shape, size 12 × 10 mm;

homogeneous structure; hyperechoic; no hilus sign; transverse. (gg) Detail of large metastatic LN in the middle part of the right neck next to IJV and CCA at level C-III: LN3 (blank arrowheads) elliptical shape, size 30 × 27 × 12 mm, volume 5 mL; homogeneous structure; hyperechoic; no hilus sign; transverse. (hh) Detail of two large metastatic LNs (blank arrowheads) of the right neck next to IJV at C-II and C-III level: LN2—elliptical shape; size 25 × 13 mm and LN3 27 × 12 mm, L/S ratio ≈ 2 (not pathological); homogeneous structure; hyperechoic; no hilus sign; longitudinal. (ii) Detail of two large metastatic LNs (blank arrowheads) of the right neck next to IJV at C-III and C-IV level, CFDS: LN2, LN3—increased mixed (peripheral and central) vascularity; lumen of small vein (v) between LNs; longitudinal. (jj) Detail of large metastatic LN4 (blank arrowheads), size 31 × 26 × 18 mm and volume 8 mL in low part of the left neck next to IJV and CCA at level C-IV: oval shape; homogeneous structure; hyperechoic; no hilus sign; compressed IJV; transverse. (kk) Detail of large metastatic LN4 (blank arrowheads) in low part of the left neck next to IJV and CCA at level C-IV, CFDS: increased mixed vascularity; minimal flow in compressed IJV; transverse. (ll) Detail of chain of small metastatic LNs in low part of the neck in front of trachea and a large one next to left CCA at level C-VI: small Ln5—Ln9 at jugulum—round shape; size from 7 to 11 mm; large LN10 (blank arrowheads)—ovoid shape, size 16 × 9 mm; homogeneous structure; hyperechoic; no hilus sign; transverse

Fig. 15.38 (aa) A 16-year-old girl with a large solitary papillary thyroid carcinoma—PTC (arrowheads) in the RL and isthmus, size 44 × 31 × 18 mm and volume 12 mL with extrathyroidal extension (ETE): solid nodule with sporadic tiny cystic cavities (≤10% of volume)—ovoid shape; inhomogeneous structure; mostly hyperechoic; sporadic microcalcifications (open arrows); tiny cystic cavities (c); microlobulated margin; tumor protrusion ventrally with contour bulging and short interrupting continuity of the capsule at place of focal hypoechoic area; Tvol 18 mL, RL 13 mL, and LL 5 mL; transverse. (bb) Detail of large solitary PTC (arrowheads) with ETE, CFDS: increased

intrnodular vascularity, *pattern II*, continuing beyond interrupted capsule into muscles (arrows); transverse. (cc) Detail of large solitary PTC (arrowheads) with ETE: solid nodule with sporadic tiny cystic cavities; ovoid shape; inhomogeneous structure; mostly hyperechoic; sporadic microcalcifications (open arrows); tiny cystic cavities (c); microlobulated margin; tumor protrusion ventrally with contour bulging and short interrupting continuity of the capsule at place of focal hypoechoic area (arrows); longitudinal. (dd) Detail of large solitary PTC (arrowheads) with ETE, CFDS: increased intranodular vascularity, *pattern II*, continuing beyond interrupted capsule into muscles (arrows); longitudinal

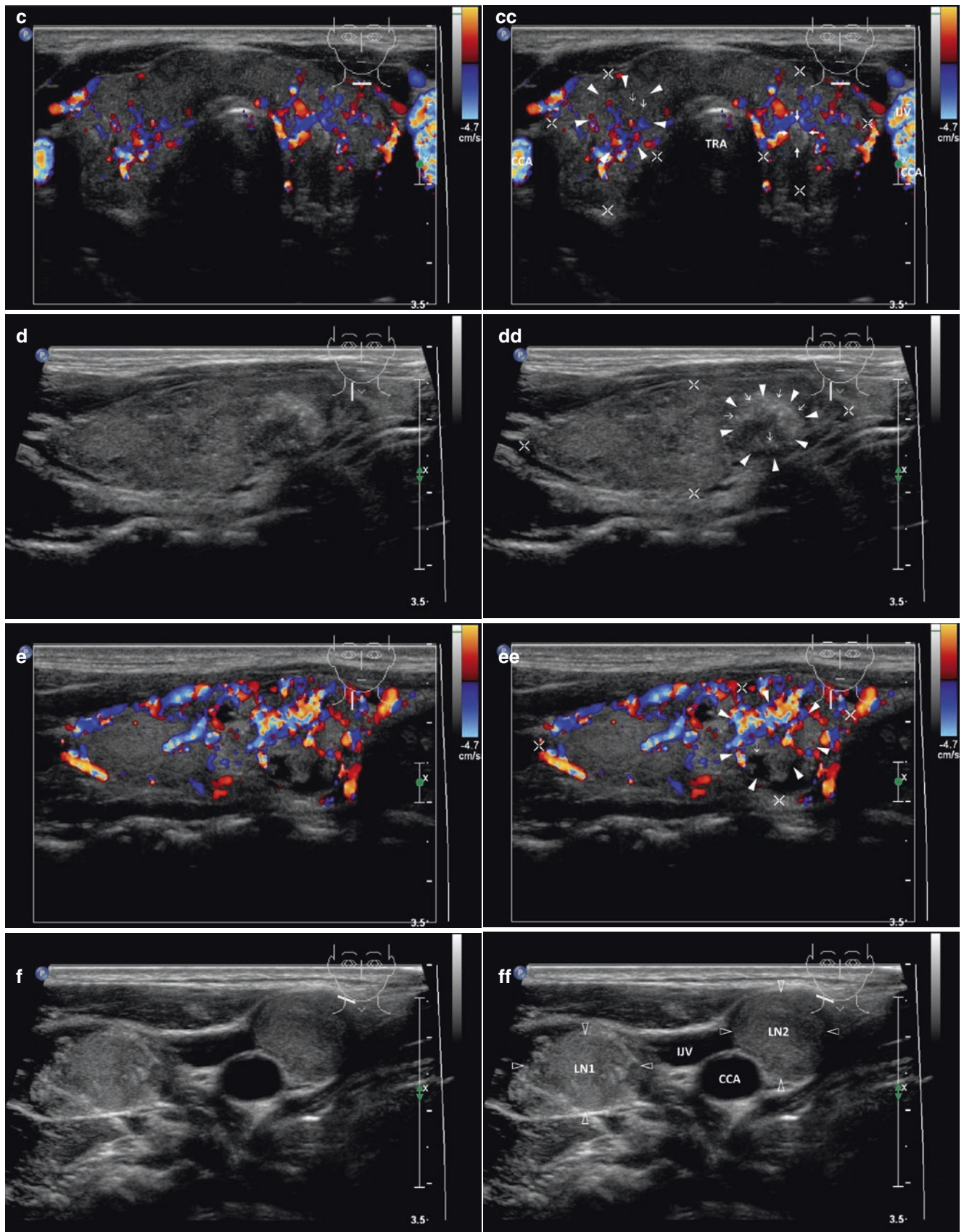
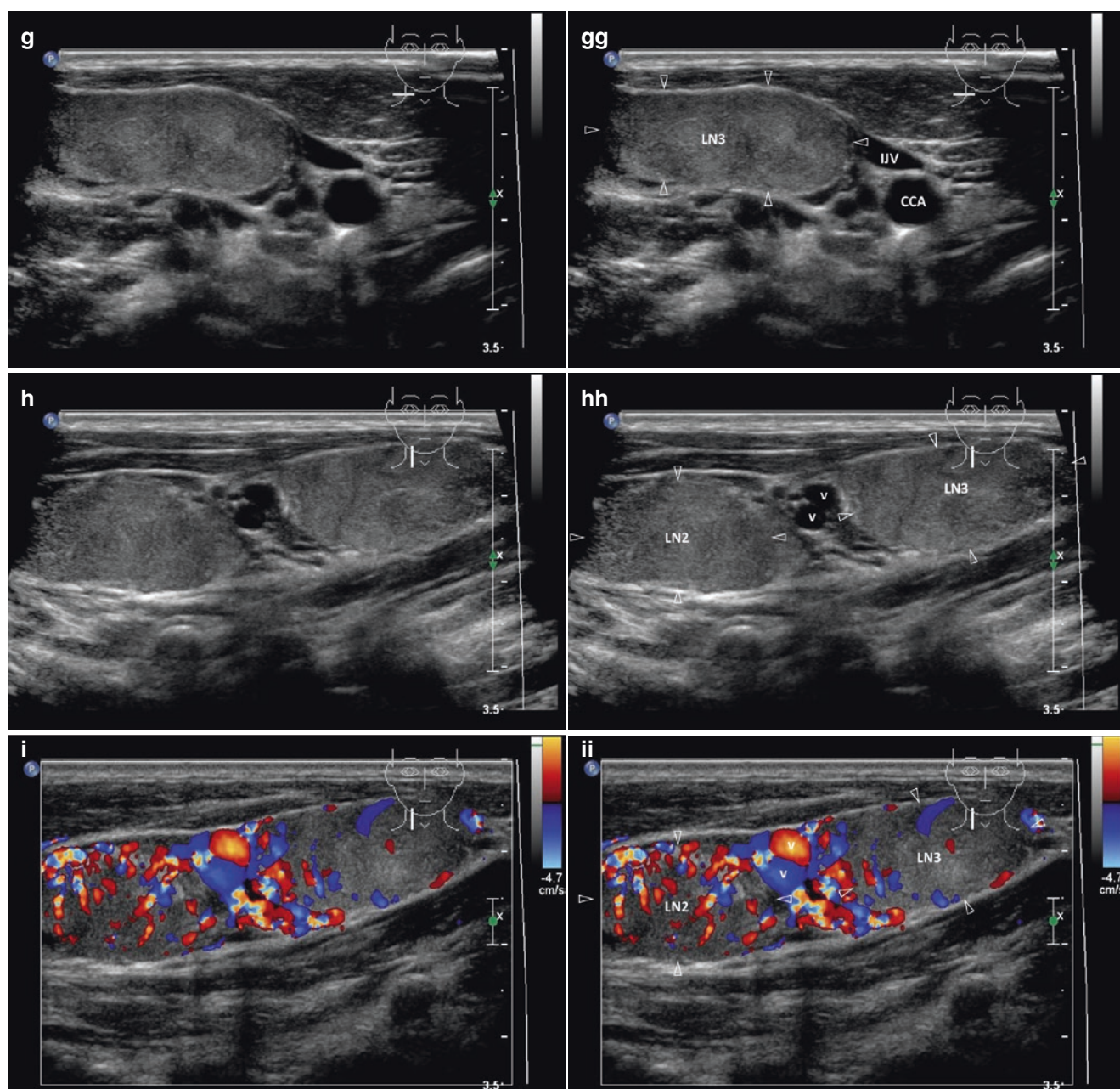


Fig. 15.39 (continued)

**Fig. 15.39** (continued)

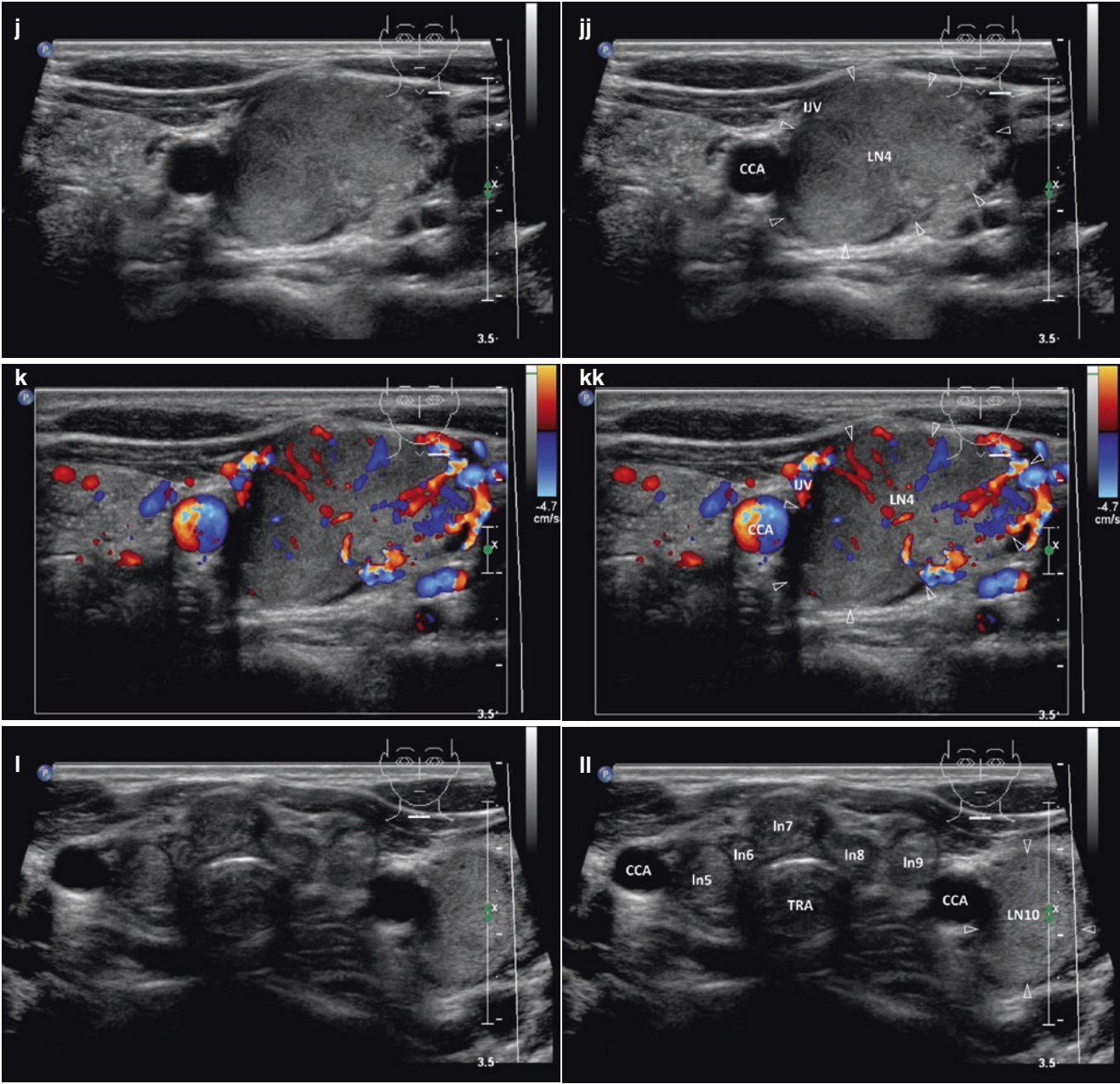


Fig. 15.39 (continued)

15.9.2 US Features of Papillary Thyroid Carcinoma in Childhood

- US classic features of high suspicion of malignancy for solid nodules according The 2015 ATA Guidelines; see Chap. 24, Table 24.1 [8].
- US findings for thyroid nodules are classified into one of three categories: probably benign, indeterminate (does not show benign or malignant features), or suspicious malignant [43].
- Based on the “Guidelines for Thyroid US” provided by the Korean Society of Thyroid Radiology (see more at Section IV. Nodular Goiter: Suspicious and Malignant Lesions) [62]:
 - Solid thyroid nodules with one or more US malignancy features (i.e., spiculated or microlobulated margin, markedly hypoechoogenic, “taller-than-wide” shape, or calcification) are considered malignant.
 - Thyroid nodules with one or two benign US features (i.e., complete cyst, predominantly a cystic lesion, cystic lesion with a comet-tail artifact, or spongiform benign cystic lesion) are considered probably benign.
- A small cohort by Koibuchi showed typical US characteristics of PTC in children. Suspicious nodules were hypoechoic with multiple marginal hyperechoic spots suggestive of psammoma bodies. The small nodules were relatively regular in shape, whereas large nodules (or after enlargement during US follow-up period) became irregular in shape. In a large nodule (a major axis of approximately 3 cm), CFDS showed abundant blood flow signals within the hypoechoic area and a presence of oval neck lymph nodes as indicative of metastasis. Moreover, there was pathologic evidence of HT as a background comorbidity [71].
- Diffusely infiltrative PTC or FTC may have all features of HT (enlargement of the thyroid, hypoechoogenicity, heterogeneity, and hypervascularity). Furthermore, patients may present with misleading thyrotoxicosis. Hashitoxicosis and may thus be mistakenly considered to have autoimmune thyroid disease (HT or GD) [43].

References

1. Enewold L, Zhu K, Ron E, Marrogi AJ, Stojadinovic A, Peoples GE, et al. Rising thyroid cancer incidence in the United States by demographic and tumor characteristics, 1980–2005. *Cancer Epidemiol Biomarkers Prev.* 2009;18(3):784–91.
2. Ito Y, Miyauchi A, Kihara M, Higashiyama T, Kobayashi K, Miya A. Patient age is significantly related to the progression of papillary microcarcinoma of the thyroid under observation. *Thyroid.* 2014;24(1):27–34.
3. Hughes DT, Haymart MR, Miller BS, Gauger PG, Doherty GM. The most commonly occurring papillary thyroid cancer in the United States is now a microcarcinoma in a patient older than 45 years. *Thyroid.* 2011;21(3):231–6.
4. Hay ID, Hutchinson ME, Gonzalez-Losada T, McIver B, Reinalda ME, Grant CS, et al. Papillary thyroid microcarcinoma: a study of 900 cases observed in a 60-year period. *Surgery.* 2008;144(6):980–7. discussion 987–8.
5. Mazzaferri EL. Management of low-risk differentiated thyroid cancer. *Endocr Pract.* 2007;13(5):498–512.
6. Qu N, Zhang L, Ji QH, Chen JY, Zhu YX, Cao YM, et al. Risk factors for central compartment lymph node metastasis in papillary thyroid microcarcinoma: a meta-analysis. *World J Surg.* 2015;39(10):2459–70.
7. Karatzas T, Vasileiadis I, Kapetanakis S, Karakostas E, Chrousos G, Kouraklis G. Risk factors contributing to the difference in prognosis for papillary versus micropapillary thyroid carcinoma. *Am J Surg.* 2013;206(4):586–93.
8. Haugen BR, Alexander EK, Bible KC, Doherty GM, Mandel SJ, Nikiforov YE, et al. 2015 American Thyroid Association Management Guidelines for adult patients with thyroid nodules and differentiated thyroid cancer: The American Thyroid Association Guidelines Task Force on thyroid nodules and differentiated thyroid cancer. *Thyroid.* 2016;26(1):1–133.
9. Wang Y, Li L, Wang YX, Feng XL, Zhao F, Zou SM, Hao YZ, et al. Ultrasound findings of papillary thyroid microcarcinoma: a review of 113 consecutive cases with histopathologic correlation. *Ultrasound Med Biol.* 2012;38(10):1681–8.
10. Aschebrook-Kilfoy B, Ward MH, Sabra MM, Devesa SS. Thyroid cancer incidence patterns in the United States by histologic type, 1992–2006. *Thyroid.* 2011;21(2):125–34.
11. Ito Y, Miyauchi A, Kobayashi K, Miya A. Prognosis and growth activity depend on patient age in clinical and subclinical papillary thyroid carcinoma. *Endocr J.* 2014;61(3):205–13.
12. Tsushima Y, Miyauchi A, Ito Y, Kudo T, Masuoka H, Yabuta T, et al. Prognostic significance of changes in serum thyroglobulin antibody levels of pre- and post-total thyroidectomy in thyroglobulin antibody-positive papillary thyroid carcinoma patients. *Endocr J.* 2013;60(7):871–6.
13. Falvo L, Catania A, D’Andrea V, Marzullo A, Giustiniani MC, De Antoni E. Prognostic importance of histologic vascular invasion in papillary thyroid carcinoma. *Ann Surg.* 2005;241(4):640–6.
14. Conzo G, Docimo G, Pasquali D, Mauriello C, Gambardella C, Esposito D, et al. Predictive value of nodal metastases on local recurrence in the management of differentiated thyroid cancer. Retrospective clinical study. *BMC Surg.* 2013;13(Suppl 2):S3.
15. Grant CS. Recurrence of papillary thyroid cancer after optimized surgery. *Gland Surg.* 2015;4(1):52–62.
16. Chow SM, Law SC, Au SK, Leung TW, Chan PT, Mendenhall WM, et al. Differentiated thyroid carcinoma: comparison between papillary and follicular carcinoma in a single institute. *Head Neck.* 2002;24(7):670–7.
17. Kamran SC, Marqusee E, Kim MI, Frates MC, Ritner J, Peters H, et al. Thyroid nodule size and prediction of cancer. *J Clin Endocrinol Metab.* 2013;98(2):564–70.
18. Kim JH, Kim NK, Oh YL, Kim HJ, Kim SY, Chung JH, et al. The validity of ultrasonography-guided fine needle aspiration biopsy in thyroid nodules 4 cm or larger depends on ultrasonography characteristics. *Endocrinol Metab (Seoul).* 2014;29(4):545–52.
19. Popowicz B, Klencki M, Lewiński A, Słowińska-Klencka D. The usefulness of sonographic features in selection of thyroid nodules for biopsy in relation to the nodule’s size. *Eur J Endocrinol.* 2009;161(1):103–11.
20. Napolitano G, Romeo A, Vallone G, Rossi M, Cagini L, Antinolfi G, et al. How the preoperative ultrasound examination and BFI of the cervical lymph nodes modify the therapeutic treatment in patients with papillary thyroid cancer. *BMC Surg.* 2013;13(Suppl 2):S52.

21. Noguchi S, Noguchi A, Murakami N. Papillary carcinoma of the thyroid. I. Developing pattern of metastasis. *Cancer*. 1970;26(5):1053–60.
22. Machens A, Hinze R, Thomusch O, Dralle H. Pattern of nodal metastasis for primary and reoperative thyroid cancer. *World J Surg*. 2002;26(1):22–8.
23. Tam AA, Özdemir D, Çuhacı N, Başer H, Aydın C, Yazgan AK, et al. Association of multifocality, tumor number, and total tumor diameter with clinicopathological features in papillary thyroid cancer. *Endocrine*. 2016;53(3):774–83.
24. Zhu F, Shen YB, Li FQ, Fang Y, Hu L, Wu YJ. The effects of Hashimoto thyroiditis on lymph node metastases in unifocal and multifocal papillary thyroid carcinoma: a retrospective Chinese cohort study. *Medicine (Baltimore)*. 2016;95(6):e2674.
25. Al Afif A, Williams BA, Rigby MH, Bullock MJ, Taylor SM, Trites J, et al. Multifocal papillary thyroid cancer increases the risk of central lymph node metastasis. *Thyroid*. 2015;25(9):1008–12.
26. So YK, Kim MW, Son YI. Multifocality and bilaterality of papillary thyroid microcarcinoma. *Clin Exp Otorhinolaryngol*. 2015;8(2):174–8.
27. Dailey ME, Lindsay S, Skahen R. Relation of thyroid neoplasms to Hashimoto disease of the thyroid gland. *AMA Arch Surg*. 1955;70(2):291–7.
28. Okayasu I, Fujiwara M, Hara Y, Tanaka Y, Rose NR. Association of chronic lymphocytic thyroiditis and thyroid papillary carcinoma. A study of surgical cases among Japanese, and white and African Americans. *Cancer*. 1995;76(11):2312–8.
29. Jeong JS, Kim HK, Lee CR, Park S, Park JH, Kang SW, et al. Coexistence of chronic lymphocytic thyroiditis with papillary thyroid carcinoma: clinical manifestation and prognostic outcome. *J Korean Med Sci*. 2012;27(8):883–9.
30. Lee JH, Kim Y, Choi JW, Kim YS. The association between papillary thyroid carcinoma and histologically proven Hashimoto's thyroiditis: a meta-analysis. *Eur J Endocrinol*. 2013;168(3):343–9.
31. Anderson L, Middleton WD, Teefey SA, Reading CC, Langer JE, Desser T, et al. Hashimoto thyroiditis: Part 2, sonographic analysis of benign and malignant nodules in patients with diffuse Hashimoto thyroiditis. *AJR Am J Roentgenol*. 2010;195(1):216–22.
32. Gul K, Dirikoc A, Kiyak G, Ersoy PE, Ugras NS, Ersoy R, et al. The association between thyroid carcinoma and Hashimoto's thyroiditis: the ultrasonographic and histopathologic characteristics of malignant nodules. *Thyroid*. 2010;20(8):873–8.
33. Durfee SM, Benson CB, Arthaud DM, Alexander EK, Frates MC. Sonographic appearance of thyroid cancer in patients with Hashimoto thyroiditis. *J Ultrasound Med*. 2015;34(4):697–704.
34. Ohmori N, Miyakawa M, Ohmori K, Takano K. Ultrasonographic findings of papillary thyroid carcinoma with Hashimoto's thyroiditis. *Intern Med*. 2007;46(9):547–50.
35. Lee J, Nam KH, Chung WY, Soh EY, Park CS. Clinicopathologic features and treatment outcomes in differentiated thyroid carcinoma patients with concurrent Graves' disease. *J Korean Med Sci*. 2008;23(5):796–801. doi:10.3346/jkms.2008.23.5.796.
36. Taneri F, Kurukahvecioglu O, Ege B, Yilmaz U, Tekin EH, Cifter C, et al. Clinical presentation and treatment of hyperthyroidism associated with thyroid cancer. *Endocr Regul*. 2005;39(3):91–6.
37. Van Sande J, Lejeune C, Ludgate M, Munro DS, Vassart G, Dumont JE, et al. Thyroid stimulating immunoglobulins, like thyrotropin activate both the cyclic AMP and the PIP2 cascades in CHO cells expressing the TSH receptor. *Mol Cell Endocrinol*. 1992;88(1–3):R1–5.
38. Viglietto G, Romano A, Manzo G, Chiappetta G, Paoletti I, Califano D, et al. Upregulation of the angiogenic factors PIGF, VEGF and their receptors (Flt-1, Flk-1/KDR) by TSH in cultured thyrocytes and in the thyroid gland of thiouracil-fed rats suggest a TSH-dependent paracrine mechanism for goiter hypervascularization. *Oncogene*. 1997;15(22):2687–98.
39. Stocker DJ, Burch HB. Thyroid cancer yield in patients with Graves' disease. *Minerva Endocrinol*. 2003;28(3):205–12.
40. Cappelli C, Braga M, De Martino E, Castellano M, Gandossi E, Agosti B, et al. Outcome of patients surgically treated for various forms of hyperthyroidism with differentiated thyroid cancer: experience at an endocrine center in Italy. *Surg Today*. 2006;36(2):125–30.
41. Inaba H, Suzuki S, Takeda T, Kobayashi S, Akamizu T, Komatsu M. Amiodarone-induced thyrotoxicosis with thyroid papillary cancer in multinodular goiter: case report. *Med Princ Pract*. 2012;21(2):190–2.
42. Saad A, Falciglia M, Steward DL, Nikiforov YE. Amiodarone-induced thyrotoxicosis and thyroid cancer: clinical, immunohistochemical, and molecular genetic studies of a case and review of the literature. *Arch Pathol Lab Med*. 2004;128(7):807–10.
43. Hong HS, Lee EH, Jeong SH, Park J, Lee H. Ultrasonography of various thyroid diseases in children and adolescents: a pictorial essay. *Korean J Radiol*. 2015;16(2):419–29.
44. Wagner B, Begic-Karup S, Raber W, Schneider B, Waldhäusl W, Vierhapper H. Prevalence of primary hyperparathyroidism in 13387 patients with thyroid diseases, newly diagnosed by screening of serum calcium. *Exp Clin Endocrinol Diabetes*. 1999;107(7):457–61.
45. Morita SY, Somervell H, Umbricht CB, Dackiw AP, Zeiger MA. Evaluation for concomitant thyroid nodules and primary hyperparathyroidism in patients undergoing parathyroidectomy or thyroidectomy. *Surgery*. 2008;144(6):862–6. discussion 866–8.
46. Heizmann O, Viehl CT, Schmid R, Müller-Brand J, Müller B, Oertli D. Impact of concomitant thyroid pathology on preoperative workup for primary hyperparathyroidism. *Eur J Med Res*. 2009;14(1):37–41.
47. Milas M, Mensah A, Alghoul M, Berber E, Stephen A, Siperstein A, et al. The impact of office neck ultrasonography on reducing unnecessary thyroid surgery in patients undergoing parathyroidectomy. *Thyroid*. 2005;15(9):1055–9.
48. Linos DA, van Heerden JA, Edis AJ. Primary hyperparathyroidism and nonmedullary thyroid cancer. *Am J Surg*. 1982;143(3):301–3.
49. Ulanovski D, Feinmesser R, Cohen M, Sulkes J, Dudkiewicz M, Shpitzer T. Preoperative evaluation of patients with parathyroid adenoma: role of high-resolution ultrasonography. *Head Neck*. 2002;24(1):1–5.
50. Nozeran S, Duquenne M, Guyetant S, Rodien P, Rohmer V, Ronceray J, et al. Diagnosis of parathyroid cysts: value of parathyroid hormone level in puncture fluid. *Presse Med*. 2000;29(17):939–41.
51. Price DL, Wong RJ, Randolph GW. Invasive thyroid cancer: management of the trachea and esophagus. *Otolaryngol Clin North Am*. 2008;41(6):1155–68.
52. Andersen PE, Kinsella J, Loree TR, Shaha AR, Shah JP. Differentiated carcinoma of the thyroid with extrathyroidal extension. *Am J Surg*. 1995;170(5):467–70.
53. McCaffrey TV, Bergstralh EJ, Hay ID. Locally invasive papillary thyroid carcinoma: 1940–1990. *Head Neck*. 1994;16(2):165–72.
54. Shah JP, Loree TR, Dharker D, Strong EW, Begg C, Vlamis V. Prognostic factors in differentiated carcinoma of the thyroid gland. *Am J Surg*. 1992;164(6):658–61.
55. Papini E, Guglielmi R, Bianchini A, Crescenzi A, Taccogna S, Nardi F, et al. Risk of malignancy in nonpalpable thyroid nodules: predictive value of ultrasound and color-Doppler features. *J Clin Endocrinol Metab*. 2002;87(5):1941–6.
56. Kobayashi K, Hirokawa M, Yabuta T, Fukushima M, Kihara M, Higashiyama T, et al. Tumor thrombus of thyroid malignancies in veins: importance of detection by ultrasonography. *Thyroid*. 2011;21(5):527–31.
57. Gross M, Mintz Y, Maly B, Pinchas R, Muggia-Sullam M. Internal jugular vein tumor thrombus associated with thyroid carcinoma. *Ann Otol Rhinol Laryngol*. 2004;113(9):738–40.
58. Chakravarthy VK, Rao ND, Chandra ST. Study of papillary carcinoma of thyroid with uncommon sites of metastasis. *Indian J Otolaryngol Head Neck Surg*. 2010;62(2):198–201.

59. Al-Jarrah Q, Abou-Foul A, Heis H. Intravascular extension of papillary thyroid carcinoma to the internal jugular vein: a case report. *Int J Surg Case Rep*. 2014;5(8):551–3.
60. Dikici AS, Yıldırım O, Er ME, Kılıç F, Tutar O, Kantarcı F, Mihmanlı I. A rare complication of the thyroid malignancies: jugular vein invasion. *Pol J Radiol*. 2015;80:360–3.
61. Sugimoto S, Doihara H, Ogasawara Y, Aoe M, Sano S, Shimizu N. Intraatrial extension of thyroid cancer: a case report. *Acta Med Okayama*. 2006;60(2):135–40.
62. Moon WJ, Baek JH, Jung SL, Kim DW, Kim EK, Kim JY, et al. Korean Society of Thyroid Radiology (KSThR); Korean Society of Radiology. Ultrasonography and the ultrasound-based management of thyroid nodules: consensus statement and recommendations. *Korean J Radiol*. 2011;12(1):1–14.
63. Kamaya A, Tahvildari AM, Patel BN, Willmann JK, Jeffrey RB, Desser TS. Sonographic detection of extracapsular extension in papillary thyroid cancer. *J Ultrasound Med*. 2015;34(12):2225–30.
64. Gupta A, Ly S, Castroneves LA, Frates MC, Benson CB, Feldman HA, et al. A standardized assessment of thyroid nodules in children confirms higher cancer prevalence than in adults. *J Clin Endocrinol Metab*. 2013;98(8):3238–45.
65. Ho WL, Zacharin MR. Thyroid carcinoma in children, adolescents and adults, both spontaneous and after childhood radiation exposure. *Eur J Pediatr*. 2016;175(5):677–83.
66. Babcock DS. Thyroid disease in the pediatric patient: emphasizing imaging with sonography. *Pediatr Radiol*. 2006;36(4):299–308.
67. Gow KW, Lensing S, Hill DA, Krasin MJ, McCarville MB, Rai SN, et al. Thyroid carcinoma presenting in childhood or after treatment of childhood malignancies: an institutional experience and review of the literature. *J Pediatr Surg*. 2003;38(11):1574–80.
68. Grigsby PW, Gal-or A, Michalski JM, Doherty GM. Childhood and adolescent thyroid carcinoma. *Cancer*. 2002;95(4):724–9.
69. Corrias A, Cassio A, Weber G, Mussa A, Wasniewska M, Rapa A, et al. Study Group for Thyroid Diseases of Italian Society for Pediatric Endocrinology and Diabetology (SIEDP/ISPED). Thyroid nodules and cancer in children and adolescents affected by autoimmune thyroiditis. *Arch Pediatr Adolesc Med*. 2008;162(6):526–31.
70. Skarpa V, Kousta E, Tertipi A, Anyfandakis K, Vakaki M, Dolianiti M, et al. Epidemiological characteristics of children with autoimmune thyroid disease. *Hormones (Athens)*. 2011;10(3):207–14.
71. Koibuchi H, Omoto K, Fukushima N, Toyotsuji T, Taniguchi N, Kawano M. Coexistence of papillary thyroid cancer and Hashimoto thyroiditis in children: report of 3 cases. *J Ultrasound Med*. 2014;33(7):1299–303.

16.1 Essential Facts

- Medullary thyroid carcinoma (MTC) constitutes approximately 2–5% of all thyroid malignancies, but it is responsible for up to 13.4% of all deaths from thyroid cancer. The prevalence is about the same in both males and females [1].
- It is a well-differentiated type of tumor that arises from the parafollicular (C cells) of the thyroid gland, and is categorized as a neuroendocrine tumor [1].
- The parafollicular cells secrete calcitonin. Serum calcitonin is greatly elevated in almost all patients with MTC. There appears to be a direct correlation of calcitonin level and the extent of thyroid involvement by MTC.
- In 80% of patients MTC occurs sporadically, as a result of a mutation involving only the somatic cells. Sporadic forms of MTC are more common in older patients (mean age at presentation about 47 years) [1].
- About 20% of patients have familial MTC, caused by germline mutation in the RET protooncogene. The hereditary forms of MTC are more common in younger patients.
- MTC is considered to be less aggressive than ATC, but more lethal than PTC and FTC.
- While most patients with MTC typically present with a palpable nodule in the upper part of the thyroid lobe, some patients may present with systemic symptoms associated with distant metastases [1].
- The clinical course of both forms of MTC is described in retrospective review of 104 patients by Kebebew; 56% of patients had sporadic MTC, 22% had familial MTC, 15% had MEN 2A, and 7% had MEN 2B [2]:
 - 32% of the patients with hereditary MTC were diagnosed by screening (genetic and/or biochemical). These patients had a lower incidence of cervical lymph node metastasis and 94.7% were cured at last follow-up compared with patients not screened.
 - Patients with sporadic MTC who had systemic symptoms (diarrhea, bone pain, or flushing) had widely metastatic MTC and 33.3% of those patients died within 5 years.
 - Overall, 49.4% of the patients were cured. In addition, 12.3% had recurrent MTC and 38.3% had persistent MTC. Patients with persistent or recurrent MTC who died of MTC lived for an average of 3.6 years.
 - Screening for MTC and early treatment (total thyroidectomy with central neck lymph node clearance) had a nearly 100% cure rate.
- Five-year recurrence-free survival varies from 20 to 73% and is related to the number of metastatic LN (Fig. 16.3hh) and postoperative calcitonin and CEA doubling times [3].

16.2 US Features of Medullary Thyroid Carcinoma

- 2015 ATA Guidelines [4] for suspect node are valid; *see more in Chap. 24*.
- Moreover, it is emphasized [5]:
 - Solid internal content (Fig. 16.1aa).
 - An ovoid-to-round shape (Fig. 16.1aa).
 - Markedly hypoechoic (52%) (Fig. 16.3aa) or hypoechoic (43%) solid lesion (Fig. 16.1aa).
 - Calcifications (52–95%) (Fig. 16.1dd, Fig. 16.2bb, Fig. 16.3bb).
- Amyloid deposits may be associated with reactive fibrosis and calcified deposits that give rise to characteristically dense, irregular foci throughout the tumor mass. In a study by Kim et al., intranodular calcifications were observed in 52% of subjects [5]. As compared to the results of the Gorman et al. (83.3%) and Saller et al. (95%) studies, Kim et al. found a low calcification rate [6, 7].

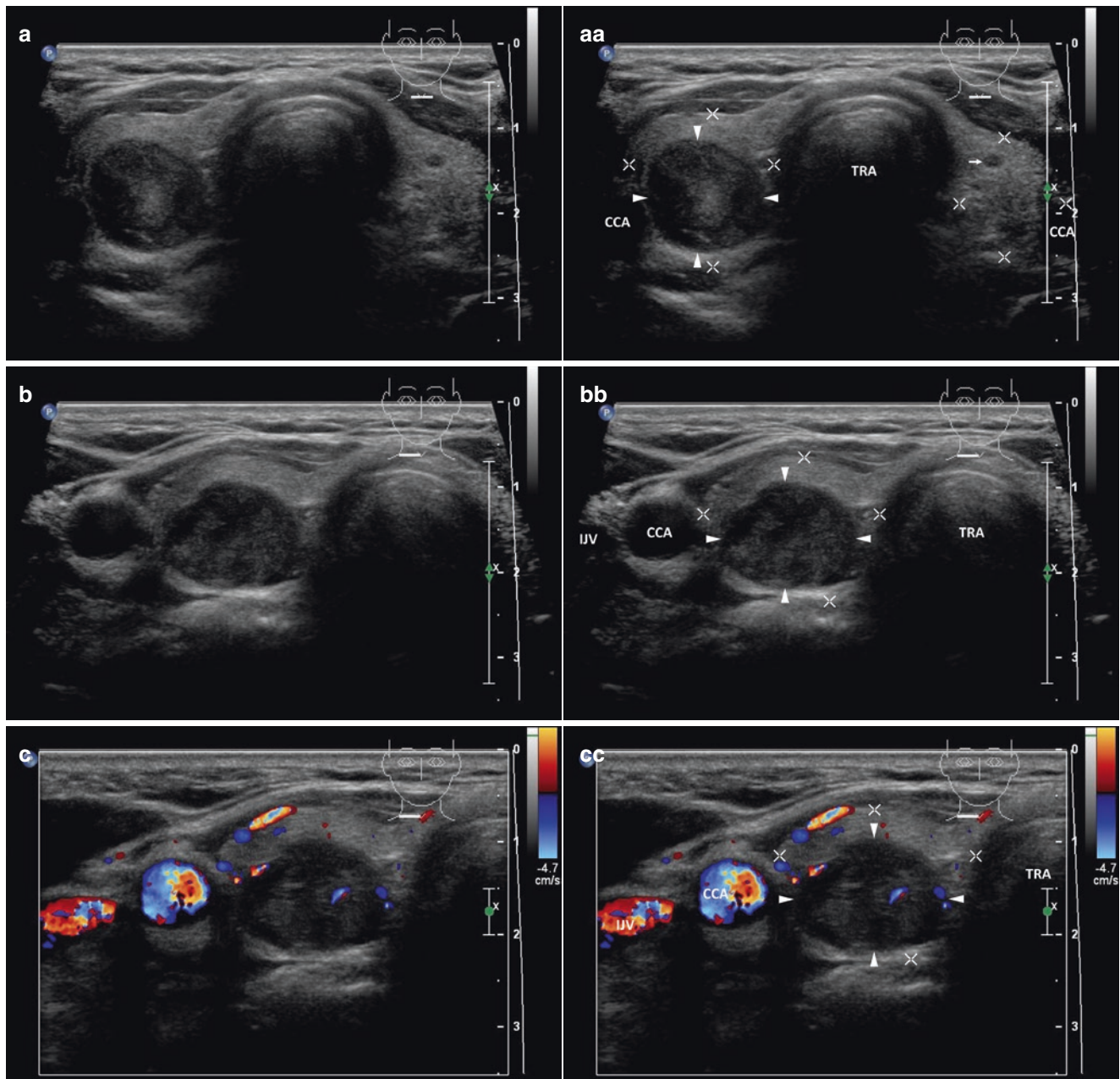


Fig. 16.1 (aa) A 39-year-old woman with a solitary small medullary thyroid carcinoma—MTC (arrowheads) in the RL, size $22 \times 16 \times 12$ mm and volume 2 mL, without metastatic cervical lymph nodes. Laboratory: serum calcitonin 1248 ng/L (normal < 11.5 ng/L). US overall view: solid nodule; round shape; inhomogeneous structure; mixed echogenicity, central isoechoic, periphery hypoechoic; well-defined margin; irregular thin halo sign; Tvol 13 mL, RL 8 mL, and LL 5 mL; transverse. (bb) Detail of small MTC (arrowheads): round

shape; mixed echogenicity; well-defined margin; transverse. (cc) Detail of small MTC (arrowheads), CFDS: minimal peripheral and central vascularity, *pattern I*; transverse. (dd) Detail of small MTC (arrowheads): ovoid shape; inhomogeneous structure; mostly isoechoic; three microcalcifications at periphery (arrows); well-defined margin; irregular thin halo sign; longitudinal. (ee) Detail of small MTC (arrowheads), CFDS: minimal peripheral and central vascularity, *pattern I*; longitudinal

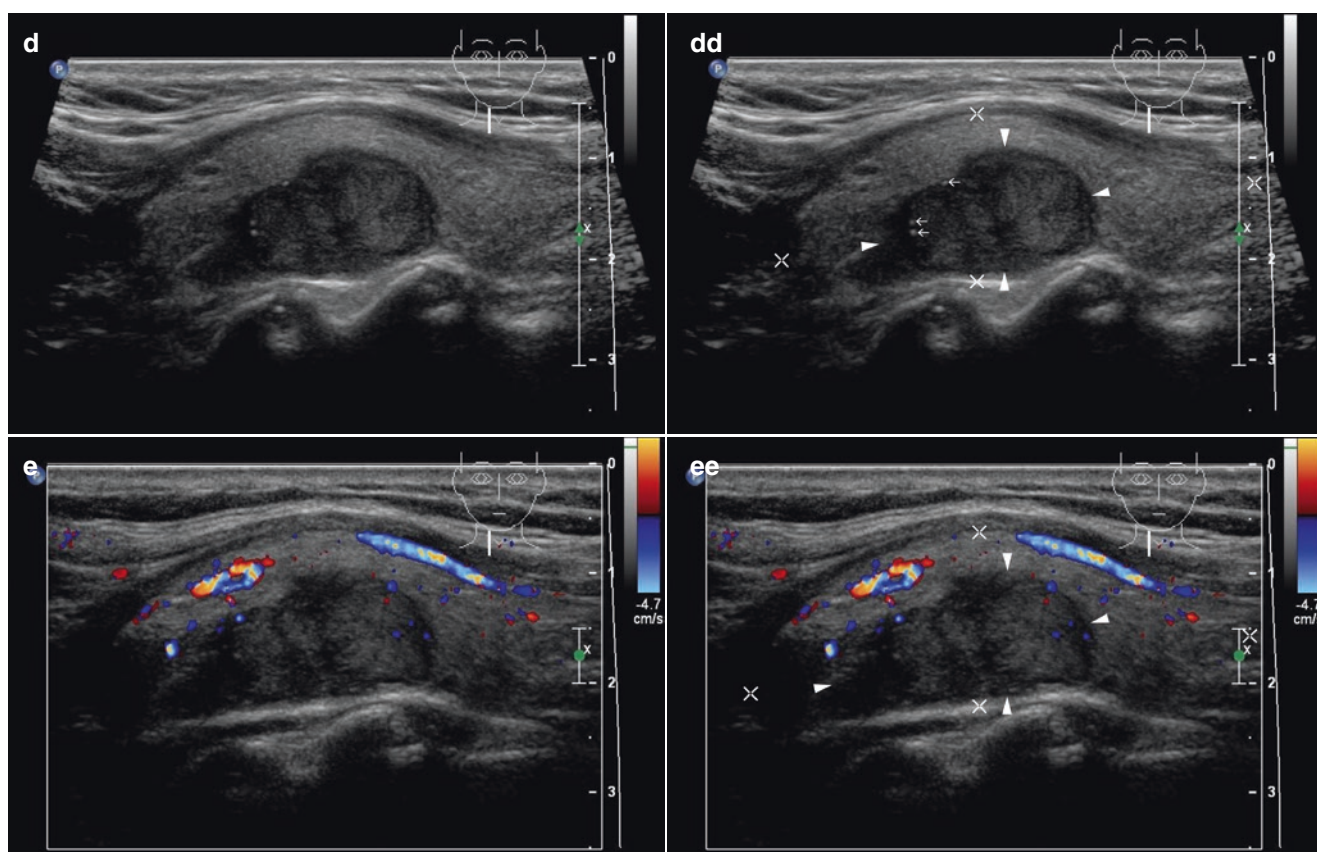


Fig. 16.1 (continued)

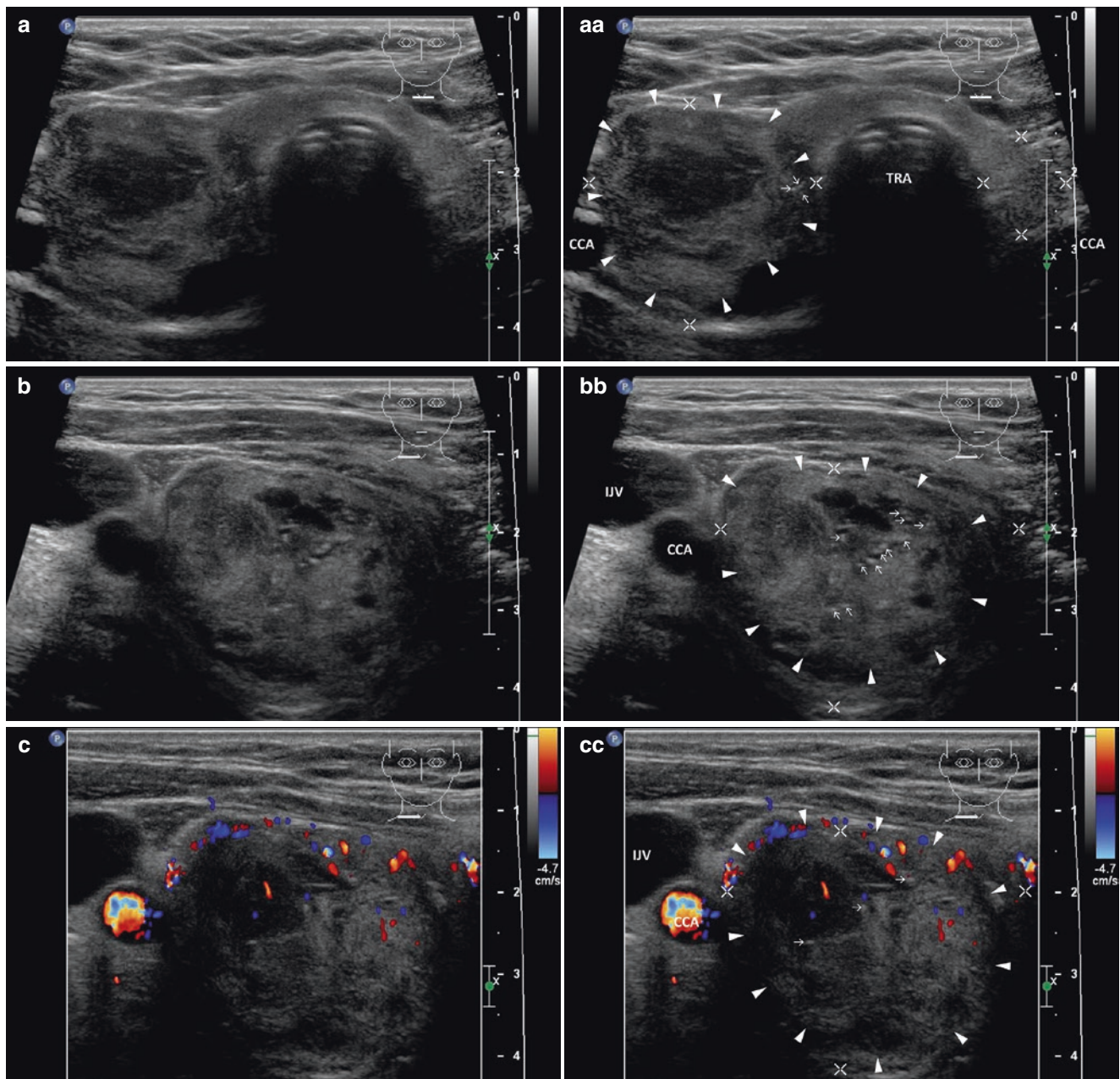


Fig. 16.2 (aa) A 57-year-old man with a solitary large medullary thyroid carcinoma—MTC (arrowheads) in the RL, size $36 \times 33 \times 28$ mm and volume 17 mL, without metastatic cervical lymph nodes. Laboratory: serum calcitonin 1858 ng/L (normal < 11.5 ng/L). US overall view: solid nodule; round shape; coarse structure; mostly hyperechoic, central ill-defined hypoechoic area; microcalcifications (arrows); ill-defined margin; Tvol 35 mL, RL 28 mL, and LL 7 mL; transverse. (bb) Detail of large MTC (arrowheads): round shape;

coarse structure; hyperechoic; microcalcifications (arrows); ill-defined margin; irregular thin halo sign; transverse. (cc) Detail of large MTC (arrowheads), CFDS: minimal peripheral and central vascularity, *pattern I*; transverse. (dd) Detail of large MTC (arrowheads): ovoid shape; coarse structure; mostly hyperechoic, central ill-defined hypoechoic area; microcalcifications (arrows); ill-defined margin; irregular thin halo sign; longitudinal. (ee) Detail of large MTC (arrowheads), CFDS: minimal peripheral and central vascularity, *pattern I*; longitudinal

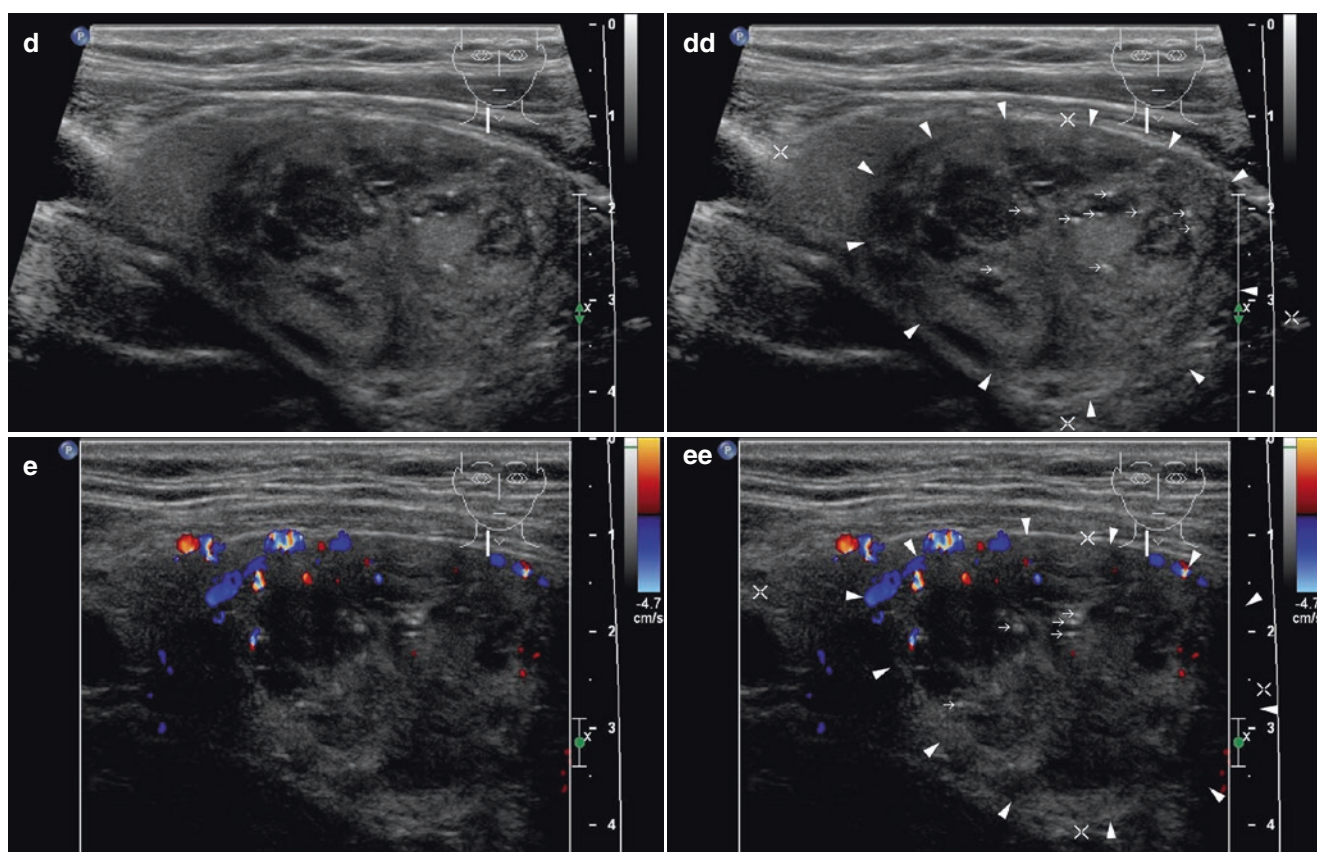


Fig. 16.2 (continued)

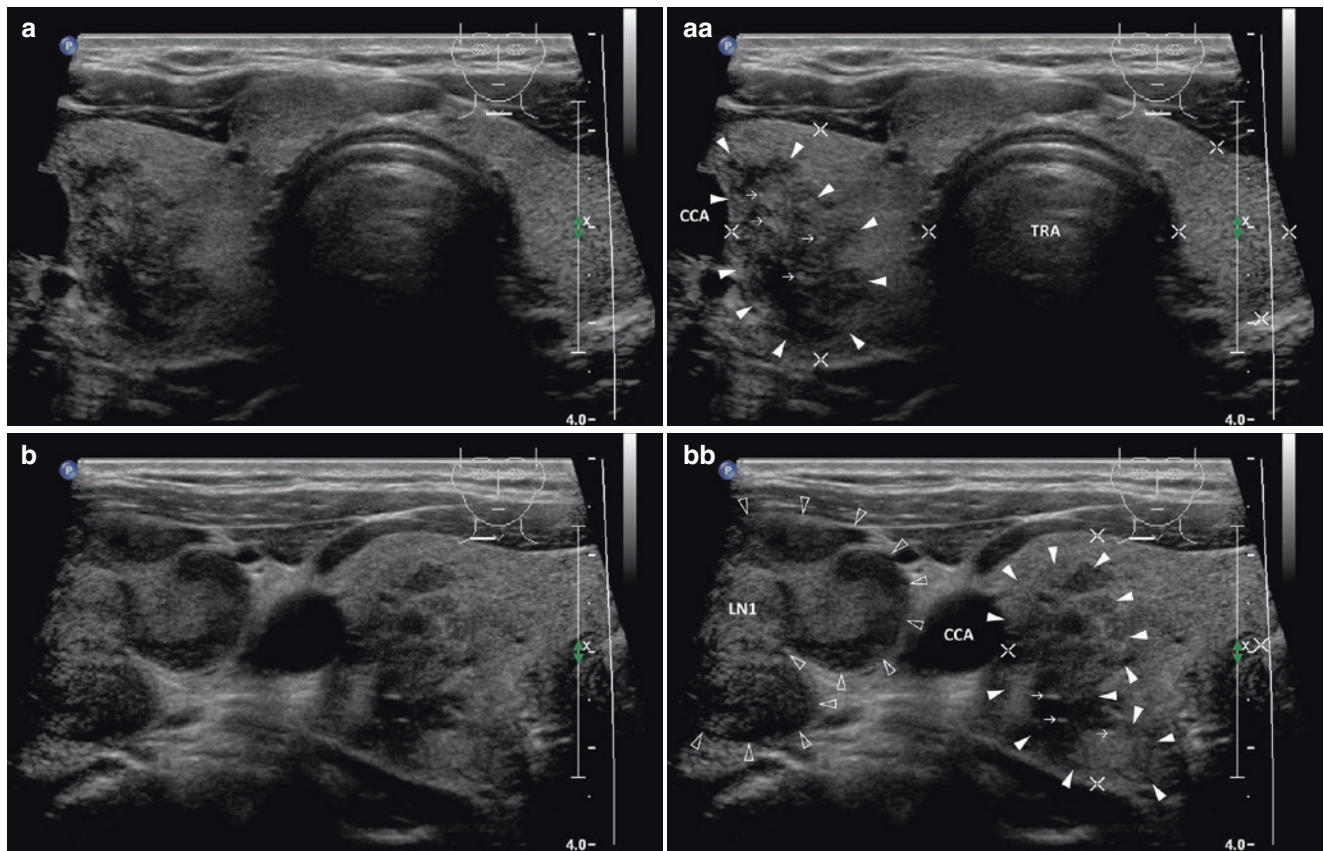
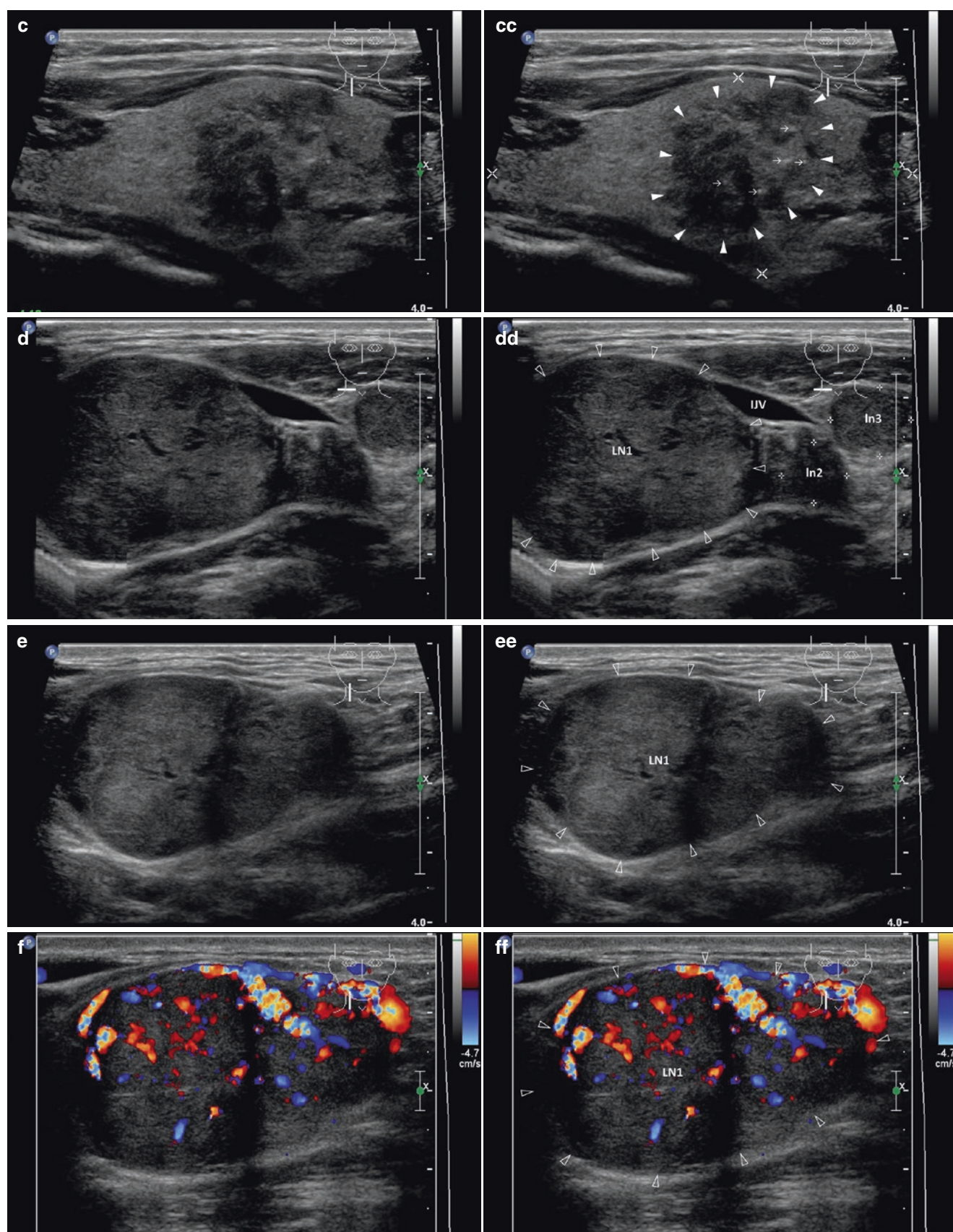


Fig. 16.3 (aa) A 43-year-old man with a solitary medium-sized medullary thyroid carcinoma—MTC (*arrowheads*) in the RL lobe, size $27 \times 20 \times 19$ mm and volume 5 mL. Moreover metastatic cervical lymph nodes (LN) along the right IJV and CCA, at levels C-III, C-IV. Laboratory: serum calcitonin >2000 ng/L (normal <11.5 ng/L). US overall view: solid nodule; irregular shape; coarse structure; mixed echogenicity with small, ill-defined hypoechoic areas; sporadic microcalcifications (*arrows*); blurred margin; Tvol 33 mL, RL 19 mL, and LL 14 mL; transverse; depth of penetration 4 cm. (bb) Detail of medium-sized MTC and large metastatic LN1 at level C-IV: suspicious nodule (*arrowheads*)—irregular shape; coarse structure; mixed echogenicity, small, ill-defined hypoechoic areas; sporadic microcalcifications (*arrows*); metastatic LN1 (*blank arrowheads*), size $36 \times 31 \times 27$ mm and volume 16 mL—oval shape; inhomogeneous structure; mixed echogenicity, central mostly hyperechoic and at periphery hypoechoic; no hilus sign; blurred margin; transverse. (cc) Detail of medium-sized MTC (*arrowheads*): irregular shape; coarse structure; mixed echogenicity with small hypoechoic areas; sporadic microcalcifications (*arrows*); blurred margin; longitudinal. (dd) Detail of large metastatic LN1, volume 16 mL and others small LNs at level C-IV: large metastatic LN1 (*blank arrowheads*)—ovoid shape; inhomogeneous structure; mostly hyperechoic; two small metastatic Ln2, Ln3 (*marks*) behind and along VJI—round shape; size ≈ 10 mm, L/S ratio ≈ 1.0 ; homogeneous structure; no hilus sign; transverse. (ee) Detail of large metastatic LN1 (*blank arrowheads*), volume 16 mL at level C-IV: ovoid shape; size 36×27 mm, L/S ratio ≈ 1.6 (pathological); inhomogeneous struc-

ture; mostly hyperechoic; no hilus sign; longitudinal. (ff) Detail of large metastatic LN1 (*blank arrowheads*), volume 16 mL, CFDS: mixed (hilar and peripheral) hypervascularity; longitudinal. (gg) Detail of large metastatic LN4, size $40 \times 26 \times 18$ mm, volume 9 mL at level C-III: large metastatic LN4 (*blank arrowheads*)—ovoid shape; inhomogeneous structure; hyperechoic; no hilus sign; another metastatic Ln5 (*marks*) behind the compressed right IJV; transverse. (hh) Detail of large metastatic LN4, volume 9 mL and five small metastatic LNs compressing the right IJV at level C-III: large LN4 (*blank arrowheads*)—elliptical shape; size 40×18 mm, L/S ratio ≈ 2 (*not pathological*); five small Ln5–Ln9—round or oval shape; hyperechoic; no hilus sign; longitudinal. (ii) Three years post thyroidectomy and radical LNs excision for MTC. Laboratory: serum calcitonin 1248 ng/L (normal <11.5 ng/L). Recurrence of disease—five small metastatic LNs on the right side along the CCA at level C-IV and one small metastatic LN on the left side along the IJV at level C-IV, size from 5 to 7 mm. US scan on the right side: two metastatic Ln1, Ln2 (*marks*)—round shape, L/S ratio ≈ 1.0 ; homogeneous structure; hyperechoic; no hilus sign; transverse. (jj) Detail of recurrence of MTC, another two small metastatic LNs on the right side at level C-IV: Ln3, Ln4 (*marks*)—round shape, L/S ratio ≈ 1.0 ; homogeneous structure; hyperechoic; no hilus sign; transverse. (kk) Detail of recurrence of MTC, one small metastatic LN on the left side along the IJV: Ln5 (*marks*)—round shape, L/S ratio ≈ 1.0 ; homogeneous structure; hyperechoic; no hilus sign; transverse

**Fig. 16.3** (continued)

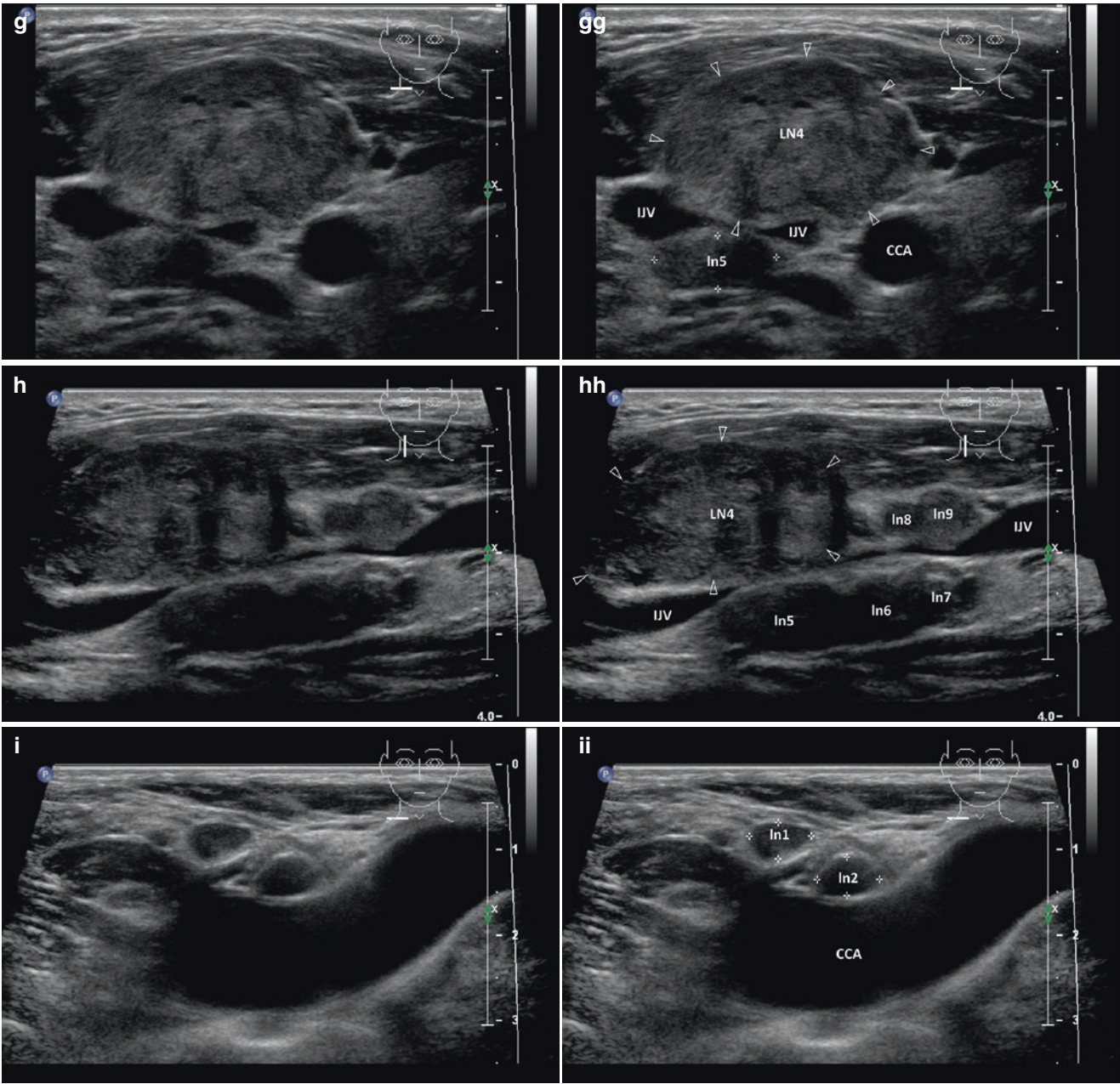


Fig.16.3 (continued)

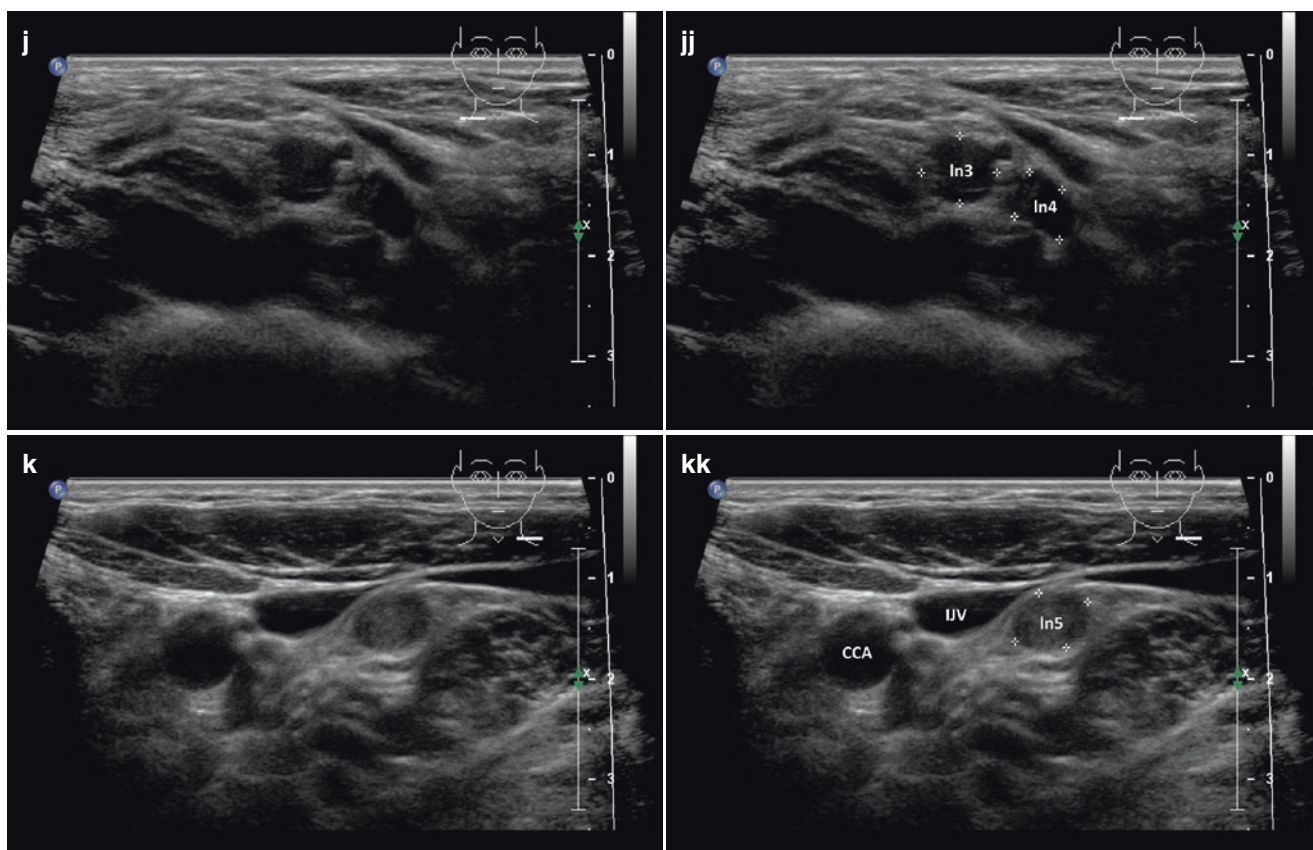


Fig. 16.3 (continued)

- The latest study by Kim et al. compared US findings of 21 MTC cases and 114 PTC cases. The mean size of MTC nodules was significantly larger than that of PTC nodules (19 ± 13.9 mm vs. 11 ± 7.5 mm). In a comparison of the US findings, 57% of MTCs and 25% of PTCs exhibited an ovoid-to-round shape, which was significantly higher for the MTC nodules. However, internal content, margin, echogenicity, and frequency of calcifications were not significantly different between MTCs and PTCs. Most MTC (80.9%) and PTC (93.9%) nodules were classified as suspicious malignant nodules [5].
- A previous study by Saller et al. included 19 patients with newly diagnosed MTC: In 17 of 19 cases (89%), lesions were hypoechoic, contained intranodular calcifications, and had no “halo sign.” In patients with MTC, intranodular blood flow was found in 11 of 14 (79%), and perinodular blood flow was found in 7 of 14 (50%). Saller defined calcifications longer than 2 mm as macrocalcifications, and reported the presence of macrocalcifications in 53% of MTC patients in their study. In conclusion, conventional US revealed a combination of hypoechogenicity, intranodular calcifications, and absence of “halo sign” in the vast majority of MTC [7].

References

1. Sajid-Crockett S, Hershman J. Thyroid nodules and cancer in the elderly. In: De Groot LJ, Beck-Peccoz P, Chrousos G, Dungan K, Grossman A, Hershman JM, Koch C, et al., editors. Endotext [Internet]. South Dartmouth, MA: MDText.com, Inc.; 2015.
2. Kebebew E, Ituarte PH, Siperstein AE, Duh QY, Clark OH. Medullary thyroid carcinoma: clinical characteristics, treatment, prognostic factors, and a comparison of staging systems. *Cancer*. 2000;88(5):1139–48.
3. Meijer JA, le Cessie S, van den Hout WB, Kievit J, Schoones JW, Romijn JA, Smit JW. Calcitonin and carcinoembryonic antigen doubling times as prognostic factors in medullary thyroid carcinoma: a structured meta-analysis. *Clin Endocrinol (Oxf)*. 2010;72(4):534–42.
4. Haugen BR, Alexander EK, Bible KC, Doherty GM, Mandel SJ, Nikiforov YE, et al. 2015 American Thyroid Association Management guidelines for adult patients with thyroid nodules and differentiated thyroid cancer: The American Thyroid Association Guidelines Task Force on thyroid nodules and differentiated thyroid cancer. *Thyroid*. 2016;26(1):1–133.
5. Kim SH, Kim BS, Jung SL, Lee JW, Yang PS, Kang BJ, et al. Ultrasonographic findings of medullary thyroid carcinoma: a comparison with papillary thyroid carcinoma. *Korean J Radiol*. 2009;10(2):101–5.
6. Gorman B, Charboneau JW, James EM, Reading CC, Wold LE, Grant CS, et al. Medullary thyroid carcinoma: role of high-resolution US. *Radiology*. 1987;162(1 Pt 1):147–50.
7. Saller B, Moeller L, Görges R, Janssen OE, Mann K. Role of conventional ultrasound and color Doppler sonography in the diagnosis of medullary thyroid carcinoma. *Exp Clin Endocrinol Diabetes*. 2002;110(8):403–7.

17.1 Essential Facts

- Anaplastic thyroid carcinoma (ATC) accounts for only 1–2% of all thyroid cancers.
- It is a very aggressive, highly malignant tumor that is most commonly seen in older people. The peak incidence of ATC is the seventh decade of life and more than two thirds of all ATC affects people over the age of 65 years.
- Women are more commonly affected than men, approximately 1.5:1.
- Clinical findings: a rapidly growing mass with tightness in the neck, dysphagia, hoarseness, dyspnea, neck pain, sore throat, and cough. Examination of the neck usually reveals a fixed, large, firm mass [1].
- ATC can be seen in several contexts: (1) a patient with DTC whose disease suddenly becomes fulminant after an interval of several years; (2) a patient with a longstanding goiter that suddenly grows at a rapid rate; (3) a patient without previous thyroid disease who develops a rapidly growing neck mass; (4) a patient whose pathological sections reveal a focus of ATC in the thyroid specimen; and (5) a patient with widespread metastases whose biopsy of an accessible metastasis suggests an ATC. In a retrospective analysis of 84 patients with ATC by Aldinger et al., 21% had a history of differentiated thyroid cancer, 37% had a longstanding goiter with sudden rapid growth, 30% had no previous thyroid disease, and 6% had widespread metastatic disease. 93% patients were presented with stage III and stage IV disease. A 5-year survival rate was only 7.1% with a mean survival period of 6.2 months from the time of diagnosis and 11.8 months from the time of onset of symptoms [2].
- In a cohort of 38 patients with ATC, systemic metastases were present in 46% of ATC patients at presentation, and 68% ATC of patients had metastases diagnosed during the course of their illness [3].
- In another retrospective cohort of 39 ATC patients, 82% died during the follow-up period of up to 10 years, 75% of these patients had distant metastases to the lung, bone, mediastinum, and peritoneum at the time of diagnosis [4].
- In a cohort of 516 patients by Kebebew et al., 8% of patients had intrathyroidal tumors, 38% had extrathyroidal tumors and/or lymph node invasion, and 43% had distant metastasis. The average tumor size was 6.4 cm (range, 1–15 cm). Age at diagnosis of ATC is a strong predictor of prognosis. There was a 28% difference in mortality between patients <60 year and those >60 years. They also reported a 45% difference in mortality at 1-year follow-up between patients who had distant metastasis and patients who had intrathyroidal ATC only [5].

17.2 US Features of Anaplastic Thyroid Carcinoma

- In a cohort of 18 cases of ATC (17 have US scan) by Suh et al., the most common US features included (Figs. 17.1aa and 17.2aa): solid mass (11 of 17, 64.7%), irregular margin (15 of 17, 88.2%), presence of cervical lymph node involvement (13 of 17, 76.4%), wider-than-tall shape (12 of 17, 70.5%), marked hypoechogenicity (9 of 17, 52.9%), and internal calcification (9 of 17, 52.9%). However, except for lymph node involvement, US findings for each group were not statistically different from other types of aggressive thyroid cancer. A correct diagnosis of ATC by initial US-FNAB was made in 9 of 18 (50%) of the cases [6].
- On computed tomography of nine patients, ATC appeared as: large size (average 4.6 cm), solid of 100%, and ill-defined of $\approx 89\%$, masses accompanied by necrosis of 100%, nodular calcification of $\approx 44\%$, direct invasion into the adjacent organs of $\approx 56\%$, and cervical lymph nodes involvement of $\approx 78\%$ [7].
- Considering the limitations of US evaluation in studying larger masses, CT or MR are more useful to obtain information on the extent and location of tumor necrosis, site of calcification in the tumor, and detecting lymph node metastases. It helps to lower false negative diagnosis by appreciating indication sites for FNAB. However, when ATC is clinically suspected, US-guided FNAB is initially performed and CT or MRI is performed after diagnosis [8].
- In a series of 113 FNAB of ATC, 3 cases (2.7%) were inadequate, 3 (2.7%) suboptimal, and 107 (94.7%) diagnostic of malignancy. On reexamination, 96 of 107 cases (89.7%) were diagnosed as ATC, 6 (5.6%) as differentiated thyroid carcinoma, and 5 (4.6%) as a malignant tumor not otherwise specified. The major diagnostic problem with fine needle aspiration biopsy (FNAB) of ATC is related to sample quality [9].

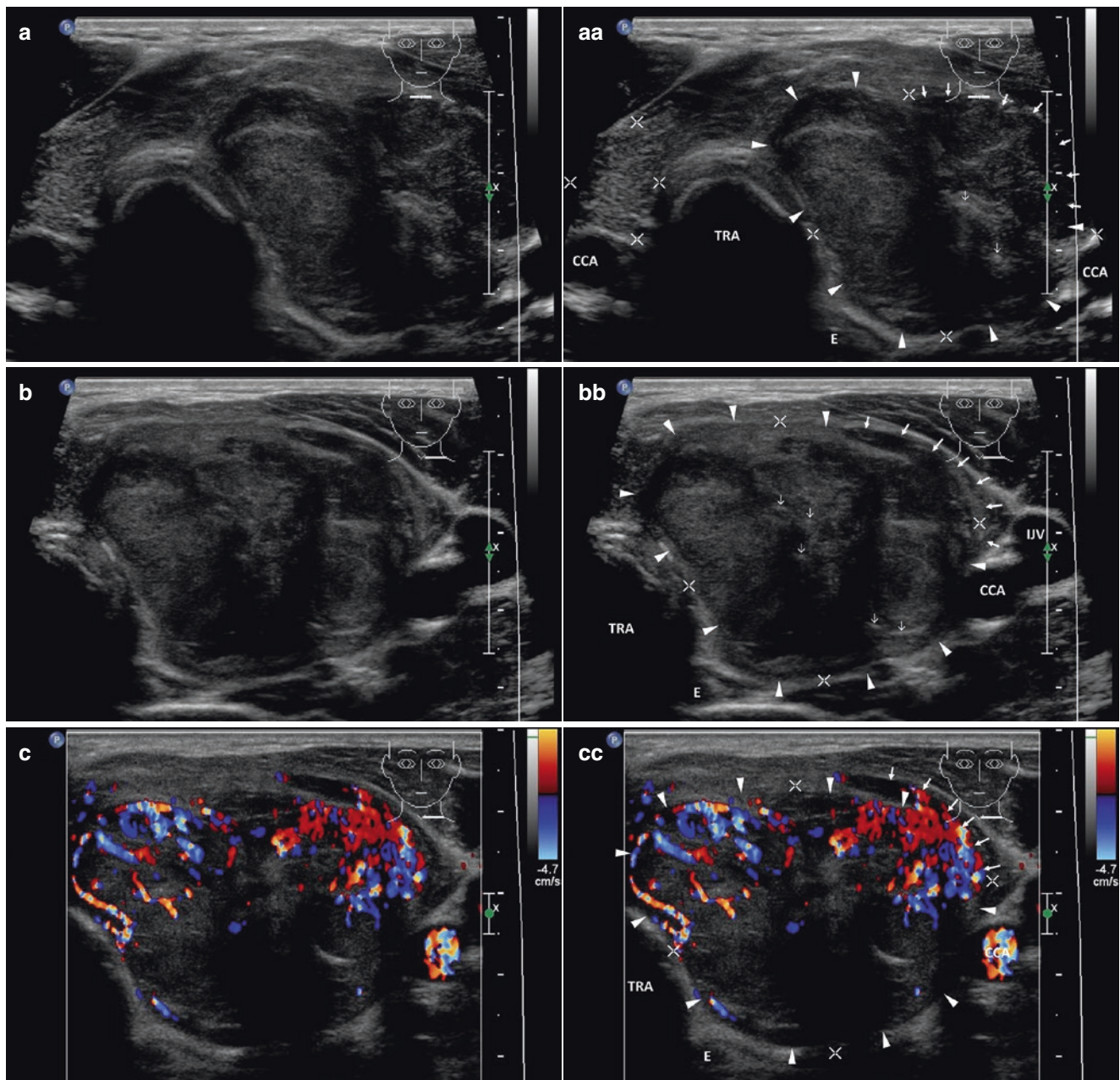


Fig. 17.1 (aa) A 41-year-old man with a large anaplastic thyroid carcinoma (ATC) in the LL and isthmus with extrathyroidal extension (ETE) into muscles, size $43 \times 38 \times 31$ mm and volume 26 mL; *without metastatic lymph nodes*: ATC (arrowheads)—solid nodule; round shape; coarse structure; mixed echogenicity with ill-defined hypoechoic areas and hyperechoic fibrous bands and sporadic microcalcifications (open arrows); microlobulated margin; tumor protrusion ventrally and laterally with interrupting continuity of the capsule and invasion into muscles (arrows); trachea deviated to the right; Tvol 50 mL, asymmetry—RL 8 mL and LL 42 mL; transverse, depth of penetration 5 cm. (bb) Another overall view large ATC (arrowheads) with ETE into muscles; tumor protrusion ventrally and laterally with interrupting continu-

ity of the capsule and invasion into muscles (arrows); another transverse view. (cc) Detail of large ATC (arrowheads) with ETE, CFDS: increased intranodular vascularity, *pattern III*, continuing beyond interrupted capsule into muscles (arrows); transverse. (dd) Detail of large ATC (arrowheads) with ETE: ovoid shape; solid nodule; coarse structure; mixed echogenicity with ill-defined hypoechoic areas and sporadic microcalcifications (open arrows); tumor protrusion ventrally interrupting continuity of the capsule into muscles (arrows); at the upper pole another small complex nodule (arrows); longitudinal. (ee) Detail of large ATC (arrowheads) with ETE, CFDS: increased intranodular vascularity, *pattern III*, continuing beyond interrupting capsule into muscles; longitudinal

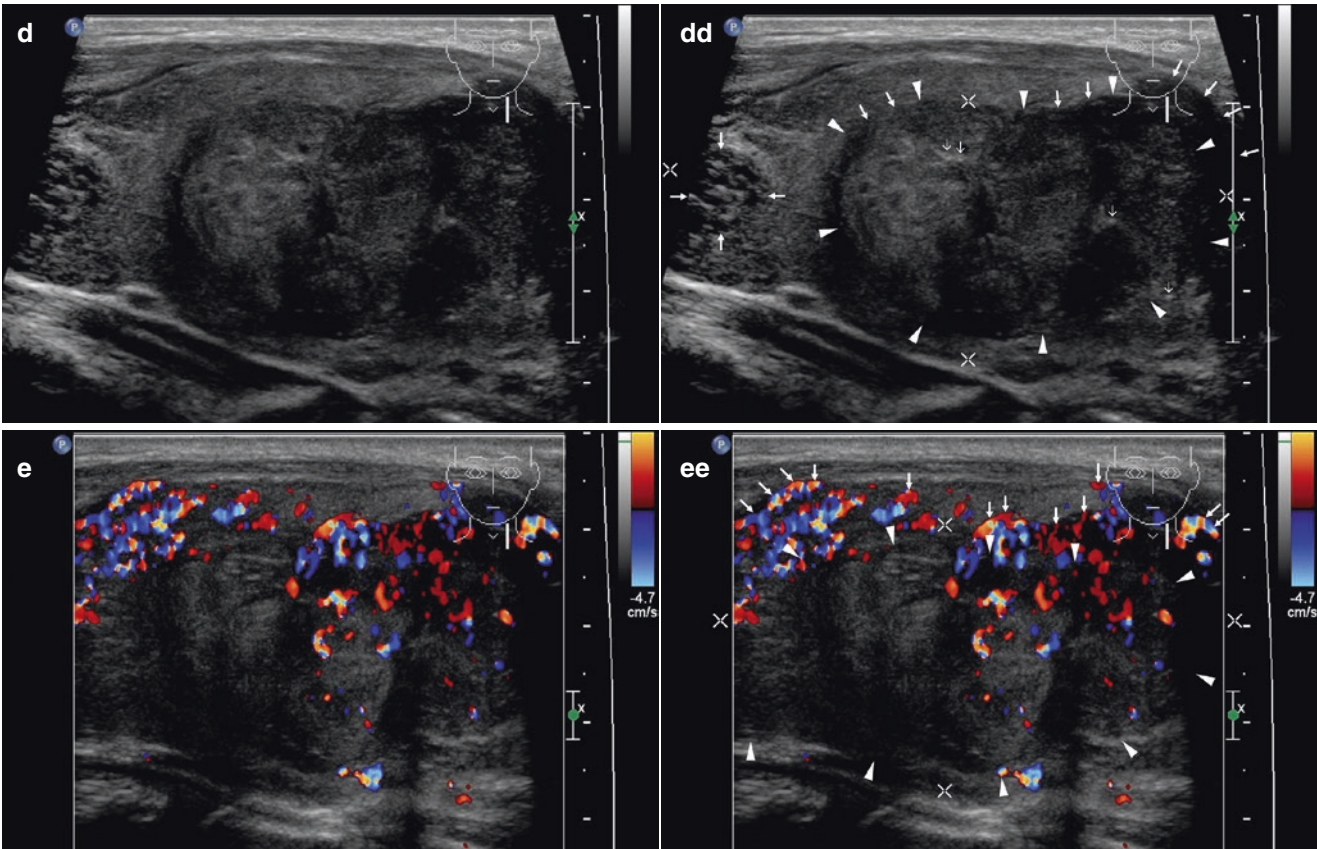


Fig. 17.1 (continued)

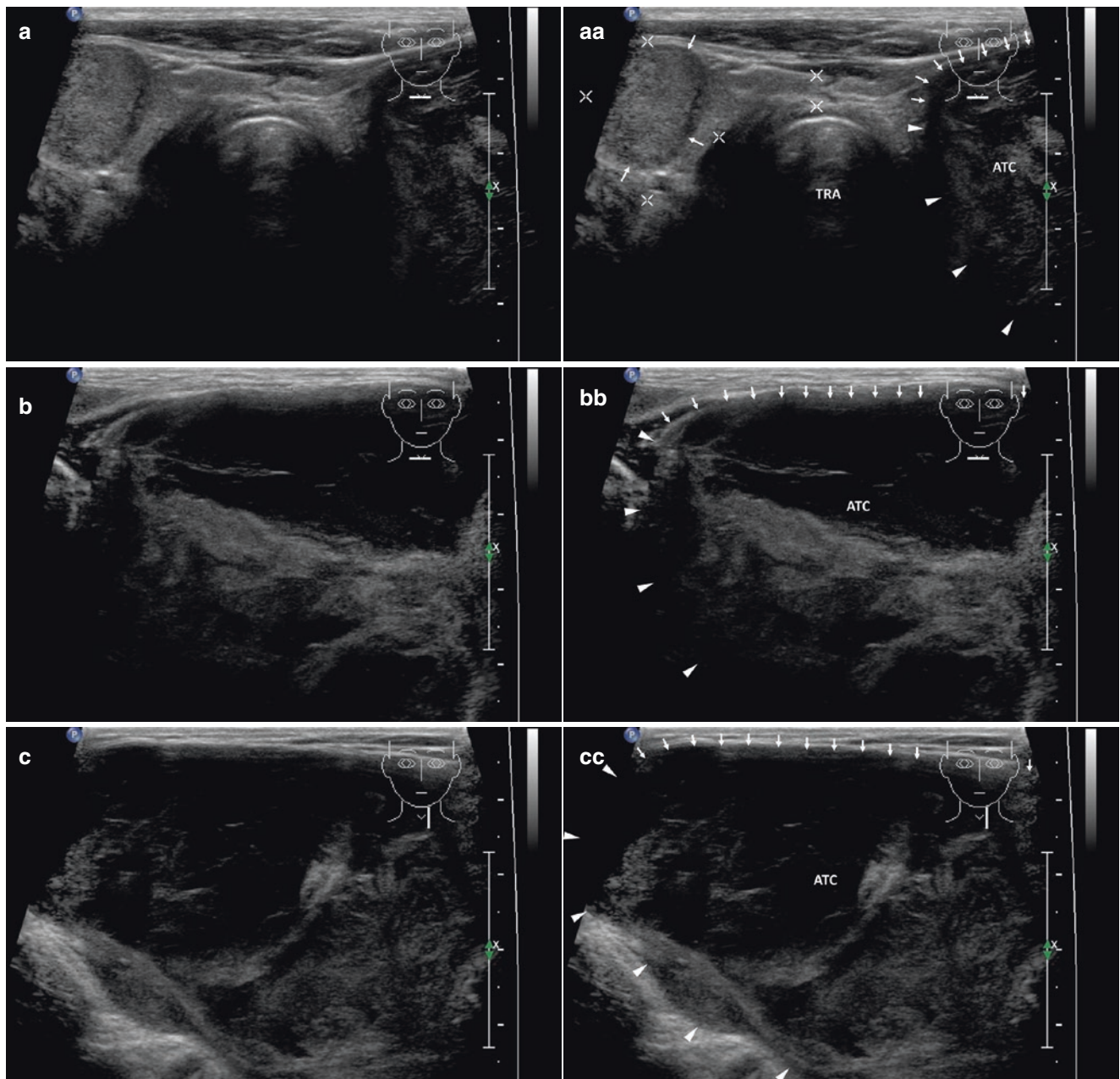


Fig. 17.2 (aa) A 56-year-old man with a giant anaplastic thyroid carcinoma—ATC (arrowheads) in the whole LL and isthmus with extra-thyroidal extension (ETE) into muscles, size $67 \times 56 \times 47$ mm and volume 90 mL, with acute thrombosis of the left IJV; *without metastatic lymph nodes*: ATC—markedly enlarged LL; coarse structure; mixed echogenicity with ill-defined hypoechoic areas and hyperechoic fibrous bands; ill-defined margin; tumor protrusion ventrally with interrupting continuity of the capsule and invasion into muscles (arrows); nonsuspicious solid nodule (arrows) in the LL; trachea deviated to the right; Tvol 106 mL, asymmetry—RL 16 mL and LL 90 mL; transverse, depth of penetration 5 cm. (bb) Detail of giant ATC (arrowheads) with ETE into muscles: solid; coarse structure; mixed echogenicity, in ventral part large hypoechoic area with hyperechoic septa (possible necrosis) and

others ill-defined hypoechoic areas in dorsal part; tumor protrusion ventrally interrupting continuity of the capsule and invasion into muscles (arrows); transverse. (cc) Detail of giant ATC (arrowheads) with ETE into muscles: solid; coarse structure; mixed echogenicity, in upper part large hypoechoic area with hyperechoic septa (possible necrosis); tumor protrusion ventrally interrupting continuity of the capsule and invasion into muscles (arrows); longitudinal. (dd) Detail of lateral part the LL with ATC (arrowheads) and acute thrombosis of the IJV: well-defined lateral border of ATC not invading into the IJV; IJV—enlarged lumen filled with markedly hypoechoic mass; non-compressible by probe; transverse. (ee) Detail of left IJV with acute thrombosis: enlarged lumen filled with markedly hypoechoic mass; non-compressible by probe; longitudinal

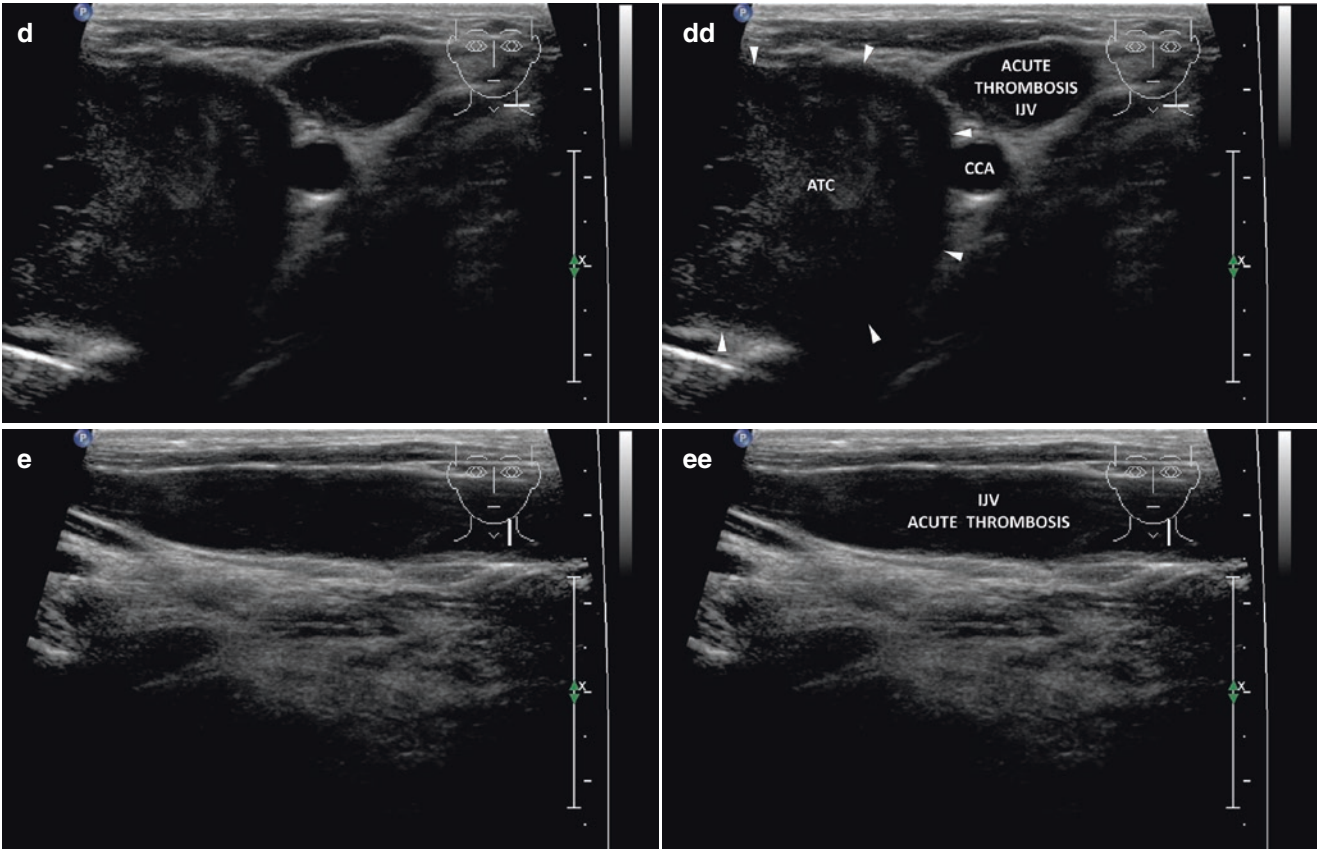


Fig. 17.2 (continued)

References

1. Sajid-Crockett S, Hershman J. Thyroid nodules and cancer in the elderly. In: De Groot LJ, Beck-Peccoz P, Chrousos G, Dungan K, Grossman A, Hershman JM, et al., editors. *Endotext* [Internet]. South Dartmouth, MA: MDText.com, Inc.; 2015.
2. Aldinger KA, Samaan NA, Ibanez M, Hill Jr CS. Anaplastic carcinoma of the thyroid: a review of 84 cases of spindle and giant cell carcinoma of the thyroid. *Cancer*. 1978;41(6):2267–75.
3. Lam KY, Lo CY, Chan KW, Wan KY. Insular and anaplastic carcinoma of the thyroid: a 45-year comparative study at a single institution and a review of the significance of p53 and p21. *Ann Surg*. 2000;231(3):329–38.
4. Lin JD, Chao TC, Chen ST, Weng HF, Lin KD. Characteristics of thyroid carcinomas in aging patients. *Eur J Clin Invest*. 2000;30(2):147–53.
5. Kebebew E, Greenspan FS, Clark OH, Woeber KA, McMillan A. Anaplastic thyroid carcinoma. Treatment outcome and prognostic factors. *Cancer*. 2005;103(7):1330–5.
6. Suh HJ, Moon HJ, Kwak JY, Choi JS, Kim EK. Anaplastic thyroid cancer: ultrasonographic findings and the role of ultrasonography-guided fine needle aspiration biopsy. *Yonsei Med J*. 2013;54(6):1400–6.
7. Lee JW, Yoon DY, Choi CS, Chang SK, Yun EJ, Seo YL, et al. Anaplastic thyroid carcinoma: computed tomographic differentiation from other thyroid masses. *Acta Radiol*. 2008;49(3):321–7.
8. Green LD, Mack L, Pasieka JL. Anaplastic thyroid cancer and primary thyroid lymphoma: a review of these rare thyroid malignancies. *J Surg Oncol*. 2006;94(8):725–36.
9. Us-Krasovec M, Golouh R, Auersperg M, Besic N, Ruparcic-Oblak L. Anaplastic thyroid carcinoma in fine needle aspirates. *Acta Cytol*. 1996;40(5):953–8.

18.1 Other Malignancies in Thyroid Gland and Cervical Lymph Nodes: Primary Thyroid Lymphoma

18.1.1 Essential Facts

- In a large Swedish retrospective study (between 1959 and 1981) of 829 patients with chronic lymphocytic thyroiditis (CLT), the risk of malignant thyroid lymphoma was greatly increased, with an estimated relative risk of 67 (4 observed vs. 0.06 expected). There was no increased risk among patients with colloid goiter [1].
- Primary thyroid lymphoma (PTL) is a rare cause of malignancy, accounting for <5% of thyroid malignancies and <2% of extranodal lymphomas, with an annual estimated incidence of 2 per 1 million. Women are more commonly affected than men (2–8:1). Patients typically present in the sixth or seventh decade of life, with men often presenting at a younger age than women [2].
- Most thyroid lymphomas are non-Hodgkin's lymphomas (NHLs) of B-cell origin. Patients with Hashimoto's thyroiditis (HT) are at greater risk for developing PTL, with a relative risk of 67 compared to those without HT [2].
- The transformation from HT to PTL occurs in about 0.5% of cases. Approximately 60–90% of PTL cases arise in a background of HT [2].
- Clinical manifestation of PTL is known as a rapidly growing mass arising in the middle-age-to-elderly phase of life, in hitherto asymptomatic female patients with a history of longstanding HT [3].
- Although PTL may grow suddenly and be life-threatening due to airway obstruction, early detection and diagnosis followed by appropriate treatment can lead to favorable prognosis [2, 3].
- In a retrospective study by Graff-Baker et al. of 1408 patients with PTL identified over 32 years of follow-up, a total of 88% had stage I–II disease; median survival was 9.3 years, a 5-year survival of 90% [4].

18.1.2 US Features of Primary Thyroid Lymphoma [3, 5]

- PTL can be divided into three types based on internal echoes, borders, and posterior echoes: nodular, diffuse, or mixed.
- Enhanced posterior echoes are present in all three types and help to distinguish lymphoma from other types of thyroid lesions.
 - In the nodular type (Fig. 18.1aa), the goiter is usually unilateral with internal hypoechoic, homogeneous, and pseudocystic lesion. Well-defined borders separate lymphomatous lesions from nonlymphomatous tissues.
 - In the diffuse type, the goiter is bilateral and diffuse heterogeneous exceedingly hypoechoic parenchyma with intervening echogenic septa-like structures. In contrast to the nodular type, the border between the lymphoma and nonlymphomatous tissue could not be clearly identified.
 - The mixed type of lymphoma shows multiple patchy, hypoechoic lesions.
- US findings of typically longstanding HT indicate atrophic or smaller thyroid glands with heterogeneous parenchyma.
- In a prospective study of 165 patients, Ota et al. suspected PTL based on the above listed US characteristics; $\approx 48\%$ were pathologically confirmed as having lymphoma. The positive predictive value of US examination was higher for the nodular type, at $\approx 65\%$, and the mixed type, at $\approx 63\%$, than for the diffuse type, at $\approx 34\%$, likely due to close resemblance to HT [5].
- In a retrospective 15-year review of US findings of 13 patients with PTL, Nam et al. [3] found that 15% showed a nodular pattern, 77% diffuse, and 8% mixed. Three patients had secondary thyroid lymphoma.
- Several studies reported that PTL had associated disease in cervical lymph nodes and the mediastinum in 69% and 73% of patients, respectively [6, 7]. To the contrary, in the Nam et al. [3] study any patient was found with a notable neck lymphadenopathy.
- Caution! Diffuse type of PTL shows US pattern, which is also typical of severe HT and hypothyroidism. A PTL can be considered only when clinical symptoms of a rapidly enlarging mass appear. Subtle US findings in asymptomatic patients make identification of thyroid lymphomas difficult [3].
- Caution! Secondary thyroid lymphomas show markedly hypoechoic masses and mimic PTC. In both cases FNAB is necessary [3].
- Caution! Sometimes PTL may behave very aggressively, e.g. show rapid growth and invasion of adjacent structures. US shows heterogeneous hypoechoic solid mass occupying the entire thyroid lobe, small internal calcifications, and irregular margin. Extrathyroidal invasion and extension to the wall of trachea or the obturation of common carotid artery is possible. These findings imply ATC with tracheal and vascular invasion [8].

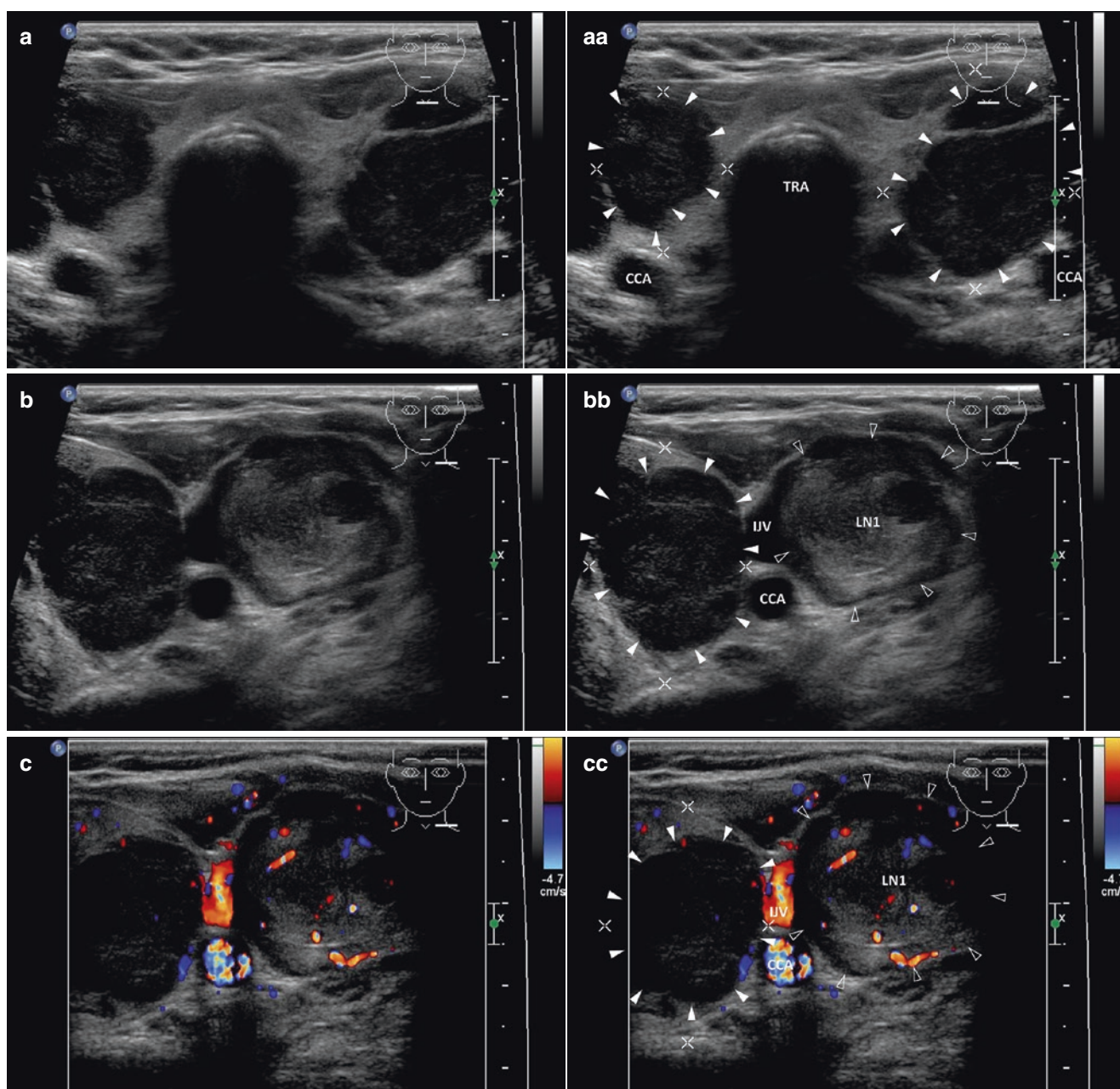


Fig. 18.1 (aa) A 70-year-old woman with secondary Non-Hodgkin lymphoma of thyroid gland and malignant cervical lymph nodes (LNs): suspicious solid nodule (*arrowheads*) in the RL, size $20 \times 18 \times 16$ mm and volume 3 mL—round shape; inhomogeneous structure; markedly hypoechoic; microlobulated margin; suspicious solid nodule (*arrowheads*) in the LL, size $33 \times 24 \times 20$ mm and volume 8 mL—ovoid shape; inhomogeneous structure; markedly hypoechoic; microlobulated margin; Tvol 48 mL, RL 21 mL, and LL 27 mL; transverse; depth of penetration 4.5 cm. (bb) Detail of a suspicious nodule in the LL and malignant LN next to the left IJV at level C-III: solid nodule (*arrowheads*)—inhomogeneous structure; markedly hypoechoic; microlobulated margin; malignant LN1 (*blank arrowheads*)—oval shape; size 23×20 mm; coarse structure; mixed echogenicity, mostly hyperechoic with hypoechoic areas; transverse. (cc) Detail of suspicious nodule in the LL and malignant LN1 next to the left IJV at level C-III, CFDS: solid nodule (*arrowheads*)—minimal vascularity, *pattern 0*; malignant LN (*blank arrowheads*)—mixed vascularity; transverse. (dd) Detail of large malignant LN2 (*blank arrowheads*), size $40 \times 27 \times 19$ mm and volume 11 mL, next left IJV at level C-II: oval shape; homogeneous

structure; markedly hypoechoic with transverse fibrous band; transverse. (ee) Detail of large malignant LN2 (*blank arrowheads*) next left IJV at level C-II, CFDS: increased hilar and central vascularity; transverse. (ff) Detail of large malignant LN2 next left IJV at level C-II: elliptical shape; size 40×19 mm, L/S ratio ≈ 2 (*not pathological*); homogeneous structure; markedly hypoechoic; next to another two small round hypoechoic LN3, LN4 size of 11 and 12 mm; longitudinal. (gg) Detail of suspicious nodule (*arrowheads*) in the RL: round shape; inhomogeneous structure; hypoechoic; microlobulated margin; transverse. (hh) Detail of suspicious nodule (*arrowheads*) in the RL, CFDS: increased hilar end peripheral vascularity, *pattern II*; transverse. (ii) One year after successful chemotherapy, large hypoechoic thyroid nodules and malignant cervical lymphadenopathy disappeared. US overall view of small multinodular goiter: small, solid, hyperechoic nodules (*arrows*) in both lobes; size from 5 to 8 mm; Tvol 18 mL, RL 9 mL, and LL 9 mL; transverse. (jj) Detail of the RL: small, solid, hyperechoic nodules (*arrows*); longitudinal. (kk) Detail of the LL: small, solid, hyperechoic nodules (*arrows*); longitudinal

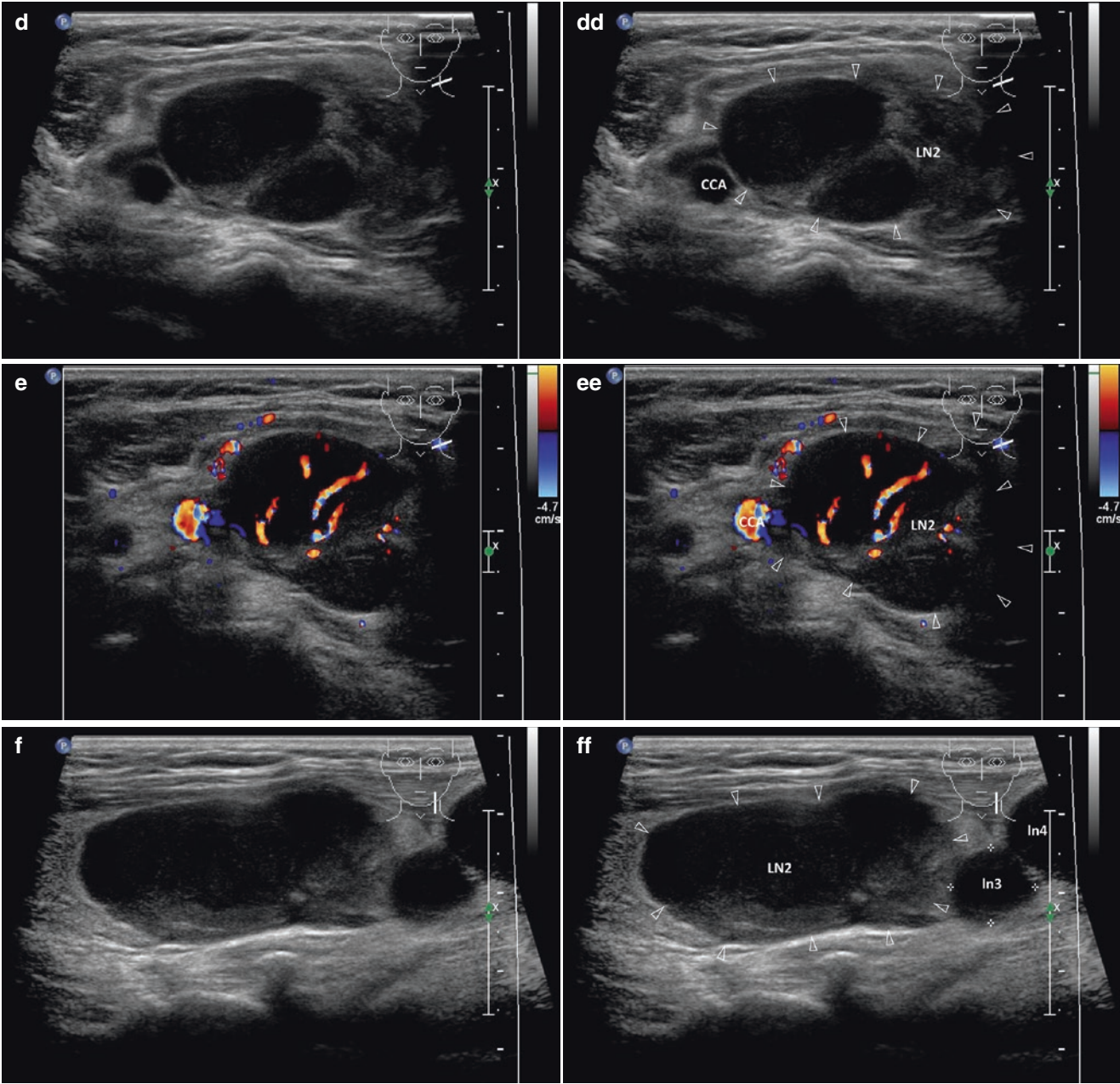
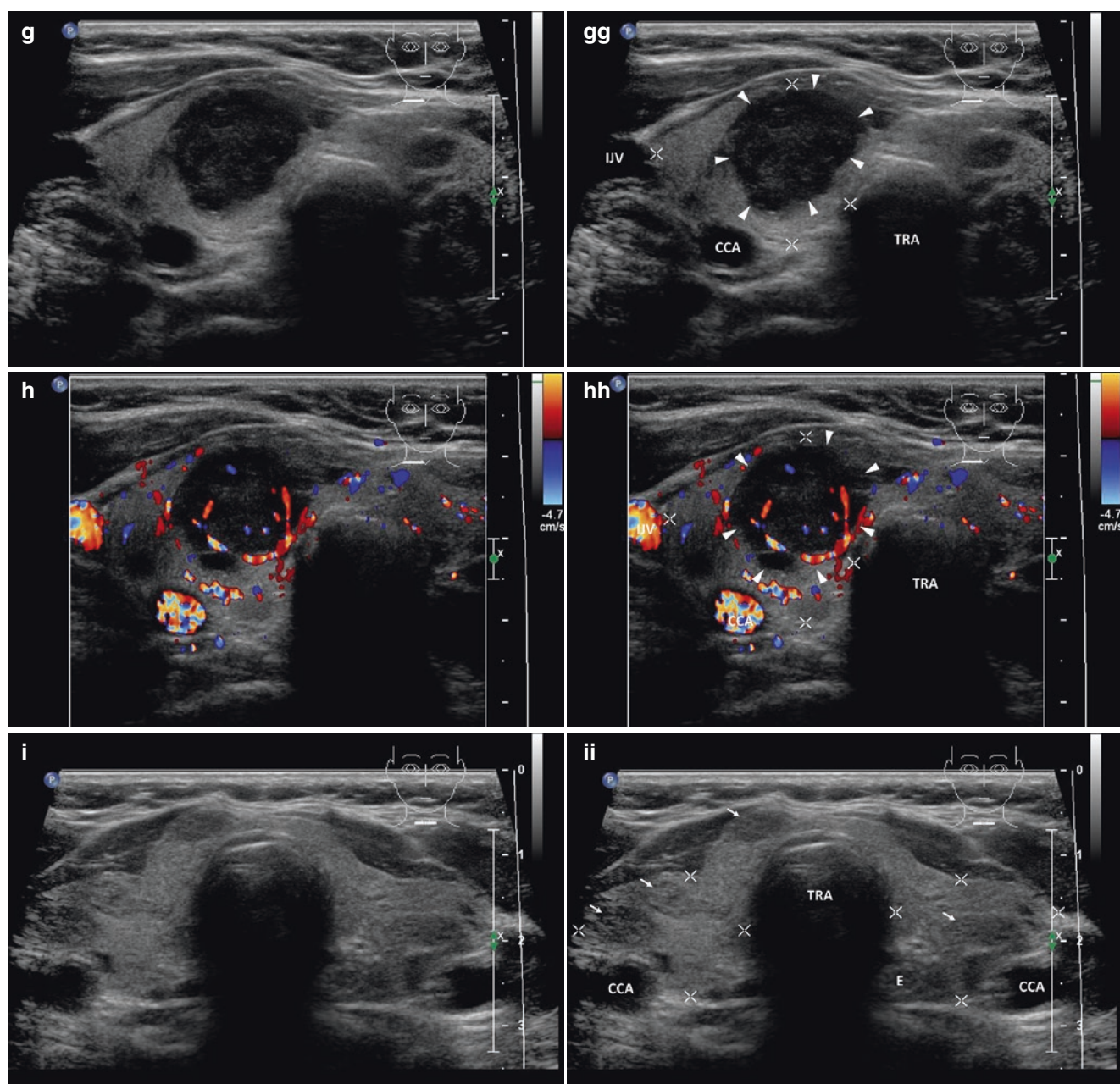


Fig. 18.1 (continued)

**Fig. 18.1** (continued)

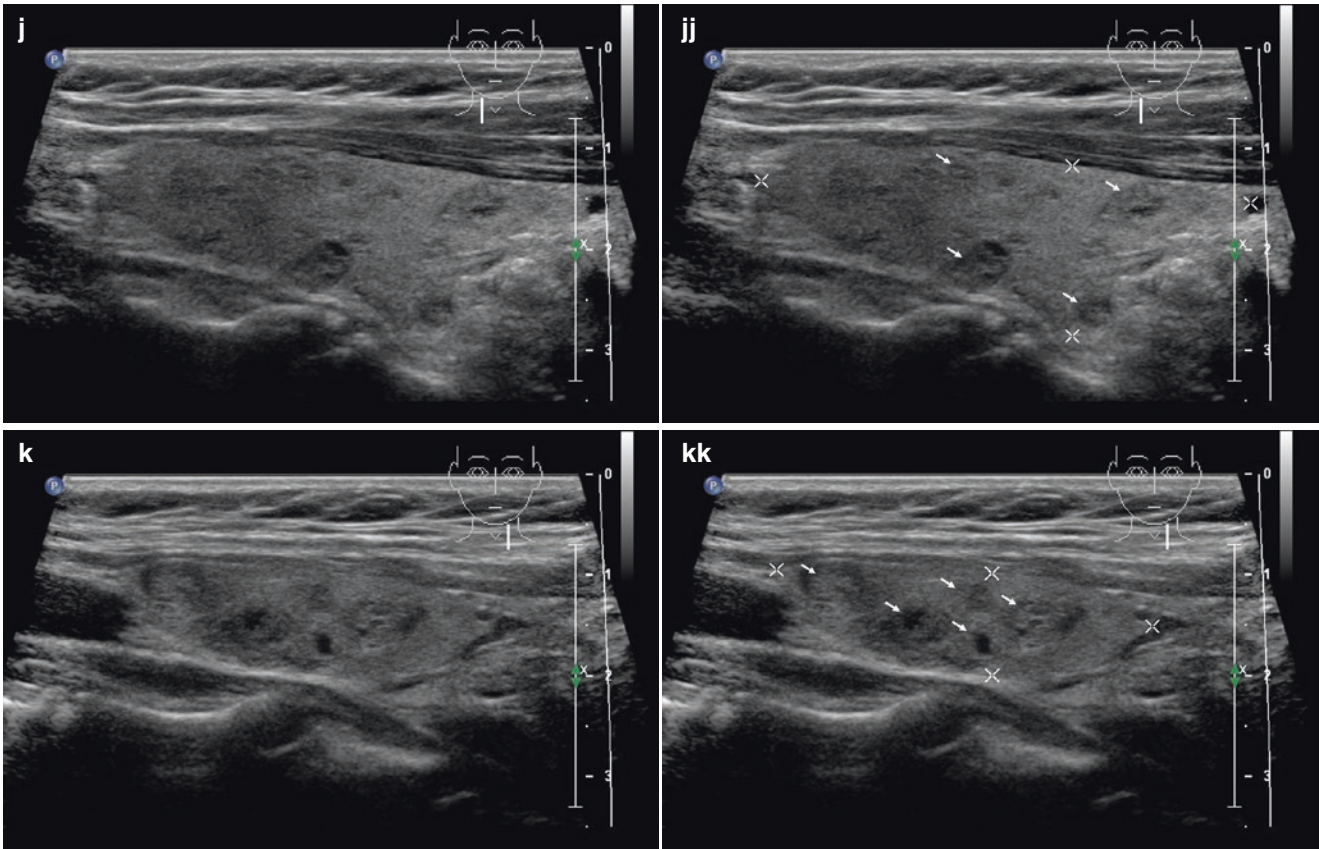


Fig. 18.1 (continued)

18.2 Other Malignancies in Thyroid Gland and Cervical Lymph Nodes: Extramedullary Plasmacytoma

18.2.1 Essential Facts

- A retrospective review by Bachar et al. analyzing 68 patients with head and neck extramedullary plasmacytoma (EMP) between 1960 and 2000 reported the 5-year local recurrence-free rate of 81%, 5-year regional recurrence of 5%, multiple myeloma development in 23% of patients, and the 5-year survival of 76% [9].
- In a study by Galieni et al. of 46 patients with EMP, the most frequent EMP localization was in the upper airways (80%). Other locations were the lymph nodes, thyroid, skin, stomach, and brain. Clinical symptoms were related to the site of presentation; the median time between appearance and diagnosis was 7.5 months. Median age at diagnosis was 55 years (range 16–80). Disorder was approximately twice as common in males as in females. Twenty-one percent of patients had a monoclonal component. Therapeutic strategy was surgery or local radiotherapy. Eighty-five percent of patients achieved complete remission. Local recurrence or recurrence at other sites occurred in 7.5% and 10%, respectively. Fifteen-year survival rate was 78%. Fifteen percent of patients developed multiple myeloma [10].
- EMP of the thyroid gland (Fig. 18.2) is a very rare disease, constituting 1.4% of the EMPs [11].
- EMPs represent less than 5% of all plasmacytomas. A fundamental condition for establishing the correct diagnosis of solitary EMP (including these of the thyroid gland) is to rule out multiple myeloma. Thus, normal bone marrow biopsy, absence of skeletal lytic lesions, and absence of a monoclonal immunoglobulin peak confirm the EMP diagnosis [12].

18.2.2 US Features of Extramedullary Plasmacytoma in the Thyroid Gland

- Our knowledge of this topic is based upon infrequent case reports. On US scan, there are present only nonspecific signs for suspicious nodules (see more in Chap. 24), as markedly hypoechoic and hypervascular lesion. US findings should be considered in context of clinical and laboratory examination.
- Case report 1: A 52-year old female with 6 months history of a progressively enlarging painless goiter with no toxic or pressure symptoms. Neck US confirmed enlargement of the thyroid gland with the presence of an 18 mm solitary isthmic nodule, heterogeneous, hypoechoic, and hypervascular, with a 20 mm lymph node on the left cervical area. Cytology from performed FNAB was consistent with a lymphoplasmacytic lymphoma or a plasmacytoma [12].
- Case report 2: A 60-year old male presented with a neck mass, hoarseness, and dysphagia of 3-month duration. On clinical examination the thyroid gland was diffusely enlarged, more prominent on the right side, firm, and painless. Thyroid profile showed hypothyroidism. US examination with large hypoechoic lesions at background of Hashimoto's thyroiditis in both lobes. Performed FNAB showed atypical epithelial cells on a background of amyloid and suggested medullary carcinoma (MTC). Histology after total thyroidectomy showed an extensive infiltration of neoplastic plasma cells against a background of Hashimoto's thyroiditis, with a bizarre Hurthle cell change. Immunohistochemistry on the histology sections confirmed the diagnosis of solitary EMP [11].
- Both cases of EMP show that cytology is challenging and misinterpretation is possible. Amyloid-like material can be associated with MTC. However other possibilities like lymphoproliferative lesions and plasmacytomas must be kept in mind [11, 12].
- EMP should be considered in the differential diagnosis of a neck mass that yields discohesive cells associated with amyloid-like material obtained by FNAB [13].

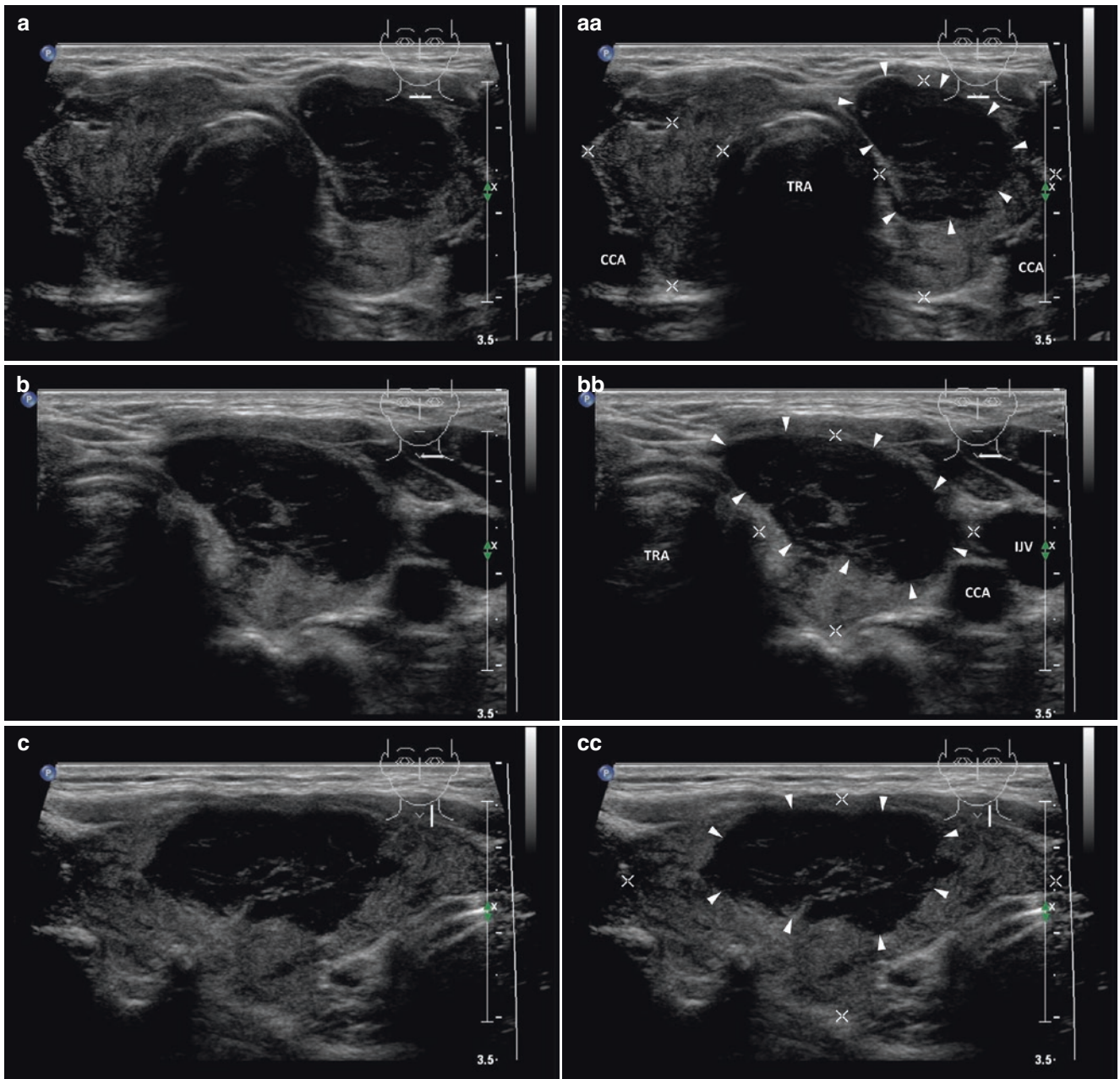


Fig. 18.2 (aa) A 58-year-old woman with Hashimoto's thyroiditis (HT) and a suspicious solitary medium-sized nodule (*arrowheads*) in the LL, size $23 \times 28 \times 17$ mm and volume 8 mL. Cytology revealed extramedullary plasmacytoma. US overall view: "taller-than-wide" shape; solid; inhomogeneous structure; markedly hypoechoic with hyperechoic fibrous septa; microlobulated margin; thyroid gland with HT—inhomogeneous, sporadically hypoechoic micronodular struc-

ture; Tvol 23 mL, RL 9 mL, and LL 14 mL; transverse. (bb) Detail of suspicious medium-sized nodule (*arrowheads*): inhomogeneous structure; markedly hypoechoic with hyperechoic fibrous septa; microlobulated margin; transverse. (cc) Detail of suspicious medium-sized nodule (*arrowheads*): inhomogeneous structure; markedly hypoechoic with hyperechoic fibrous septa; microlobulated margin; longitudinal

18.3 Other Malignancies in Thyroid Gland and Cervical Lymph Nodes: Malignant Cervical Lymph Nodes, Primary Outside the Thyroid Gland

18.3.1 Essential Facts

- Malignant cervical lymph nodes (LN) are either found in hematological malignancies or as metastases of head and neck tumors (including thyroid cancer) [14].
- In patient with confirmed head and neck tumor, presence of a unilateral metastatic LN reduces the 5-year survival rate by 50%, whereas the presence of bilateral metastatic LN reduces the 5-year survival rate to 25% [15].
- Oral cancer is one of the most common types of tumor in the head and neck (38%) and local metastatic LN occurs in about 40% of this entity [16].
- Lymphoma (Figs. 18.7 and 18.8) is the second-most common neoplasm of the head and neck region and should be considered in the differential diagnosis of any lesion in this region. As the treatment options differ, accurate identification of the nature of the diseases is essential [14, 17].
- In a study by Jones et al., the primary site of secondary metastatic cervical LNs was discovered mostly in the head and neck region, in $\approx 76\%$ of patients. Primary sites other than head and neck occurred in $\approx 11\%$ and no primary tumor was found in $\approx 13\%$ of patients [18].
- For patients with post-radiation neck fibrosis, US examination is highly beneficial compared to clinical examination, with sensitivity $\approx 97\%$ resp. $\approx 73\%$ [19].
- US of suspicious LN is characterized by high sensitivity $\approx 97\%$ and low specificity $\approx 32\%$. However, when US findings are combined with US-FNAB, the specificity is as high as 93% [20].
- PET/CT has the best results in evaluation of metastatic cervical LN, sensitivity of $\approx 92\%$, specificity of $\approx 99\%$, and accuracy of $\approx 97\%$, and PET/CT has higher accuracy of $\approx 85\%$ for the pathologic nodal classification over the clinical examinations of $\approx 68\%$ or PET of $\approx 70\%$ [21].
- Common primary LN metastatic sites of head and neck tumors are [14]:
 - Along the internal jugular vein: thyroid carcinomas; pharyngeal, laryngeal, and esophageal tumors.
 - Below the mandible: oral squamous cell carcinoma of the tongue and tonsils.
 - The upper neck area and the posterior triangle: nasopharyngeal carcinoma.
- Above the clavicle and behind the sternocleidomastoid muscle (posterior triangle): adenocarcinomas in the chest and abdominal cavity—breast (Fig. 18.4), lung (Fig. 18.6), gastrointestinal (Fig. 18.3), and genitourinary tracts (Fig. 18.5).

18.3.2 US Features of Metastatic Lymph Nodes [14]

- Size:
 - Larger LNs tend to have a higher risk of malignancy.
 - Caution! Reactive LNs can be as large as metastatic.
 - Different cut-offs of the nodal size to differentiate reactive and metastatic nodes have been reported (5 mm, 8 mm, and 10 mm).
 - LNs size follow-up is useful in two clinical situations: (1) increase in nodal size on serial examinations in a patient with a known carcinoma is highly suspicious for metastatic involvement; (2) serial reduction in nodal size is a useful indicator in monitoring patient's response to treatment.
- Shape:
 - Metastatic LNs are spherical, short-to-long axis ratio (S/L ratio) ≈ 1.0 [14], or long-to-short axis ratio (L/S) ≈ 1.0 (Fig. 18.4bb) [22, 23].
 - Eccentric cortical hypertrophy, due to focal tumor infiltration within the LN.
 - Caution! Submandibular benign and reactive LNs are also often oval-to-spherical.
- Border:
 - Metastatic LNs tend to have sharp borders (Fig. 18.4bb).
 - Advanced stages may demonstrate ill-defined borders, indicating extracapsular spread.
- Echogenicity:
 - Metastatic LNs are predominantly hypoechoic relative to the adjacent musculature (Fig. 18.4bb).
 - Caution! To the contrary, metastatic LNs from PTC are usually hyperechoic.
- Hilus sign:
 - Metastatic lymph nodes usually do not show any echogenic hilus (Fig. 18.4bb).
 - Caution! Echogenic hilus may also be found in malignant LN. Therefore, the presence/absence of echogenic hilus cannot be used as the sole criterion for evaluation of cervical LNs.
- Intrnodal necrosis:
 - Cystic necrosis (Figs. 15.21ff, 19.5, and 19.10) is the more common form, which appears as an echolucent area within LN.
 - Coagulative necrosis is the less common sign, and appears as an echogenic focus within LN, and does not produce acoustic shadowing.
 - Intrnodal necrosis may be found in metastatic or tuberculous LNs.
- Calcifications:
 - Calcification within LN is uncommon.
 - Caution! To the contrary, metastatic cervical LN from PTC tend to show microcalcifications (punctate calcification), located on periphery with acoustic shadowing.

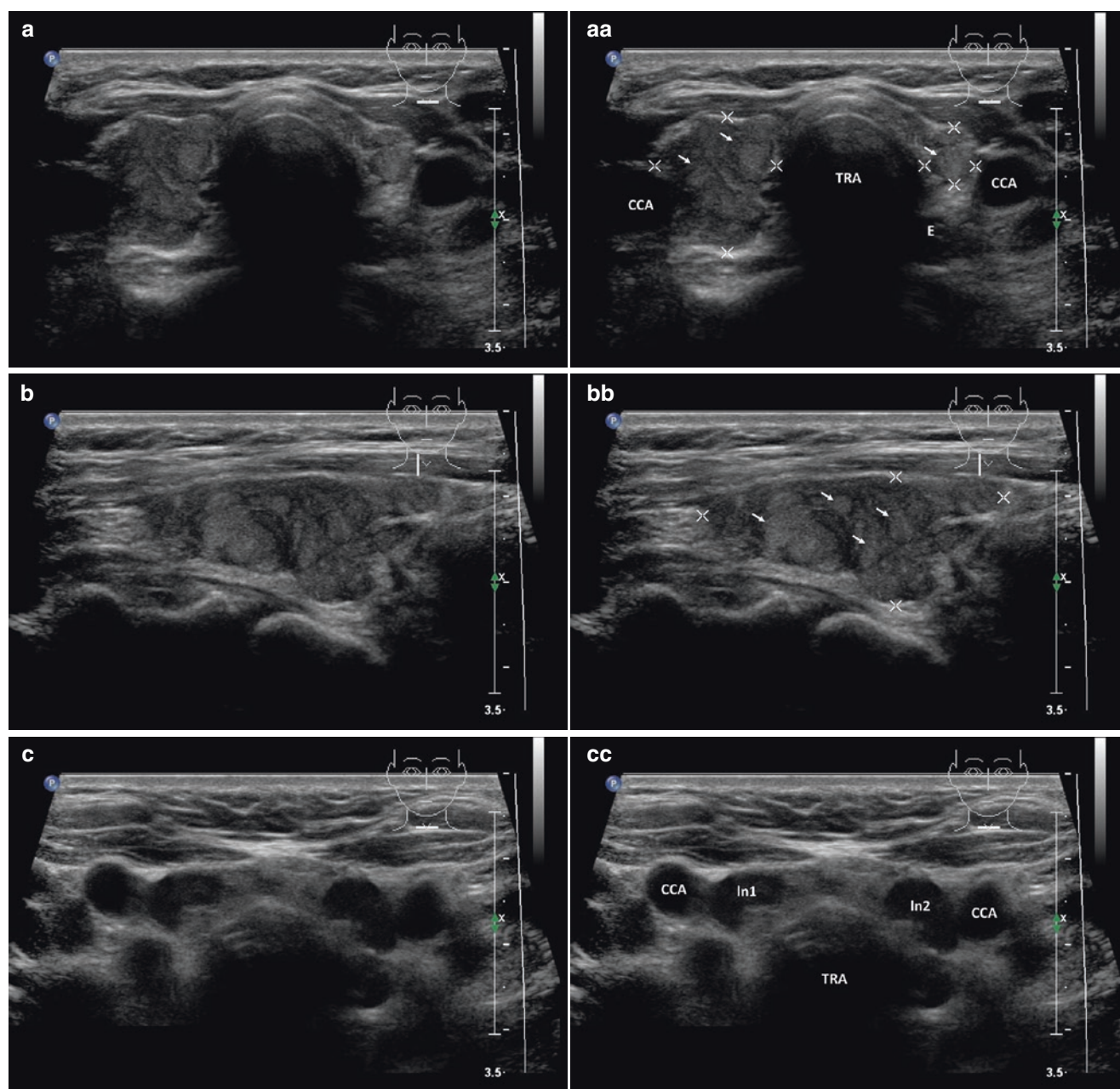


Fig. 18.3 (aa) A 57-year-old woman with a gastric cancer and metastatic cervical and supraclavicular lymph nodes (LN). US appearance of small Hashimoto's thyroiditis (HT) with non-suspicious solid nodules (FNAB not performed): inhomogeneous hypoechoic micronodular structure; sporadically small, solid, hyperechoic nodules (*arrows*); Tvol 7 mL, asymmetry—RL 5 mL and LL 2 mL; transverse. (bb) Detail of RL with HT and nodules: sporadically small, solid, hyperechoic nod-

ules (*arrows*), size from 5 to 10 mm; longitudinal. (cc) Detail of two metastatic LNs at jugulum at level C-VII: Ln1, Ln2—elliptical shape; homogeneous structure; hypoechoic; no hilus sign; size 9×6 mm and 9×7 mm; transverse. (dd) Detail of the five metastatic LNs in left supraclavicular region: Ln3–Ln6—elliptical or oval shape; homogeneous structure; hypoechoic, no hilus sign; size 9×6 mm and 9×7 mm; transverse

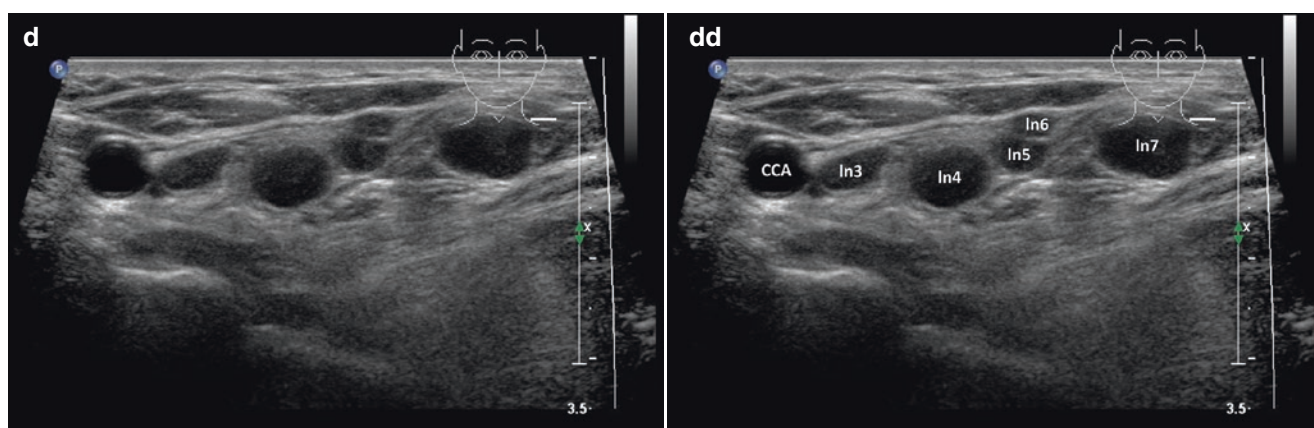


Fig. 18.3 (continued)

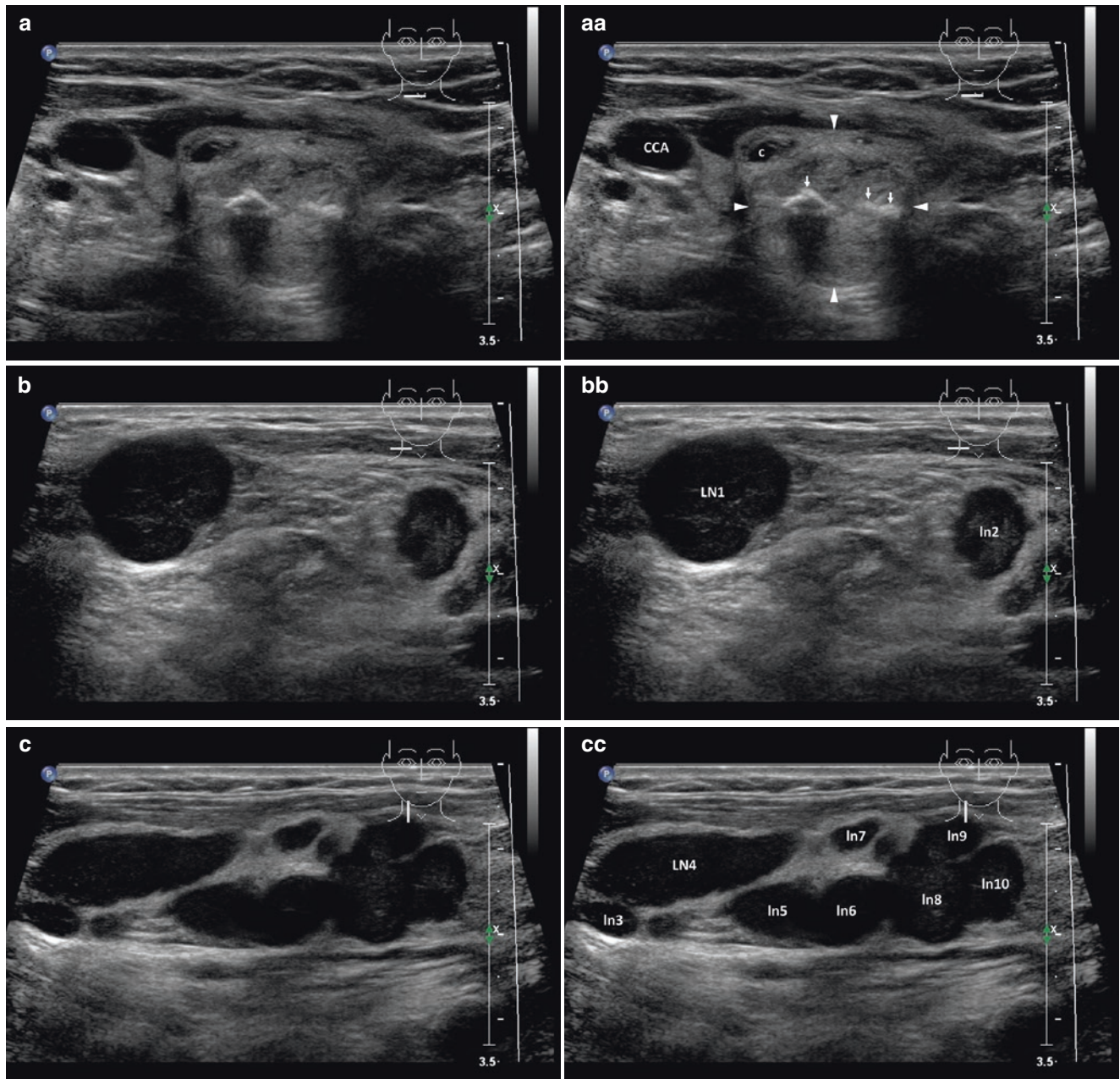


Fig. 18.4 (aa) A 57-year-old woman post right breast mastectomy for cancer and with metastatic lymph nodes (LN) in the right neck region. US finding of solitary non-suspicious complex nodule (*arrowheads*) with calcifications in the RL, size $17 \times 17 \times 16$ mm and volume 2 mL (FNAB—benign cytology): round shape; coarse structure; hyperechoic; intranodular curvilinear calcifications (*arrows*) with acoustic shadow; transverse. (bb) Detail of the two metastatic LNs, large LN1 size

$22 \times 18 \times 15$ mm and volume 3 mL and small LN2 size 11×7 mm at level C-V: oval shape; homogeneous structure; hypoechoic; no hilus sign; transverse. (cc) Detail of cluster of approximately eight metastatic LNs size from 5 mm to 25 mm at level C-II, III, IV: LN3–LN10—elliptical or oval shape; homogeneous structure; hypoechoic, no hilus sign; longitudinal

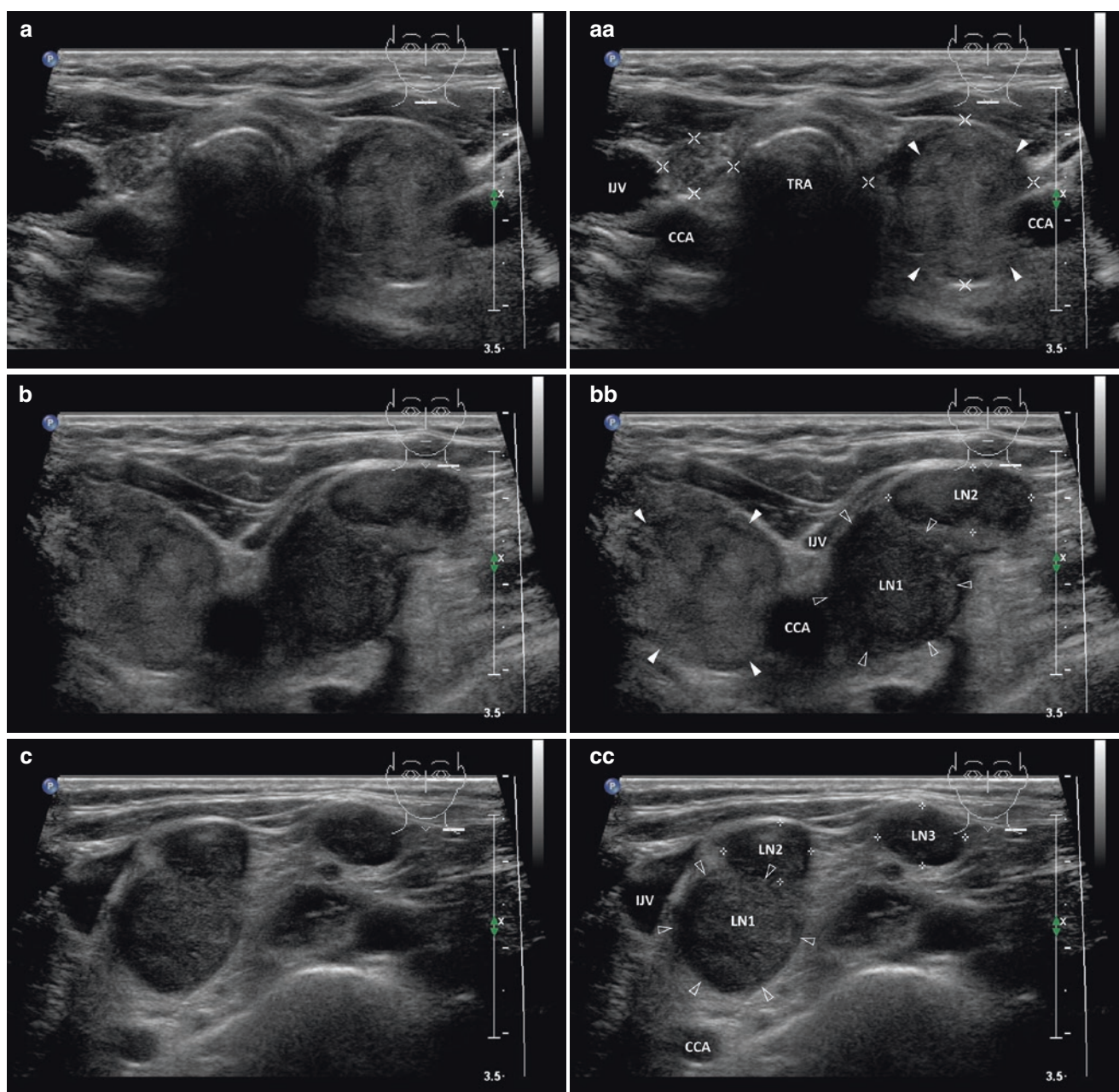


Fig. 18.5 (aa) A 66-year-old woman after right nephrectomy for cancer and with metastatic lymph nodes (LN) in the left low neck at level C-IV and supraclavicular region. US appearance of small Hashimoto's thyroiditis (HT) with solitary non-suspicious medium-sized solid nodule (*arrowheads*) in the LL, size $27 \times 16 \times 15$ mm and volume 3.5 mL (FNAB—benign cytology): round shape; coarse structure; hyperechoic, irregular thin halo sing; RL—structure of atrophic HT; Tvol 11 mL, asymmetry—RL 3 mL and LL 8 mL; transverse. (**bb**) Detail of solitary medium-sized nodule in the LL and two metastatic LNs next to the left CCA and IJV at level C-IV: solid nodule (*arrowheads*)—coarse struc-

ture; hyperechoic, irregular thin halo sing; metastatic LN1 (*blank arrowheads*)—round shape, size 16×15 mm; metastatic LN2 (*marks*)—elliptical shape, size 16×7 mm; homogeneous structure; slightly hypoechoic; no hilus sign; both LNs compress the left IJV; transverse. (**cc**) Detail of three metastatic LNs—LN1, LN2 at level C-IV and LN3 at left supraclavicular region: LN1, LN2 next to the left IJV—oval and elliptical shape; LN1 (*blank arrowheads*) hyperechoic, LN2 (*marks*) slightly hypoechoic; no hilus sign; small LN3 (*marks*), size 10×7 mm—oval shape; homogeneous structure; hypoechoic; no hilus sign; transverse

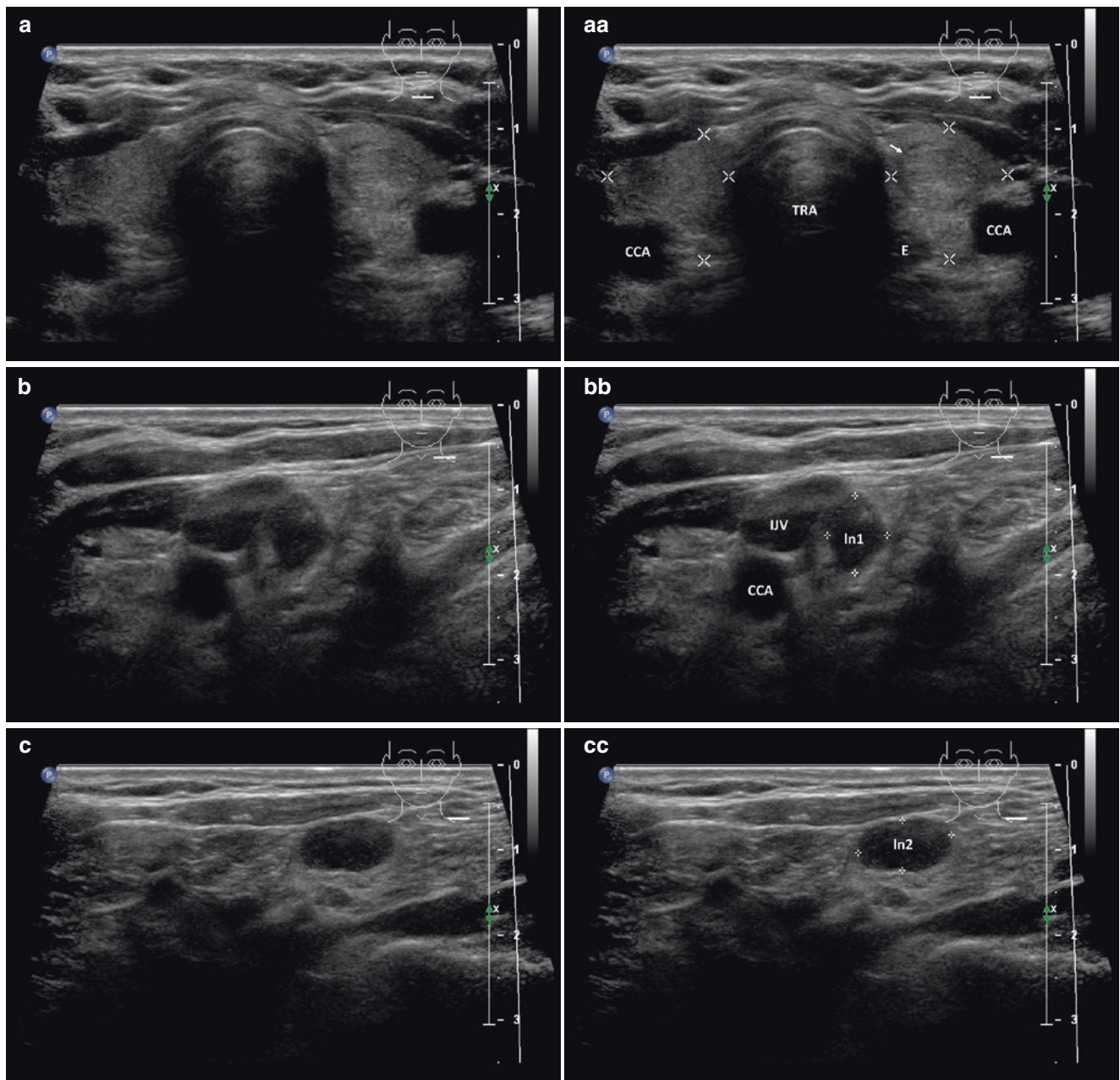
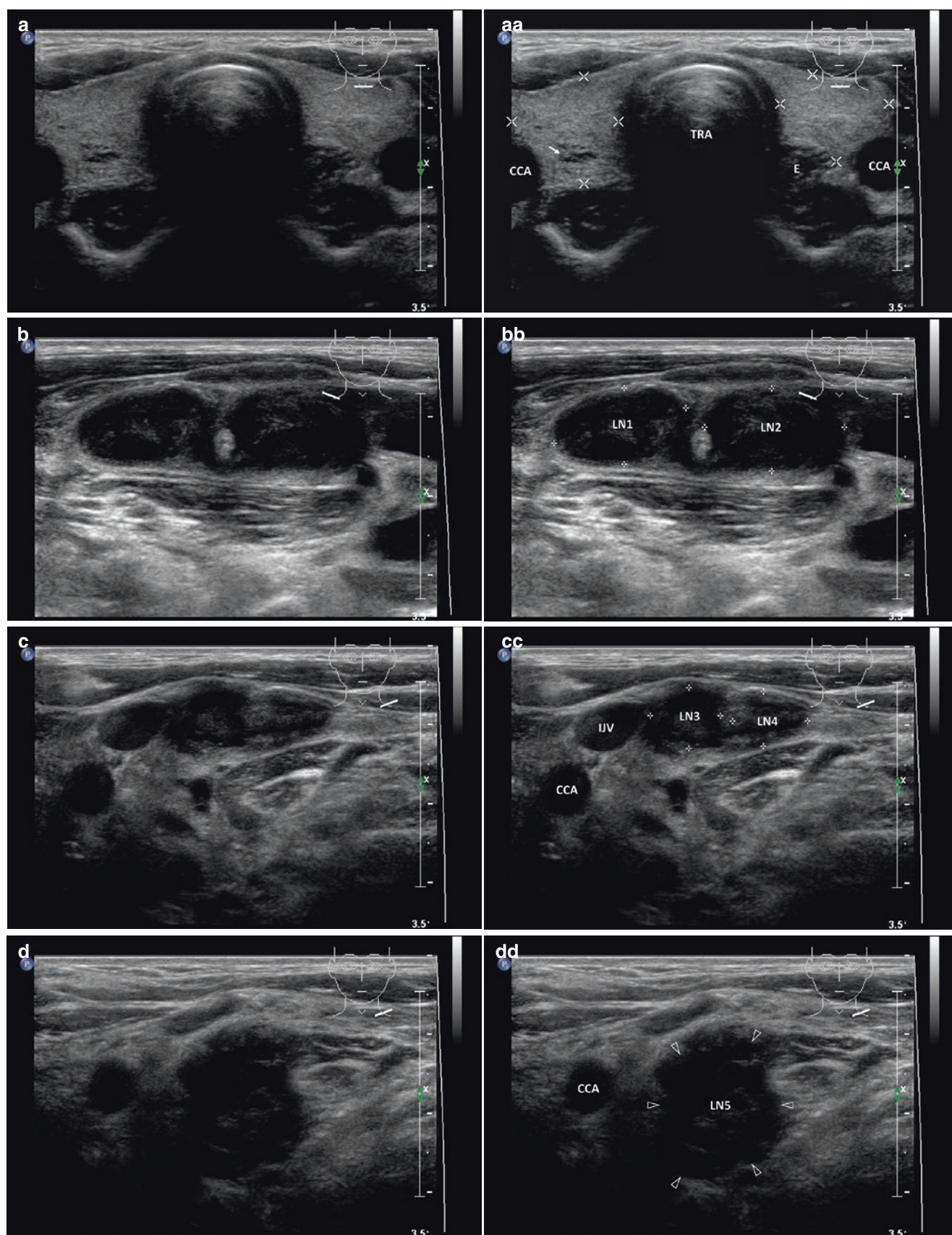


Fig. 18.6 (aa) A 63-year-old woman with left bronchial cancer and with metastatic lymph nodes (LN) in the left low neck at level C-IV and supraclavicular region. US finding of solitary non-suspicious small solid nodule (*arrow*) in the LL, size $12 \times 10 \times 8$ mm and volume 0.5 mL (FNAB—benign cytology); round shape; homogeneous structure; hyperechoic, thin halo sing; Tvol 10 mL, RL 5 mL and LL 5 mL; trans-

verse. (bb) Detail of small metastatic LN, size $9 \times 7 \times 5$ mm, volume 0.2 mL next to the left IJV at level C-IV: Ln1 (*marks*)—oval shape; homogeneous structure; hypoechoic; no hilus sign; transverse. (cc) Detail of small metastatic LN, size $12 \times 10 \times 6$ mm, volume 0.4 mL at left supraclavicular region: Ln2 (*marks*)—elliptical shape; homogeneous structure; hypoechoic; no hilus sign; transverse

Fig. 18.7 (aa) A 35-year-old woman with Hodgkin lymphoma and with malignant lymph nodes (LN) in right and left low neck at level C-IV and supraclavicular regions. US appearance of solitary non-suspicious small solid nodule (*arrow*) in the RL, size $7 \times 6 \times 4$ mm and volume 0.1 mL (FNAB not performed): ovoid shape; inhomogeneous structure; hyperechoic; sporadic tiny cystic cavities; thin halo sing; Tvol 14 mL, RL 7 mL, and LL 7 mL; transverse. (bb) Detail of two malignant LNs in the right supraclavicular region: elliptical shape, LN1 (*marks*) size of 18×10 mm, L/S ratio > 2 and LN2 (*marks*) size

21×12 mm, L/S ratio > 2 (*not pathological*); homogeneous structure; hypoechoic; no hilus sign; transverse. (cc) Detail of two malignant LNs in the left supraclavicular region: oval shape, LN3 (*marks*) size 11×10 and LN4 (*marks*) size 9×7 mm; homogeneous; hypoechoic; no hilus sign; transverse. (dd) Detail of another one malignant LN5 (*blank arrowheads*) deep in the jugulum next to the left CCA at level C-VII: ovoid shape, size 18×15 mm; inhomogeneous structure; hypoechoic; no hilus sign; lobulated margin; transverse



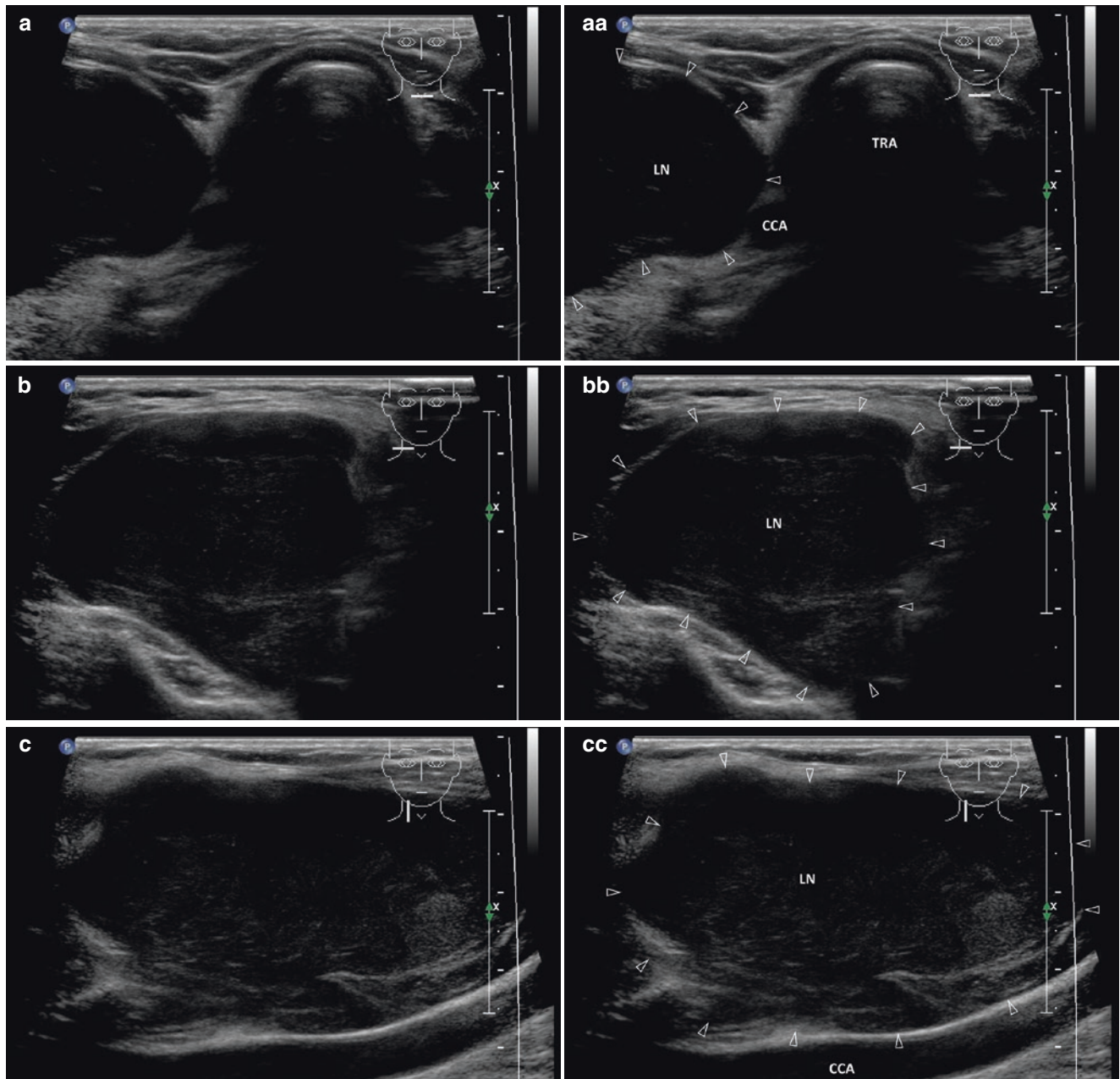


Fig. 18.8 (aa) A 64-year-old woman with Non-Hodgkin lymphoma and a large mass palpable for approximately 2 weeks in the right low neck region. Patient's history: 26 years post total thyroidectomy for multinodular goiter. US appearance of giant malignant lymph node—LN (*blank arrowheads*), size $69 \times 44 \times 37$ mm and volume 60 mL located in front of the right CCA at C-III, IV level and extends into the right thyroid bed as far as trachea: oval shape; solid; inhomogeneous structure; mostly hypoechoic; no hilus sign; empty left thyroid bed

without thyroid remnants; transverse. (bb) Detail of giant malignant LN (*blank arrowheads*) in front of the right CCA and extending into the right thyroid bed: oval shape; solid; inhomogeneous structure; mostly hypoechoic; no hilus sign; transverse. (cc) Detail of giant malignant LN (*blank arrowheads*) in front of the right CCA and extending into the right thyroid bed: ovoid shape; solid; inhomogeneous structure; mostly hypoechoic; sporadic fibrous bands; no hilus sign; longitudinal

owing (Fig. 15.16bb). Metastatic LNs from MTC may also show calcification, but its incidence is substantially lower (Fig. 16.3bb).

- Vascularity
 - Peripheral.
 - Mixed vascularity (presence of both hilar and peripheral vascularity); Mixed vascularity disappear at later stage of malignant process.

18.3.3 US Features of Malignant Lymph Nodes in Lymphomas [14]

- Lymphomatous nodes tend to be enlarged with a minimal transverse diameter of 10 mm or larger. Progressive and substantial reduction in nodal size is a useful indicator of good treatment response.
- Lymphomatous nodes tend to be round in shape, well-defined, appear hypoechoic and usually without an echogenic hilus.
- These features are similar for most metastatic LNs. Therefore, nodal shape, border sharpness, echogenicity, and presence/absence of an echogenic hilus may not be useful sonographic criteria to differentiate lymphoma from metastases.
- Lymphomatous nodes rarely show cystic necrosis unless the patient received previous radiation therapy, chemotherapy, or has advanced disease.
- Intranodal calcification is uncommon in lymphomatous lymph nodes. However, calcification may be found in lymphomatous nodes after treatment; these calcifications are usually dense with posterior acoustic shadowing.
- Lymphomatous nodes tend to have both hilar (in 62%) and peripheral (in 90%) vessels.
- Caution! None of above-mentioned criteria alone can be used to distinguish reactive from metastatic LNs.
- Linear echogenic hilus seen within LN on US examination has been proposed but not confirmed as a sign of benignity. Samples of 46 patients with linear echogenic hilus were examined; malignancy was confirmed in 59%, tuberculosis in 15%, and 26% of samples were benign; linear echogenic hilus should therefore not be regarded as a sole criterion for benignity [24].
- Above-mentioned US criteria of the LN are useful for the differential diagnosis of the cervical LN. In a study by Takeuchi et al. sensitivity, specificity, and accuracy rate were $\approx 97\%$, 100% , and $\approx 99\%$ respectively. False positive rate and false negative rate were zero percent and 1.4% , respectively. The short-axis diameter and shape of metastatic nodes were larger and rounder than those of non-metastatic ones. Of the metastatic nodes, 69% showed hypoechoic and 31% isoechoic levels, and 78% exhibited

punctate bright hyperechogenic spots. Of non-metastatic nodes, 92% showed hypoechoic and 8% isoechoic levels, and none of them showed hyperechogenic spots. Hilus echogenic line was not present in any metastatic node, but was seen in 58% of non-metastatic ones. Of the metastatic nodes, 19% exhibited a cystic pattern; none of the non-metastatic nodes showed the pattern [25].

- In a study by Ahuja and Ying, 286 patients with cervical lymphadenopathy were evaluated. Metastatic, lymphomatous, and tuberculous LN were round in 63–94% and without echogenic hilus in 57–91%. Sharp borders were found in metastatic and lymphomatous LN in 56–100%, but uncommon in tuberculosis in 49%. Capsular or mixed vascularity is common in metastatic, lymphomatous, and tuberculous LN, but not found in reactive ones. Except metastatic LN of PTC that showed low resistance, metastatic LN had a higher vascular resistance than reactive LN. Micronodular echo pattern is common in lymphomatous LN. Hyperechogenicity and punctate calcification are typical features for metastatic LN of PTC. Intranodal cystic necrosis, adjacent soft tissue edema, matting, and displaced hilar vascularity are common features of tuberculosis [26].
- Location of cervical lymph nodes—numerical classification system [27]; see more in Chap. 19.
- US-guided FNAB is an accurate method for neck nodes evaluation, with sensitivity of 89–98%, specificity of 95–98%, and overall accuracy of 95–97% [28].

References

1. Holm LE, Blomgren H, Löwhagen T. Cancer risks in patients with chronic lymphocytic thyroiditis. *N Engl J Med*. 1985;312(10):601–4.
2. Stein SA, Wartofsky L. Primary thyroid lymphoma: a clinical review. *J Clin Endocrinol Metab*. 2013;98(8):3131–8.
3. Nam M, Shin JH, Han BK, Ko EY, Ko ES, Hahn SY, et al. Thyroid lymphoma: correlation of radiologic and pathologic features. *J Ultrasound Med*. 2012;31(4):589–94.
4. Graff-Baker A, Roman SA, Thomas DC, Udelsman R, Sosa JA. Prognosis of primary thyroid lymphoma: demographic, clinical, and pathologic predictors of survival in 1,408 cases. *Surgery*. 2009;146(6):1105–15.
5. Ota H, Ito Y, Matsuzuka F, Kuma S, Fukata S, Morita S, et al. Usefulness of ultrasonography for diagnosis of malignant lymphoma of the thyroid. *Thyroid*. 2006;16(10):983–7.
6. Belal AA, Allam A, Kandil A, El Hussein G, Khafaga Y, Al Rajhi N, et al. Primary thyroid lymphoma: a retrospective analysis of prognostic factors and treatment outcome for localized intermediate and high grade lymphoma. *Am J Clin Oncol*. 2001;24(3):299–305.
7. Skarsgard ED, Connors JM, Robins RE. A current analysis of primary lymphoma of the thyroid. *Arch Surg*. 1991;126(10):1199–203. discussion 1203–4
8. Kim EH, Kim JY, Kim TJ. Aggressive primary thyroid lymphoma: imaging features of two elderly patients. *Ultrasonography*. 2014;33(4):298–302.

9. Bachar G, Goldstein D, Brown D, Tsang R, Lockwood G, Perez-Ordóñez B, et al. Solitary extramedullary plasmacytoma of the head and neck—long-term outcome analysis of 68 cases. *Head Neck*. 2008;30(8):1012–9.
10. Galieni P, Cavo M, Pulsoni A, Avvisati G, Bigazzi C, Neri S, et al. Clinical outcome of extramedullary plasmacytoma. *Haematologica*. 2000;85(1):47–51.
11. Bhat V, Shariff S, Reddy RA. Extramedullary plasmacytoma of thyroid—a mimicker of medullary carcinoma at fine needle aspiration cytology: a case report. *J Cytol*. 2014;31(1):53–6.
12. Ridal M, Ouattassi N, Harmouch T, Amarti A, Alami MN. Solitary extramedullary plasmacytoma of the thyroid gland. *Case Rep Otolaryngol*. 2012;2012:282784.
13. Boutsos EP, Bedrossian CW, De Frias DV, Nayar R. Thyroid plasmacytoma mimicking medullary carcinoma: a potential pitfall in aspiration cytology. *Diagn Cytopathol*. 2000;23(5):354–8.
14. Ahuja AT, Ying M, Ho SY, Antonio G, Lee YP, King AD, et al. Ultrasound of malignant cervical lymph nodes. *Cancer Imaging*. 2008;25(8):48–56.
15. Som PM. Detection of metastasis in cervical lymph nodes: CT and MR criteria and differential diagnosis. *AJR Am J Roentgenol*. 1992;158(5):961–9.
16. Noguti J, De Moura CF, De Jesus GP, Da Silva VH, Hossaka TA, Oshima CT, et al. Metastasis from oral cancer: an overview. *Cancer Genomics Proteomics*. 2012;9(5):329–35.
17. DePeña CA, Van Tassel P, Lee YY. Lymphoma of the head and neck. *Radiol Clin N Am*. 1990;28(4):723–43.
18. Jones AS, Cook JA, Phillips DE, Roland NR. Squamous carcinoma presenting as an enlarged cervical lymph node. *Cancer*. 1993;72(5):1756–61.
19. Bruneton JN, Normand F. Cervical lymph nodes. In: Bruneton JN, editor. *Ultrasonography of the neck*. Berlin: Springer-Verlag; 1987. p. 81.
20. Baatenburg de Jong RJ, Rongen RJ, Laméris JS, Harthoorn M, Verwoerd CD, Knecht P. Metastatic neck disease. Palpation vs ultrasound examination. *Arch Otolaryngol Head Neck Surg*. 1989;115(6):689–90.
21. Jeong HS, Baek CH, Son YI, Ki Chung M, Kyung Lee D, Young Choi J, et al. Use of integrated 18F-FDG PET/CT to improve the accuracy of initial cervical nodal evaluation in patients with head and neck squamous cell carcinoma. *Head Neck*. 2007;29(3):203–10.
22. Solbiati L, Rizzatto G, Bellotti E, Montali G, Cioffi V, Croce F. High-resolution sonography of cervical lymph nodes in head and neck cancer: criteria for differentiation of reactive versus malignant nodes. *Radiology*. 1988;169(P):113–6.
23. Steinkamp HJ, Cornehl M, Hosten N, Pegios W, Vogl T, Felix R. Cervical lymphadenopathy: ratio of long- to short-axis diameter as a predictor of malignancy. *Br J Radiol*. 1995;68(807):266–70.
24. Evans RM, Ahuja A, Metreweli C. The linear echogenic hilus in cervical lymphadenopathy—a sign of benignity or malignancy? *Clin Radiol*. 1993;47(4):262–4.
25. Takeuchi Y, Suzuki H, Omura K, Shigehara T, Yamashita T, Okumura K, et al. Differential diagnosis of cervical lymph nodes in head and neck cancer by ultrasonography. *Auris Nasus Larynx*. 1999;26(3):331–6.
26. Ahuja A, Ying M. An overview of neck node sonography. *Investig Radiol*. 2002;37(6):333–42.
27. Chong V. Cervical lymphadenopathy: what radiologists need to know. *Cancer Imaging*. 2004;4(2):116–20.
28. Ying M, Bhatia KS, Lee YP, Yuen HY, Ahuja AT. Review of ultrasonography of malignant neck nodes: greyscale, Doppler, contrast enhancement and elastography. *Cancer Imaging*. 2014;13(4):658–69.

19.1 Essential Facts

- The risk factors influencing recurrence after the initial operation on PTC includes male sex, extrathyroid extension, metastatic lymph nodes (LN), distant metastasis, tumor size greater than 2 cm, subtotal thyroidectomy and without postoperative radioiodine ^{131}I -therapy (RIT) [1].
- Relapse of PTC can occur in three forms: distant metastasis, “true” local recurrence, and disease within metastatic lymph nodes. It is estimated that 90% of disease relapse in PTC are metastatic LNs. Because of the typically indolent nature of the disease, relapse is typically identified within the first 3–4 years [2].
- Persistent or recurrent metastatic disease in patients with PTC detected during the follow-up period was found to be 20–28% [3].
- In a study by Mazzaferri and Jhiang in the mid-1990s, post-treatment recurrence rates among PTC patients were 43.3% after more than 5 years of follow-up, and 19.3% more than 10 years after the original treatment [4].
- A later study by Durante et al. [2] reported that recurrences more than 5 years after surgery were discovered in 23% of patients (Figs. 19.6, 19.7 and 19.10). The differences between the findings of these two studies are largely a reflection of the changing demography of the differentiated thyroid carcinoma. Today’s PTCs are much more likely to be diagnosed at a subclinical stage than those treated in 1960s to the 1990s.
- Follow-up of low risk patients with PTC remains questionable. Neck US, serum thyroglobulin (Tg), and whole-body scan after L-thyroxin withdrawal are performed.
- Torlontano et al. reported that up to 50% of metastatic LNs were <1 cm and not palpable; negative predictive value of both negative Tg and US at first follow-up was 98.8% [5].

19.2 US Features of Metastatic Lymph Nodes

- For a detailed description of US features, *see Sect. 18.3 of Chap. 18*.
- Metastatic LNs tend to be round (Figs. 19.2 and 19.8), hypoechoic (Figs. 19.1 and 19.9), and hyper vascularized (Fig. 19.6) with a loss of hilar architecture (all figures in this chapter), and in differentiated thyroid cancer—PTC, FTC (Fig. 19.2aa, bb) they may also demonstrate specific features such as hyperechoic punctuations (Figs. 19.3 and 19.4) or microcalcifications and cystic appearance (Figs. 19.5 and 19.7) [3].
- LN round shape was reported to have an excellent specificity in 86%, but low sensitivity in 53% (likely partial or initial involvement of LN does not change the LN shape). In addition, some normal LNs may be rounded, especially in the parotid and submandibular regions [3].
- Absence of echogenic hilum is a US sign with higher sensitivity of 92%, but with low specificity of 52% compared to LN round shape [6].
- Presence of a hyperechoic hilum of the nodes is usually considered as a strong diagnostic criterion for benign LNs. However, it has been reported that 84–92% of benign nodes, but less than 5% of metastatic nodes, have a hyperechoic hilum [6].
- A recent study compared roles of US, CT, and PET-CT in the evaluation of cervical recurrence in DTC, by correlating findings with sample pathology. Sensitivity, specificity, and accuracy were $\approx 69\%$, $\approx 90\%$, and $\approx 80\%$ for US; $\approx 63\%$, $\approx 95\%$, and $\approx 80\%$ for CT; and $\approx 54\%$, $\approx 79\%$, and $\approx 67\%$ for PET-CT, respectively. Sensitivity and specificity of ultrasound and CT were higher than reported for PET-CT [7].
- PET-CT is a valid imaging modality for the diagnosis of iodine-negative lesions on iodine scan [8].
- Location of cervical lymph nodes—numerical classification system [9]:
 - C-IA—Submental lymph nodes.
 - C-IB—Submandibular lymph nodes.
 - C-II—Internal jugular (deep cervical) chain from the base of the skull to the inferior border of the hyoid bone.
 - C-III—Internal jugular (deep cervical) chain from the hyoid bone to the inferior border of the cricoid arch.
 - C-IV—Internal jugular (deep cervical) chain between the inferior border of the cricoid arch and the supraclavicular fossa.
 - C-V—Posterior triangle or spinal accessory nodes.
 - C-VI—Central compartment nodes from the hyoid bone to the suprasternal notch.
 - C-VII—Nodes inferior to the suprasternal notch in the upper mediastinum.

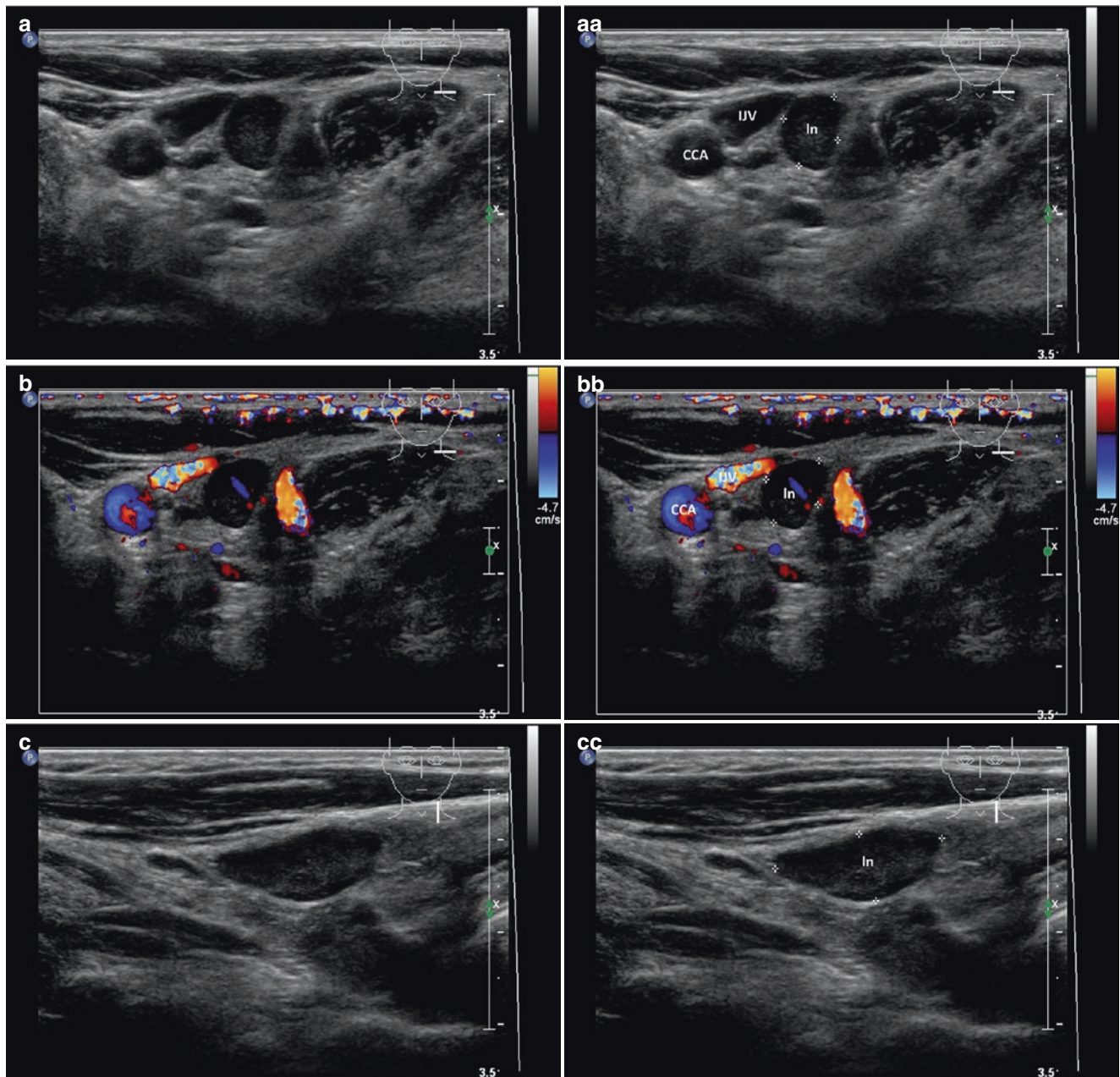


Fig. 19.1 (aa) A 39-year-old woman, 10 years post thyroidectomy for papillary thyroid carcinoma (PTC). Small solitary metastatic lymph node (LN) along the left internal jugular vein (IJV) at level C-IV, size $18 \times 8 \times 6$ mm and volume 0.5 mL. US scans: In (marks)—elliptical shape; homogeneous structure; hypoechoic; no hilus sign; transverse.

(bb) Detail of solitary metastatic LN, CFDS: In (marks)—hilar vascularity, one central vessel branch; transverse. (cc) Detail of solitary metastatic LN: In (marks)—elliptical shape, size 18×8 mm, L/S ratio > 2 (not pathological); no hilus sign; longitudinal

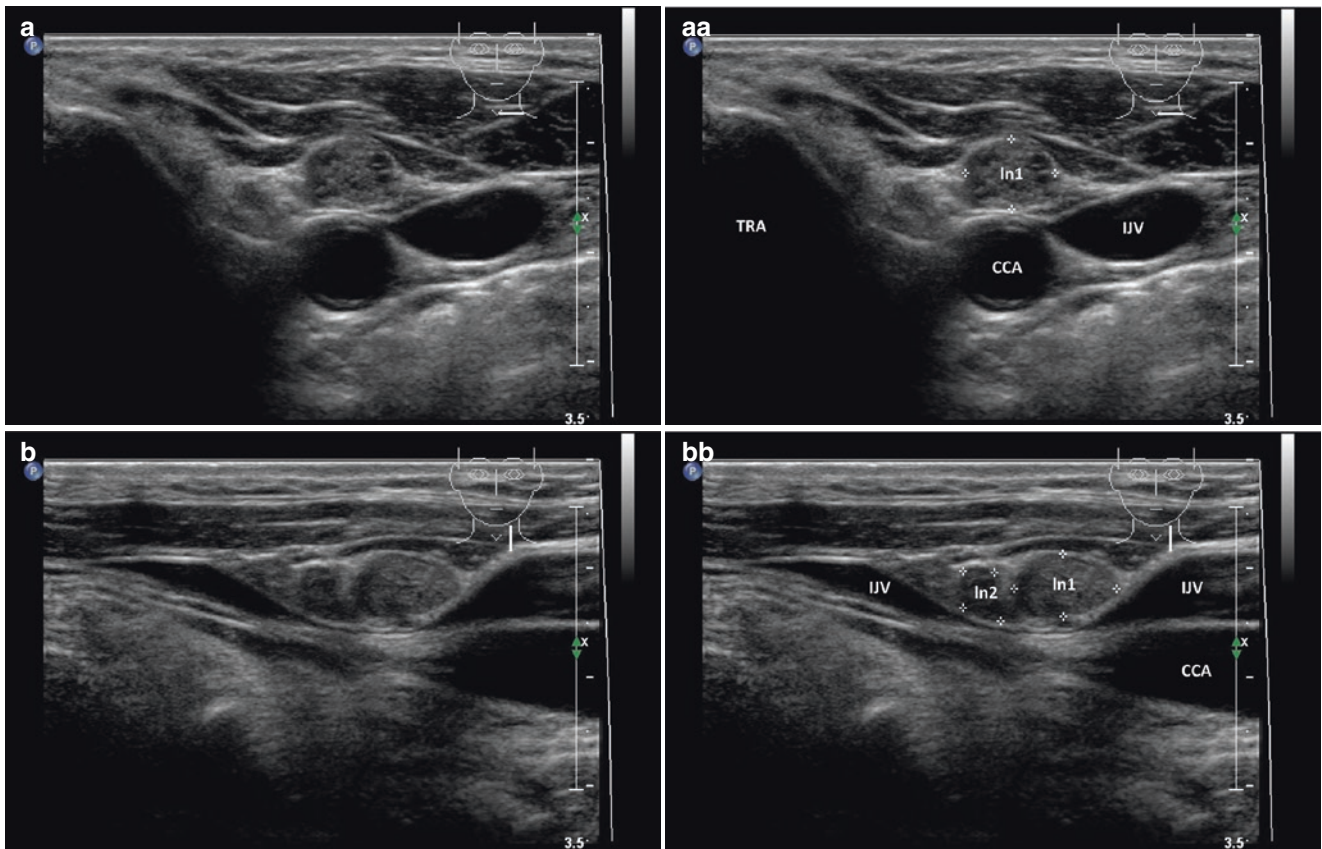
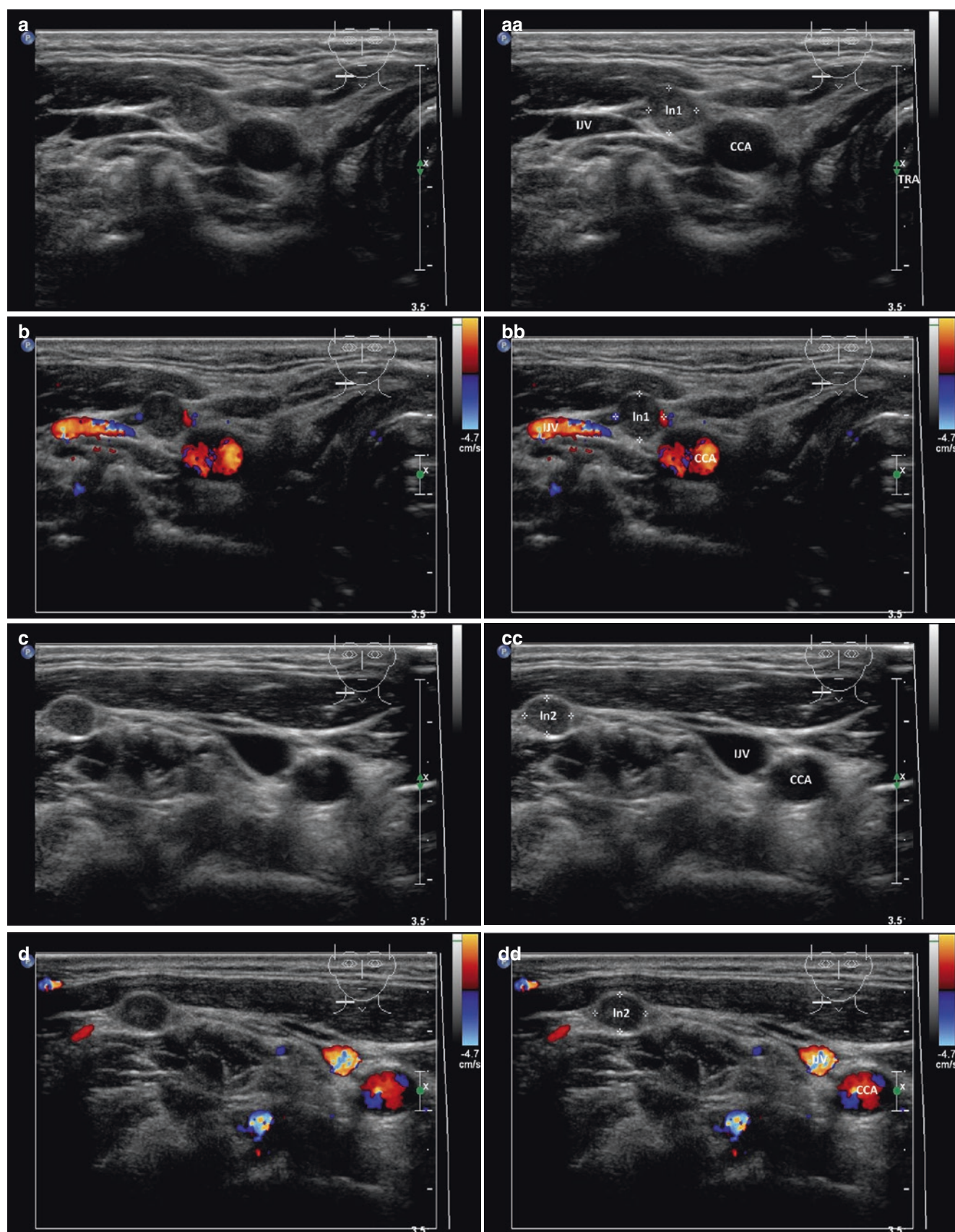


Fig. 19.2 (aa) An 83-year-old man, 13 years post thyroidectomy for papillary thyroid carcinoma (PTC). Two small metastatic lymph nodes (LN) along the left internal jugular vein (IJV) at level C-III—small NL size $10 \times 9 \times 6$ mm, volume 0.3 mL and tiny NL size 6×5 mm. US scan: Ln1 (marks)—round shape; homogeneous structure; hyperechoic;

no hilus sign; transverse. (bb) Detail of two metastatic LNs: both Ln1 and Ln2 (marks)—round shape, L/S ratio ≈ 1.0 ; homogeneous structure; hyperechoic; no hilus sign; vein compression by US probe; longitudinal

Fig. 19.3 (aa) A 36-year-old woman, 2 years post thyroidectomy for papillary thyroid carcinoma (PTC). Two tiny metastatic lymph nodes (LN) along the left IJV at levels C-II and C-III. US scan of tiny metastatic LN at level C-II, size 6×6 mm, volume < 0.1 mL: Ln1 (marks)—round shape, L/S ratio ≈ 1.0 ; homogeneous structure; hyperechoic; no hilus sign; transverse. (bb) Detail of tiny metastatic LN at level C-II,

CFDS: Ln1 (marks)—minimal peripheral vascularity; transverse. (cc) Detail of tiny metastatic LN at level C-III, size 6×5 mm, volume < 0.1 mL: Ln2 (marks)—round shape, L/S ratio ≈ 1.0 ; homogeneous structure; hyperechoic; no hilus sign; transverse. (dd) Detail of tiny metastatic LN at level C-III, CFDS: Ln2 (marks)—avascular; transverse



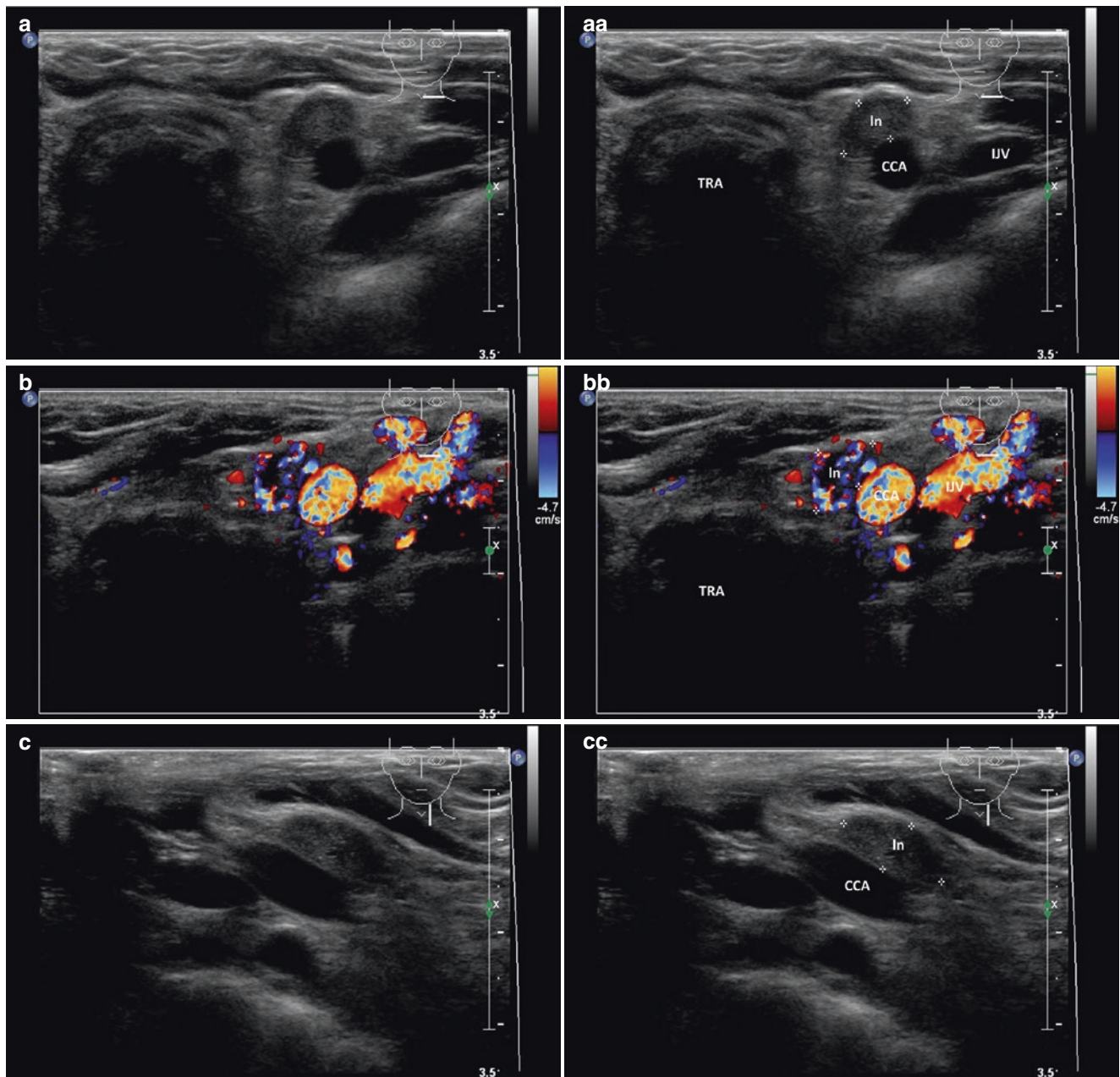


Fig. 19.4 (aa) A 38-year-old woman, 10 years post thyroidectomy for medullary thyroid carcinoma (MTC) and 8 years post metastatic lymph nodes (LN) excision. Recurrence of small metastatic LN on the left side in front of CCA at level C-VI, size $15 \times 8 \times 5$ mm and volume 0.3 mL. US scans: In (marks)—elliptical shape; homogeneous structure; hyperechoic; no hilus sign; transverse. (bb) Detail of small meta-

static LN at level C-VI, CFDS: In (marks)—mixed (hilar and peripheral) hypervascularity; transverse. (cc) Detail of small metastatic LN at level C-VI: In (marks)—elliptical shape, size 15×8 mm, L/S ratio ≈ 2 (not pathological); no hilus sign; longitudinal. (dd) Detail of small metastatic LN at level C-VI, CFDS: In (marks)—mixed (hilar end peripheral) hypervascularity; longitudinal

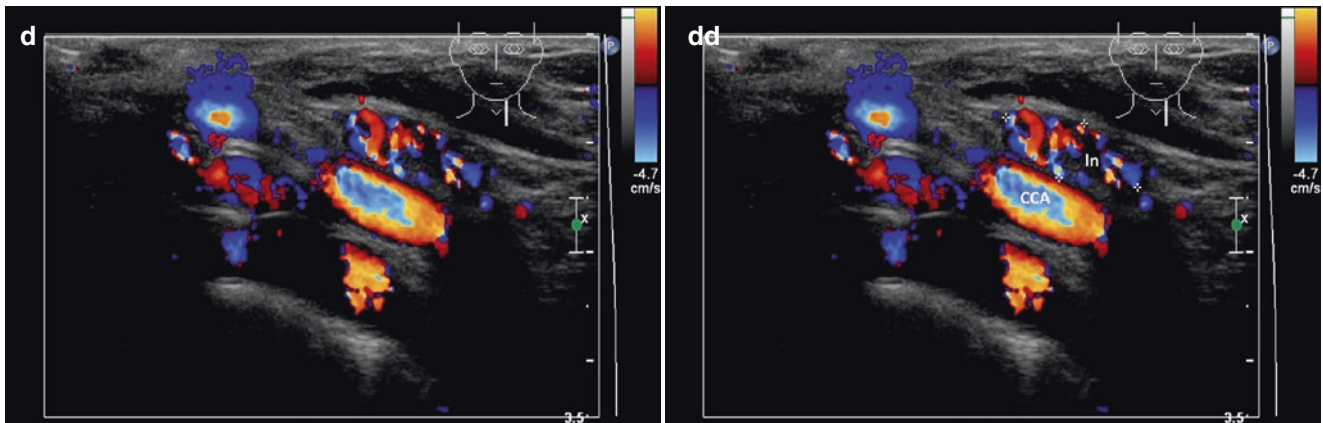


Fig. 19.4 (continued)

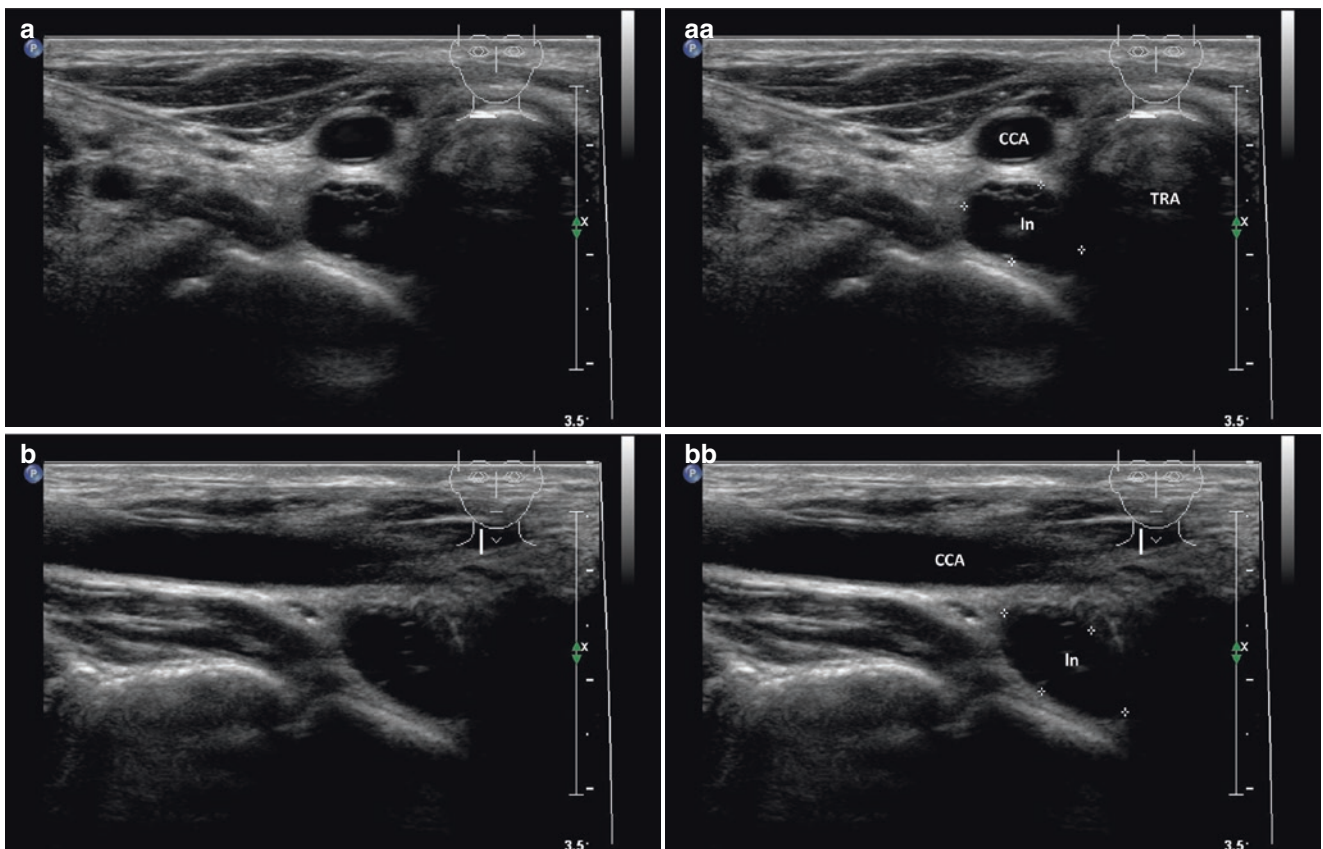


Fig. 19.5 (aa) A 26-year-old woman, 8 years post thyroidectomy for papillary thyroid carcinoma (PTC). Small solitary metastatic lymph node (LN) with cystic necrosis located deep behind the right CCA at level C-IV, size $15 \times 12 \times 8$ mm and volume 0.7 mL. US scans: In (marks)—elliptical shape; inhomogeneous structure; anechoic areas

with short hyperechoic septa; no hilus sign; transverse. (bb) Detail of small metastatic LN at level C-IV: In (marks)—elliptical shape, size 15×8 mm, L/S ratio ≈ 2 (not pathological); no hilus sign; longitudinal

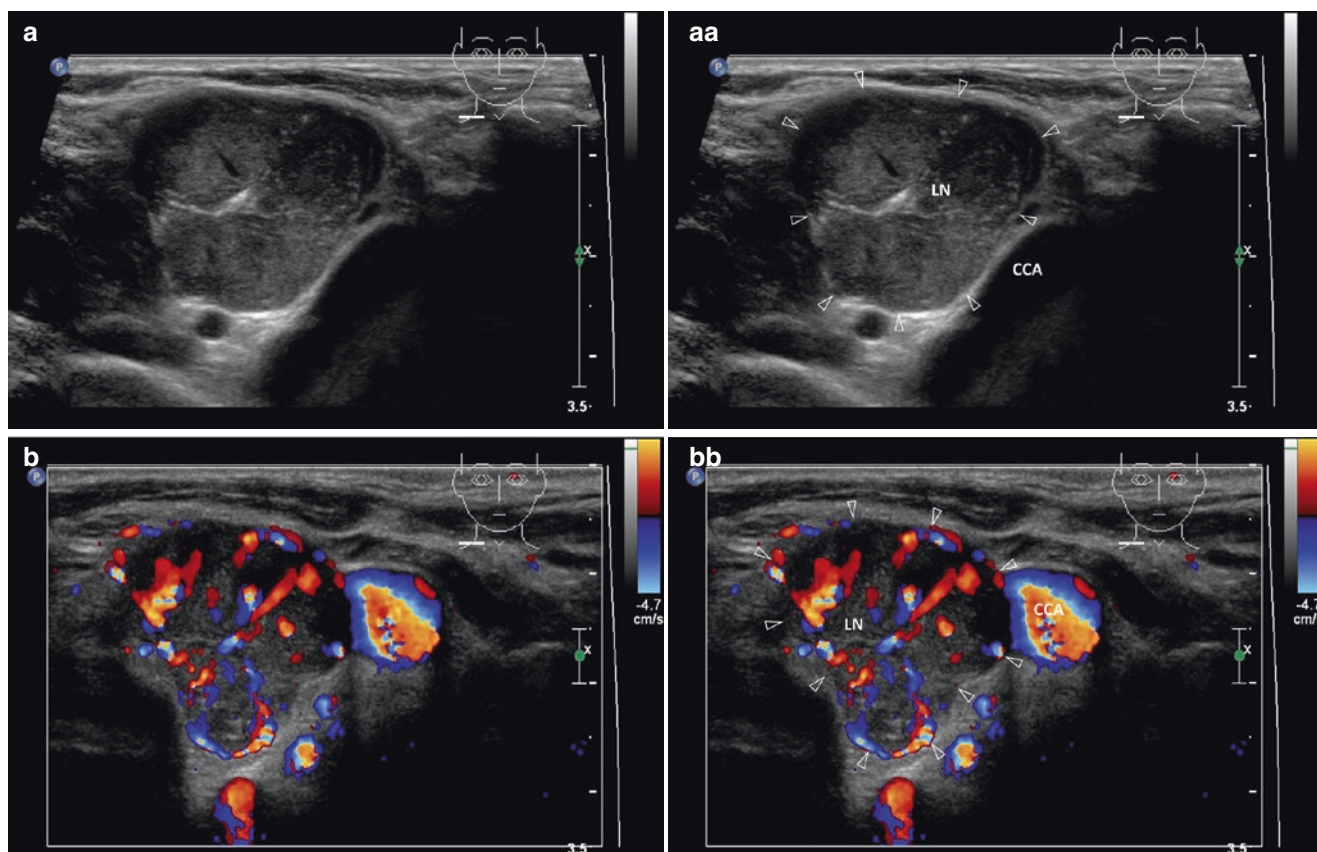


Fig. 19.6 (aa) A 70-year-old man, 16 years post thyroidectomy for papillary thyroid carcinoma (PTC) with two month palpable resistance. Solitary large metastatic lymph node (LN) on the right side along CCA at level C-IV, size $25 \times 23 \times 22$ mm and volume 6 mL. US scans: LN (*blank arrowheads*)—round shape, L/S ratio ≈ 1.0 ; coarse structure;

transverse hyperechoic septum in central part; no hilus sign; transverse. (bb) Detail of solitary large metastatic LN at level C-IV, CFDS: LN (*blank arrowheads*)—mixed (hilar end peripheral) hypervascularity; longitudinal

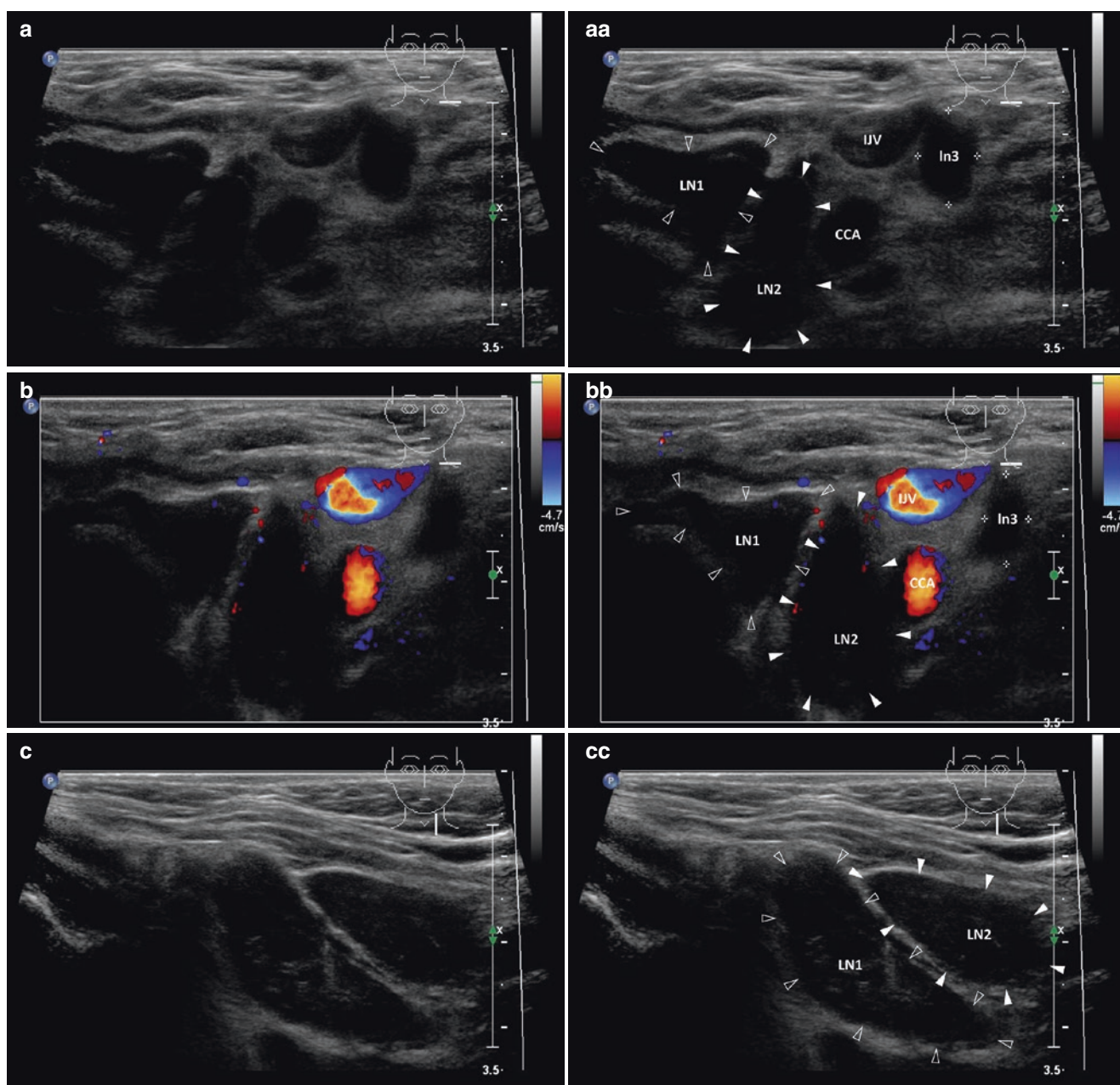


Fig. 19.7 (aa) An 83-year-old woman, 15 years post thyroidectomy for papillary thyroid carcinoma (PTC). Three metastatic lymph nodes (LN) on the left side, two between trachea and CCA at level C-VI; LN1 (blank arrowheads) size $31 \times 20 \times 12$ mm, volume 4.5 mL, LN2 (arrowheads) size $26 \times 21 \times 11$ mm, volume 3 mL and one small LN3 (marks) along the IJV at level C-IV, size $10 \times 6 \times 6$ mm, volume 0.2 mL. US scans: all LNs have the same cyst-like pattern—elliptical shape; homogeneous structure; markedly hypoechoic; no hilus sign;

transverse. (bb) Detail of large metastatic LNs in C-VI and small at level C-IV, CFDS: in LN1 (blank arrowheads) and LN2 (arrowheads) minimal peripheral vascularity; LN3 (marks) avascular; transverse. (cc) Detail of two large metastatic LNs in C-VI: both LNs—elliptical shape, LN1 (blank arrowheads) size 31×12 mm and LN2 (arrowheads) size 26×11 mm, L/S ratio > 2 (not pathological); inhomogeneous structure; mostly hypoechoic with small fibrous areas; no hilus sign; longitudinal

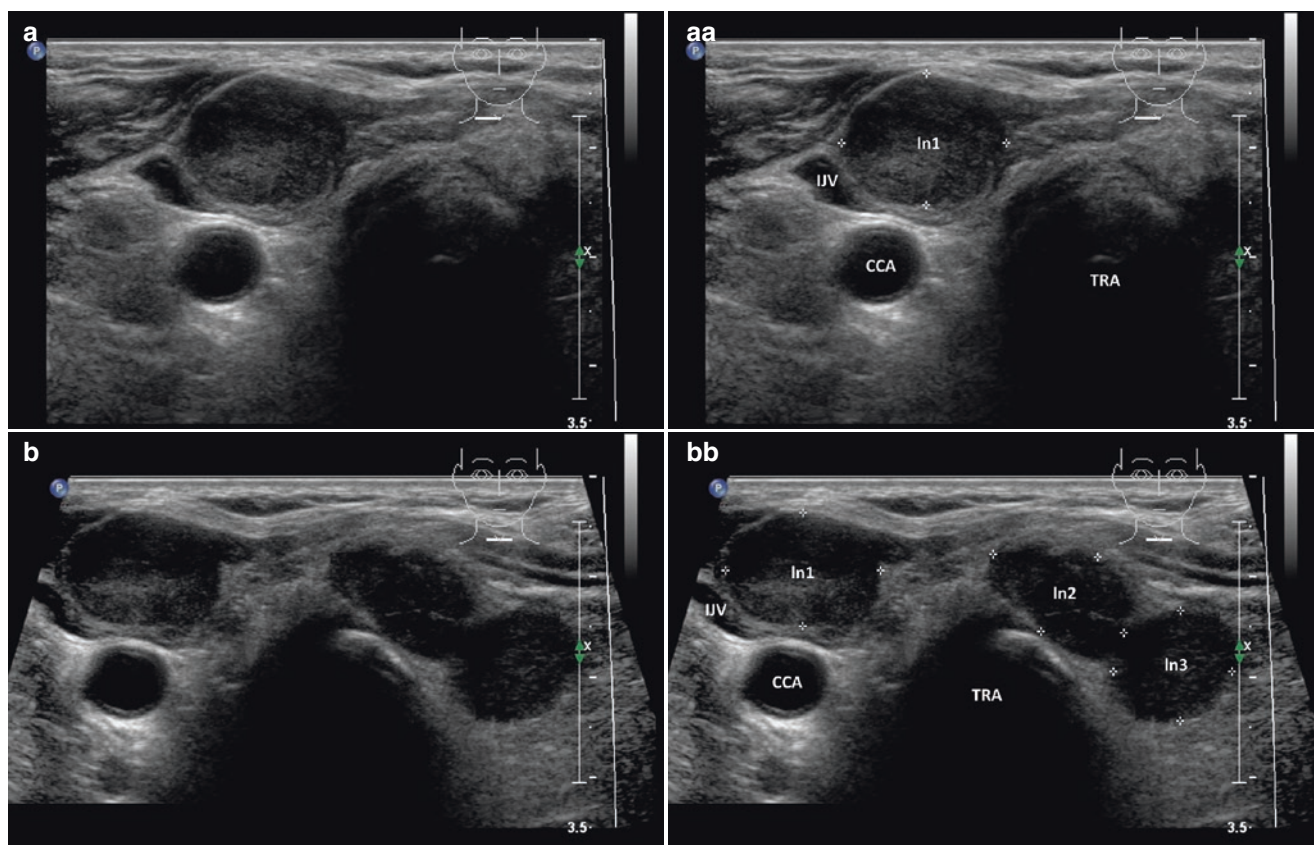


Fig. 19.8 (aa) A 76-year-old man, 3 years post thyroidectomy for papillary thyroid carcinoma (PTC). Three metastatic lymph nodes (LN) deep in the neck. First in front of the right CCA and two on the left side in front of the trachea at level C-VI. US scan of first metastatic LN, size 14×12 mm: Ln1 (marks)—round shape, L/S ratio ≈ 1.0 ; coarse struc-

ture; mostly hyperechoic; no hilus sign; causing compression of the right IJV; transverse. (bb) Overall view of all metastatic LNs, two in front of the trachea, Ln2 (marks)—size 14×10 mm and Ln3 (marks)—size 12×10 mm: round shape, L/S ratio ≈ 1.0 ; coarse structure; mixed echogenicity; no hilus sign; transverse

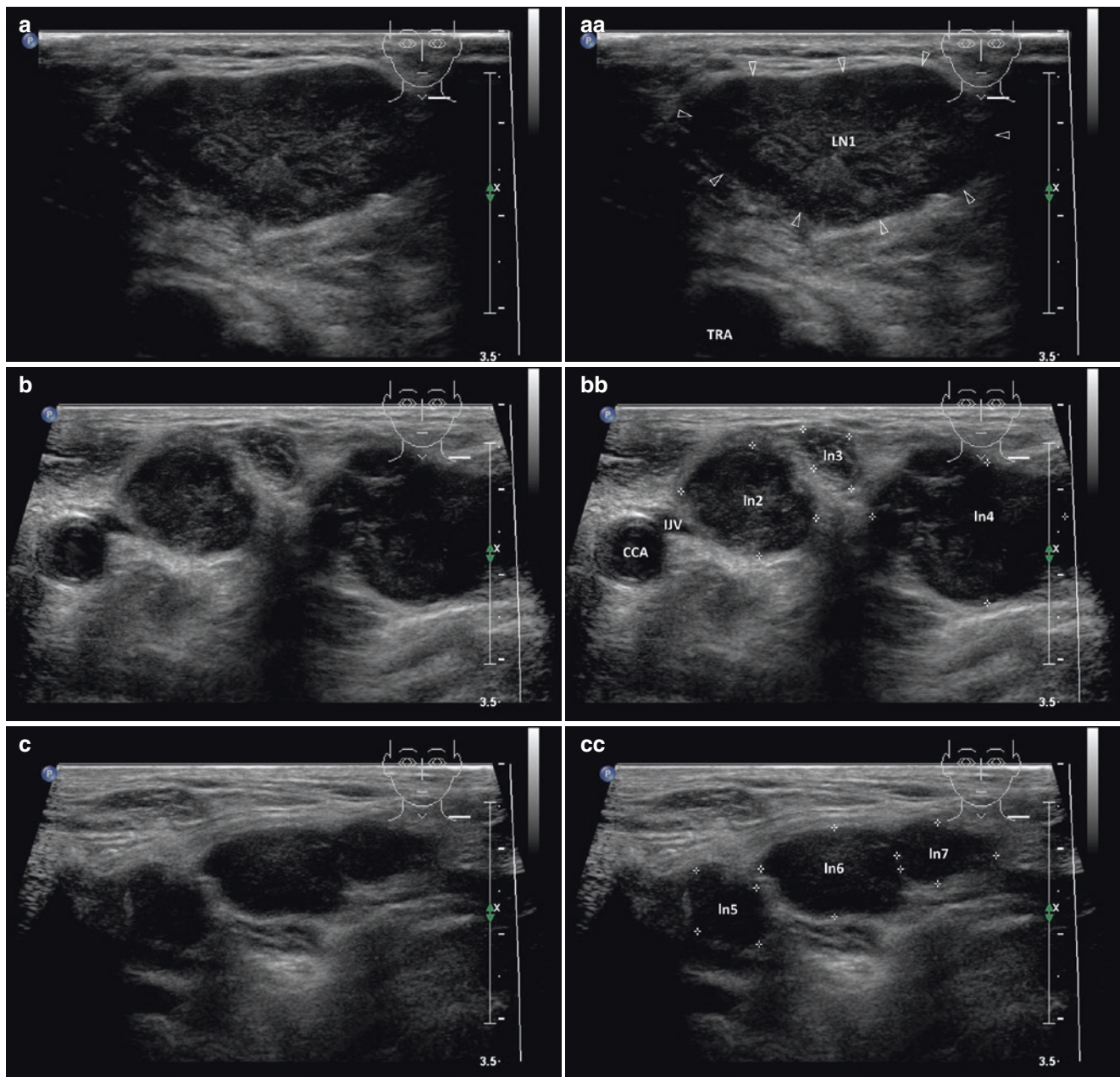


Fig. 19.9 (aa) A 79-year-old man, 1 year post thyroidectomy for anaplastic thyroid carcinoma (ATC). Multiple metastatic lymph nodes (LN) on the left side, the largest in the lower anterior neck in front of trachea at level C-VI, the others outside of CCA at level C-IV and follow further into left supraclavicular area, altogether seven LNs. The largest metastatic LN at level C-VI, size $32 \times 31 \times 17$ mm and volume 9 mL; LN1 (*blank arrowheads*)—elliptical shape, L/S ratio ≈ 2 (*not pathological*); inhomogeneous structure; mostly hypoechoic with fibrotic areas; no hilus sign; transverse. (**bb**) Detail of three metastatic

LNs next to the left CCA at level C-IV and in medial supraclavicular area; Ln2, 3, 4 (*marks*) size with maximal diameter 19 mm, 8 mm and 27 mm, Ln2 causing compression of the left IJV; round or oval shape, L/S ratio ≈ 1.0 ; inhomogeneous structure; mostly hypoechoic with fibrotic areas; no hilus sign; transverse. (**cc**) Detail of three metastatic LNs in left lateral supraclavicular area; Ln 5, 6, 7 (*marks*) size with maximal diameter 15 mm, 25 mm and 15 mm; round or oval shape, L/S ratio ≈ 1.0 ; homogeneous structure; hypoechoic; no hilus sign; transverse

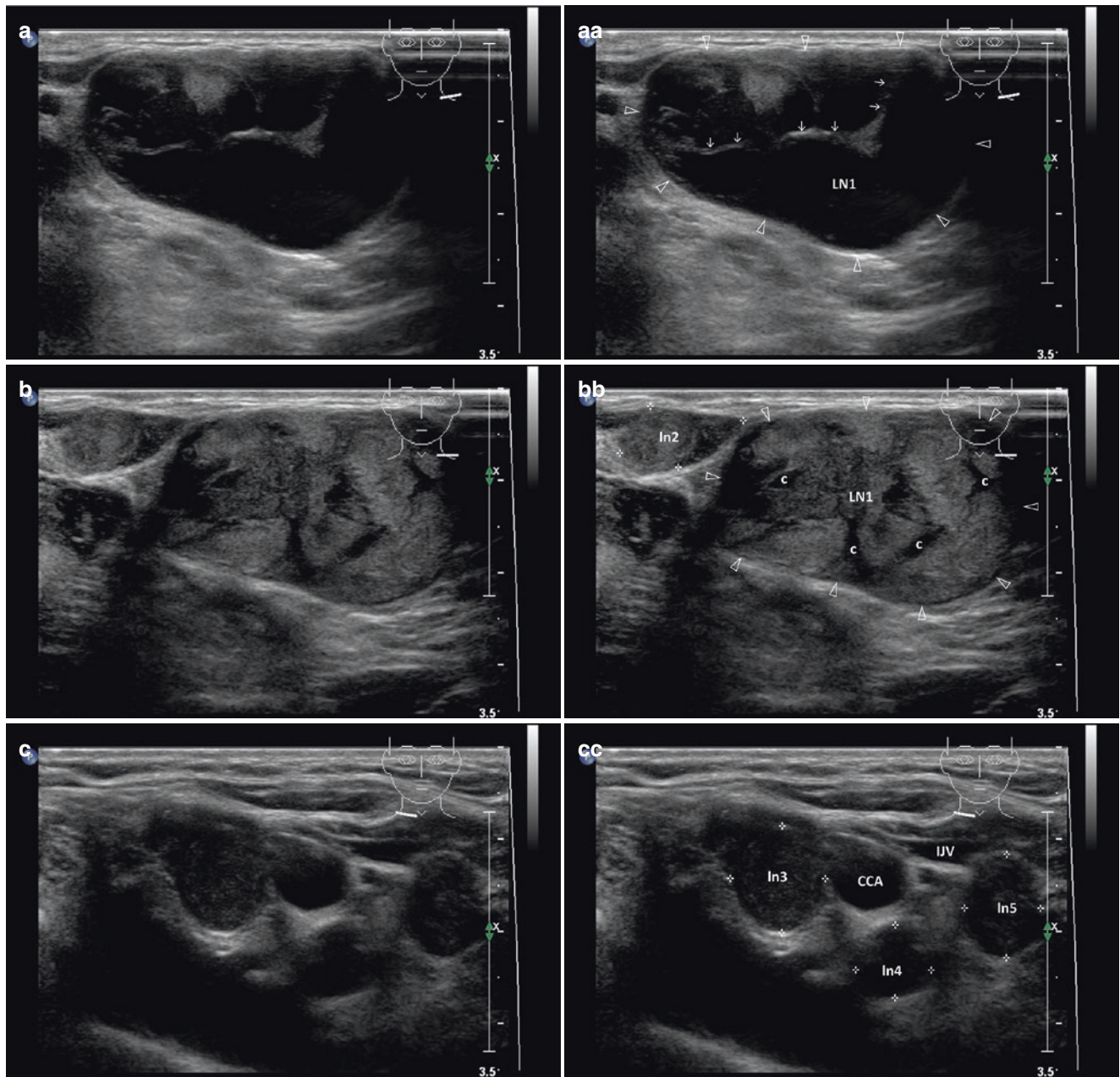


Fig. 19.10 (aa) A 73-year-old woman, 8 years post thyroidectomy for papillary thyroid carcinoma (PTC). Multiple metastatic lymph nodes (LNs) deep in the lower anterior neck bilaterally. Large metastatic LN with cystic necrosis next to the left IJV at level C-IV, size $36 \times 33 \times 22$ mm and volume 14 mL: LN1 (*blank arrowheads*)—elliptical shape; anechoic content with debris; internal thick hyperechoic septum and thin septa (*open arrows*); transverse. (bb) Detail of large metastatic LN in left C-IV level post FNAB and evacuation of liquid

part; residual solid part, size 31×19 mm: LN1 (*blank arrowheads*)—oval shape; coarse structure; hyperechoic with tiny cystic cavities (*c*); no hilus sign; next to another small metastatic Ln2 (*marks*) size 8×7 mm—round shape; hyperechoic; no hilus sign; transverse. (cc) Detail of three small metastatic LNs (*marks*) along the right CCA at level C-IV, Ln3 size 16×12 mm, Ln4 size 10×8 mm and Ln 5 size 12×8 mm: oval shape; solid; inhomogeneous structure; slightly hyperechoic; no hilus sign; transverse

References

1. Guo K, Wang Z. Risk factors influencing the recurrence of papillary thyroid carcinoma: a systematic review and meta-analysis. *Int J Clin Exp Pathol*. 2014;7(9):5393–403.
2. Durante C, Montesano T, Torlontano M, Attard M, Monzani F, Tumino S, et al. PTC Study Group. Papillary thyroid cancer: time course of recurrences during postsurgery surveillance. *J Clin Endocrinol Metab*. 2013; 98(2): 636–642.
3. Napolitano G, Romeo A, Vallone G, Rossi M, Cagini L, Antinolfi G, et al. How the preoperative ultrasound examination and BFI of the cervical lymph nodes modify the therapeutic treatment in patients with papillary thyroid cancer. *BMC Surg*. 2013;13 Suppl 2:S52.
4. Mazzaferri EL, Jhiang SM. Differentiated thyroid cancer long-term impact of initial therapy. *Trans Am Clin Climatol Assoc*. 1995;106:151–70.
5. Torlontano M, Attard M, Crocetti U, Tumino S, Bruno R, Costante G, et al. Follow-up of low risk patients with papillary thyroid cancer: role of neck ultrasonography in detecting lymph node metastases. *J Clin Endocrinol Metab*. 2004;89(7):3402–7.
6. Reginelli A, Pezzullo MG, Scaglione M, Scialpi M, Brunese L, Grassi R. Gastrointestinal disorders in elderly patients. *Radiol Clin N Am*. 2008;46(4):755–71, vi.
7. Seo YL, Yoon DY, Baek S, Ku YJ, Rho YS, Chung EJ, et al. Detection of neck recurrence in patients with differentiated thyroid cancer: comparison of ultrasound, contrast-enhanced CT and (18) F-FDG PET/CT using surgical pathology as a reference standard: (ultrasound vs. CT vs. (18)F-FDG PET/CT in recurrent thyroid cancer). *Eur Radiol*. 2012;22(10):2246–54.
8. Razfar A, Branstetter 4th BF, Christopoulos A, Lebeau SO, Hodak SP, Heron DE, et al. Clinical usefulness of positron emission tomography-computed tomography in recurrent thyroid carcinoma. *Arch Otolaryngol Head Neck Surg*. 2010;136(2):120–5.
9. Chong V. Cervical lymphadenopathy: what radiologists need to know. *Cancer Imaging*. 2004;4(2):116–20.

Part V

Miscellanea

20.1 Essential Facts

- Total thyroidectomy (TT) has an important role in the management of patients with thyroid malignancy and benign disease involving both lobes of the thyroid gland. This approach avoids disease recurrence and the increased risk of morbidity associated with secondary operation. The incidence of complications with TT is similar to that with other techniques (subtotal and “near” total thyroidectomy). Therefore, TT is considered the gold standard of thyroid surgery [1].
- Bron et al., between 1988 and 2002, performed 834 total thyroidectomies (706 women, 128 men) for clinically benign disease. Indications for surgery were 730 (87%) euthyroid multinodular goiter (MNG), 57 (7%) toxic MNG, and 47 (6%) Graves’ disease. A total of 74 patients had previously undergone partial thyroidectomy. The incidence of temporary recurrent laryngeal nerve palsy was 2.3% and the incidence of temporary hypoparathyroidism was 14.4%. Permanent recurrent laryngeal nerve palsy occurred in 1.1%, and 2.4% of patients had permanent hypoparathyroidism. Neither the initial clinical diagnosis nor a history of previous surgical treatment significantly influenced the rate of complications. The incidence of malignancy, other than incidental microscopic papillary carcinoma, was 4.6% [2].
- The extent of thyroidectomy in Grave’s disease (GD) is still controversial. TT requires thyroxine replacement therapy throughout the patient’s life. The subtotal thyroidectomy aims to maintain long-term euthyroidism without thyroxine replacement therapy. However, these remnants entail the risk of hyperthyroidism recurrence. The surgical outcomes of Sugino et al. showed: patients with thyroid remnant of 7 g, 6 g, or 5 g had the relapse in 14.1%, 12.6%, and 10.9% respectively. None of the patients with remnant that weighed <2 g developed recurrent hyperthyroidism. Subtotal thyroidectomy leaving 3 to 4 g remnant tissue is a suitable surgical option for GD to avoid permanent hypothyroidism, and has low risk of recurrence rate 4% [3].
- Primary treatment of differentiated thyroid carcinomas (DTCs) generally comprises a combination of surgery and radioiodine ¹³¹I ablation. This intensive approach consists of TT and central lymphadenectomy in all cases, completed by modified lateral lymphadenectomy. Thyroid remnant radioiodine ablation is routinely given to the vast majority of, if not all, DTC patients to destroy every source of uptake. Adjuvant radioiodine should be given, however, to complete, not to replace, total thyroidectomy [4].
- Thyroid remnants with volume <2 mL could be seen on US at the earliest a month after the total or near-thyroidectomy. Thyroid remnants smaller than 2 g (<2 mL) facilitate use of postoperative radioiodine ablation [5, 6].
- Lobectomy (Fig. 20.3) was previously used for solitary benign nodules. Endoscopic neck surgery for the parathyroid and thyroid was developed by Gagner and Huscher in 1996 and 1997, respectively. This method is currently known as minimally invasive video-assisted technique (MIVAT). Generally, endoscopic thyroid surgery has been thought to be appropriate for benign thyroid disease. Initially, it was indicated for nodules ≤3 cm, benign or low-grade follicular lesion, and papillary carcinoma, with contraindications for previous neck surgery, large goiter, local metastases, previous neck irradiation, thyroiditis, and hyperthyroidism. These indications during the development of this technique slightly changed. Nowadays it could be performed nodules ≥5 cm, for Graves’ disease, and thyroiditis. The role of endoscopy for carcinoma is still under debate [7].
- Preoperative US with precise volume measurement of thyroid, lobe, or node, and subsequent FNAB and cytology are crucial for the choice of surgical approach.

20.2 US Findings of Thyroid Remnants

- Post thyroidectomy, the carotid artery and jugular vein slide medially into the space previously occupied by the thyroid gland. The normal postoperative thyroid bed should have a uniform echogenic texture owing to fibrofatty connective tissue (Fig. 20.2). The left thyroid bed is often occupied by the esophagus [8].
- TT and “near” total thyroidectomy (“near” TT) are associated with a low rate of recurrence. Subtotal thyroidectomy, in which a portion of the thyroid gland is deliberately left in the thyroid bed, has a considerably higher rate of recurrence. The incidence of complications with TT and “near” TT is similar to that with other techniques of thyroid surgery. However, despite the radical intent of surgeons, a real TT is not always carried out. The complete removal of all the thyroid tissue employing TT is not the norm, and micro/macrosopic remnants almost always remain. D’Andrea et al., in a US and CFDS study of 102 patients who had undergone TT for benign thyroid pathologies, demonstrated significant thyroid tissue remnants in the thyroid lodge in 34 cases ($\approx 33\%$). Therefore, out of a total of 102 so-called “total thyroidectomies,” only 68 ($\approx 66\%$) were really total, whereas 12 patients ($\approx 12\%$) had near-total thyroidectomy, leaving tissue remnants <1 cm, and 22 patients ($\approx 22\%$) had subtotal thyroidectomy, with tissue remnants ≥ 1 cm [1].
- Recommendation for US follow-up after thyroidectomy [1]: all patients should be re-examined 6 months after the operation with a US and CFDS of the thyroid lodge and reclassified on the basis of tissue remnants as follows:
 - Total Thyroidectomy (TT) = absence of macroscopic thyroid tissue remnants (Fig. 20.1).
 - Near Total Thyroidectomy (“near” TT) = presence of thyroid tissue remnants <1 cm (Figs. 20.4, 20.5, and 20.7).
 - Subtotal Thyroidectomy = presence of thyroid tissue remnants ≥ 1 cm (Figs. 20.6 and 20.8).

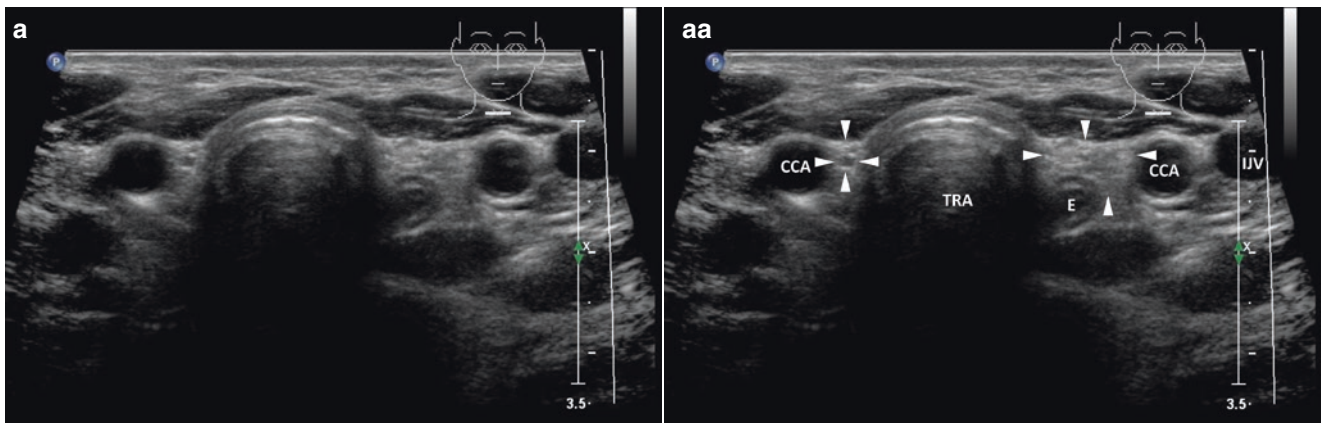


Fig. 20.1 (aa) US of thyroid bed 2 years post total thyroidectomy for PTC: uniform echogenic texture of an empty thyroid bed bilaterally (arrowheads); no thyroid remnants; right common carotid artery slides close to the trachea; left thyroid bed is occupied by the esophagus; transverse

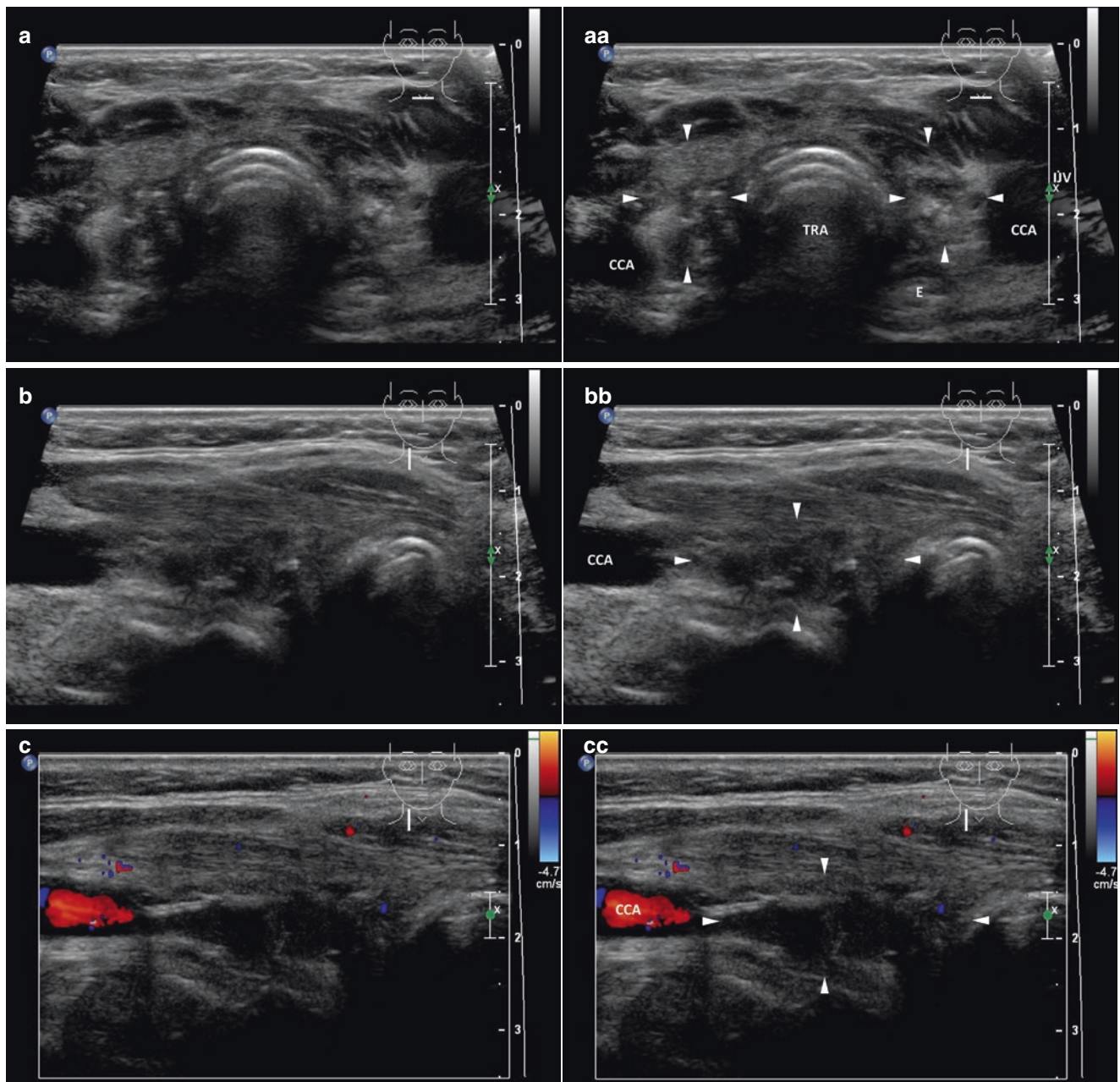


Fig. 20.2 (aa) US of thyroid bed 1 month post thyroidectomy with resorption of post-thyroidectomy hematoma and formation of fibrofatty connective tissue, which may mimic thyroid remnants (arrowheads): inhomogeneous mass; mixed echogenicity with small hyperechoic (fibrotic) areas; ill-defined blurred margin; transverse. (bb) Detail of the right thyroid bed (arrowheads): ill-defined fibrofatty connective tissue; longitudinal.

(cc) Detail of the right thyroid bed (arrowheads), CFDS: avascular tissue; longitudinal. (dd) Detail of the left thyroid bed (arrowheads): ill-defined fibrofatty connective tissue; longitudinal. (ee) Detail of the left thyroid bed (arrowheads), CFDS: avascular tissue; longitudinal

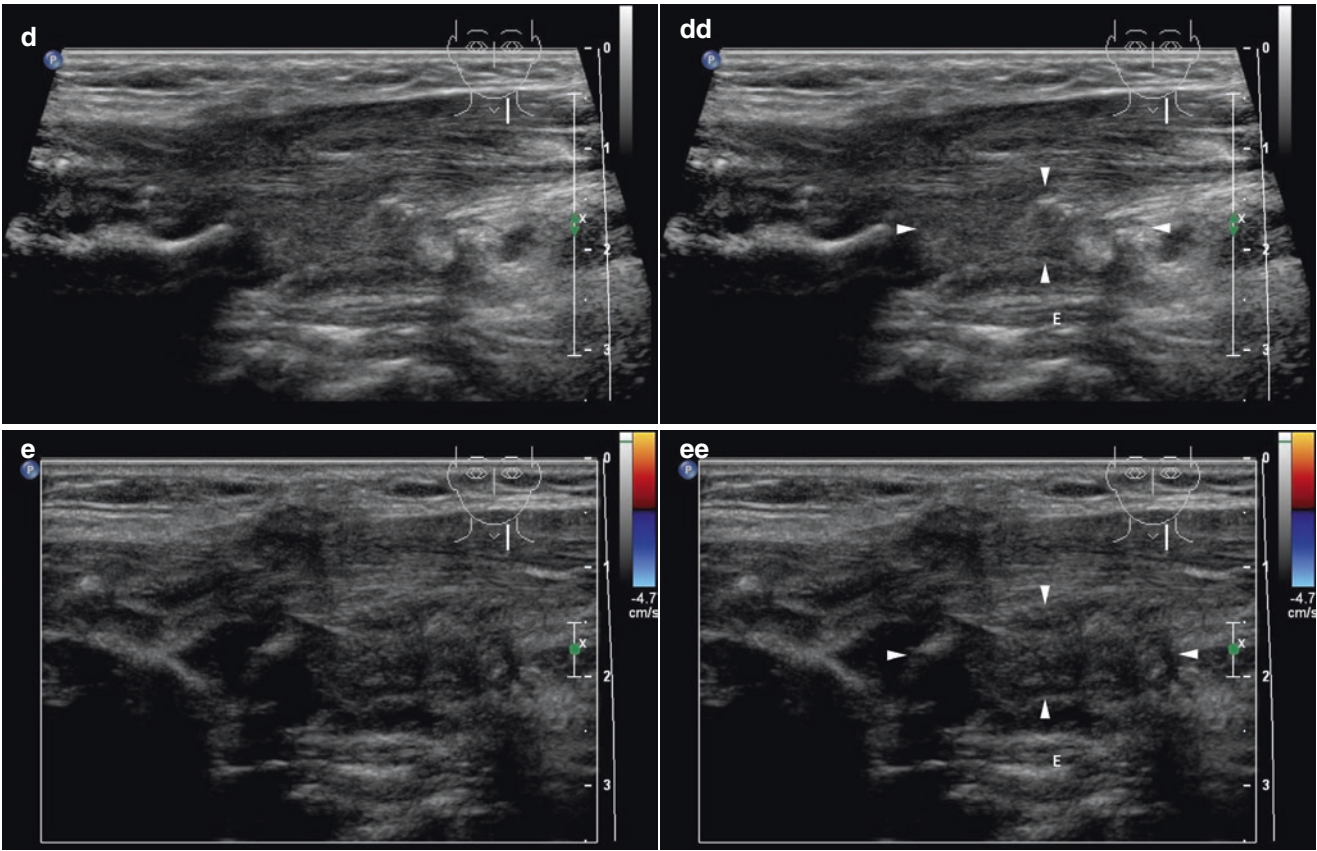


Fig. 20.2 (continued)

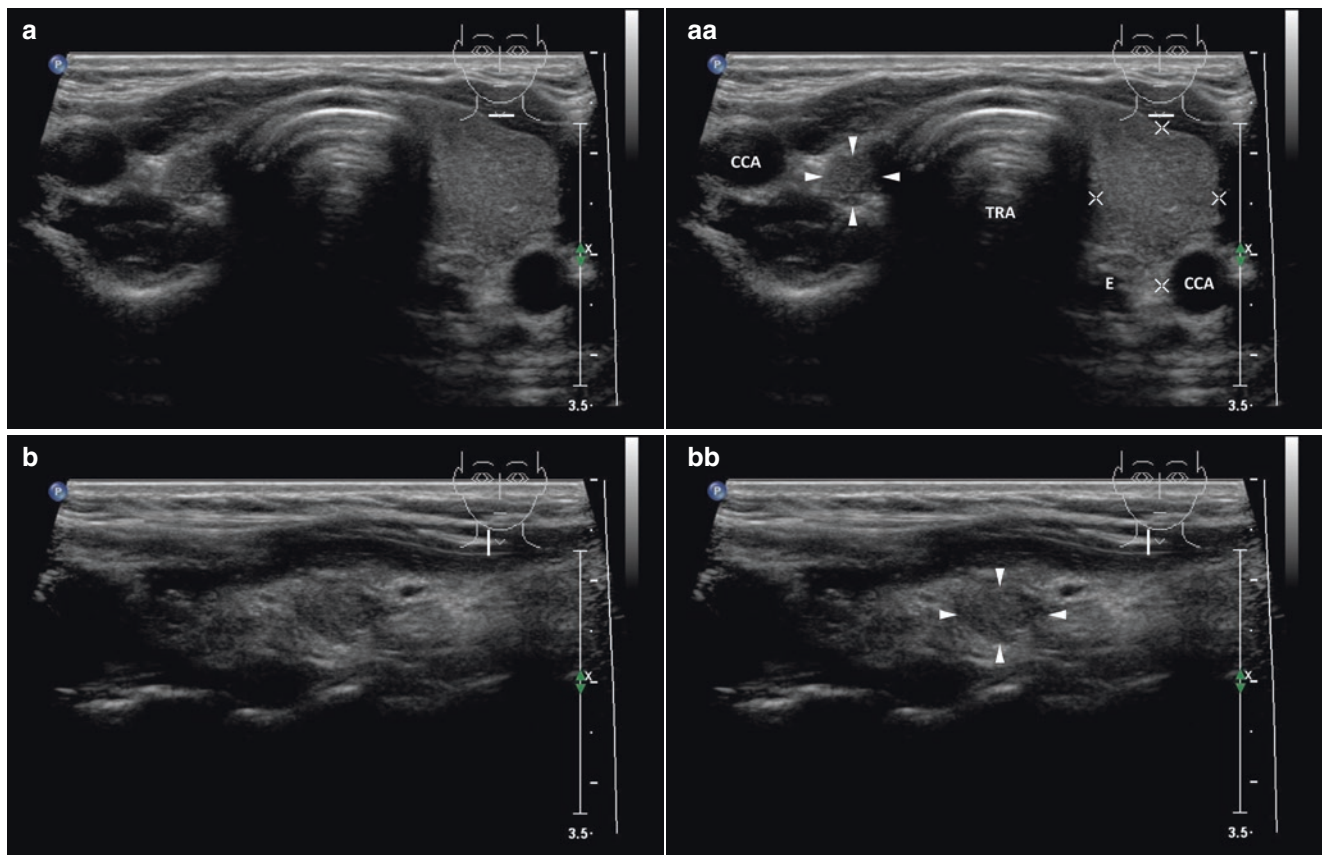


Fig. 20.3 (aa) 3 year post right lobectomy for a solitary complex nodule; tiny remnant (*arrowheads*), size $9 \times 7 \times 5$ mm and volume 0.2 mL in the right thyroid bed: round shape; homogeneous structure; isoechoic;

well-defined smooth margin; normal LL volume 6 mL; transverse. (bb) Detail of tiny remnant (*arrowheads*): oval shape; homogeneous structure; isoechoic; well-defined smooth margin; longitudinal

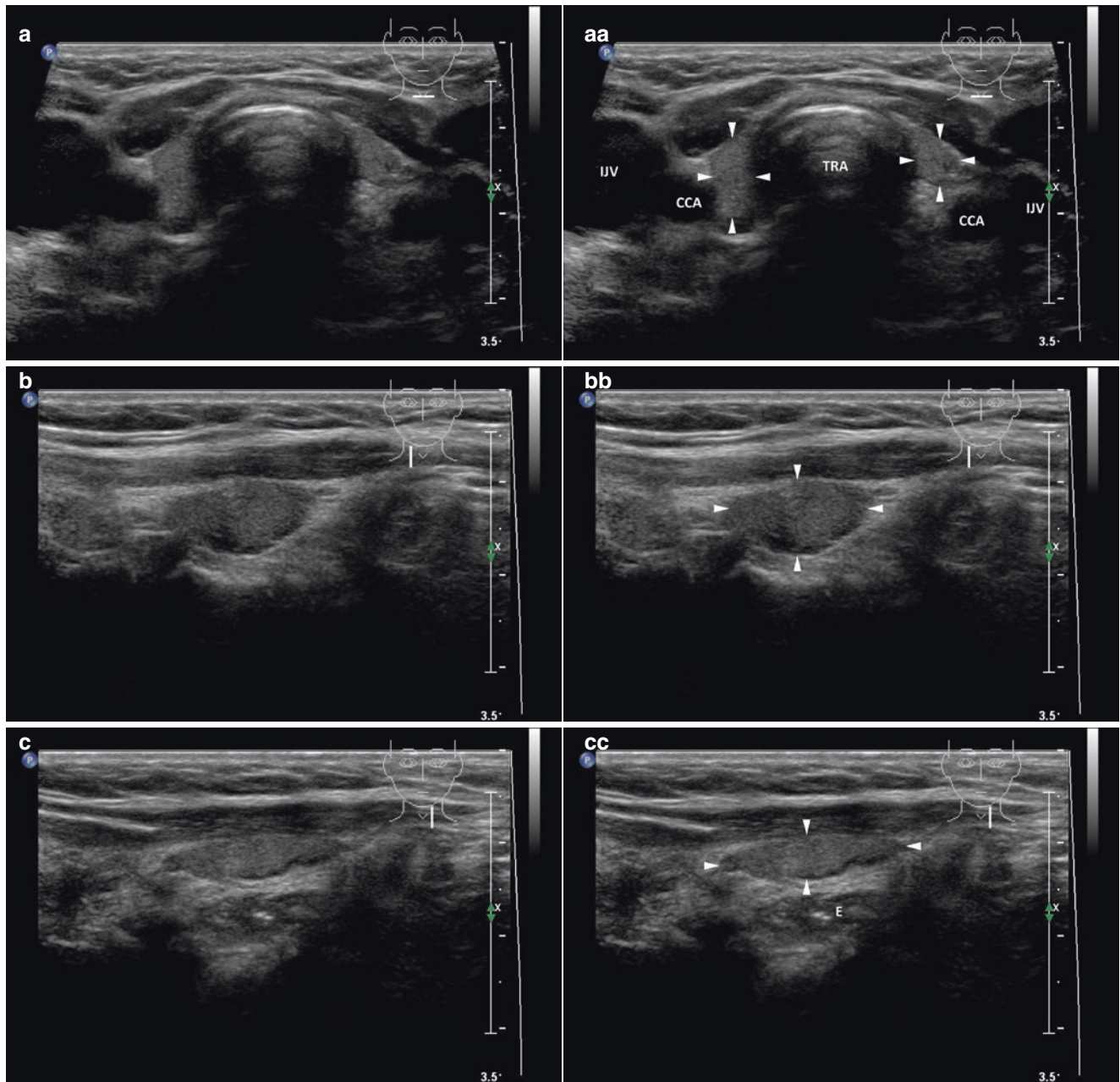


Fig. 20.4 (aa) 3 year post “near” total thyroidectomy for multinodular goiter, tiny remnants (*arrowheads*) in thyroid bed: remnant size $17 \times 9 \times 7$ mm and volume 0.5 mL in the right thyroid bed and remnant size $15 \times 8 \times 6$ mm and volume 0.3 mL in the left thyroid bed: oval shape; homogeneous structure; isoechoic; transverse. (bb) Detail of

tiny remnant (*arrowheads*) in the right thyroid bed: ovoid shape; homogeneous structure; isoechoic; well-defined margin; longitudinal. (cc) Detail of tiny remnant (*arrowheads*) in the left thyroid bed: elliptical shape; homogeneous structure; isoechoic; well-defined, dorsally microlobulated margin; longitudinal

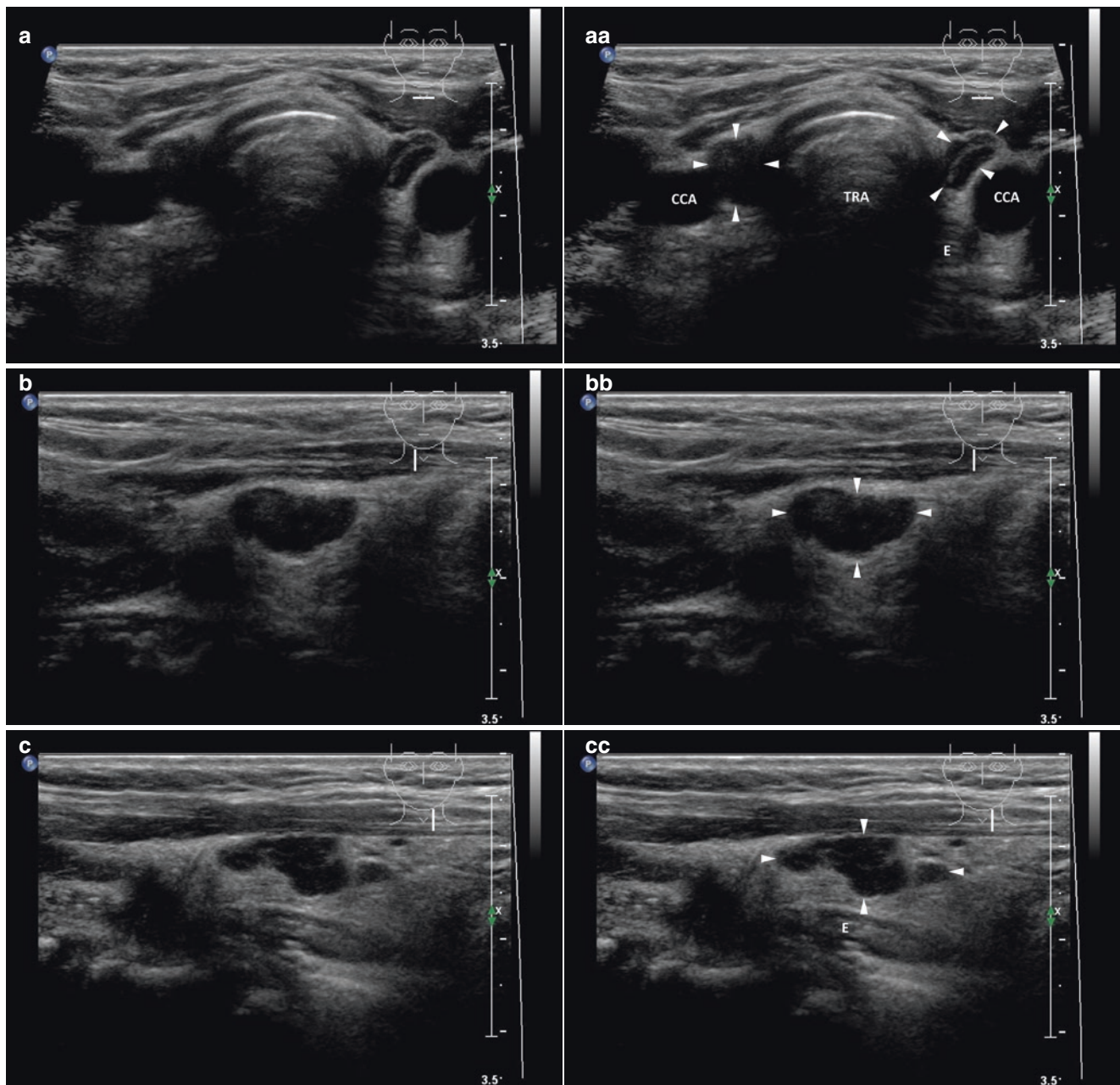


Fig. 20.5 (aa) 12 year post “near” total thyroidectomy for Hashimoto’s thyroiditis, remnants in thyroid bed (*arrowheads*): small remnant—size $17 \times 11 \times 9$ mm and volume 0.8 mL in the right thyroid bed, inhomogeneous hypoechoic structure; tiny remnant—size $14 \times 9 \times 7$ mm and volume 0.5 mL in the left thyroid bed, inhomogeneous hypoechoic structure with coarse echogenic fibrous septum; transverse. (bb) Detail

of small remnant (*arrowheads*) in the right thyroid bed: inhomogeneous hypoechoic structure; microlobulated margin; longitudinal. (cc) Detail of tiny remnant (*arrowheads*) in the left thyroid bed: inhomogeneous hypoechoic micronodular structure with hyperechoic fibrous septa; microlobulated margin; longitudinal

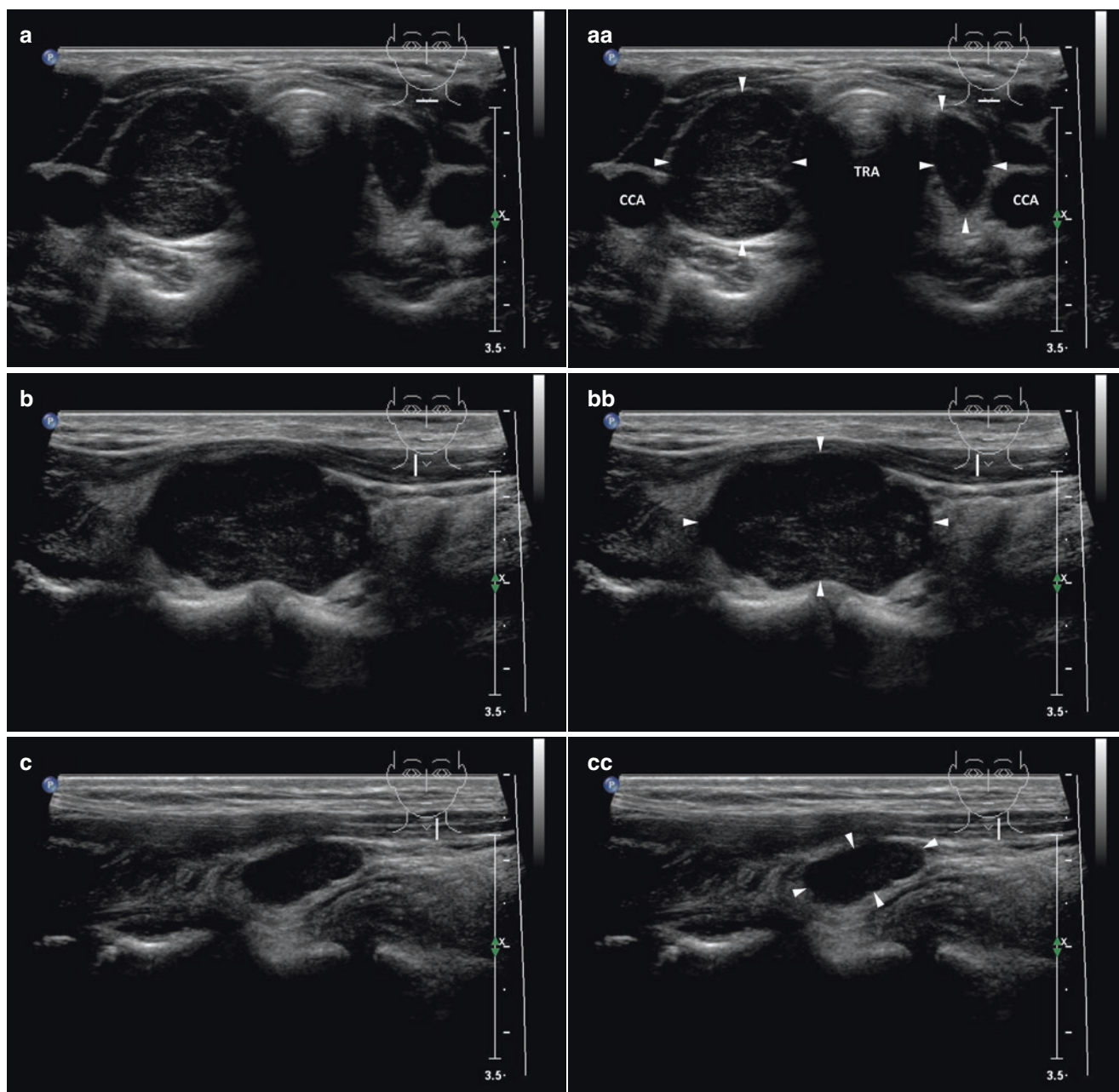
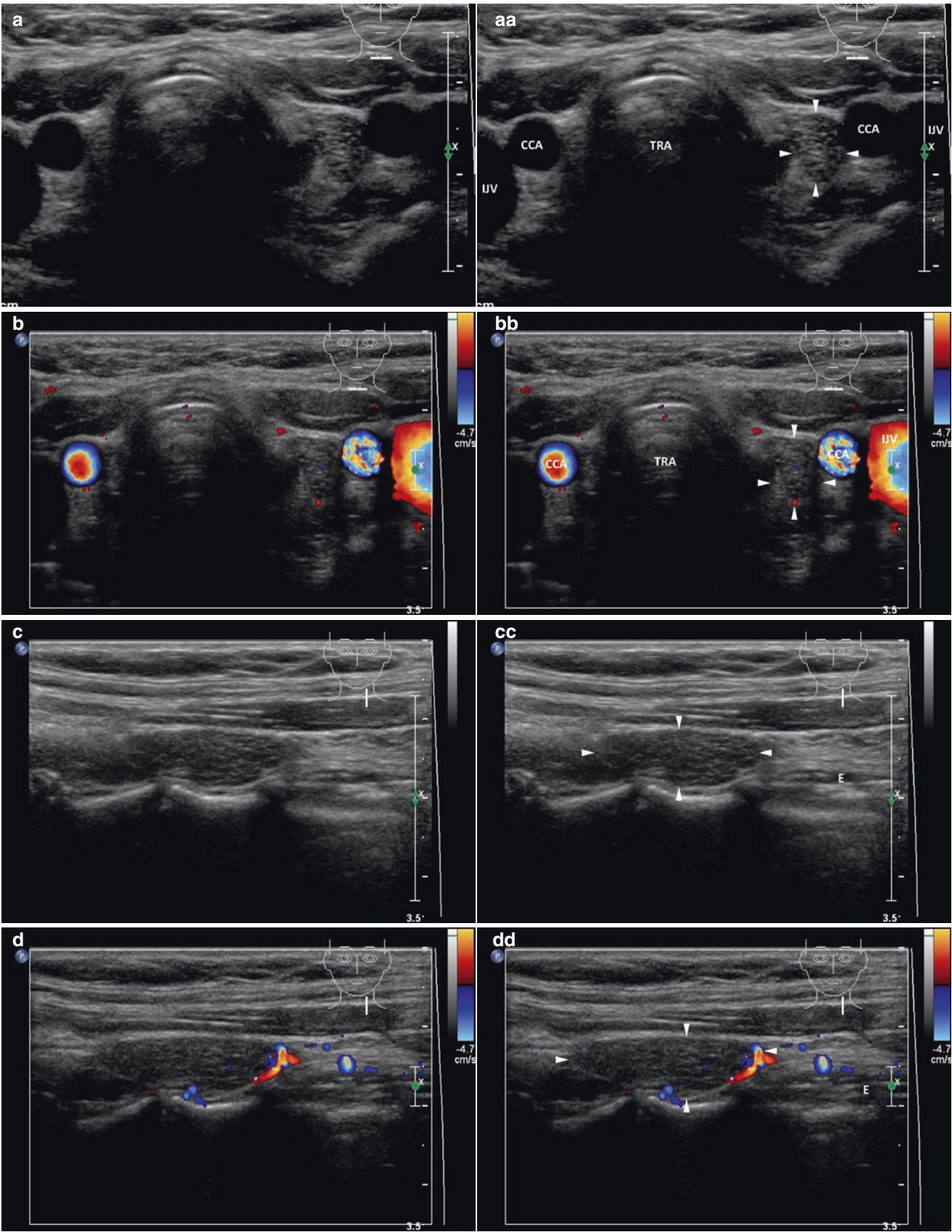


Fig. 20.6 (aa) 14 year post subtotal thyroidectomy for Hashimoto's thyroiditis, remnants in thyroid bed: large remnant (*arrowheads*)—size $29 \times 17 \times 16$ mm and volume 4 mL in the right thyroid bed, inhomogeneous hypoechoic micronodular structure with hyperechoic fibrous septa; small remnant (*arrowheads*)—size $12 \times 12 \times 5$ mm and volume 1 mL in the left thyroid bed, homogeneous, markedly hypoechoic struc-

ture; transverse. (bb) Detail of large remnant (*arrowheads*) in the right thyroid bed: inhomogeneous hypoechoic micronodular structure with hyperechoic fibrous septa; microlobulated margin; longitudinal. (cc) Detail of small remnant (*arrowheads*) in the left thyroid bed: homogeneous markedly hypoechoic structure; smooth margin; longitudinal

Fig. 20.7 (aa) 4 year post “near” total thyroidectomy for Graves' disease (GD), small remnant (*arrowheads*) size $18 \times 8 \times 7$ mm and volume 0.6 mL in the left thyroid bed: oval shape; inhomogeneous hypoechoic micronodular structure with echogenic fibrous septa; well-defined margin; right CCA slides close to the trachea; transverse. (bb) Detail of small remnant (*arrowheads*) in the left thyroid bed, CFDS: minimal

vascularity, *pattern 0*; transverse. (cc) Detail of small remnant (*arrowheads*) in the left thyroid bed: elliptical shape; inhomogeneous hypoechoic micronodular structure with echogenic fibrous septa; well-defined margin; longitudinal. (dd) Detail of small remnant (*arrowheads*) in the left thyroid bed, CFDS: minimal peripheral vascularity, *pattern I*; longitudinal



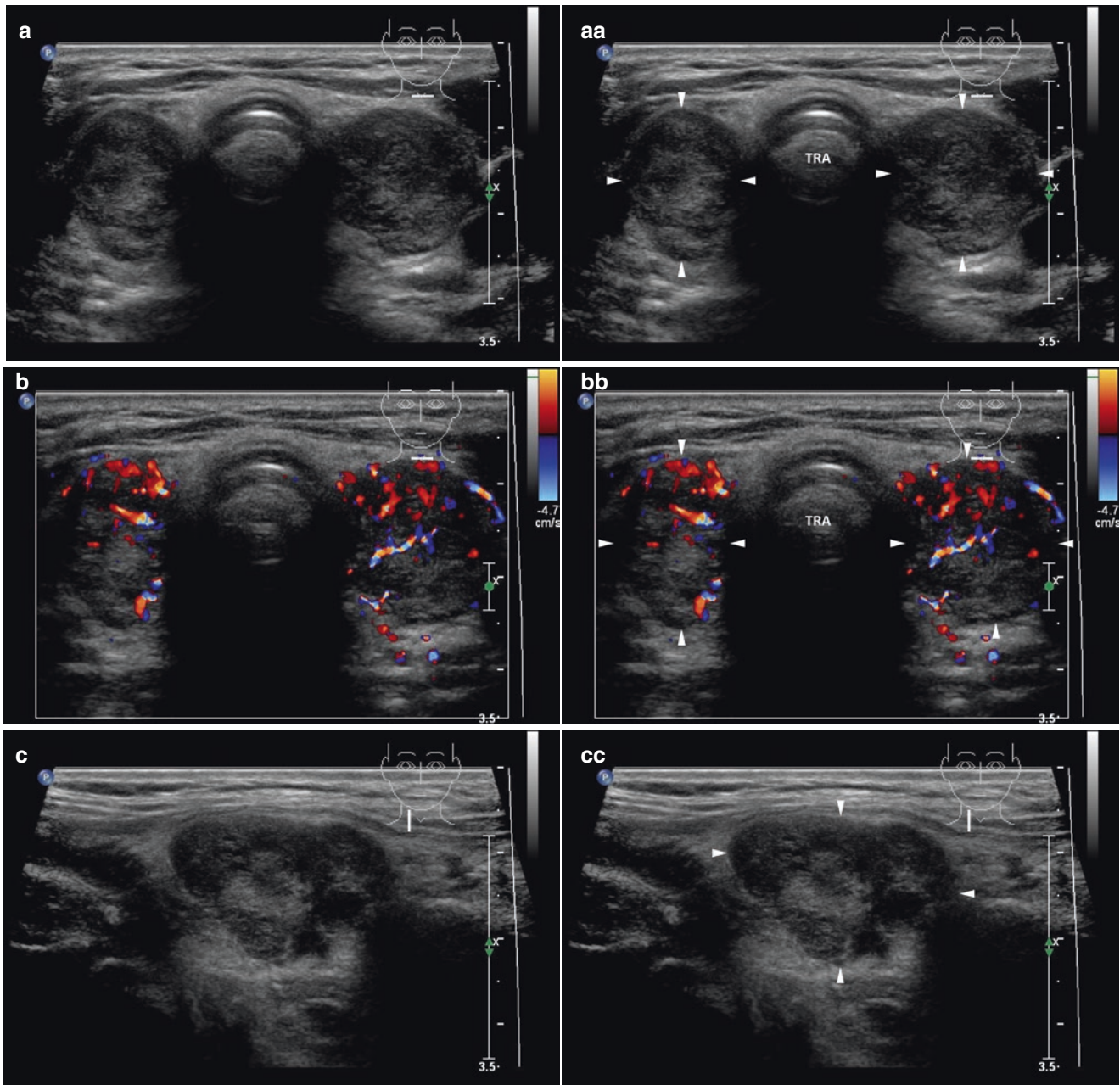


Fig. 20.8 (aa) 20 year post subtotal thyroidectomy for Graves' disease (GD), large remnants (arrowheads) in thyroid bed—size $27 \times 19 \times 18$ mm, volume 5 mL on the right and size $31 \times 22 \times 20$ mm, volume 7 mL on the left: coarse micronodular structure; mixed echogenicity; transverse. (bb) Both remnants (arrowheads) overall view, CFDS: hypervascularity, *pattern III*; transverse. (cc) Detail of remnant (arrowheads) in the right thyroid bed: ovoid shape; coarse micronodu-

lar structure; mixed echogenicity; longitudinal. (dd) Detail of remnant (arrowheads) in the right thyroid bed, CFDS: hypervascularity, *pattern III*; longitudinal. (ee) Detail of remnant (arrowheads) in the left thyroid bed: ovoid shape; coarse micronodular structure; mixed echogenicity; longitudinal. (ff) Detail of remnant (arrowheads) in the left thyroid bed, CFDS: hypervascularity, *pattern III*; longitudinal

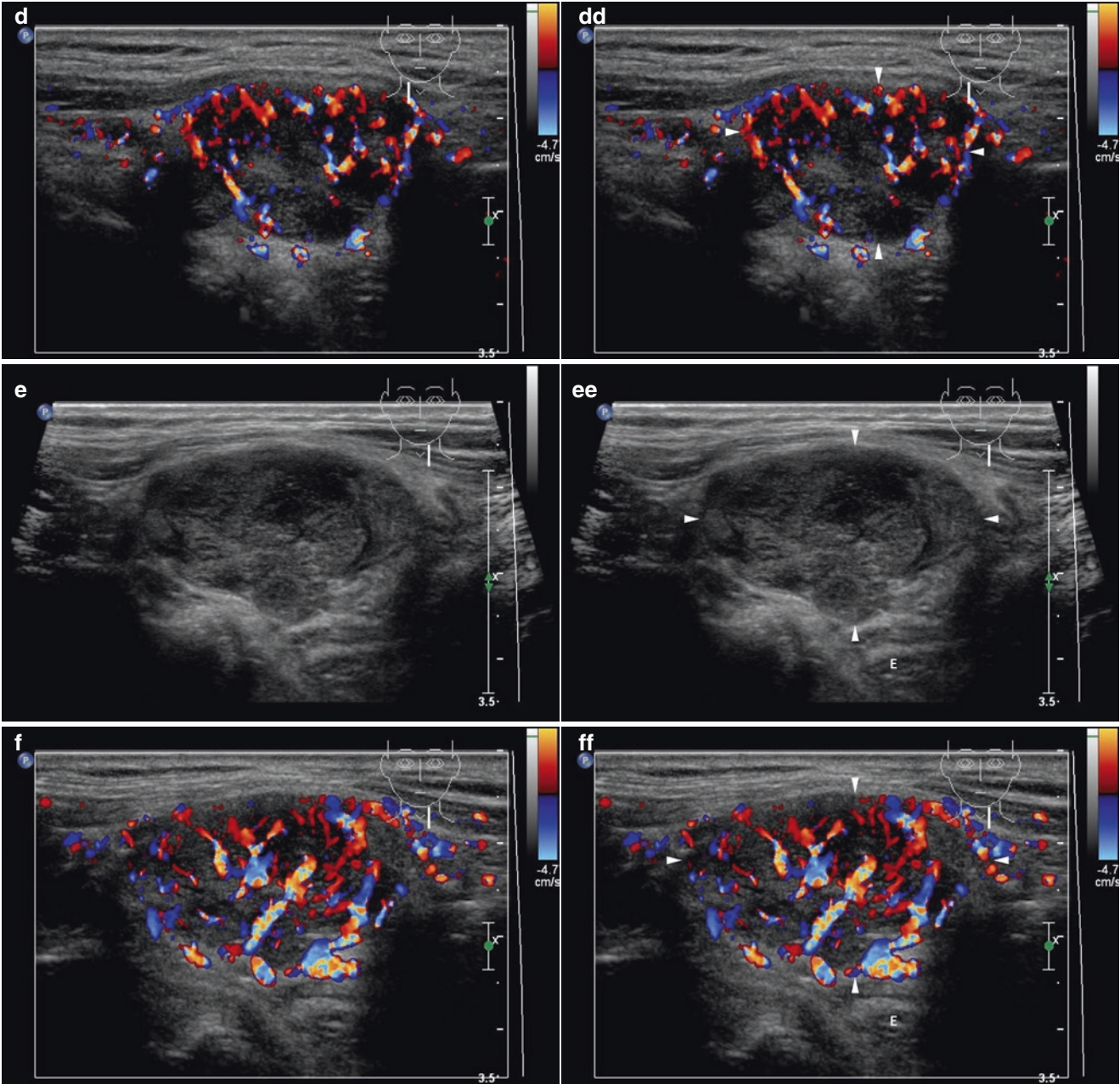


Fig.20.8 (continued)

References

1. D'Andrea V, Cantisani V, Catania A, Di Matteo FM, Sorrenti S, Greco R, et al. Thyroid tissue remnants after "total thyroidectomy". *G Chir*. 2009;30(8–9):339–44.
2. Bron LP, O'Brien CJ. Total thyroidectomy for clinically benign disease of the thyroid gland. *Br J Surg*. 2004;91(5):569–74.
3. Sugino K, Ito K, Nagahama M, Kitagawa W, Shibuya H, Ito K. Surgical management of Graves' disease—10-year prospective trial at a single institution. *Endocr J*. 2008;55(1):161–7.
4. Jarzab B, Handkiewicz-Junak D, Wloch J. Juvenile differentiated thyroid carcinoma and the role of radioiodine in its treatment: a qualitative review. *Endocr Relat Cancer*. 2005;12(4):773–803.
5. Maxon HR. Quantitative radioiodine therapy in the treatment of differentiated thyroid cancer. *Q J Nucl Med*. 1999;43(4):313–23.
6. Mazzaferri EL, Kloos RT. Clinical review 128: current approaches to primary therapy for papillary and follicular thyroid cancer. *J Clin Endocrinol Metab*. 2001;86(4):1447–63.
7. Irawati N. Endoscopic right lobectomy axillary-breast approach: a report of two cases. *Int J Otolaryngol*. 2010;2010:958764.
8. Zaheer S, Tan A, Ang ES, Loke KS, Kao YH, Goh A, et al. Post-thyroidectomy neck ultrasonography in patients with thyroid cancer and a review of the literature. *Singap Med J*. 2014;55(4):177–82.

21.1 Essential Facts

- Thyroid hemiagenesis (Fig. 21.1aa) is a rare congenital abnormality of the thyroid gland, characterized by the absence of one lobe. The true prevalence of this congenital abnormality is not known because the absence of one thyroid lobe usually does not cause clinical symptoms by itself. In 2000, Shabana et al. performed a systematic US study of the thyroid gland volume for the evaluation of iodine deficiency in 2845 normal Belgian schoolchildren and found an absence of the left lobe in six children (four girls and two boys). There was no association with other thyroid malformations or dysfunction. The prevalence of thyroid hemiagenesis was established of 0.2% and confirmed the female predominance and higher incidence of agenesis of the left lobe [1].
- A large retrospective study between 1970 and 2010 in Sicily by De Sanctus et al. found 329 (1.3%) cases of thyroid hemiagenesis in 24,032 unselected schoolchildren from 11 to 14 years old. It is interesting to note that most cases have an agenesis of the left lobe (80%) followed by

the isthmus (44–50%), and the girl-to-boy ratio was 1:1.4, contrary to other studies that document a higher prevalence in women. The hemiagenesis is mostly diagnosed when a patient presents a lesion in the remaining/functioning lobe. The solitary functioning lobe can be a site of pathological changes similar to a normally developed thyroid gland [2].

- Lipomas arise in almost 50% of all soft tumors. The neck lipomas are rare tumors that may present as painless masses with slow growth in the lateral portions of the neck [3].
- Branchial cleft remnants, which arise from the incomplete obliteration of any branchial tract, accounts for the majority of branchial cleft anomalies. Clinically they can present as different morphologic patterns: approximately 70% are hypoglossal duct sinuses and cysts, 25% are branchial cysts and sinuses, and 5% are cystic hygromas [4].
- Branchial cleft cysts (BCCs) can first come to clinical attention usually in a child or young adult in the second through fourth decades of life. They present clinically as smooth, soft, ovoid, cystic masses in the lateral part of the

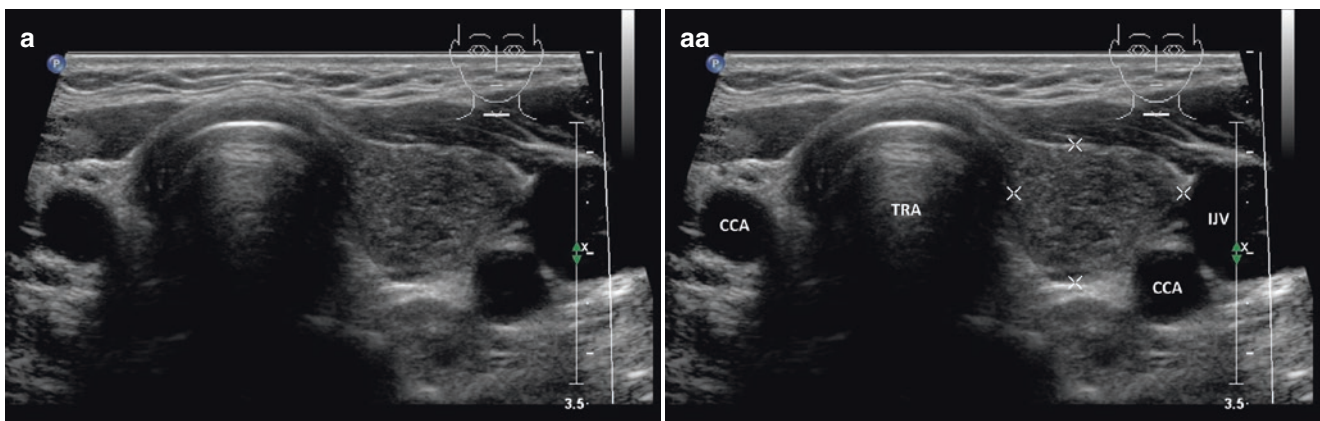


Fig. 21.1 (aa) A 71-year-old woman with hemiagenesis of the RL and isthmus, Hashimoto's thyroiditis (HT) in the solitary LL. The diagnosis was established in middle-age, when she presented with features of hypothyroidism and anti-thyroid antibodies positive for HT. US appear-

ance: empty right thyroid bed; LL—inhomogeneous with hypoechoic micronodular structure and thin hyperechoic fibrous septa; volume 5 mL; transverse

neck, behind the angle of the mandible, and anterior to the sternocleidomastoid muscle [5, 6].

- Dermoid cysts (DCs) are benign lesions histologically composed of tissues originating from the ectoderm and the mesoderm, but never from the endoderm. Approximately 7% of all DCs are seen in the head and neck area (the third most common site, after the coccyx in 44% and the ovary in 42%), and they are located most often in superficial subcutaneous tissues. DCs can occur at any age with no gender predilection, but more than 50% of all cases are detected by the age of 6 years. DCs are generally asymptomatic unless they grow enough to be conspicuous, causing cosmetic problems or compressive effects. Congenital cysts arise from a rest of embryonic epithelium such as bronchial cleft cyst, and are acquired as a result of traumatically implanted skin in the deeper tissues. The lumen of the cyst contains amorphous material with a few hair shafts [7].
- Other non-thyroid cystic neck masses include lymphatic malformation, ranula, and parathyroid cyst (Fig. 22.10aa). US-guided sclerotherapy (by sclerosant agents 96% ethanol or OK-432) is an alternative treatment for all benign non-thyroid cystic neck masses [8].
- Intravascular extension of tumor cells by direct intraluminal spread is more commonly encountered in anaplastic thyroid carcinoma. Invasion of internal jugular vein (IJV) by thyroid cancer indicates a poor outcome. Differentiated thyroid carcinomas (DTC) as papillary and more often follicular and Hurthle cell carcinomas have well-documented microscopic characteristics of microinvasion affecting the great cervical veins. Direct extraluminal vascular invasion with DTCs is extremely rare. Cervical and arm edema and pain are the most common presentations of IJV thrombosis [9, 10].
- The cellulitis—phlegmon and superficial abscess are acute processes of neck swelling. Clinically, there are general differences between the two. The pain caused by cellulitis tends to be more severe and generalized than the localized pain associated with an abscess. Cellulitis often presents with swelling, warmth, erythema, and tenderness over the affected area and equates to the descriptive Latin terms “*tumor*,” “*calor*,” “*rubor*,” and/or “*dolor*.” The firmness of the cellulitis can range from doughy to indurate. The borders of cellulitis are typically large, smooth, ill-defined, and do not contain pus. An abscess usually has a small and well-circumscribed borders with signs of inflammation, and is soft or fluctuant to palpation, indicating a pus-filled cavity. Patients with systemic infections often have fever [11].
- Differentiating a soft tissue abscess from cellulitis is important because each of these disorders requires a different treatment approach. Whereas cellulitis responds to systemic antibiotics, an abscess must be drained surgically. Diagnosis is complicated by the fact that abscesses often begin as cellulitis and therefore the two conditions frequently coexist [12].
- Squire et al. investigated 135 patients with soft tissue infection (76 with abscess and 59 with cellulitis). Comparison of clinical examination alone with US examination for superficial abscess showed the sensitivity 86% vs. 98% and the specificity 70% vs. 88%, the positive predictive value 81% vs. 93%, and the negative predictive value 77% vs. 97%. In 18 cases, US was not consistent with the clinical examination, but US finding was correct in 17 (94%) of the cases. However, three patients with false-positive findings of abscess on US turned out to have hematomas. Concluding, bedside US improves accuracy in detection of superficial abscesses [12].
- Postoperative hemorrhage is a well-known complication of thyroid surgery. It requires special attention because it may represent a life-threatening situation due to acute airway obstruction from the deep hematoma. The reported incidence of post-thyroidectomy hemorrhage varies from 0.36 to 4.3%. The etiology of post-thyroidectomy hemorrhage has been described as slipping of the major vessel ligature, reopening of the cauterized veins, retching and bucking of the patient during recovery, a Valsalva maneuver, increased blood pressure and oozing from the thyroid cut area. Neck swelling is frequently identified as a representative clinical sign of post-thyroidectomy hemorrhage. The ecchymosis is often identified in cases of superficial hematoma, but rare in cases of deep hematoma [13].

21.2 US Findings of Lesions at the Anterior Neck Space Mimicking Thyroid

- US findings of branchial cysts (Fig. 21.5bb): a well-defined cystic mass [6].
- US findings of dermoid and epidermoid cysts (Fig. 21.6aa): cyst has an internal echo, with a solid appearance with only slight or no posterior echo enhancement. Amorphous keratinous debris from keratinizing stratified squamous epithelium fills the lumen of each cyst, producing the internal echoes. Caution! Lipomas are indistinguishable from these cysts. US-FNAB clarifies the cystic nature, cytological evaluation reveals benign-appearing squamous cells and amorphous cellular debris [14].
- US findings of lipoma (Fig. 21.3bb): an elongated isoechoic or hyperechoic mass in the subcutaneous tissues (very much like those of subcutaneous fat tissue). The existence of striated echoes in the tumor corresponding to the septa increases the possibility of lipoma. US is useful for acquiring information about the nature, size, and depth of the lesion as well as its relationship to adjacent vessels and other structures, especially the thyroid gland [3]. Caution! US can reveal lipoma and coexisting MNG (Fig. 21.4aa).
- US findings of a thrombus in the internal jugular vein (Fig. 21.7aa): the vein is expanded and contained a thrombus of heterogeneous, dominantly hyperechoic structure [15].
- US findings of a tumor thrombus in the internal jugular vein (Fig. 15.36aa): cancer mass of thyroid lobe (often with multiple areas of necrosis) extending and invading the jugular vein wall; the cancer and thrombus are hypervascular in CFDS. Moreover, CFDS demonstrates a totally or partially absent flow in IJV [9].
- US findings of superficial abscess: spherical in shape with poorly defined borders, content forms heterogenic, anechoic, or hypoechoic mass containing a variable amount of internal echoes. Compression of the mass with the transducer may demonstrate movement or “swirling” of pus [12].
- US findings of cellulitis—phlegmon (Fig. 21.9aa): a thickening and diffuse hyperechogenicity of the subcutaneous fat with obliteration of the interface between the echogenic fat and the dermis. This is commonly referred to as “cobblestoning.” There are increased local reactive LNs. CFDS helps differentiate soft tissue infections by demonstrating diffuse hypervascularity in areas of inflammation [12].
- US findings of hematomas (Fig. 21.8dd): the echogenicity of blood contained within a hematoma is variable and depends largely on time of stasis. Initially blood appears anechoic, but over several hours, as the blood begins to coagulate, it appears more and more echogenic. Pus also appears echogenic but is differentiated from congealed blood by its heterogeneity. Clotted blood appears uniformly echogenic, while pus has a variable echogenic pattern [12]. Superficial hematoma indicates a hematoma located between the subplatysmal dissection plane and the strap muscles, while deep hematoma indicates a hematoma between the strap muscles and the thyroid bed [13].
- US of the scare after tracheostomy (Figs. 21.11aa and 23.2cc): an interrupting the continuity of the isthmus, deformed trachea with indentation of the wall [16].

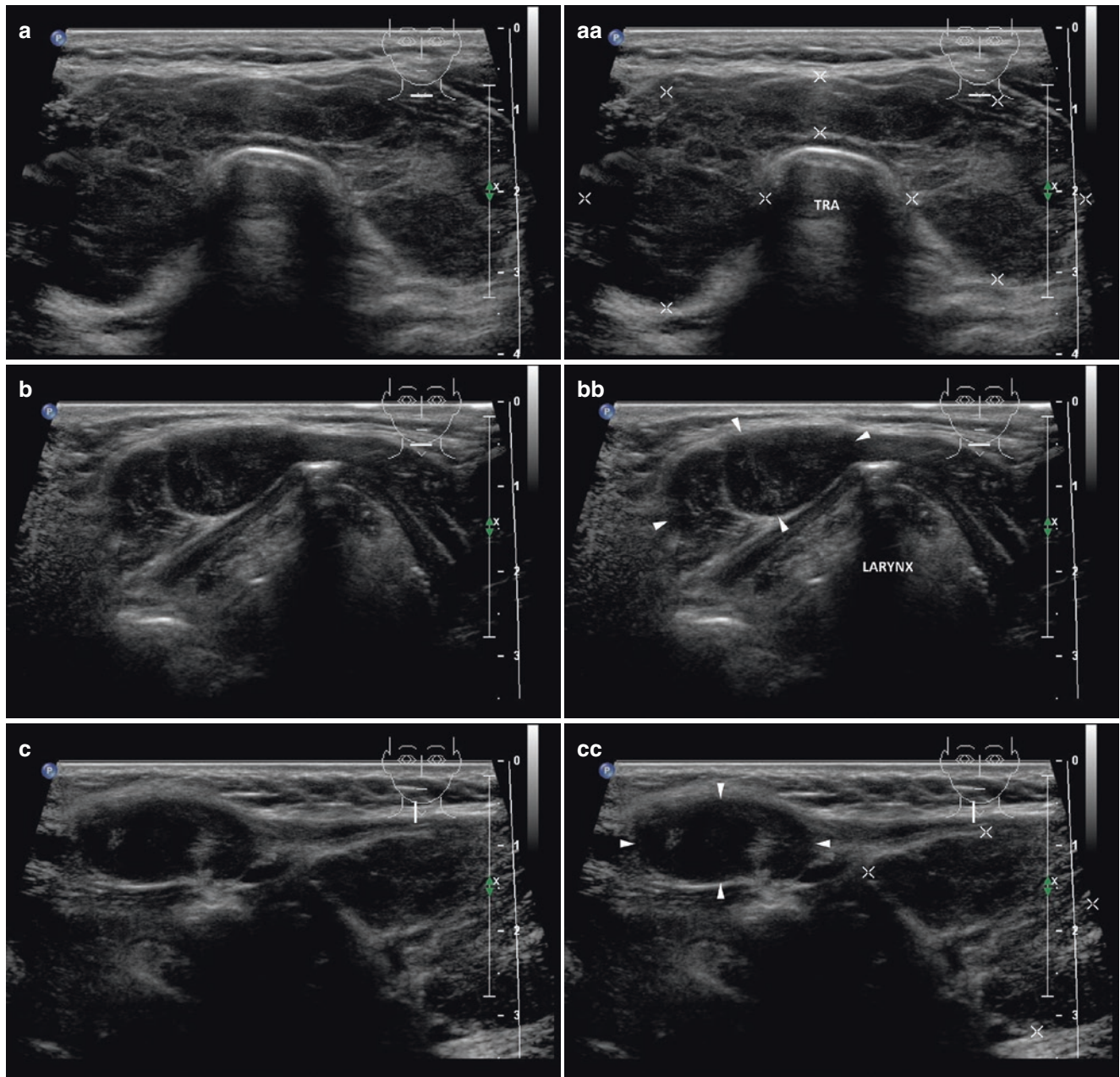


Fig. 21.2 (aa) A 65-year-old woman presented with 5 years palpable painless mass next to the right laryngeal cartilage. Since middle-age she has been treated for hypothyroidism and anti-thyroid antibodies positive for the Hashimoto's thyroiditis (HT). US demonstrates large pyramidal lobe, size $25 \times 23 \times 12$ mm and volume 3.5 mL and HT: enlarged thyroid gland—coarse structure; mixed echogenicity; hypoechoic micronodular structure with thick hyperechoic fibrous septa and areas; microlobulated margin; Tvol 37 mL, RL 20 mL, and LL 17 mL;

transverse. (bb) Detail of large pyramidal lobe (arrowheads); confirmed by US-FNAB: inhomogeneous hypoechoic micronodular structure with echogenic fibrous septa; US appearance similar to Hashimoto's goiter; transverse. (cc) Detail of large pyramidal lobe (arrowheads): space visible between pyramidal lobe and upper pole of the RL; longitudinal. (dd) Detail of large pyramidal lobe (arrowheads), CFDS: diffusely increased vascularity of both, pyramidal lobe and the RL, pattern II; longitudinal

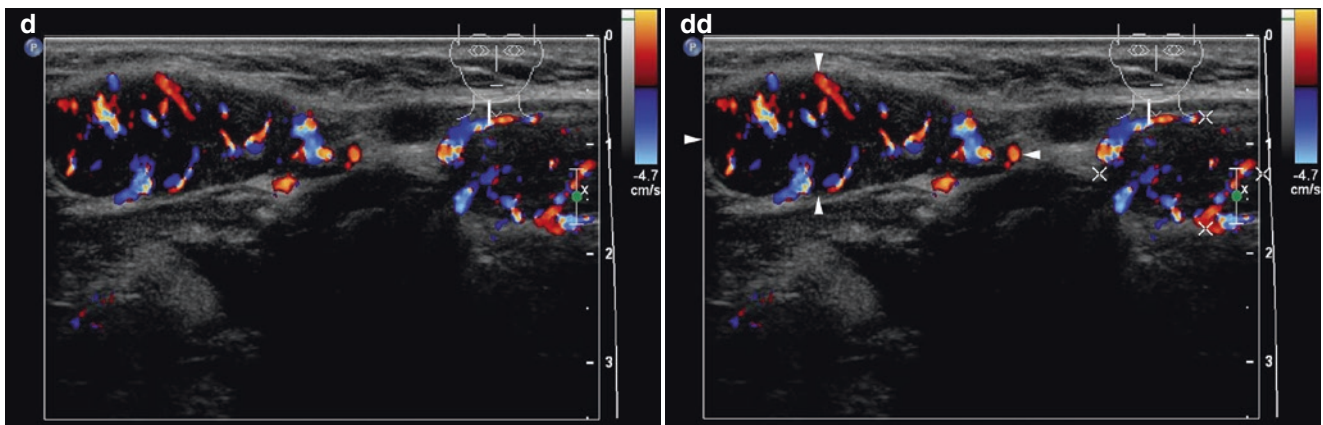


Fig. 21.2 (continued)

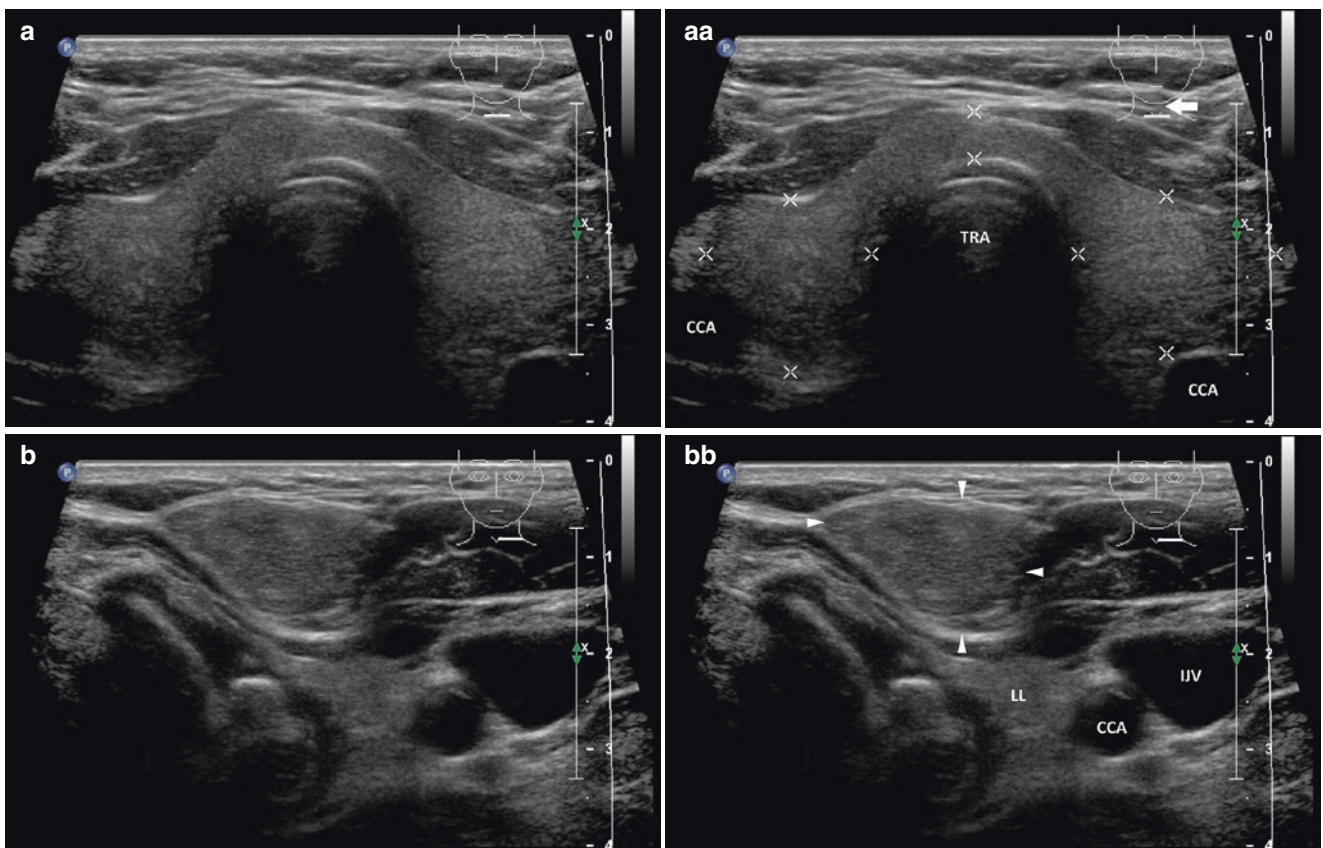


Fig. 21.3 (aa) A 66-year-old man, presented with 1 year palpable painless mass next to the left laryngeal cartilage. US showed separated lipoma (confirmed by US-FNAB), volume 4 mL, localized ventrally in front of the upper pole of the LL. US overall view of thyroid gland: the normal thyroid gland; Tvol 20 mL, RL 9 mL, and LL 11 mL; transverse. Note: pictogram—*thick arrow* indicates location of lipoma (*not shown*)—cranially from the current probe position. (bb) Detail of lipoma (*arrowheads*), ventrally in front of the upper pole of the LL:

well-defined solid mass; homogeneous structure; hyperechoic; transverse. (cc) Overall view of the lipoma (*arrowheads*) and thyroid gland: lipoma clearly separated from the upper pole of the LL by a thin strip of muscle (*arrows*); there are shown upper poles of both thyroid lobes, LL pushed dorsally; transverse. (dd) Detail of lipoma (*arrowheads*): lipoma clearly separated from anterior part of the LL by thin strip of muscle (*arrows*); longitudinal

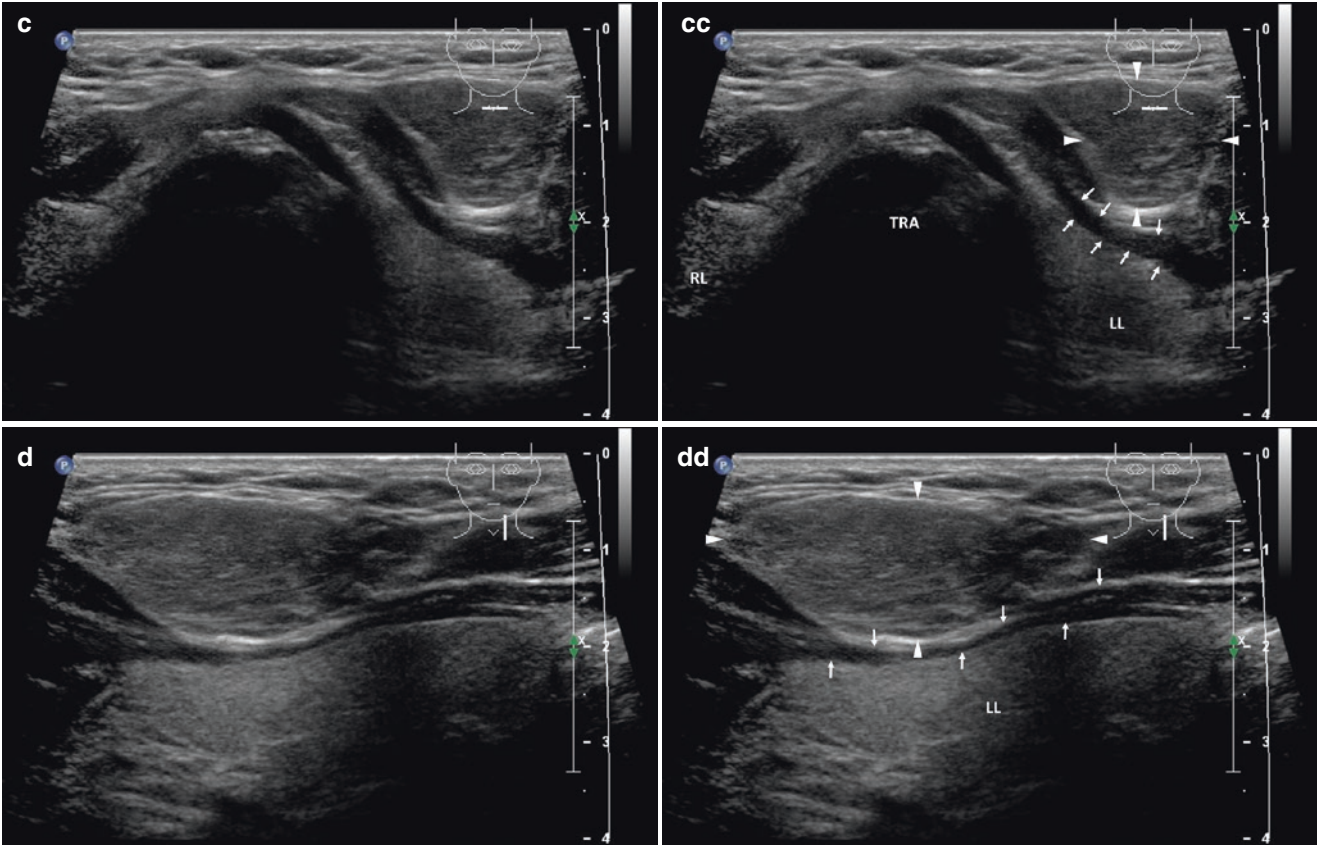


Fig. 21.3 (continued)

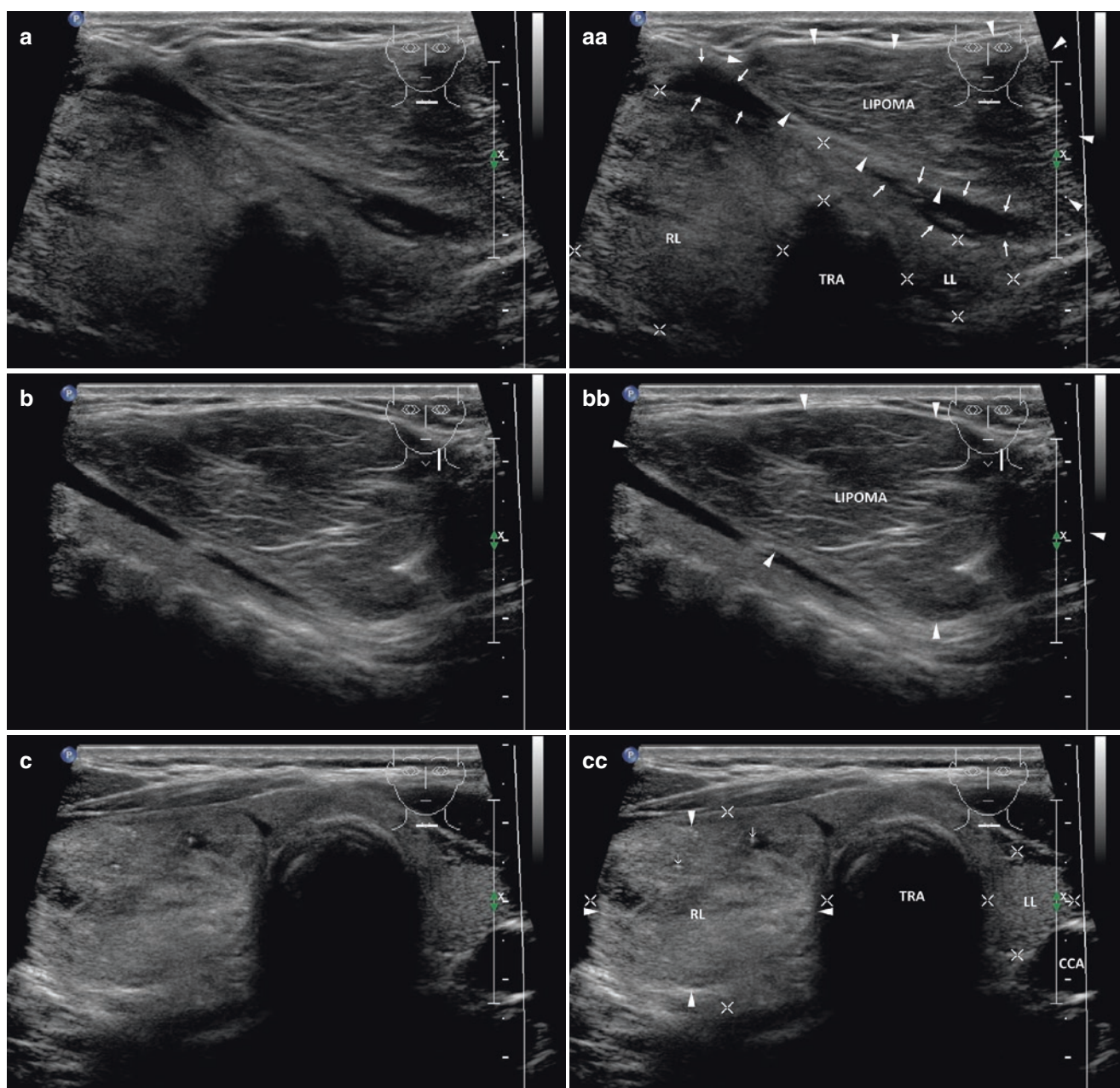


Fig. 21.4 (aa) A 72-year-old man, presented with 5 years palpable painless mass under the laryngeal cartilage in the midline and on the left side. Palpable mass was for many years considered as a goiter. US revealed coexisting multinodular goiter (MNG) palpable on the right side, and large lipoma (confirmed by US-FNAB), size $51 \times 50 \times 24$ mm, volume 32 mL, palpable on the left side and imitating goiter. US overall view of lipoma (arrowheads) and thyroid gland: lipoma localized ventrally in front of the LL, clearly separated from the anterior part by thin strip of muscle (arrows) and pushes LL dorsally; coexisting

MNG—enlarged RL; coarse structure; hyperechoic; Tvol 39 mL, asymmetry—RL 32 mL and LL 7 mL; transverse. (bb) Detail of lipoma (arrowheads): well-defined solid, hyperechoic mass; longitudinal. (cc) Detail of the thyroid gland with large solid nodule (arrowheads), size $36 \times 33 \times 30$ mm and volume 17 mL in the RL: round shape; more wide than tall (non-suspicious); coarse structure; hyperechoic; sporadic tiny cystic cavities (c) and microcalcifications (open arrows); well-defined margin with thin halo sign; transverse

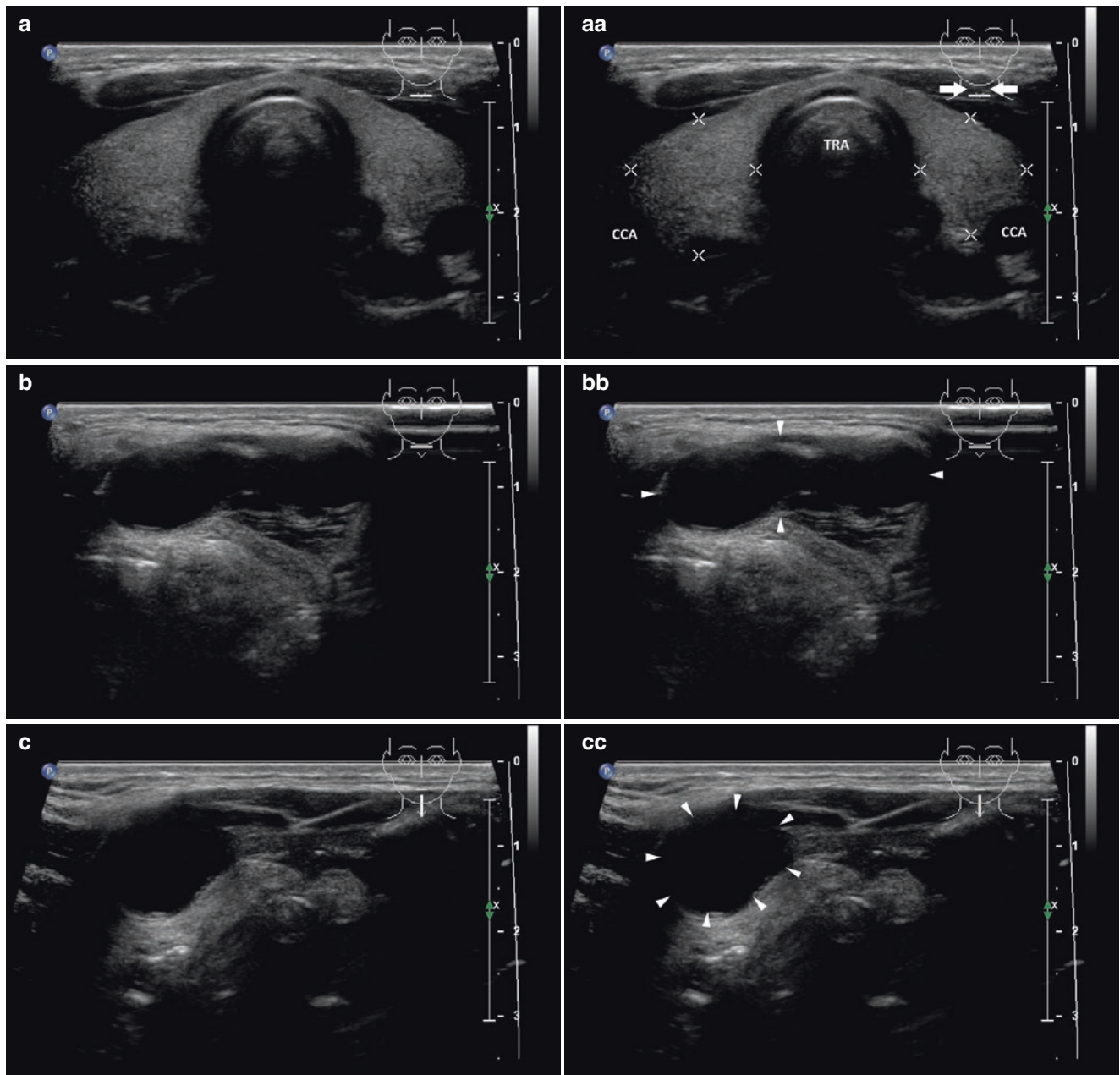
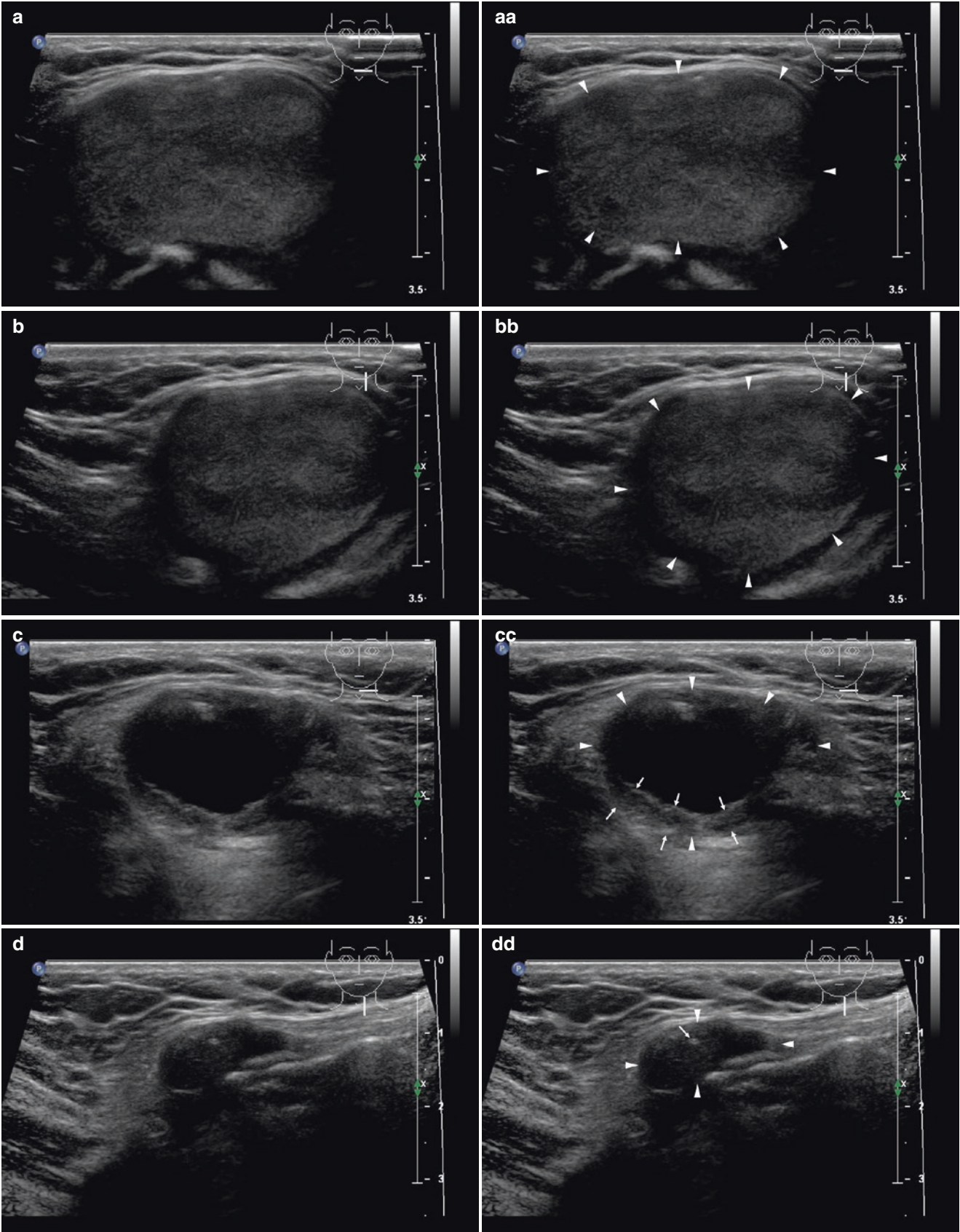


Fig. 21.5 (aa) A23-year-old woman with branchial cleft cyst (BCC), diagnosed in the childhood at age 11. FNAB and evacuation were performed once, but the cyst relapsed. Now is manifested as palpable mass in the central neck above the laryngeal cartilage. US revealed cyst sized $33 \times 17 \times 10$ mm, volume 3 mL; normal thyroid gland; Tvol 11 mL, RL 6 mL, and LL 5 mL; transverse. Note: pictogram—*thick*

arrow indicates location of BCC (*not shown*)—cranially from the current probe position. (bb) Detail of BCC (*arrowheads*): well-defined transversally elongated lesion with anechoic content and fine wall; transverse. (cc) Detail of BCC (*arrowheads*): well-defined ovoid lesion with anechoic content and fine wall; longitudinal

Fig. 21.6 (aa) A 50-year-old man with more than 10 years visible and palpable mass in the central neck above the laryngeal cartilage. In order to hide this resistance, he chose to wear a full beard. US showed large apparently solid lesion (*arrowheads*), size $36 \times 35 \times 23$ mm and volume 15 mL; ovoid, well-defined, homogeneous, hyperechoic mass; distant from the normal thyroid gland (*not shown*); transverse. The initial US view suggested large lipoma. But FNAB was performed and aspiration surprisingly yielded 15 mL of dense café au lait fluid. The

final cytologic diagnosis was dermoid cyst. (bb) Detail of dermoid cyst (*arrowheads*): homogeneous, hyperechoic mass; longitudinal. (cc) Detail of dermoid cyst (*arrowheads*) 1 month post evacuation: cyst relapsed to volume 3.5 mL; thick hyperechoic wall (*arrows*); anechoic contents; transverse. (dd) Detail of shrunken dermoid cyst (*arrowheads*) 6 months after successful PEIT: solid, inhomogeneous hypoechoic mass, size $19 \times 12 \times 12$ mm and volume 1.5 mL; dotted area of fibrosis in the center (*arrow*); longitudinal



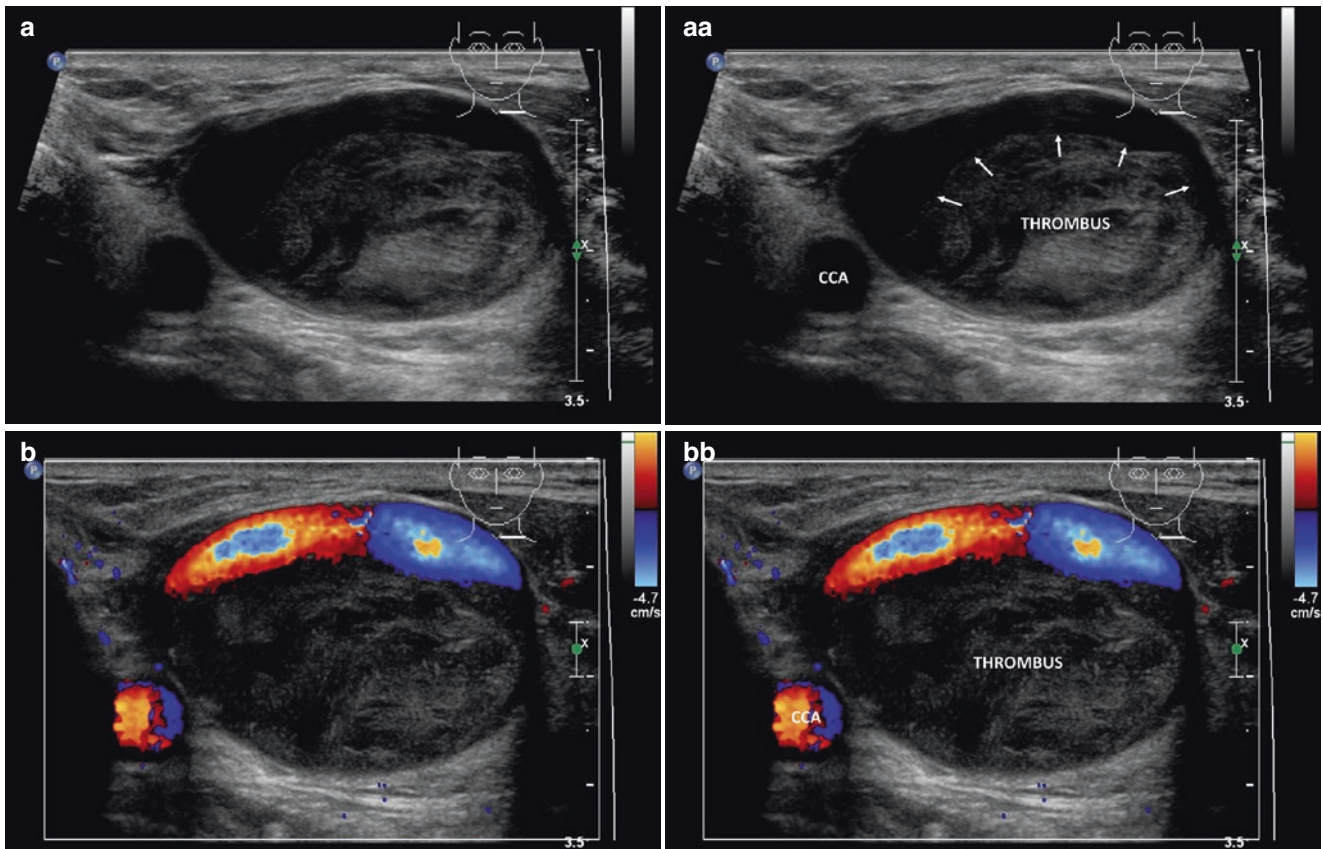


Fig. 21.7 (aa) A 58-year-old woman 7 years post thyroidectomy for PTC with 1 month palpable resistance in the thyroid region left side. Metastasis of PTC was considered. However, large thrombus in the left internal jugular vein (IJV) was detected on US: expanded vein with mostly hyperechoic solid mass filling almost the whole lumen; anechoic crescent-shaped lumen preserved along the wall of IJV (*arrows*); no remnants in the thyroid lodge; transverse. (bb) Detail of hyperechoic

thrombus, CFDS: preserved flow through crescent-shaped lumen; transverse. (cc) Detail of large, almost complete thrombosis, left IJV: mostly hyperechoic thrombus and preserved anechoic lumen (*arrows*) along the anterior wall; longitudinal. (dd) Detail of hyperechoic thrombus, CFDS: preserved flow through crescent-shaped lumen; longitudinal

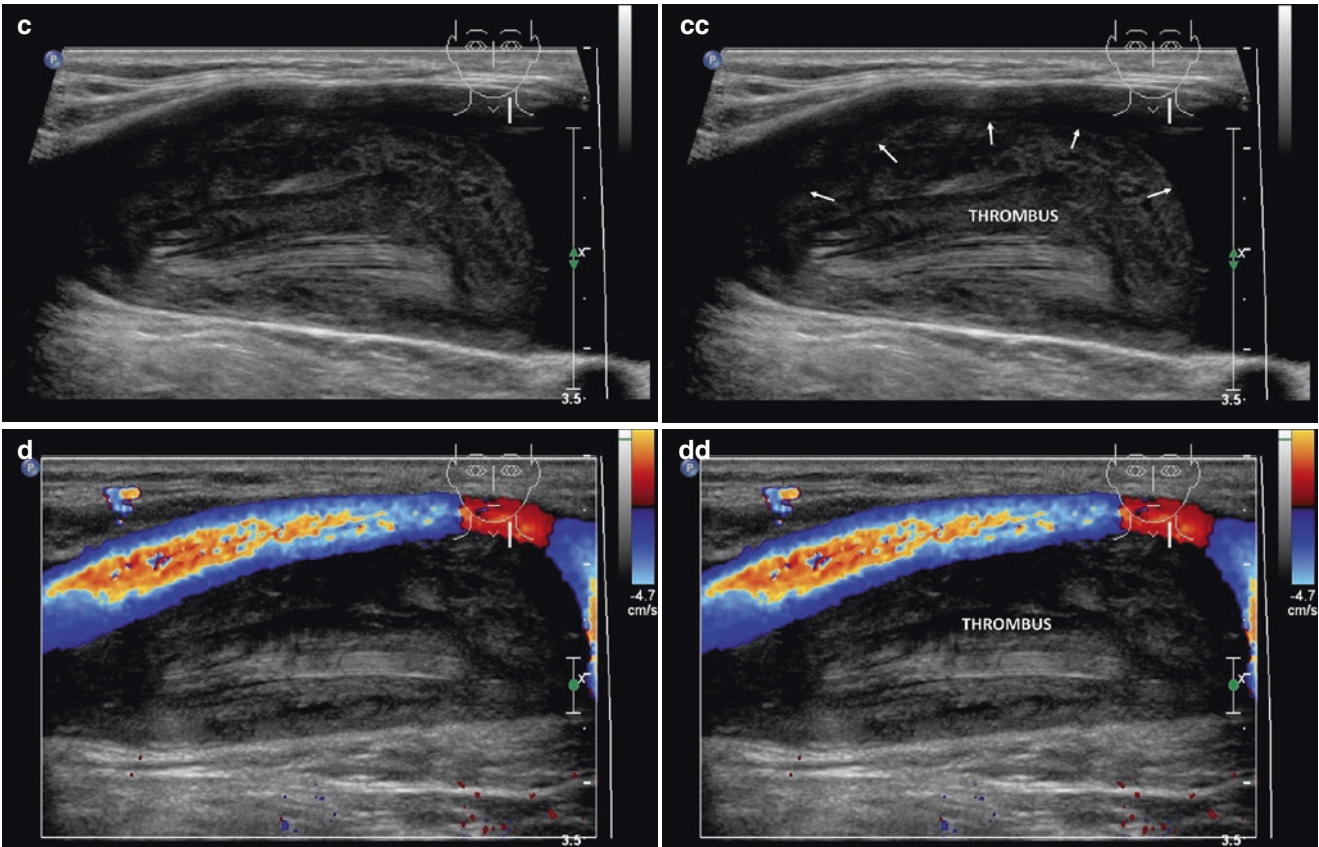


Fig. 21.7 (continued)

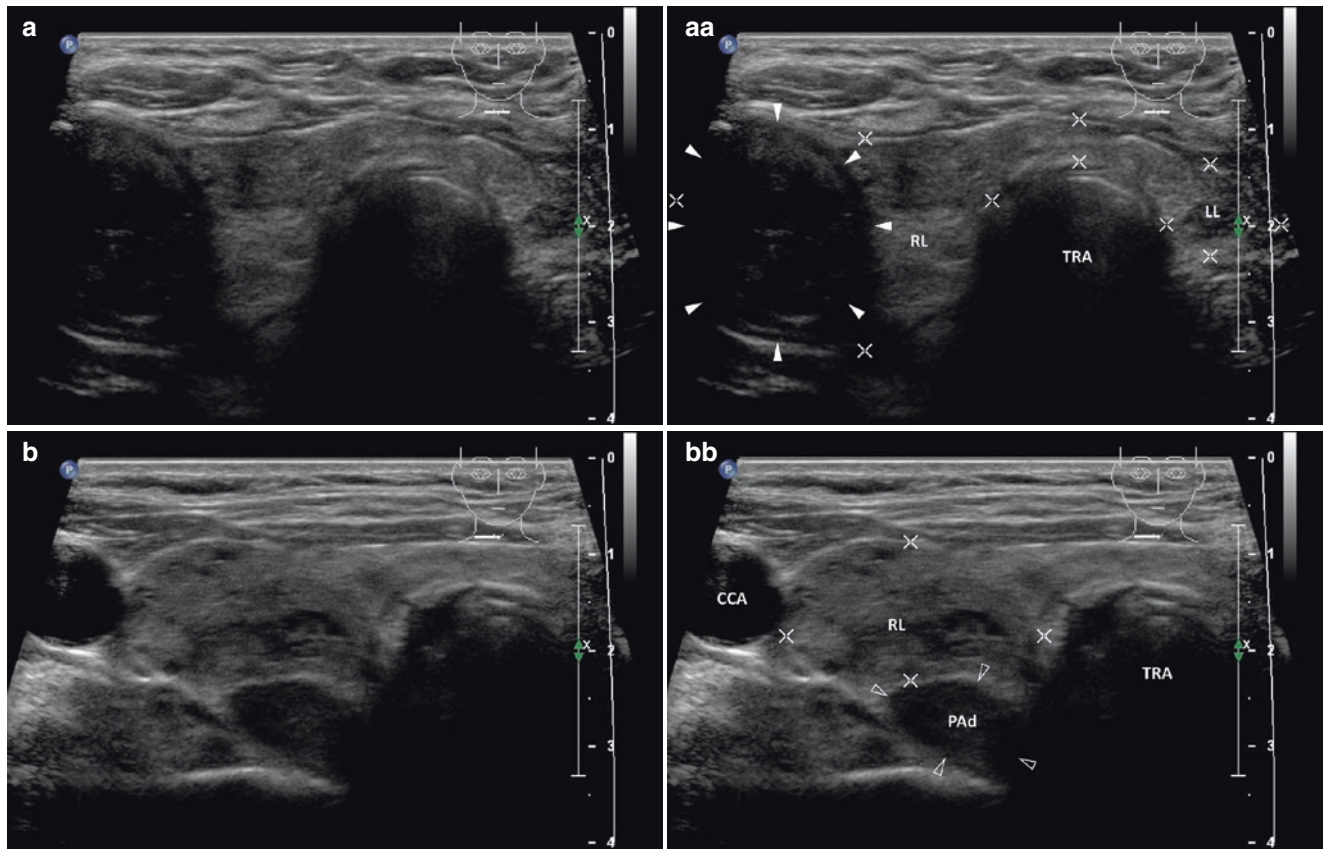


Fig. 21.8 (aa) Case of large acute postoperative hematoma post total thyroidectomy and parathyroidectomy. A 69-year-old man, polymorbid patient with history of myocardial infarction, permanent atrial fibrillation with anticoagulant therapy, and end stage kidney disease on renal replacement therapy with secondary hyperthyroidism, presented with palpable resistance in the right jugulum. US appearance prior to surgery—multinodular goiter with large complex nodule (*arrowheads*), size $31 \times 26 \times 23$ mm and volume 10 mL in the RL: inhomogeneous structure; septated cystic cavities; Tvol 32 mL, asymmetry—RL 22 mL and LL 10 mL; transverse. (bb) US appearance prior to surgery—detail of superior parathyroid adenoma (PAd) behind the RL (*blank arrowheads*), size $23 \times 17 \times 9$ mm and volume 1.8 mL: elliptical shape; homogeneous structure; hypoechoic; transverse. (cc) US appearance prior to surgery—detail of complex nodule (*arrowheads*) and superior PAd (*blank arrowheads*): complex nodule in the central part of the RL and elliptical PAd behind the RL; longitudinal. (dd) Ten days after surgery there was a great resistance in the operating field. The long-term anticoagulation therapy was discontinued 1 week before surgery and low-molecular-weight heparin was initiated postoperatively. However, US revealed large acute post-thyroidectomy hematoma (*arrowheads*) in the thyroid lodge (confirmed by computed tomography). US overall

view: heterogeneous mass in both thyroid beds; mixed echogenicity; fluid-fluid level (*arrows*) in the right bed; hematoma in the right thyroid bed—size $52 \times 47 \times 36$ mm and volume 46 mL, hematoma in the left thyroid bed—size $44 \times 25 \times 25$ mm and volume 14 mL; transverse. (ee) Detail of acute post thyroidectomy hematoma in the right thyroid bed (*arrowheads*): well-defined mass; inhomogeneous structure; mostly hyperechoic; in central part is seen fluid-fluid level (*arrows*) with anechoic fluid and organized hyperechoic clot formation; transverse. (ff) Detail of acute post-thyroidectomy hematoma in the right thyroid bed (*arrowheads*): well-defined mass; inhomogeneous structure; mostly hyperechoic; in central part is seen fluid-fluid level (*arrows*) with anechoic fluid and organized hyperechoic clot formation; longitudinal. (gg) Detail of acute post-thyroidectomy hematoma in the left thyroid bed (*arrowheads*): well-defined mass; inhomogeneous structure; mostly hyperechoic; in central part is seen fluid-fluid level (*arrows*) with anechoic fluid and organized hyperechoic clot formation; transverse. (hh) Detail of acute post-thyroidectomy hematoma in the left thyroid bed (*arrowheads*): well-defined mass; inhomogeneous structure; mostly hyperechoic; in central part is seen fluid-fluid level (*arrows*) with anechoic fluid and organized hyperechoic clot formation; longitudinal

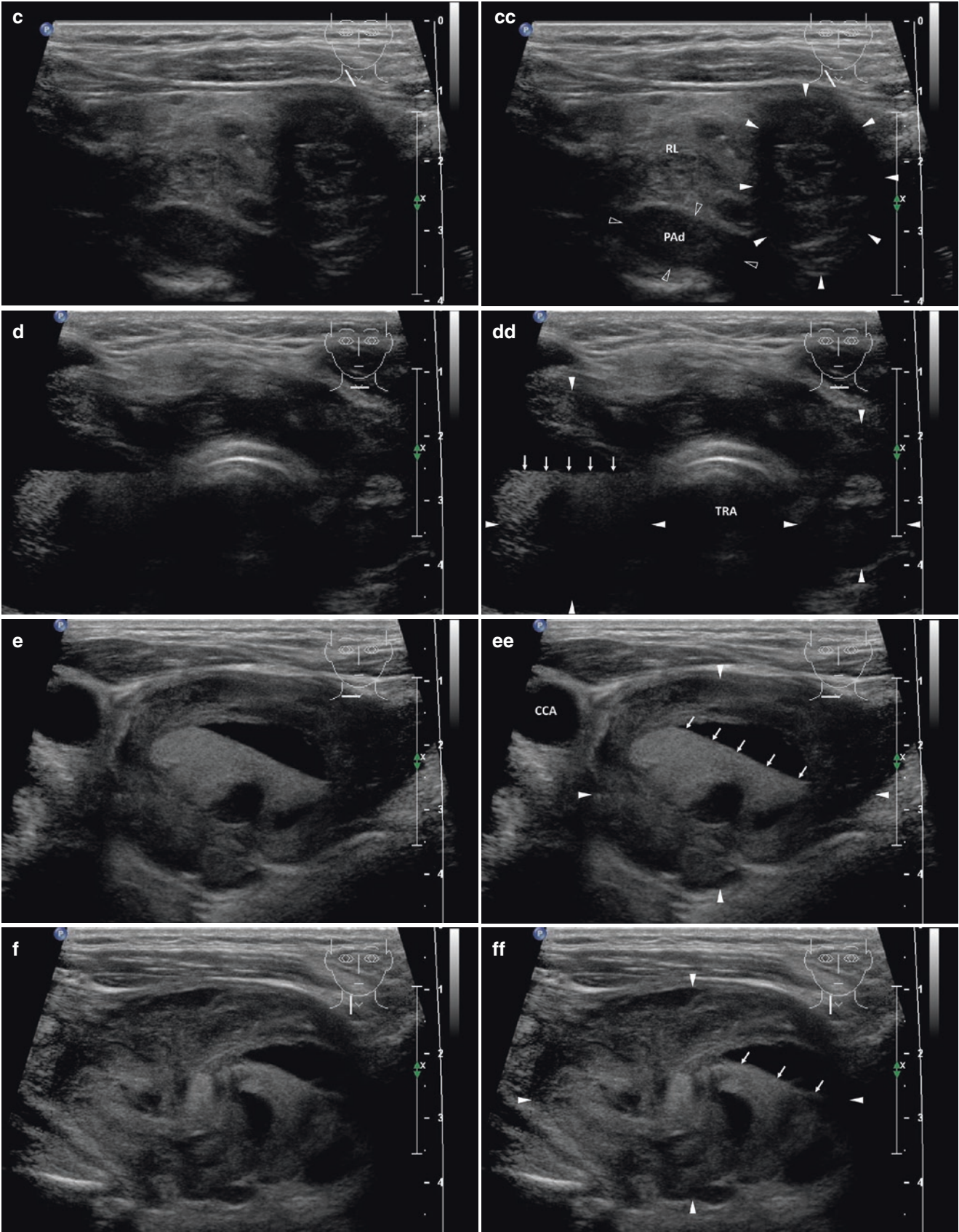


Fig. 21.8 (continued)

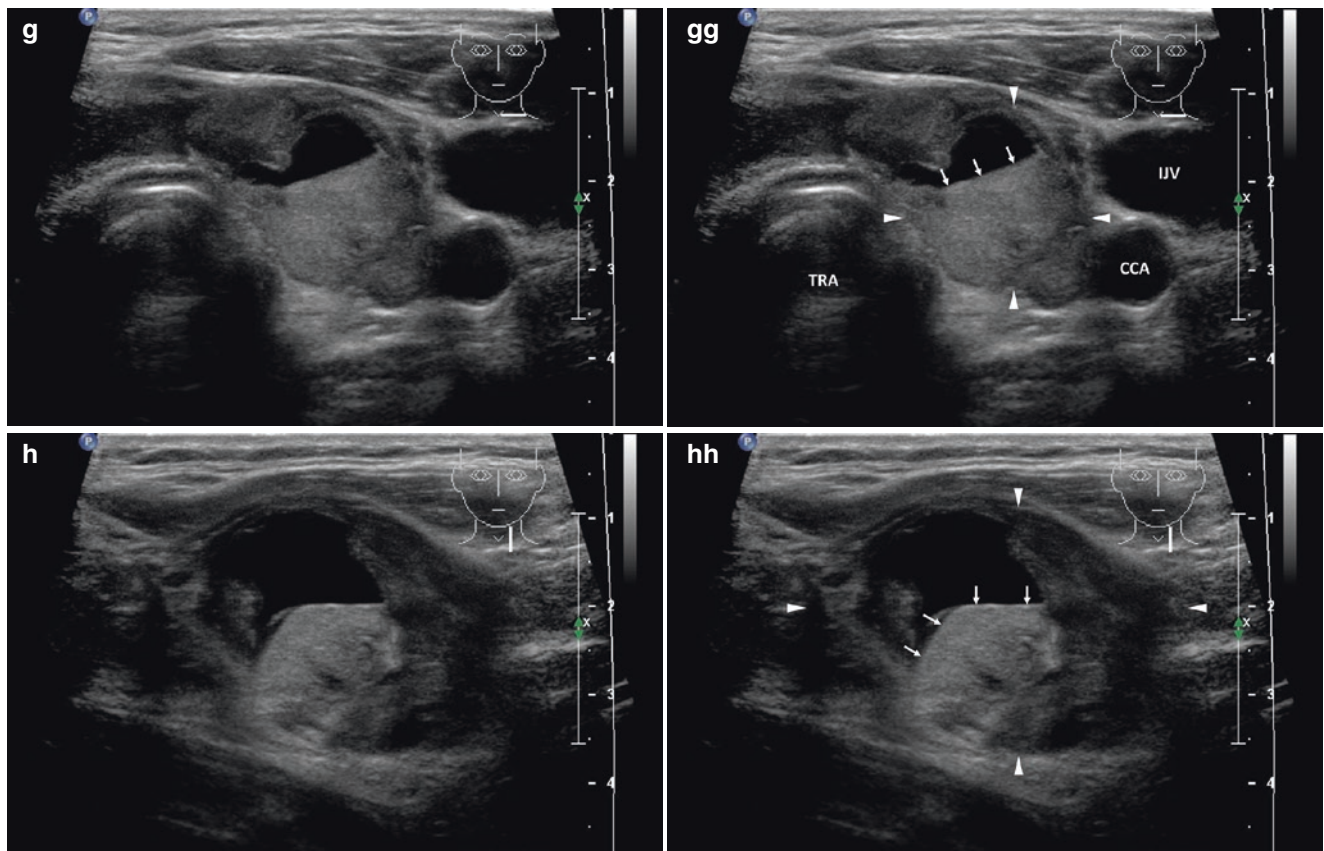


Fig. 21.8 (continued)

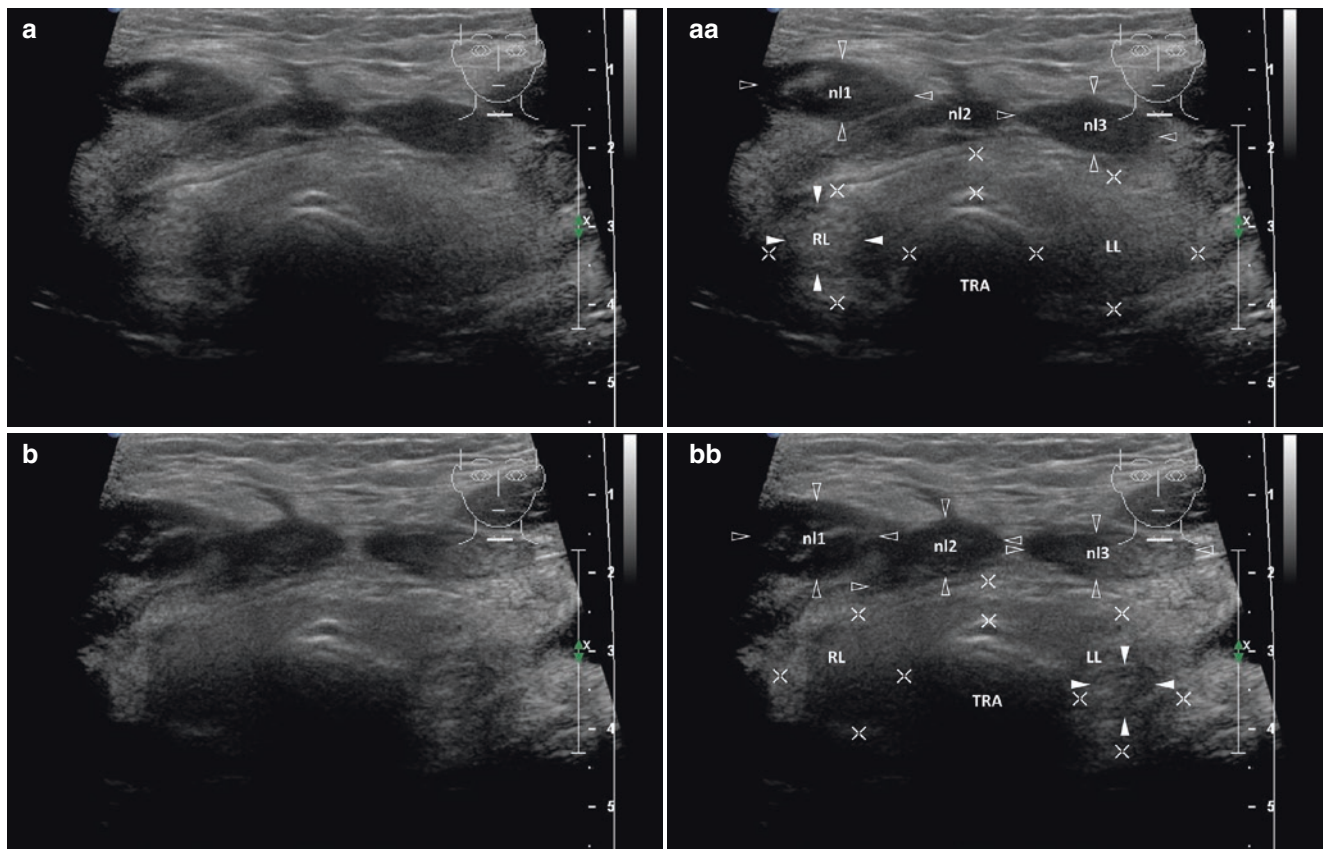


Fig. 21.9 (aa) A 69-year-old woman with acute myeloid leukemia. She had markedly painful edema and erythema in the anterior neck including the thyroid region and high fever for the last 4 days. The clinical findings imitated acute thyroiditis. However, US showed phlegmon of the neck—subcutaneous layer considerably thickened up to 20–25 mm; inhomogeneous; mostly hyperechoic with thin hypoechoic bands; several reactive lymph nodes—ln1, 2, 3 (blank arrowheads);

elliptical shape; hypoechoic; ln1 hyperechoic hilus sign; the thyroid gland—small multinodular goiter pushed dorsally; small, solid, hypoechoic nodule (arrowheads) in the RL; Tvol 10 mL, RL 4 mL, and LL 6 mL; transverse. (bb) Detail of phlegmon and the LL: small, solid, hyperechoic nodule (arrowheads); no signs of thyroid abscess; transverse

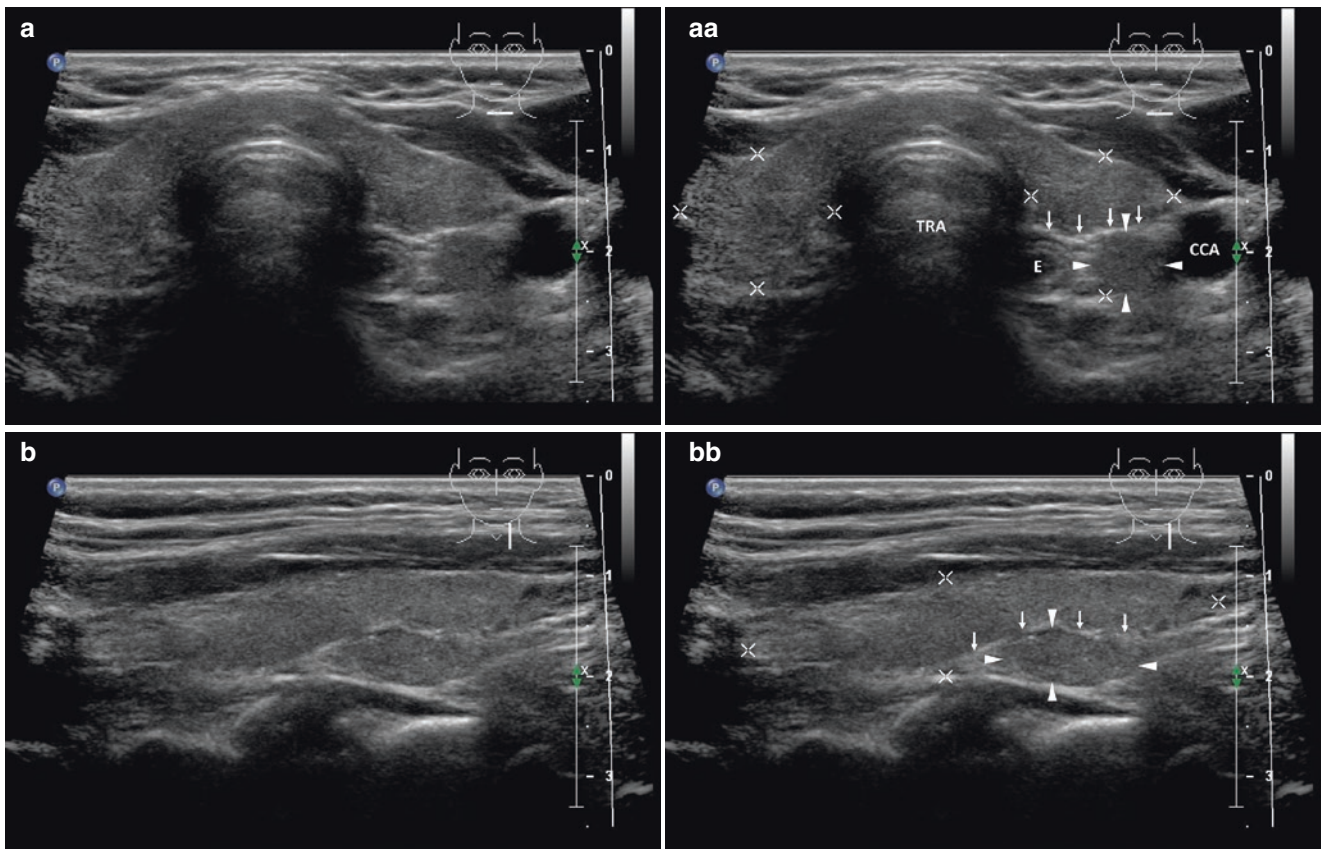


Fig. 21.10 (aa) Pseudo-lesion caused by posterior hyperechoic thyroid septum: transverse septum (*arrows*) at the posterior part of the LL forms an image of the solid isoechogenic nodule, so-called “*pseudo-nodule*”; Tvol 10 mL, RL 5 mL, and LL 5 mL; transverse. (bb) Detail

of thyroid septum (*arrows*) at longitudinal view: pseudo-lesion may be misdiagnosed as “*pseudo-nodule*” or “*parathyroid adenoma*,” but the tissue is isoechoic with the thyroid gland

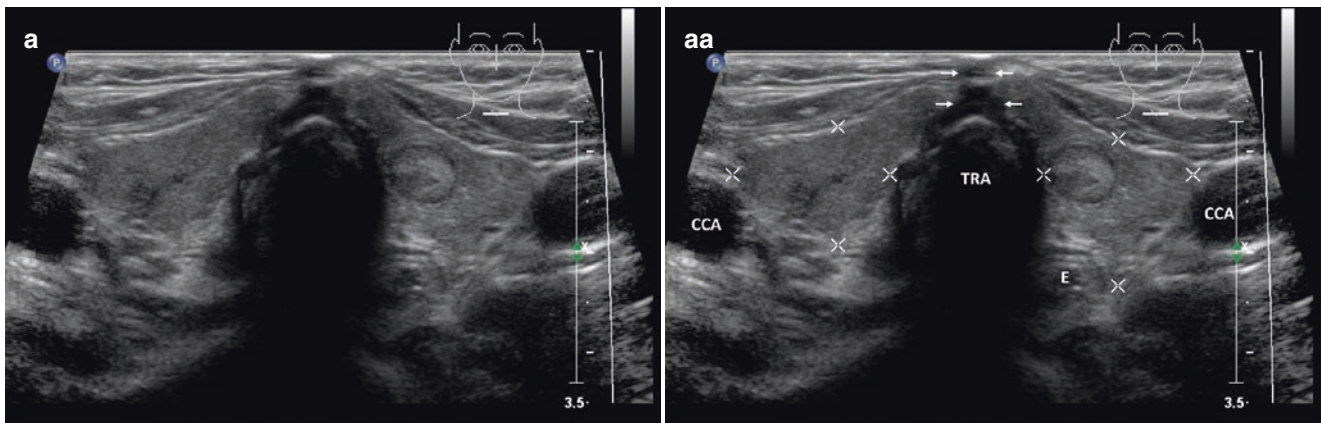


Fig. 21.11 (aa) US view of the scar after tracheostomy: in the midline is an interruption of isthmus continuity (*arrows*) and deformed trachea with indentation of the wall; furthermore, small solid isoechogenic

nodule with thin halo sign in the LL; Tvol 12 mL, RL 6 mL, and LL 6 mL; transverse

21.3 US Findings of Artifacts [17]

- Edge shadowing from thyroid cystic lesion at tangential angle—“ears” (similarly hepatic cysts, gall-bladder); see more in [Chap. 7](#) (Fig. 7.10cc).
- So-called “comet tails” as bright hyperechoic reverberation artifacts (the condensed colloid proteins); see more in [Chap. 7](#) (Fig. 7.9aa).
- Posterior acoustic enhancement behind cyst (similarly hepatic cysts, gall-bladder); see more in [Chap. 7](#) (Fig. 7.4aa).

- A “mirror-image” artifact arises when there is a highly reflective surface. Typically hepatic cyst is reflected back to the highly reflective surface, e.g. diaphragm. A similar situation may occur in locating a cystic nodule in the midline in the isthmus (Fig. 21.12aa), and a “mirror-image” can be seen beyond the tracheal wall (the most hyperechoic arc-shape line is the interface of the tracheal wall and air in the tracheal lumen).

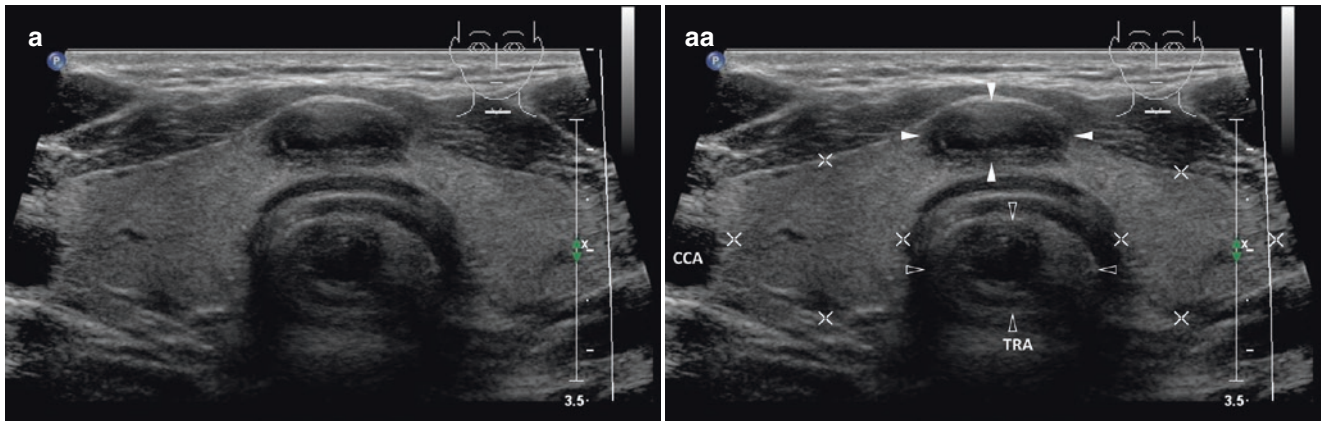


Fig. 21.12 (aa) “Mirror-image” artifact back to the tracheal wall: complex cyst (arrowheads) with thickened wall and anechoic content, size $16 \times 14 \times 7$ mm, volume 1 mL, located in the middle of the isthmus;

slightly enlarged “mirror artifact” (blank arrowheads) of the cyst mirrored into the trachea; Tvol 23 mL, RL 11 mL, and LL 10 mL; transverse

21.4 US Findings of Normal Anatomic Structure of Thyroid Gland Mimic a Lesion [18]

- There are two often-seen findings of normal structures within thyroid gland that may influence examination and can potentially mimic pathological lesions.
- Approximately 40% of individuals have a pyramidal lobe (Fig. 21.2cc) arising from the isthmus that extends toward the hyoid bone. This may be misinterpreted as a pathological mass when it is enlarged.
- The echogenic septum within the thyroid gland. The septum extends at the posterior part of the lobe and in transverse section forms a “*pseudo-nodule*” (Fig. 21.10aa) and in longitudinal section often creates separated “*tongue*” (Fig. 21.10bb). The septum makes a posterior shadow resulting in a posterior “*hypoechoic lesion*.” This finding may be misdiagnosed as parathyroid lesion or suspicious thyroid nodule.

References

1. Shabana W, Delange F, Freson M, Osteaux M, De Schepper J. Prevalence of thyroid hemiagenesis: ultrasound screening in normal children. *Eur J Pediatr*. 2000;159(6):456–8.
2. De Sanctis V, Soliman AT, Di Maio S, Elsedfy H, Soliman NA, Elalaily R. Thyroid hemiagenesis from childhood to adulthood: review of literature and personal experience. *Pediatr Endocrinol Rev*. 2016;13(3):612–9.
3. Grecchi F, Zollino I, Candotto V, Gallo F, Rubino G, Bianchi R, et al. A case of lipoma of lateral anterior neck treated with surgical enucleation. *Dent Res J (Isfahan)*. 2012;9(Suppl 2):S225–8.
4. Panchbhai AS, Choudhary MS. Branchial cleft cyst at an unusual location: a rare case with a brief review. *Dentomaxillofac Radiol*. 2012;41(8):696–702.
5. Choo MJ, Kim YJ, Jin HR. A case of second branchial cleft cyst with oropharyngeal presentation. *J Korean Med Sci*. 2002;17(4):564–5.
6. Chauhan A, Tiwari S, Pathak N. Primary branchiogenic carcinoma: report of a case and a review of the literature. *J Cancer Res Ther*. 2013;9(1):135–7.
7. Yigit N, Karslioglu Y, Yildizoglu U, Karakoc O. Dermoid cyst of the parotid gland: report of a rare entity with literature review. *Head Neck Pathol*. 2015;9(2):286–92.
8. Kim JH. Ultrasound-guided sclerotherapy for benign non-thyroid cystic mass in the neck. *Ultrasonography*. 2014;33(2):83–90.
9. Dikici AS, Yildirim O, Er ME, Kılıç F, Tutar O, Kantarcı F, Mihmanlı I. A rare complication of the thyroid malignancies: jugular vein invasion. *Pol J Radiol*. 2015;80:360–3.
10. Taib NA, Hisham AN. Follicular thyroid carcinoma with direct tumour extension into the great cervical veins and right atrium: is transcervical thrombectomy a safe option? *Asian J Surg*. 2007;30(3):216–9.
11. Shah A, Ahmed I, Hassan S, Samoon A, Ali B. Evaluation of ultrasonography as a diagnostic tool in the management of head and neck facial space infections: a clinical study. *Natl J Maxillofac Surg*. 2015;6(1):55–61.
12. Squire BT, Fox JC, Anderson C. ABSCESS: applied bedside sonography for convenient evaluation of superficial soft tissue infections. *Acad Emerg Med*. 2005;12(7):601–6.
13. Lee HS, Lee BJ, Kim SW, Cha YW, Choi YS, Park YH, et al. Patterns of post-thyroidectomy hemorrhage. *Clin Exp Otorhinolaryngol*. 2009;2(2):72–7.
14. Yasumoto M, Shibuya H, Gomi N, Kasuga T. Ultrasonographic appearance of dermoid and epidermoid cysts in the head and neck. *J Clin Ultrasound*. 1991;19(8):455–61.
15. Yoshikawa H, Suzuki M, Nemoto N, Hara H, Hashimoto G, Otsuka T, et al. Internal jugular thrombophlebitis caused by dermal infection. *Intern Med*. 2011;50(5):447–50.
16. Shih JY, Lee LN, Wu HD, Yu CJ, Wang HC, Chang YL, et al. Sonographic imaging of the trachea. *J Ultrasound Med*. 1997;16(12):783–90.
17. Kremkau FW, Taylor KJ. Artifacts in ultrasound imaging. *J Ultrasound Med*. 1986;5(4):227–37.
18. Choi SH, Kim EK, Kim SJ, Kwak JY. Thyroid ultrasonography: pitfalls and techniques. *Korean J Radiol*. 2014;15(2):267–76.

22.1 Essential Facts

- Primary hyperparathyroidism (pHPT) is the third most common endocrine disease and the frequency of its detection gradually increases. According to data from 2009, worldwide prevalence ranges from 0.1 to 0.7% [1].
- Asymptomatic cases of pHPT prevail at present. It is defined by moderately elevated serum calcium levels (s-Ca), often borderline or slightly elevated levels of serum parathyroid hormone (s-PTH), and lack of clinical symptoms. A 10-year follow-up (without specific pharmacotherapy) showed that 25% of patients developed overt disease and fulfilled the indication criteria for parathyroidectomy. In the rest of the patients, the laboratory values and bone mineral density remained unchanged [2].
- In the United States and many other developed countries, for the last 30 years, asymptomatic form represents up to three-fourth of all diagnosed pHPT cases. The ratio of men to women is 3:1, with maximal incidence at the age of 50–60 years [2].
- Eighty percent of pHPT cases are caused by a solitary parathyroid adenoma (PAd), 2–4% are caused by multiple parathyroid adenomas, 15% are caused by hyperplasia of all the four parathyroid glands, and about 0.5% of cases are caused by parathyroid carcinoma (PCa) [2].
- Contrary to PAd, clinical signs and laboratory findings of PCa are usually severe and impressive. In PCa, s-PTH levels are three to ten times higher than normal, in contrast to the average twofold increase seen in PAd. As for serum calcium levels, these often range from 3.5 to 3.75 mmol/L in PCa, but are not that high in PAd, usually increasing by only 0.25–0.5 mmol/L above the normal [3].
- In various studies the most portable and less invasive US imaging has a sensitivity of 56–100% and specificity of 40–99% in accurate localization of the PAd. ^{99m}Tc -MIBI SPECT/CT shows sensitivity of 56–100% and specificity of 83–99%. In a study by Noda, US scan, ^{99m}Tc -MIBI planar scan, and ^{99m}Tc -MIBI SPECT/CT showed accurate localization in 77.0% (47/61), 75.4% (46/61) and 88.5% (46/52) of the evaluable cases, respectively. Combination of US and ^{99m}Tc -MIBI SPECT/CT certainly contributes to the preoperative planning by indicating correct localization of single PAd [4].
- Use of preoperative imaging is advantageous for identifying parathyroid lesions in ectopic locations. In those cases sensitivity of US scan was reported as 22.2%, and that of ^{99m}Tc -MIBI SPECT/CT 100% [4].
- Preoperative localization of an abnormal parathyroid gland was successfully performed with US in 83.7%, with MIBI in 67.3%, with SPECT in 72.4%, while MRI in only 61.2%.
- Sensitivity, specificity, and diagnostic accuracy values were 87.2%, 25.0%, and 83.0%; 70.2%, 50.0%, and 69.4%; 75.5%, 50.0%, and 74.5%; 63.8%, 50.0%, and 63.3% for US, MIBI, SPECT, and MRI, respectively [5].
- Combining US and MIBI as imaging methods for preoperative imaging of pHPT often provides more satisfactory results. While the accuracy of US is relatively low in the ectopic localizations, the size of the lesion can be an important factor in the accuracy achieved with MIBI. The respective values for sensitivity, specificity, and diagnostic accuracy were 94.9%, 25.0%, and 91.1% when US was combined with MIBI [5].
- Ectopic parathyroid glands (Fig. 22.9cc) result from aberrant migration during the early stages of embryonic

development and lack of their successful identification may lead to lack of success in parathyroid surgery. They represent a common source of persistent or recurrent hyperparathyroidism, when missed at initial diagnosis. Their prevalence is about 2–43% in anatomical series and up to 16% and 14% in patients with primary and secondary hyperparathyroidism, respectively. Ectopic inferior parathyroids are most frequently found in the anterior mediastinum, in association with the thymus or the thyroid gland, while the most common position for ectopic superior parathyroids is the tracheoesophageal groove and retroesophageal region [6].

- In current large series of 656 patients, incidence of ectopic PAd was 1.4%, which is lower than in previously reported. Eleven patients showed ectopic uptake suspicious of PAd on ^{99m}Tc -MIBI. CT confirmed diagnosis of ectopic PAd in seven patients and MRI showed PAd in two patients. Surgical and histopathological findings confirmed diagnosis of ectopic PAd in nine patients. Sensitivity and specificity of US were 11% and 100%, respectively. ^{99m}Tc -MIBI had sensitivity, specificity, positive and negative predictive values of 100%, 86%, 98% and 65%, respectively. Combination of ^{99m}Tc -MIBI with CT or MRI yielded the correct diagnosis in all cases, giving a sensitivity and specificity of 100% [7].
- Of a series of 231 patients operated on for pHPT, 37 (16%) had ectopic PAd. Ectopic inferior PAd were 23 (62%): intrathymic, 7 (30%); anterosuperior mediastinal, 5 (22%); intrathyroidal, 5 (22%); within thyrothymic ligament, 4 (17%); and submandibular, 2 (9%). Ectopic superior PAd were 14 (38%): in the tracheoesophageal groove, 6 (43%); retroesophageal, 3 (22%); posterosuperior mediastinal, 2 (14%); intrathyroidal, 1 (7%); in the carotid sheath, 1 (7%); and paraesophageal, 1 (7%). ^{99m}Tc -MIBI scans were true-positive in 81%, identifying 13 of 16 retrosternal glands, and false-negative in 19%. A 16% incidence of ectopic PAd and a 100% positive predictive value of sestamibi scintigraphy underscore the importance of sestamibi imaging in patients with pHPT [8].
- Presence of supernumerary parathyroid gland in the autopsy series is 5%, and presence of more than five glands is 1.25%. In the pHPT series, cases related to supernumerary parathyroid glands are rare, reported at about 0.7%. About 60% of supernumerary parathyroid glands are located in the mediastinum, the majority in thymus [9].

22.2 US Features of Parathyroids

- Localizations of normal parathyroid glands [10]:
 - Parathyroid glands are located on the posterior face of the thyroid lobes, in extra capsular position.
 - There are four glands, two on each side.
 - Superior parathyroid glands are located at the level of the superior third to half of the lobes (Fig. 22.1aa).
 - Inferior parathyroid glands are located at the inferior poles of the lobes (Fig. 22.1cc).
 - Normal parathyroid glands are small (3/4/5 mm) and identifiable only with high frequency transducers (Fig. 22.1aa, cc).
- US findings typical for parathyroid adenoma (Fig. 22.2aa) [11]:
 - PADs are localized in the area of superior (Fig. 22.2cc) or inferior (Fig. 22.3cc) parathyroid gland.
 - Solid.
 - Homogeneous.
 - Hypoechoic.
 - Average size of 16–19 mm (range 4–63 mm).
 - Hypervascularization confirmed by CFDS (Fig. 22.6ee).
 - Oval (Figs. 22.9aa and 22.11bb), elliptical (Fig. 22.3aa), or bean-like shape (Figs. 22.4aa and 22.5cc), elongated (Figs. 22.6dd and 22.7bb), lentil-like (Figs. 22.7 and 22.8), triangular (Fig. 22.13).
- US scan of parathyroid carcinoma (Fig. 22.12, year 2010, older generation of US device; Fig. 22.17, year 2017 latest generation of US device) differentiating from parathyroid adenoma [12]:
 - Size usually about 3 cm.
 - Nonhomogeneous structure.
 - Frequent degenerative changes—pseudocystic cavities and calcifications Echogenicity of PCa could be hyperechoic and also hypoechoic, depending on presence of areas of bleeding or necrosis.
 - Irregular borders.
- However, rarely seen large degenerated PAd (Fig. 22.11bb) may be also of hyperechoic US image, thus in these cases FNAB is recommended. In transverse US scan the most of PCa have the depth/width ratio ≥ 1 , contrary to the ratio < 1 characteristic for PAd [12].
- In the case of a US scan of large or atypical PAd, or in case of parathyroid cyst (Fig. 22.10aa), PTH analysis of punctate is pivotal to confirm the diagnosis [13, 14].
- The critical size for parathyroid gland detected by US in uremic patients with sHPT [15]:
 - Diffuse hyperplasia - PAd size < 0.5 mL or < 1 cm (Figs. 22.13 and 22.16aa).
 - Nodular hyperplasia - PAd size > 0.5 mL or > 1 cm (Figs. 22.14 and 22.15); usually resistant to medical therapy.

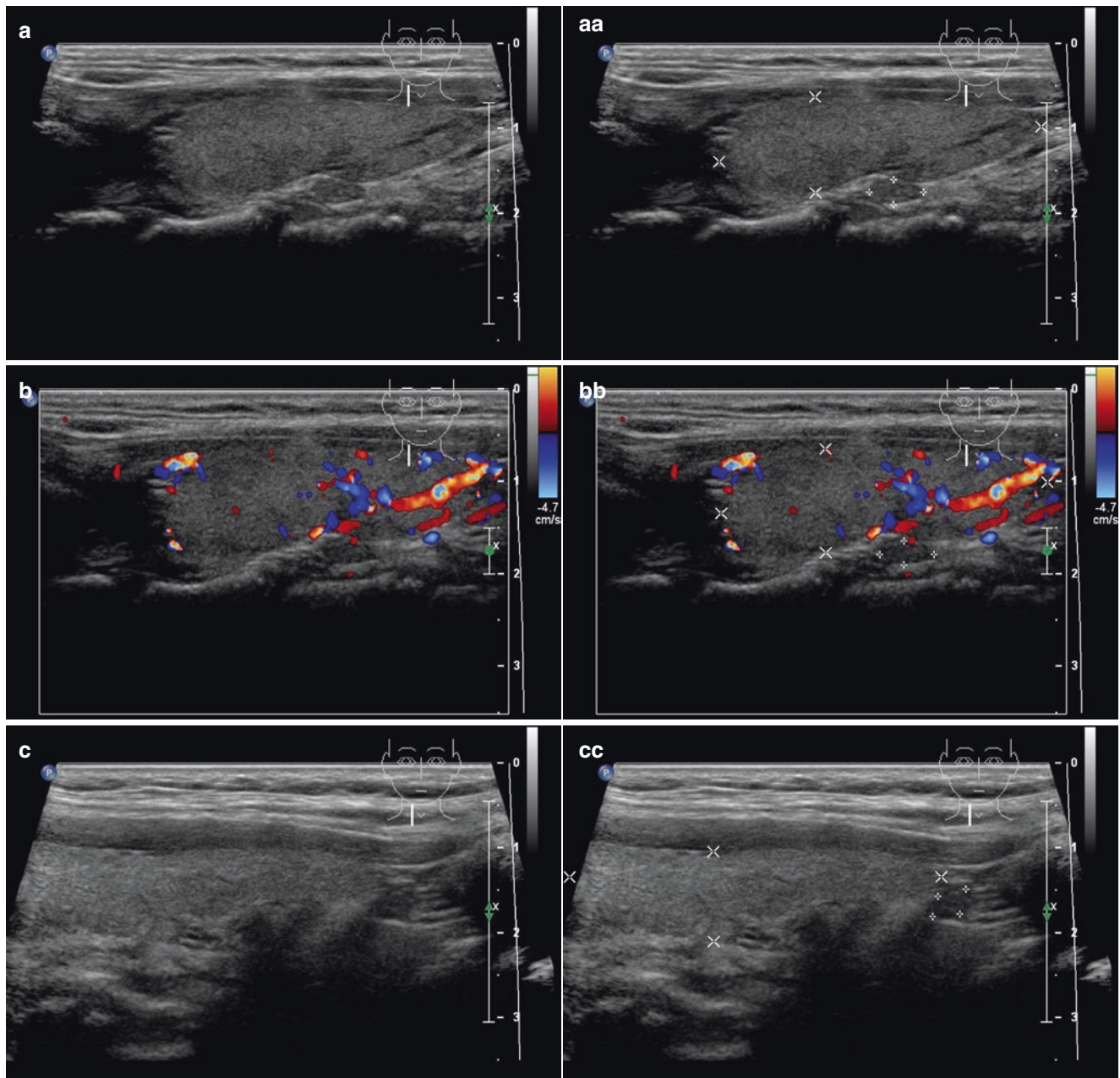


Fig. 22.1 (aa) Normal right superior parathyroid gland (*marks*) just behind the middle of RL, well shown in longitudinal section: lentil-like shape; small size 6×3 mm; homogeneous structure; isoechoic with thyroid gland. (bb) Normal right superior parathyroid gland (*marks*), CFDS: hilar vascularity; longitudinal. (cc) Normal right inferior para-

thyroid gland (*marks*) just behind the lower pole of RL, well shown in longitudinal section: lentil-like shape; small size 5×3 mm; homogeneous structure; isoechoic with thyroid gland. (dd) Normal right inferior parathyroid gland (*marks*), CFDS: hilar vascularity; longitudinal

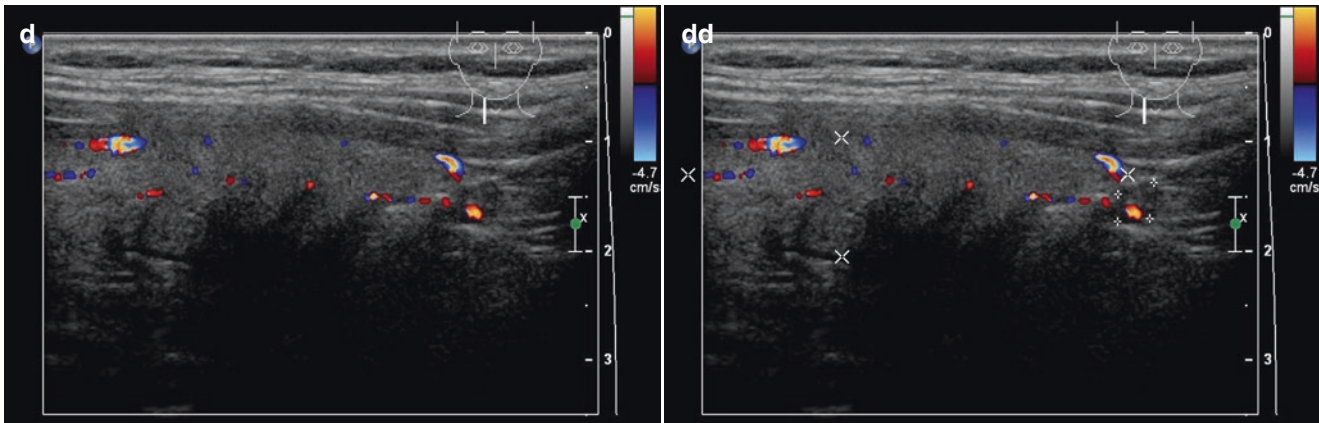


Fig. 22.1 (continued)

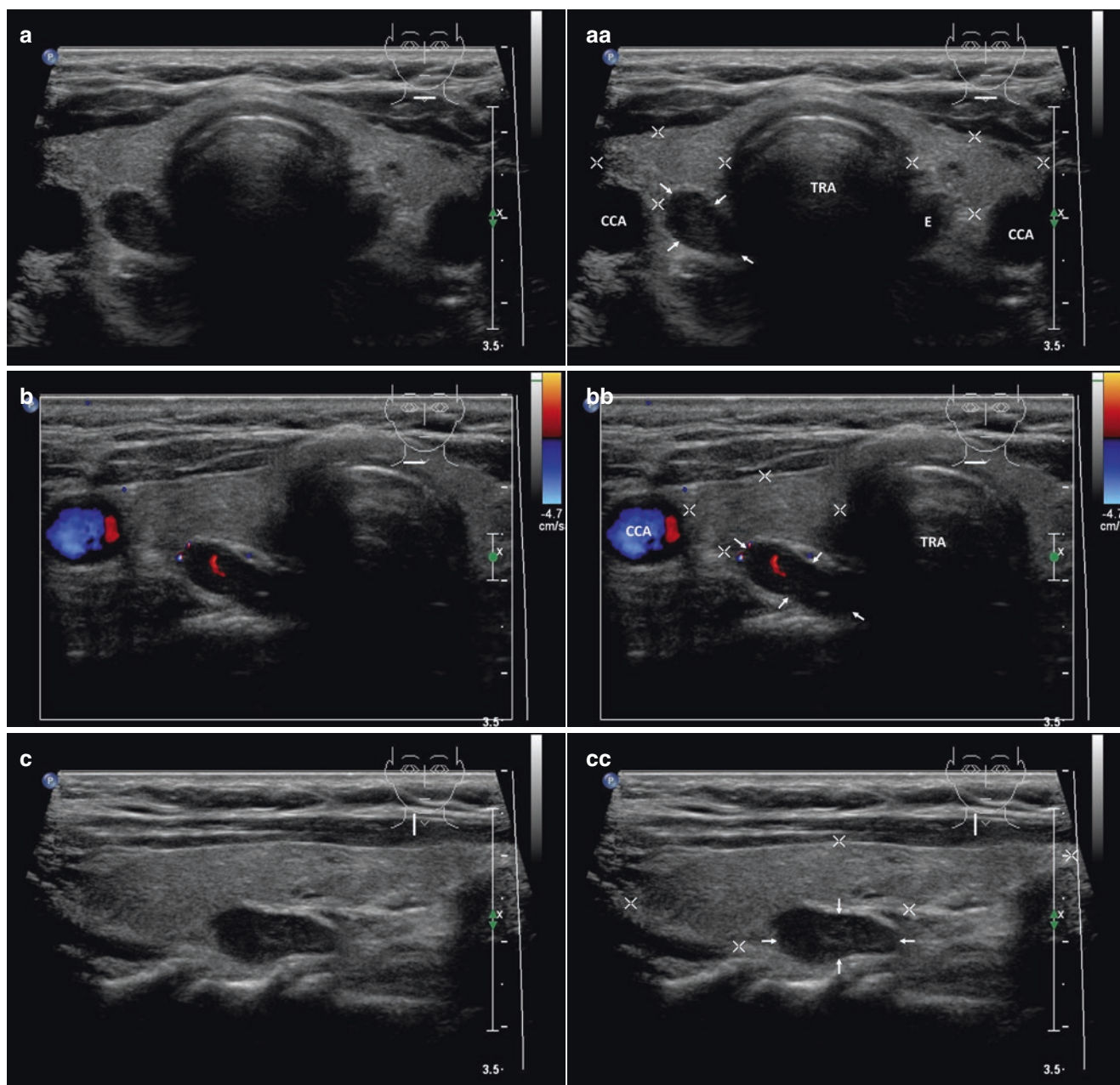


Fig. 22.2 (aa) A 63-year-old woman with asymptomatic pHPT, laboratory: mild hypercalcemia, s-Ca 2.6 mmol/L (normal: 2.15–2.55), mild elevation of parathyroid hormone, s-PTH 82 ng/L (normal: 12–65). Small right superior parathyroid adenoma—PAd (arrows), size $15 \times 11 \times 5$ mm and volume 0.4 mL: bean-like shape; slightly inhomogeneous; hypoechoic; normal thyroid gland; transverse. (bb) Detail of superior PAd (arrows), CFDS: flat central vascularity; transverse. (cc) Detail of superior PAd (arrows): located behind the middle of the right thyroid lobe; bean-like shaped; longitudinal. (dd) Detail of superior PAd (arrows), CFDS: flat central vascularity; longitudinal

geneous; hypoechoic; normal thyroid gland; transverse. (bb) Detail of superior PAd (arrows), CFDS: flat central vascularity; transverse. (cc) Detail of superior PAd (arrows): located behind the middle of the right thyroid lobe; bean-like shaped; longitudinal. (dd) Detail of superior PAd (arrows), CFDS: flat central vascularity; longitudinal

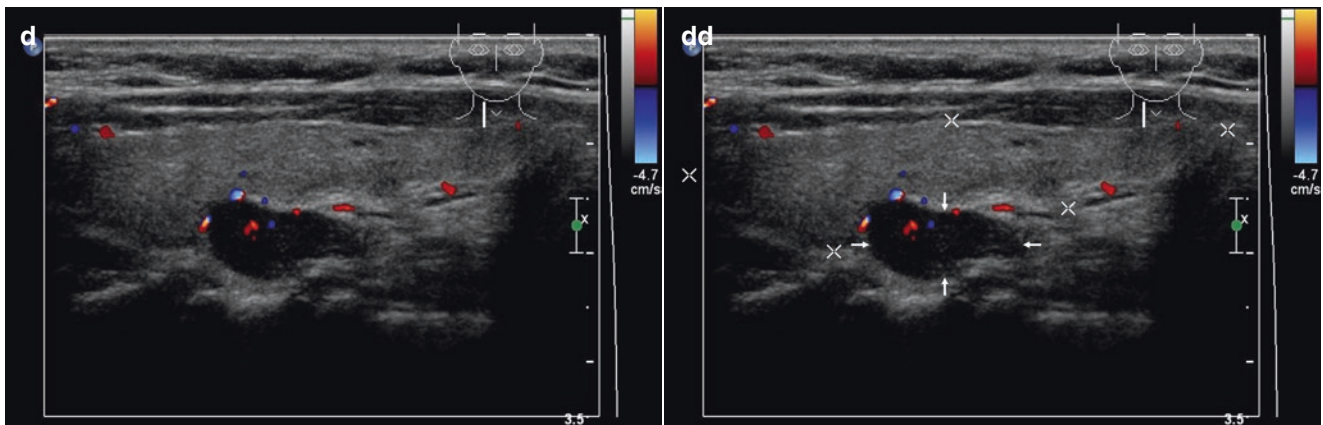


Fig. 22.2 (continued)

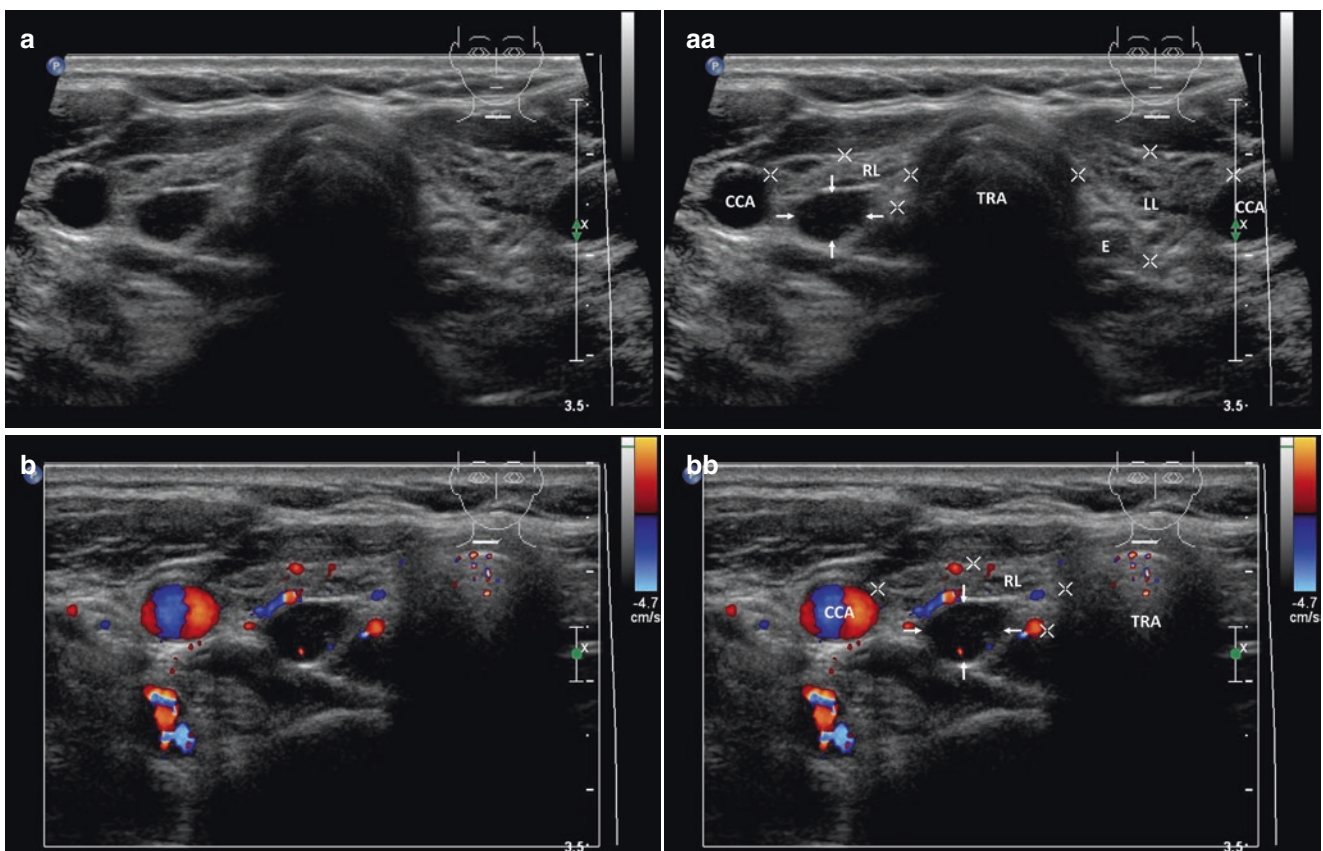


Fig. 22.3 (**aa**) A 50-year-old woman with asymptomatic pHPT, laboratory: mild hypercalcemia, s-Ca 2.67 mmol/L (normal: 2.15–2.55), moderate elevation of parathyroid hormone, s-PTH 103 ng/L (normal: 12–65). Small right inferior parathyroid adenoma—PA (arrows), size 12 × 8 × 7 mm and volume 0.4 mL: elliptical shape; homogeneous; hypoechoic; thyroid gland—Hashimoto’s thyroiditis; Tvol 14 mL, RL

7 mL, and LL 7 mL; transverse. (**bb**) Detail of small inferior PAD (arrows), CFDS: flat hilar vascularity; transverse. (**cc**) Detail of tiny inferior PAD (arrows): elliptical shape; longitudinal. (**dd**) Detail of small inferior PAD (arrows), CFDS: flat hilar and peripheral vascularity; longitudinal

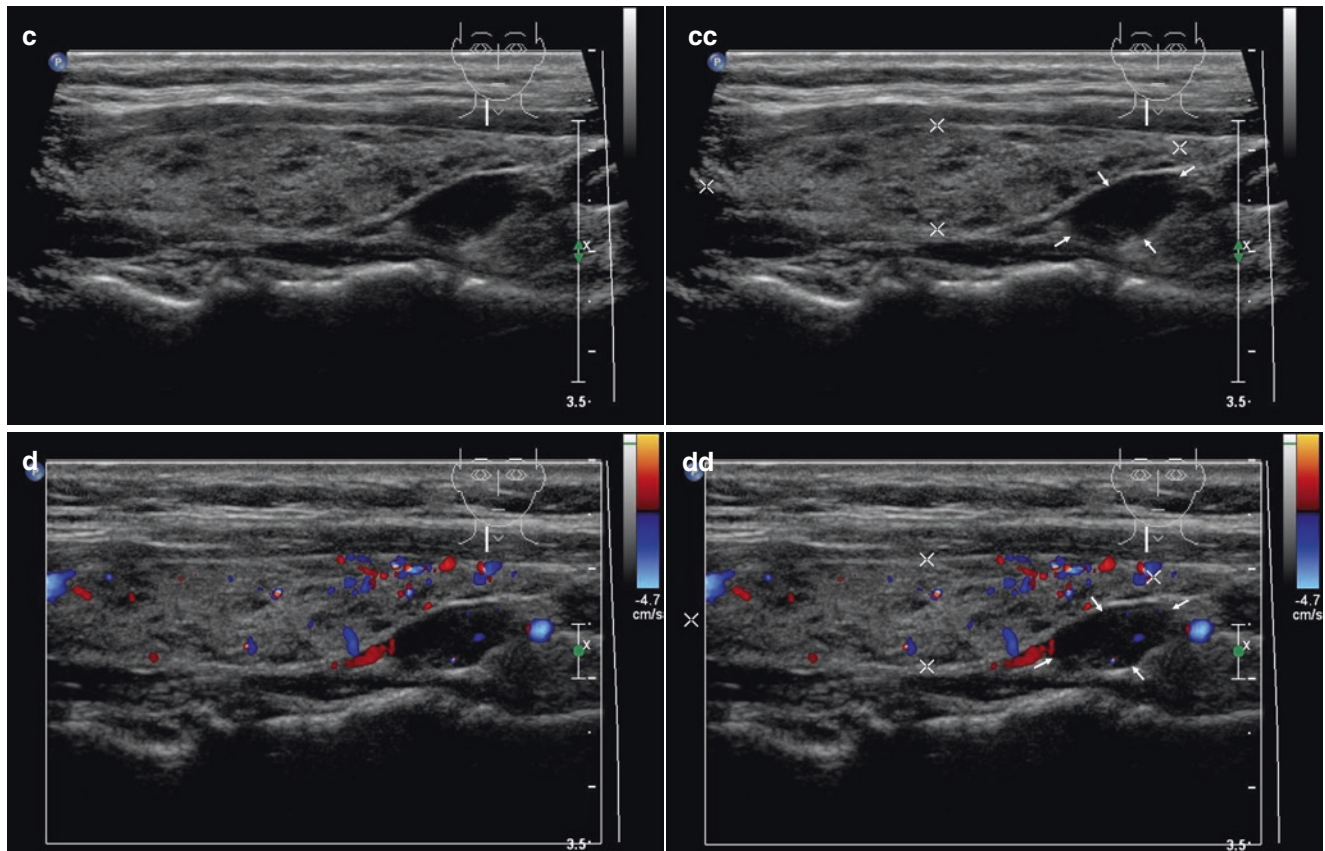
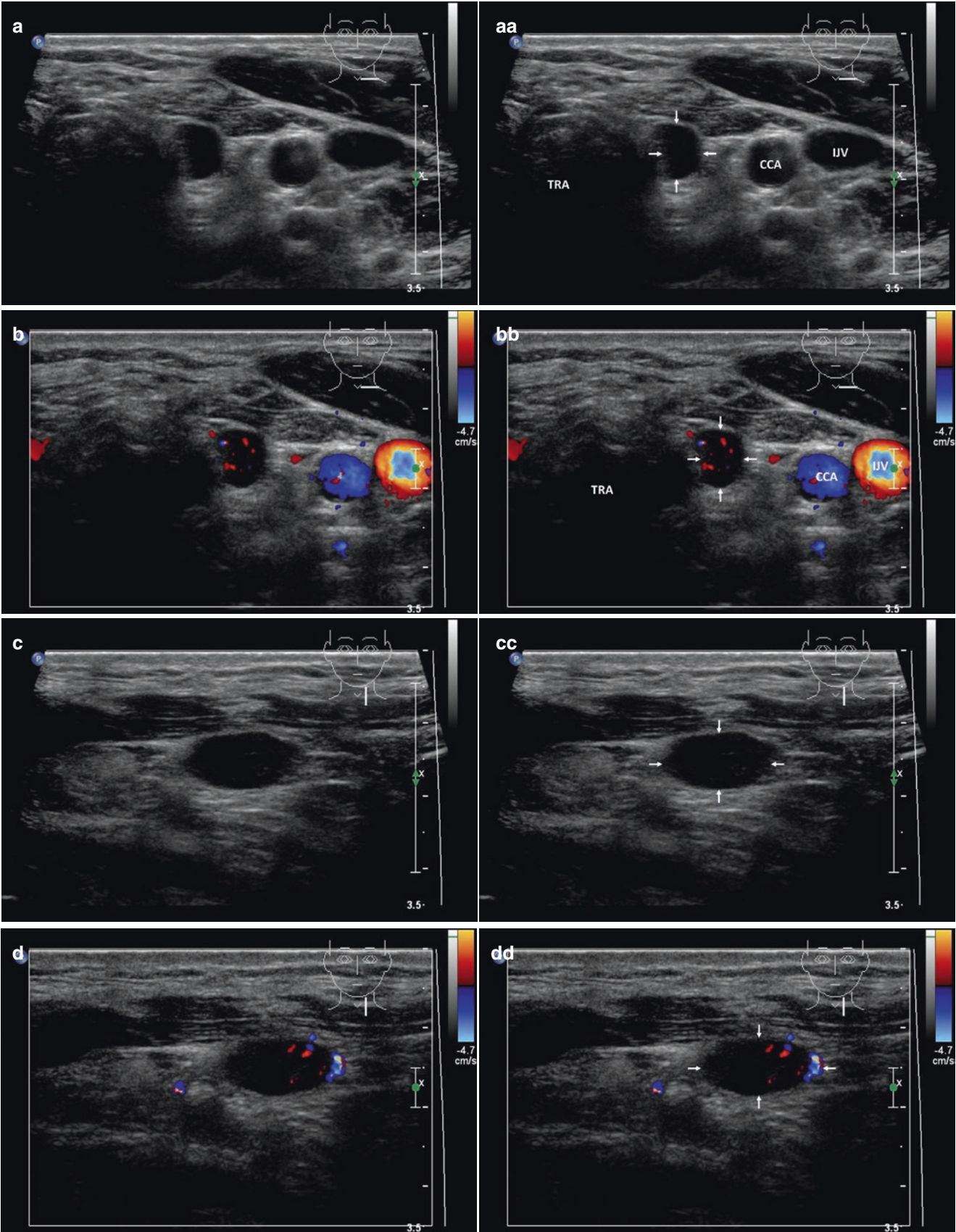


Fig. 22.3 (continued)

Fig. 22.4 (aa) A 43-year-old man with asymptomatic pHPT, laboratory: moderate hypercalcemia, s-Ca 3.04 mmol/L (normal: 2.15–2.55), high elevation of parathyroid hormone, s-PTH 255 ng/L (normal: 12–65). Personal history: 20 years post total thyroidectomy for papillary thyroid carcinoma. Small left parathyroid adenoma—PAd (arrows), size 15 × 8 × 5 mm and volume 0.4 mL, confirmed by ^{99m}Tc -MIBI, as a

suspicious lesion in the left thyroid bed: bean-like shape; homogeneous structure; markedly hypoechoic; transverse. (bb) Detail of the left PAd (arrows), CFDS: increased peripheral vascularity; transverse. (cc) Detail of the left PAd (arrows): elliptical shape; longitudinal. (dd) Detail of the left PAd (arrows), CFDS: focally increased peripheral vascularity; longitudinal



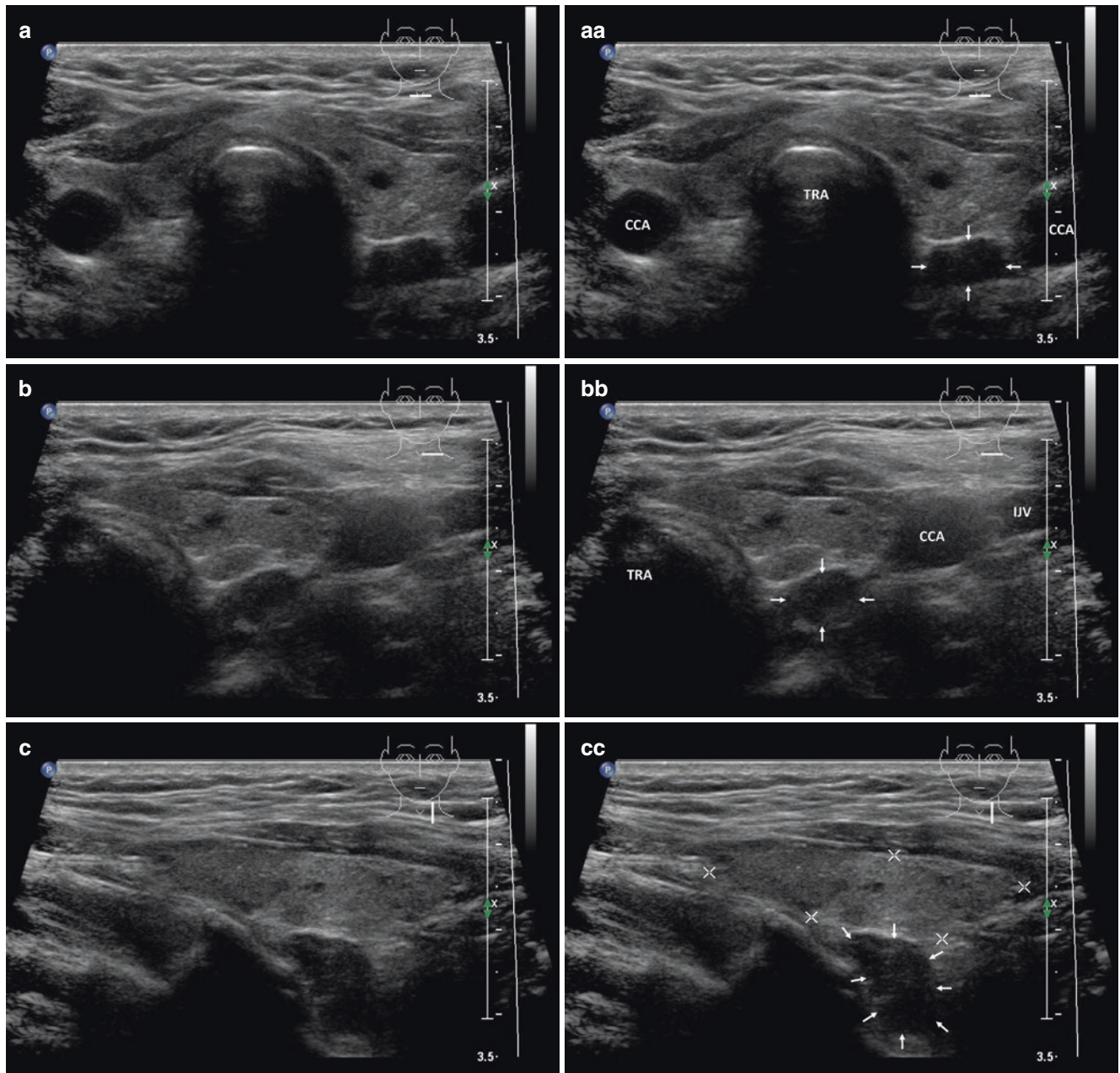


Fig. 22.5 (aa) A 75-year-old woman with pHPT, laboratory: moderate hypercalcemia, s-Ca 2.86 mmol/L (normal: 2.15–2.55), moderate elevation of parathyroid hormone, s-PTH 110 ng/L (normal: 12–65). Personal history: severe osteoporosis. Small left inferior parathyroid adenoma (PAd), size 15 × 14 × 7 mm and volume 0.7 mL directed

towards the prevertebral space, overall US view: elliptical; inhomogeneous; hypoechoic; transverse. (bb) Detail of small inferior PAd: bean-like shaped; directed back towards the prevertebral space; transverse. (cc) Detail of small inferior PAd: bean-like shaped; directed back towards the prevertebral space; longitudinal

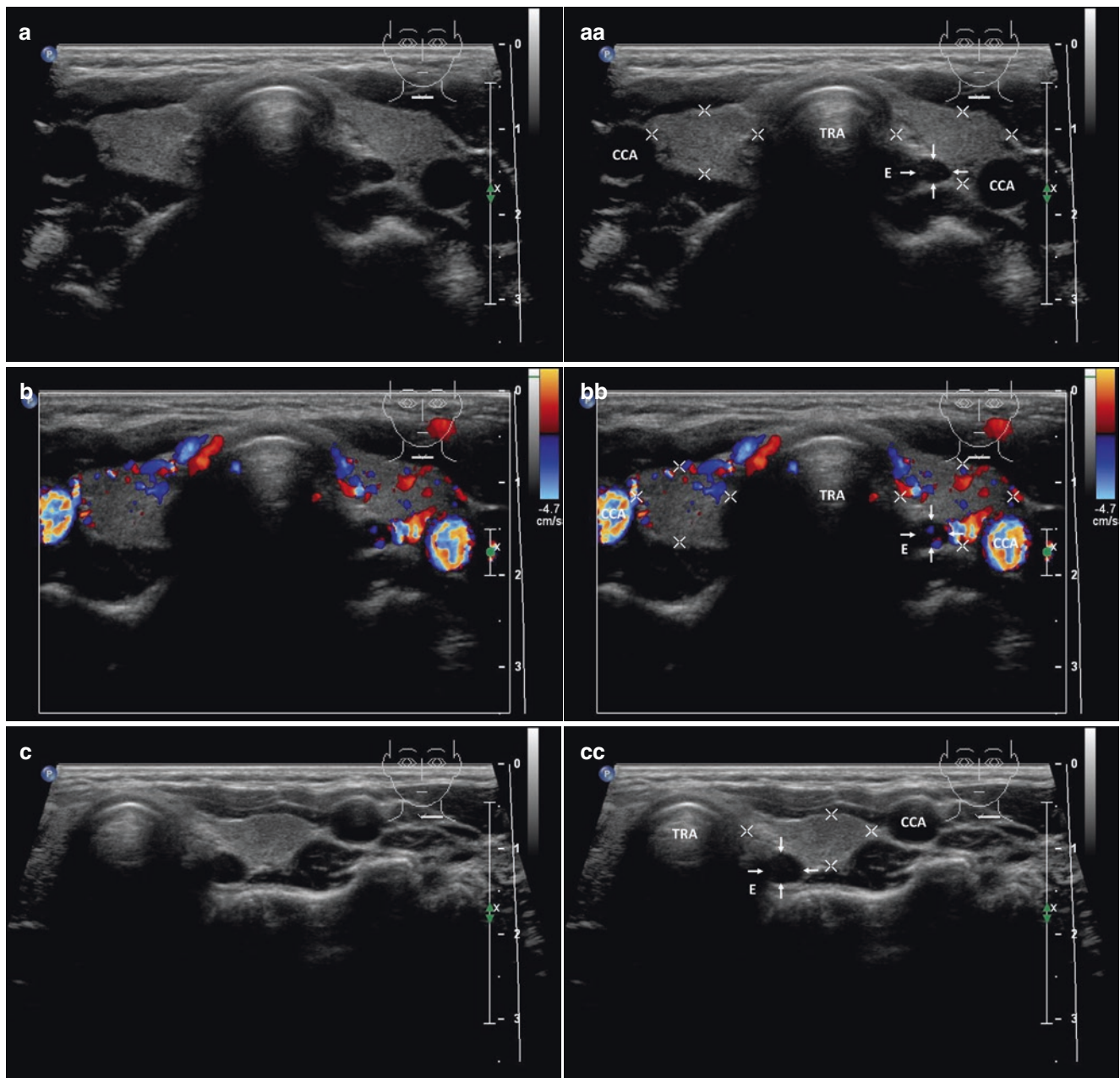


Fig. 22.6 (aa) A 10-year-old boy with pHPT, laboratory: severe hypercalcemia, s-Ca 2.86 mmol/L (normal: 2.15–2.55), moderate elevation of parathyroid hormone, s-PTH 110 ng/L (normal: 12–65). Personal history: nephrocalcinosis and growth retardation. Small elongated left superior parathyroid adenoma—PAd (arrows), size $12 \times 5 \times 4$ mm and volume 0.2 mL: lentil-like shape; homogeneous structure; hypoechoic; small thyroid gland—homogeneous structure, isoechoic, Tvol 4 mL; transverse. (bb) Overall view of thyroid gland and small elongated left

superior PAd (arrows), CFDS: diffusely increased vascularity; thyroid gland—normal vascularity, *pattern I*; transverse. (cc) Detail of small elongated left superior PAd (arrows): lentil-like shape; homogeneous structure; hypoechoic; transverse. (dd) Detail of small elongated left superior PAd (arrows): markedly elongated hypoechoic PAd along posterior wall of the upper part of LL; longitudinal. (ee) Detail of small elongated left superior PAd (arrows), CFDS: diffusely increased vascularity; longitudinal

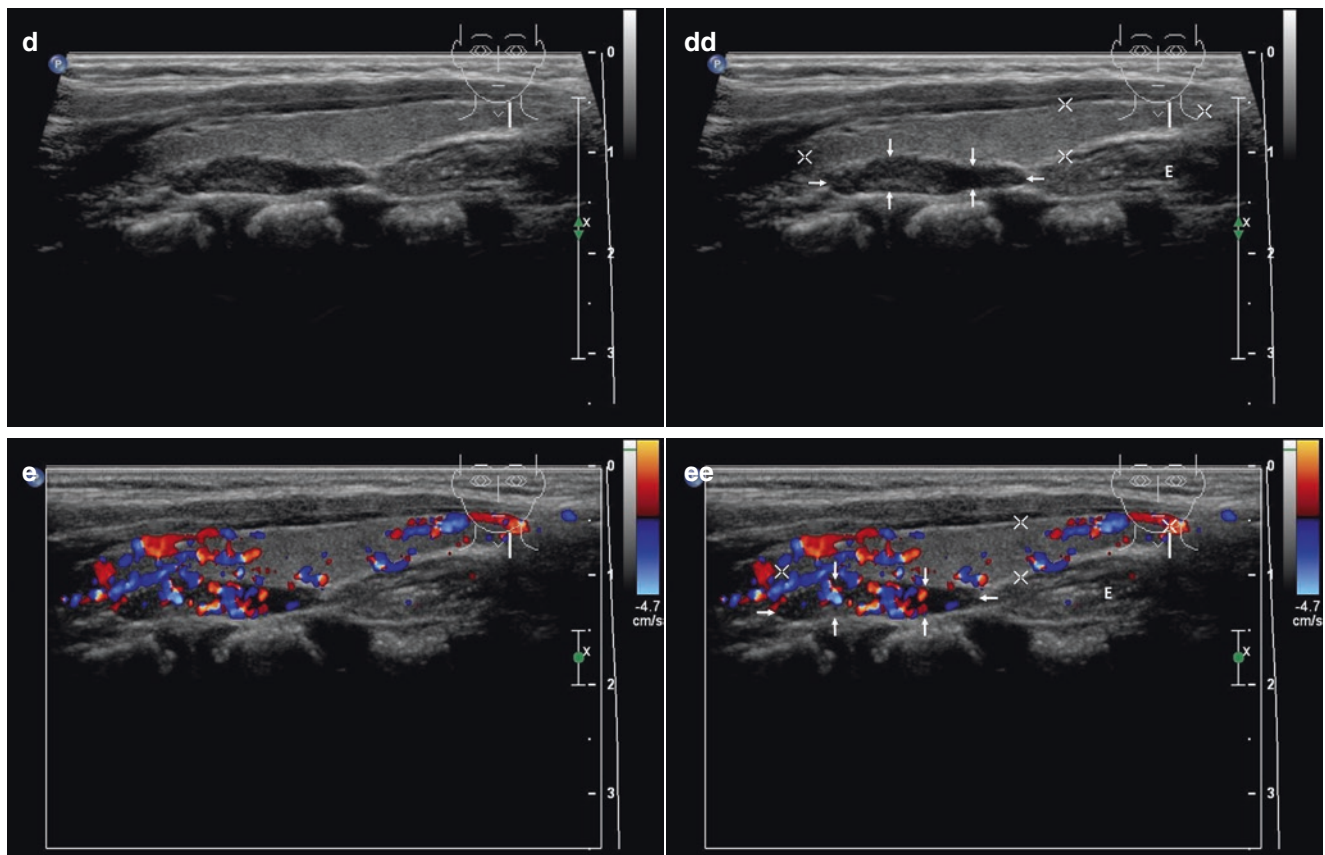


Fig. 22.6 (continued)

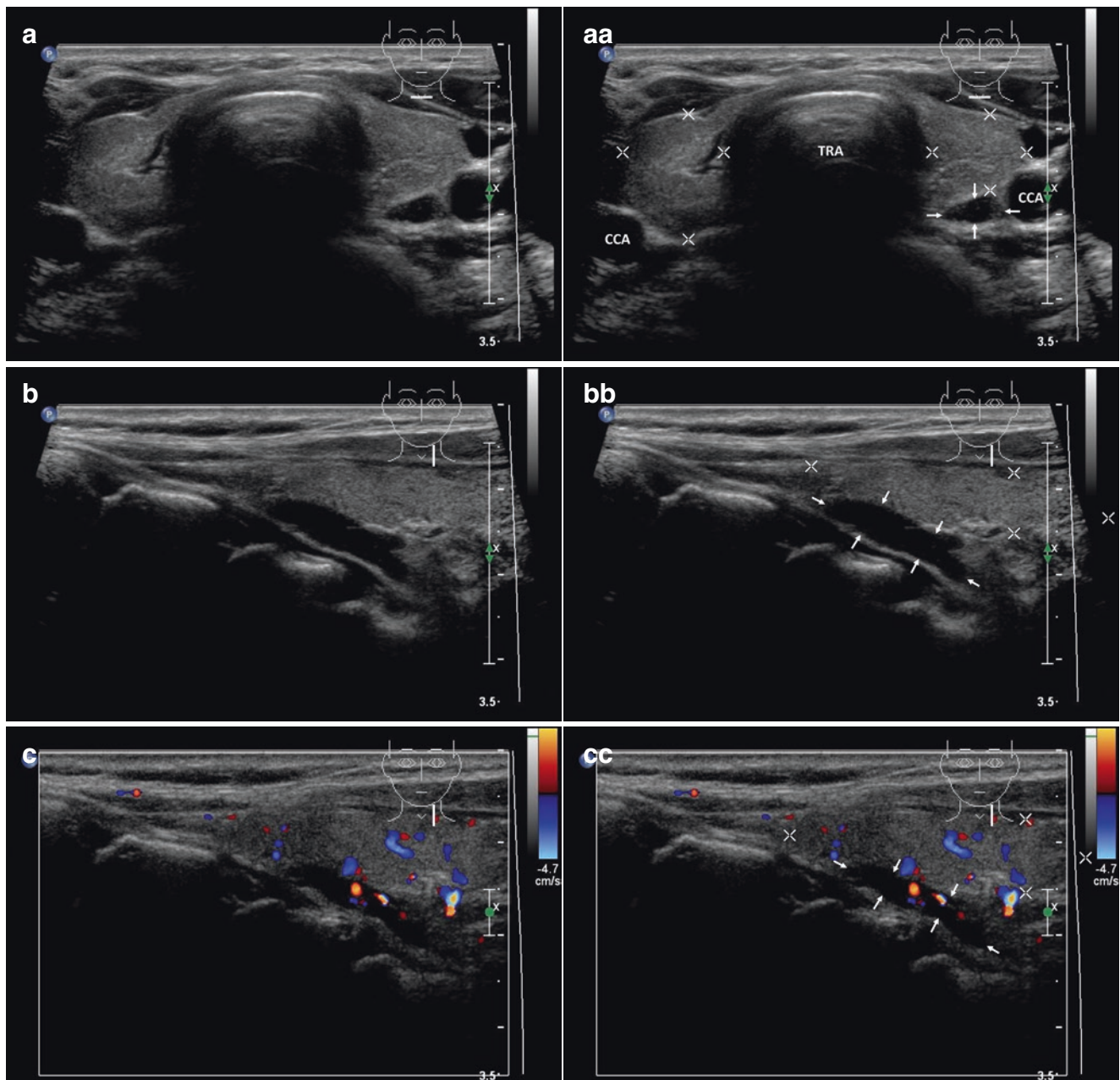


Fig. 22.7 (aa) A 69-year-old woman with symptomatic pHPT, laboratory: mild hypercalcemia, s-Ca 2.74 mmol/L (normal: 2.15–2.55), moderate elevation of parathyroid hormone, s-PTH 105 ng/L (normal: 12–65). Personal history: urolithiasis. Small elongated left superior parathyroid adenoma—PAd (*arrows*), size 18 × 7 × 3 mm and volume

0.2 mL: lentil-like shape; homogeneous structure; hypoechoic; normal thyroid gland; transverse. (bb) Detail of elongated superior PAd (*arrows*): markedly elongated hypoechoic PAd along posterior wall of the upper part of LL; longitudinal. (cc) Detail of elongated superior PAd (*arrows*), CFDS: hilar and peripheral vascularity; longitudinal

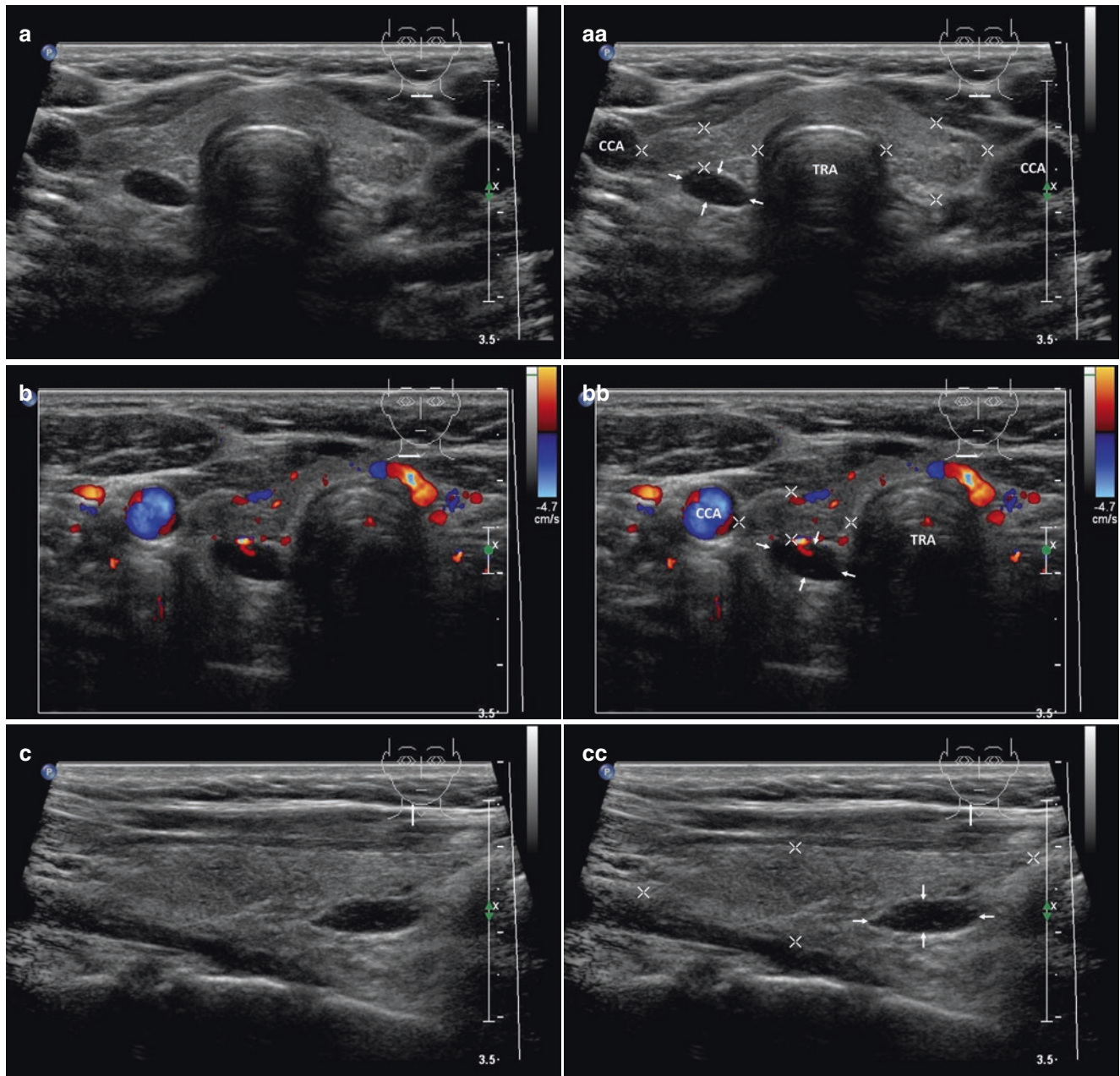


Fig. 22.8 (aa) A 53-year-old woman with pHPT, laboratory: moderate hypercalcemia, s-Ca 2.82 mmol/L (normal: 2.15–2.55), moderate elevation of parathyroid hormone, s-PTH 127 ng/L (normal: 12–65). Personal history: urolithiasis. Tiny right inferior parathyroid adenoma—PAd (arrows), size 11 × 7 × 5 mm and volume 0.2 mL: lentil-like shape; homogeneous; hypoechoic; thyroid gland—flat features of

Hashimoto's thyroiditis, slightly inhomogeneous, mostly isoechoic, sporadic hypoechoic micronodules; Tvol 8 mL, RL 4 mL, and LL 4 mL; transverse. (bb) Detail of tiny inferior PAd (arrows), CFDS: hilar vascularity; transverse. (cc) Detail of tiny inferior PAd (arrows): lentil-like shape; longitudinal. (dd) Detail of tiny inferior PAd (arrows), CFDS: hilar and central vascularity; longitudinal

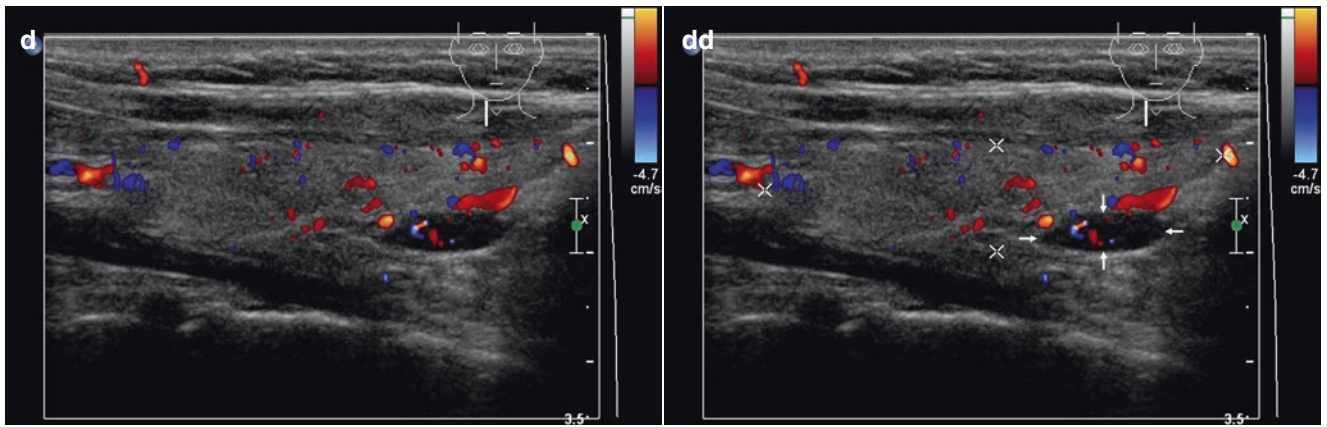


Fig. 22.8 (continued)

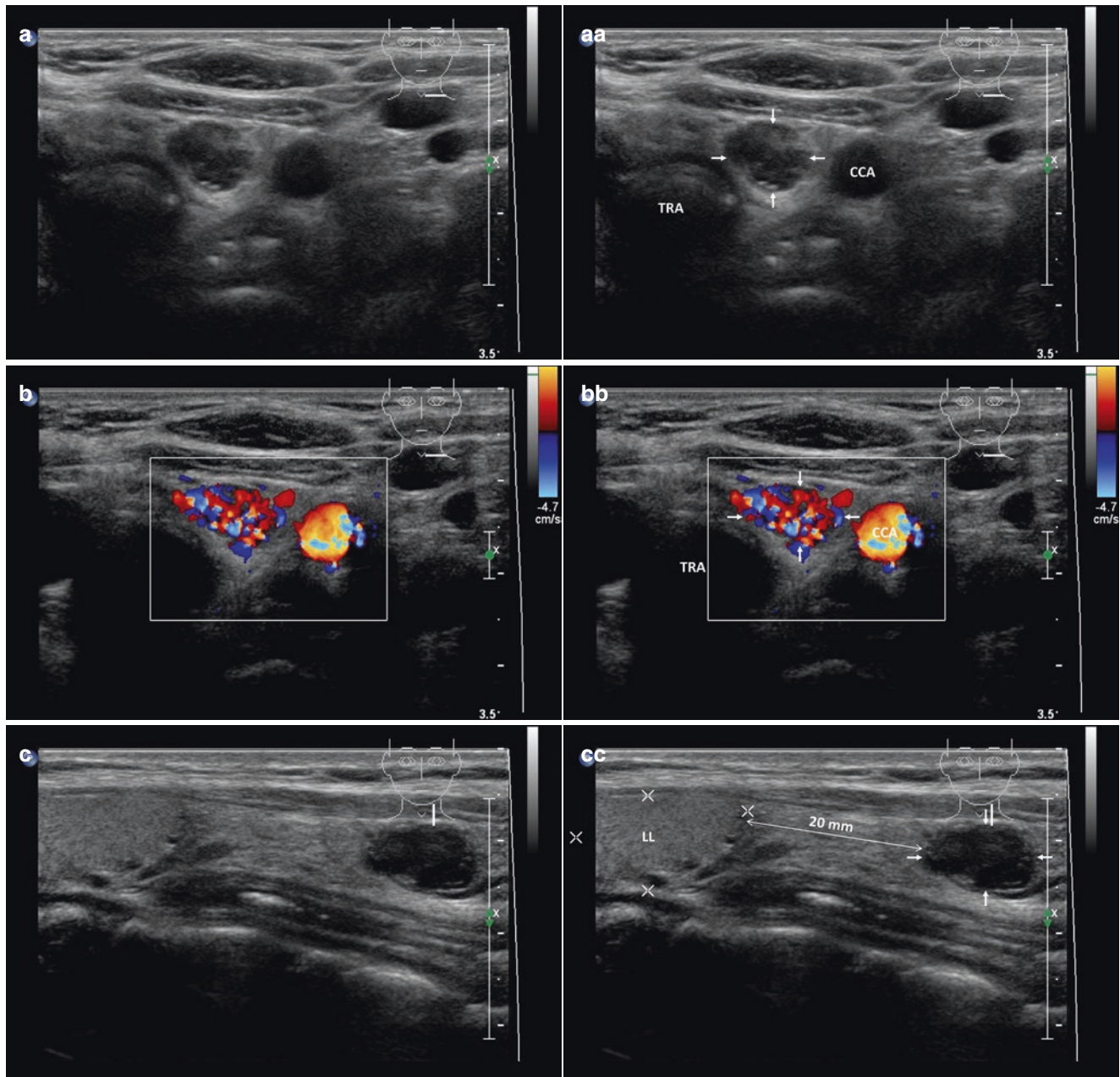


Fig. 22.9 (aa) A 29-year-old woman with pHPT, laboratory: moderate hypercalcemia, s-Ca 3.03 mmol/L (normal: 2.15–2.55), high elevation of parathyroid hormone, s-PTH 215 ng/L (normal: 12–65). Personal history: urolithiasis. Ectopic left inferior parathyroid adenoma—PAd (arrows), size 13 × 9 × 8 mm and volume 0.5 mL located deep in the lower neck approximately 2 cm under the lower pole of LL: oval shape; inhomogeneous structure; mostly hypoechoic; *thyroid gland not seen*;

transverse. (bb) Detail of the ectopic left inferior PAd (arrows), CFDS: diffusely hypervascularity; transverse. (cc) Detail of the ectopic left inferior PAd (arrows): 2 cm space between the lower pole of LL and PAd; longitudinal. (dd) Detail of the ectopic left inferior PAd (arrows), CFDS: normal vascularity in the thyroid, *pattern I*; diffusely hypervascularity of the PAd; longitudinal

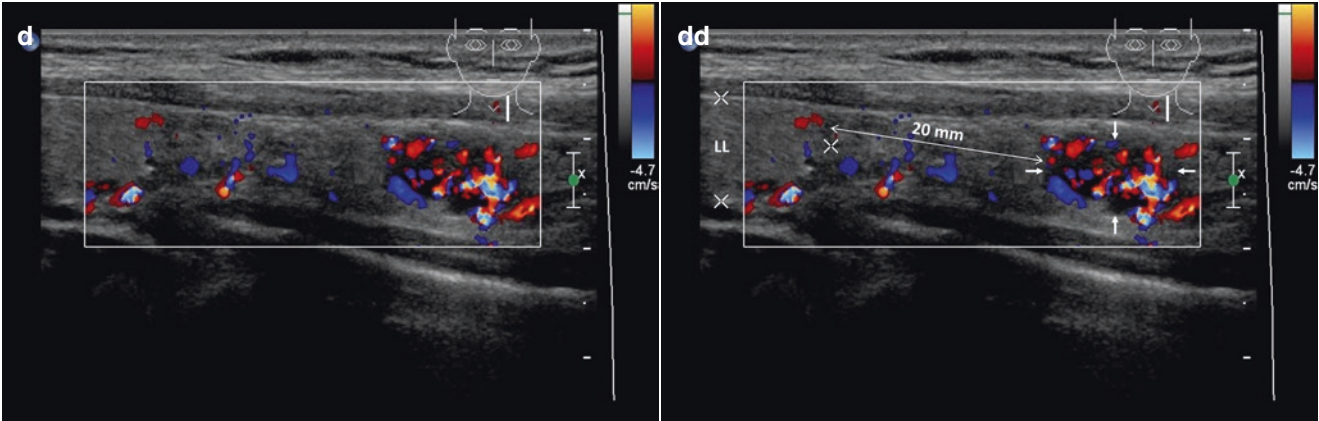


Fig. 22.9 (continued)

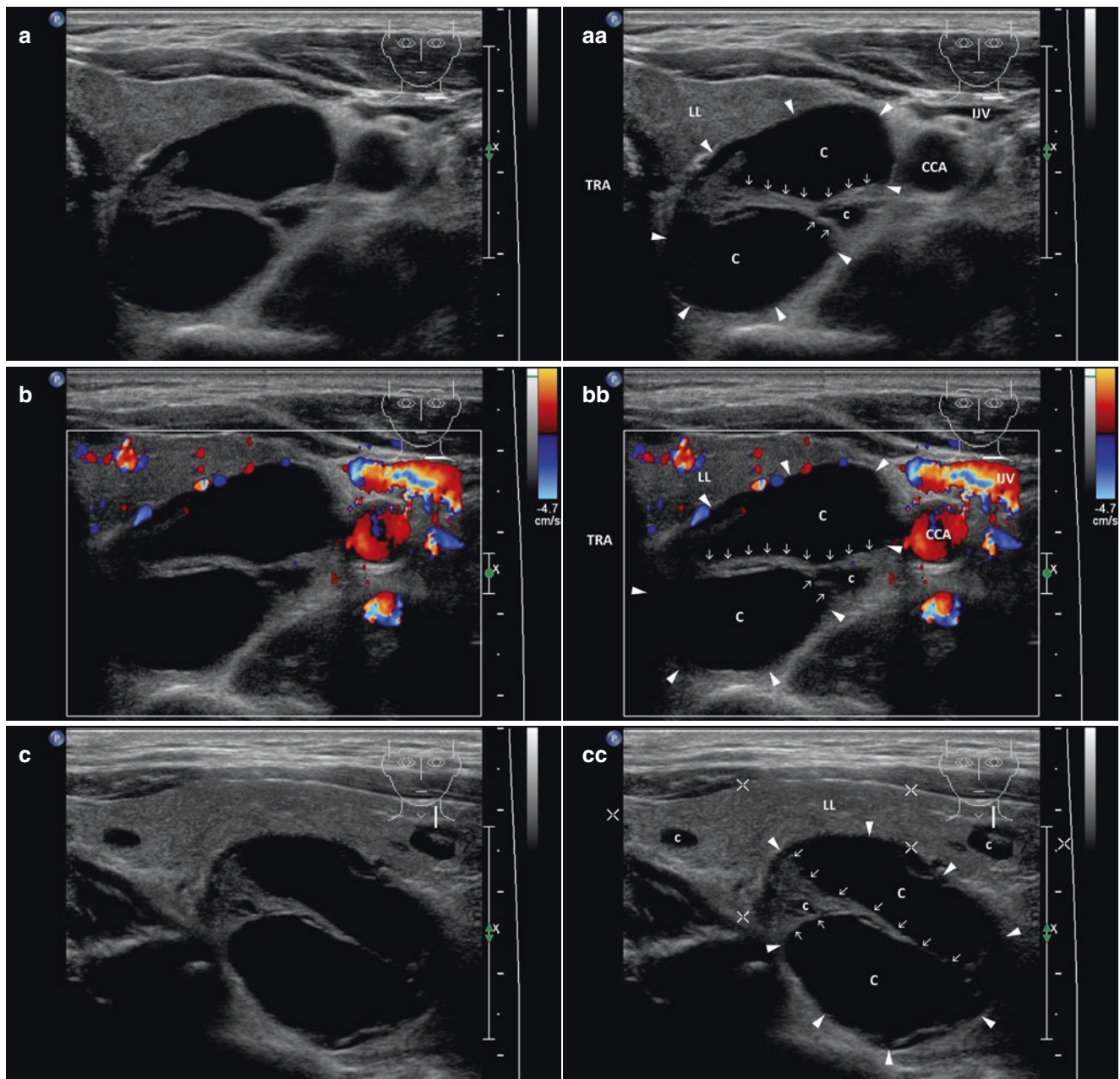


Fig. 22.10 (aa) A 76-year-old man with pHPT, laboratory: severe hypercalcemia, s-Ca 3.93 mmol/L (normal: 2.15–2.55), very high elevation of parathyroid hormone, s-PTH 802 ng/L (normal: 12–65). Personal history: urolithiasis. Large septated left inferior parathyroid cyst (arrowheads), size 38 × 31 × 24 mm and volume 14 mL: elliptical shape; thin smooth wall; anechoic content (C) with coarse branched

septum (open arrows); transverse; depth of penetration 4.5 cm. (bb) Detail of parathyroid cyst (arrowheads), CFDS: minimal vascularity in the wall; transverse. (cc) Detail of parathyroid cyst (arrowheads) located behind the low part of the LL pushes the lobe ventrally: elliptical shape; thin smooth wall; anechoic content (C) with coarse branched septum (open arrows); longitudinal

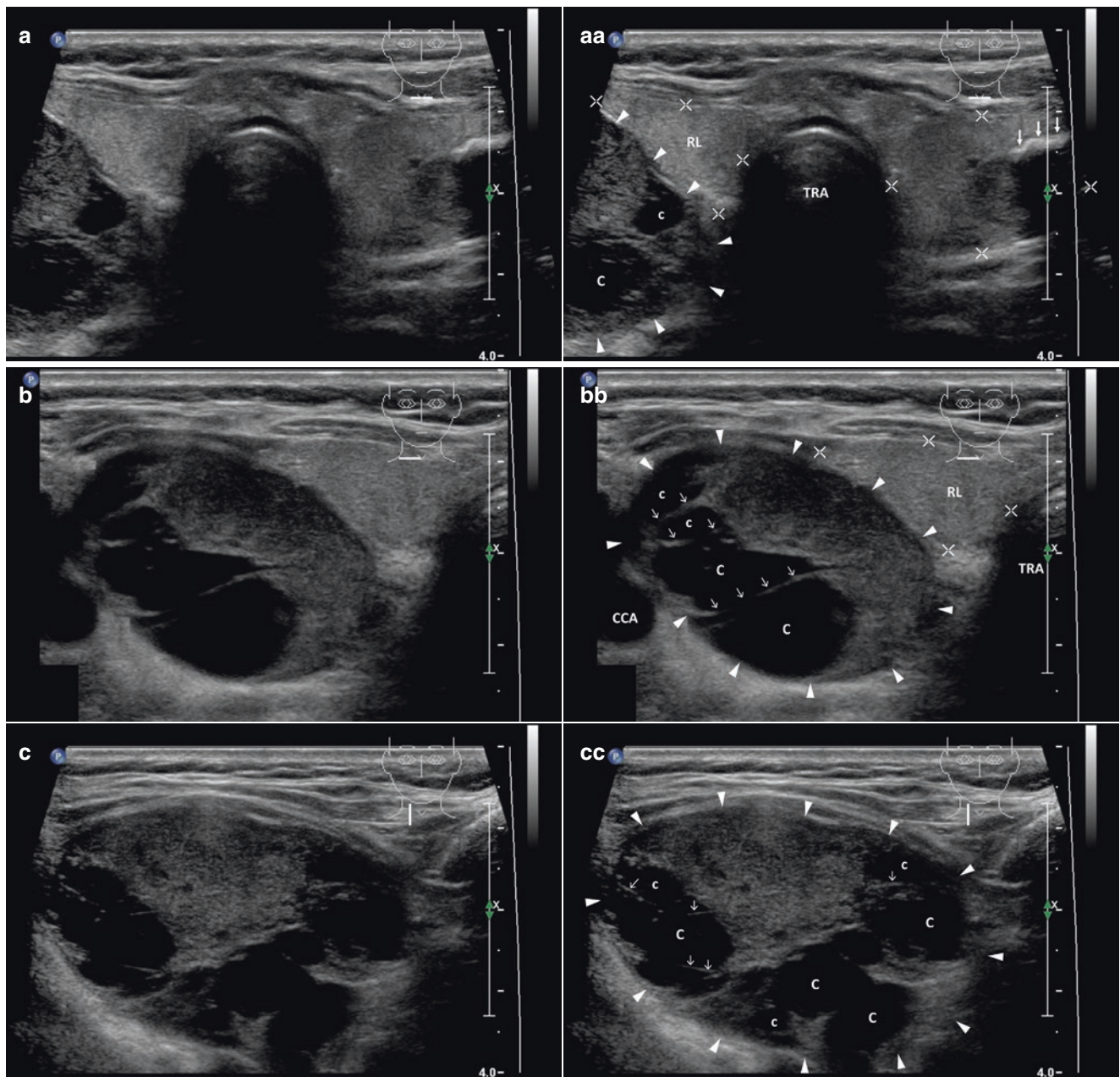


Fig. 22.11 (aa) An 82-year-old woman with pHPT, laboratory: severe hypercalcemia, s-Ca 3.13 mmol/L (normal: 2.15–2.55), high elevation of parathyroid hormone, s-PTH 335 ng/L (normal: 12–65). Personal history: urolithiasis, osteoporosis. Giant right inferior parathyroid adenoma—PAd (arrowheads), size 45 × 33 × 25 mm and volume 20 mL, with degenerative changes—cystic degeneration with septa: PAd localized behind the lower half of the dislocated and deformed RL; oval shape; coarse structure; hyperechoic; small (c) and large cystic cavities (C) with anechoic content; thyroid gland—multinodular goiter; solid

nodule of volume 1 mL with coarse rim calcification (arrows) and acoustic shadows in the LL; Tvol 48 mL, RL 31 mL, and LL 16 mL; transverse; depth of penetration 4 cm. (bb) Detail of giant right inferior PAd (arrowheads) with degenerative changes: about half of adenoma forms prominent cystic cavities (C) with anechoic content and hyper-echoic septa (open arrows); transverse. (cc) Detail of giant right inferior PAd with degenerative changes: ovoid shape; about half of adenoma forms prominent cystic cavities (C) with anechoic contents and hyper-echoic septa (open arrows); longitudinal

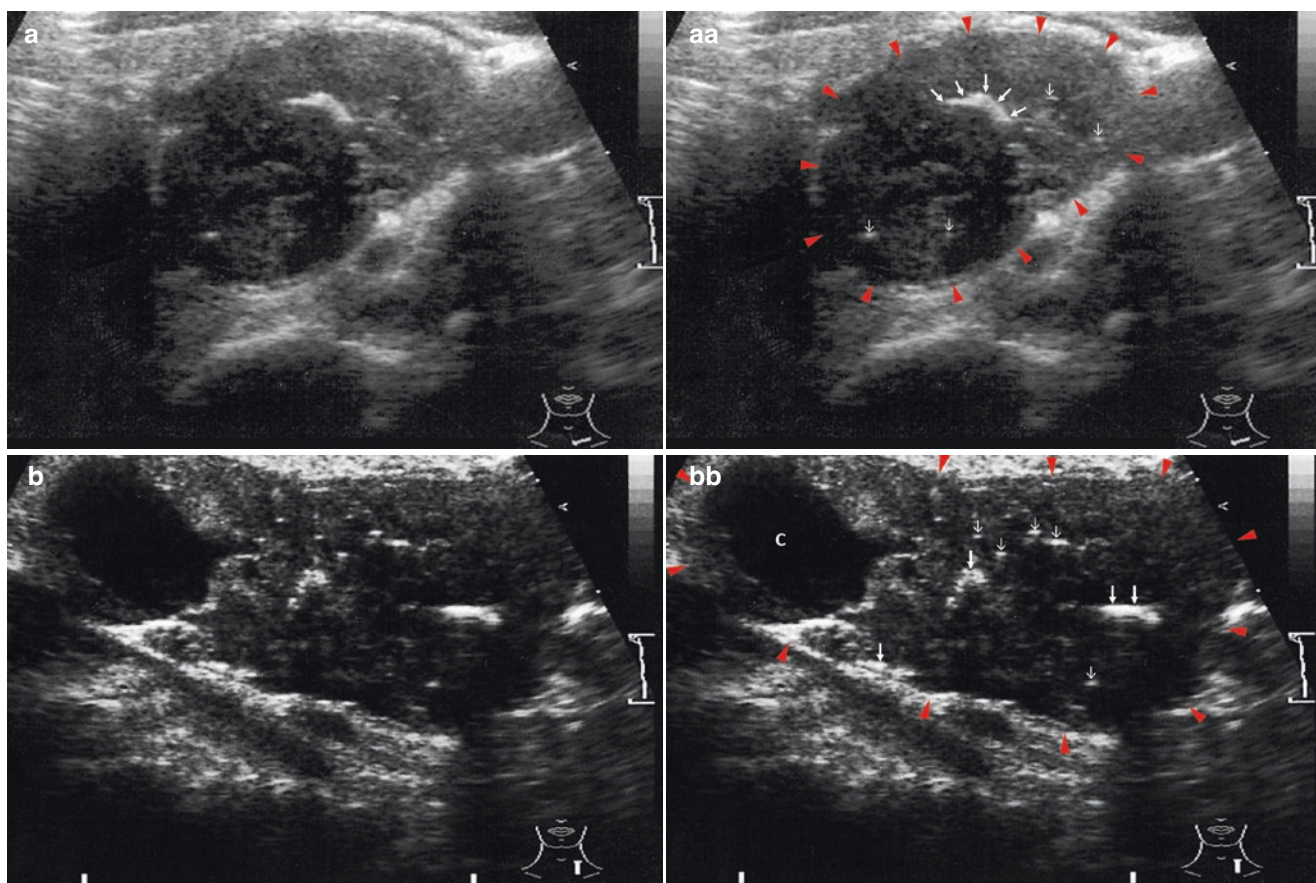
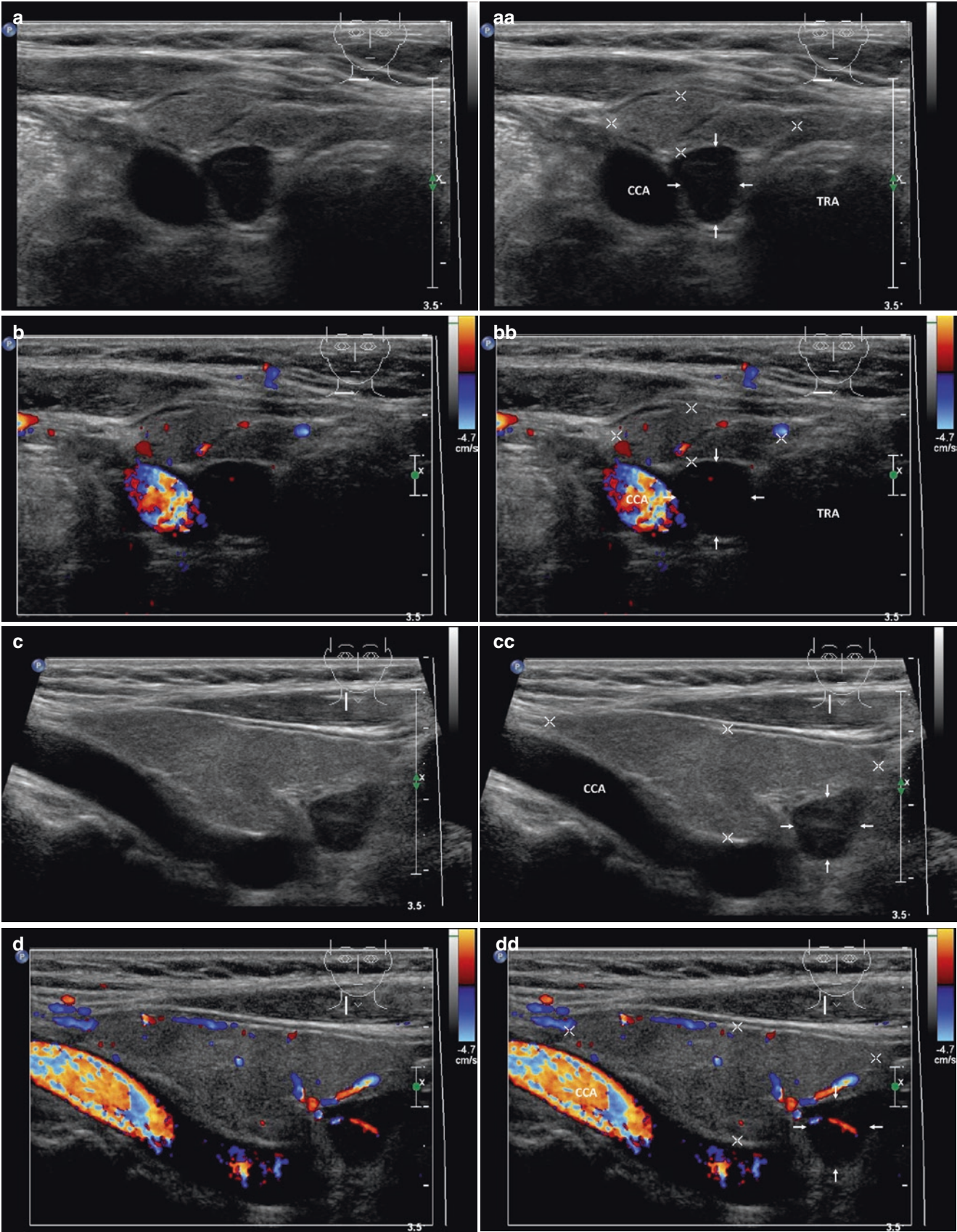


Fig. 22.12 (aa) A 61-year-old woman with severe pHPT, laboratory: severe hypercalcemia, s-Ca 3.47 mmol/L (normal: 2.15–2.55), very high elevation of parathyroid hormone, s-PTH 2070 ng/L (normal: 12–65). US showed normal thyroid gland; large tumour (red arrowheads), size $44 \times 25 \times 18$ mm and volume 10 mL in the left inferior parathyroid localization. Cytological examination suggested parathyroid carcinoma (PCa), moreover PTH level of more than 2500 pg/mL were determined in the aspirate. US scans: well-defined lesion; oval

shape; coarse structure; mostly hypoechoic; degenerative changes—coarse calcification (arrows) in the central part and diffusely microcalcifications (open arrows) on the periphery; transverse. (bb) Detail of the PCa (red arrowheads): elongated elliptical shape; degenerative changes—cystic cavity in the upper part; two coarse calcifications (arrows) in the central and lower parts and diffusely several microcalcifications (open arrows); longitudinal (year 2010, older generation of US device)

Fig. 22.13 (aa) A 65-year-old woman, end stage kidney disease patient on renal replacement therapy with sHPT, laboratory: normal calcemia, s-Ca 2.52 mmol/L (normal: 2.15–2.55), normal phosphatemia, s-P 0.99 mmol/L (normal: 0.81–1.45), high levels of parathyroid hormone, s-PTH 289 ng/L (normal: 12–65), urea 16.9 mmol/L, creatinine 260 μ mol/L. Small right inferior parathyroid adenoma—PAd

(arrows), size $11 \times 9 \times 8$ mm and volume 0.5 mL: triangular shape; homogeneous; hypoechoic; transverse. (bb) Detail of small inferior PAd (arrows), CFDS: flat hilar vascularity; transverse. (cc) Detail of small inferior PAd (arrows): triangular shape; homogeneous; hypoechoic; longitudinal. (dd) Detail of small inferior PAd (arrows), CFDS: hilar and prominent central vessel branch; longitudinal



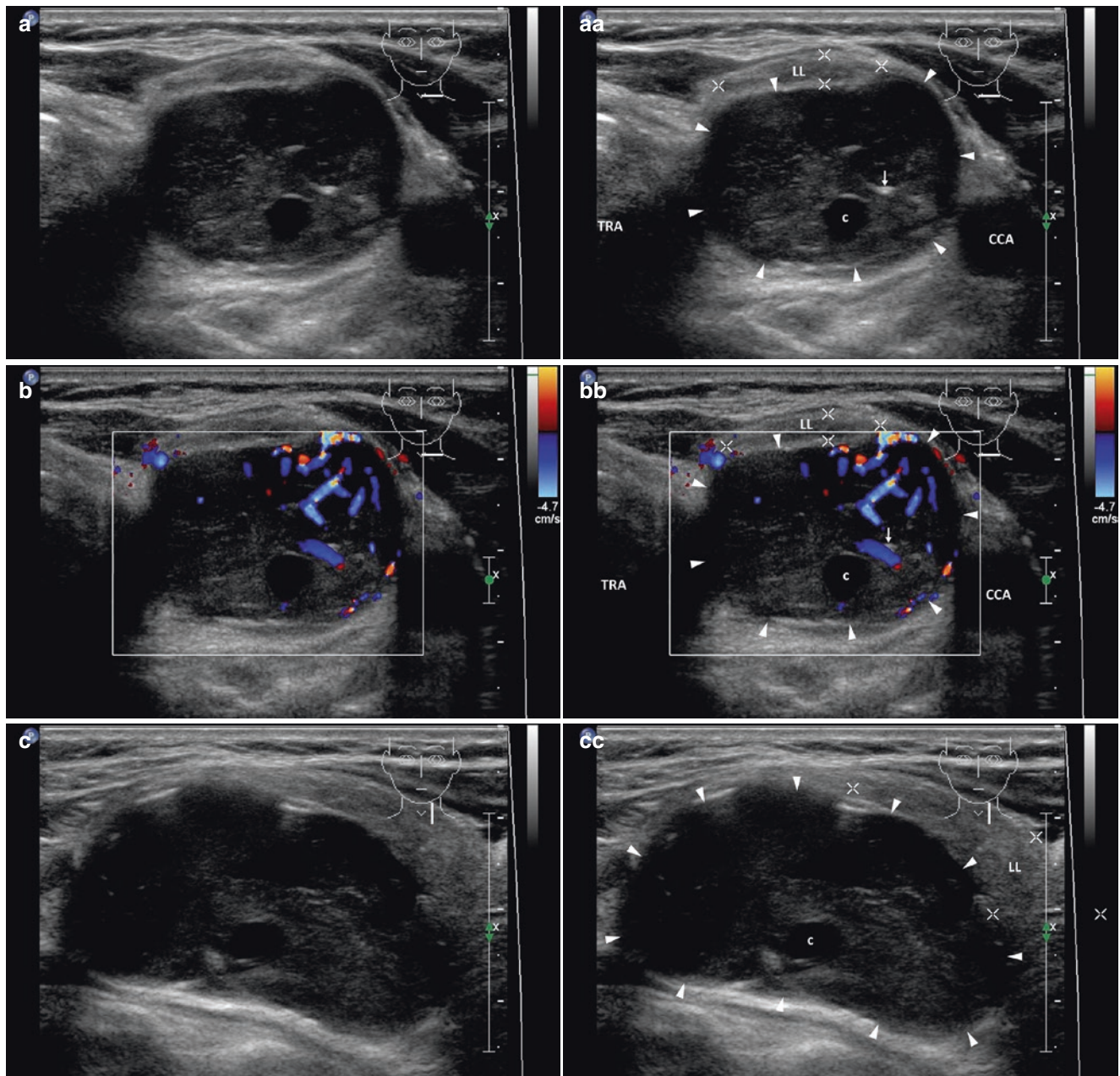


Fig. 22.14 (aa) A 65-year-old woman, end stage kidney disease patient on renal replacement therapy with sHPT, laboratory: hypocalcemia, s-Ca 1.65 mmol/L (normal: 2.15–2.55), elevated phosphatemia, s-P 2.89 mmol/L (normal: 0.81–1.45), very high level of parathyroid hormone, s-PTH > 2000 ng/L (normal: 12–65), urea 12.3 mmol/L, creatinine 493 μ mol/L. Large left superior parathyroid adenoma—PAD (arrowheads), size $40 \times 27 \times 19$ mm and volume 11 mL, with degenerative changes: round shape; coarse structure; small cystic cavity (c) and

coarse spot calcification (arrows); transverse; depth of penetration 4 cm. (bb) Detail of large left superior PAD (arrowheads), CFDS: peripheral and central hypervascularity; transverse. (cc) Detail of large left superior PAD (arrowheads): ovoid shape; small cystic cavity (c); longitudinal. (dd) Detail of large left superior PAD (arrowheads), CFDS: hilar and central vascularity, vessel arch at the periphery; longitudinal

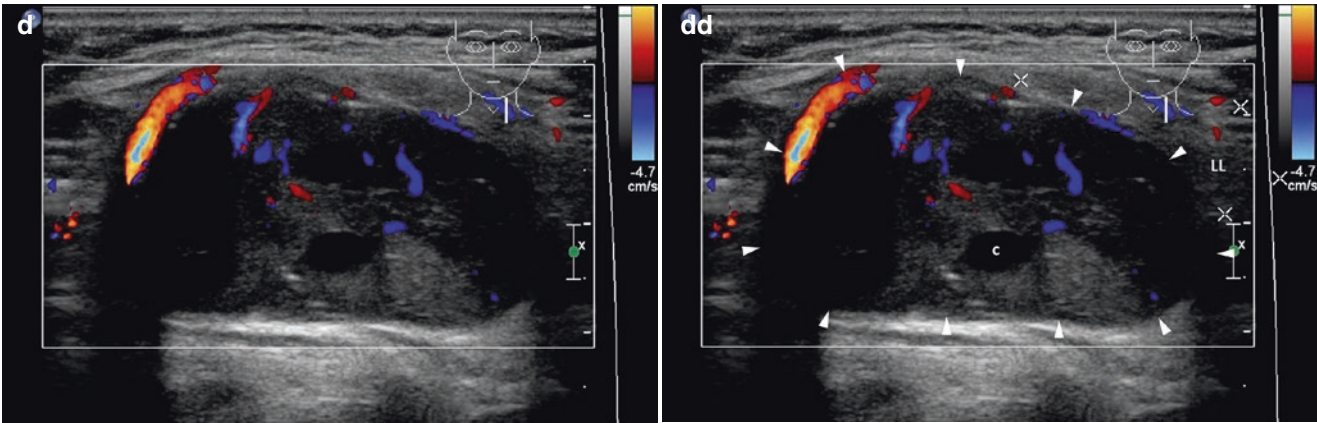


Fig. 22.14 (continued)

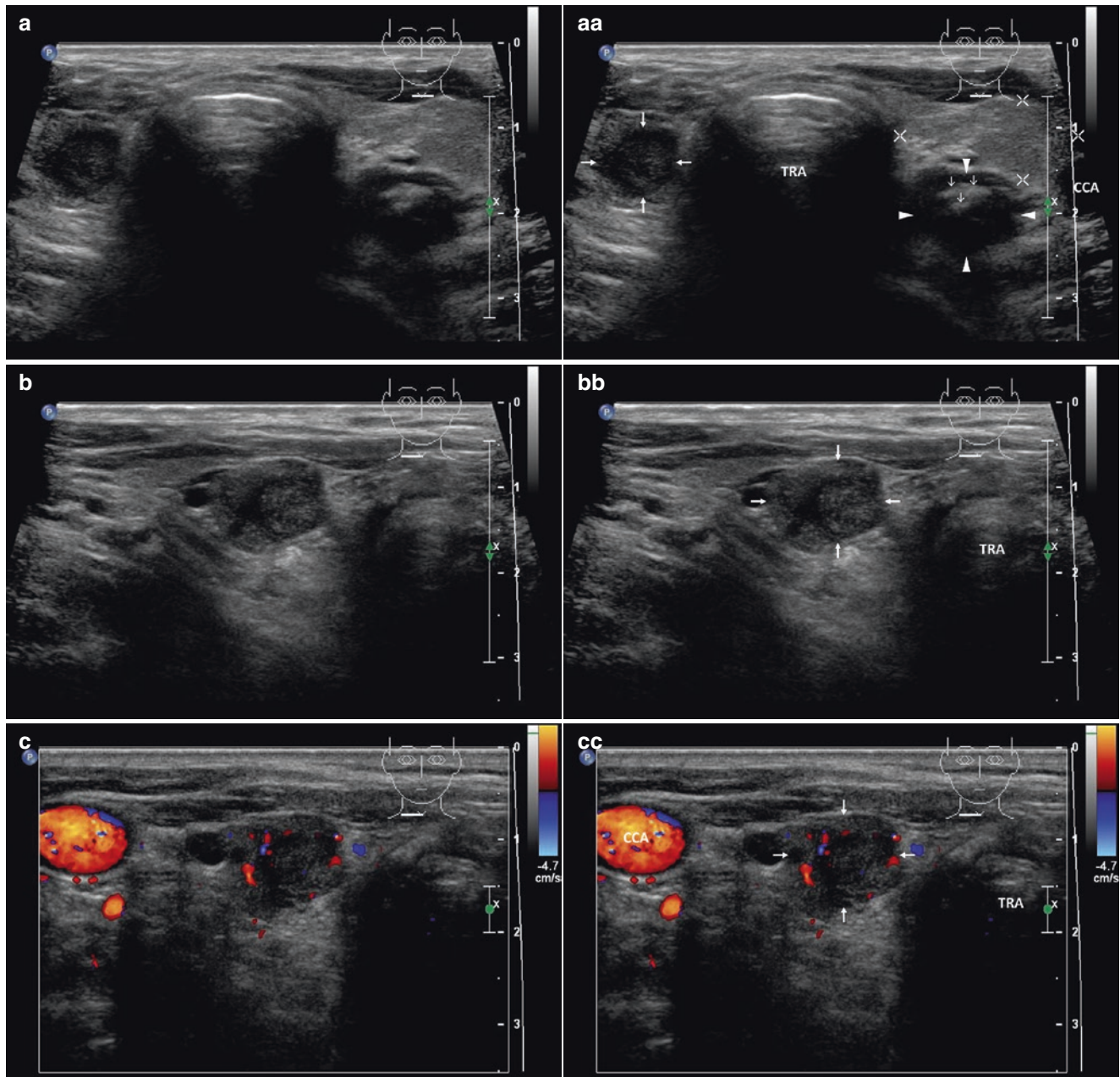


Fig. 22.15 (aa) A 61-year-old man, end stage kidney disease patient on renal replacement therapy with sHPT, laboratory: normal calcemia, s-Ca 2.43 mmol/L (normal: 2.15–2.55), elevated phosphatemia, s-P 2.19 mmol/L (normal: 0.81–1.45), high level of parathyroid hormone, s-PTH 610 ng/L (normal: 12–65), urea 9.2 mmol/L, creatinine 316 μ mol/L. Two parathyroid adenomas (PAd), small right inferior PAd, size 14 \times 13 \times 10 mm, volume 1.0 mL, and medium-sized left inferior PAd, size 17 \times 15 \times 12 mm, volume 1.6 mL, with degenerative changes. US overall view: right PAd (*arrows*)—round shape; homogeneous structure; hypoechoic; left PAd (*arrowheads*)—round shape; inhomogeneous; mostly hypoechoic; cluster of coarse calcifications at the periphery (*open arrows*); normal thyroid gland; transverse. (bb) Detail of right inferior PAd (*arrows*): round shape; homogeneous struc-

ture; hypoechoic; transverse. (cc) Detail of right inferior PAd (*arrows*), CFDS: peripheral vascularity; transverse. (dd) Detail of right inferior PAd (*arrows*): oval shape; homogeneous structure; hypoechoic; longitudinal. (ee) Detail of right inferior PAd (*arrows*), CFDS: increased hilar and central vascularity; longitudinal. (ff) Detail of left inferior PAd (*arrowheads*): round shape; inhomogeneous structure; mostly hypoechoic; cluster of coarse calcifications (*open arrows*); transverse. (gg) Detail of left inferior PAd (*arrowheads*), CFDS: minimal peripheral vascularity; transverse. (hh) Detail of left inferior PAd (*arrowheads*): ovoid shape; inhomogeneous structure; mostly hypoechoic; two coarse calcifications in the periphery (*open arrows*); next to PAd tiny complex thyroid nodule (*marks*); longitudinal

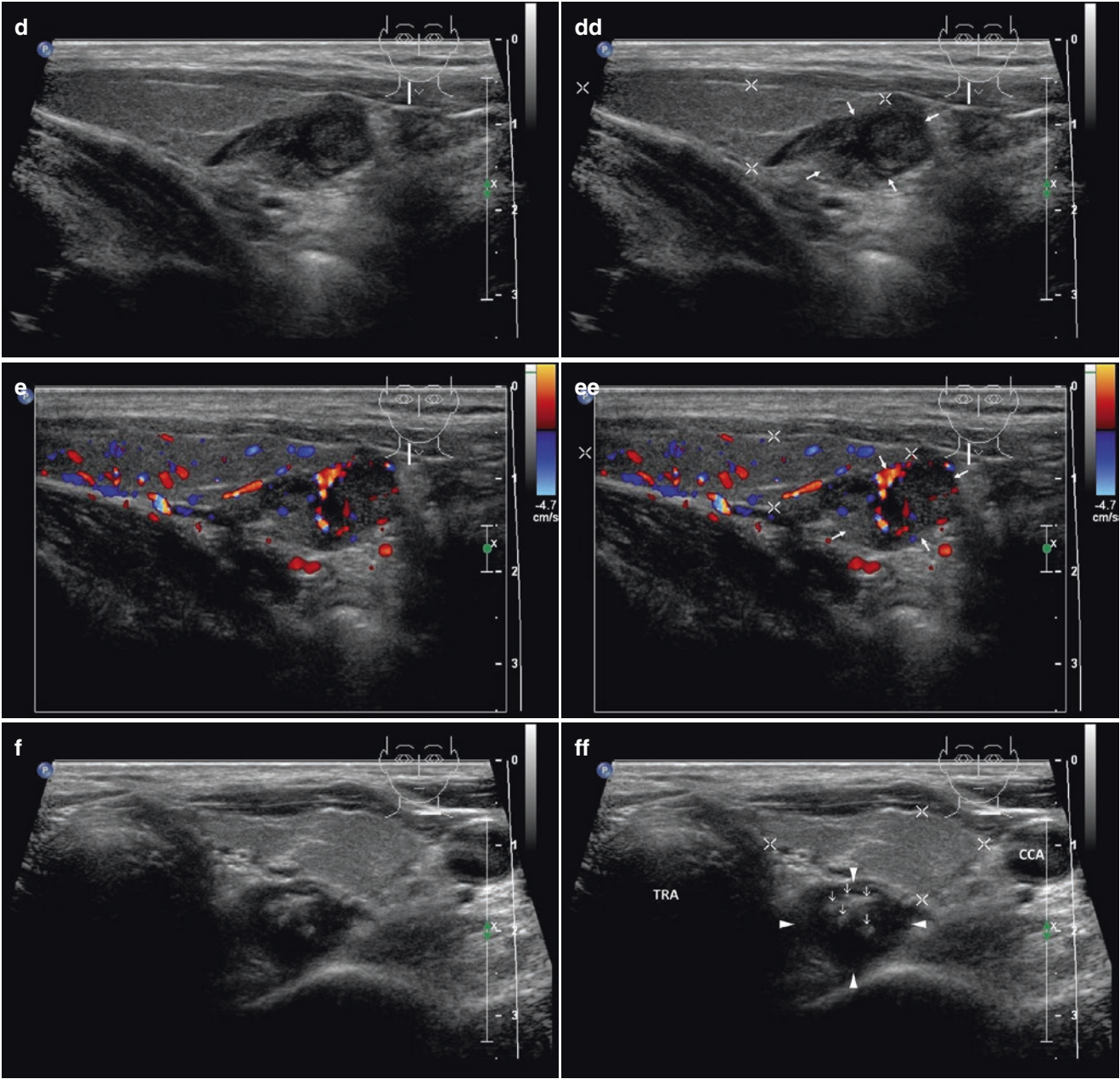


Fig. 22.15 (continued)

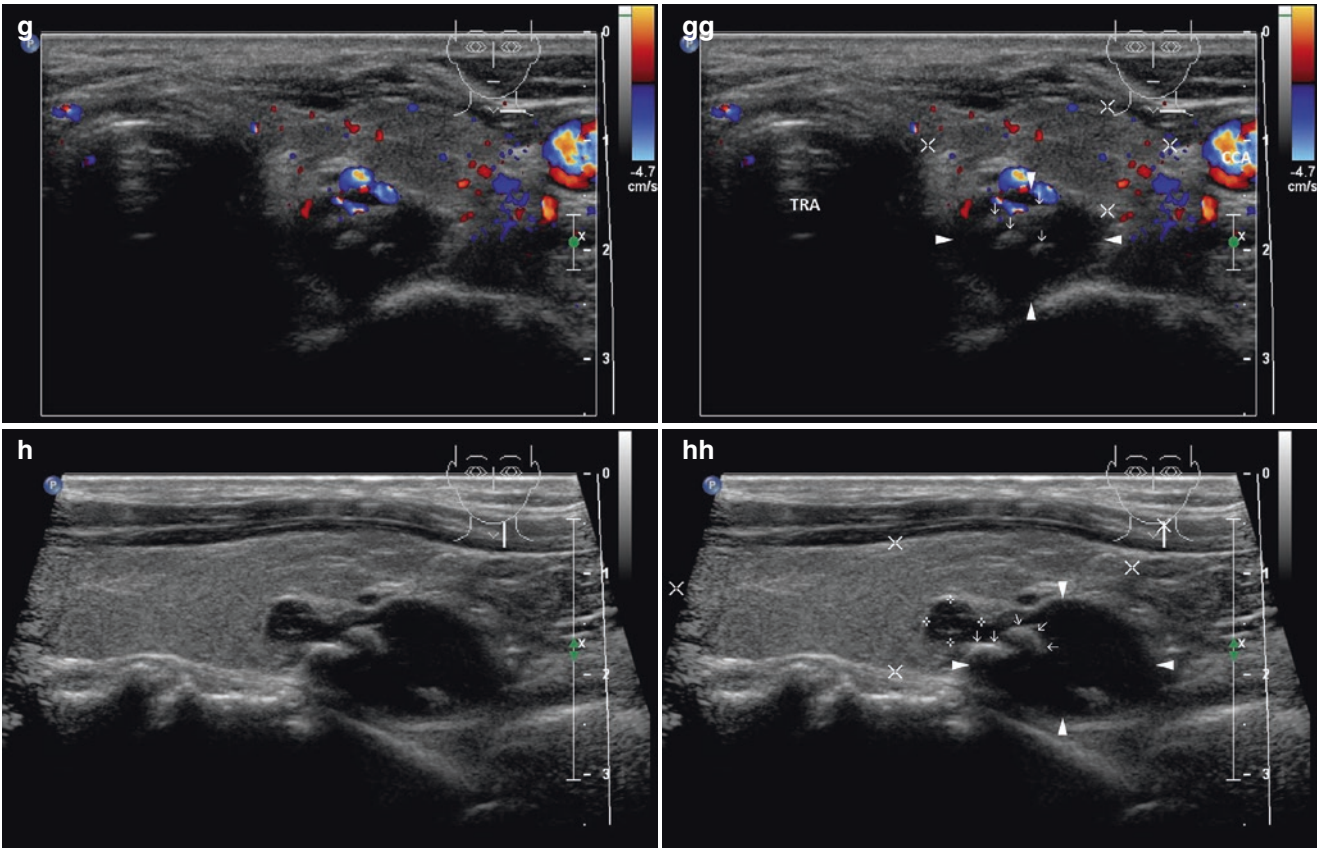


Fig. 22.15 (continued)

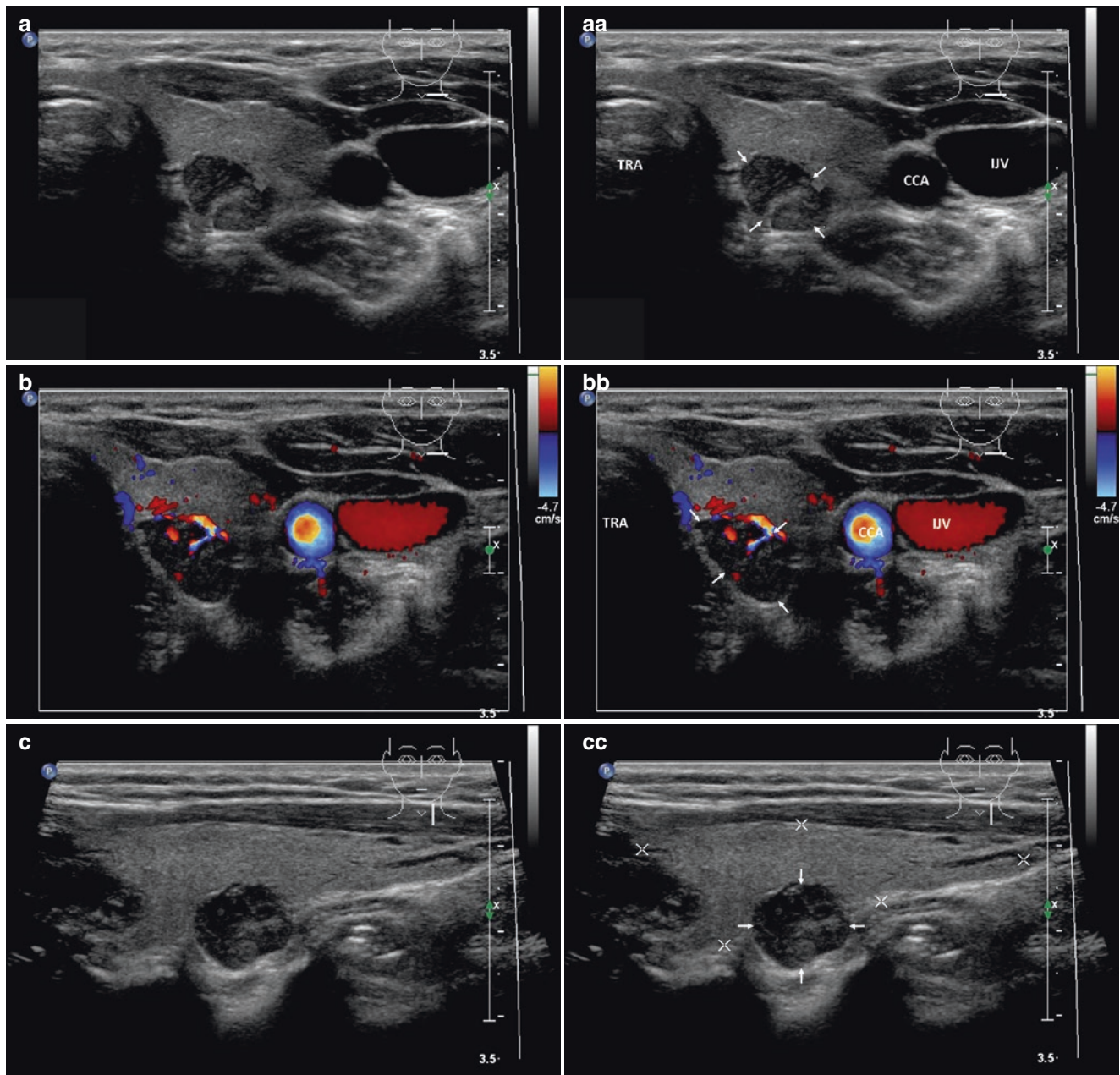


Fig. 22.16 (aa) A 53-year-old woman, end stage kidney disease patient on renal replacement therapy with sHPT, laboratory: normal calcemia, s-Ca 2.18 mmol/L (normal: 2.15–2.55), elevated phosphatemia, s-P 1.76 mmol/L (normal: 0.81–1.45), high levels of parathyroid hormone, s-PTH 805 ng/L (normal: 12–65), urea 19.1 mmol/L, creatinine 526 μ mol/L. Multiple parathyroid adenomas (PAd). Total of three small PAd's localized in right inferior, left superior and left inferior site. US scan of the left superior PAd (*arrows*), size 13 \times 11 \times 8 mm and volume 0.5 mL: oval shape; inhomogeneous structure; mostly hypoechoic with central coarse fibrous area; transverse. (bb) Detail of the left superior PAd (*arrows*), CFDS: hilar and peripheral vascularity; transverse. (cc) Detail of the left superior PAd (*arrows*): oval shape; longitudinal. (dd) Detail of the left superior PAd (*arrows*), CFDS: increased hilar and central vascularity; longitudinal. (ee) US scan of the left inferior PAd (*arrows*), size 15 \times 10 \times 8 mm and volume 0.6 mL: oval shape; coarse structure; mixed echogenicity; transverse. (ff) Detail

of the left inferior PAd (*arrows*), CFDS: hilar vascularity; transverse. (gg) Detail of the left inferior PAd (*arrows*): elliptical shape; longitudinal. (hh) Detail of the left inferior PAd (*arrows*), CFDS: increased hilar, peripheral and central vascularity; longitudinal. (ii) Detail of both the left superior 0.5 mL and inferior 0.6 mL PAd's (*arrows*): the upper located behind the middle and the lower behind the low pole of the LL; longitudinal. (jj) US scan of the right inferior PAd (*arrows*), size 16 \times 11 \times 8 mm and volume 0.8 mL: oval shape; inhomogeneous structure; mixed echogenicity; transverse. (kk) Detail of the right inferior PAd (*arrows*), CFDS: peripheral vascularity; transverse. (ll) Detail of the right inferior PAd (*arrows*): elliptical shape; longitudinal. (mm) Detail of the right inferior PAd (*arrows*), CFDS: hilar and central vascularity; longitudinal. (nn) Detail of two inferior PAd's (*arrows*), the right of 0.8 mL and left of 0.6 mL: the right—elliptical shape; mixed echogenicity and the left—oval shape; mostly isoechoic; transverse

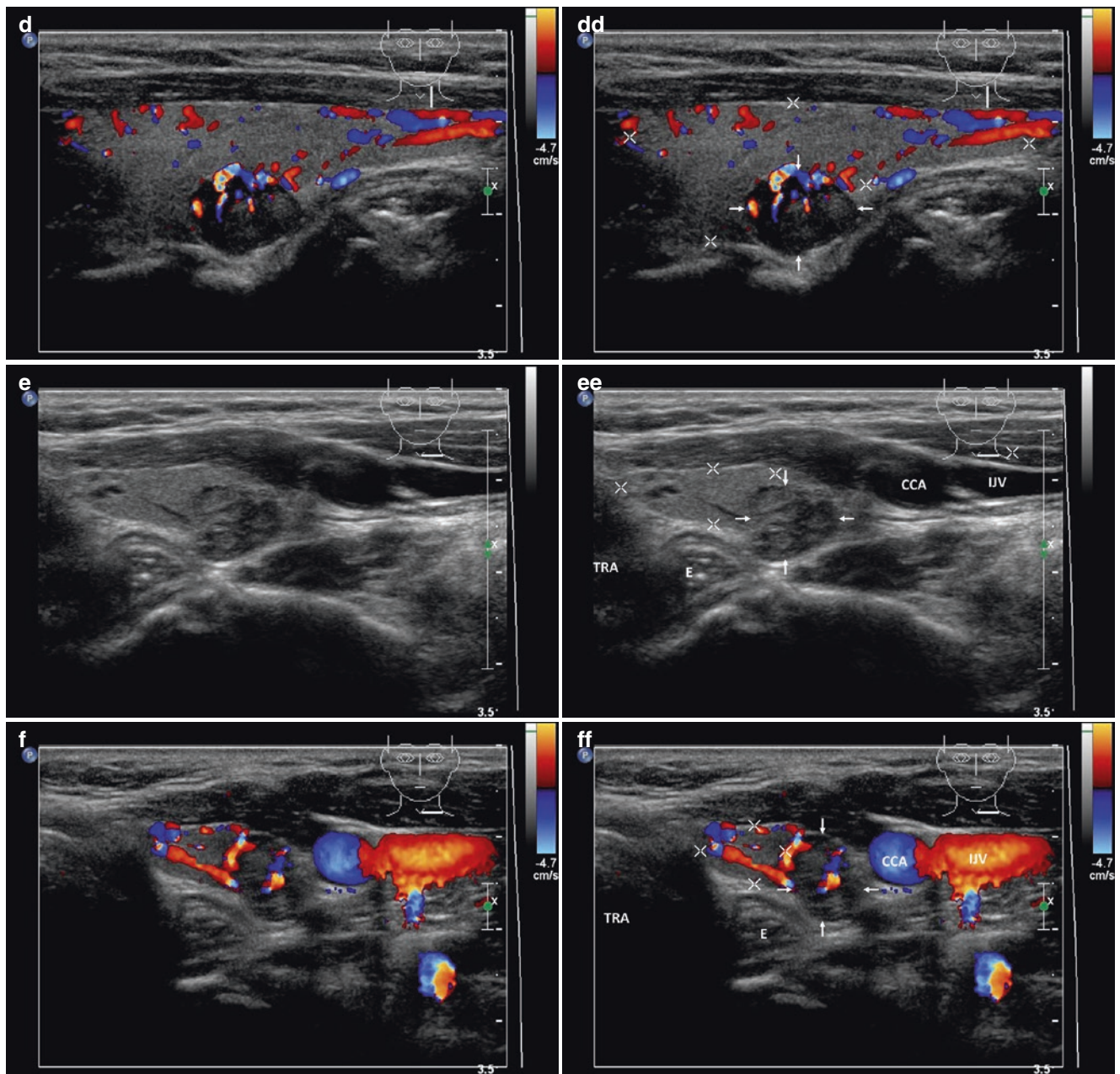


Fig. 22.16 (continued)

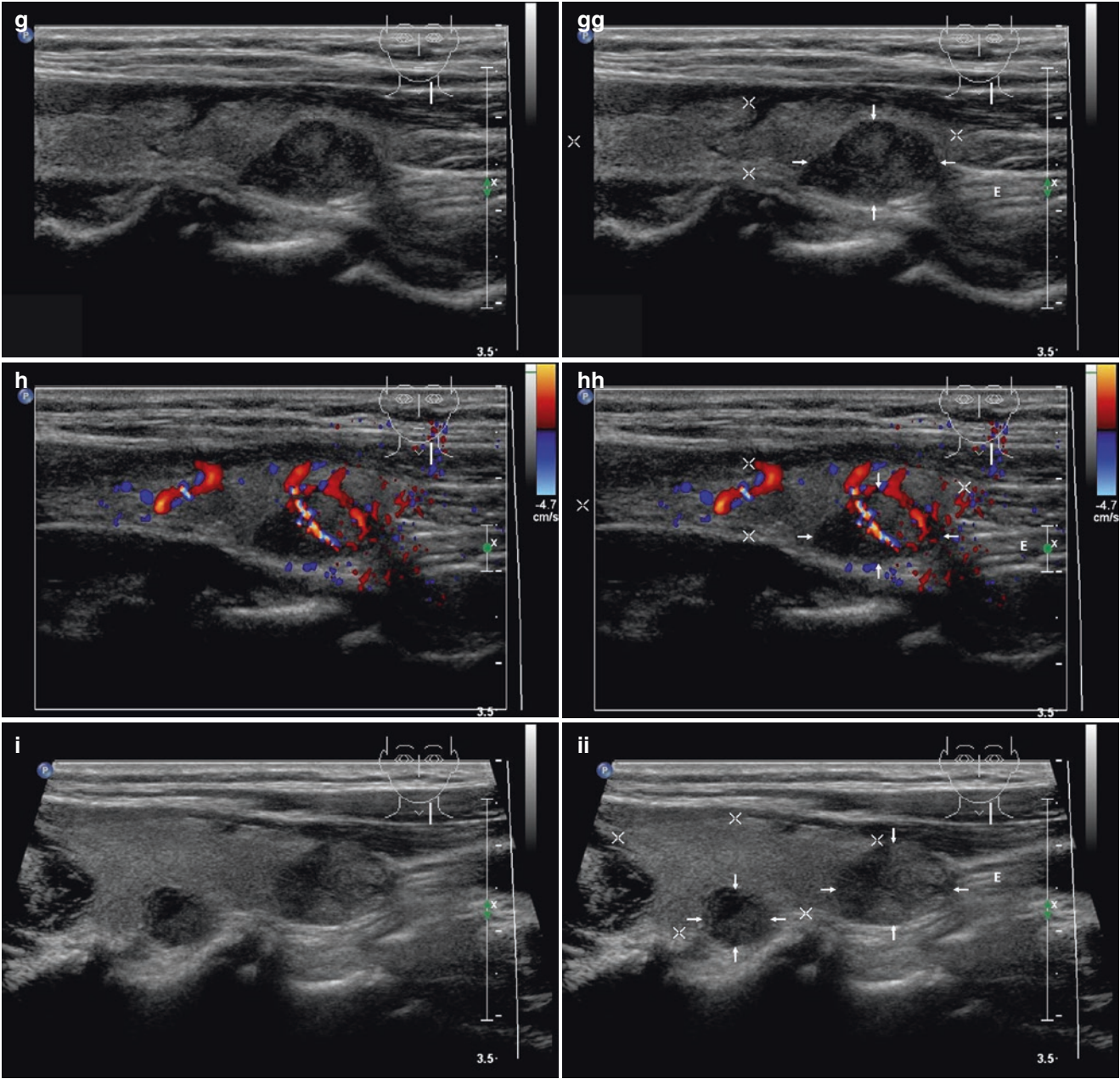


Fig. 22.16 (continued)

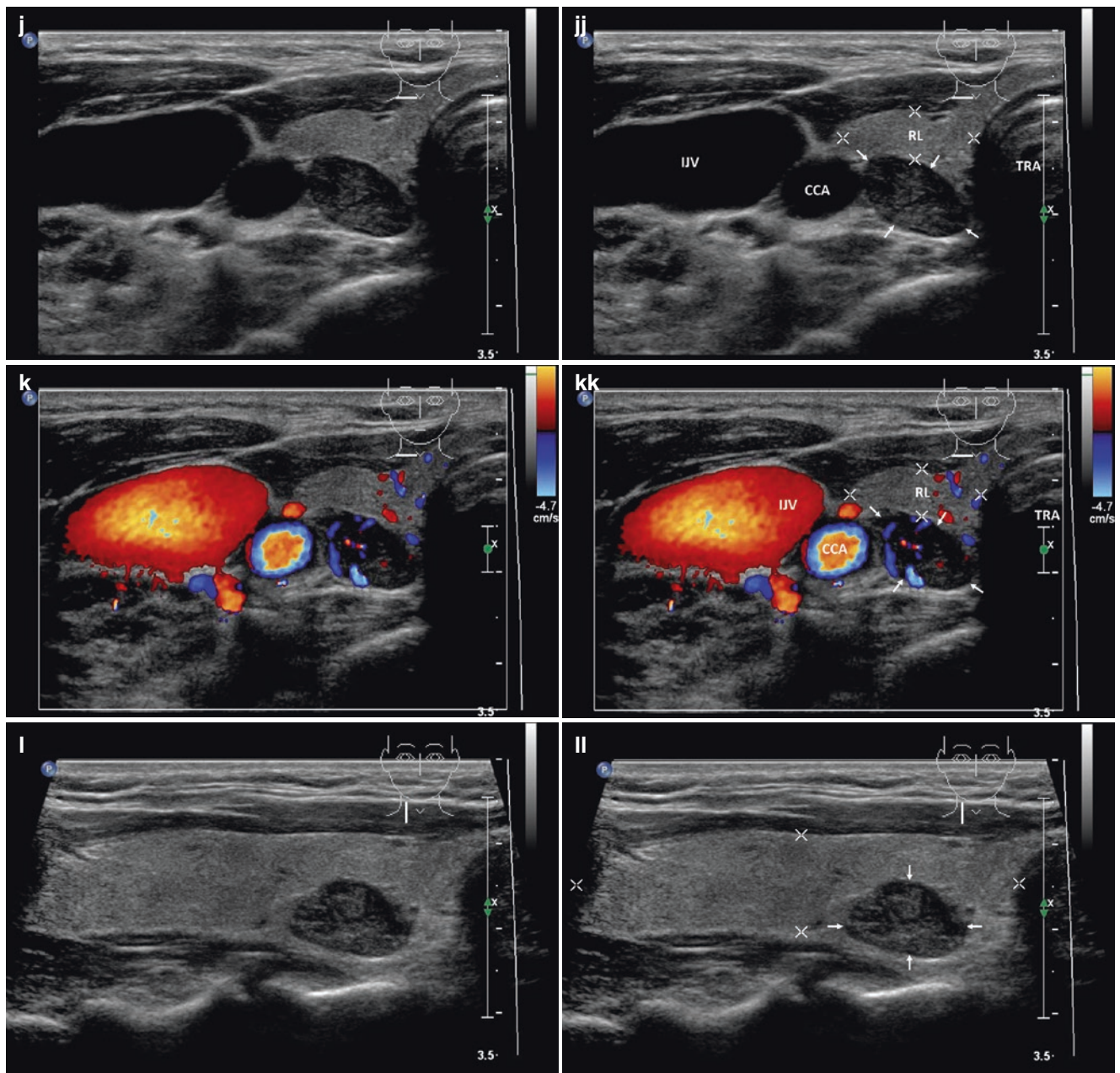


Fig. 22.16 (continued)

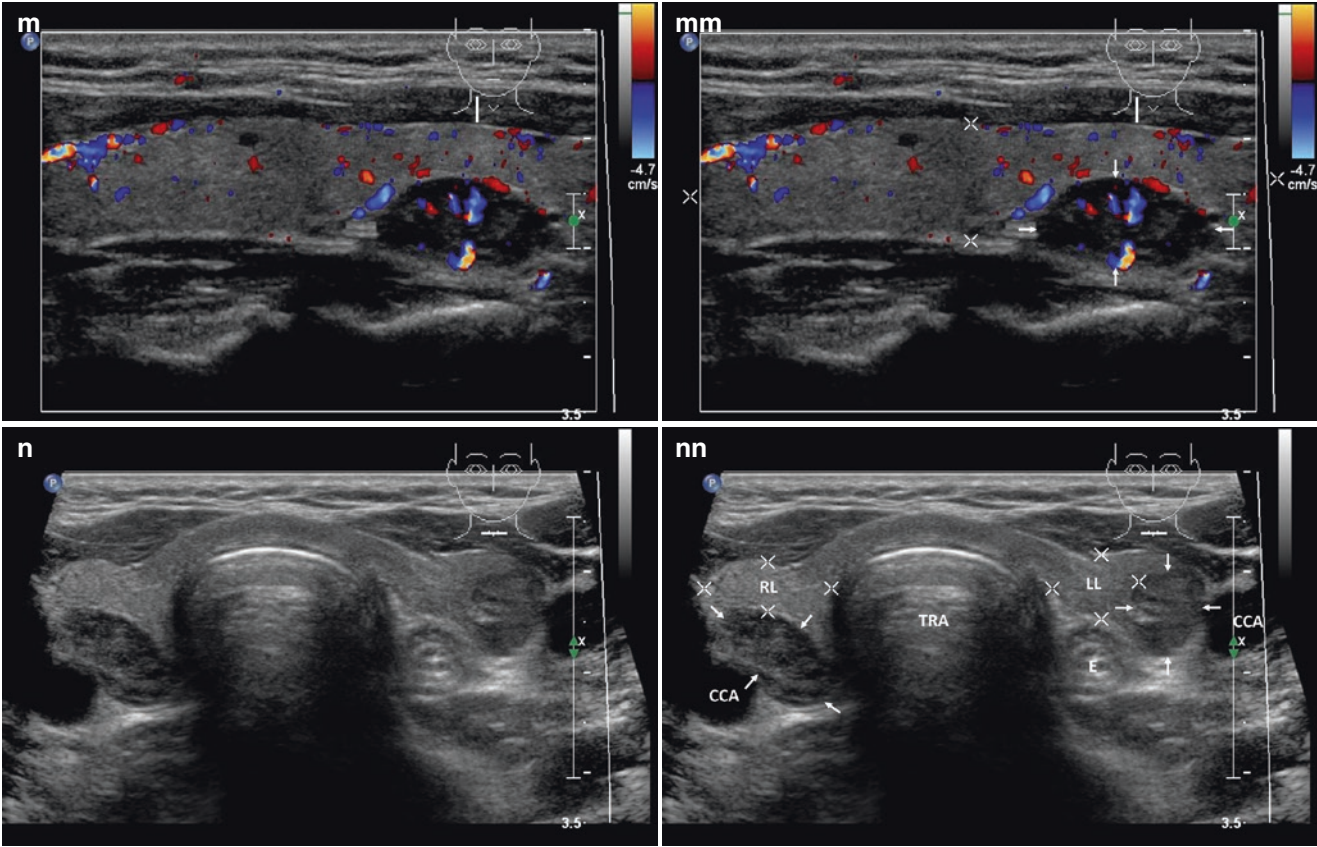


Fig. 22.16 (continued)

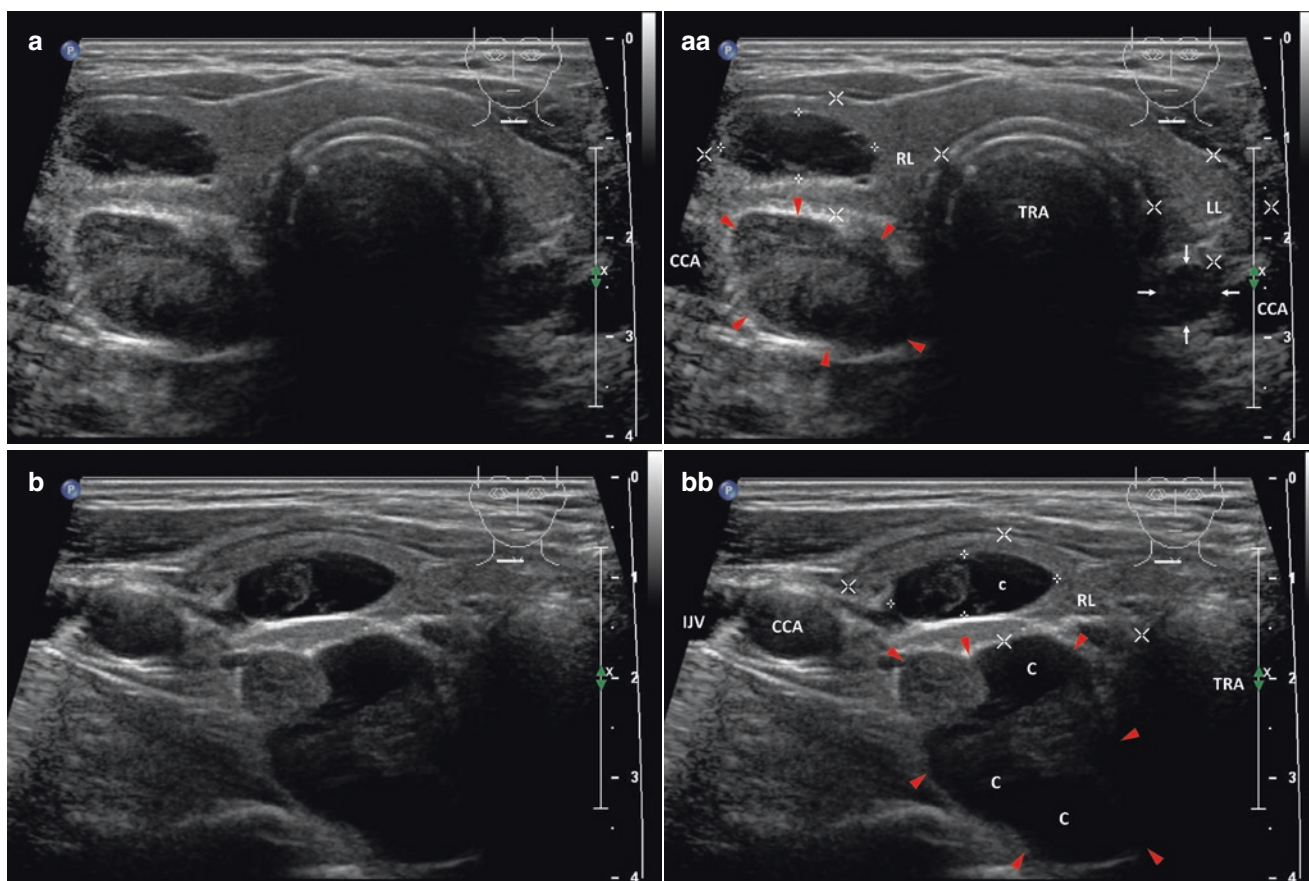


Fig. 22.17 (aa) A 60-year-old man with severe pHPT, laboratory: severe hypercalcemia, s-Ca 3.75 mmol/L (normal: 2.15-2.55), very high elevation of parathyroid hormone, s-PTH 988 ng/L (normal: 12-65). Personal history: skeletal symptoms, osteoporosis. US show three parathyroid lesions! – Large parathyroid carcinoma (PCa) (red arrowheads) of volume 8 mL in the right inferior parathyroid localization and two small parathyroid adenomas (PAD); all confirmed by postoperative histology. Overall US view: PCa (red arrowheads) – oval shape; solid part with inhomogeneous hyperechoic structure; small intrathyroidal PAD (marks) in the low pole of RL – complex lesion with cystic degeneration; small left inferior PAD (arrows) in typical localization – elliptical shape; homogeneous structure; hypoechoic; Tvol 20 mL, RL 13 mL, and LL 7 mL; transverse. **(bb)** Detail of the PCa (red arrowheads), size 32 × 23 × 20 mm and volume 8 mL: well-defined complex lesion; oval shape; inhomogeneous structure; hyperechoic solid part; degenerative changes – large cystic cavities (C); small intrathyroidal PAD (marks), size 17 × 16 × 7 mm and volume 1.2 mL in the RL, originally considered as complex thyroid nodule: complex lesion with cystic degeneration (c); transverse. **(cc)** Detail of the PCa (red arrowheads):

well-defined complex lesion; oval shape; inhomogeneous structure; hyperechoic solid part; degenerative changes – large cystic cavities (*C*); lobulated margin; small intrathyroidal PAd (*marks*) in the RL: complex lesion with cystic degeneration (*c*); longitudinal. (**dd**) Detail of the PCa (*red arrowheads*), CFDS: sporadic peripheral vascularity in solid part; small intrathyroidal PAd (*marks*) in the RL CFDS: hilar vascularity and one peripheral vessel branch; longitudinal. (**ee**) Detail of “classic” small left inferior PAd (*arrows*), size $13 \times 9 \times 6$ mm and volume 0.4 mL: elliptical shape; homogeneous structure; hypoechoic; transverse. (**ff**) Detail of “classic” small left inferior PAd (*arrows*): elliptical shape; homogeneous structure; hypoechoic; longitudinal. (**gg**) Detail of “classic” small left inferior PAd (*arrows*), CFDS: one hilar and one central vessel branches; longitudinal. (h) CT transverse view: large PCa (*red arrowheads*) located behind RL and trachea; two PAd: in the low pole of RL and in small left inferior PAd (*white arrows*). (Figure courtesy of Pavel Koranda, MD, PhD) (**hh**) ^{99m}Tc -MIBI SPECT transverse view: minimal uptake in PCa (*red arrowheads*); increased uptake in intrathyroidal PAd (*white arrows*) in the low pole of RL and in small left inferior PAd (*white arrows*). (Figure courtesy of Pavel Koranda, MD, PhD)

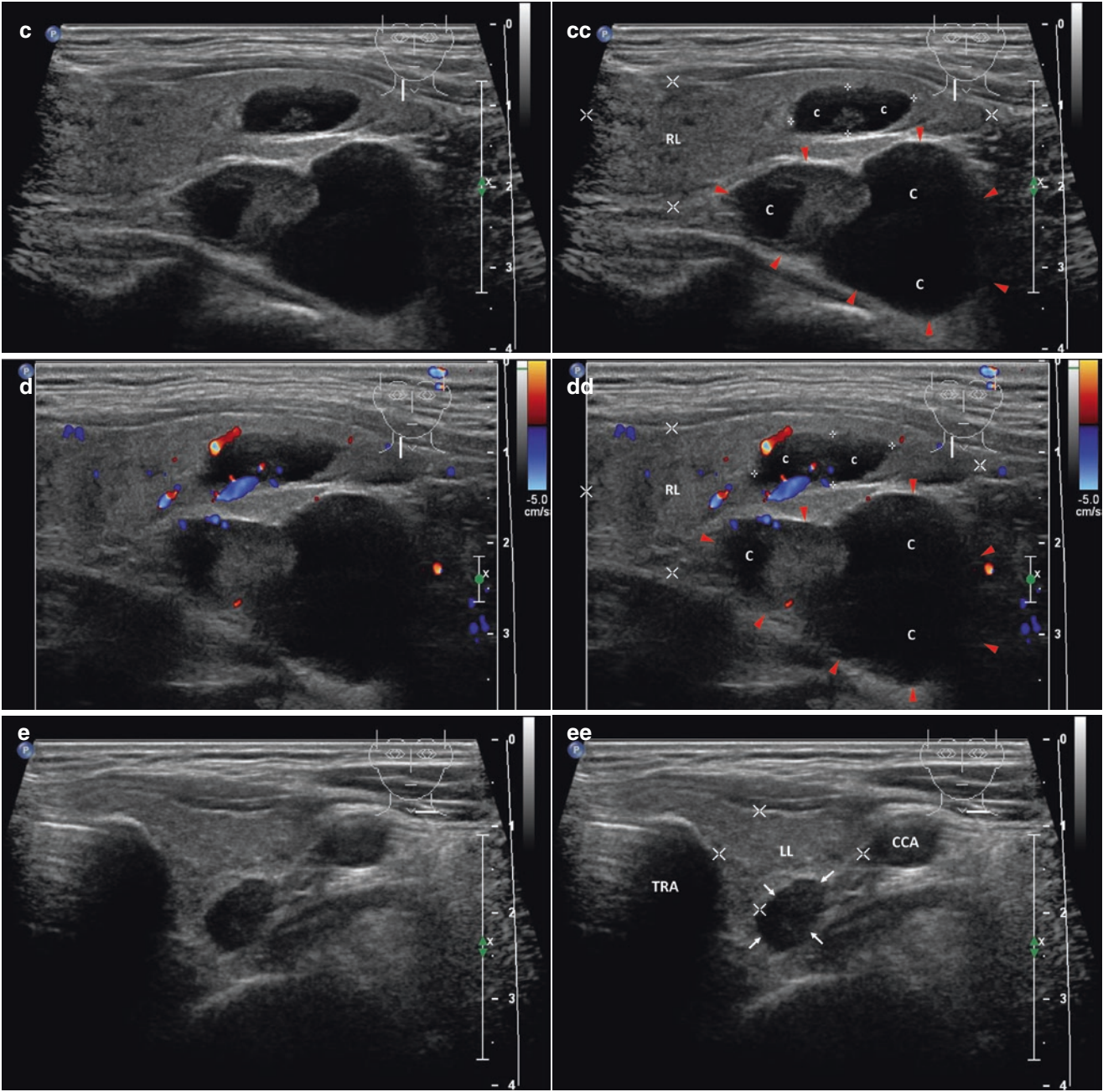


Fig. 22.17 (continued)

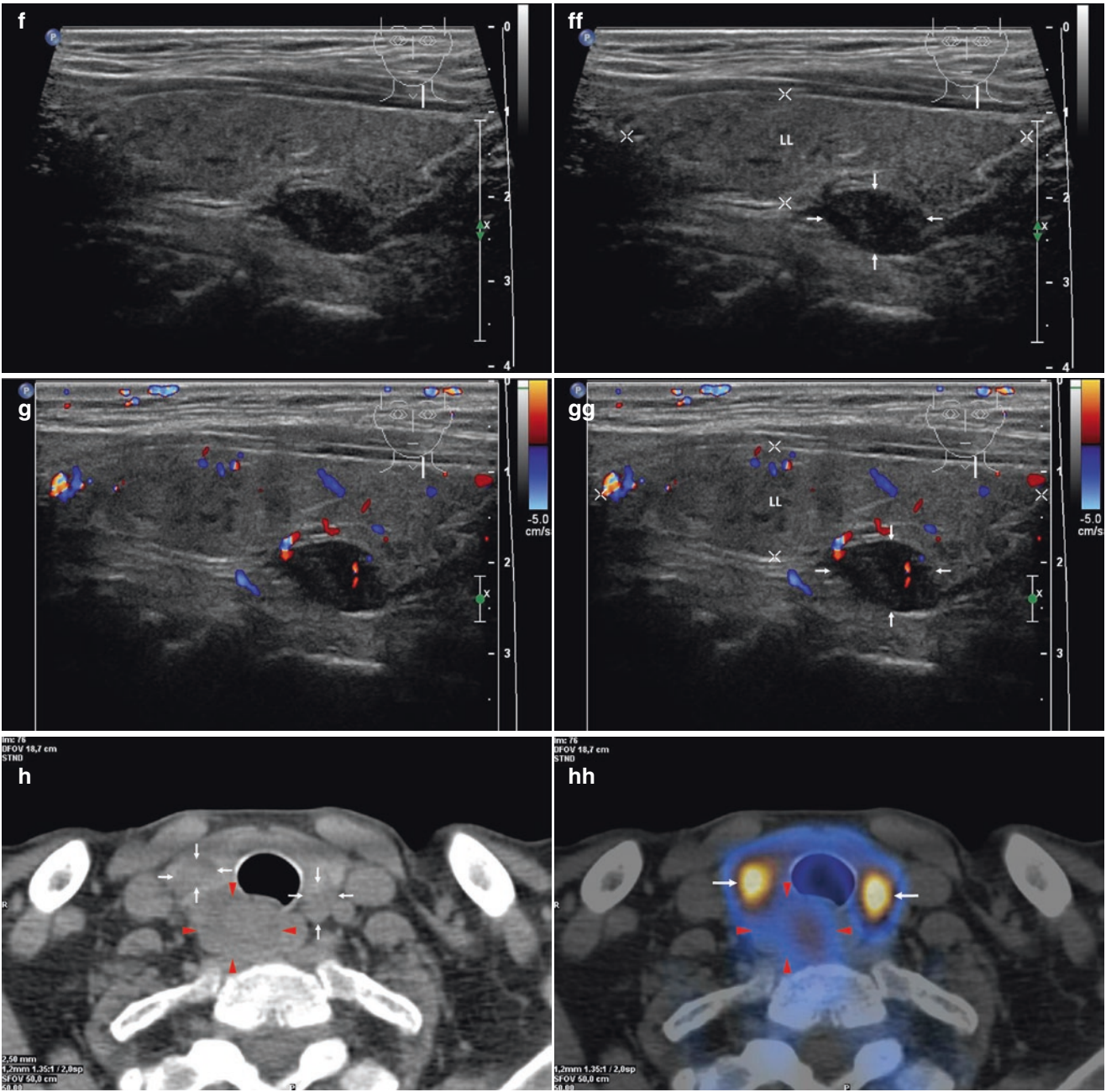


Fig. 22.17 (continued)

References

1. Fraser WD. Hyperparathyroidism. *Lancet*. 2009;374(9684):145–58.
2. Bilezikian JP, Khan AA, Potts Jr JT, Third International Workshop on the Management of Asymptomatic Primary Hyperthyroidism. Guidelines for the management of asymptomatic primary hyperparathyroidism: summary statement from the third international workshop. *J Clin Endocrinol Metab*. 2009;94(2):335–9.
3. Cordeiro AC, Montenegro FL, Kulcsar MA, Dellanegra LA, Tavares MR, Michaluart Jr P, Ferraz AR. Parathyroid carcinoma. *Am J Surg*. 1998;175(1):52–5.
4. Noda S, Onoda N, Kashiwagi S, Kawajiri H, Takashima T, Ishikawa T, et al. Strategy of operative treatment of hyperparathyroidism using US scan and (99m)Tc-MIBI SPECT/CT. *Endocr J*. 2014;61(3):225–30.
5. Akbaba G, Berker D, Isik S, Aydin Y, Ciliz D, Peksoy I, et al. A comparative study of pre-operative imaging methods in patients with primary hyperparathyroidism: ultrasonography, 99mTc sestamibi, single photon emission computed tomography, and magnetic resonance imaging. *J Endocrinol Investig*. 2012;35(4):359–64.
6. Noussios G, Anagnostis P, Natsis K. Ectopic parathyroid glands and their anatomical, clinical and surgical implications. *Exp Clin Endocrinol Diabetes*. 2012;120(10):604–10.
7. Zerizer I, Parsai A, Win Z, Al-Nahhas A. Anatomical and functional localization of ectopic parathyroid adenomas: 6-year institutional experience. *Nucl Med Commun*. 2011;32(6):496–502.
8. Phitayakorn R, McHenry CR. Incidence and location of ectopic abnormal parathyroid glands. *Am J Surg*. 2006;191(3):418–23.
9. Uludag M, Isgor A, Yetkin G, Atay M, Kebudi A, Akgun I. Supernumerary ectopic parathyroid glands. Persistent hyperparathyroidism due to mediastinal parathyroid adenoma localized by preoperative single photon emission computed tomography and intraoperative gamma probe application. *Hormones (Athens)*. 2009;8(2):144–9.
10. Ghervan C. Thyroid and parathyroid ultrasound. *Med Ultrason*. 2011;13(1):80–4.
11. Ulanovski D, Feinmesser R, Cohen M, Sulkes J, Dudkiewicz M, Shpitzer T. Preoperative evaluation of patients with parathyroid adenoma: role of high-resolution ultrasonography. *Head Neck*. 2002;24(1):1–5.
12. Hara H, Igarashi A, Yano Y, Yashiro T, Ueno E, Aiyoshi Y, et al. Ultrasonographic features of parathyroid carcinoma. *Endocr J*. 2001;48(2):213–7.
13. Nozeran S, Duquenne M, Guyetant S, Rodien P, Rohmer V, Ronceray J, et al. Diagnosis of parathyroid cysts: value of parathyroid hormone level in puncture fluid. *Presse Med*. 2000;29(17):939–41.
14. Halenka M, Frysak Z, Koranda P, Kucerova L. Cystic parathyroid adenoma within a multinodular goiter: a rare cause of primary hyperparathyroidism. *J Clin Ultrasound*. 2008;36(4):243–6.
15. Fukagawa M, Kazama JJ, Shigematsu T. Management of patients with advanced secondary hyperparathyroidism: the Japanese approach. *Nephrol Dial Transplant*. 2002;17(9):1553–7.

23.1 Method, Indications, and Complications of PEIT

- Percutaneous ethanol injection therapy (PEIT) is a minimally invasive procedure that may be performed as an alternative to surgery for the treatment of thyroid cysts, parathyroid adenoma (PAd) and, less frequently, toxic thyroid nodules [1, 2]. Most recently, PEIT of metastatic lymph nodes is gaining interest as a nonsurgical directed therapy for patients with recurrent differentiated thyroid carcinoma (PTC and FTC) [3].
- Absolute ethanol (96%) induces cellular dehydration, protein denaturation, and thrombosis in the capillary bed. This is followed by coagulation necrosis and reactive fibrosis in parathyroid adenoma or at the cyst wall, resulting in their shrinkage [4, 5].
- PEIT is suitable procedure for elderly patients with comorbidities and high surgical risk. For anxious patients or those not willing to undergone surgery PEIT may be method of choice [2, 6].
- We require FNAB before performing PEIT of large PAd (in small PAd <1 mL and in PAd with typical US features malignancy is not expected) or the thickened wall of a complex cyst, including the examination of evacuated fluid. PEIT is only performed if there is no suspicion of malignant lesion.
- The risk of overlooking thyroid malignancy, including PTC and FTC microadenomas, in those treated with minimally invasive techniques exists, but must be very small. During long-term follow-up (> 5 years), no patient operated on due to growth and/or pressure symptoms has been diagnosed with thyroid malignancy after PEIT [7].
- Complications can be caused by leakage of ethanol into the surrounding tissue [4, 5]:
 - No serious, life-threatening complications were reported in any published series of patients.
 - Mild localized pain for 24–48 h after application is typically noted.
 - Dysphonia or temporary vocal fold paresis; permanent paresis is rare; in the largest sample of 432 patients with thyroid cysts undergoing percutaneous ethanol injection therapy, temporary paresis was noted in 0.7% [8].
 - Small hematoma.
 - Periglandular fibrosis following repeated percutaneous ethanol injection therapy, complicating potential later surgery.
 - Frequency of PEIT complications is lower in thyroid cysts [5].
- PEIT is relatively effective, often offering the same results as surgery. It is safe, inexpensive, may be repeated and carried out on outpatient basis.
- PEIT is mostly performed without local anesthesia [5].
- It must be stressed that PEIT is not a routine procedure and is only performed in selected patients. It should be carried out by a specialist routinely performing FNAB of thyroid nodules and PEIT.

23.2 Ultrasound-Guided Percutaneous Ethanol Injection Therapy (US-PEIT) of Thyroid Cysts

- At US, 15–25% of solitary thyroid nodules are found to be cystic or predominantly cystic [6, 9].
- Simple aspiration of the cystic portion of the nodule can reduce pressure-related symptoms and cosmetic problems. Although aspiration can induce collapse of the cystic portion, there is a high risk of fluid recurrence 10% up to 80% [6, 10].
- Larger cystic nodules recur more frequently after aspiration than small nodules [9, 11].
- Previously, Treece et al. in 1983 or Edmonds et al. in 1987 successfully used instillation of intracystic tetracycline hydrochloride as sclerosant to treat recurrent pure thyroid cyst [12, 13].
- PEIT of thyroid cyst was first successfully performed by Croatian physician Rozman in 1989 [14].
- US-PEIT is indicated in patients with recurrent thyroid cysts with volumes ≥ 3 mL causing symptoms of compression or cosmetic complaints [6].
- For the purpose of PEIT, cyst can be divided according to US pattern, size, and liquid character obtained by FNAB [5, 6, 9, 11]:
 - Pure cysts (Fig. 23.1aa)—US scan showing a cystic component of more than 90%, anechoic content, and smooth internal wall; drained fluid is viscous, clear, or pale yellow.
 - Complex cysts (Fig. 23.2bb, dd)—US scan showing a fluid component of 60–90% of the volume, anechoic or flocculated contents, roughened wall and septa in some cysts; aspirated fluid is mostly brown with debris, or dark yellow, viscous-to-gelatinous, or hemorrhagic.
- Regarding size, cysts are mostly divided into small (3–10 mL), medium (11–40 mL), and large (> 40 mL).
- Criteria of complete therapeutic success [6]:
 - shrinkage of the cyst (near disappearance) and no recurrence of the fluid component (Figs. 23.1dd, 23.2gg).
 - or marked ($> 50\%$ of initial volume) size reduction.
- Reported success rate ranges from 68 to 100% [5, 15].
- During one application, amount of instilled ethanol is equal to 23–100% of the initial cyst volume but preferably no more than 10 mL. Based on ultrasound findings, procedure is repeated at intervals of 2 weeks to 1 month [16, 17].
- A special issue presents in viscous cysts with thick gelatinous content, which cannot be aspirated with an 18-gauge needle. These required different techniques:
 - Most commonly used is a two-stage ethanol ablation technique. During the first session, ethanol is injected into the cyst (1 mL for each 10 mL of cyst volume) to reduce density of the viscous fluid. At the second session (2–4 weeks after the first), the cystic fluid is aspirated from the nodule, and ethanol is injected [11, 18].
 - Sung et al. attempted a one-step ethanol ablation technique with thick gelatinous content aspiration through large-bore needle or a catheter connected to a suction pump following the ethanol injection [15].
 - Cystic fluid is aspirated as completely as possible and then ethanol is instilled into the cavity to a volume of 40–100% of the volume of aspirated fluid [5].
- Evaluating more than 20 years of experiences, PEIT is considered in the United States and Europe by the 2010 AACE/AME/ETA Guidelines as a standard nonsurgical, minimally invasive procedure in management of recurrent thyroid cysts [19].

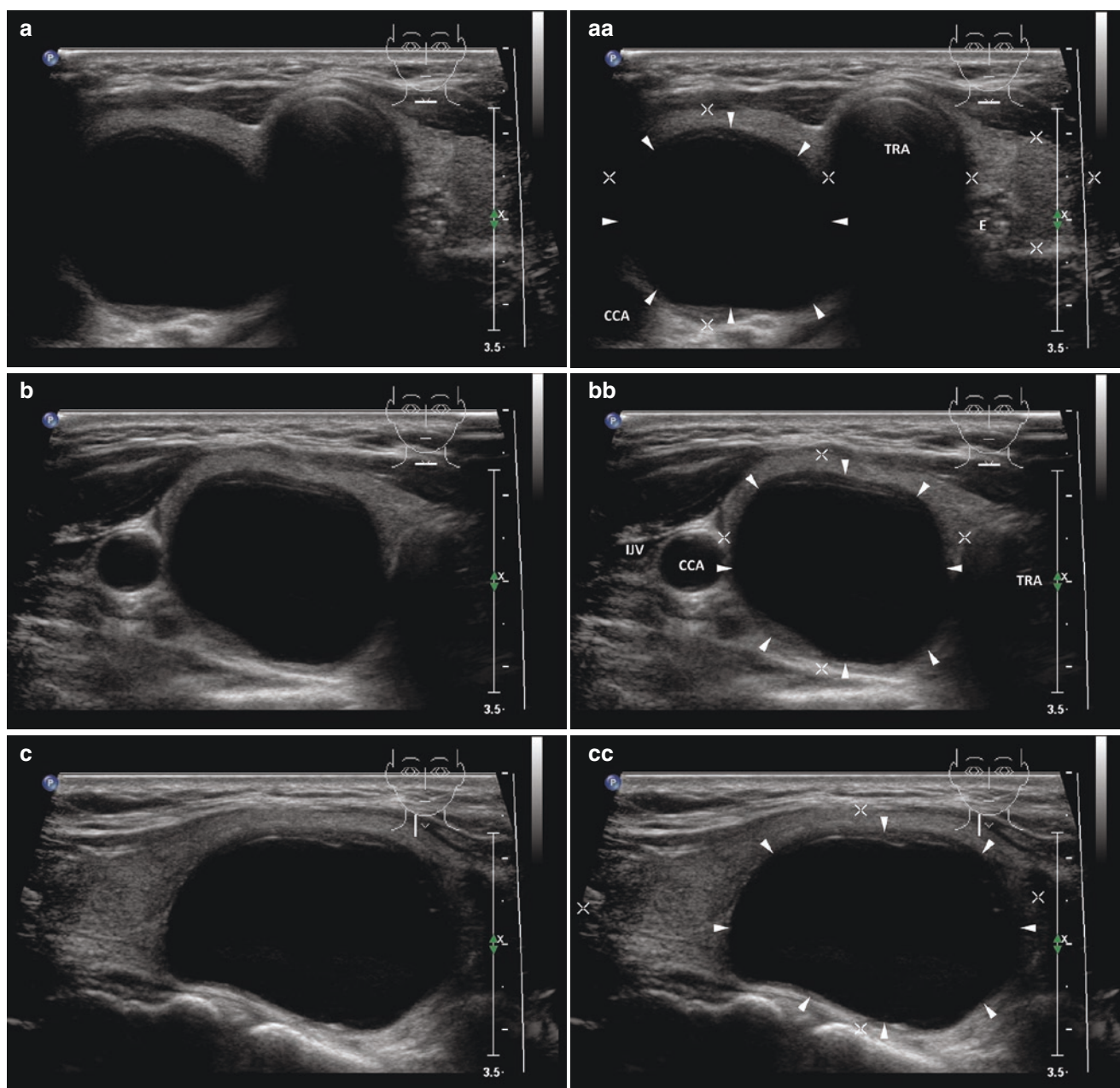


Fig. 23.1 (aa) A 59-year-old woman with a 1 month palpable resistance on the neck. Solitary pure cyst (arrowheads), size $35 \times 27 \times 22$ mm and volume 11 mL in the RL prior to PEIT: smooth wall; anechoic contents; Tvol 24 mL, RL 20 mL and LL 4 mL; transverse. (bb) Detail of pure cyst (arrowheads): smooth wall; anechoic contents; transverse. (cc) Detail of pure cyst (arrowheads): smooth wall; anechoic contents; longitudinal. (dd) Six months post PEIT—small solid nodule (arrows), size $10 \times 8 \times 6$ mm and volume 0.3 mL as

residue of cyst: inhomogeneous structure; mostly isoechoic, focally hypoechoic areas; no recurrence of the liquid component; Tvol 12 mL, RL 7 mL, and LL 5 mL; transverse. (ee) Detail of small solid residue (arrows): inhomogeneous structure; mostly isoechoic, focally hypoechoic areas; no recurrence of the liquid component; transverse. (ff) Detail of small solid residue (arrows): inhomogeneous structure; mostly isoechoic, focally hypoechoic areas; no recurrence of the liquid component; longitudinal

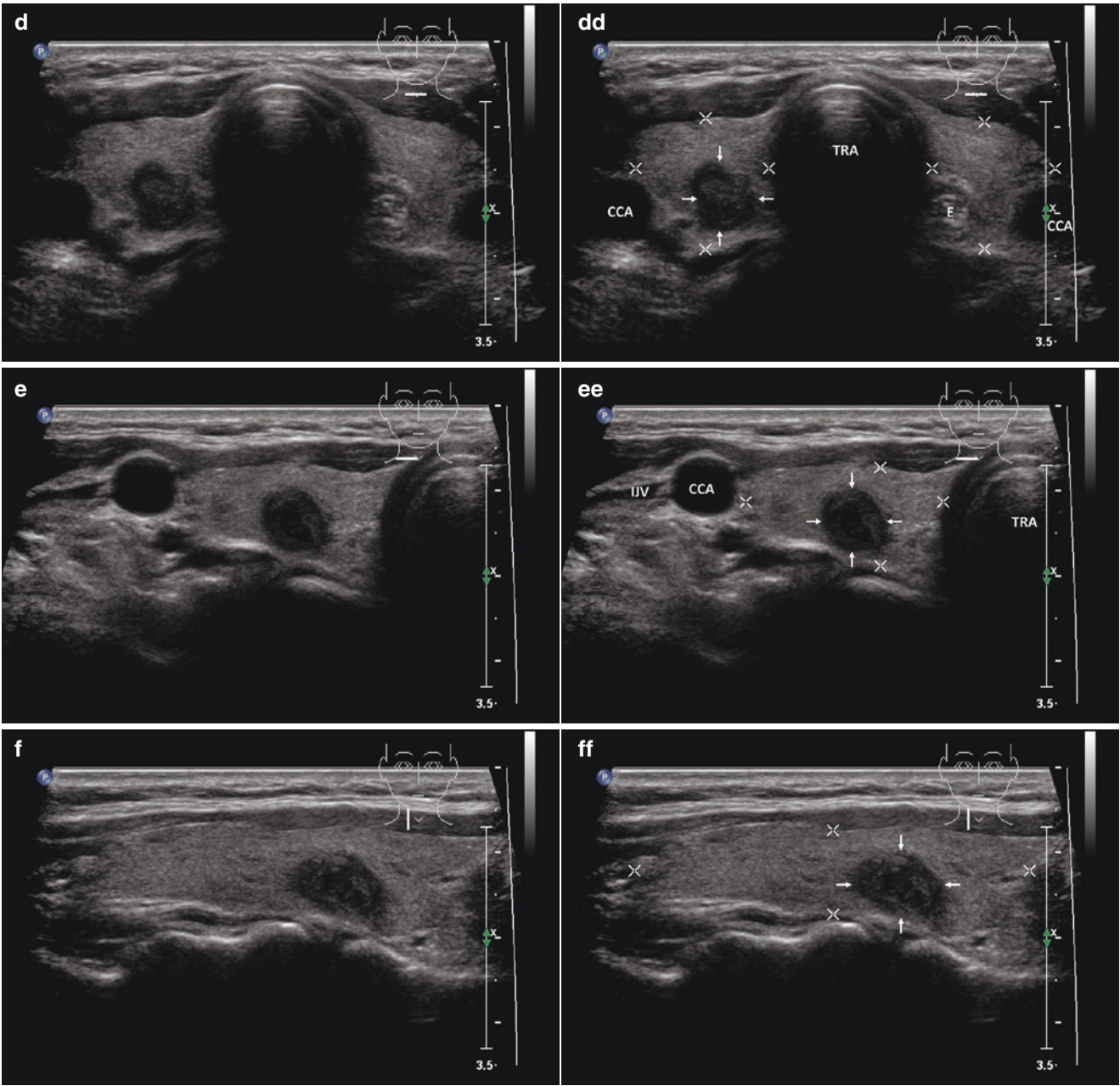


Fig. 23.1 (continued)

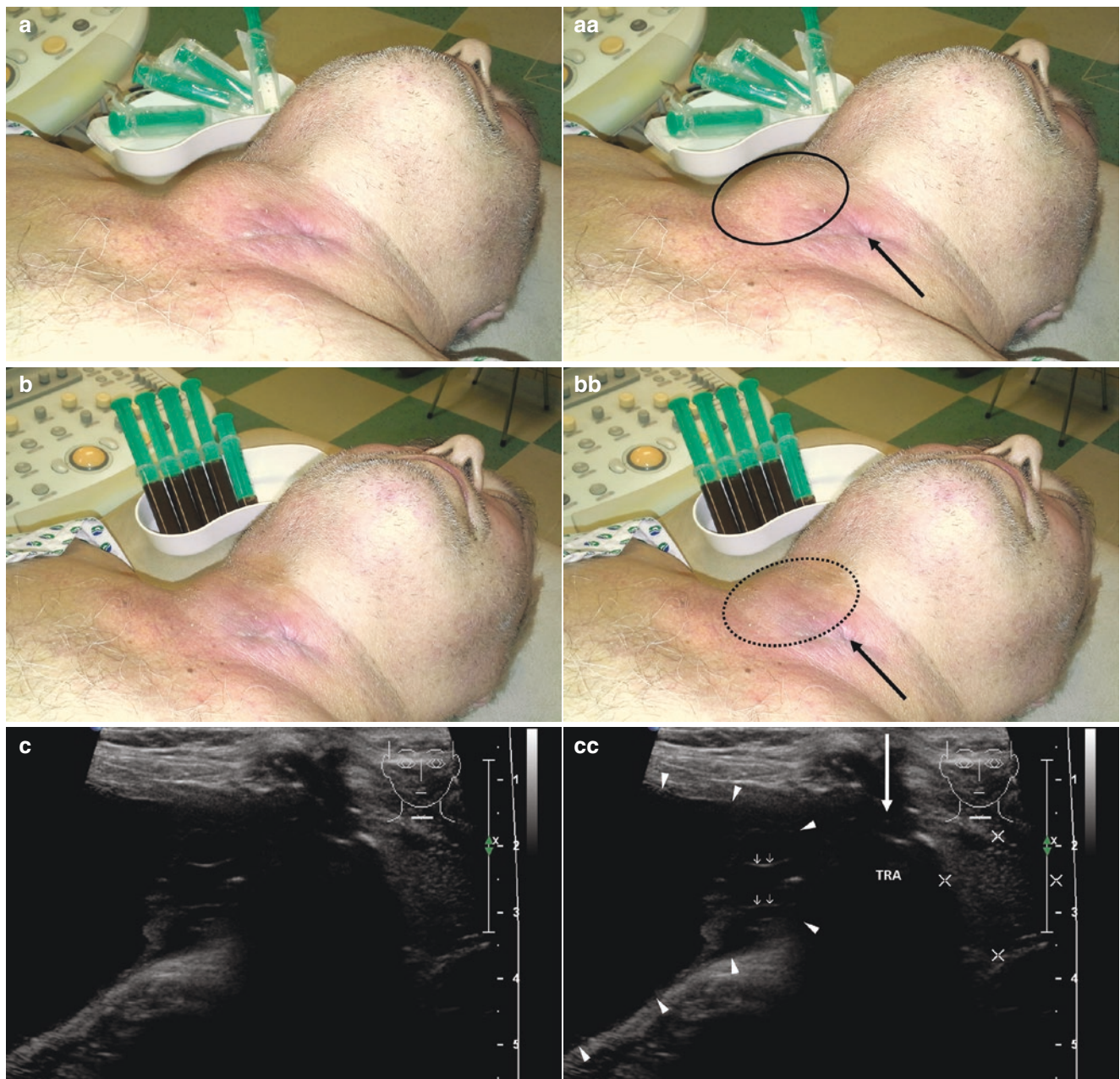


Fig. 23.2 (aa) A 63-year-old man with a 2 months progressively increasing, palpable resistance (*full black line*) on the right side of the neck. Personal history: myocardial infarction and cardiopulmonary resuscitation with tracheotomy—scar (*long black arrow*). US revealed giant complex cyst volume 102 mL in the RL. Patient is lying before evacuation with visible resistance, also visible scar post tracheotomy. (bb) Lying patient post evacuation and first PEIT, visible resistance (*dotted black line*) disappeared. Five filled 20 mL syringes with brownish content. (cc) Overall US view of giant complex cyst (*arrowheads*), occupying whole RL, size $76 \times 63 \times 41$ mm, volume 102 mL and normal sized LL: smooth wall with short thick peripheral septa (*open arrows*); anechoic content; scar after tracheotomy (*long arrows*)—interrupting continuity of the isthmus and deformed trachea with indentation of the wall; Tvol 110 mL, asymmetry—RL 102 mL and LL

8 mL; transverse. (dd) Detail of giant complex cyst (*arrowheads*): smooth wall with short thick peripheral septa (*open arrows*); anechoic contents; transverse. (ee) Detail of giant complex cyst (*arrowheads*): smooth wall without septa; anechoic contents; longitudinal. (ff) Twelve months post PEIT—small solid nodule (*arrows*), size $15 \times 11 \times 9$ mm and volume 0.3 mL as residue of cyst: solid; inhomogeneous; mostly hypoechoic; tiny bands and punctuations of fibrosis (*open arrows*); no recurrence of the liquid component; shrunken scar post tracheotomy (*long arrows*); Tvol 19 mL, RL 11 mL, and LL 8 mL; transverse. (gg) Detail of small solid residue (*arrows*): solid; inhomogeneous structure; mostly hypoechoic; thin bands and areas of fibrosis (*open arrows*); transverse. (hh) Detail of small solid residue (*arrows*): solid; inhomogeneous structure; mostly hypoechoic; thin bands and areas of fibrosis (*open arrows*); longitudinal

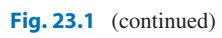


Fig. 23.1 (continued)

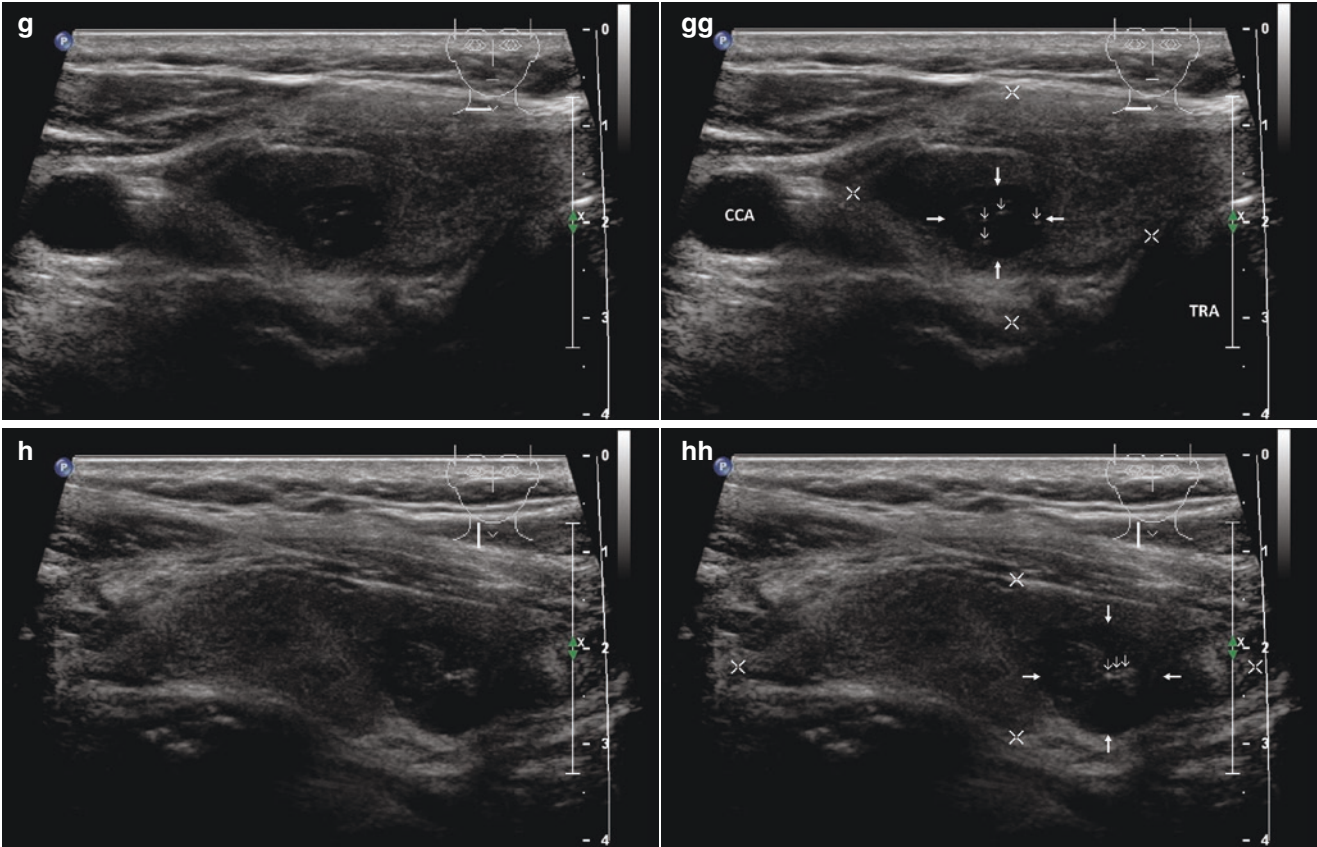


Fig. 23.2 (continued)

23.3 Ultrasound-Guided Percutaneous Ethanol Injection Therapy (US-PEIT) of the Parathyroid Gland

- Another term often used for this method is Percutaneous Alcohol Ablation of the Parathyroid gland (PAAP) [20].
- First, it should be noted that surgery is the gold standard and permanently effective therapy for patients with primary hyperparathyroidism (pHPT). Therapeutic effect of conventional exploration and minimally invasive parathyroidectomy for pHPT for both is about 97% [21].
- Surgery is indicated in all symptomatic patients with PHPT.
- In 2013, The Fourth International Workshop on the Management of Asymptomatic Primary Hyperparathyroidism published revised guidelines for asymptomatic primary hyperparathyroidism [22]:
 - Laboratory: threshold value for serum calcium, $s\text{-Ca} > 0.25 \text{ mmol/L}$ ($> 1 \text{ mg/dL}$) above the upper normal limit.
 - Skeletal guidelines: A. BMD by DXA: T-score < -2.5 at lumbar spine, total hip, femoral neck, or distal 1/3 radius; B. Vertebral fracture by X-ray, CT, MRI, or VFA (vertebral fracture assessment) utilizing DXA technology.
 - Renal guidelines: A. Creatinine clearance $< 60 \text{ cc/min}$; B. 24-h urine for calcium $> 400 \text{ mg/d}$ ($> 10 \text{ mmol/d}$) and increased stone risk by biochemical stone risk analysis; C. Presence of nephrolithiasis or nephrocalcinosis by X-ray, ultrasound, or CT.
 - Age < 50 years.
- For secondary and primary hyperparathyroidism, US-PEIT was firstly successfully performed by Solbiati in 1985 and by Müller-Gärtner in 1987 [23, 24].
- Danish physician Karstrup was the first to investigate this procedure on a larger scale. In 1989 he treated 20 patients with pHPT with a success rate of 44% [25]. Then in 1993 two sets, the first of 18 patients with a success rate of 56%, and second of 14 patients with a success rate of 79%. The difference between the sets of patients was the interval between applications: 1 month vs. 1 week [4].
- Complete therapeutic success:
 - achievement of normal serum calcium and parathormone concentration.
 - reduced volume of PAd and no vascularity on CFDS (Fig. 23.3dd, ee).
 - negative ^{99m}Tc -MIBI scintigraphy at the end of follow-up period (Fig. 23.3gg).
- Reported success rate has ranged from 33 to 89% [20, 26].
- During one application, the amount of instilled ethanol is equal to 50–85% of the parathyroid adenoma volume [4, 20, 26].
- There is no strict time schedule for individual PEIT procedures and intervals between check-ups following ethanol application. For example, the reported intervals as follows: 24 h by Harman [20], 2 weeks by Stratigis [26], 1 week and 1 month by Karstrup [4].
- Effect of the PEIT procedure on the calcium level might not be persistent. Both pHPT and sHPT may recur due to either revival of sclerotized PAd, development of new PAd, or due to diffuse hyperplasia of all four parathyroid glands [20].
- US-PEIT may be used as a nonsurgical alternative in selected cases, especially elderly patients with comorbidities who are ineligible for surgery. It may be beneficial in patients with previous thyroidectomy or unsuccessful parathyroidectomy in whom another surgery in that area would increase the risk of complications (Fig. 23.4aa, ee, ii) [20, 26].
- In Japan, PEIT is a standard therapy of secondary hyperparathyroidism in patients with end stage kidney disease requiring dialysis to treat dominant parathyroid adenoma resistant to therapy (Fig. 23.5aa, ee, hh). The first guidelines, originally published in 2000 in Japan by the Japanese Working Group of PEIT of the Parathyroid, were novelized in 2003 as “Guidelines for Percutaneous Ethanol Injection Therapy (PEIT) of the Parathyroid Glands in Chronic Dialysis Patients.” Indications for PEIT [27]:
 - Parathyroid hormone (PTH) concentration $\geq 400 \text{ pg/mL}$.
 - Verification of osteitis fibrosa or high-turnover bone using X-ray images and bone metabolism markers.
 - Enlarged parathyroid glands detectable by US.
 - Patients resistant to medical therapy.

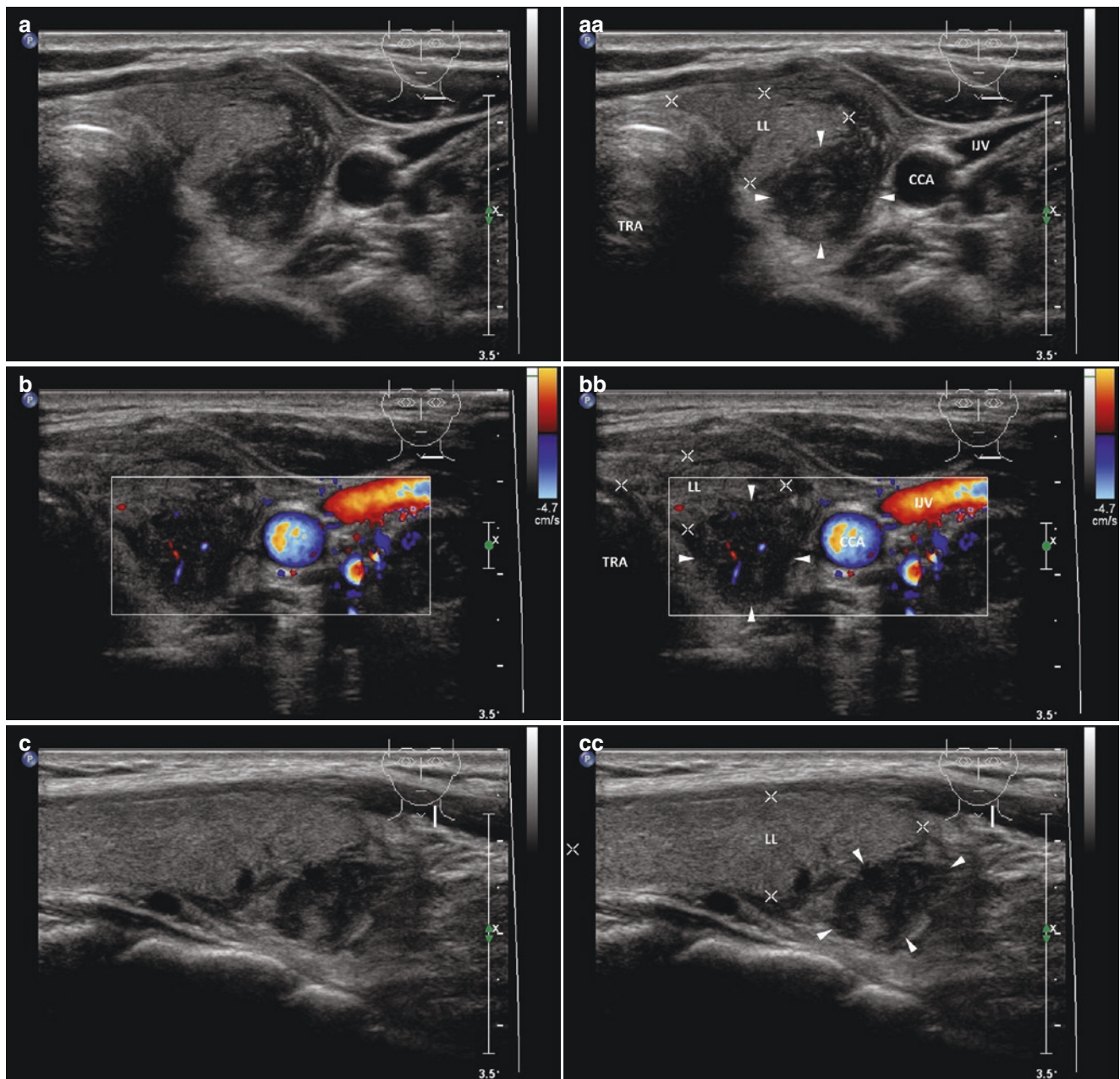


Fig. 23.3 (aa) A 49-year-old woman with asymptomatic pHPT, laboratory: mild hypercalcemia, s-Ca 2.71 mmol/L (normal: 2.15–2.55), moderately elevated level of parathyroid hormone, s-PTH 170 ng/L (normal: 12–65). Personal history: healthy anxious patient refusing surgery; PEIT as method of patient's choice. Left inferior parathyroid adenoma (PAd), size 15 × 12 × 9 mm and volume 1 mL, confirmed by ^{99m}Tc -MIBI scintigraphy. US scans prior to PEIT, PAd (arrowheads) located behind the lower pole of the LL: solid; oval shape; inhomogeneous structure; slightly hypoechoic; transverse. (bb) Detail of left inferior PAd (arrowheads), CFDS: sporadic central vascularity; transverse. (cc) Detail of left inferior PAd (arrowheads) located behind the lower pole of the LL: solid; oval shape; inhomogeneous structure; slightly hypoechoic; longitudinal. (dd) Three months post PEIT, laboratory: normal levels of

s-Ca 2.29 mmol/L and s-PTH 47 ng/L. US shows shrunken left inferior PAd (arrows), size 7 × 4 × 3 mm and volume 0.1 mL: lentil-like shape; inhomogeneous structure; mixed echogenicity; tiny bands and punctuations of fibrosis; transverse. (ee) Detail of shrunken left inferior PAd (arrows), CFDS: without vascularity; transverse. (ff) Detail of shrunken left inferior PAd (arrows): elliptical shape; inhomogeneous structure; mixed echogenicity; tiny bands and punctuations of fibrosis; longitudinal. (g) ^{99m}Tc -MIBI scintigraphy prior to PEIT: radioisotope uptake in PAd (thick arrow) in the left jugular region. (Figure courtesy of Pavel Koranda, MD, PhD) (gg) ^{99m}Tc -MIBI scintigraphy 12 months post PEIT: without uptake of the radioisotope (blank thick arrow). (Figure courtesy of Pavel Koranda, MD, PhD)

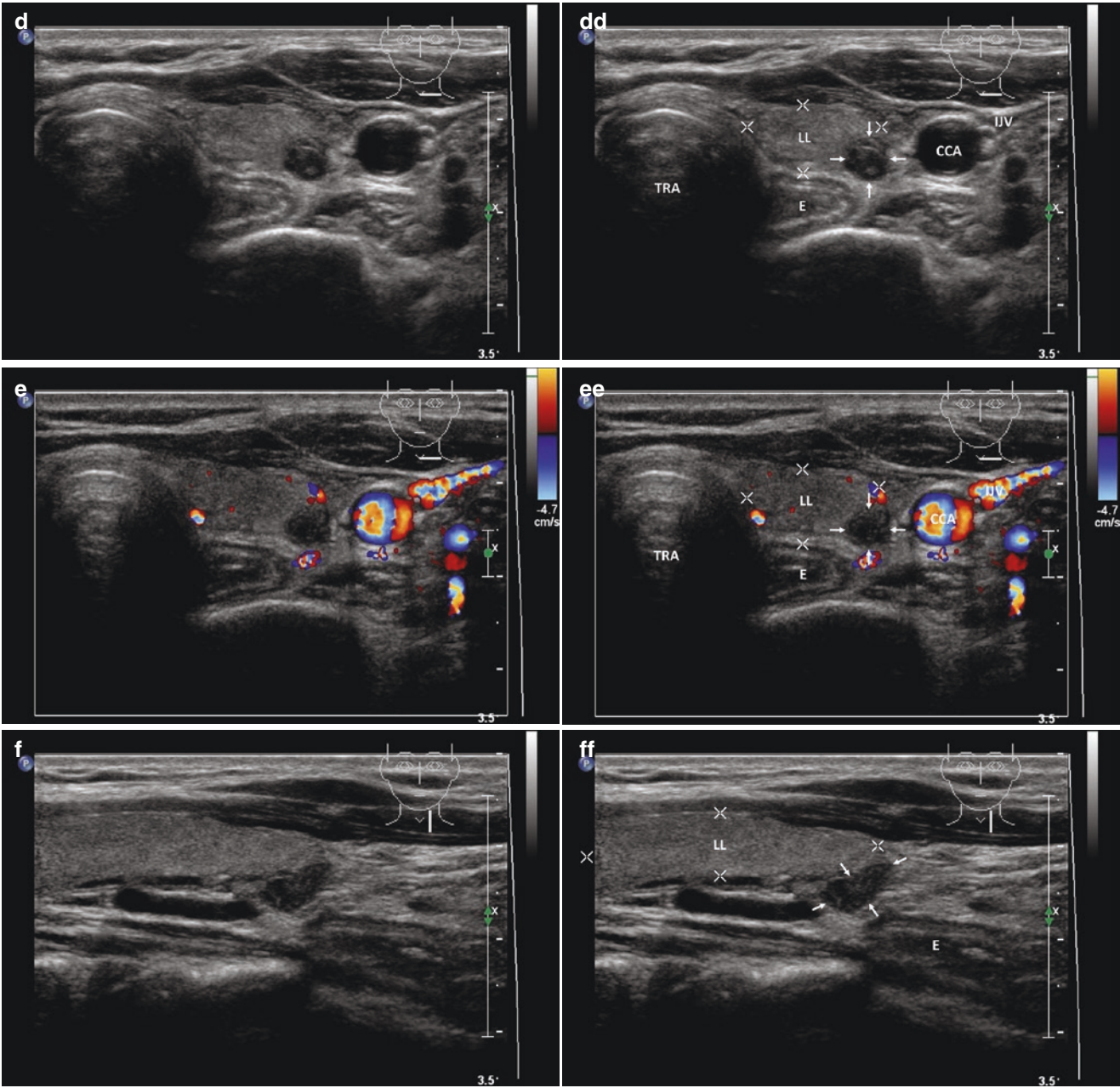


Fig. 23.3 (continued)

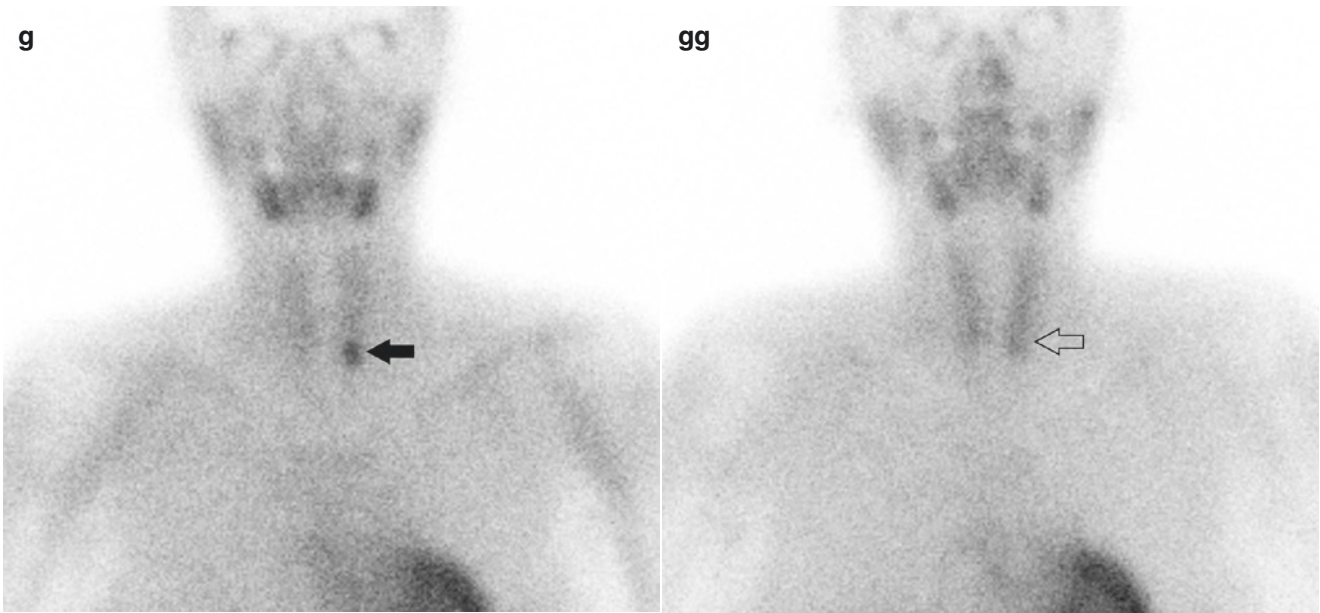


Fig. 23.3 (continued)

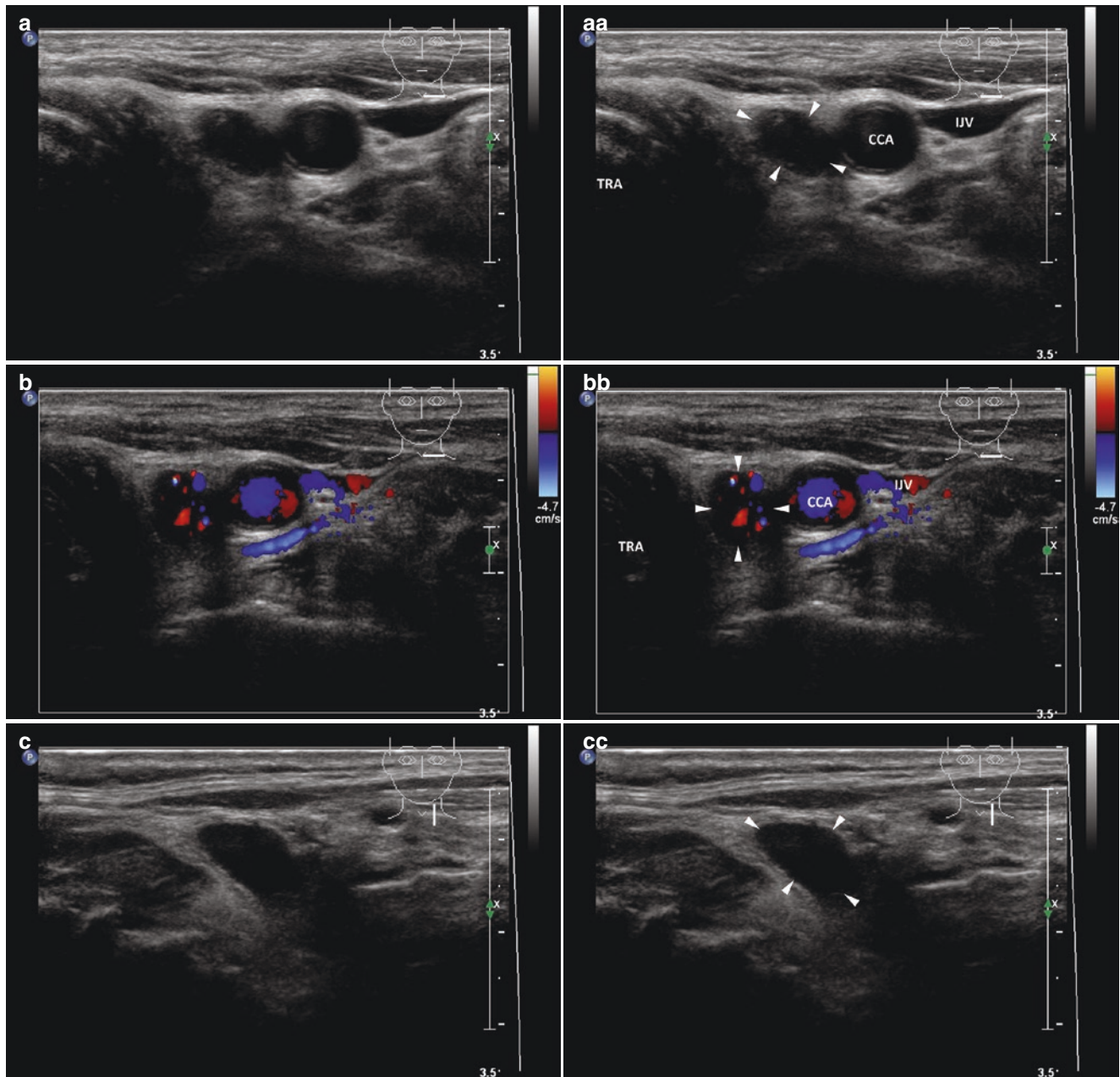


Fig. 23.4 (aa) A 92-year-old man with asymptomatic pHPT, laboratory: mild hypercalcemia, s-Ca 2.72 mmol/L (normal: 2.15–2.55), moderately elevated level of parathyroid hormone, s-PTH 112 ng/L (normal: 12–65). Personal history: coronary heart disease with paroxysmal atrial fibrillation, hypertension, 3 years post total thyroidectomy for papillary thyroid carcinoma. Lesion in the left thyroid bed—left parathyroid adenoma (PAD), size 14 × 12 × 7 mm and volume 0.6 mL; confirmed by ^{99m}Tc -MIBI scintigraphy. US scans prior to PEIT, PAD (arrowheads) located in left thyroid bed: bean-like shape; homogeneous structure; hypoechoic; transverse. (bb) Detail of left PAD (arrowheads), CFDS: diffusely increased vascularity; transverse. (cc) Detail of left PAD (arrowheads): bean-like shape; longitudinal. (dd) Detail of left PAD (arrowheads), CFDS: diffusely increased vascu-

larity; longitudinal. (ee) Twelve months post PEIT, laboratory: normal levels of s-Ca 2.22 mmol/L and s-PTH 62 ng/L. Tiny shrunken left PAD (arrows), size 7 × 6 × 3 mm and volume 0.1 mL: lentil-like shape; inhomogeneous; mixed echogenicity; tiny bands and punctuations of fibrosis; transverse. (ff) Detail of shrunken left PAD (arrows), CFDS: without vascularity; transverse. (gg) Detail of shrunken left PAD (arrows): lentil-like shape; longitudinal. (hh) Detail of shrunken left PAD (arrows), CFDS: without vascularity; transverse; longitudinal. (i) ^{99m}Tc -MIBI scintigraphy prior to PEIT: radioisotope uptake in PAD (thick arrow) in the left jugular region. (Figure courtesy of Pavel Koranda, MD, PhD) (ii) ^{99m}Tc -MIBI scintigraphy 12 months post PEIT: without uptake of the radioisotope (blank thick arrow). (Figure courtesy of Pavel Koranda, MD, PhD)

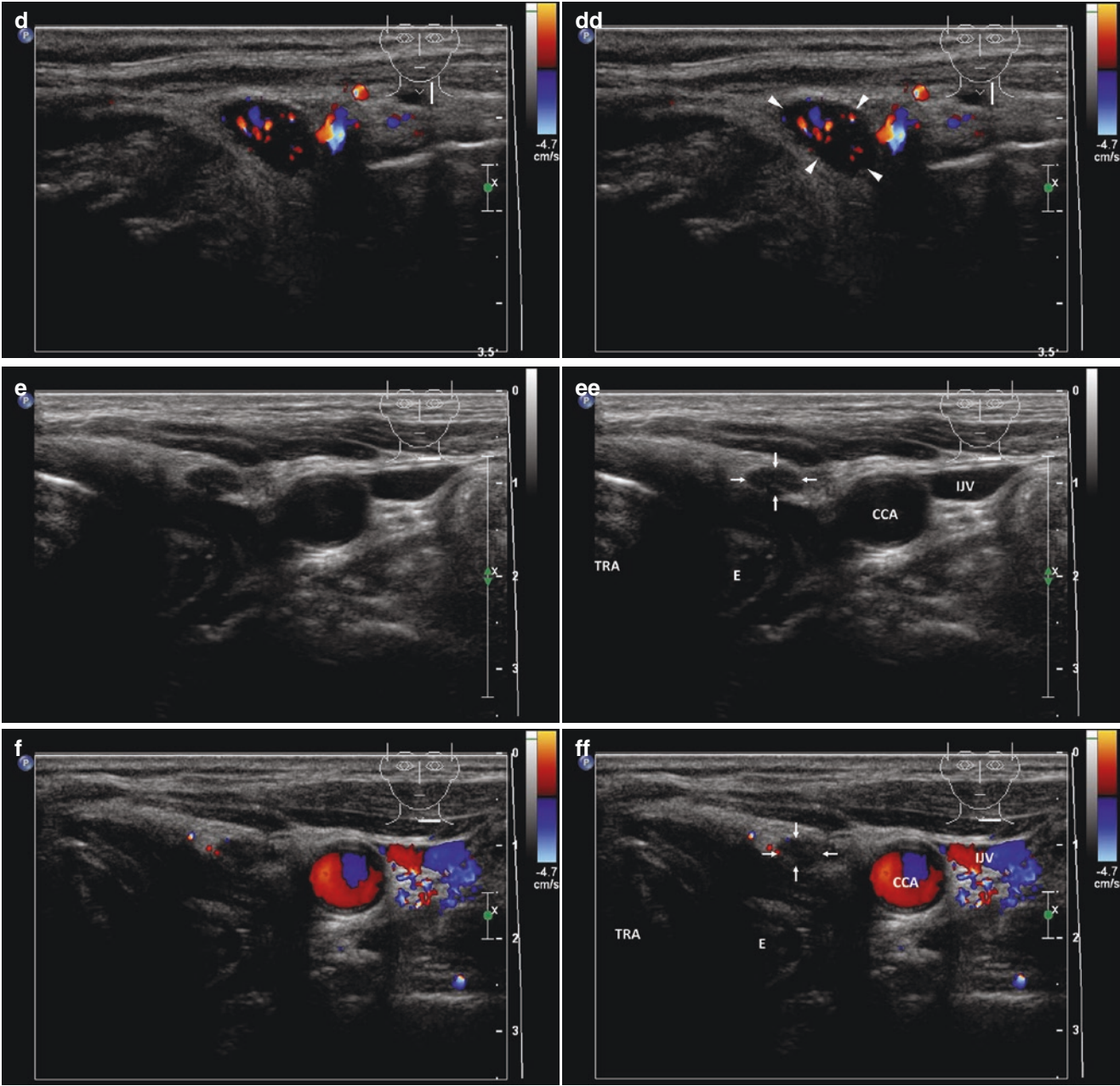


Fig. 23.4 (continued)

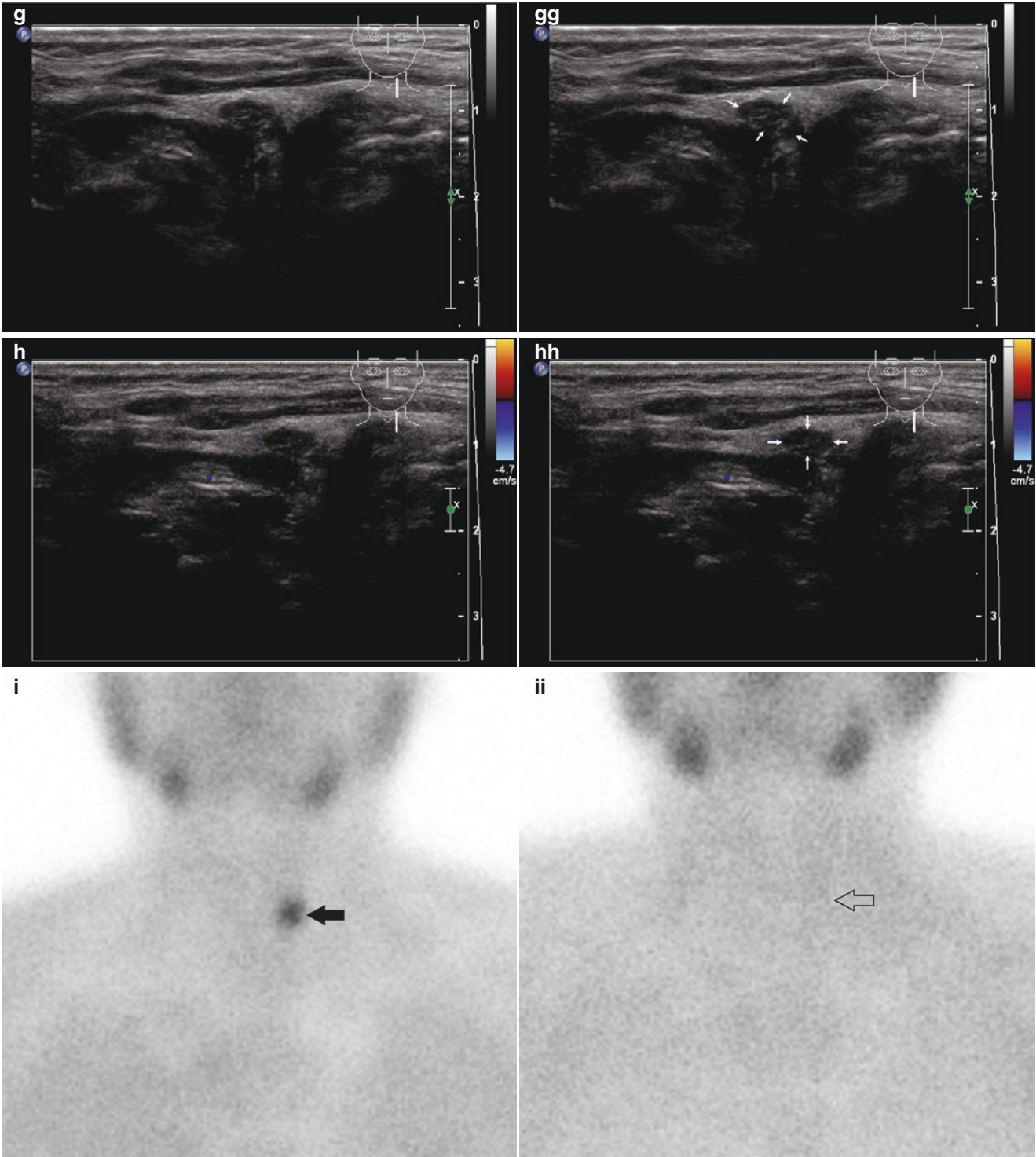


Fig. 23.4 (continued)

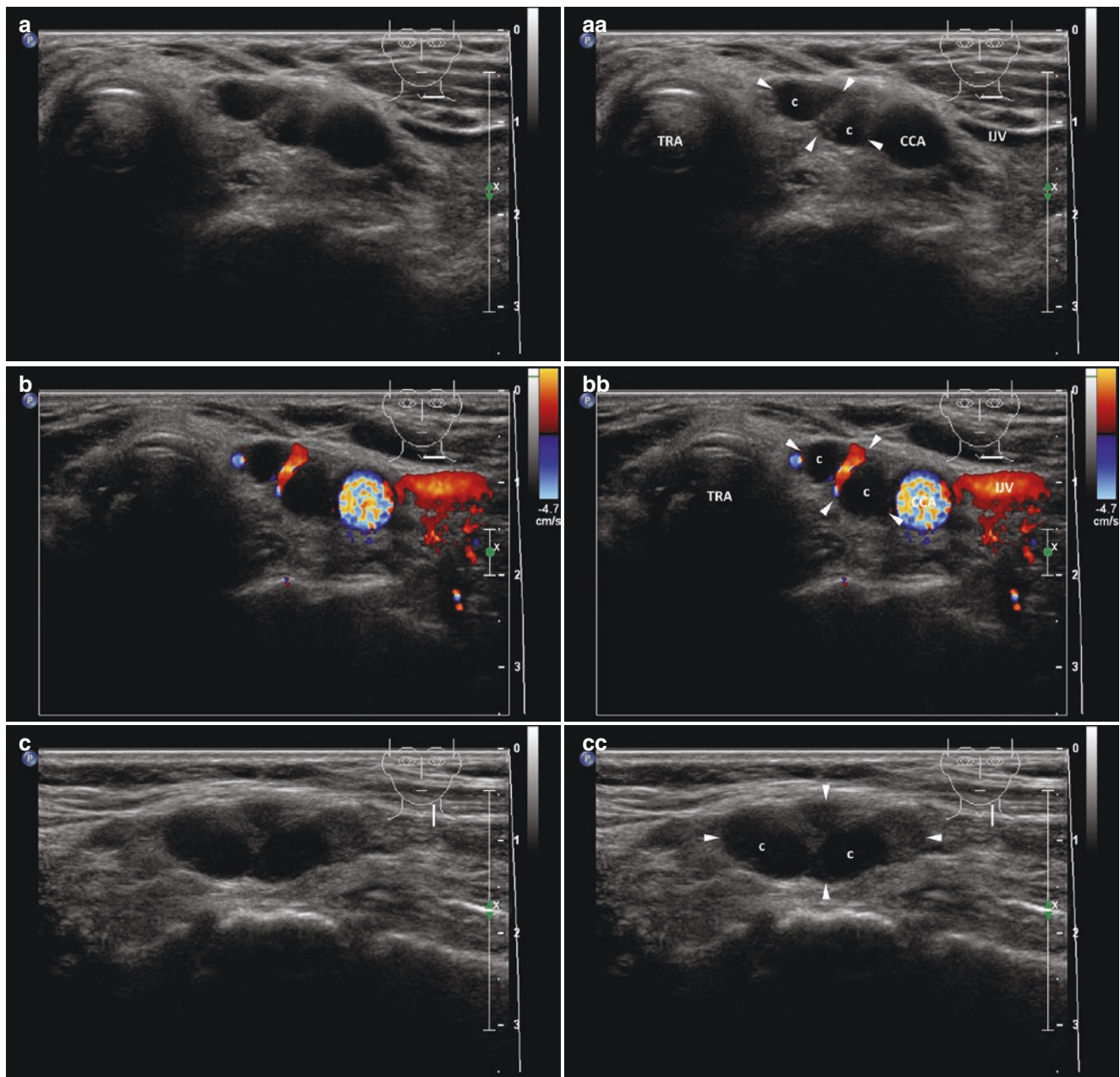


Fig. 23.5 (aa) A 61-year-old woman, end stage kidney disease on renal replacement treatment with sHPT, laboratory: mild hypercalcemia, s-Ca 2.63 mmol/L (normal: 2.15–2.55), high level of parathyroid hormone, s-PTH 314 ng/L (normal: 12–65), urea 19.8 mmol/L, creatinine 192 μ mol/L. Personal history: diabetes mellitus type 2, coronary artery heart disease with paroxysmal atrial fibrillation, 30 years post subtotal thyroidectomy for benign multinodular goiter, 16 years post total thyroidectomy of remnants and 5 years post parathyroidectomy on the right side. New lesion in the left thyroid bed—left parathyroid adenoma (PAD) with degenerative changes, size 24 \times 12 \times 7 mm and volume 1 mL; confirmed by 99m Tc-MIBI scintigraphy. US scan prior to PEIT, PAD (arrowheads) located in left thyroid bed: bean-like shape; inhomogeneous structure; two cystic cavities (c) and thick hyperechoic septum in the middle part; transverse. (bb) Detail of left PAD (arrowheads), CFDS: hilar vascularity and vessel in septum; transverse. (cc) Detail of left PAD (arrowheads): two cystic cavities (c) and thick hyperechoic septum in the middle part; longitudinal.

(dd) Detail of left PAD (arrowheads), CFDS: hilar vascularity and vessel in septum, minimal on periphery; longitudinal. (ee) Twelve months post PEIT, laboratory: normal level s-Ca 2.15 mmol/L (normal: 2.15–2.55), moderate elevated level s-PTH 121 ng/L (normal: 12–65), urea 19.5 mmol/L, creatinine 195 μ mol/L. Tiny shrunken left PAD (arrows), size 8 \times 6 \times 3 mm and volume 0.1 mL: lentil-like shape; inhomogeneous structure; mixed echogenicity; tiny bands and punctuations of fibrosis; transverse. (ff) Detail of shrunken left PAD (arrows), CFDS: without vascularity; transverse. (gg) Detail of shrunken left PAD (arrows): lentil-like shape; inhomogeneous structure; mixed echogenicity; tiny bands and punctuations of fibrosis; longitudinal. (h) 99m Tc-MIBI scintigraphy prior to PEIT: radioisotope uptake in PAD (thick arrow) in the left jugular region. (Figure courtesy of Pavel Koranda, MD, PhD) (hh) 99m Tc-MIBI scintigraphy 12 months post PEIT: without uptake of the radioisotope (blank thick arrow). (Figure courtesy of Pavel Koranda, MD, PhD)

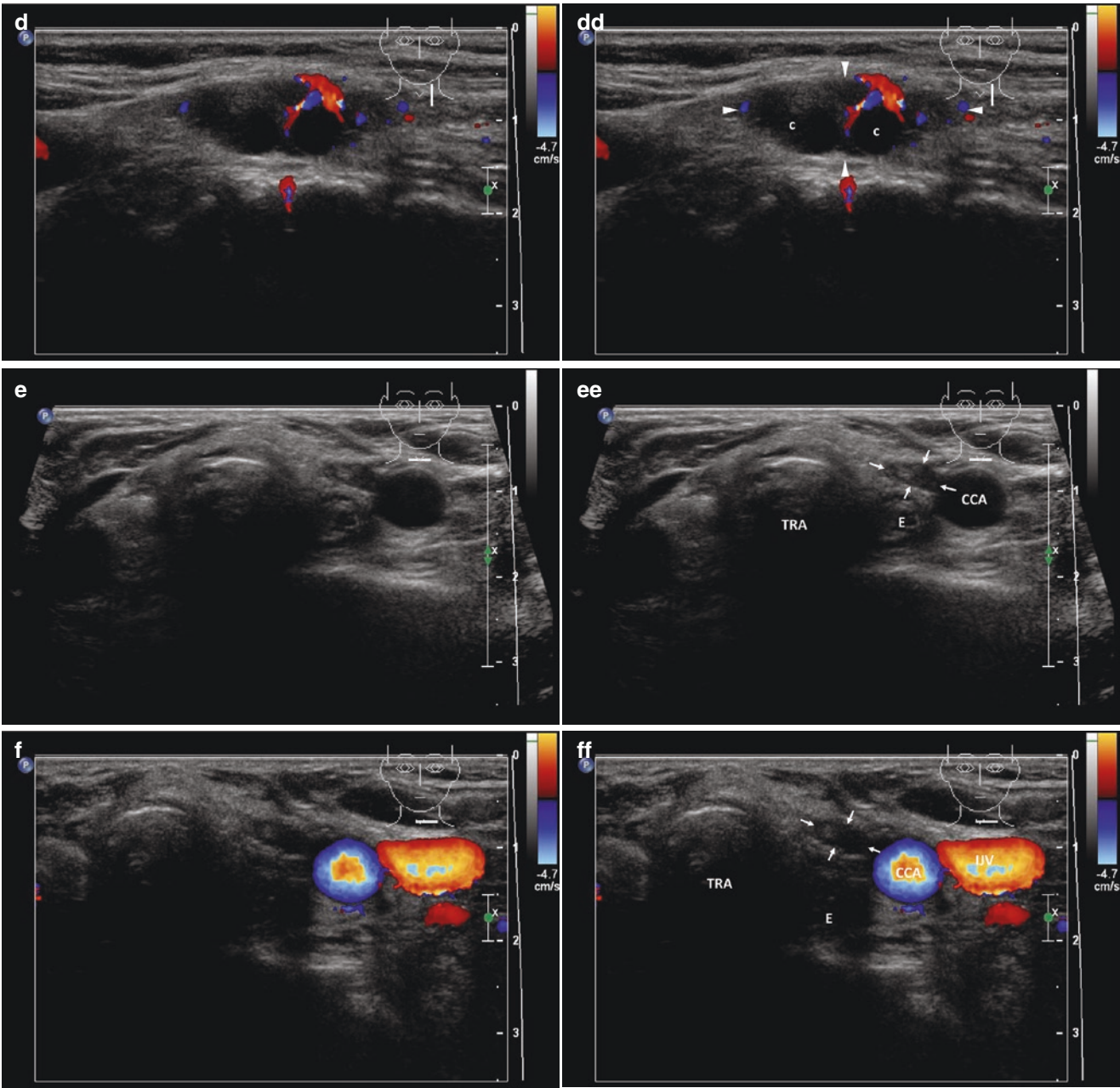


Fig.23.5 (continued)

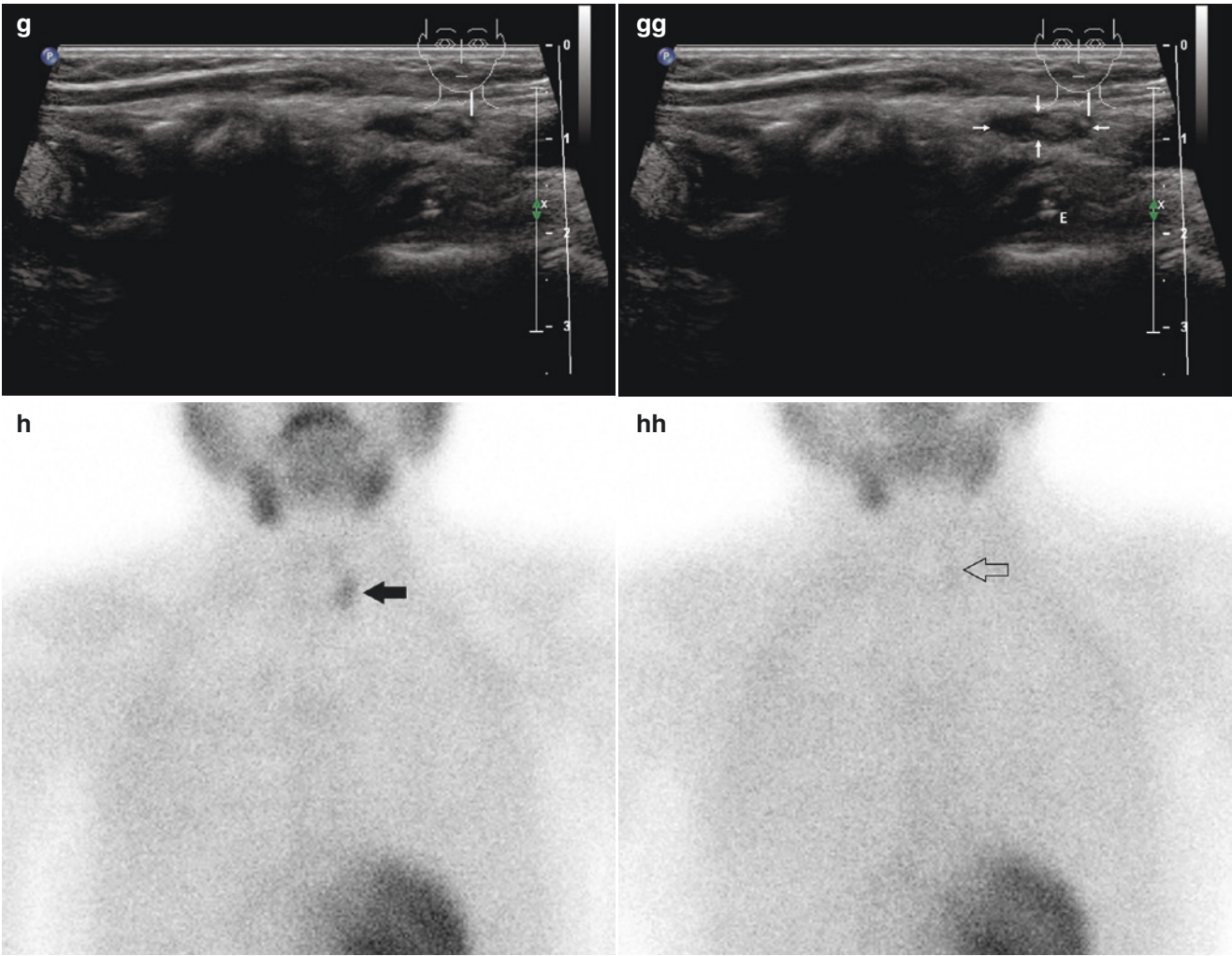


Fig.23.5 (continued)

References

1. Bennedbaek FN, Karstrup S, Hegedüs L. Percutaneous ethanol injection therapy in the treatment of thyroid and parathyroid diseases. *Eur J Endocrinol*. 1997;136(3):240–50.
2. Kim JH, Lee HK, Lee JH, Ahn IM, Choi CG. Efficacy of sonographically guided percutaneous ethanol injection for treatment of thyroid cysts versus solid thyroid nodules. *AJR Am J Roentgenol*. 2003;180(6):1723–6.
3. Haugen BR, Alexander EK, Bible KC, Doherty GM, Mandel SJ, Nikiforov YE, et al. 2015 American Thyroid Association management guidelines for adult patients with thyroid nodules and differentiated thyroid cancer: the American Thyroid Association guidelines task force on thyroid nodules and differentiated thyroid cancer. *Thyroid*. 2016;26(1):1–133.
4. Karstrup S, Hegedüs L, Holm HH. Acute change in parathyroid function in primary hyperparathyroidism following ultrasonically guided ethanol injection into solitary parathyroid adenomas. *Acta Endocrinol*. 1993;129(5):377–80.
5. Cho YS, Lee HK, Ahn IM, Lim SM, Kim DH, Choi CG, et al. Sonographically guided ethanol sclerotherapy for benign thyroid cysts: results in 22 patients. *AJR Am J Roentgenol*. 2000;174(1):213–6.
6. Bennedbaek FN, Hegedüs L. Treatment of recurrent thyroid cysts with ethanol: a randomized double-blind controlled trial. *J Clin Endocrinol Metab*. 2003;88(12):5773–7.
7. Gharib H, Hegedüs L, Pacella CM, Baek JH, Papini E. Clinical review: nonsurgical, image-guided, minimally invasive therapy for thyroid nodules. *J Clin Endocrinol Metab*. 2013;98(10):3949–57.
8. Lee SJ, Ahn IM. Effectiveness of percutaneous ethanol injection therapy in benign nodular and cystic thyroid diseases: long-term follow-up experience. *Endocr J*. 2005;52(4):455–62.
9. Del Prete S, Caraglia M, Russo D, Vitale G, Giuberti G, Marra M, et al. Percutaneous ethanol injection efficacy in the treatment of large symptomatic thyroid cystic nodules: ten-year follow-up of a large series. *Thyroid*. 2002;12(9):815–21.
10. Yasuda K, Ozaki O, Sugino K, Yamashita T, Toshima K, Ito K, et al. Treatment of cystic lesions of the thyroid by ethanol instillation. *World J Surg*. 1992;16(5):958–61.
11. Zingrillo M, Torlontano M, Ghiggi MR, D'Aloiso L, Nirchio V, Bisceglia M, et al. Percutaneous ethanol injection of large thyroid cystic nodules. *Thyroid*. 1996;6(5):403–8.
12. Treece GL, Georgitis WJ, Hofeldt FD. Resolution of recurrent thyroid cysts with tetracycline instillation. *Arch Intern Med*. 1983;143(12):2285–7.
13. Edmonds CJ, Tellez M. Treatment of thyroid cysts by aspiration and injection of sclerosant. *Br Med J (Clin Res Ed)*. 1987;295(6597):529.
14. Rozman B, Bence-Zigman Z, Tomic-Brzac H, Skreb F, Pavlinovic Z, Simonovic I. Sclerosation of thyroid cysts by ethanol. *Period Biol*. 1989;91:1116–8.
15. Sung JY, Baek JH, Kim YS, Jeong HJ, Kwak MS, Lee D, et al. One-step ethanol ablation of viscous cystic thyroid nodules. *AJR Am J Roentgenol*. 2008;191(6):1730–3.
16. Kim DW, Rho MH, Kim HJ, Kwon JS, Sung YS, Lee SW. Percutaneous ethanol injection for benign cystic thyroid nodules: is aspiration of ethanol-mixed fluid advantageous? *AJNR Am J Neuroradiol*. 2005;26(8):2122–7.
17. Halenka M, Karasek D, Frysak Z. Ultrasound-guided percutaneous ethanol injection of small and medium-sized thyroid cysts with relatively small amounts of ethanol. *Biomed Pap Med Fac Univ Palacky Olomouc Czech Repub*. 2015;159(3):417–21.
18. Zieleznik W, Kawczyk-Krupka A, Barlik MP, Cebula W, Sieroń A. Modified percutaneous ethanol injection in the treatment of viscous cystic thyroid nodules. *Thyroid*. 2005;15(7):683–6.
19. Gharib H, Papini E, Paschke R, Duick DS, Valcavi R, Hegedüs L, AACE/AME/ETA Task Force on Thyroid Nodules, et al. American association of clinical endocrinologists, associazione medici endocrinologi, and europeanthyroid association medical guidelines for clinical practice for the diagnosis and management of thyroid nodules. *Endocr Pract*. 2010;16(Suppl 1):1–43.
20. Harman CR, Grant CS, Hay ID, Hurley DL, van Heerden JA, Thompson GB, et al. Indications, technique, and efficacy of alcohol injection of enlarged parathyroid glands in patients with primary hyperparathyroidism. *Surgery*. 1998;124(6):1011–9. discussion 1019–20.
21. Grant CS, Thompson G, Farley D, van Heerden J. Primary hyperparathyroidism surgical management since the introduction of minimally invasive parathyroidectomy: Mayo Clinic experience. *Arch Surg*. 2005;140(5):472–8. discussion 478–9.
22. Bilezikian JP, Brandi ML, Eastell R, Silverberg SJ, Udelman R, Marcocci C, et al. Guidelines for the management of asymptomatic primary hyperparathyroidism: summary statement from the fourth international workshop. *J Clin Endocrinol Metab*. 2014;99(10):3561–9.
23. Solbiati L, Giangrande A, De Pra L, Bellotti E, Cantù P, Ravetto C. Percutaneous ethanol injection of parathyroid tumors under US guidance: treatment for secondary hyperparathyroidism. *Radiology*. 1985;155(3):607–10.
24. Müller-Gärtner HW, Beil FU, Schneider C, Ringe JD, Greten H. Percutaneous transthyroidal instillation treatment of parathyroid adenoma with ethanol in primary hyperparathyroidism. *Dtsch Med Wochenschr*. 1987;112(38):1459–61.
25. Karstrup S, Transbøl I, Holm HH, Glenthøj A, Hegedüs L. Ultrasound-guided chemical parathyroidectomy in patients with primary hyperparathyroidism: a prospective study. *Br J Radiol*. 1989;62(744):1037–42.
26. Stratigis S, Stylianou K, Mamalaki E, Perakis K, Vardaki E, Tzenakis N, et al. Percutaneous ethanol injection therapy: a surgery-sparing treatment for primary hyperparathyroidism. *Clin Endocrinol*. 2008;69(4):542–8.
27. Fukagawa M, Kitaoka M, Tominaga Y, Akizawa T, Kakuta T, Onoda N, Japanese Society for Parathyroid Intervention, et al. Guidelines for percutaneous ethanol injection therapy of the parathyroid glands in chronic dialysis patients. *Nephrol Dial Transplant*. 2003;18(Suppl 3):iii31–3.

24.1 Essential Facts

- Diagnosis of thyroid nodules by needle biopsy was first described by Martin and Ellis in 1930; they used an 18-gauge-needle aspiration technique. Scandinavian investigators introduced “*small-needle*” aspiration biopsy of the thyroid in the 1960s, and this technique came into widespread use in North America in the 1980s [1, 2].
- The diagnostic accuracy of US-guided FNAB (Fig. 24.1) vs. “*free-hand*” FNAB is 88% resp. 76% [3].
- Nondiagnostic results are inconclusive; further evaluation by repeated FNAB, ultrasound-guided biopsy, or radionuclide scanning is necessary.
- Suspicious cytologic results are also inconclusive and are associated with a 20% chance of malignant involvement; surgical treatment is necessary for clarification.
- FNAB is a safe, inexpensive, minimally invasive, highly accurate, and cost-effective means in the diagnosis of nodular thyroid disease.
- The procedure has a central role in the management of thyroid nodules and should be used as the initial diagnostic test.
- The introduction of FNAB had a substantial effect on the management of patients with thyroid nodules. The percentage of patients undergoing thyroidectomy decreased by 25%, and the yield of carcinoma in patients who undergo surgery increased from 15% to at least 30%. FNAB decreased the cost of care by 25% [5].

24.2 Importance and Benefits of FNAB in the Diagnosis of Nodular Thyroid Disease in the Beginning of the 1990s by Gharib [4]

- Efficacy of Fine-Needle Aspiration Biopsy (FNAB) and its role in the management of a nodular goiter was clearly established. Accuracy of cytologic diagnosis approached 95%.
- FNAB is a reasonable approach for thyroid nodules; its costs have decreased substantially because it facilitates selection of patients needing to undergo surgical excision.
- Selecting patients for operation on the basis of results of FNAB has more than doubled the yield of carcinoma.
- Limitations of cytologic examination, nondiagnostic results, and cellular follicular neoplasms should be remembered but need not negate continued use of FNAB.
- Negative (benign) and positive (malignant) cytologic results are conclusive; careful clinical follow-up of benign nodules and surgical excision of malignant nodules are recommended.

24.3 Diagnostic Yield of FNAB in the Diagnosis of Nodular Thyroid Disease in the Beginning of the 1990s by Gharib [5]

- Four cytologic diagnostic categories are used. Prevalence of these categories: benign, 69%; suspicious, 10%; malignant, 4%; and nondiagnostic, 17%.
- Analysis of FNAB data suggests false-negative rate of 1–11%, false-positive rate of 1–8%, sensitivity of 65–98%, and specificity of 72–100%.
- Limitations of FNAB are related to the skills of the aspirator, the expertise of the cytologist, and the difficulty in distinguishing some benign cellular adenomas from their malignant counterparts.

24.4 Current FNAB Experience by Dean and Gharib [6]

- Thyroid FNAB is the most accurate test to determine malignancy, and is an integral part of current thyroid nodule evaluation. Results are superior when US-guided FNAB is performed.
- FNAB results are classified as diagnostic (satisfactory) or nondiagnostic (unsatisfactory). Unsatisfactory smears (5–10%) result from hypocellular specimens usually caused by cystic fluid, bloody smears, or suboptimal preparation.
- Diagnostic smears are conventionally subclassified into benign, indeterminate, or malignant categories:
 - Benign cytology (60–70%) is negative for malignancy, and includes cysts, colloid nodule, or Hashimoto's thyroiditis.
 - Malignant cytology (5%) is almost always positive for malignancy, and includes primary thyroid tumors or nonthyroid metastatic cancers.
 - Indeterminate or suspicious specimens (10–20%) include atypical changes, Hurthle cells, or follicular neoplasms.
- The new Bethesda Cytologic Classification has a six-category classification, further subdividing indeterminate by risk factors. Overall, the indeterminate category has anywhere from 15% up to 60% risk of malignancy.
- Recent development of molecular markers should help to further separate benign from malignant nodules with an indeterminate cytology.
- Caution! Benign lesions on FNAB have an approximate 3% risk of malignancy, and may be followed with US. Repeating FNAB decreases the risk of a false negative result to 1.3% [7].

24.5 The Large Analysis of the Brigham and Women's Hospital and Harvard Medical School with a Total of 1985 Patients and FNAB of 3483 Nodules [8]

- Typical malignant nodule: solid (14.3%), hypoechoic (15.2%), with punctuate calcifications (23.3%), solitary (14%).
- Prevalence of thyroid cancer was similar between the patients with solitary nodule (14.8%) and the patients with multiple nodules (4.9%).
- Solitary nodules represent twice the risk of malignancy when compared to nonsolitary nodules and more than 1.5 times higher in a man than in a woman.
- In patients with multiple nodules ≥ 10 mm, cancer was multifocal in 46%, and 72% of cancers occurred in the largest nodule.
- Risk ranges from a 48% likelihood of malignancy in a solitary solid nodule with punctate calcifications in a man to less than 3% in a noncalcified predominantly cystic nodule in a woman.
- In patients with one or more thyroid nodules ≥ 10 mm, likelihood of thyroid cancer per a patient is independent of number of nodules, whereas likelihood per nodule decreases with increasing number of nodules.
- In patients with two or more nodules, aspiration of only the largest nodule would have missed almost one-third of the malignancies. For exclusion of cancer in a thyroid with multiple nodules ≥ 10 mm, up to four nodules should be considered for FNAB. Sonographic characteristics can be used to prioritize nodules for FNAB based on their individual risk of cancer.

24.6 Recommendations for Diagnostic FNAB of a Thyroid Nodules Based on US Pattern According to the 2015 ATA Guidelines [9]

- Features with the highest specificity (median > 90%) for thyroid cancer are microcalcifications, irregular margins, and taller-than-wide shape.
- Diagnostic FNAB of a nodule <10 mm should be performed only in suspicious cases or in patients with personal history of radiation exposure or familial thyroid cancer.
- US patterns and FNAB guidance for thyroid nodules: see Table 24.1.

Table 24.1 Sonographic patterns, estimated risk of malignancy, and US-FNAB guidance for thyroid nodules

Sonographic pattern	US features	Estimated risk of malignancy, %	FNA size cutoff (largest dimension)
High suspicion	Solid hypoechoic nodule or solid hypoechoic component of a partially cystic nodule with one or more of the following features: irregular margins (infiltrative, microlobulated), microcalcifications, taller-than-wide shape, rim calcifications with small extrusive soft tissue component, evidence of ETE	>70–90	Recommend FNAB at ≥ 1 cm
Intermediate suspicion	Hypoechoic solid nodule with smooth margins without microcalcifications, ETE, or taller-than-wide shape	10–20	Recommend FNAB at ≥ 1 cm
Low suspicion	Isoechoic or hyperechoic solid nodule, or partially cystic nodule with eccentric solid areas, without microcalcification, irregular margin or ETE, or taller than wide shape	5–10	Recommend FNAB at ≥ 1.5 cm
Very low suspicion	Spongiform or partially cystic nodules without any of the sonographic features described in low, intermediate, or high suspicion patterns	<3	Consider FNAB at ≥ 2 cm Observation without FNAB is also a reasonable option
Benign	Purely cystic nodules (no solid component)	<1	No biopsy ^a

Modified from the 2015 ATA Guidelines [10]

ETE extrathyroidal extension

^aAspiration of the cyst may be considered for symptomatic or cosmetic drainage

24.7 The Bethesda System for Reporting Thyroid Cytopathology [9, 10]

- Since 2010, the Bethesda System for Reporting Thyroid Cytopathology has been used to eliminate significant variability in reporting of cytological findings in thyroid FNAB samples. See Table 24.2.
- Recent studies applying the criteria and terminology of the Bethesda System to large series of patients have shown relatively good concordance in reporting FNAB cytology, with 89–95% of samples being satisfactory for interpretation and 55–74% reported as definitively benign and 2–5% as definitively malignant.
- The remaining samples were cytologically indeterminate, including AUS/FLUS in 2–18% of nodules, FN in 2–25%, and SUSP in 1–6%.
- In most cases, a repeated FNAB result in a more definitive interpretation; only about 20% of nodules are repeatedly AUS.

Table 24.2 The 2010 Bethesda system for reporting thyroid cytopathology (modified from the 2015 ATA guidelines [10])

Diagnostic category	Estimated/predicted risk of malignancy by the Bethesda system (%)	Actual risk of malignancy in nodules surgically excised, % median (range)	Clinical management
I—Nondiagnostic or unsatisfactory	1–4	20 (9–32)	Repeat FNAB in 3 months
II—Benign	0–3	2.5 (1–10)	US follow-up Nodules with significant growth or “suspicious” US changes, repeat FNAB
III—Atypia of undetermined significance (AUS) or follicular lesion of undetermined significance (FLUS)	5–15	14 (6–48)	Observe clinically and repeat FNAB in three months, or refer patient directly for surgery without repeating FNAB
IV—Follicular neoplasm (FN) or suspicious for a follicular neoplasm	15–30	25 (14–34)	Lobectomy, if malignancy is proven complete thyroidectomy
V—Suspicious for malignancy (SUSP)	60–75	70 (53–97)	Lobectomy or thyroidectomy
VI—Malignant	97–99	99 (94–100)	Thyroidectomy ^a

^aExceptions: metastatic tumors, non-Hodgkin lymphomas, and undifferentiated carcinomas

24.8 Basic Equipment Needed for US-FNAB

- Syringe holder (Fig. 24.2) or syringe pistol.
- 10 or 20 mL plastic syringes.
- Fine or thin needles (20- to 22-gauge).
- For the evacuation of cysts with dens colloid and debris, a thicker needle (18-gauge) is often necessary.
- Glass slides to prepare smears for cytologic examination (six to eight pieces).
- 1% lidocaine for those who prefer biopsy with local anesthesia.



Fig. 24.1 High-resolution ultrasound device with linear probe 10 MHz, footpad 5 cm (preferable to measure the length of the thyroid lobe)

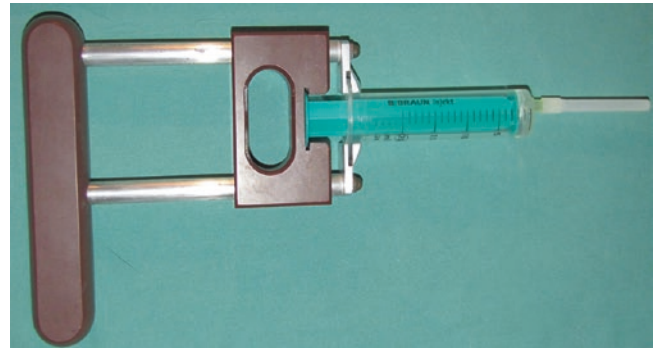


Fig. 24.2 Equipment for US-FNAB: syringe holder 20 mL syringe, 20-gauge needle

24.9 Description of US-Guided FNAB

- US-FNAB (Fig. 24.3) is usually performed on an outpatient basis, in a darkened room with a nurse available to assist with the procedure.
- The patient is placed supine with neck hyperextended to expose thyroid.
- The patient is asked not to breathe deeply, swallow, talk, or move during the procedure.
- Start with disinfection of the puncture site.
- When performing US-guided FNAB, after focusing the nodule by US, the needle should be rapidly inserted through the skin into the nodule. Once the needle tip is visible in the nodule, gentle suction is applied while the needle is moved in and out within the nodule vertically. FNAB takes 5–10 s.
- Once the needle tip is visible in the nodule, gentle suction is applied while the needle is moved in and out within the nodule vertically. FNAB takes 5–10 s.
- In cases of large thyroid cyst evacuation, the procedure takes longer. It occasionally requires replacement of the syringe maintaining the needle in the cyst.
- After biopsy has been completed, firm pressure should be maintained above the biopsy site.
- Observe the patient for a few minutes as occasionally patients have dizziness or pain. If no problems are noted, they are allowed to leave.



Fig. 24.3 Performance of the US-FNAB

24.10 Hemorrhage as a FNAB Complication

- The source of bleeding is usually the sum of abnormal vessels within the capsule of thyroid nodule with frequent artero-venous shunts.
 - Minor hematomas are the most common FNAB complication, but their morbidity is usually negligible [11].
 - Major hematomas are rare, but life-threatening. Only a few cases of post-FNAB uncontrolled bleeding accompanied by acute respiratory distress requiring an urgent surgery has been reported [12, 13].
- Hemorrhagic risk factors:
- Anticoagulation therapy; should be discontinued 4–5 days prior to FNAB.
 - Antiplatelet therapy; should be discontinued 7–10 days prior to FNAB.
 - Thrombocytopenia and hemostasis abnormalities.
 - Caution! Full medical history and coagulation parameters in risk patients should be obtained before performing FNAB.
 - Post-FNAB hematoma (Fig. 24.4cc) is typically self-limiting with a mild neck discomfort and well managed with mild ice compression (Fig. 24.4ff). Hematoma usually resorbs within a few days (Fig. 24.4gg).

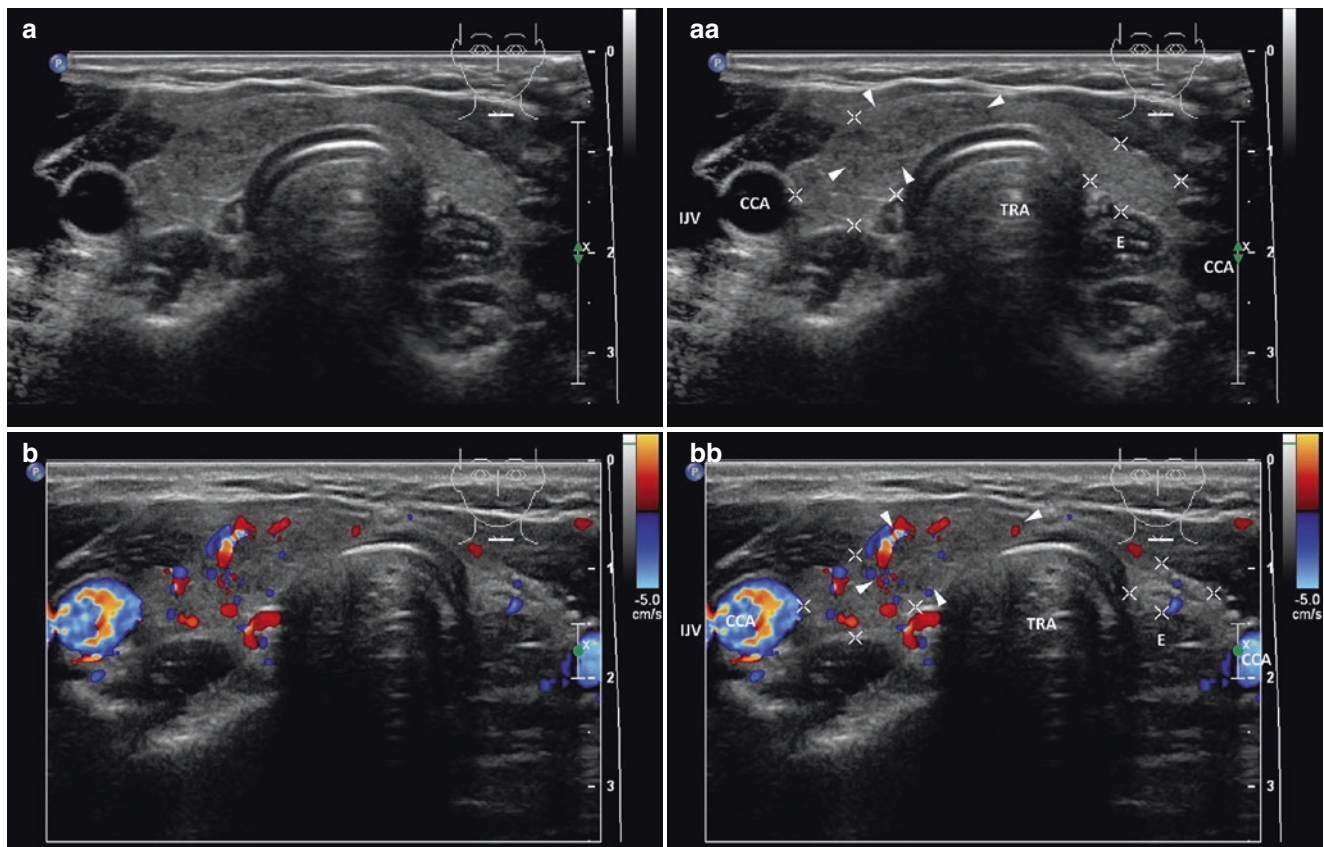


Fig. 24.4 (aa) A 27-year-old woman with a solitary solid nodule (arrowheads), size $21 \times 17 \times 7$ mm and volume 1.5 mL in the RL extending into the right branch of isthmus, US scan: elliptical shape, “more wide than tall”; inhomogeneous structure; isoechoic; ill-defined, no halo sign; Tvol 9 mL, RL 5 mL, and LL 4 mL; transverse. (bb) Detail of a solitary solid nodule (arrowheads), CFDS before FNAB: focally increased vascularity at periphery and sporadic parenchymal vascularity, *pattern I*; transverse. (cc) A few minutes after FNAB, patient complained of neck discomfort. US revealed an acute hematoma (blank arrowheads) next to the RL, size $55 \times 18 \times 16$ mm and volume 8 mL: well-defined, homogeneous, slightly hypoechoic mass between the RL and the right CCA; transverse. Patient had no anticoagulant or antiplatelet medication, but due to migraine used a large dose of ibuprofen. (dd) Detail of an acute hematoma (blank arrowheads) a few min-

utes after FNAB: well-defined, homogeneous, slightly hypoechoic mass compressing the RL; transverse. (ee) Detail of an acute hematoma (blank arrowheads) a few minutes after FNAB: well-defined, homogeneous, slightly hypoechoic mass spreading cranially above the RL; longitudinal. (ff) Detail of an acute hematoma (blank arrowheads); after 2 h of ice compression—hematoma slightly diminished, size $55 \times 17 \times 13$ mm and volume 6.5 mL: well-defined, homogeneous, almost isoechoic mass still compressing the RL; transverse. Post-FNAB coagulation tests revealed no abnormality. Patient did not experience any further difficulties and was discharged. (gg) An acute hematoma (blank arrowheads) 2 days after FNAB (outpatient examination, ice applied at home); hematoma substantially diminished, size $23 \times 14 \times 7$ mm and volume 1.2 mL: well-defined, homogeneous, almost isoechoic mass without compressing the RL; transverse

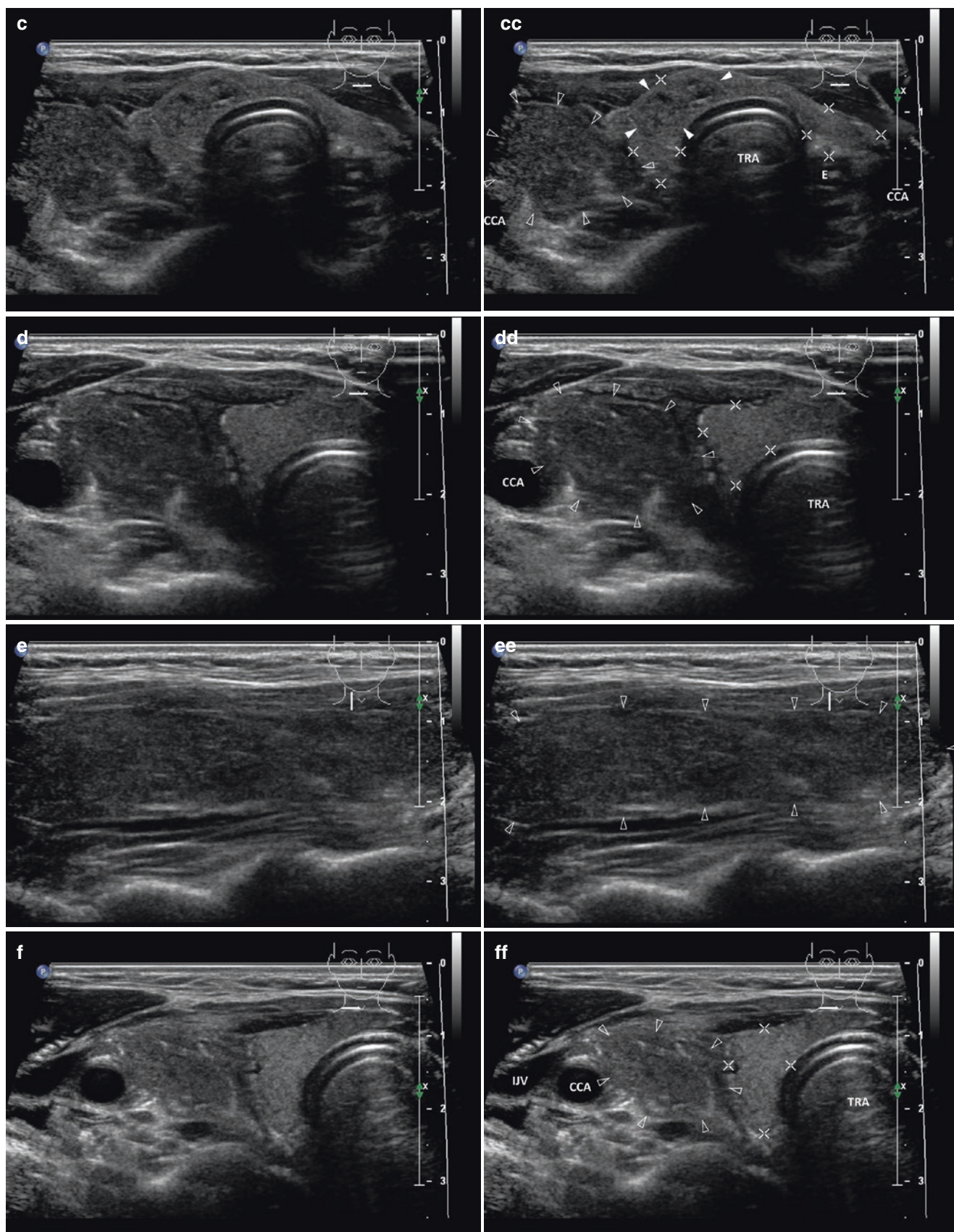


Fig. 24.4 (continued)

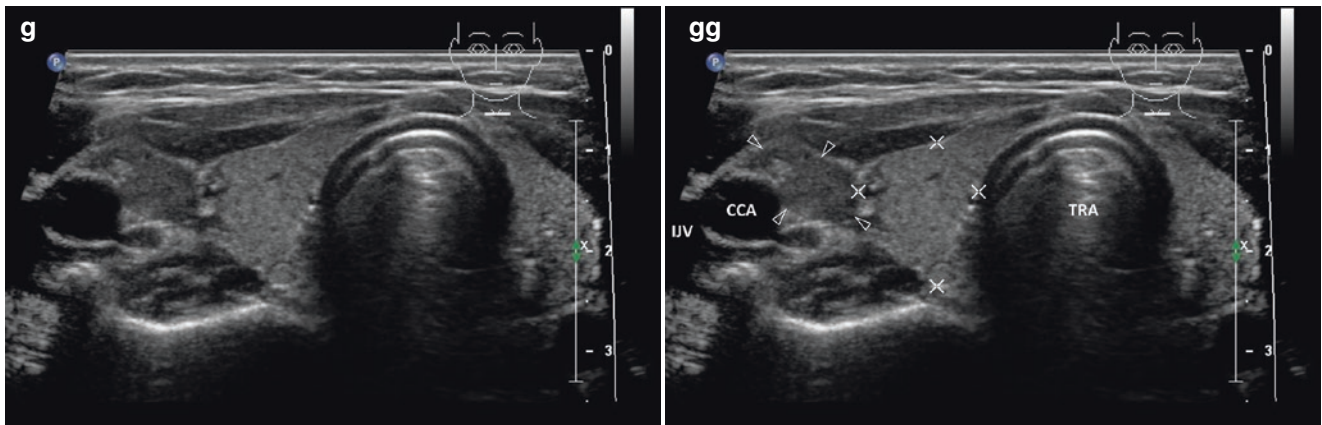


Fig. 24.4 (continued)

References

1. Martin HE, Ellis EB. Biopsy by needle puncture and aspiration. *Ann Surg.* 1930;92(2):169–81.
2. Bäckdahl M, Wallin G, Löwhagen T, Auer G, Granberg PO. Fine-needle biopsy cytology and DNA analysis. Their place in the evaluation and treatment of patients with thyroid neoplasms. *Surg Clin North Am.* 1987;67(2):197–211.
3. Krishnappa P, Ramakrishnappa S, Kulkarni MH. Comparison of free hand versus ultrasound-guided fine needle aspiration of thyroid with histopathological correlation. *J Environ Pathol Toxicol Oncol.* 2013;32(2):149–55.
4. Gharib H. Fine-needle aspiration biopsy of thyroid nodules: advantages, limitations, and effect. *Mayo Clin Proc.* 1994;69(1):44–9.
5. Gharib H, Goellner JR. Fine-needle aspiration biopsy of the thyroid: an appraisal. *Ann Intern Med.* 1993;118(4):282–9.
6. Dean DS, Gharib H. Fine-needle aspiration biopsy of the thyroid gland. In: De Groot LJ, Beck-Peccoz P, Chrousos G, Dungan K, Grossman A, Hershman JM, et al., editors. *Endotext* [Internet]. South Dartmouth, MA: MDText.com, Inc.; 2015.
7. Bomeli SR, LeBeau SO, Ferris RL. Evaluation of a thyroid nodule. *Otolaryngol Clin N Am.* 2010;43(2):229–38.
8. Frates MC, Benson CB, Doubilet PM, Kunreuther E, Contreras M, Cibas ES, et al. Prevalence and distribution of carcinoma in patients with solitary and multiple thyroid nodules on sonography. *J Clin Endocrinol Metab.* 2006;91(9):3411–7.
9. Crippa S, Mazzucchelli L, Cibas ES, Ali SZ. The Bethesda System for reporting thyroid fine-needle aspiration specimens. *Am J Clin Pathol.* 2010;134(2):343–4.
10. Haugen BR, Alexander EK, Bible KC, Doherty GM, Mandel SJ, Nikiforov YE, et al. 2015 American Thyroid Association Management guidelines for adult patients with thyroid nodules and differentiated thyroid cancer: The American Thyroid Association Guidelines Task Force on thyroid nodules and differentiated thyroid cancer. *Thyroid.* 2016;26(1):1–133.
11. Polyzos SA, Anastasilakis AD. Systematic review of cases reporting blood extravasation-related complications after thyroid fine-needle biopsy. *J Otolaryngol Head Neck Surg.* 2010;39(5):532–41.
12. Donatini G, Masoni T, Ricci V, D’Elia M, Guadagni A, Baldetti G, et al. Acute respiratory distress following fine needle aspiration of thyroid nodule: case report and review of the literature. *G Chir.* 2010;31(8–9):387–9.
13. Hor T, Lahiri SW. Bilateral thyroid hematomas after fine-needle aspiration causing acute airway obstruction. *Thyroid.* 2008;18(5):567–9.

Thyroid Abscess as a Complication of Fine-Needle Aspiration Biopsy: A Case Report

25

25.1 Essential Facts

- Acute thyroiditis with abscess formation is an extremely rare condition with a rapid (usually several days), possibly dramatic and life-threatening course (several hours).
- Clinical presentation:
 - General symptoms—fever, chills.
 - Local manifestations—classical signs of inflammation: heat, pain, redness and swelling—firm induration over the affected thyroid lobe, painful on palpation, erythema over the mass.
 - Suddenly formed large abscess leads to tracheal deviation and compression and may cause severe dyspnea requiring intubation and emergency surgical treatment.
- Symptoms: pain on palpation or persistent pain at the site of the mass, limited neck movement, difficulty swallowing, dyspnea and dysphonia, even inspiratory stridor in case of dramatic course [1].
- Most common causes of abscess formation according to patient age:
 - In children, abscess is usually formed in the setting of the normal thyroid gland due to spread of infection by pathological communication in congenital abnormalities of the oropharynx-fistula of processus piriformis or persistent thyroglossal duct [2].
 - In adults, abscess is usually formed in the setting of multinodular goiter:
 - In immunocompromised patients, by haematogenous spread of infection in sepsis from another primary source (the gastrointestinal or genitourinary tracts) [3].
 - Mechanical insult—swallowing of sharp foreign body (e.g. a bone) and subsequent perforation through the esophageal wall [4], or iatrogenic causes (after fine-needle aspiration biopsy) [5, 6].
 - Invasion of carcinoma from neighboring organs—larynx, esophagus [7], or in thyroid carcinoma itself [8].
- Most common infectious agents: skin pathogens—*Staphylococcus aureus*, *Streptococcus pyogenes*, pathogens of the gastrointestinal and genitourinary tracts—*Escherichia coli*, *Pseudomonas* spp. [9, 10].
- Treatment: broad-spectrum antibiotics, excision and drainage of the abscess, thyroidectomy is sometimes necessary, with removal of the surrounding soft tissues infiltrated with inflammation [1].

25.2 The Case Report [11]

- 80-year-old female patient with a long history of large multinodular goiter of 38 mL followed-up by ultrasound.
- Personal history: cholecystectomy many years ago, no history of diabetes mellitus, no immunity influencing drugs.
- At a local radiology center, US-FNAB from the right lobe was performed, with benign cytology results.
- Three days after the FNAB, painful mass suddenly formed at the right neck site of puncture.
- Over the next days, the mass enlarged, with increasing pain and local erythema development (Fig. 25.1). Patient suffered from increased body temperature of 37.0 °C, dysphagia, dyspnea, and later stridor.
- Eight days after the FNAB, patient was examined in outpatient endocrinology center of university hospital:
 - US (Figs. 25.2 and 25.3) and computed tomography findings (Fig. 25.4) demonstrated a large abscess in the right thyroid lobe, with a volume of 60 mL, causing tracheal deviation and compression.
 - Laboratory findings—high C-reactive protein (128 mg/mL); high white cell count of $15.9 \times 10^9/L$.
 - Cytological examination of the puncture fluid—polymorphonuclears; culture of the puncture fluid—*Escherichia coli*.
 - Blood and urine culture negative.
 - Normal levels of serum TSH (thyroid-stimulating hormone) and fT4 (free thyroxine).
- Patient was surgically revised with removal of the abscess, adjacent soft tissues, and inflamed muscles; antibiotic therapy followed (piperacillin + tazobactam).
- At inspection 5 month later the patient was without any complains (Fig. 25.5) with normal thyroid function tests.
- Caution! Strict aseptic measures are necessary even in for routine and minimally invasive FNAB procedure.



Fig. 25.1 An 80 year-old-woman with a thyroid abscess, physical findings 8 days post FNAB from the RL: local palpable mass and erythema in the right lower neck and upper chest

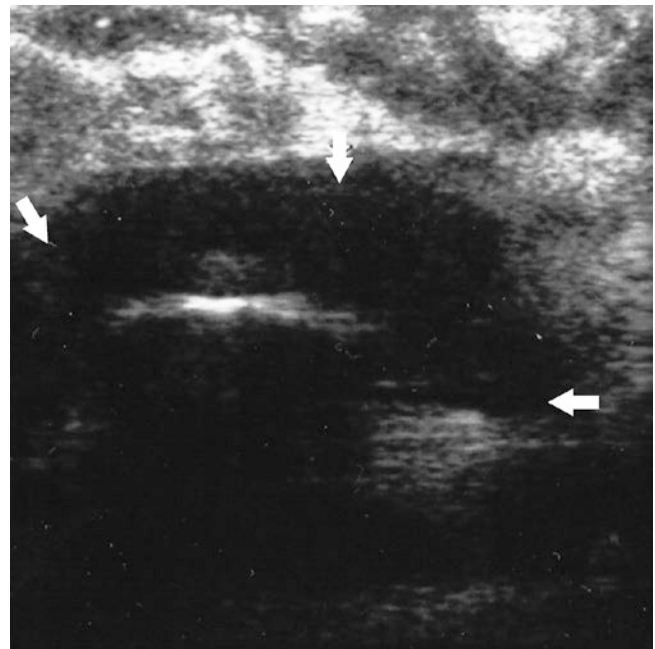


Fig. 25.2 US scan of thyroid abscess in the RL—large cystic nodule, size approximately $65 \times 55 \times 35$ mm and volume 62 mL: subcutaneous phlegmon ventrally—subcutaneous layer thickened up to 20 mm; inhomogeneous; mostly hyperechoic with hypoechoic, ill-defined areas; thyroid abscess in the RL—large cystic lesion (thick arrows); mostly anechoic contents; hyperechoic band in the center; ill-defined; probe pressure creates swirling; transverse, depth of penetration 4 cm (year 2007, older generation of US device)

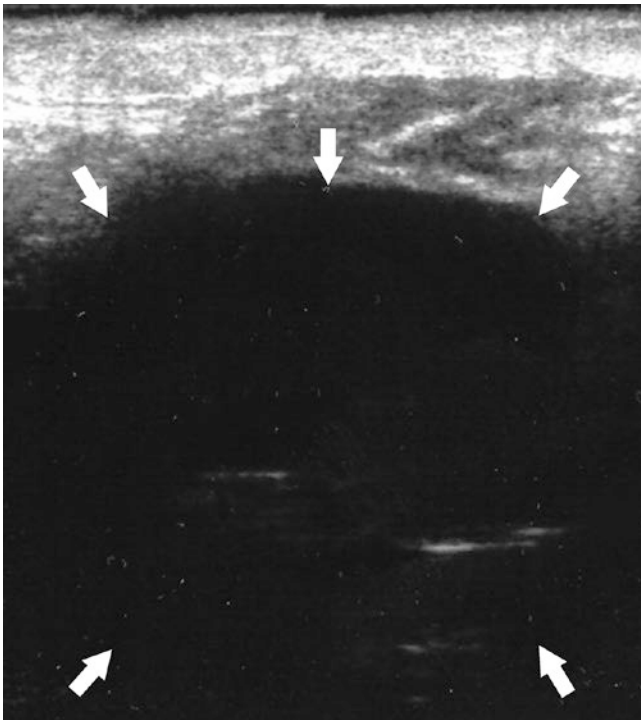


Fig. 25.3 US scan of thyroid abscess in the RL—large cystic nodule, volume 62 mL; subcutaneous phlegmon ventrally; the subcutaneous layer thickened to as much as 20 mm; an abscess in the right thyroid lobe—thyroid abscess in the RL—large cystic lesion (*thick arrows*); mostly anechoic contents; sporadic hyperechoic bands; longitudinal; depth of penetration 8 cm (year 2007, older generation of US device)



Fig. 25.5 Patient, physical findings 6 months after surgery: a large scar after excision of the thyroid abscess and sternocleidomastoid muscle



Fig. 25.4 CT of the thyroid abscess: the enlarged RL extends into the right mediastinum; large lobular cavity, size 72 × 52 × 30 mm; no presence of gas; trachea considerable deviated to the left side; inflammation of surrounding soft tissue and muscular structures; reactive lymphadenopathy; transverse

References

1. Kale SU, Kumar A, David VC. Thyroid abscess—an acute emergency. *Eur Arch Otorhinolaryngol*. 2004;261(8):456–8.
2. Mali VP, Prabhakaran K. Recurrent acute thyroid swellings because of pyriform sinus fistula. *J Pediatr Surg*. 2008;43(4):e27–30.
3. Vandjme A, Pageaux GP, Bismuth M, Fabre JM, Domergue J, Perez C, et al. Nocardiosis revealed by thyroid abscess in a liver—kidney transplant recipient. *Transpl Int*. 2001;14(3):202–4.
4. Lin ZH, Teng YS, Lin M. Acute thyroid abscess secondary to oesophageal perforation. *J Int Med Res*. 2008;36(4):860–4.
5. Wang YC, Yeh TS, Lin JD. Gram-negative thyroid abscess resulting from fine-needle aspiration in an immunosuppressed patient. *Clin Infect Dis*. 1997;25(3):745–6.
6. Chen HW, Tseng FY, Su DH, Chang YL, Chang TC. Secondary infection and ischemic necrosis after fine needle aspiration for a painful papillary thyroid carcinoma: a case report. *Acta Cytol*. 2006;50(2):217–20.
7. Piñero Madrona A, Illana Moreno J, Parrilla Paricio P. Thyroid abscess due to fistulization of hypopharyngeal carcinoma. *Med Clin (Barc)*. 1999;113(13):518–9.
8. Ohno Y, Ilo K, Imamura M, Aoki N. A case of acute suppurative thyroiditis associated with thyroid papillary carcinoma. *Nihon Naibunpi Gakkai Zasshi*. 1993;69(9):1003–12.
9. Nishihara E, Miyauchi A, Matsuzuka F, Sasaki I, Ohye H, Kubota S, et al. Acute suppurative thyroiditis after fine-needle aspiration causing thyrotoxicosis. *Thyroid*. 2005;15(10):1183–7.
10. Sicilia V, Mezitis S. A case of acute suppurative thyroiditis complicated by thyrotoxicosis. *J Endocrinol Investig*. 2006;29(11):997–1000.
11. Halenka M, Skodova I, Horak D, Kucerova L, Karasek D, Frysak Z. Thyroid abscess as a complication of fine-needle aspiration biopsy. *Endocrinologist*. 2008;18(6):263–5.

Index

A

- AACE/AME/ETA Guidelines, 362
- Acute myeloid leukemia, 325
- AIT. *See* Amiodarone-induced thyrotoxicosis (AIT)
- American Thyroid Association (ATA) Guidelines, 77, 93, 141–142, 173, 191, 231, 242, 381
- Amiodarone-induced thyrotoxicosis (AIT), 228–229
 - classification, 71
 - class III antiarrhythmic drug, 71
 - diagnostic criteria
 - AIT type 1, 71–73, 76
 - AIT type 2, 71, 74–76
 - incidence, 71
 - mixed form, 71
 - occurrence, 71
 - prevalence, 71
- Anaplastic thyroid carcinoma (ATC)
 - age at diagnosis, 257
 - clinical findings, 257
 - incidence of, 257
 - metastatic cervical lymph nodes, 293
 - retrospective analysis, 257
 - US features
 - computed tomography, 258
 - ETE, 258–262
 - FNAB, 258
 - giant ATC, 258, 261–262
 - large ATC, 258–260
- Anterior neck space mimicking thyroid, lesions at
 - branchial cysts, 313, 318
 - cellulitis—phlegmon, 313, 325
 - dermoid and epidermoid cysts, 313, 318–319
 - hematomas, 313, 322–324
 - internal jugular vein, thrombus in, 234–235, 313, 320–321
 - lipoma, 313, 315–316
 - MNG, 313, 317
 - scar after tracheostomy, 313, 326, 365–367
 - superficial abscess, 313
- Anti-inflammatory medication therapy, 55
- Arc/linear calcification, 106, 113–114
- ATC. *See* Anaplastic thyroid carcinoma (ATC)
- Atrophic gland, 30–34
- Autoimmune thyroid diseases (AITD)
 - Amsterdam cohort study, 18
 - genetic factors, 17
 - prevalence, 17
- Autoimmune thyroiditis (AT). *See* Hashimoto's thyroiditis (HT)

B

- BCC. *See* Branchial cleft cysts (BCCs)
- Benign cytology, 380
- Bethesda Cytologic Classification, 380

- Bethesda System, 382
- Branchial cleft cysts (BCCs), 311–312, 318
- Branchial cleft remnants, 311
- Brunn method, 3

C

- Calcifications
 - complex nodule
 - acoustic shadows, 106, 115
 - arc/linear, 106, 113–114
 - benign and malignant nodules, with malignancy rates, 105
 - coarse, 106, 110
 - curvilinear, irregular margin, 106, 110
 - curvilinear, smooth margin, 106, 111
 - eggshell, 106, 112, 115, 116
 - incidence, 105
 - linear, 106, 111
 - malignancy, risk of, 106
 - papillary thyroid carcinoma, 106
 - peripheral dystrophic, 105, 106
 - psammomatous, 105
 - rim peripheral, 106, 116
 - stippled, fine/coarse nonlinear particles, 106, 113
 - MTC, 247, 248, 250, 251, 252
 - thyroid nodules, 78
- Cat's eye artifact, 80, 83
- Cervical lymph nodes
 - benign/reactive, 6
 - malignancy
 - border, 275, 276
 - calcifications, 275
 - cancer, right nephrectomy for, 277
 - echogenicity, 275, 276
 - hilus sign, 275, 276
 - Hodgkin lymphoma, 278–279
 - intranodal necrosis, 275
 - left bronchial cancer, 278
 - in lymphomas, 274, 280–281
 - non-Hodgkin lymphoma, 266–270
 - oral cancer, 274
 - primary site, 274–275
 - shape, 275, 276
 - size, 275
 - vascularity, 275
 - metastatics
 - ATC, 293
 - location of, 284
 - MTC, 288–289
 - PET-CT, 284
 - PTC, 190, 284–287, 289–292, 294
 - round shape, 284
- PTL (*see* Primary thyroid lymphoma (PTL))

Chronic lymphocytic thyroiditis (CLT), 214, 265. *See also* Hashimoto's thyroiditis (HT)

Coarse calcification, 106, 110

Cobblestoning, 313

Color-flow Doppler sonography (CFDS), 46, 56, 331, 368

- AIT, 71, 76
- blood flow, absence of, 80
- differentiate soft tissue infections, 313
- ETE, 233
- pattern, 51
- thyroid remnants, 300
- toxic multinodular goiter/solitary toxic adenoma, 135, 136, 138
- tumor thrombus, 313

Comet tail artifact, 80, 327

Complex cysts, 362, 365–367

Complex nodule

- with calcification
 - acoustic shadows, 106, 115
 - arc/linear, 106, 113–114
 - benign and malignant nodules, with malignancy rates, 105
 - coarse, 106, 110
 - curvilinear, irregular margin, 106, 110
 - curvilinear, smooth margin, 106, 111
 - eggshell, 106, 112, 115, 116
 - incidence, 105
 - linear, 106, 111
 - malignancy, risk of, 106
 - papillary thyroid carcinoma, 106
 - peripheral, 106
 - peripheral dystrophic, 105, 106
 - psammomatous, 105
 - rim peripheral, 106, 116
 - stippled, fine/coarse nonlinear particles, 106, 113
- with cystic degeneration
 - cystic nodule, 105, 107
 - solid nodule, 105, 108–109
 - spongiform nodule, 105, 109

Computed tomography (CT)

- ATC, 258
- thyroid abscess, 390, 391

Corticosteroids therapy, 55

Cystic degeneration

- cystic nodule, 105, 107
- solid nodule, 105, 108–109
- spongiform nodule, 105, 109

Cysts, thyroid. *See* Thyroid cysts

D

DCs. *See* Dermoid cysts (DCs)

de Quervain's diseases. *See* Subacute granulomatous thyroiditis (SGT)

Dermoid cysts (DCs), 312, 313, 318–319

Differentiated thyroid cancer (DTC), 155, 225, 231, 232, 257, 284, 299, 312

Diffuse goiter, 12–13

- definition, 11
- epidemiologic study, 11
- iodine deficiency endemic area, 11
- local sex-specific reference values, 11
- palpation, 11
- prevalence, 11–12
- thyroid volume measurement
 - age, 12
 - body surface area, 12

- long-term iodine sufficiency, 12, 13
- US features, 15
- WHO/ICCIDD-recommended reference, 11, 12

DTC. *See* Differentiated thyroid cancer (DTC)

Dystrophic calcification, 105–106

E

Ecchymosis, 312

Echogenicity, 3, 6, 78

Echogenic septum, 328

Echotexture, 3

Ectopic parathyroid glands, 329–330, 344

Eggshell calcification, 106, 112, 115, 116

Epidermoid cysts, 313, 318–319

ETE. *See* Extrathyroidal extension (ETE)

Extramedullary plasmacytoma (EMP), 274

Extrathyroidal extension (ETE), 232

- capsule vascularity, 233, 259–260
- CFDS, 234–235
- contour bulging, 223–224, 233
- echogenic capsule, loss of, 232–234, 259–262
- giant ATC, 258, 261–262
- large ATC, 258–260
- large solitary PTC, 236–237
- patients, survival of, 231
- probe, non-compressible by, 233, 261
- solid hyperechoic mass, 233–235

F

Fine-needle aspiration biopsy (FNAB)

- ATA Guidelines, 381
- ATC, 258
- benign lesions on, 380
- diagnostic smears, 380
- diagnostic yield of, 379
- EMP, 274
- equipment for, 383
- hemorrhage, 385–387
- importance and benefits of, 379
- nondiagnostic smears, 380
- PAd, 331
- PEIT, 361, 362
- PTC, 225, 266
- thyroid abscess
 - in adults, 389
 - in children, 389
 - clinical presentation, 389
 - infectious agents, 389
 - large multinodular goiter, 390–391
 - symptoms, 389
 - treatment, 389

US-FNAB

- Bethesda System for Reporting Thyroid Cytopathology, 382
- equipment for, 383
- performance of, 384

Focal lymphocytic thyroiditis (FLT), 19

Follicular thyroid carcinoma (FTC), 93

- Hashimoto's thyroiditis, 160–161
- HCC, 161–162
- incidence, 155
- medium-sized, 159
- MI-FTC, 155
- PTC, 172, 190, 232, 234–235, 242, 243
- survival rate, 155

- two FTC, 157–158
- US features, 156
- WI-FTC, 155
- Follicular variant of papillary carcinoma (FVPTC), 172, 173, 184–185, 191, 202–203, 225
- FTC. *See* Follicular thyroid carcinoma (FTC)
- FVPTC. *See* Follicular variant of papillary carcinoma (FVPTC)

G

- Gastric cancer, 272–273
- Gestational transient thyrotoxicosis (GTT), 1–2
- Glandular vascularity, 3
- Goiter
 - diffuse, 12–13
 - age, 12
 - body surface area, 12
 - definition, 11
 - epidemiologic study, 11
 - iodine deficiency endemic area, 11
 - local sex-specific reference values, 11
 - long-term iodine sufficiency, 12, 13
 - palpation, 11
 - prevalence, 11–12
 - US features, 15
 - WHO/ICCIDD-recommended reference, 11, 12
 - Hashimoto's thyroiditis
 - asymmetric fibrotic goiter volume, 26
 - “Delphian” lymph node, 29
 - giant goiter volume, 24–25
 - LL, with classic HT, 23, 24, 26–28
 - markedly fibrotic goiter, 27
 - multinodular goiter, 28
 - RL, with classic HT, 23, 24, 26–28
 - multinodular
 - in adults, 119
 - dominant giant complex cyst, 91
 - dominant medium-sized complex cyst, 89–90
 - giant complex nodule, 127
 - giant right lobe, 124–125
 - large complex nodule, 126
 - left lobe, with solid and complex nodules, 124
 - medium-sized complex nodule, 122–123
 - medium-sized solid nodule, 120–121
 - RIT, 119
 - US features, 128
 - substernal
 - essential facts, 129
 - primary, 129–131
 - secondary, 129, 132–133
 - US characteristics, 134
- Graves' disease (GD), 299
 - clinical findings, 1
 - diffuse heterogeneous/coarse echotexture, 2–4, 6
 - diffuse hypoechoic, 2–4, 6
 - enlarged gland, with round-shaped lobes, 2–4
 - giant goiter, 2, 9–10
 - history, 1
 - hyperthyroidism, 1–2
 - hypoechoic micronodular structure, with short fibrous septa, 6–8
 - incidence, 1
 - inferior thyroid artery, 2, 6
 - laboratory findings, 1
 - near TT, 306–307
 - prevalence, 1
 - PTC, 225–227

- subtotal thyroidectomy, 299, 308–309
- thyroid inferno, 2, 11
- TT, 299

H

- Hashimoto's thyroiditis (HT), 243
 - Amsterdam AITD cohort study, 18
 - annual incidence, 17, 18
 - atrophic gland, 30–34
 - clinical findings, 17
 - definition, 17
 - diagnosis, 17
 - FTC, 160–161
 - goiter
 - asymmetric fibrotic goiter volume, 26
 - “Delphian” lymph node, 29
 - giant goiter volume, 24–25
 - left lobe, with classic HT, 23, 24, 26–28
 - markedly fibrotic goiter, 27
 - multinodular goiter, 28
 - right lobe, with classic HT, 23, 24, 26–28
- hashitoxicosis
 - biochemical characterization, 35
 - CFDS qualitative parameters, 35, 36
 - CFDS quantitative parameters, 35
 - definition, 35
 - inferior thyroid artery, 35
 - peak systolic velocity, 35, 36, 38
 - thyroid scintigraphy, 35
- history, 17
- hypertrophic autoimmune hypothyroidism, 18
- and multifocal papillary thyroid carcinoma, 238–241
- organ-specific autoimmune disease, 17
- prevalence, 18
- primary atrophic variant, 18
- PTC
 - blurred margin, 214, 218, 223–224
 - cervical metastatic LNs, 214, 221–224
 - CLT, 214
 - diffuse sclerosing variant, PTC, 214, 223–224
 - hypoechoic, 214–217
 - ill-defined margin, 214, 218, 223–224
 - intranodal microcalcifications, 214, 220
 - microcalcifications, peripheral arc of, 214, 219
 - multifocal PTC, 214, 219
 - with smooth margins, 214–217
 - solid nodule, 214–217
 - thick halo sign, 214, 219
 - without “halo” sign, 214–217
 - without internal calcifications, 214–217
- PTL, 265
- and solitary tiny papillary thyroid microcarcinoma, 236
- suspicious solitary medium-sized nodule, 271
- thyroid remnants, 305, 306
- US features
 - coarse septations from fibrous bands, 19
 - diffusely heterogeneous, coarse echotexture, 19, 20, 23
 - enlarged gland, 19, 23, 24
 - FLT, 19
 - high-resolution sonography instruments, 19
 - microlobulated margin, 19–21, 23
 - multiple discrete hypoechoic micronodules, 19, 20, 23
 - nodular HT, 19
 - perithyroidal satellite lymph nodes, 19, 29
 - positive predictive value, 19
 - thyroid size and echotexture assessment, 19

- Hashitoxicosis
 - biochemical characterization, 35
 - CFDS
 - qualitative parameters, 35, 36
 - quantitative parameters, 35
 - definition, 35
 - inferior thyroid artery, 35
 - peak systolic velocity, 35, 36, 38
 - thyroid scintigraphy, 35
 - Hematomas, 313, 322–324
 - Hemorrhage, 385–387
 - Hilus sign, 275, 276
 - Hodgkin lymphoma, 278–279
 - HT. *See* Hashimoto's thyroiditis (HT)
 - Human chorionic gonadotropin (hCG), 1
 - Hürthle cell carcinoma (HCC), 140, 155, 161, 190, 232
 - Hyperechoic debris, 80, 91
 - Hyperthyroidism, 1–2
- I**
- Inferior thyroid artery (ITA), 2, 6, 35
 - Intermediate suspicion, of malignancy
 - ATA guidelines, 145
 - medium-sized solid nodule, 151–152
 - small solid nodule, 146–147, 149–150
 - US findings, 148
 - Internal jugular vein (IJV), 232, 285, 286, 312, 313, 320–321
 - Iodine deficiency disorders (IDD), 8, 11
- L**
- Linear calcification, 106, 111
 - Lipoma, 311, 313, 315–316
 - Lobectomy, 299, 303
 - Lymph nodes, cervical
 - benign/reactive, 6
 - malignancy
 - border, 275, 276
 - calcifications, 275
 - cancer, right nephrectomy for, 277
 - echogenicity, 275, 276
 - hilus sign, 275, 276
 - Hodgkin lymphoma, 278–279
 - intranodal necrosis, 275
 - left bronchial cancer, 278
 - in lymphomas, 274, 280–281
 - non-Hodgkin lymphoma, 266–270
 - oral cancer, 274
 - primary site, 274–275
 - shape, 275, 276
 - size, 275
 - vascularity, 275
 - metastatics
 - ATC, 293
 - location of, 284
 - MTC, 288–289
 - PET-CT, 284
 - PTC, 190, 284–287, 289–292, 294
 - round shape, 284
 - PTL (*see* Primary thyroid lymphoma (PTL))
- M**
- Magnetic resonance imaging (MRI), 128, 258, 329, 330
 - Malignant cervical lymph nodes
 - border, 275, 276
 - calcifications, 275
 - cancer, right nephrectomy for, 277
 - echogenicity, 275, 276
 - hilus sign, 275, 276
 - Hodgkin lymphoma, 278–279
 - intranodal necrosis, 275
 - left bronchial cancer, 278
 - in lymphomas, 274, 280–281
 - Non-Hodgkin lymphoma, 266–270
 - oral cancer, 274
 - primary site, 274–275
 - shape, 275, 276
 - size, 275
 - vascularity, 275
 - Malignant cytology, 380
 - Medullary thyroid carcinoma (MTC), 274, 288–289
 - calcifications, 247, 248, 250, 251, 252
 - clinical course, 247
 - hereditary forms, 247
 - hypoechoic, 247, 252
 - ovoid-to-round shape, 247–249
 - prevalence, 247
 - screening, 247
 - serum calcitonin, 247
 - solid internal content, 247–249
 - solid lesion, 247, 248
 - with solitary large MTC, 247, 250–251
 - with solitary medium-sized MTC, 247, 252–255
 - with solitary small MTC, 247–249
 - sporadic forms, 247
 - Metastatic cervical lymph nodes
 - location of, 284
 - PET-CT, 284
 - post thyroidectomy, for thyroid carcinoma
 - ATC, 293
 - MTC, 288–289
 - PTC, 190, 284–287, 289–292, 294
 - round shape, 284
 - MIBI, 329
 - Mild hypercalcemia, 334, 335, 341, 369–377
 - Minimally invasive, targeted parathyroidectomy (MIP), 231
 - Minimally invasive video-assisted technique (MIVAT), 299
 - “Mirror-image” artifact, 327
 - MNG. *See* Multinodular goiter (MNG)
 - Moderate hypercalcemia, 336, 338, 342, 344
 - MTC. *See* Medullary thyroid carcinoma (MTC)
 - Multinodular goiter (MNG), 194, 225, 304, 313, 317
 - in adults, 119
 - dominant giant complex cyst, 91
 - dominant medium-sized complex cyst, 89–90
 - giant complex nodule, 127
 - giant right lobe, 124–125
 - large complex nodule, 126
 - left lobe, with solid and complex nodules, 124
 - medium-sized complex nodule, 122–123
 - medium-sized solid nodule, 120–121
 - RIT, 119
 - US features, 128
- N**
- NHLs. *See* Non-Hodgkin's lymphomas (NHLs)
 - Nodular goiter
 - suspicious and malignant lesions
 - ATA guidelines, 141–142
 - clinical assessment, 142
 - cystic thyroid nodules, 142
 - incidence and mortality, 141
 - malignant nodules, 142–143
 - for solid nodules, high-suspicion, 142
 - US characteristics, 142

- thyroid nodules
 - calcifications, 78
 - echogenicity, 78
 - FNAB (*see* Fine-needle aspiration biopsy (FNAB))
 - Halo sign, 78
 - internal content, 77–78
 - margin, 78
 - shape, 77
 - size, 77
 - vascularity, 78
- Nodules
 - mixed predominantly cystic nodule, 79
 - solid (*see* Solid nodule)
 - thyroid
 - calcifications, 78
 - echogenicity, 78
 - FNAB (*see* Fine-needle aspiration biopsy (FNAB))
 - Halo sign, 78
 - internal content, 77–78
 - margin, 78
 - shape, 77
 - size, 77
 - vascularity, 78
- Non-Hodgkin's lymphomas (NHLs), 265–270
- O**
 - One-step ethanol ablation technique, 362
 - Oral cancer, 274
 - Ord disease, 18
- P**
 - Papillary thyroid carcinoma (PTC), 93, 106, 230
 - AIT, 228–229
 - in children and adolescents, 242–243
 - DTC, 231, 232
 - ETE, 232
 - capsule vascularity, 233, 259–260
 - CFDS, 234–235
 - contour bulging, 223–224, 233
 - echogenic capsule, loss of, 232–234, 259–262
 - large solitary PTC, 236–237
 - patients, survival of, 231
 - probe, non-compressible by, 233, 261
 - solid hyperechoic mass, 233–235
 - GD, 225–227
 - HT
 - blurred margin, 214, 218, 223–224
 - cervical metastatic LNs, 214, 221–224
 - CLT, 214
 - diffuse sclerosing variant, PTC, 214, 223–224
 - hypoechoic, 214–217
 - ill-defined margin, 214, 218, 223–224
 - intranodal microcalcifications, 214, 220
 - microcalcifications, peripheral arc of, 214, 219
 - multifocal PTC, 214, 219
 - with smooth margins, 214–217
 - solid nodule, 214–217
 - thick halo sign, 214, 219
 - without “halo” sign, 214–217
 - without internal calcifications, 214–217
 - medium-sized and large nodules
 - blurred margin, 191, 204–206
 - cervical metastatic LNs, 191–197
 - cystic degeneration, 191, 198–199, 204–206
 - “daughter” small PTC, 191, 200–201
 - degenerative and necrotic changes, 191, 198–199, 204–206
 - elliptical shape, 191, 198–199
 - FVPTC, 191, 202–203
 - hyperechoic, 191, 196–197
 - ill-defined margin, 191, 204–206
 - intranodular hypervascularity, 191–195, 198–199
 - ipsilateral cervicolateral compartment, 190
 - irregular margins, 191, 198–199
 - irregular shape, 191, 204–206
 - lobulated margin, 191, 204–206
 - metastatic LNs, 190
 - microcalcifications, 191–193, 196–197, 202–203
 - mixed echogenicity, 191, 194–195
 - oval shape, 191, 196–197
 - rarely complete/incomplete halo sign, 191, 196–199
 - rarely marked hypoechogenicity, 191, 200–201
 - rarely well-defined margin, 191, 200–201
 - rim/intranodal macrocalcifications, 191, 194–195, 198–199, 204–206
 - round shape, 191, 194–195
 - slightly hypoechoic, 191–193
 - US-FNAB, 190
 - metastatic LN, 280, 283–287, 289–292
 - multifocal
 - HT, 207
 - US findings, 208–213
 - and parathyroid adenoma, 231
 - small solitary nodule, 181
 - complete/incomplete halo sign, 172, 182–183, 186–187
 - cystic degeneration, 173, 188–189
 - vs. FTC, 172
 - FVPTC, 173, 184–185
 - incidence of, 172
 - intranodular hypervascularity, 173, 186–189
 - irregular margins, 173, 178–179
 - marked hypoechogenicity, 172–173, 175
 - microcalcifications, 173, 178–180, 184–185
 - prognosis, 172
 - “taller-than-wide” shape, 173, 176–180
 - threshold effect, 190
 - vascular invasion, 172
 - thyroid remnants, 300
 - Papillary thyroid microcarcinomas (PTMC), 210
 - AIT, 228
 - cervical metastatic LNs, 166, 170–171
 - halo sign, 166, 169–171
 - heterogeneous echogenicity, 165, 170–171
 - HT, 214–215
 - isoechogenicity, 165, 169, 170
 - microcalcifications, 166, 167, 168
 - post-surgical follow-up of patients, 165
 - prevalence of, 165
 - subclinical low-risk, 165
 - thyroid tissue, 166, 168, 170–171
 - Parathyroid adenoma (PA), 230, 361, 375–377
 - ectopic inferior parathyroids, 330, 344–345
 - large degenerated, 331, 347
 - large left superior, 349–351, 355–359
 - left inferior, 352–359, 369–371
 - parathyroid cyst, 331, 346
 - pHPT, 329
 - right inferior, 347, 352–359
 - shrunk left, 372–374
 - small elongated left superior, 339–341
 - small inferior, 338
 - small left, 336–337
 - s-PTH levels, 329
 - synchronous papillary thyroid carcinoma, 231
 - ^{99m}Tc-MIBI scan, 330
 - tiny right inferior, 342–343
 - US findings, 331, 334–336

Parathyroid carcinoma (PCa)
 cytological examination, 348
 pHPT, 329
 s-PTH levels, 329
 US scan, 331, 348
 Parathyroid cyst, 347
 Parathyroid gland
 preoperative localization, 329
 US-PEIT
 complete therapeutic success, 368
 left inferior PAd, 369–371
 sHPT, renal replacement treatment with, 368, 375–377
 shrunken left PAd, 372–374
 Percutaneous ethanol injection therapy
 complications, 361
 indications, 361
 method, 361
 US-PEIT (*see* Ultrasound-guided percutaneous ethanol injection therapy (US-PEIT))
 Percutaneous ethanol injection therapy (PEIT) studies, 79
 Peripheral dystrophic calcifications, 105, 106
 Plummer's disease. *See* Toxic multinodular goiter (TMNG)
 Postoperative hemorrhage, 312
 Primary atrophic variant, 18
 Primary hyperparathyroidism (pHPT), 329, 330
 PAd and PCa, 334, 335, 336, 369
 percutaneous ethanol injection therapy, 368–374
 supernumerary parathyroid glands, 330
 Primary thyroid lymphoma (PTL)
 clinical manifestation, 265
 HT, 265
 incidence, 265
 retrospective study, 265
 US features
 borders, 266
 gastric cancer, 272–273
 HT and suspicious solitary medium-sized nodule, 271
 internal echoes, 266
 metastatic cervical and supraclavicular lymph nodes, 272–273
 NHL and malignant cervical lymph nodes, 266–270
 posterior echoes, 266
 Psammomatous calcification, 105
 PTC. *See* Papillary thyroid carcinoma (PTC)
 PTL. *See* Primary thyroid lymphoma (PTL)
 PTMC. *See* Papillary thyroid microcarcinomas (PTMC)
 Pure cysts, 362–364
 Pyramidal lobe, 314, 328

R

Radioiodine ¹³¹I-therapy (RIT), 2
 cervical compression, 119
 cosmetic discomfort, 119
 hyperthyroidism, 42
 inspiratory capacity, 119
 post-RIT thyroid gland, 52
 tracheal compression, 119
 Renal replacement therapy, 348, 350, 352, 355
 Retrosternal goiter (RSG), 129
 Riedel's thyroiditis, 17
 Rim peripheral calcification, 106, 116
 RSG. *See* Retrosternal goiter (RSG)

S

School-age children (SAC), 8
 Scintigraphy with ^{99m}Tc-MIBI, 369–371, 375–377

Secondary hyperparathyroidism (sHPT), 348, 350, 352, 355, 368, 375–377
 Serum parathyroid hormone (s-PTH), 329, 369
 sHPT. *See* Secondary hyperparathyroidism (sHPT)
 Small-needle aspiration biopsy, 379
 Solid nodule
 benign
 coarse structure, 93, 98
 elliptical, 93, 96–97
 homogeneous, 93–95
 hyperechogenicity, 93, 98
 isoechogenicity, 93–95
 ovoid, 93–95
 perinodular vascularity, 93, 94
 round shape, 93, 98
 sporadic tiny cystic cavities, 93, 98–100
 partially cystic nodule, 93
 Solitary toxic adenoma (STA), 225
 clinical findings, 135
 prevalence, 135
 radioactive iodine treatment, 135
 US findings, 135–137
 Sporadic tiny cystic cavity
 large solitary solid nodule, 99–100
 medium-sized solitary solid nodule, 98
 s-PTH. *See* Serum parathyroid hormone (s-PTH)
 SSG. *See* Substernal goiter (SSG)
 STA. *See* Solitary toxic adenoma (STA)
 Struma lymphomatosa, 17
 Subacute granulomatous thyroiditis (SGT)
 clinical findings, 55
 course after therapy, 55
 history, 55
 incidence, 55
 laboratory findings, 55
 physical examination, 55
 US features
 bilateral thyroid involvement, 56–65
 characteristic findings, 56
 cytopathological examination, 56
 ill-defined hypoechoic areas, 56, 62–64
 minimal vascularity pattern, 57–61
 thyroid carcinoma, 56, 65–67
 unilateral thyroid involvement, 56, 65–67
 Substernal goiter (SSG)
 essential facts, 129
 primary, 129–131
 secondary, 129, 132–133
 US characteristics, 134
 Subtotal thyroidectomy, 300
 GD, 299, 308–309
 Hashimoto's thyroiditis, 306
 Superficial abscess, 312, 313
 Superior parathyroid gland, 331–333
 Supernumerary parathyroid gland, 330
 Supraclavicular lymph nodes, 272–273
 Suspicious medium-sized nodule, 151, 271

T

“Taller-than-wide” shape, 77, 105, 142, 143, 145, 148, 157, 168, 170, 173, 176, 178, 191, 208, 210, 212, 220, 226, 228, 230, 232, 243, 271, 381
^{99m}Tc-technetium-pertechnetate, 140
 Thyroglobulin antibodies (Tg-Ab), 17–18
 Thyroid abscess, FNAB
 in adults, 389

- in children, 389
 - clinical presentation, 389
 - infectious agents, 389
 - large multinodular goiter, 390–391
 - symptoms, 389
 - treatment, 389
 - Thyroid cysts
 - complex cysts
 - dominant complex septated cyst, 80, 88
 - dominant giant complex cyst, 80, 91
 - dominant medium-sized complex cyst, 80, 86, 91
 - hyperechoic debris, 80, 91
 - small complex septated cyst, 80, 84, 85, 88
 - solitary medium-sized complex septated cyst, 80, 87
 - nodules, 79
 - primary cysts, 79
 - pure cysts
 - cat's eye artifact, 80, 83
 - comet tails, 80
 - with large cyst, 80, 81
 - with multiple tiny cysts, 80, 83
 - with small cyst, 80, 82
 - US-PEIT
 - AACE/AME/ETA Guidelines, 362
 - complex cysts, 362, 365–367
 - cystic fluid, 362
 - cyst size, 362
 - one-step ethanol ablation technique, 362
 - pure cysts, 362–364
 - simple aspiration, 362
 - two-stage ethanol ablation technique, 362
 - Thyroidectomy, 105
 - Thyroid hemiagenesis
 - diagnosis, 311
 - prevalence of, 311
 - Thyroid inferno, 2, 4, 11, 35, 42, 46, 47, 49, 51
 - Thyroid, margin of, 3
 - Thyroid nodules
 - calcifications, 78
 - echogenicity, 78
 - FNAB (*see* Fine-needle aspiration biopsy (FNAB))
 - Halo sign, 78
 - internal content, 77–78
 - margin, 78
 - shape, 77
 - size, 77
 - vascularity, 78
 - Thyroid peroxidase antibodies (TPO-Ab), 17–18
 - Thyroid remnants
 - DTC, 299
 - endoscopic thyroid surgery, 299
 - near TT, 299, 300
 - Graves' disease, 306–307
 - Hashimoto's thyroiditis, 305
 - multinodular goiter, 304
 - post right lobectomy, 303
 - post thyroidectomy, 300
 - fibrofatty connective tissue, formation of, 301–302
 - post-thyroidectomy hematoma, resorption of, 301–302
 - PTC, 300
 - subtotal thyroidectomy, 300
 - Graves' disease, 299, 308–309
 - Hashimoto's thyroiditis, 306
 - TT
 - complications, incidence of, 299
 - Graves' disease, 299
 - MNG, 299
 - permanent recurrent laryngeal nerve palsy, 299
 - temporary recurrent laryngeal nerve palsy, 299
 - Thyroid-stimulating hormone (TSH), 225
 - Thyroxin replacement therapy, 299
 - TMNG. *See* Toxic multinodular goiter (TMNG)
 - Total thyroidectomy (TT), 299, 300
 - complications, incidence of, 299
 - Graves' disease, 299, 306–307
 - Hashimoto's thyroiditis, 305
 - multinodular goiter, 299, 304
 - permanent recurrent laryngeal nerve palsy, 299
 - temporary recurrent laryngeal nerve palsy, 299
 - Toxic multinodular goiter (TMNG), 225
 - diagnosis, 135
 - laboratory findings, 135
 - physical examination, 135
 - prevalence, 135
 - radioactive iodine treatment, 135
 - US findings, 135, 138–139
 - TSH. *See* Thyroid-stimulating hormone (TSH)
 - TT. *See* Total thyroidectomy (TT)
 - Two-stage ethanol ablation technique, 362
- U**
- Ultrasound-guided fine-needle aspiration biopsy (US-FNAB)
 - ATC, 258
 - Bethesda System, for Reporting Thyroid Cytopathology, 382
 - equipment for, 383
 - parathyroid adenoma, 231
 - performance of, 384
 - PTC, 190, 231
 - Ultrasound-guided percutaneous ethanol injection therapy (US-PEIT)
 - of parathyroid gland
 - complete therapeutic success, 368
 - left inferior PAd, 369–371
 - sHPT, renal replacement treatment with, 368, 375–377
 - shrunk left PAd, 372–374
 - of thyroid cysts
 - AACE/AME/ETA Guidelines, 362
 - complex cysts, 362, 365–367
 - cystic fluid, 362
 - cyst size, 362
 - one-step ethanol ablation technique, 362
 - pure cysts, 362–364
 - simple aspiration, 362
 - two-stage ethanol ablation technique, 362
 - Ultrasound guided sclerotherapy, 312
 - US-FNAB. *See* Ultrasound-guided fine-needle aspiration biopsy (US-FNAB)
 - US-PEIT. *See* Ultrasound-guided percutaneous ethanol injection therapy (US-PEIT)
- W**
- WHO/ICCIDD-recommended reference, 11, 12